Université de Toulouse

THÈSE

En vue de l'obtention du

DOCTORAT DE L'UNIVERSITÉ DE TOULOUSE

Délivré par :

Université Toulouse 3 Paul Sabatier (UT3 Paul Sabatier)

Présentée et soutenue par :
Cécile FORMOSA

le lundi 22 septembre 2014

Titre :

Comprehension of the mechanisms of action of antimicrobial molecules using nanobiotechnologies

---

École doctorale et discipline ou spécialité :

ED SDM : Nano-physique, nano-composants, nano-mesures - COP 00

Unité de recherche :

LAAS-CNRS UPR 8001 - SRSMC-CNRS UMR 7565

Directeur(s) de Thèse :

Dr. Etienne DAGUE
Prof. Raphaël E. DUVAL

Jury :

Dr. Sandor KASAS, scientific collaborator, EPFL, Switzerland
Prof. John R. DUTCHER, professor, University of Guelph, Ontario, Canada
Dr. David ALSTEENS, postdoctoral fellow, ETHZ, Switzerland
Prof. Christine ROQUES, professor, University of Toulouse, France
Dr. Marion GRARE, scientific collaborator, University of Toulouse, France

Abstract

My PhD work consists in using Atomic Force Microscopy (AFM) techniques to study pathogenic microorganisms, and to probe their interactions with antimicrobials. During the last three decades, microbial resistance has dramatically increased and spread around the world. Pathogenic bacteria and yeasts have developed several ways to resist against almost all antimicrobials used. These pathogens can cause a wide range of superficial infections, but are also the cause of life-threatening infections in some patients. There are therefore two emergencies; the first one is to find new antimicrobial molecules, with an innovative mechanism of action. To reach this goal, it is mandatory to get further fundamental knowledge on the microbial cell wall, in order to identify original targets at the cell surface for new molecules. Therefore the second emergency is to develop techniques to explore microbial surfaces from a different angle, which requires an original experimental approach. In this context, biophysical approaches still remain underexploited in clinical microbiology. In my PhD, we took advantage of a technology coming from physics, and adapted to biological conditions, AFM. Its principle relies on the measure of a force between a sharp tip and a surface; by keeping this force constant while scanning the sample, it is possible to get a three dimensional image of it. An advantage of AFM is the possibility to work in liquid on living cells, which allowed us to image the elongation of live bacterial cells of *P. aeruginosa* treated by ticarcillin, a cell wall targeting antibiotic, and the removal of capsular polysaccharides from *K. pneumoniae* upon treatment with colistin, a last chance antibiotic. Nevertheless, sample immobilization is often a challenge that must be addressed for each kind of microorganisms studied. It represents an entire field of research, and led us to engineer a microstructured polydimethylsiloxane (PDMS) stamp to immobilize round cells of different sizes such as yeasts. Once this step accomplished, AFM can be used in classic imaging and force spectroscopy modes (contact mode, oscillating mode, force volume mode), but also in advanced modes in order to acquire multiparametric set of data on living cells. Indeed, AFM is also a highly sensitive force machine, able to record force distance curves that give access to nanomechanical and adhesive properties of living cells. We therefore used the multiparametric imaging mode, QI^{TM} from JPK Instruments, to image and quantify the nanomechanical/adhesive properties of microorganisms as well as mammalian cells and their isolated nucleus. We could then observe the modifications of the adhesive properties of the yeast *C. albicans*, treated or not by caspofungin, a last chance antifungal. Finally, to get further in the architecture of microorganisms cell wall, it is possible to functionalize AFM tips with biomolecules. A strategy that we have developed has consisted in grafting antibodies targeted against a peptide on the AFM tip while tagging proteins with the same peptide at the surface of living cells. This allowed mapping the localization of specific proteins at the surface of living yeasts and mammalian cells. Another strategy we developed has consisted in directly grafting on the AFM tip a biomolecule that naturally interacts with cell wall components. We used this last strategy to probe the bacterial cell wall of *P. aeruginosa* submitted to treatment by an innovative antibacterial, Cx1, and better understand the structure of its peptidoglycan. In conclusion, during my PhD, we especially addressed the contribution of biophysics in clinical microbiology. We developed original techniques to immobilize samples, to functionalize AFM tips, and used advanced multiparametric AFM modes to acquire original data on the surface of pathogenic microorganisms, in native conditions or in interaction with antimicrobials.

Summary

List of publications

1. **Formosa C.**, Grare M., Duval R. E., Dague E. Nanoscale effects of antibiotics on *P. aeruginosa*, *Nanomed. NBM* 8, 12-16 (2012). (IF=5.978)

2. **Formosa C.**, Grare M., Jauvert E., Coutable A., Regnouf-de-Vains J. B., Mourer M., Duval R. E., Dague E. Nanoscale analysis of the effects of antibiotics and CX1 on a *Pseudomonas aeruginosa* multidrug-resistant strain, *Sci. Rep.* 2, 575 (2012). (IF=5.078)

3. Pillet F., Sanchez A., **Formosa C.**, Séverac M., Trévisiol E., Bouet J. Y., Anton-Leberre V. Dendrimer functionalization of gold surface improves the measurements of protein-DNA interactions by surface plasmon resonance imaging, *Biosens. Bioelectronics.* 43, 148-154 (2013). (IF=6.451)

4. Chopinet L.*, **Formosa C.***, Rols M. P., Duval R. E., Dague E. Imaging living cells surface and quantifying its properties at high resolution using AFM in QITM mode, *Micron* 48, 26-33 (2013). (IF=2.062)
   *co-first authors

5. **Formosa C.**, Schiavone M., Martin-Yken H., François J. M., Duval R. E., Dague E. Nanoscale effects of Caspofungin against two yeasts species *; Saccharomyces cerevisiae* and *Candida albicans*. *Antimicrob Agents Chemother.* 57, 3498-3506 (2013). (IF=4.451)

6. Sapet C., **Formosa C**., Sicard F., Bertosio E., Zelphati O., Laurent N. 3D-fection: cell transfection within 3D scaffolds and hydrogels. *Ther. Deliv.* 4:6, 673-685 (2013).

7. François J. M., **Formosa C**., Schiavone M., Pillet F., Martin-Yken H., Dague E. Use of Atomic Force Microscopy (AFM) to explore cell wall properties and response to stress in the yeast *Saccharomyces cerevisiae. Curr. Genet.* 59, 187-196 (2013). (IF=1.712)

8. Beauvais A., Bozza S., Kniemeyer O., **Formosa C.**, Balloy V., Henry C., Roberson R. W., Dague E., Chignard M., Brakhage A. A., Romani L., Latgé J. P. Deletion of the α1,3 glucan synthase induces a restructuration of the conidial cell wall responsible for the avirulence of *Aspergillus fumigatus. Plos Path.* 9:11 (2013). (IF=9.127)

9. Pillet F., Chopinet L., **Formosa C.**, Dague E. Atomic Force Microscopy and pharmacology; from microbiology to cancerology. *BBA-Gen. Subjects* 1840:3, 1028-1050 (2014). (IF=3.829)

10. Pillet F., Lemonier S., Schiavone M., **Formosa C.**, Martin-Yken H., François J. M., Dague E. Uncovering by Atomic Force Microscopy of an original circular structure at the yeast cell surface in response to heat shock. *BMC Biol.*, 12:6 (2014). (IF=7.430).

11. **Formosa C.**, Schiavone M., Boisrame A., Richard M. L., Duval R. E., Dague E. Multiparametric imaging of adhesive nanodomains at the surface of *Candida albicans* by Atomic Force Microscopy. *Nanomed. NBM, in press.*

12. **Formosa C**., Lachaize V., Galés C., Rols M. P., Martin-Yken H., François J. M., Duval R. E., Dague E. Mapping HA-tagged protein at the surface of living cells by Atomic Force Microscopy. *J. Mol. Recognit., accepted*.

13. Schiavone M., Vax A., **Formosa C**., Martin-Yken H., Dague E., François J. M. A combined chemical and enzymatic method to determine quantitatively the polysaccharide components in the cell wall of yeasts. *FEMS Yeast. Res., in press*.

14. **Formosa C**., Pillet F., Schiavone M., Duval R. E., Ressier L., Dague E. A versatile tool to generate living cells arrays for Atomic Force Microscopy studies. *Nat. Protoc. accepted.*

15. **Formosa C.**, Duval R. E., Dague E. Unravelling of a mechanism of resistance to colistin in *Klebsiella pneumoniae* thanks to Atomic Force Microscopy. *JAC, under review*.

16. **Formosa C**., Dague E. Imaging living yeast cells and quantifying their biophysical properties by Atomic Force Microscopy. *Book Chapter submitted to Springer's Advanced Microscopy in Mycology.*

List of communications

1. AFMBioMed Conference, Paris (France), August 23-27, 2011. **Formosa C.**, Grare M., Duval R. E., Dague E. Nanoscale effects of antibiotics on *P. aeruginosa* multidrug resistant. **Poster presentation.**

2. 51st ICAAC (Interscience Conference on Antimicrobial Agents and Chemotherapy), Chicago (IL, USA), September 17-20, 2011. **Formosa C.**, Grare M., Duval R. E., Dague E. An application of nanotechnologies in microbiology: probing nanoscale effects of antibiotics on living bacteria. **Poster presentation**.

3. LMO Conference (Levures, Modèles, Outils), Toulouse (France), April 2-4, 2012. **Formosa C.**, Elsztein C., de Morais Jr M. A., François J. M., Dague E. Nanoscale effects of ethanol on wild type and yap1 mutant of *Saccharomyces cerevisiae*. **Poster presentation**.

4. 52nd ICAAC (Interscience Conference on Antimicrobial Agents and Chemotherapy), San Francisco (CA, USA), September 9-12, 2012. **Formosa C.**, Grare M., Duval R. E., Dague E. Nanoscale analysis of the effects of a new antibacterial, CX1, on a multidrug-resistant Pseudomonas aeruginosa. **Poster presentation**.

5. Linz Winter Workshop (Advances in Single-Molecule Research for Biology and Nanoscience), Linz (Austria), February 16-18, 2013. **Formosa C.**, Grare M., Duval R. E. and Dague E. AFM for clinical microbiology; the example of Cx1 and *Pseudomonas aeruginosa*. **Oral presentation.**

6. Advances in Biodetection and Biosensors Conference, Barcelona (Spain), March 5-6, 2013. Pillet F., Sanchez A., **Formosa C.**, Séverac M., Trévisiol E., Bouet J. Y., Anton-Leberre V. Dendrimer functionalization of gold surface to improve SPRi measurement of the Centromere binding specificity in assembly of the F plasmid partition complex. **Poster presentation.**

7. PYFF5 Conference (Physiology of Yeast and Filamentous Fungi), Montpellier (France), June 4-7, 2013. **Formosa C**., Schiavone M., Elsztein C., Martin-Yken H., De Morais Jr M. A., Duval R. E., François J. M., Dague E. The yeast response to external stress investigated by Atomic Force Microscopy. **Poster presentation.**

8. 53rd ICAAC (Interscience Conference on Antimicrobial Agents and Chemotherapy), Denver (CO, USA), September 10-13, 2013. Dague E., **Formosa C.**, Grare M., Duval R. E. Atomic Force Microscopy for microbes investigation and antimicrobial agent evaluation. **Poster presentation honored as "George McCracken Infectious Disease Fellow."**

9. Forum de l'Innovation de la Direction Générale de l'armement, Paris (France), November 21st, 2013. **Formosa C**., Duval R. E., Dague E. Comprendre les cibles d'actions de nouvelles molécules antibactériennes à l'aide des bionanotechnologies. **Invited poster presentation.**

10. Linz Winter Workshop (Advances in Single-Molecule Research for Biology and Nanoscience), Linz (Austria), January 31st-February 3rd, 2014. **Formosa C**., Schiavone M., Duval R. E. and Dague E. Imaging of adhesive nanodomains at the surface of Candida albicans by Atomic Force Microscopy. **Poster presentation.**

11. Linz Winter Workshop (Advances in Single-Molecule Research for Biology and Nanoscience), Linz (Austria), January 31st-February 3rd, 2014. Pillet F., **Formosa C.**, Teissié J., Rols M. P. and Dague E. Observation by AFM of cell-wall damages induced on bacteria by pulsed electric field. **Poster presentation.**

12. Linz Winter Workshop (Advances in Single-Molecule Research for Biology and Nanoscience), Linz (Austria), January 31st-February 3rd, 2014. Schiavone M., **Formosa C.**, Martin-Yken H., François J. M. and Dague E. Impact of caspofungin and gene deletions on yeast cell wall architecture. **Oral presentation.**

13. Forum des Microscopies à Sondes Locales, Montauban (France), March 17-21, 2014. **Formosa C.**, Schiavone M., Duval R. E., Dague E. Biophysique des nanodomaines adhésifs à la surface de *Candida albicans* par Microscopie à Force Atomique. **Oral presentation.**

14. Forum des Microscopies à Sondes Locales, Montauban (France), March 17-21, 2014. Schiavone M., **Formosa C.**, Martin-Yken H., François J. M., Dague E. Nanoarchitecture de la paroi des levures stressées. **Poster presentation**.

15. 54th ICAAC (Interscience Conference on Antimicrobial Agents and Chemotherapy), Washington (DC, USA), September 9-12, 2014. **Formosa C.,** Duval R. E., Dague E. Unraveling of a mechanism of resistance to colistin in *Klebsiella pneumoniae* thanks to Atomic Force Microscopy. **Oral presentation**.

List of abbreviations

AFM: Atomic Force Microscopy

AMP: AntiMicrobial Peptide

ANS: Anilino-1-Naphtalene-Sulfonic acid

APTES: 3-AminoPropylTriEToxySilane

ATCC: American Type Culture Collection

BSA: Bovine Serum Albumine

CHO: Chinese Hamster Ovaries

CWI: Cell Wall Integrity

CX1: para-guanidinoethylcalix-[4]-arene

DNA: DesoxyriboNucleic Acid

ECDC: European Center for Disease prevention and Control

EMEA: European MEdecines Agency

ESBL: Extended Spectrum β-Lactamase

FDA: Food and Drug Administration

FS: Force Spectroscopy

FV: Force Volume

HaCaT: cell line Human Keratinocyte

HS-AFM: High Speed Atomic Force Microscopy

KPC: *Klebsiella pneumonia*e Carbapenemase

LPS: LipoPolySaccharide

MDR: MultiDrug Resistant

MRC-5: cell line Human Fetal Lung Fibroblast

PALM: PhotoActivated Localization Microscopy

PDMS: PolyDiMethylSiloxane

PEI: PolyEthylenImine

PEG: PolyEthylene Glycol

QI™: Quantitative Imaging

RNA: RiboNucleic Acid

SEM: Scanning Electron Microscopy

SMFS: Single Molecule Force Spectroscopy

STORM: STochastic Optical Reconstruction Microscopy

XDR: eXtreme Drug Resistant

List of figures

Introduction

This PhD has for subject the "Comprehension of the mechanisms of action of antimicrobial molecules thanks to nanobiotechnologies". Its aim has been to use Atomic Force Microscopy (AFM) techniques to study pathogenic microorganisms, and to probe their interactions with antimicrobials. During the last three decades, microbial resistance has dramatically increased and has spread around the world. Pathogenic bacteria and yeasts have developed several ways to resist against almost all antimicrobials used. These pathogens can cause a wide range of superficial infections, but are also the cause of life-threatening infections in immunocompromised patients. There are therefore two emergencies; the first one is to find new antimicrobial molecules, with an innovative chemical structure, and if possible an innovative mechanism of action. But to reach this goal, it is mandatory to get further fundamental knowledge on the microbial cell wall, in order to identify original targets at the cell surface for new molecules. Therefore the second emergency is to develop techniques to explore microbial surfaces from a different angle, which requires an original experimental approach. In this context, biophysical approaches still remain underexploited in clinical microbiology[1–3].

During this PhD, we took advantage of AFM, a technology coming from physics, and adapted to biological conditions[4]. We used this powerful tool to get new fundamental data on the surface properties of yeasts and bacteria, in interactions with antimicrobials. The yeast model studied has been *Candida albicans*, a versatile opportunist pathogen, which is by far the most common human fungal pathogen. Because of its plasticity, *i.e.* its ability to grow both as unicellular budding cells or as filamentous hyphae, it can cause a wide range of infections, from surface infections to mucosal and blood-stream infections[5,6]. As for bacterial models, we focused on Gram-negative bacteria, and more specifically on the species *Pseudomonas aeruginosa* and *Klebsiella pneumoniae*. *P. aeruginosa* is an invasive opportunistic pathogen that causes severe

infections including bacteremia, pneumonia, meningitis or urinary tract and wound infections[7]. The particularity of this bacterial species is to be naturally resistant to multiple antibiotics, which is due to a natural lower outer membrane permeability and to many adaptive resistance mechanisms[8,9]. *K. pneumoniae* is well known as a cause of community-acquired bacterial pneumonia. However, its role as a common healthcare-associated pathogen causing infections of the urinary tract, bloodstream, pneumonia and intra-abdominal infections has become exceedingly common[10,11]. The particularity of *K. pneumoniae* is to produce extended spectrum β-lactamases (ESBLs), enzymes capable of hydrolyzing penicillins, cephalosporins of the first, second, third and fourth generations, and the monobactam aztreonam[12–14]. The goal of this PhD has been to increase the amount of fundamental data on the cell wall of these pathogenic microorganisms, but also to probe their interactions with antimicrobials. To this end, we worked with antibiotics such as ticarcillin, a β-lactam targeting the synthesis of the cell wall peptidoglycan, and tobramycin, an aminoglycoside inhibiting protein synthesis by binding with the bacterial ribosome, that we used to treat cells of *Pseudomonas aeruginosa*[15]. We also studied the interactions of last-chance molecules, used only in cases of severe infections when no other treatments are efficient with pathogenic microorganisms. In the case of *Klebsiella pneumoniae*, we used colistin (polymyxin E), a polypeptidic bactericidal agent which mechanism of action remains poorly characterized[16,17]. In the case of *Candida albicans*, we focused on the effects of caspofungin, a lipopeptide of the echinocandin class, which mechanism of action is to inhibit the synthesis of β-1,3-glucans, a major component of the yeast cell wall[18]. Finally the last antimicrobial studied during this PhD has been an innovative molecule, a cationic calixarene called CX1 that we used to treat a multidrug-resistant strain of the bacterial species *P. aeruginosa*, with the aim of understanding its unknown mechanism of action[19]. Figure 1 shows a schematic representation of the three axis developed during this PhD, that are the microorganisms

studied, the antimicrobial molecules used to treat them, and AFM, the tool used to explore the interactions between them.

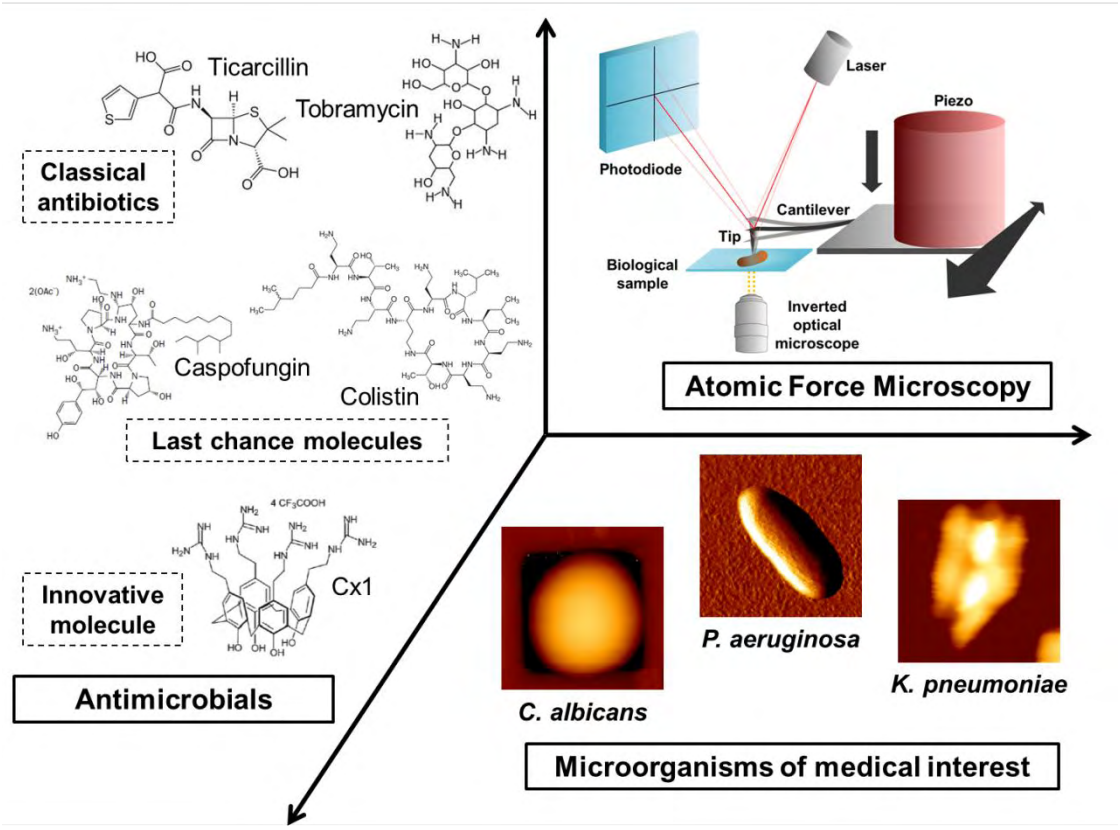

Figure 1. Recapitulative schema of the three axis "question", "biological models" and "tool" of this PhD. The effects of antibiotics, of last chance or innovative molecules were evaluated on different bacterial and yeast species of medical interest, thanks to Atomic Force Microscopy.

The present document is composed of 3 chapters. The first chapter is a general overview. It will first introduce the subject of the PhD, and place it in proper context. Then it will review the work performed during the three years of the PhD and discuss the main results obtained. After the general conclusions, are presented chapters 2 and 3, composed of my publications. In chapter 2 are presented 3 reviews focusing on the use of Atomic Force Microscopy for pharmacological studies, as well as for the study of yeast cells. In chapter 3 are presented research articles on the

work performed during this PhD. Chapter 3.1 presents the technological developments that were realized to adapt AFM techniques to biological samples. The first publication presents a protocol that was developed to immobilize round shaped cells such as yeast. The second publication describes the use of a multiparametric imaging mode (QI^{TM} from JPK Instruments) to study bacteria, yeast and eukaryotic cells. In the third publication is presented a method to localize specific proteins at the surface of living cells, by functionalizing AFM tips with antibodies targeted against a peptide used to tag proteins in cells. Chapter 3.2 is dedicated to the work performed on yeast cells. A first publication studies of the adhesive properties of *Candida albicans*, and shows high resolution and multiparametric data on aggregated proteins at its surface. A second publication presents the effects of caspofungin on the same yeast species, and how this molecule modulates the adhesive and nanomechanical properties of its cell wall. In chapter 3.3 are presented the results obtained on bacteria. The first publication describes the nanoscale effects of ticarcillin and tobramycin on the cell wall of *P. aeruginosa*. In the second publication, colistin is used to treat sensitive and colistin-resistant strains of *K. pneumoniae*, which allowed the unravelling of a new mechanism of resistance to colistin. The third publication shows how AFM has been used to understand the mechanism of action of an innovative antibacterial molecule, CX1, on the cell wall of a multidrug-resistant strain of *P. aeruginosa*. The appendices at the end of the document are composed of research articles in which I have participated, but that are not directly related to the PhD subject.

This PhD has been co-funded by the DGA (Direction Générale de l'Armement) and by the ANR (Agence Nationale de la Recherche). It was supervised by Etienne Dague, CNRS searcher at LAAS (Laboratoire d'Analyse et d'Architecture des Systèmes), CNRS (Centre National de la Recherche Scientifique), Toulouse, France, and Prof. Raphaël E. Duval, professor

of clinical microbiology at the University of Lorraine, and searcher at SRSMC (Laboratoire de Structure et Réactivité des Systèmes Moléculaires Complexes), CNRS, Nancy, France. Most of the experimental work has been performed in LAAS in Toulouse. This PhD is also the result of fruitful collaborations with Jean-Marie François and Hélène Martin-Yken, searchers at LISBP (Laboratoire d'Ingénierie des Systèmes Biologiques et des Procédés) and specialists of the genetics of yeasts cells, with Marion Grare, searcher at CHU Purpan (Centre Hospitalier Universitaire), specialist in clinical microbiology and pathogenic bacteria, and with Céline Galés, searcher at INSERM (Institut National de la Santé et de la Recherche Médicale), specialist of molecular biology and mammalian cell surface receptors. During these three years, I have worked with Post-Docs (Flavien Pillet) but also with PhD students (Louise Chopinet, Marion Schiavone, Véronique Lachaize), with whom I have exchanged every day, and participated to each other's works. Finally this work has been performed thanks to the work of Sandrine Assié-Souleille and Charline Blatché, technicians of the laboratory, responsible of the equipment used.

Chapter 1

General Overview

Chapter 1.1: General context, the return to the "pre-antibiotic era"

1.1.1 Antimicrobials and pathogens resistance

1.1.2 How to get out of this situation?

1.1.3 Technologies to study pathogens

Chapter 1.2: Review of the PhD work: technological developments and fundamental studies of microorganism's cell walls.

1.2.1 Introduction

1.2.2 Technological developments to study the cell wall of microorganisms by AFM

1.2.3 A nanoscale view of the yeast cell wall of Candida albicans and Saccharomyces cerevisiae

1.2.4 Nanoscale behavior of the bacterial cell wall submitted to antibacterials

1.2.5 AFM to understand the mechanism of action of a new antibacterial molecule

Chapter 1.3: Discussion: contribution of "nanomicrobiology" to clinical microbiology; does it help?

1.3.1 AFM as a useful tool for clinical microbiology

1.3.2 Cell surface properties of Candida albicans

1.3.3 Probing the effects of antibiotics on the cell wall of bacteria

Chapter 1.1: General context: the return to the "pre-antibiotic era"

1.1.1 Antimicrobials and pathogens resistance

Most pathogenic bacteria and yeasts are part of the human natural flora. But in some cases, these commensal bacteria become pathogenic, particularly in immunocompromised patients. To fight against these bacteria, antibiotics were developed. An antibiotic is defined as a substance that inhibits the growth or destroys microorganisms. The history of antibiotics starts in the early 1900s, when a man named Ehrlich, a German scientist, decided to find a molecule to cure syphilis, a sexually transmitted disease, caused by the spirochete *Treponema pallidum* that was endemic and incurable at that time. To this end, Ehrlich synthesized hundreds of compounds and tested them on syphilis infected rabbits. In 1909, the sixth compound in the 600th series tested, numbered 606, cured syphilis infected rabbits, and showed significant promise for the treatment of patients. The drug was then marketed in 1910 under the name of Salvarsan, and knew a great success by becoming the most-prescribed drug, until the 1940s[20]. Amazingly, the mechanism of action of this drug is still unknown, and its chemical structure has been solved only recently[21]. This screening approach introduced by Ehrlich then became the cornerstone of the early ages of the antibiotic research. It led to the discovery of sulfa drug, namely Prontosil, which was synthesized by Bayer chemists in 1935. The active part of Prontosil, sulfanilamide, was then produced massively, which led to the broad dissemination of the first bacterial resistances, to sulfa drug[20,22]. Penicillin effects were first observed by Ernest Duchesne, a French medicine doctor, in 1896. His observation was that *Penicillium glaucum* could neutralize the bacterial proliferation of *Escherichia coli* cells. However, this discovery remained silent until Alexander Fleming observed the same phenomenon in 1928. For 12 years after its observation of the antimicrobial activity of *Penicillium*, Fleming was trying to get chemists to purify the active

substance of *Penicillium*. He finally abandoned this idea in 1940, but in the same year, Florey and Chain published a paper describing the purification of penicillin for clinical testing[23]. Their protocol led to the massive production and distribution of penicillin in 1945[20,22], which led to the appearance of resistant strains capable to inactivate the molecule. However, the discovery of these first three drugs, Salvarsan, Prontosil and penicillin set up the paradigms for drug discovery research. These paths led to a number of new antibiotics, between the 1950s and the 1970s, the golden era of discovery of novel antibiotics classes.

As for antifungals, their development was extremely slow since the first antifungal agent, Nystatin, (also known as mycostatin) was discovered only in 1949, by two scientists named Hazen and Brown[24]. The reasons believed for this slow development is due to the nature of fungus: they are eukaryotic species and thus are biologically similar to human hosts[25]. This means that developing a drug to fight fungal disease without affecting the human host is a difficult task. However the isolation of Nystatin from the mold *Streptomyces nursei* set the stage for the discovery of amphotericin, in 1955, by Oura *et al*[26]. This substance was found to be the product of *Streptomyces nodosus*. The two forms of amphotericin, named A and B, were polyene antifungals with an *in vitro* effect on a wide variety of fungi[27]. In 1957, 5-Fluorocytosine, also known as flucytosine, was discovered by Duschinski, Pleven and Heidelberger[28], but its antifungal activity was first reported in 1964 by Gruneberg *et al*[29]. It must be noted that nowadays, the gold standard therapy for cryptococcal meningitis, a disease that kills more than 650 000 per year world-wide, in based on these two last molecules; amphotericin B and flucytosine[30]. Then, in the early 1960s however, Griseofulvin, the first orally antifungal was used to treat superficial fungal infections of the skin[31,32]. In 1963, the first broad-spectrum antifungal, haloprogin, was synthesized by Seki, a Japanese chemist, and used to treat dermatophytic infections in humans[33]. The late 1960s heralded the discovery of azoles antifungal agents, with

the introduction of clotrimazole (developed by Bayer), miconazole and econazole (developed by Janssen Pharmaceutica). But because of their poor response rates, the frequent recurrences of major fungal infections, and the toxicity associated with these molecules, scientists started the search for a new chemical group of azoles derivates, the triazoles. In general the triazoles demonstrated a broader spectrum of antifungal activity and reduced toxicity. However these recent years, as a result of the massive use of triazoles in critically ill patients, clear patterns of azole resistance have emerged[34]. To date, only these three classes of antifungal drugs have been available for systemic fungal infections: polyenes (amphotericin B), azoles and triazoles, and flucytosine. Although many of these drugs have advanced the management of fungal infections, failure rates remain high, and emergence of intrinsically resistant fungi is a growing problem. In this context, a new class of antifungal has been developed, the echinocandins[18]. The lead compound anidulafungin was identified in 1974[35]. In 1989, the compound that led to caspofungin was reported[36], and the precursor of micafungin was identified in 1990[37]. It is only in 2002 that caspofungin was approved by the FDA (Food and Drug Administration) to be used as an antifungal agent. The target of the echinocandins is the cell wall enzyme complex β-1,3-D-glucan synthase; this is the only class of antifungal that targets the cell wall of fungi. But even with this last class of echinocandins, the repertoire of antifungal agents is still very limited, particularly in comparison with the number of agents available for bacterial infections, and the search for new antifungals continues[30].

However the increased availability and use of antimicrobial agents in the recent years have led to the development of resistant strains. Indeed, most of the bacterial pathogens associated with epidemics of human disease have evolved into MultiDrug-Resistant (MDR) forms, *i.e.* into forms that are non-susceptible to at least one antimicrobial agent in three or more antimicrobial categories. Strains that are non-susceptible to at least one antimicrobial agent in all antimicrobials

categories except two or fewer are classified as eXtreme Drug Resistant (XDR) strains[38]. In this context, antifungal resistance is no exception; resistance to many antifungal drugs in use has also emerged these recent years. Drug resistance not only poses a major threat to public health, it also has striking economic consequences. Indeed, drug-resistant infections double the duration of hospital stay, double mortality and morbidity, compared with drug-susceptible infections[39]. But what is the cause of drug-resistance? The resistance problem is dependent on two components; the antimicrobial drug that inhibits susceptible organism and selects resistant ones, and the genetic resistance determinants in microorganisms selected by the antimicrobial drug[40]. Drug resistance emerges when these two components come together in an environment or host, which can lead to a clinical problem. Then, resistance genes and their hosts spread and propagate under continued antimicrobial pressure to amplify and extend to other hosts and locations. Indeed, drug resistance is mobile, as the genes for resistance can be transferred among microorganisms of different taxonomic and ecological groups, by the mean of mobile genetic elements such as plasmids, or naked DNA, among others[25,41]. In the absence of mobile genetic elements, a progression to drug resistance can occur through sequential mutations in chromosomes, which represents less than 20% of the bacterial resistances[42].

For bacteria, the mechanisms of resistance can be classified as antibiotic target related or antibiotic related (Figure 2). Antibiotic targets can be: (i) protected by modification (mutation in RNA polymerase confers resistance to rifampin), (ii) modified by an enzyme (methylation of an adenine residue in 23S rRNA makes it insensitive to macrolides), (iii) protected at cellular and population levels (formation of protective barriers by secretion of exopolysaccharides, alteration or decrease in the number of porins in Gram-negative bacteria). Antibiotics can be: (i) modified so the efficiency is lost (modifying enzymes inactivate chloramphenicol and aminoglycosides),

(ii) destroyed (β-lactamases destroy penicillin and cephalosporins), (iii) pumped out of the cell (via efflux pumps)[20,22,40,43,44].

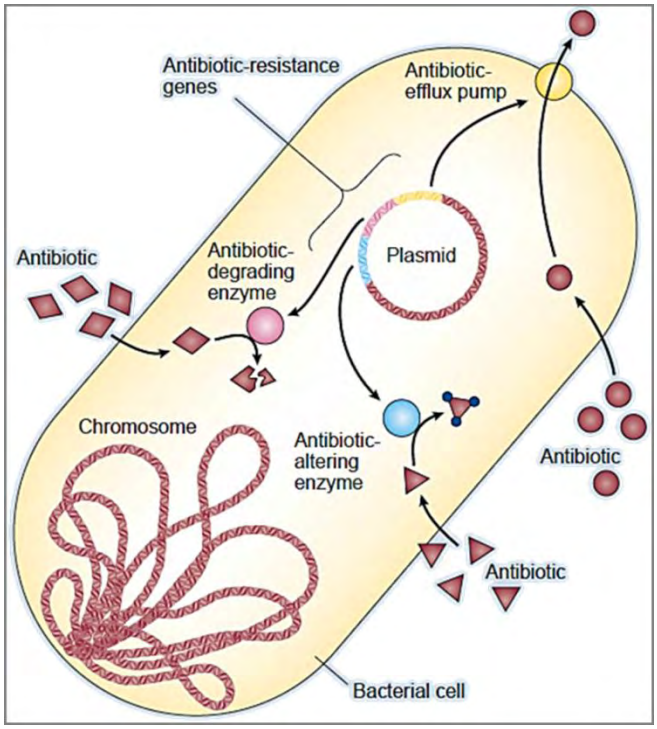

Figure 2. Schematic representation of the biological mechanisms of resistance of bacteria. Some mechanisms of resistance are directed at the antibiotic, while other target how the drug is transported. A third type of mechanism not shown alters the intracellular target of the drug, making the drug unable to inhibit a vital function in the microbial cell. Reprinted from[40].

As for yeast cells, the molecular mechanisms of resistance are also well-known; they are: (i) the increased efflux of antifungals (mutation in transcriptional regulators), (ii) alteration of the target protein of the antifungal, (iii) overexpression of the protein target (even in the presence of the drug, there are enough protein for maintaining a sufficient activity), (iv) alteration of the metabolism (loss of the enzyme activity prevents from the accumulation of a toxic product in the presence of the drug)[25,45–47]. In both cases, bacteria and fungi, known mechanisms of resistance do not explain all the resistances observed. Additional mechanisms are probably waiting for discovery.

Reviewing the history of the development of antimicrobial drugs, and of the mechanisms of resistance pathogens have developed against these drugs force us to acknowledge the present situation, which can be summarized by the sentence "bad bugs, no drugs"[48]. Indeed, the mortality rates due to multidrug resistant bacteria are high; each year, 25 000 patients in the European Union die from an infection caused by a MDR bacteria (European Center for Disease Prevention and Control (ECDC)/ European Medicines Agency (EMEA) Joint working group, 2009). In parallel, we can contribute to an "innovation gap" in the pharmaceutical industry (Figure 3). Since 2000 only three new classes of antibiotics have been introduced to the market for human use, and one of those is limited to topical use[44]. In the case of fungi, the problem is even more concerning for the long-term, since the number of fundamentally different types of antifungal agents that are available for treatment remains extremely limited, due to the biological proximity between humans and fungal pathogens[25].

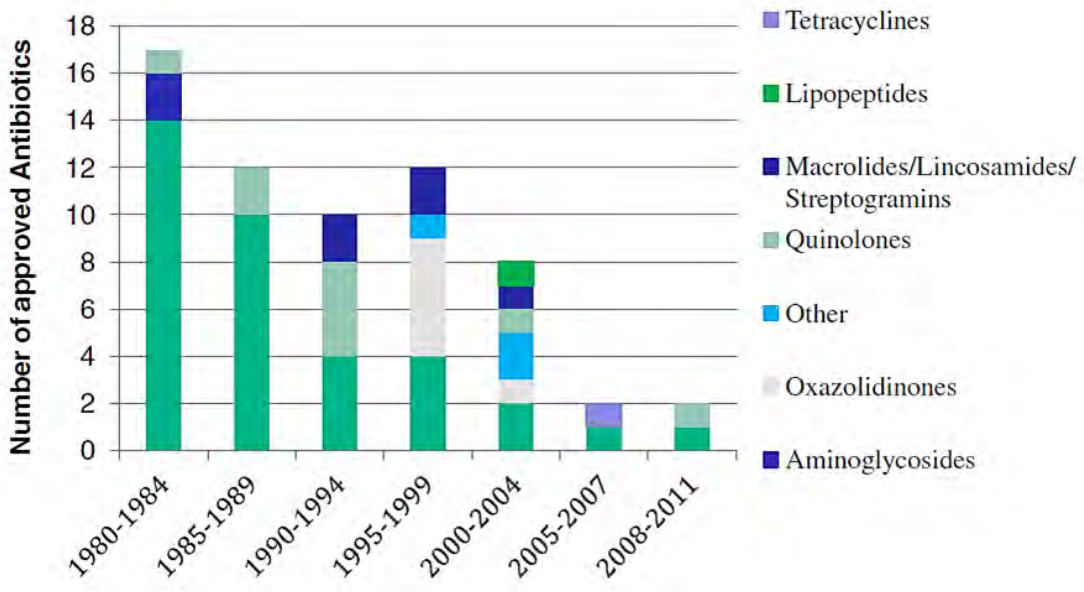

Figure 3. Number of approved antibiotics during the last 30 years. Reprinted from [44].

1.1.2 How to get out of this situation?

Bacterial and fungal infections are the cause of an enormous disease and societal burden. The increasing number of antimicrobial resistant microorganisms motivates prospective research toward discovery of new antimicrobial substances. Indeed, the need for new antimicrobial agents is high, and if no new agents are discovered, many of the current therapies will no longer work in the future, even for common infections. The two historical lines of antimicrobial drug discovery, synthetic chemical efforts *versus* isolation of new natural product scaffolds are both still in play. Since 2000, 22 antibiotics were launched and approved. Among them, 12 were antibiotics belonging to two new natural product classes such as daptomycin and retapamulin, and 9 of them were of synthetic origin[49–51]. Natural product classes are mainly represented by AntiMicrobial Peptides (AMPs) that are antibiotics produced by various organisms such as mammals, arthropods, plants and bacteria. Originally, their mechanisms of action were thought to consist solely of an increase in the pathogen cell membrane permeability, but it has been showed that they also exert their effects by inhibiting processes such as cell wall synthesis or enzyme activity[52–54]. However microbial pathogens have evolved different systems to resist to these antimicrobials, for example by destruction of the peptides by proteolytic digestion, change of the peptide target (modification of the cell envelope), and removal of antimicrobial peptides from their site of action via efflux pumps[55]. As for synthetic antimicrobials, there are the results of the modification of the molecular characteristics of existing molecules, to make them better in terms of reduced side-effects and avoidance of resistance[56]. A good example is the 4H-4-oxoquinolizine derivatives, developed in response to growing bacterial resistance to quinolones among Gram-positive and -negative bacteria and anaerobic pathogens. The modifications brought to these quinolones improved the antibacterial efficiency and spectrum, as well as their pharmacokinetic properties[57]. But as antimicrobial resistance increases, the race will intensify between microbes

and novel drug discovery and development efforts. Moreover, there are controversies concerning the cost-effectiveness of such research. Therefore new strategies have to be developed to overcome pathogen resistance.

One of these strategies developed for bacteria is the analysis of the bacterial genome. The resistance of pathogens has been going on in nature before antibiotics were used for chemotherapy. Indeed, in addition to the ability of microorganisms to acquire resistance, they are also intrinsically resistant to different classes of antimicrobials. This is a trait that is universally found within the genome of bacterial species, that is not dependent from the antimicrobial selective pressure, and that is not due to gene transfer[58]. The molecular basis of this phenomenon is the presence of the Gram-negative outer membrane that is impermeable to many molecules and exhibits many efflux pumps. In addition to this intrinsic resistance, studies have shown that a number of additional genes and genetic loci also contribute to the level of intrinsic susceptibility[59,60]. Combined, these different elements encompass the intrinsic "resistome". The study of this intrinsic resistome is of relevance for predicting evolution of microorganisms, for understanding the linkage between resistance and other virulence processes or metabolisms, and for defining novel targets which inactivation makes microorganisms susceptible to antibiotics[61]. However, genome-wide analysis of the intrinsic resistome of a given microorganism requires using high-throughput technologies.

1.1.3 Technologies to study pathogens

The study of the resistome of the bacteria is a way to identify new targets, by looking at the "inside" of the bacteria, *i. e.* at their chromosomes and plasmids. However, what about the "outside" of bacteria? And what about yeast cells? To combat drug resistance, it is necessary to develop new technologies that allow the study of the cell envelope of bacteria and pathogenic

yeasts, since this is where components that are unique and essential for the microorganisms, but not found in hosts, are. In this work, the type of technology that we have chosen to work with is Atomic Force Microscopy[4], a technology adapted from physics to the field of microbiology. Indeed, AFM is particularly well suited to the study of microorganisms because it combines a high-resolution imaging capacity with little sample preparation required, compared to other types of microscopy such as Scanning Electronic Microscopy[62]. In addition, samples can be imaged in fluid environments, which provides possibilities for monitoring live microbes in real-time. Nevertheless, the very first prerequisite is the bacterial or fungal cell immobilization. This point is critical in the development of AFM in microbiology[63]. The researchers have to deal with the paradox of a firm but not denaturing immobilization method. A lot of work is achieved by drying the sample, but that unfortunately leads to dead cells. The immobilization of living cells is therefore a research area that should not be neglected.

AFM is not only an imaging technology. It is also a highly sensitive force machine, able to measure forces as small as 10 to 20 pN. An AFM is therefore able to record force distance curves, where the force experienced by the probe is plotted as a function of the probe-sample separation distance, and which give access to the biophysical properties of the living material. Nanomechanical properties and nanoadhesive properties of the samples can be measured using the AFM as a force machine. The results of such experiments create new paradigms in life science, and the interpretations in term of structure functions relationships are promising. This technology allows the nanoscale study of the cell envelopes of yeasts and bacteria, and therefore will help in getting fundamental knowledge on the cell wall of pathogenic microorganisms, with the aim of identifying new targets for antimicrobial drugs at their surface. The bibliographic analysis of the use of AFM technologies for microbiology is presented in Chapter 2, under the form of two review articles and of one book chapter.

Chapter 1.2: Review of the PhD work: technological developments and fundamental studies of microorganism's cell walls.

1.2.1 Introduction

This work consists in using Atomic Force Microscopy (AFM) techniques to study the cell wall of pathogenic microorganisms, and to probe their interactions with antimicrobials. During the last three decades, microbial resistance has increased and propagated around the world. Pathogenic microbes have developed different ways to resist almost all antibacterial and antifungal available. These pathogens can cause a wide range of superficial infections, but are also the cause of life-threatening infections in immunocompromised patients. There are therefore two emergencies; the first one is to discover new antimicrobial molecules, with an innovative chemical structure, and mechanism of action. However to reach this goal, it is essential to get new fundamental knowledge on the microbial cell wall, in order to identify new targets at the cell surface for new cell wall targeting molecules. Therefore the second emergency is to develop techniques to explore microbial surfaces, which requires an original experimental approach. In this context, biophysical approaches still remain underexploited in clinical microbiology. In my PhD, we took advantage of AFM, a technology coming from physics, and adapted to biological conditions. Its principle for contact imaging is to maintain the AFM tip in continuous contact with the surface when translated over the sample. Recording of the cantilever deflection as the tip is scanned over the surface gives access a three dimensional image of the sample[64] (contact mode, Figure 4). AFM can also be used in Force Spectroscopy (FS) mode, where the cantilever deflection is recorded as the AFM tip is pushed towards the sample, and retracted from it (Figure 4 and 5).

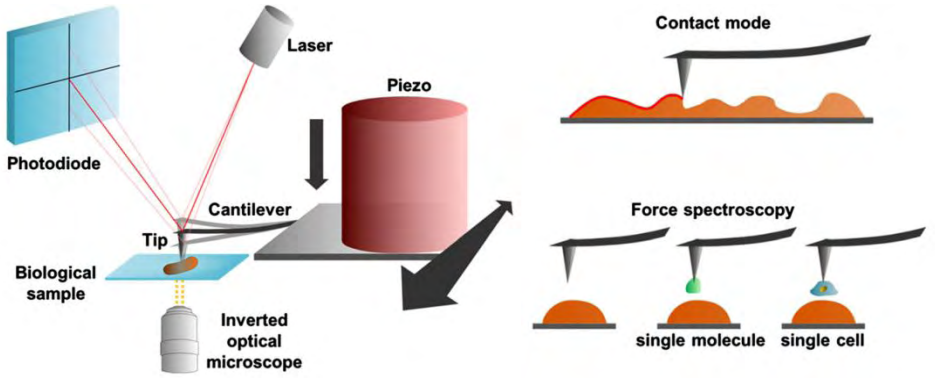

Figure 4. Schema introducing the AFM technology. A sharp tip is mounted on a cantilever that can be moved in the x, y, and z direction thanks to a piezo electric ceramic. The deflection of the cantilever is monitored on a 4 square photodiode using the reflection of a laser beam, aligned at the end of the, usually gold coated, cantilever. The AFM can be used to produce topographical images (like in contact mode) or to measure forces (in the force spectroscopy mode) between a bare or a functionalized tip (with a biomolecule or a single cell) and the sample. Reprinted from [64].

An advantage of AFM is the possibility to work in liquid on living cells, which allowed us for example to image the elongation of live bacterial cells of *P. aeruginosa* treated by ticarcillin, a cell wall targeting antibiotic[65] (Chapter 3.3.1, p233). We could also image the disappearing of the capsule of the bacteria *Klebsiella pneumoniae* under colistin treatment, a "last chance" antibacterial with a poorly known mechanism of action (Chapter 3.3.2, p240). Nevertheless, sample immobilization is often a challenge that must be addressed for each kind of microorganisms studied. Indeed, samples must be immobilized firmly enough to withstand AFM tips lateral forces, but without denaturing them. It represents an entire field of research, and led us to engineer a microstructured polydimethylsiloxane (PDMS) stamp, with holes of different sizes, to immobilize round cells of different sizes such as yeasts (Chapter 3.1.1, p146). Once this step accomplished, AFM can be used in classic imaging and force spectroscopy modes (Figure 4, contact mode, oscillating mode, force volume mode), but also in advanced modes in order to acquire high resolution or multiparametric set of data on living cells[66]. We have used for example

the multiparametric imaging mode, called Quantitative Imaging mode (QI™), from JPK Instruments, to image and quantify the nanomechanical/adhesive properties of microorganisms (*Candida albicans*, *Escherichia coli*, *Aspergillus fumigatus*), as well as mammalian cells (CHO, Chinese Hamster Ovaries) and their isolated nucleus (Chapter 3.1.2, p165).

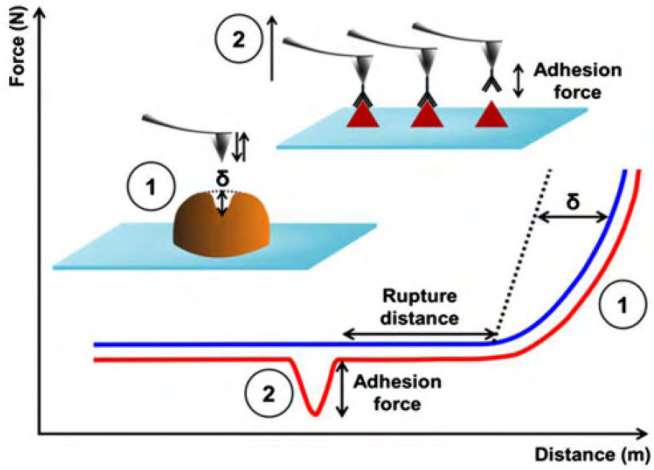

Figure 5. Schematic representation of AFM used in Force Spectroscopy mode. Force spectroscopy gives access to force curves that can be analyzed in two different ways. (1) Indentation (δ) is read on the force curve and represents the nanomechanical properties of the cell wall of yeasts. (2) single molecule force spectroscopy (SMFS) uses functionalized AFM tips with biomolecules or ligand; the interaction between a ligand chemically fixed on the AFM tip and the protein at the surface is given by the adhesion forces on the retracted force curve (red curve). Reprinted from [67]

But AFM is not only an imaging technology; it is also a highly sensitive force machine. An AFM is therefore able to record force distance curves, which give access to the nanomechanical and adhesive properties of the living material probed (Figure 5). Thanks to this possibility, we could study the adhesive properties of the pathogenic yeast *Candida albicans* (Chapter 3.2.1, p201) and show at its surface the presence of proteins able to aggregate into nanodomains and form amyloid plaques. We also could observe the modifications of these adhesive properties under caspofungin treatment[68], an antifungal used only as a last resort in life-threatening infections (Chapter 3.2.2, p221). Finally, to get further into the architecture of microorganisms cell wall, it is possible to

functionalize AFM tips with biomolecules (Figure 4 and 5). We used this strategy to functionalize AFM tips with Concanavalin A, a lectin that specifically binds to carbohydrates present in the bacterial cell wall[69]. These experiments allowed us to demonstrate the resistance of a multidrug-resistant strain of *Pseudomonas aeruginosa* to classical antibiotics, but also to understand the mechanism of action of an innovative molecule, CX1, on this species, thanks to the study of its peptidoglycan structure[70] (Chapter 3.3.3, p260). We then used this same technique to localize specific proteins expressed at the tip of the mating projections of *Saccharomyces cerevisiae*. To this end, we created a recognition system based on the antigen-antibody interaction, by functionalizing AFM tips with an antibody targeted against a peptide, used to label proteins of interest. This system was validated on model surfaces; its versatility was confirmed on living mammalian cells CHO (Chapter 3.1.3, p175).

1.2.2 Technological developments to study the cell wall of microorganisms by AFM

A prerequisite for AFM experiments is the immobilization of the biological samples probed[63]. However, immobilizing living microorganisms is often a challenge; samples must be immobilized firmly enough to withstand the lateral forces exerted by the AFM tip, but without denaturing them. Several techniques have been already used to immobilize living cells. Microorganisms can be chemically fixed on a solid substrate using glutaraldehyde or APTES[71], or immobilized on gelatin coated surfaces[72]. However these techniques can respectively modify the interface of the biological sample, or pollute the AFM tips, leading to artifacts. Another strategy takes advantage of the electrostatic interactions between a positively charged surface, such as a PolyEthylenImine (PEI) coated glass slides, and a negatively charged sample, such as bacteria[73]. In this work, this strategy has been used to immobilize living *Pseudomonas aeruginosa* and *Klebsiella pneumoniae* cells. Finally a strategy to immobilize round shaped cells

such as bacterial cocci and yeasts cells is to trap them in the pores of polycarbonate membranes[74]. This technique has been widely used over the recent years[75–78], although it is time-consuming and cells can be submitted to mechanical forces when trapped in the pores. To circumvent these problems, a strategy was developed in our team in 2011, consisting in trapping rounds shaped cells such as yeasts or spores of *Aspergillus fumigatus* in microstructured PDMS stamps[79]. This strategy is composed of three different steps. First, a glass/chromium mask harboring microstructured patterns is generated, and these patterns are then transferred onto a silicon wafer by photolithography and deep reactive ion etching. Then PDMS stamps are fabricated; for that, a PDMS prepolymer solution containing a mixture of PDMS oligomers and a reticular agent in a 10:1 mass ratio is cured on the silicon master for 1 hour at 80°C. The PDMS polymer can then be demolded to obtain a microstructured PDMS stamp. Finally cells are assembled into the microstructured PDMS stamp by convective/capillary deposition. This consists in dragging a drop of a cell suspension onto the PDMS stamp at a given temperature, humidity and translation speed. This procedure can also be performed manually in the case organized arrays of cells are not needed. An overview of this technique is presented in figure 6, where the three different steps are represented.

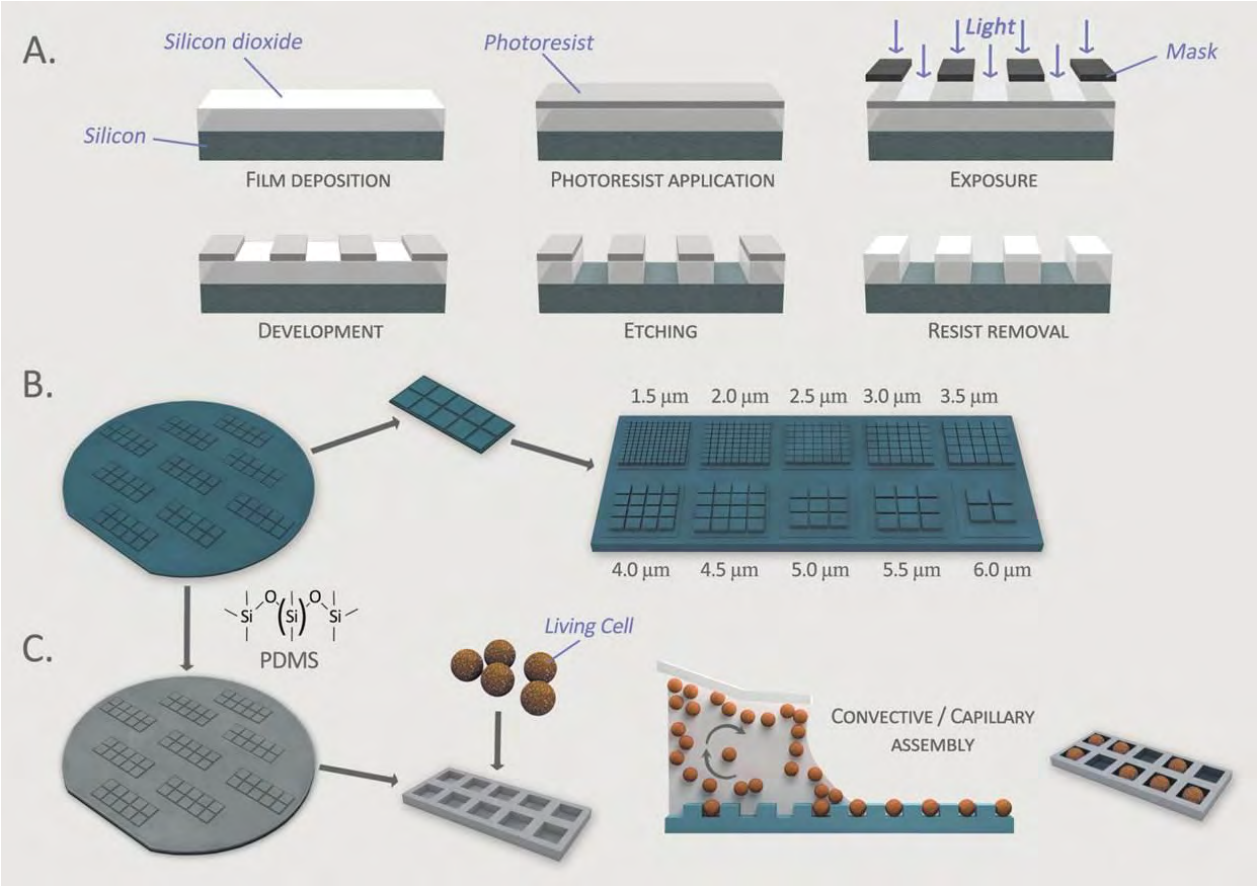

Figure 6. Schematic representation of the PDMS immobilization protocol. The first step (a) consists in generating a silicon master presenting the negative geometry desired for the PDMS stamp. The second step (b) is dedicated to the stamp molding. Liquid PDMS is flowed over the silicon master and reticulated for 1h at 80°C. Finally (c) cells are assembled in the microstructured PDMS stamp by convective/capillary deposition forming cell array. To be published.

In 2011, the first PDMS stamp was developed in our team[79]. It presented square patterns 5 µm wide, with a depth of 2.1 µm. However the use of this stamp was limited to microorganisms with a diameter of 5 µm approximately. During this PhD, we have developed a new PDMS stamp with square patterns ranging from 1.5 to 6 µm wide, with a pitch of 0.5 µm and a depth ranging from 1 to 4 µm. Characterization by AFM of these patterns on the PDMS stamp is presented in figure 7b. This new geometry allows immobilizing a wide broad of microorganisms of different sizes, without denaturing them as no chemicals are required. This immobilization method, soon to be published and presented in Chapter 3.1.1 (p146) , has been used during these three years to image

yeasts cells of *Candida albicans* (Figure 7a and c), and to study their adhesive properties, or their behaviors when submitted to an antifungal stress (Chapter 3.2, p200). It has also been used in collaborative studies to immobilize yeast cells of *Saccharomyces cerevisiae* submitted to thermal stress (Appendix 1, p272), or to study the effects of a mutation on the adhesive properties of spores of *Aspergillus fumigatus* (Appendix 2, p285).

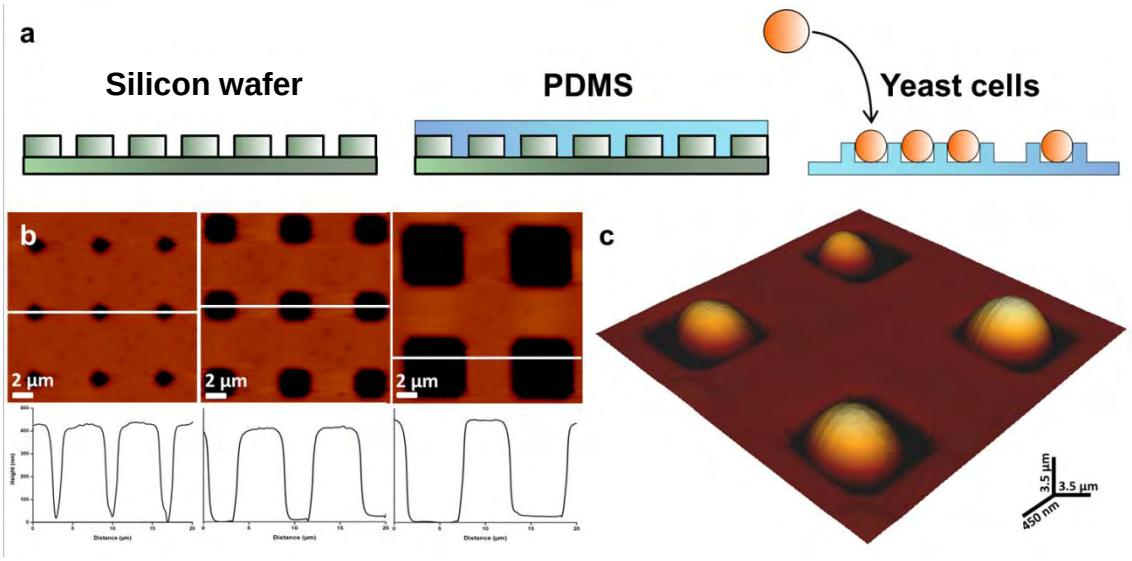

Figure 7. Immobilization of living yeast cells. (a) Schematic representation of yeast cells in PDMS microstructured stamps. (b) Height AFM images and corresponding cross-sections of the microstructured PDMS stamps. The structures ranged from 1.5 to 6.0 µm large and 2 to 3 µm deep. (c) *S. cerevisiae* cells trapped in microstructured PDMS stamps as imaged by Atomic Force Microscopy. Reprinted from [67]

Once this step of immobilizing living round cells was accomplished, the next challenge was to find an imaging mode where lateral forces were reduced, that could give high-resolution data and ideally also quantitative ones. Given our needs, we interested ourselves in the new advanced mode from JPK Instruments, named Quantitative Imaging™ (QI™) mode[66,80,81]. This mode is based on force curve acquisition across the sample surface, like a force-volume mode (FV), but processed quicker, as the tip, while retracting, moves laterally to the next point before

approaching again. In this mode, the time to record a single force curve is up to 1.0 ms, and the resolution up to 512 pixel², which is well suited for biological samples and kinetic studies on these samples. A comparison of QI™ with contact mode or Force Volume (FV) mode is presented in figure 8.

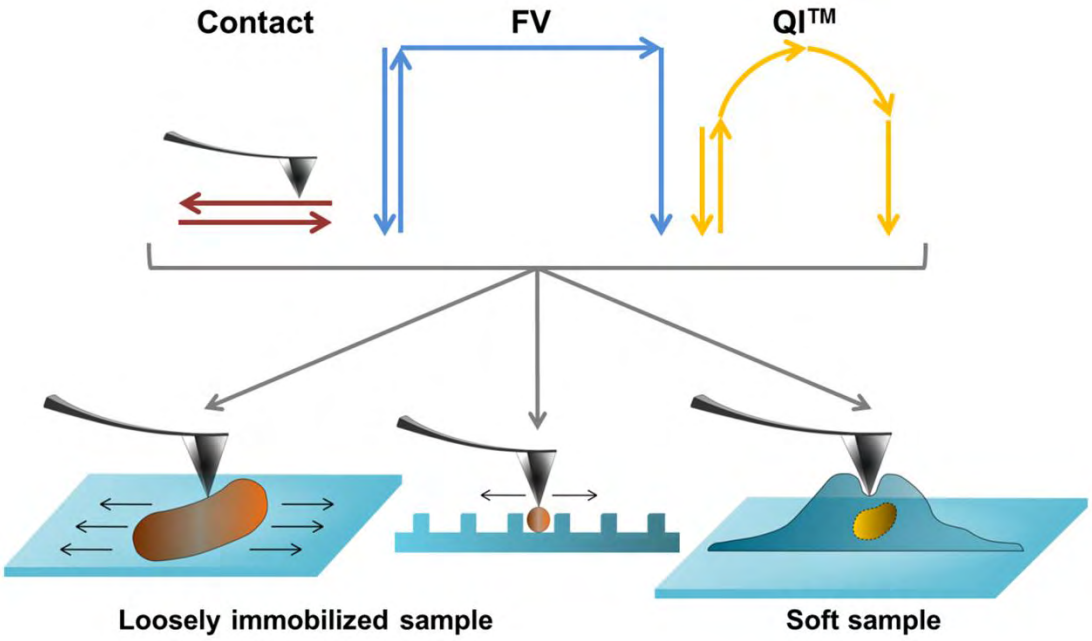

Figure 8. AFM modes comparison. For each mode, contact, Force-Volume (FV) and Quantitative Imaging™ (QI™) mode, the movement of the AFM tip is represented. These modes were applied to different kinds of samples: loosely immobilized samples and soft samples. QI™ is the best suited for these kind of samples. Reprinted from [66].

In this mode, during acquisition, a force curve is recorded for each pixel, therefore giving access to the "true" surface topography of the sample, by extracting the zero-force contact point from each curve. Each extent force curves can also be analyzed individually through theoretical models giving therefore access to the nanomechanical properties of the sample, such as elasticity or stiffness. Finally, each retract force curve can be extracted to measure the adhesion forces between the tip, biofunctionalized or not, and the biological sample. We have demonstrated in this work that this AFM mode was useful to image loosely bound samples, as well as soft

samples as no lateral forces are exerted by the tip during acquisition (Figure 8). Furthermore, we showed that it was possible thanks to this mode to map at high-resolution the nanomechanical properties of the samples, as well as their adhesive properties. These results, published in Micron, are presented in chapter 3.1.2 (p165). Therefore, during this PhD, we took advantage of this technology, and used it to image and quantify the nanomechanical/adhesive properties of different microorganisms such as *C. albicans*[68] (Chapter 3.2, p200), *S. cerevisiae*[68] (Appendix 1, p272) *A. fumigatus*[82] (Appendix 2, p285), and *K. pneumoniae* (Chapter 3.3.2, p240).

In order to access significant adhesive data on living cells, AFM can be used in QI™ or FV mode with functionalized AFM tips; this is called Single Molecule Force Spectroscopy (SMFS). In this technique, AFM tips interact with biomolecules immobilized on innate substrates or artificial biomembranes (*in vitro* studies), or present at the surface of living cells (*in vivo* studies), to understand the intra- and inter-molecular interactions of biomolecular systems[83,84]. Although this technique has been widely used *in vitro*[85–87], only few reports have used it on living cells; such experiments are often challenging, because of the heterogeneity of the cellular surfaces. For example, the yeast cell wall is composed of heterogeneous components (mannans, mannoproteins, glucans, chitin), that are structurally organized among the cell wall depth. This heterogeneity and complex molecular organization is essential for maintaining a functional cell wall that protects the cell from the environment, and allows morphogenic events to take place[88]. However, during SMFS experiments, all these different components at the surface of the living cells can cause non-specific interactions with the AFM tip (hydrophobic interactions, electrostatic…), hiding therefore the interactions of interest. In this context, it is necessary to functionalize AFM tips with specific antibodies targeting only one molecule in particular at the surface of the cells. But the huge lack of antibodies recognizing native membrane proteins with

high specificity largely prevents the use of functionalized AFM tips to explore the behavior of these proteins at the cell surface. To bypass these problems, biologists developed a genetic strategy consisting in labelling proteins to their amino (N-) or carboxy (C-) terminus with specific small tags and then expressing these tagged-proteins in living cells. Several and general epitope tags such as Human influenza hemagglutinin (HA) tag (YPYDVPDYA), FLAG tags (DYKDDDDK) or myc tags (EQKLISEEDL) and corresponding high specific antibodies recognizing these epitopes have been thus developed and are commonly used by the biology community, therefore offering the possibility to follow the protein of interest with high accuracy. We took advantage of these specific antibodies and functionalized an AFM tip with an antibody targeted against the HA epitope-tag. Many strategies to functionalize AFM tips with biomolecules have been described so far. Some of them consist in the nonspecific adsorption of proteins, for example BSA (Bovine Serum Albumin), to the silicon nitride surface of AFM tips[89], or in the chemical fixation of biomolecules by sulfur-gold bonds to gold-coated AFM tips. This last strategy has been successfully used for measuring interactions forces between complementary DNA strands[90], or between fibronectin and bacterial cells[91]. However, in the first case, the adsorption is nonspecific, and in the second case, the gold-coating of AFM tips modifies the spring constant of the cantilevers where the tips are fixed. To avoid these problems, it is possible to covalently link a molecule containing amino groups directly to the silicon nitride AFM tip. To this end, AFM tips must be first amino-functionalized either by esterification with ethanolamine[92] or silanization with aminopropyl-triethoxysilane (APTES)[93]. Then, the amino-functionalized tip has to be bridged to the biomolecule of interest. This can be achieved by different ways[94], for example through the use of heterobifunctionalized PolyEthylene Glycol (PEG)[94–96], or, as we decided in our study, through the use of an aldehyde-phosphorus dendrimer. This strategy developed in our team in 2012[69], has already been used for probing the surface of

live bacteria[70], and consists in making "dendritips" by reacting amino-functionalized AFM tips with dendrimers, therefore leading to dendrimer-activated tips. This strategy is described in figure 9. Then, the free aldehyde functions at the surface of the dendrimers are available to react with amino-functions present on every protein and on many biomolecules. Using this strategy we are able to measure specific interactions between a biomolecule immobilized on the AFM tip and a biomolecule immobilized on an abiotic surface, or at the surface of living cells, without modifying the spring constant of the cantilever.

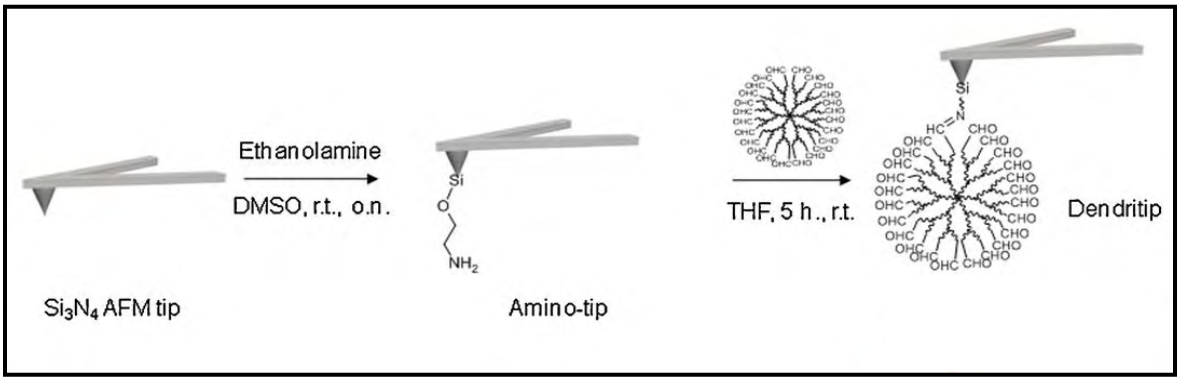

Figure 9. Schematic representation of Dendritip fabrication. Amino groups are introduced on the AFM tip and the dendrimer bearing 96-aldehyde en groups is attached via imine bond formation. Reprinted from [69].

In this work, we have used this strategy and developed AFM tips functionalized with an anti-HA (peptide YPYDVPDYA) antibody. At first the designed experiments also consisted in functionalizing AFM tips with anti-V5 (peptide GKPIPNPLLGLDST) and anti-Histidine (amino acid H) antibodies. However, optimizing the chemistry on the AFM tip and on model surfaces so that the antibodies and epitopes are presented with the right orientation for specific recognition, optimizing the concentrations in antibodies on the AFM tip to avoid multiple binding events, and finally tagging proteins with the right epitopes tags using biomolecular techniques are difficult and time-consuming procedures. Therefore we chose to focus on the couple HA-anti HA, and

developed biological models with surface proteins exhibiting HA tags. The first step for developing the HA-antiHA system was to validate our tip on model surfaces functionalized with HA epitopes, as presented in figure 10. For that, we performed blocking experiments (figure 10b), loading rate experiments (figure 10c), as well as contact time experiments (figure 10d). These experiments allowed us to show the specificity of the interaction between the antibody grafted on the AFM tip and the HA epitope on the surface model, and to characterize it thermodynamically by calculating the dissociation kinetic constant (Koff).

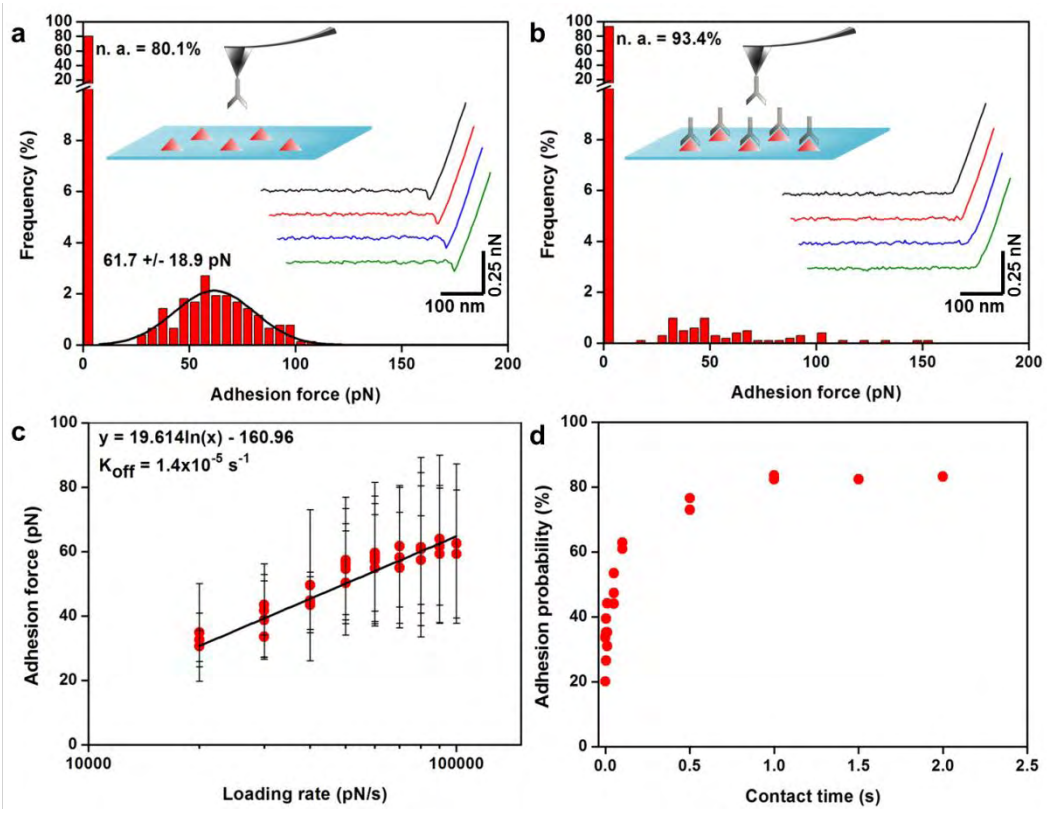

Figure 10. Single Molecule Force Spectroscopy with HA and HA antibody-functionalized AFM tips (HA-tip). (a) single molecule interactions between HA peptide immobilized on epoxy glass slide, and HA-antibodies immobilized on an AFM tip, at a loading rate of 70 nN/s. (b) blocking of HA specific sites by HA-antibodies and single-molecule force spectroscopy with HA antibody AFM tips. (c) Loading-rate dependence of interaction forces between HA and HA antibodies, and (d) contact-time dependence of the adhesion probability. Results accepted for publication in Journal of Molecular Recognition.

Then, after validation, we used this system on yeast cells over-expressing a cell wall protein called Ccw12 labelled with the HA epitope. This protein, involved in the remodeling of the cell wall, could be mapped only at the surface of cells in a particular morphogenic state during mating process. This led us to image for the first time by AFM yeasts cells as "shmoos", *i.e.* in mating projections. The results obtained with the HA tip on these shmoos open new perspectives to study the remodeling of the cell wall in yeasts. Finally to show the versatility of our system, we used it on mammalian cells CHO, and unfolded from their surface a G-coupled protein receptor, the β2-adrenergic receptor, labelled with HA epitope at its N-terminal. These results, soon to be published in Journal of Molecular Recognition, are presented in Chapter 3.1.3 (p175).

1.2.3 A nanoscale view of the yeast cell wall of Candida albicans and Saccharomyces cerevisiae

The first type of microorganisms studied during my PhD was yeast cells, especially *Candida albicans,* the most common human pathogenic fungal species, and *Saccharomyces cerevisiae*, also known as the baker yeast. Yeast cells are surrounded by a thick, mechanically strong cell wall which serves several key physiological functions, namely maintaining cell shape and cell integrity, and protecting cell interior from harmful compounds from the environment. The cell wall also harbors several proteins that are implicated in molecular recognition and adhesion[97]. The chemical composition of the yeast cell wall, presented in figure 11, is well known[88]. It consists in a microfibrillar network of β-glucans (β-1,3 and β-1,6-glucans) that represents 50 to 60 % of the cell wall mass, overlaid by highly glycosylated proteins decorated by long chains of mannose residues representing 40-50 % of the cell wall mass. Chitin, a linear

polysaccharide of β-linked *N*-acetylglucosamine, is the third component of the yeast cell wall and represents 1 to 3 % of the cell wall mass.

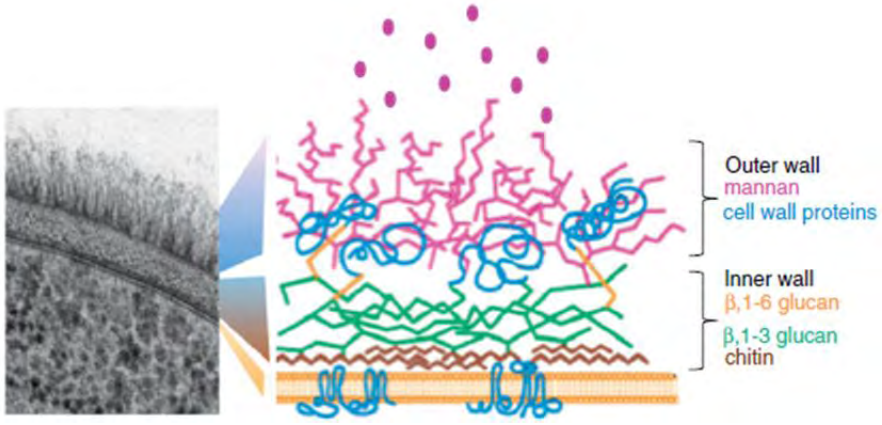

Figure 11. Cell wall composition of yeast cells. Transmission electron micrograph showing a section of the *C. albicans* cell wall, and a cartoon showing the arrangement of the major components of the cell wall. Adapted from [5].

Over the last 15 years, the complexity of the cell wall architecture has emerged from detailed genetic, molecular and biochemical studies, which led to the discovery of several interconnections among these various wall components to form macromolecular complexes[98,99]. In addition, the molecular architecture of the cell wall is not static but constantly remodeled depending on growth conditions, morphological development as well as response to cell surface stresses[98]. Therefore, AFM, which allows direct visualizing and probing the ultrastructure of the cell wall, is perfectly suited for the study of its dynamic structure and its molecular modification in different conditions[100,101].

The yeast *Candida albicans* has emerged as a major public health problem these last two decades. This opportunistic pathogen causes a wide range of infections from skin infections, to mucosal and blood-stream infections[5]. Whereas mucosal infections are common and occur in healthy organisms, blood-stream infections are observed only in immunocompromised patients

and are life-threatening. This type of infections, also known as candidaemia, can develop into disseminated candidiasis when the infection spreads to internal organs, leading to high mortality rates[6]. But in order to colonize and subsequently to disseminate in the blood stream, *C. albicans* first needs to adhere to different substrates. This first stage of infection[102] is mediated by adhesins that are found on the surface of the yeast cell wall. Many of these adhesins are mannoproteins, and among them, the adhesin family identified as having a major role in host cell attachment is the Als (Agglutinin-like Sequences) family[103]. The Als were initially reported as having homologies with the proteins responsible for auto-agglutination in the baker yeast *Saccharomyces cerevisiae*. Eight Als have been identified, they all are primarily involved in host-pathogen interactions[104]. It was found that there were amyloid-forming sequences in the Als adhesins of *Candida albicans*[105]. Amyloids are insoluble fibrillar protein aggregates whose core consists in crystalline arrays of identical sequence in many molecules of the amyloid protein[106,107]. Cells expressing the Als proteins can rapidly aggregate, and the aggregation has amyloid-like properties. Like amyloid formation, aggregation ability propagates through the adherent cell population and depends on conformational changes of the Als protein. This transition of the conformational state to an aggregative state of the proteins is characterized by the formation of hydrophobic nanodomains on the entire surface of the cell[108]. Different techniques can be used to visualize these nanodomains at the surface of *C. albicans*: fluorescence microscopy[105,107,108], or Atomic Force Microscopy. This last technology has been used by Alsteens *et al.* to image the formation and propagation of nanodomains in living yeast cells[109] and also to unfold amyloid proteins from the yeast surface using single molecule force spectroscopy[110–112]. In this work, we have used Quantitative Imaging™ mode to image, as showed in figure 12, and quantify at the same time the nanomechanical properties, the adhesiveness (force and nature of the interaction), the size and the thickness of the nanodomains at high resolution[66,113].

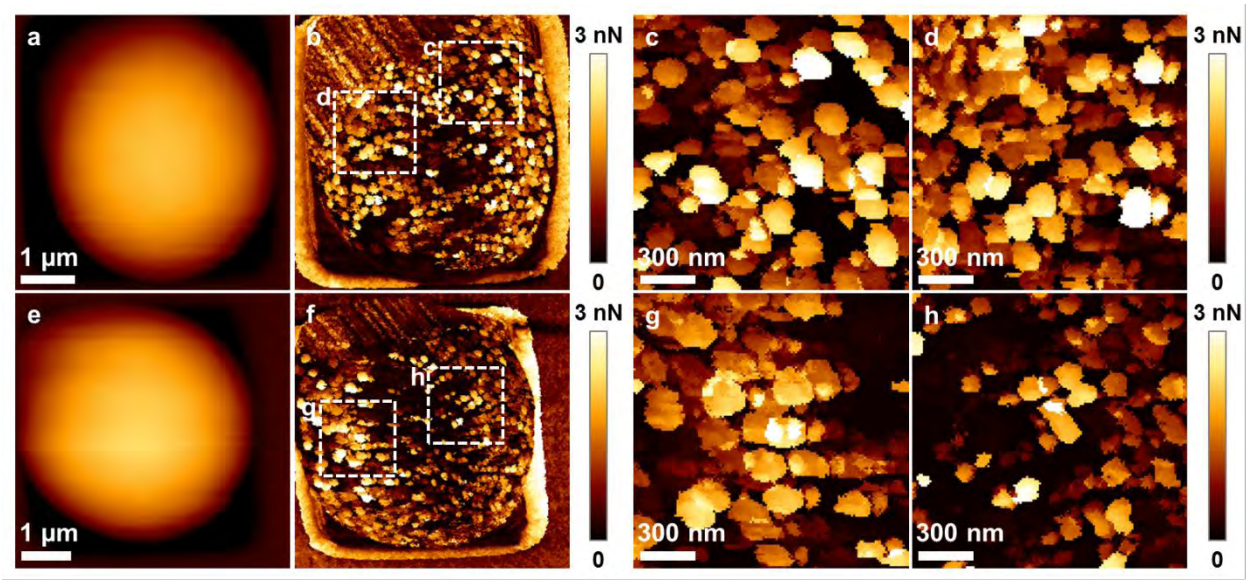

Figure 12. Imaging of the adhesive domains of *Candida albicans*. (a and e) Height images (z-range = 2.5 µm) of two *C. albicans* cells in polydimethylsiloxane (PDMS) stamps, and (b and f) adhesion images corresponding to the height images. (c, d, g and h) Adhesion images of small areas on top of the cell, represented by the white squares in b and f. Results accepted for publication in Nanomedicine NBM.

The data collected showed that these nanodomains are localized differently at the surface of the cell, depending on the structures featured by the cells (bud scars, buds). This illustrates the amazing plasticity of this species[6] able to grow as a commensal or as a pathogen[5,114], in all the parts of the intestinal tract, but also on the vaginal mucosa, as unicellular budding cells or as filamentous hyphae. We also showed that there were degrees of adhesiveness, depending on whether the amyloid proteins had totally aggregated (hydrophobic nanodomains) or not, and that these degrees of aggregation were directly correlated to the stiffness of the yeast cell wall. We then went further in the study, using functionalized AFM tips, and were able to determine that the less adhesive nanodomains were formed by mannoproteins that can interact specifically with Concanavalin A. Using force measurements and amyloid forming or inhibiting peptides, we could show that these mannoproteins were able to aggregate to form the adhesive nanodomains, because of their amyloid properties. These results, accepted for publication in Nanomedicine

NBM (chapter 3.2.1, p201), show the plasticity of *C. albicans*[25] and participate to explain its remarkable adaptation and pathogenicity.

The yeast cell wall is also the target of choice for antifungal agents since it is a specific armor that does not exist in mammalian cells, and its damaging leads to cell death[115,116]. Due to the essential function of the cell wall, exposure of yeasts to antifungals such as caspofungin, a specific inhibitor of the β-glucan synthase[18], induces activation of cell wall remodeling through the Cell Wall Integrity (CWI) pathway[117], which culminates into transcriptomic and metabolic responses aiming at counteracting the disastrous effects caused by this drug on the cell wall. We complemented these molecular data using AFM, and studied the effects of caspofungin on the yeasts *Candida albicans* and *Saccharomyces cerevisiae*, as a model yeast species[68]. Using our innovative method to immobilize yeasts cells into PDMS stamps, in combination with the Quantitative Imaging™ mode that allows acquiring high-resolution force maps on challenging samples, we could collect AFM data on different cells in a reasonable period of time. In parallel of these experiments, we quantified the different components of the yeast cell wall (glucans, mannans and chitin) in native conditions, and upon treatment, using acid hydrolysis method[118]. We found that administration of caspofungin induced a deep cell wall remodeling in both yeast species showed by an increase in the elasticity of the cell wall as a function of the caspofungin dose. The changes in the cell wall composition, however, were more pronounced for *C. albicans*, with notably a more elevated rise in chitin as a function of the caspofungin dose, concurrent with the increase of the elasticity of the cell wall. In addition, at low dose of caspofungin, the cell surface of *C. albicans* exhibited adhesions, that could potentially be due to the presence of mannoproteins such as adhesins of the Als family. On the other hand, treatment of *S. cerevisiae*

cells with high doses of caspofungin resulted in an impairment of cytokinesis. Figure 13 shows a summary of these results, which are published in Antimicrobial Agents and Chemotherapy and presented in Chapter 3.2.2 (p221).

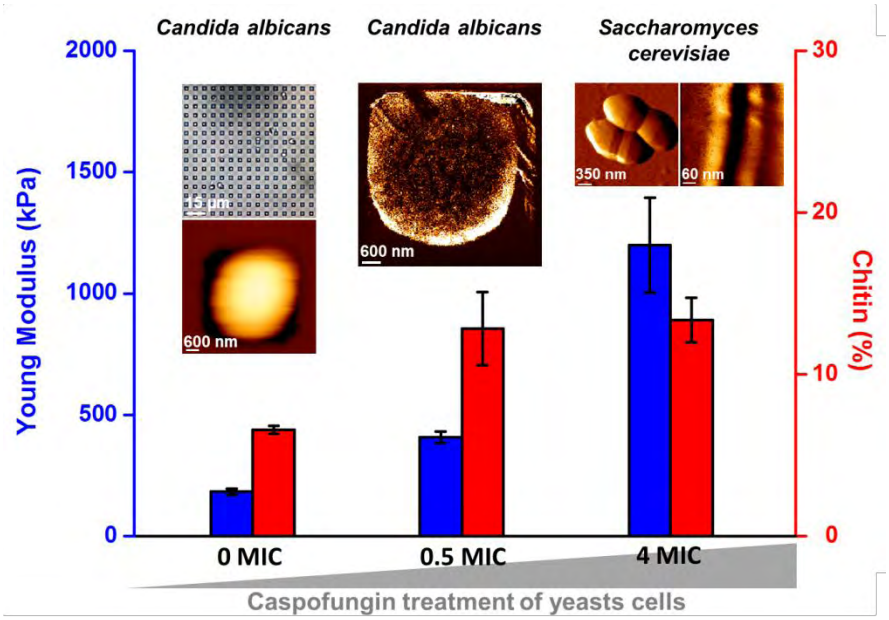

Figure 13. Overview of the effects of caspofungin on *Candida albicans* and *Saccharomyces cerevisiae*. Young modulus values of the cell wall of probed cells of *C. albicans* increase with the dose of caspofungin, which can be directly correlated to the increase in the chitin content of the cell wall. *C. albicans* cells have modified adhesive properties upon treatment by caspofungin at 0.5 MIC, whereas *S. cerevisiae* morphology is modified at a high dose of caspofungin. Adapted from [68].

The use of AFM unraveled unexpected effects of antifungal agents on fungal adhesion properties and cell growth of two different species. These results may help in understanding the molecular basis of microbes-drugs interactions and opens new avenues for developing new therapeutic agents.

Finally we used AFM to probe the cell wall of stressed yeast cells, in order to directly visualize the morphological, structural and biophysical changes of the yeast cell wall happening during a heat shock. For these experiments, we used *Saccharomyces cerevisiae*, and submitted

this strain to a biotechnologically relevant stress; thermal stress. The group of G. Walker in Scotland has pioneered this research and published several papers where AFM was used to evaluate the effects of thermal and osmotic stress[119], ethanol shock[120], and oxidative stress[121], on the cell wall of *S. cerevisiae* and *Schizosaccharomyces pombe.* However, in these studies, the method of immobilization consists in air drying a cell suspension deposited on a glass slide, before AFM experiments. This immobilization method can lead to the modification of the interface of the cells, leading to different results than in liquid on living cells. In this work, we evaluated the effects of thermal stress on the cell wall of *Saccharomyces cerevisiae*. We showed that a shift of temperature from 30 to 42°C induced in less than 1 hour the formation of a circular structure, taking its origin on the cell wall, and evolving in concentric rings on the cell surface, as showed on the high-resolution image of the *S. cerevisiae* cell wall presented in Figure 14.

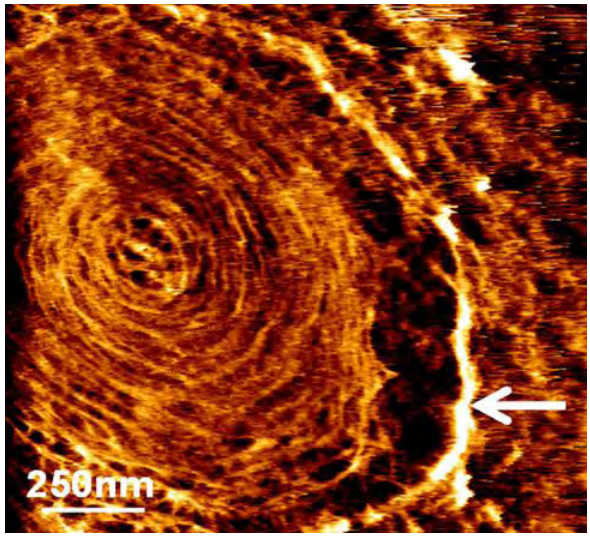

Figure 14. Exploring the ultrastructure of yeast cell surface in response to a thermal stress by AFM. Exponential growing yeast cells were subjected to a temperature shift from 30 to 42°C. After a 1 h exposure, cells were imaged by AFM in contact mode at a very low applied force (0.1 nN). High-resolution deflection image shows a succession of concentric rings, ended with a major ring (ring with the larger diameter, white arrow). Reprinted from [122].

In parallel, the cell wall Young modulus of heated cells was increased by twofold compared to native cells, and this was observed in parallel of a twofold increase in the content level of chitin in the cell wall. This morphological process was found to be dependent on genes required for the budding process and under the control of the CWI signaling pathway. From these genetic results, we came to the suggestion that the formation of these circular rings arose from a defective bud scar or bud emergence site during the temperature stress[122] (Appendix 1, p272). However more work has now to be performed, in order to understand the decrease in the cell wall elasticity, and to link it with a biological process of cell wall remodeling.

Altogether, these results show how AFM technology can bring new fundamental data on the cell wall of yeast cells. We could explore the adhesive and nanomechanical properties of the pathogenic yeast species *Candida albicans* and show the presence of amyloid plaques at its surface, that disappeared after the cells were treated with an antifungal drug, caspofungin. We then used AFM to probe the effects of thermal stress on the cell wall, and showed that *S. cerevisiae* cells had an increased cell wall elasticity after a temperature shift from 30 to 42°C. This reflects the complexity of the molecular mechanisms ensuring maintenance of the cell wall, and its assembly.

1.2.4 Nanoscale behavior or the bacterial cell wall submitted to antibacterials

We then studied a second type of microorganism, bacteria, and specifically Gram-negative bacteria. The bacterial cell wall is a complex multilayered structure that (i) serves to protect bacteria from their environment, (ii) plays an essential role during cell division, and (iii) forms a selective passage for nutrients from the outside and waste products from the inside[123,124]. The cell walls of bacteria are divided into two major groups. Gram-negative bacteria, as described in

figure 15, are surrounded by a thin peptidoglycan layer, which is surrounded by an outer membrane containing lipopolysaccharide. Gram-positive bacteria do not possess an outer membrane but are surrounded by layers of peptidoglycan thicker than for Gram-negative.

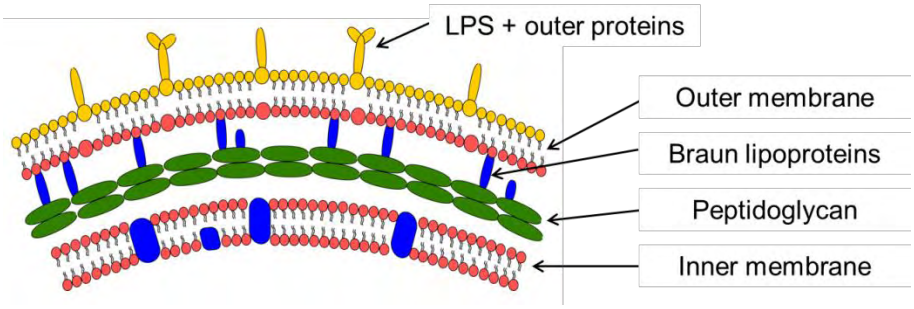

Figure 15. Representative schema of the cell envelope of Gram-negative bacteria. Adapted from [70].

The outer membrane is a distinguishing feature of Gram-negative bacteria. It is a lipid bilayer composed of proteins and glycolipids, notably the lipopolysaccharide (LPS), that ensures a critical role in the barrier function of the outer membrane. The LPS is also known as an endotoxin and provokes endotoxic shocks associated with septicemia caused by Gram-negative bacteria[125]. The outer membrane is covalently bound to the peptidoglycan layer by lipoproteins called Braun's lipoproteins[126]. The peptidoglycan is made up of repeating units of the disaccharide N-acetyl glucosamine-N-acetyl muramic acid, which are cross-linked by penta-peptide side chains[127]. The peptidoglycan sacculus is a rigid structure that determines the shape of bacteria. The outer membrane and the inner membrane delimit a compartment called the periplasm, which contains proteins such as harmful degradative enzymes (RNAse or alkaline phosphatase), periplasmic binding proteins (sugar and amino acid transport and chemotaxis), and chaperone-like molecules (role in envelope biogenesis)[128,129]. Finally the inner membrane is a phospholipidic bilayer that contains all the proteins with roles in the energy production, lipid

biosynthesis, protein secretion and transport[123,130]. Because the bacterial cell wall is a unique feature of Gram-negative bacteria, with components such as peptidoglycan and LPS that are not found in any other cells, and because of its crucial role in the surviving of bacterial cells, it represents a perfect target for antibacterials. It is then of first interest to probe the bacterial cell wall with AFM, in order to get new fundamental knowledge about this complex dynamic structure, to understand its nanoscale behavior in interaction with antimicrobials, and therefore to identify new targets for innovative antibacterial molecules in the future.

The first species we worked on is *Pseudomonas aeruginosa*. This bacterial species is a "superbug"; infections associated with multidrug-resistant *P. aeruginosa* have a substantial impact on mortality rates. *P. aeruginosa* is an invasive, Gram-negative opportunistic pathogen that causes a wide range of infections including bacteraemia, pneumonia, meningitis, urinary tract and wound infections. Moreover, *P. aeruginosa* is naturally resistant to antibiotics due to its natural low outer membrane permeability and to many adaptive resistance mechanisms (loss of porins, surexpression of efflux pumps, presence of β-lactamase …)[8,9,131–133]. The common way to fight against bacteria is to use antibiotics. We therefore studied the effects of two reference antibiotics, ticarcillin and tobramycin, that are active on *P. aeruginosa*, and widely used in therapeutics[65]. Ticarcillin is a β-lactam that inhibits the bacterial transpeptidases and transglycosylases responsible for the assembly of the cell wall peptidoglycan[134]. The second molecule, tobramycin, is an aminoglycoside that works by binding to the 30S and 50S units of the bacterial ribosome, preventing formation of the 70S complex. As a result, mRNA cannot be translated into protein. Our results showed significant morphology modification of bacteria treated by both antibiotics. Bacteria grown in the presence of ticarcillin formed filaments, a morphology already observed by Scanning Electron Microscopy[135], and explained by the fact that β-lactamins activate the SOS system of the bacteria, leading to the inhibition of cell division[136].

Tobramycin-treated cells did not elongate but presented a deformed cell wall, due to the fact that tobramycin treatment leads to the synthesis of abnormal proteins that are incorporated into the cell wall, which therefore loses its integrity. These results, presented in figure 16, are published in Nanomedicine NBM and presented in chapter 3.3.1 (p233).

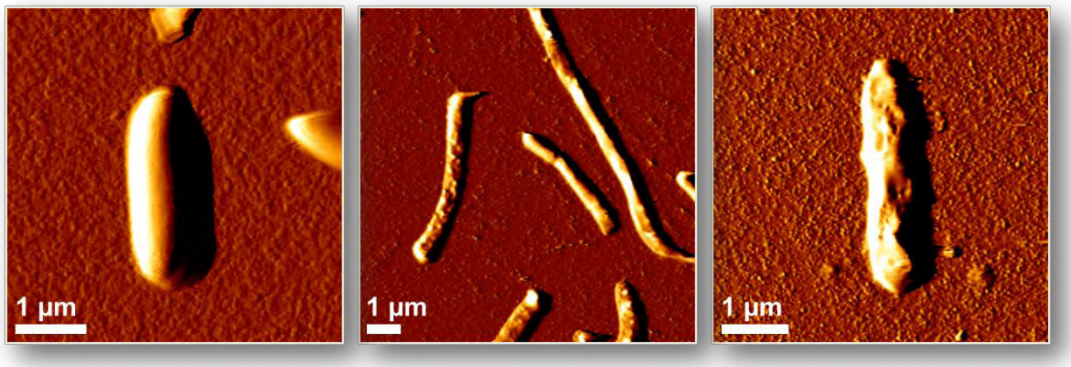

Figure 16. Morphological modifications of *Pseudomonas aeruginosa* cells induced by antibiotic treatments. Deflection images of cells in native conditions (left panel), under ticarcillin treatment (middle panel), and under tobramycin treatment (right panel). Adapted from [65].

This first set of data allowed us to demonstrate that looking at the bacterial biophysical properties upon antimicrobial treatment was rich in information concerning the mechanism of action of these molecules; this method could therefore be used to probe the effects of other antimicrobial agents on the cell wall of multidrug resistant species.

We then probed the effects of another antibacterial molecule, polymyxin E, also known as colistin, on the cell wall of multidrug resistant strains of the Gram-negative bacterial species, *Klebsiella pneumoniae*. *K. pneumoniae* has been recognized over 100 years ago as a cause of community-acquired pneumonia[11]. But the vast majority of *Klebsiella* infections are associated with hospitalizations; *K. pneumoniae* infections of the urinary tract, bloodstream, lungs and abdominal cavity have now became common. Numerous virulence factors have been described for *K. pneumoniae*. Among others, extracellular capsules are essential to virulence; indeed, the

capsular material forms thick bundles of fibrillous structures that cover the bacterial surface in massive layers[10]. This protects the bacteria from phagocytosis and prevents killing by bactericidal serum factors[13]. Another important feature of *K. pneumoniae* is its ability to resist a large number of antibiotics. Indeed, within a few years after the introduction of cephalosporins, a type of β-lactamins, *K. pneumoniae* strains within hospitals were showed to produce β-lactamases able to inactivate these agents. These β-lactamases were in fact ESBL, for Extended-Spectrum β-Lactamases. ESBLs are plasmid mediated enzymes that hydrolyze oxymino-β-lactamins agents. These plasmids also carry resistance genes to other antibiotics, including aminoglycosides, chloramphenicol, sulfonamides…. Thus, *K. pneumoniae* strains containing these plasmids are multidrug resistant[10,13,137]. However, ESBLs are readily inhibited by the commercially available β-lactamases inhibitors (clavulanic acid, tazobactam and sulbactam)[14], which serves as an important phenotypic test to identify ESBLs. During this PhD, we have specifically worked on the characterized *K. pneumoniae* ATCC 700603 strain, a clinical isolate obtained from a patient in the USA in 1994, which produces an ESBL called SHV-18[12,138]. Because this ESBL is sensitive to clavulanic acid, it has been used as a reference strain for quality control in ESBL detection.

Management and treatment of ESBL-producing *K. pneumoniae* infections can be challenging. Currently, carbapenems are the only class of antibiotics that have consistently been effective against ESBL-producing *K. pneumoniae*. However, bacteria have developed carbapenemases (KPC), which are ESBL-like enzymes that confer resistance to extended-spectrum cephalosporins and carbapenems[11,14]. Therefore, clinicians had to turn back to an old antibiotic of the polymyxin class, colistin, as a last resort agent for the treatment of infections caused by multidrug resistant *Klebsiella pneumoniae*. Polymyxins are cyclic lipodecapeptides that are strongly cationic. They were discovered as early as 1947[139], and widely used at that time.

But, following reports on nephrotoxicity and neurotoxicity in the 1970s, they were largely replaced by other better-tolerated antibiotics[16,140]. Polymyxin B and polymyxin E (colistin) are the main antibiotics of this group, and the only ones used clinically. They are bactericidal, and act rapidly and specifically on Gram-negative bacteria. We will focus on colistin, the polymyxin used in this work. Its initial target is the lipid A of the LPS of the outer membrane of Gram-negative bacteria. Thanks to its positive charges, colistin interacts electrostatically with these molecules, and competitively displace divalent cations from them, causing disruption of the membrane. This results in an increase of the permeability of the cell wall, leakage of cell contents, and subsequently, cell death[141,142]. However, some authors argue that interaction with membranes is a part of the polymyxin activity, but not actually the lethal event[143]. Therefore the precise mechanism of action of colistin still remains contentious[144]. In this study, we have used Atomic Force Microscopy to probe the effects of colistin on *K. pneumoniae* ATCC 700603, and on its colistin-resistant derivate named Kpm[145], with the aim of better understanding the mechanism of action of this molecule. The effects of this molecule have already been showed by AFM on air-dried cells of *Pseudomonas aeruginosa* and *Acinetobacter baumannii*[146–148], but no work have been performed on live cells of *Klebsiella pneumoniae*.

Our results show for the first time the capsule of *K. pneumoniae*, at the nanometric scale, and its nanomechanical properties. On the ATCC strain, we showed that colistin had a detergent-like effect by removing the mucus off the bacteria. On the Kpm strain, imaging data showed that the capsule was different from the ATCC strain, by being tightly bound to the cells, instead of being spread on large surfaces around cells, as it is the case for the ATCC strain. Upon treatment with colistin, even at high doses (12 µg/mL), the capsule was not removed from the surface of Kpm cells. We therefore could hypothesize that this strain had a modified capsule, conferring it resistance to colistin. A further analysis of the force curves obtained on both strains showed that

in the case of the ATCC strain, the AFM was first pushing through the layer of capsular polysaccharide, then through the bacteria, before reaching the glass slide. On the Kpm strain, the tip goes first through multiple layers of polysaccharide, before reaching the bacteria, and then the glass slide. The colistin-resistant strain therefore presents a capsule's nanoarchitecture in superposed layers. But despite this organization, and the fact that cells resist the colistin effects, their capsule is still affected; nanomechanical data showed that the Young modulus of Kpm capsule increased with the dose of colistin. In the case of the sensitive strain, the Young modulus of the capsule in native conditions is lower (3.6 ± 0.8 kPa) than for the resistant strain (21.3 ± 4.7 kPa), allowing us to infer between each strain's capsular polysaccharide organizations. And since capsule was removed in presence of colistin from the sensitive strain, no conclusions on the effects of colistin on the nanomechanical properties of the cells could be drawn. Figure 17 below presents the hypothesis that could made using the overall data, on the architecture of the capsule of the sensitive strain (Figure 17a) and of the resistant strain (Figure 17b).

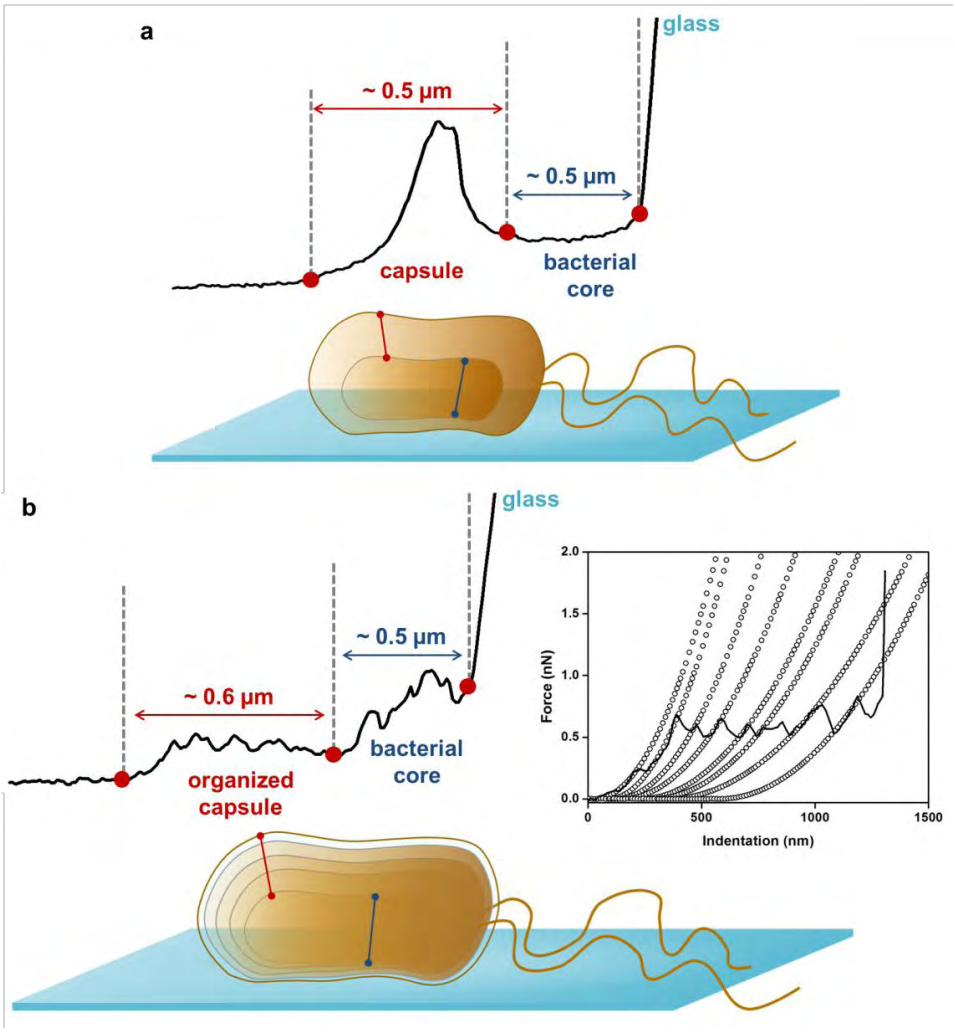

Figure 17. Schematic representation of the hypothesis formulated on the capsular architecture of *Klebsiella pneumoniae*. (a) capsule organization of *K. pneumoniae* ATCC 700603, and (b) capsule organization of *K. pneumoniae* colistin resistant (Kpm). The graphic in (b) shows an indentation curve recorded on top of a Kpm cell in native conditions (grey line), in which each spike has been fitted using the Hertz model. To be published in Journal of Antimicrobial Chemotherapy (manuscript in revision).

Altogether, these results allowed us to bring new insights into the mechanism of resistance of Kpm to colistin. Indeed, we could hypothesize that Kpm cells were resisting the effects of the polymyxin thanks to the particular nanoarchitecture of its capsule, in superposed layers that each represent a barrier to colistin. Therefore the molecule cannot reach its target, *i. e.* the LPS and the cytoplasmic membrane. In the ATCC cells, because of the "leaky" structure of the capsular

polysaccharides, colistin can reach LPS and therefore kill cells. These results are to be published in Journal of Antimicrobial Chemotherapy and are presented in Chapter 3.3.2 (p240).

1.2.5 AFM to understand the mechanism of action of a new antibacterial molecule

But colistin being still a toxic molecule for kidneys and neurons, and Gram-negative bacteria still gaining resistance mechanisms, there is an urgent need for new antibacterials, with an innovative mechanism of action. Among various approaches to develop new antibacterial agents is one dedicated to polycationic calixarene-based guanidinium compounds that display an intrinsic antimicrobial activity. Calixarenes, first characterized in 1940 by Niederl and Vogel[149], are macrocycle (cycle oligomer) composed of *n* phenolic units (usually 4 to 8). It has been demonstrated that their excellent organizing behavior into rigid structures gives them many functionalities. Given the fact that bacteria are negatively charged, and focusing on this organizing behavior, the introduction of positive charges on the calixarene core leads to a constrained oligomeric polycation. As antimicrobial agents, the guanidinium derivatives have been modestly studied these last years, and most of the investigated compounds are poly-guanidinium species derived from synthalin A[150]. However, a remarkable gain of antibacterial properties in the spatial organization of the monomeric para-guanidinoethylphenol into its tetrameric calixarenic isomer[151] was recently observed. Further studies have confirmed and expanded the above findings: Grare *et al* in 2006 showed an important antibacterial activity for the calixarene presented in figure 18 *in vitro*, both on Gram-positive and Gram-negative bacteria, to a lesser degree for *E. faecalis* and *P. aeruginosa*[152]. In a similar study conducted in 2007, the calixarene showed no apparent cytotoxicity on MRC-5 and HaCaT eukaryotic cell lines compared to other antibacterial molecules (hexamidine and synthalin A)[19].

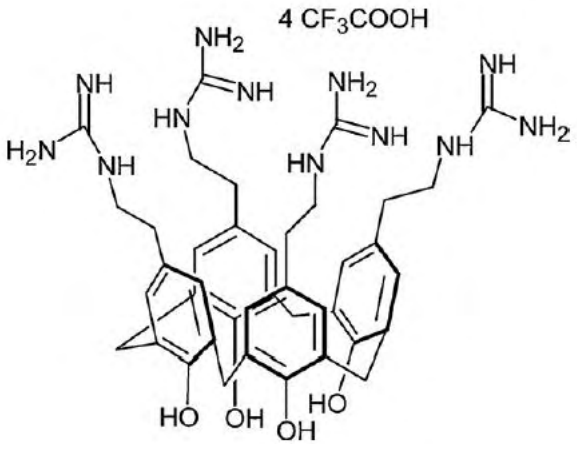

Figure 18. Chemical structure of *para*-guanidinoethylcalix[4]arene (CX1). Reprinted from [151]

Thus, the *para*-guanidinoethylcalix[4]arene (CX1) is a new cationic antibacterial drug, with a broad spectrum, not toxic, with a possible parietal target, but with an unknown kind of activity (*i.e.* bactericidal or bacteriostatic). The initial hypothesis concerning its mechanism of action was that the introduction of positive charges on the calixarene core could lead to the disorganization of the bacterial cell wall. Since *P. aeruginosa* possesses a highly negatively charged outer membrane, it was a good candidate to study the interaction with CX1 using AFM. We therefore developed a strategy to evaluate the nanoscale effects of CX1 on the bacterial cell wall, and to elucidate its mechanism of action. To this end, we worked with a sensitive strain of *P. aeruginosa* (ATCC 27853), but also with a multidrug resistant one, *P. aeruginosa*, which is resistant, among others, to ticarcillin and tobramycin. Since the mechanisms of action of these two antibiotics are well known, by comparing the effects caused by them with the ones caused by CX1, we will be able to get a better understanding of the mechanism of action of CX1 and determine its bacterial target. This strategy is schematically summarized in figure 19.

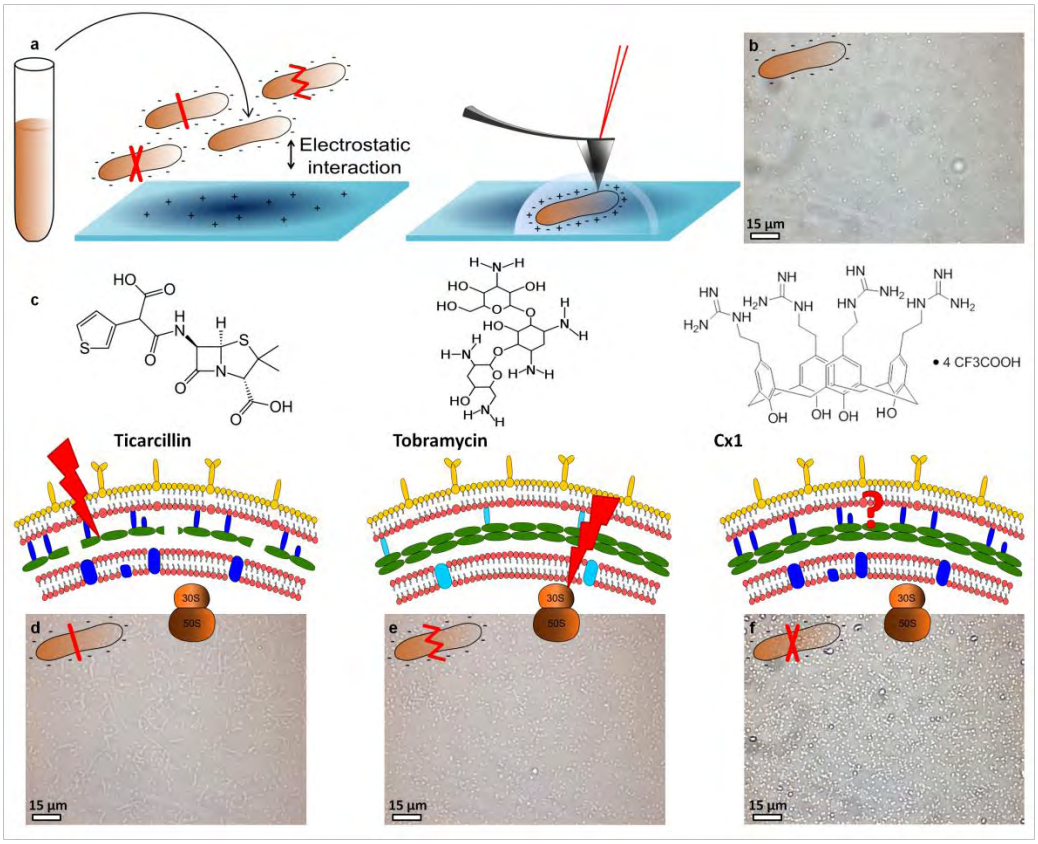

Figure 19. Schematic representation of the strategy used to study the mechanism of action of CX1. (a) cells cultivated in Mueller Hinton broth for 20 hours at 35°C are immobilized on a polyethylenimine coated glass slide for AFM experiments. (b) optical image of the surface covered with immobilized untreated *P. aeruginosa*. (c) molecules used in the study and their targets. (d) optical images of *P. aeruginosa* treated by ticarcillin (4 mg/mL), (e) by tobramycin (0.25 mg/mL) and (f) by CX1 (32 mg/mL). Reprinted from [70].

The results showed that on a multidrug resistant strain of *Pseudomonas aeruginosa*, CX1 caused a dramatic decrease of the cell wall Young modulus, which was not the case when cells were treated with ticarcillin or tobramycin. These results showed that CX1 was efficient on such a bacterial strain, and that its action destabilized the cell wall of the bacteria. To go further into the mechanism of action, we probed the cell wall of treated and untreated bacteria with an AFM tip functionalized with Concanavalin A, a lectin that binds to carbohydrates. These single molecule force spectroscopy experiments revealed that the lectin could unfold a molecule 6 µm long only on CX1 treated cells. Experiments performed on phospholipidic bilayers submitted to a

treatment by CX1 during one hour showed that the antibacterial caused the creation of holes of approximately 0.5 to 1 µm in diameter in the bilayers. Similar holes were also observed at the surface of the CX1 treated cells. At this stage, we had learned that CX1 was causing a deep destabilization of the cell wall of bacteria (Young modulus decreased, unfolding of long molecules, holes observed at the surface of cells) and was creating holes in bilayers that mimic the outer membrane of Gram-negative bacteria. We could therefore make the following hypothesis on the mechanism of action of CX1: this molecule interacts with the surface of the Gram-negative bacteria and creates holes in the outer membrane. This gives access to the functionalized AFM tip to a molecule that is under the outer membrane; this molecule could possibly be the peptidoglycan, which was showed to form a super-coiled rope coiled all around the cell envelope in Gram-positive cells of *Bacillus subtilis*[153,154], explaining perhaps the fact that it was unfolded on such long distances. These results are published in Scientific Reports, and can be found in Chapter 3.3.3 (p260).

The next step of such a study is now to understand how this molecule can be used in synergy with other antibiotics, and if it can restore the action of the antibiotics on multidrug resistant strains.

Chapter 1.3: Discussion: contribution of "nanomicrobiology" to clinical microbiology; does it help?

1.3.1 AFM as a useful tool for clinical microbiology

Microbiology is a scientific field that focuses on microorganisms and the activities that characterize them. More specifically, microbiology has a role in the identification and

characterization of microorganisms, in the study of their origins and evolution, in the understanding of the interactions they have between them and with their natural or artificial environment. In comparison, clinical microbiology is a branch of medicine that has the role to identify and characterize microorganisms (bacteria, viruses, fungi and parasites) that cause human disease, to provide a diagnostic and a therapeutic support for the clinical management of patients, and to prevent the transmission of infectious diseases both in the health-care system and in the community[155]. Atomic Force Microscopy has long been used for microbiology studies now. The yeast and bacteria cell wall probed by AFM has been the subject of many publications, that have been reviewed already several times[1–3,156,100,157,101,158–161]. Indeed, AFM is a powerful technology that presents different distinguishing features: (i) the physical interaction at the basis of AFM is not limited by the light wavelength, and therefore AFM permits the resolution for molecular and atomic events imaging, (ii) AFM allows three dimensional imaging, (iii) AFM can image samples under physiological conditions, and (iv) the tip of the AFM can be modified chemically or biochemically to identify specific structures and the measurement of specific interactions. These features make AFM an ideal tool to address microbiological questions, *i.e.* to characterize microorganisms and their interactions with other cells or with their environments.

What I would like to emphasize in this thesis is the relevance of such a technology in the field of clinical microbiology. AFM is a technology that cannot be used to cover all the components of clinical microbiology, but it can, however, be a powerful tool to characterize pathogenic microorganisms, at the nanoscale level, in order to identify new potential drug targets. AFM can also have a role in the "diagnostic and treatment" component of clinical microbiology, since it is a way to evaluate the effects of antimicrobial molecules, and therefore their efficiency, on medically important microorganisms. This is what this work is about, characterizing pathogenic microorganisms, and evaluating the efficiency of different antimicrobial treatments on these

microorganisms. Indeed, AFM was used here to characterize at the nanoscale the morphology, the nanomechanical and adhesive properties of the bacterial species *Pseudomonas aeruginosa*, *Klebsiella pneumoniae*, of multidrug resistant strains of these two species, and of the fungal species *Candida albicans* and *Saccharomyces cerevisiae*. For each microorganisms, fundamental knowledge on their surface properties was acquired, and the effects of antimicrobial drugs, such as antibiotics (ticarcillin, tobramycin, colistin), an innovative noncommercial calixarene (CX1) and antifungals (caspofungin), were probed. Therefore, this thesis clearly is a brick to the clinical microbiology "wall". But it has needed technological developments; this part constitutes almost half of the work, as there are no scientific discoveries without technological developments. AFM is not a "push-button" technology; technical details must be considered to ensure the success of the experiments, then results must be analyzed with great care. Indeed, it is easy to make results show what we want, and a look from "above" must be taken constantly to keep the presented results accurate. However, these considerations are the same for all advanced technologies, such as the real-time genomics techniques used in clinical microbiology laboratories to characterize isolated pathogens from patients. The technological developments made during this PhD allowed us to get new fundamental data on bacteria and yeasts, treated or not with antimicrobials. The main results will be discussed in detail, in the following paragraphs.

1.3.2 Cell surface properties of Candida albicans

We have showed, using AFM, the presence of adhesive nanodomains at the surface of round cells of the pathogenic yeast *Candida albicans*. These nanodomains, probably composed of the aggregated Als1 or 5 adhesin protein, had already been imaged using AFM, by Alsteens *et al.* in 2010[109]. In this pioneering work, the authors show that formation of nanodomains is force-induced at the surface of *S. cerevisiae* cells overexpressing the Als5 protein. They use the AFM

in the force-volume mode to acquire arrays of 32 by 32 force curves, therefore presenting adhesion images of a resolution of 1024 pixels². In our study, *C. albicans* wild-type cells were probed using Quantitative Imaging™ mode. In this fast force volume based mode, we could record adhesion images of the surface of cells with a resolution of 16 384 pixels². This resolution on this type of measures (adhesion images) on living wild-type cells was never reached before. Compared to the results presented by Alsteens *et al*. in 2010, the aggregation of amyloid proteins is observed in both cases; the difference lies in the resolution of the images, and in the characterization of the nanodomains (nanomechanical properties, size, and molecular nature) on the whole cells. Therefore advanced technologies like QI™, combined with relevant biological models such as *C. albicans*, allow visualizing dynamic events, like the apparition of amyloid plaques on a whole cell. Other techniques could be used to visualize such nanodomains at the surface of cells. Indeed, Lipke and his team have showed the presence of amyloid nanodomains at the surface of yeast cells by fluorescence microscopy, using fluorescent dyes, thioflavin T or 8-anilino-1-naphtalene-sulfonic acid (ANS)[105,107,108,162]. However the resolution of such images is quite poor, even if fluorescence microscopy is a highly sensitive technique. In order to increase the resolution using fluorescence, techniques such as super-resolution fluorescence microscopy can be used. These techniques achieve spatial resolution not limited by diffraction by modulating close-by fluorescent molecules into different states, thus distinguishing their fluorescence signal. One approach to achieve this distinction is based on stochastically switching individual fluorescent molecules between a fluorescent and a dark state, which was invented under the name of stochastic optical reconstruction microscopy (STORM)[163], or photoactivated localization microscopy (PALM)[164]. This approach collects a series of fluorescent images, each containing a sparse subset of fluorophores activated into the fluorescent state. A super-resolution image is then reconstructed by determining the positions of individual activated fluorophores[165,166]. But since

formation and propagation of nanodomains is a dynamic process, single-molecule super-resolution imaging technique can be used. This approach determines the positions of different copies of labelled molecules. If these labelled copies are incorporated into a larger structure, then their positions randomly sample this structure and thereby provide information about its overall shape and position in the cell. A point-by-point reconstruction can then be assembled by combining the localized positions of all detected molecules in a computational post-processing step[167,168]. This technique provides information about the precise motion of individual proteins, that could be fluorescent labelled Als protein, and therefore is useful for the investigation of protein dynamics, like their aggregation into amyloid plaques, in living cells. However these techniques are still emerging and only a few papers use them to study microorganisms. In one example[169], the authors have used super-resolution imaging combined with single-molecule tracking to visualize single fluorescent labeled DNA polymerase and ligase molecules in live cells of *Escherichia coli*. Their study allowed providing new data of the enzymes reaction rates, substrate search times and diffusion coefficients, before and during DNA damage response. This led to the description of model DNA repair pathway *in vivo*[169]. However this technique remains an imaging technique, even if the number of fluorescent molecules and their brightness distribution can be measured, in comparison, AFM has enabled us to quantitatively characterize the nanodomains observed, in terms of adhesiveness, stiffness, and height. A combination of these two nanoscopic techniques would allow unravelling the mysteries surrounding the formation of amyloid plaque by amyloid proteins at the surface of live *C. albicans* cells.

This possibility, to directly image the adhesive properties of *C. albicans* cells, has also been useful to unravel the unsuspected effects of caspofungin on this yeast species. Indeed, caspofungin is an echinocandin known for inhibiting the synthesis of glucans of the cell wall of yeasts, therefore leading to cell death. Our study, using QI™ mode, allowed us to show that

caspofungin had also an effect on the adhesive properties of this yeast that are an important feature for its pathogenesis. Indeed, if caspofungin is used at a low dose, the cells answer by modifying their adhesive properties *i.e.* by exhibiting a homogeneously distributed adhesiveness all over the cell. However, if the cells are submitted to a treatment with a high dose of caspofungin, then the cells display much lower adhesiveness. A similar study, performed by El-Kirat-Chatel and coworkers in the same year as our study, showed that the treatment by caspofungin induced the massive exposure of the cell adhesion protein Als1 on the cell surface, leading to increased hydrophobicity[170]. Their results are therefore in line with our observations, and it is likely probable that the adhesiveness that we have witnessed with low doses of caspofungin is due to the overexpression of the Als1 protein. The important point to emphasize here is that a technology like Atomic Force Microscopy allowed showing that caspofungin not only had effects on the cell wall synthesis, but also caused modification of the expression of surface adhesins. This is indeed an important point since these surface adhesins are a characteristics of pathogenic yeast species, compared to non-pathogenic ones like *Saccharomyces cerevisiae*, and are essential for the cells to adhere to surfaces, and therefore to infect them. On this point further studies could be performed. For example, genetic studies aiming at quantifying the expression of each adhesin-coding gene under treatment with different doses of caspofungin could complement the results obtained by AFM. Using this type of experiments, we could conclude on which genes expression' is modulated by the drug; indeed, Als1 seems to be involved, but perhaps other Als proteins or other surface adhesins could be involved too. Another example of experiments that could be performed is to use AFM on mutated *C. albicans* strains for the different Als proteins. With this kind of experiment, the adhesive properties of each strain could be visualized under caspofungin treatments; this would help in the understanding of which Als are modulated by the antifungal drug. However these experiments would be difficult to

interpret since it has been shown that when one Als is missing, others compensate for its loss[103,171,172].

Altogether, the results obtained on *Candida albicans* are relevant for clinical microbiology. Indeed, even if the dynamics of the nanodomains would need working with different technologies, AFM used in a multiparametric mode, QI™, allowed their direct visualization and quantifying of their nanomechanical properties. Then, while treating the cells with caspofungin, we could show that these surface adhesive properties were modified by the antifungal drug, and that this modification was dose-dependent. Therefore, this work has brought significant new fundamental knowledge on the cell wall properties of this pathogen that could be used in further works to develop new antifungal drugs, targeting for example the expression of the surface adhesins. We have showed that their expression could be modulated by an external drug, and since their expression is essential for the pathogen to realize the first stages of infections, *i.e.* adhesion to the host's surface, it then represents a perfect target for an antifungal drug.

1.3.3 Probing the effects of antibiotics on the cell wall of bacteria

During this PhD, we probed the effects of two well-known antibiotics, ticarcillin, a β-lactam that targets the cell wall, and tobramycin, an aminoglycoside that targets the protein synthesis, on the cell wall of the Gram-negative bacteria *Pseudomonas aeruginosa*. The main results from these experiments showed spectacular morphology modification of the bacilli treated by ticarcillin, with inhibition of the cell morphology and the formation of long filaments. Observations of such filaments formed by Gram-negative bacilli, under the presence of antibiotics, were reported as long ago as 1964, by Chang and Weinstein[173]. In this study, the authors showed the formation of filaments by *Proteus vulgaris* after 4 hours of treatment by cephalotin, an antibiotic of the cephalosporin class. In a later study, Ellis *et al.*, in 1976, used

scanning electron microscopy to show the elongation of *Pseudomonas aeruginosa* cells treated by a penicillin and two cephalosporins[174]. Compared to scanning electron microscopy, that requires a complicated preparation of the samples, AFM offers the possibility to work in liquid on living cells. Our results are the first one showing the cell elongation on *P. aeruginosa* cells treated by a penicillin, on living cells, since the dose of ticarcillin used was of 0.5 × MIC, at the nanoscale. But how can be explained this elongation? Antimicrobials can induce the SOS response in bacteria, *i.e.* a conserved regulatory network that is induced in response to DNA damage. SOS response activation promotes the transfer and expression of foreign resistance genes, but also induces spontaneous chromosomal mutation frequency[175–177]. In the case of treatment by β-lactams such as ticarcillin, the defective cell wall synthesis occurring during treatment triggers a two-component signal transduction system that induces the SOS response. This leads to a temporarily inhibition of the cell division, which has the effect to enable bacteria to survive and limit the bactericidal effects of these drugs[178]. Thus we have showed by AFM that a low dose of ticarcillin on *P. aeruginosa* had the effect to activate the SOS response, leading to the bacterial tolerance of this drug. In the context of drug resistance, particularly important for *P. aeruginosa*[8], these results are of great significance, and show how AFM can participate in the characterization of the stress-response mechanisms of bacteria submitted to antibiotics, and therefore how it can help in the treatment process of these microorganisms. To go further in the characterization of this resistance mechanism, the dynamics of it could be studied. For that, recent developments of the AFM into High-Speed AFM could be used. HS-AFM was first developed in 2008 by Ando's team[179] in order to visualize structure dynamics and dynamics of biological molecules in physiological conditions at a subsecond to sub-100 ms temporal resolution and a 2 nm lateral and a 0.1 nm vertical resolution[180]. This new type of microscopy has already been used to study biological processes, such as the dynamic behavior of myosin V

molecules translocating along actin filaments[181], or the crystalline cellulose degradation by individual cellulases enzymes[182]. In 2010, Fantner's team used this technology to investigate the kinetic of individual bacterial cell death under treatment by an antimicrobial peptide CM15[183]. This pioneering study allowed characterizing the early stages of the action of the antimicrobial peptide on the cell surface of living *Escherichia coli* cells. Such a technology could be used in our case, to further characterize the effects of antibiotics on the cell wall of *P. aeruginosa*, and therefore better understand how this bacterial strain withstands antibiotic treatment. Recent developments have allowed the implementation of HS-AFM coupled with an optical fluorescence microscope[184], which would be a great tool to visualize the morphological changes induced by antibiotics on the surface of individual cells[185], from a dynamic perspective.

The second part of the work performed on bacteria has consisted in using AFM to understand the mechanism of action of antimicrobial molecules. This strategy was used first with an already used molecule, colistin, then with an innovative one, CX1, on two different species of multidrug-resistant Gram-negative bacteria. Therefore in this last part, a further step was taken, since AFM was not used solely to characterize the effects of antimicrobials, but also to decipher the mechanism of actions of antimicrobials, which is an important step in the drug discovery process. For colistin, an old polymyxin reused nowadays for infections caused by XDR bacteria, AFM experiments performed on the bacterial species *Klebsiella pneumoniae*, allowed us to show that one of its action was to remove the capsule off the bacteria. Indeed, with colistin-resistant bacteria (strain named Kpm), we observed, for the first time in liquid conditions, a capsule that was structured in several layers, compared to the sensitive strain. This particular architecture kept colistin from removing the capsule from the bacteria, even at high doses, suggesting that this particular structure was a way for the bacteria to resist the entry of colistin into the cell wall, a way to keep colistin from reaching its supposed target, in Gram-negative, the lipid A of LPS.

This study allowed us to show how Kpm was able to resist the effects of colistin. However, it did not lead us to better understand the mechanism of action of the molecule, as it was initially our purpose. Indeed, the way colistin kills bacterial cell is still a debated subject. Colistin is known to interact with LPS present at the surface of the outer membrane of Gram-negative bacteria, leading to outer membrane disruption and therefore cell death[141]. However, some studies have showed that colistin was interacting with phospholipids and LPS present on the outer membrane of Gram-negative bacteria, which would disturb membrane permeability, to let the molecule bind to phospholipids at the surface of the cytoplasmic membrane, leading to cell death[186,187]. Other authors argue that interactions of colistin with membranes of Gram-negative bacteria are probably not the lethal event, and that colistin may have multiple targets, and also intracellular ones[188–190]. It has also been shown that colistin was efficient against *Mycobacterium aurum*, that do not display LPS at its surface, but mycolic acids and phospholipids[191]. However colistin is not efficient on Gram-positive bacteria, that do not display LPS nor phospholipids at their surface, but peptidoglycans[141]. Following this, we could think that the target of colistin is phospholipids, since *Mycobacterium aurum* presents phospholipids on its surface. However, studies have showed that strains modified for their LPS were becoming resistant to colistin[192–194]. What I would like to emphasize with this paragraph, is that colistin mechanism is more complicated than we could think, as regard of the literature on this subject. The feeling that we can get out of the literature is that there might be multiple targets to colistin, and that more work has to be done on this subject. Therefore, determining its mechanism of action using AFM was a complicated task that we could only contribute to.

As for CX1, an innovative antibacterial calixarene presenting positively charged groups, we probed its effects on the morphology and on the cell wall nanomechanical properties of a multidrug-resistant strain of *Pseudomonas aeruginosa*, and compared them to the ones of

ticarcillin and tobramycin. This allowed us to better understand its mechanism of action. But in this study, the experiments that really were pertinent to understand the mechanism of action of CX1 were of two kinds. In the first kind, we used functionalized AFM tips to probe the molecular architecture of the cell wall of treated cells. To this end, the lectin Concanavalin A that specifically binds to carbohydrates was covalently linked to the AFM tip. The results obtained with this tip on CX1 treated cells showed retract unfoldings on long distances (up to 6 µm). Comparison with the literature, and especially with the works of André and Hayhurst on the structure of the peptidoglycan of Gram-positive bacilli[153,154], allowed us to hypothesize that the unfolded molecule was in fact the peptidoglycan of the bacteria. But how could this molecule, found between the inner and the outer membrane of the cell wall of Gram-negative bacteria, be unfolded from the cell wall of CX1 treated cells? To answer this question, a second type of experiments, on phospholipidic biomembranes mimicking the outer membrane of Gram-negative bacteria, was performed. These experiments realized using an advanced tapping mode, HyperDrive™, showed that CX1 could create holes in the membranes. Back to the bacterial context, in fact CX1 perforates the outer membrane of the bacteria, and this is why we could then access the peptidoglycan with the functionalized AFM tip. Working with functionalized AFM tips on bacteria to probe the effects of antimicrobials, or working on the effects of antimicrobials molecules on artificial biomembranes are strategies that have already been used before. For example, in a study realized by Gilbert *et al.*, AFM tips were functionalized with an antibiotic, vancomycin, and used to probe the cell wall of *Lactococcus lactis*[78]. Their results showed how single-molecule force spectroscopy could be used to characterize the binding forces between vancomycin and the D-Ala-D-Ala motif of the peptidoglycan, and allowed mapping of the distribution of single D-Ala-D-Ala ligands on living bacteria. The authors used AFM in force spectroscopy mode with functionalized AFM tips in order to map the target of the antibiotic at

the surface of living cells. Then, in another study using AFM technology on supported lipid bilayers[195,196], the authors have probed the effects of oritavancin, a new lipoglycopeptide derived from vancomycin, and showed that oritavancin caused a remodeling of the lipid organization of phospholipidic bilayers[197]. However, these strategies have never been used in combination, like we did in our study, in order to understand the mechanism of action of a new innovative antibacterial drug. And this is the originality of our work, to use AFM in different modes (imaging and force spectroscopy), with bare and biomodified AFM tips, and on different substrates (living bacteria and supported lipid bilayers), to participate in the development of a molecule, and bring it closer to clinical use. This study has showed that AFM can be used beyond the clinical microbiology, with participating in the drug discovery process, by showing the mechanism of action of a promising molecule. The next step is now to understand the activity of this molecule in synergy with antibiotics. Indeed, it has been showed in our team (unpublished results) that this molecule, used with antibiotics on multidrug-resistant strains, was able to restore the activity of the antibiotics. AFM studies of the nanoscale mechanism of this synergetic action on MDR bugs will need to be performed, in the near future. And CX1 being efficient also on Gram-positive bacteria[19], studies on a model Gram-positive bacterial species could also be performed. Since the two types of bacteria have a different cell wall organization, it is likely probable that CX1 has effects different from the ones it has on Gram-negative bacteria. For this type of study, *Staphylococcus aureus* could be a good candidate since it is the Gram-positive bacteria that is the most frequently found in infections acquired in the health-care system.

Taken together, the fundamental data obtained using AFM technology on the cell wall of Gram-negative bacteria allowed us to characterize the effects of known antibiotics at the nanoscale, but also to better understand the mechanism of action of older and innovative antibacterial molecules. This data is of relevance in the field of clinical microbiology, but also in

the field of drug discovery, since CX1 is a new molecule that is not used yet in clinics. Therefore, the answer to the question asked in the title of this discussion is yes, AFM used for nanomicrobiology studies is indeed a useful tool in clinical microbiology.

Bibliographic references

1. Firtel, M. & Beveridge, T. J. Scanning probe microscopy in microbiology. *Micron* **26,** 347–362 (1995).
2. Dufrêne, Y. F. Atomic Force Microscopy, a Powerful Tool in Microbiology. *J. Bacteriol.* **184,** 5205–5213 (2002).
3. Liu, S. & Wang, Y. Application of AFM in microbiology: a review. *Scanning* **32,** 61–73 (2010).
4. Binnig, G., Quate, C. F. & Gerber, C. Atomic Force Microscope. *Phys. Rev. Lett.* **56,** 930–934 (1986).
5. Gow, N. A. & Hube, B. Importance of the Candida albicans cell wall during commensalism and infection. *Curr. Opin. Microbiol.* **15,** 406–412 (2012).
6. Poulain, D. *Candida albicans* , plasticity and pathogenesis. *Crit. Rev. Microbiol.* 1–10 (2013). doi:10.3109/1040841X.2013.813904
7. Hauser, A. R. Pseudomonas aeruginosa: So Many Virulence Factors, So Little Time. *Crit. Care Med.* **39,** 2193–2194 (2011).
8. Strateva, T. & Yordanov, D. Pseudomonas aeruginosa – a phenomenon of bacterial resistance. *J. Med. Microbiol.* **58,** 1133–1148 (2009).
9. Breidenstein, E. B. M., de la Fuente-Núñez, C. & Hancock, R. E. W. Pseudomonas aeruginosa: all roads lead to resistance. *Trends Microbiol.* **19,** 419–426 (2011).
10. Podschun, R. & Ullmann, U. Klebsiella spp. as nosocomial pathogens: epidemiology, taxonomy, typing methods, and pathogenicity factors. *Clin. Microbiol. Rev.* **11,** 589–603 (1998).
11. Keynan, Y. & Rubinstein, E. The changing face of Klebsiella pneumoniae infections in the community. *Int. J. Antimicrob. Agents* **30,** 385–389 (2007).
12. Rasheed, J. K. *et al.* Characterization of the Extended-Spectrum β-Lactamase Reference Strain, Klebsiella pneumoniae K6 (ATCC 700603), Which Produces the Novel Enzyme SHV-18. *Antimicrob. Agents Chemother.* **44,** 2382–2388 (2000).
13. Gupta, A., Ampofo, K., Rubenstein, D. & Saiman, L. Extended spectrum beta lactamase-producing Klebsiella pneumoniae infections: a review of the literature. *J. Perinatol. Off. J. Calif. Perinat. Assoc.* **23,** 439–443 (2003).
14. Perez, F., Endimiani, A., Hujer, K. M. & Bonomo, R. A. The continuing challenge of ESBLs. *Curr. Opin. Pharmacol.* **7,** 459–469 (2007).
15. Jehl, F., Chomarat, M., Weber, M. & Gérard, A. *De l'antibiogramme à la prescription*. (2004).
16. Nation, R. L. & Li, J. Colistin in the 21st Century. *Curr. Opin. Infect. Dis.* **22,** 535–543 (2009).
17. Biswas, S., Brunel, J.-M., Dubus, J.-C., Reynaud-Gaubert, M. & Rolain, J.-M. Colistin: an update on the antibiotic of the 21st century. *Expert Rev. Anti Infect. Ther.* **10,** 917–934 (2012).
18. Denning, D. W. Echinocandin antifungal drugs. *The Lancet* **362,** 1142–1151 (2003).
19. Grare, M. *et al.* In vitro activity of para-guanidinoethylcalix[4]arene against susceptible and antibiotic-resistant Gram-negative and Gram-positive bacteria. *J. Antimicrob. Chemother.* **60,** 575–581 (2007).
20. Aminov, R. I. A Brief History of the Antibiotic Era: Lessons Learned and Challenges for the Future. *Front. Microbiol.* **1,** (2010).

21. Lloyd, N. C., Morgan, H. W., Nicholson, B. K. & Ronimus, R. S. The Composition of Ehrlich's Salvarsan: Resolution of a Century-Old Debate. *Angew. Chem. Int. Ed.* **44,** 941–944 (2005).
22. Davies, J. & Davies, D. Origins and Evolution of Antibiotic Resistance. *Microbiol. Mol. Biol. Rev.* **74,** 417–433 (2010).
23. Chain, E. *et al.* the classic: penicillin as a chemotherapeutic agent. 1940. *Clin. Orthop.* **439,** 23–26 (2005).
24. Hazen, E. L. & Brown, R. Two antifungal agents produced by a soil actinomycete. *Science* **112,** 423 (1950).
25. Anderson, J. B. Evolution of antifungal-drug resistance: mechanisms and pathogen fitness. *Nat. Rev. Microbiol.* **3,** 547–556 (2005).
26. Oura, M., Sternberg, T. H. & Wright, E. T. A new antifungal antibiotic, amphotericin B. *Antibiot. Annu.* **3,** 566–573 (1955).
27. Dutcher, J. D. The discovery and development of amphotericin B. *Dis. Chest* **54,** Suppl 1:296–298 (1968).
28. Heidelberger, C. *et al.* Fluorinated pyrimidines, a new class of tumour-inhibitory compounds. *Nature* **179,** 663–666 (1957).
29. Baum, G. L. Antifungal therapy, 1978. *Postgrad. Med. J.* **55,** 587–592 (1979).
30. Butts, A. & Krysan, D. J. Antifungal Drug Discovery: Something Old and Something New. *PLoS Pathog* **8,** e1002870 (2012).
31. Flint, A., Forsey, R. R. & Usher, B. Griseofulvin, A New Oral Antibiotic for the Treatment of Fungous Infections of the Skin. *Can. Med. Assoc. J.* **81,** 173 (1959).
32. Wrong, N. M., Rosset, M., Hudson, A. L. & Rogers, S. Griseofulvin in the treatment of superficial fungous infections. *Can. Med. Assoc. J.* **81,** 167–173 (1959).
33. Harrison, E. F. *et al.* Haloprogin: a Topical Antifungal Agent. *Appl. Microbiol.* **19,** 746 (1970).
34. Maertens, J. A. History of the development of azole derivatives. *Clin. Microbiol. Infect.* **10,** 1–10 (2004).
35. Nyfeler, R. & Keller-Schierlein, W. [Metabolites of microorganisms. 143. Echinocandin B, a novel polypeptide-antibiotic from Aspergillus nidulans var. echinulatus: isolation and structural components]. *Helv. Chim. Acta* **57,** 2459–2477 (1974).
36. Masurekar, P. S., Fountoulakis, J. M., Hallada, T. C., Sosa, M. S. & Kaplan, L. Pneumocandins from Zalerion arboricola. II. Modification of product spectrum by mutation and medium manipulation. *J. Antibiot. (Tokyo)* **45,** 1867–1874 (1992).
37. Iwamoto, T. *et al.* WF11899A, B and C, novel antifungal lipopeptides. I. Taxonomy, fermentation, isolation and physico-chemical properties. *J. Antibiot. (Tokyo)* **47,** 1084–1091 (1994).
38. Magiorakos, A.-P. *et al.* Multidrug-resistant, extensively drug-resistant and pandrug-resistant bacteria: an international expert proposal for interim standard definitions for acquired resistance. *Clin. Microbiol. Infect.* **18,** 268–281 (2012).
39. Holmberg, S. D., Solomon, S. L. & Blake, P. A. Health and economic impacts of antimicrobial resistance. *Rev. Infect. Dis.* **9,** 1065–1078 (1987).
40. Levy, S. B. & Marshall, B. Antibacterial resistance worldwide: causes, challenges and responses. *Nat. Med.* **10,** S122–S129 (2004).
41. Alekshun, M. N. & Levy, S. B. Molecular Mechanisms of Antibacterial Multidrug Resistance. *Cell* **128,** 1037–1050 (2007).

42. Wang, H., Dzink-Fox, J. L., Chen, M. & Levy, S. B. Genetic characterization of highly fluoroquinolone-resistant clinical Escherichia coli strains from China: role of acrR mutations. *Antimicrob. Agents Chemother.* **45,** 1515–1521 (2001).
43. Fernández, L., Breidenstein, E. B. M. & Hancock, R. E. W. Creeping baselines and adaptive resistance to antibiotics. *Drug Resist. Updat.* **14,** 1–21 (2011).
44. Bassetti, M., Merelli, M., Temperoni, C. & Astilean, A. New antibiotics for bad bugs: where are we? *Ann. Clin. Microbiol. Antimicrob.* **12,** 22 (2013).
45. Sanglard, D. & Odds, F. C. Resistance of Candida species to antifungal agents: molecular mechanisms and clinical consequences. *Lancet Infect. Dis.* **2,** 73–85 (2002).
46. Sanglard, D. Resistance of human fungal pathogens to antifungal drugs. *Curr. Opin. Microbiol.* **5,** 379–385 (2002).
47. Cowen, L. E. The evolution of fungal drug resistance: modulating the trajectory from genotype to phenotype. *Nat. Rev. Microbiol.* **6,** 187–198 (2008).
48. Boucher, H. W. *et al.* Bad Bugs, No Drugs: No ESKAPE! An Update from the Infectious Diseases Society of America. *Clin. Infect. Dis.* **48,** 1–12 (2009).
49. Butler, M. S. & Cooper, M. A. Antibiotics in the clinical pipeline in 2011. *J. Antibiot. (Tokyo)* **64,** 413–425 (2011).
50. Butler, M. S., Blaskovich, M. A. & Cooper, M. A. Antibiotics in the clinical pipeline in 2013. *J. Antibiot. (Tokyo)* **66,** 571–591 (2013).
51. Walsh, C. T. & Wencewicz, T. A. Prospects for new antibiotics: a molecule-centered perspective. *J. Antibiot. (Tokyo)* **67,** 7–22 (2014).
52. Cruz, J., Ortiz, C., Guzmán, F., Fernández-Lafuente, R. & Torres, R. Antimicrobial Peptides: Promising Compounds Against Pathogenic Microorganisms. *Curr. Med. Chem.* (2014).
53. Tavares, L. S. *et al.* Strategies and molecular tools to fight antimicrobial resistance: resistome, transcriptome, and antimicrobial peptides. *Front. Microbiol.* **4,** 412 (2013).
54. Jenssen, H., Hamill, P. & Hancock, R. E. W. Peptide Antimicrobial Agents. *Clin. Microbiol. Rev.* **19,** 491–511 (2006).
55. Guilhelmelli, F. *et al.* Antibiotic development challenges: the various mechanisms of action of antimicrobial peptides and of bacterial resistance. *Antimicrob. Resist. Chemother.* **4,** 353 (2013).
56. Antibacterial and antifungal drug discovery. *Nat. Biotechnol.* **18,** IT24–IT26 (2000).
57. Ma, Z. *et al.* Synthesis and antimicrobial activity of 4H-4-oxoquinolizine derivatives: consequences of structural modification at the C-8 position. *J. Med. Chem.* **42,** 4202–4213 (1999).
58. Cox, G. & Wright, G. D. Intrinsic antibiotic resistance: Mechanisms, origins, challenges and solutions. *Int. J. Med. Microbiol.* **303,** 287–292 (2013).
59. Fajardo, A. *et al.* The neglected intrinsic resistome of bacterial pathogens. *PloS One* **3,** e1619 (2008).
60. Wright, G. D. The antibiotic resistome. *Expert Opin. Drug Discov.* **5,** 779–788 (2010).
61. Olivares Pacheco, J. A. *et al.* The intrinsic resistome of bacterial pathogens. *Antimicrob. Resist. Chemother.* **4,** 103 (2013).
62. Liu, S. & Wang, Y. Application of AFM in microbiology: a review. *Scanning* **32,** 61–73 (2010).
63. El Kirat, K., Burton, I., Dupres, V. & Dufrene, Y. F. Sample preparation procedures for biological atomic force microscopy. *J. Microsc.* **218,** 199–207 (2005).

64. Pillet, F., Chopinet, L., Formosa, C. & Dague, É. Atomic Force Microscopy and pharmacology: From microbiology to cancerology. *Biochim. Biophys. Acta BBA - Gen. Subj.* **1840,** 1028–1050 (2014).
65. Formosa, C., Grare, M., Duval, R. E. & Dague, E. Nanoscale effects of antibiotics on P. aeruginosa. *Nanomedicine Nanotechnol. Biol. Med.* **8,** 12–16 (2012).
66. Chopinet, L., Formosa, C., Rols, M. P., Duval, R. E. & Dague, E. Imaging living cells surface and quantifying its properties at high resolution using AFM in QI^{TM} mode. *Micron* **48,** 26–33 (2013).
67. Francois, J. M. *et al.* Use of atomic force microscopy (AFM) to explore cell wall properties and response to stress in the yeast Saccharomyces cerevisiae. *Curr. Genet.* **59,** 187–196 (2013).
68. Formosa, C. *et al.* Nanoscale Effects of Caspofungin against Two Yeast Species, Saccharomyces cerevisiae and Candida albicans. *Antimicrob. Agents Chemother.* **57,** 3498–3506 (2013).
69. Jauvert, E. *et al.* Probing single molecule interactions by AFM using bio-functionalized dendritips. *Sens. Actuators B Chem.* **168,** 436–441 (2012).
70. Formosa, C. *et al.* Nanoscale analysis of the effects of antibiotics and CX1 on a Pseudomonas aeruginosa multidrug-resistant strain. *Sci Rep* **2,** (2012).
71. Louise Meyer, R. *et al.* Immobilisation of living bacteria for AFM imaging under physiological conditions. *Ultramicroscopy* **110,** 1349–1357 (2010).
72. Doktycz, M. J. *et al.* AFM imaging of bacteria in liquid media immobilized on gelatin coated mica surfaces. *Ultramicroscopy* **97,** 209–216 (2003).
73. Francius, G., Tesson, B., Dague, E., Martin-Jézéquel, V. & Dufrêne, Y. F. Nanostructure and nanomechanics of live Phaeodactylum tricornutum morphotypes. *Environ. Microbiol.* **10,** 1344–1356 (2008).
74. Kasas, S. & Ikai, A. A method for anchoring round shaped cells for atomic force microscope imaging. *Biophys. J.* **68,** 1678–1680 (1995).
75. Francius, G., Domenech, O., Mingeot-Leclercq, M. P. & Dufrêne, Y. F. Direct Observation of Staphylococcus aureus Cell Wall Digestion by Lysostaphin. *J. Bacteriol.* **190,** 7904–7909 (2008).
76. Alsteens, D. *et al.* Structure, cell wall elasticity and polysaccharide properties of living yeasts cells, as probed by AFM. *Nanotechnology* 384005 (2008).
77. Dague, E., Alsteens, D., Latgé, J.-P. & Dufrêne, Y. F. High-Resolution Cell Surface Dynamics of Germinating Aspergillus fumigatus Conidia. *Biophys. J.* **94,** 656–660 (2008).
78. Gilbert, Y. *et al.* Single-Molecule Force Spectroscopy and Imaging of the Vancomycin/d-Ala-d-Ala Interaction. *Nano Lett.* **7,** 796–801 (2007).
79. Dague, E. *et al.* Assembly of live micro-organisms on microstructured PDMS stamps by convective/capillary deposition for AFM bio-experiments. *Nanotechnology* **22,** (2011).
80. JPK Instruments. QITM mode- Quantitative Imaging with the Nanowizard 3 AFM. at <www.jpk.com>
81. JPK Instruments AG - Application Reports / Technical Reports - AFM. at <http://www.jpk.com/afm.230.en.html>
82. Beauvais, A. *et al.* Deletion of the α-(1,3)-Glucan Synthase Genes Induces a Restructuring of the Conidial Cell Wall Responsible for the Avirulence of Aspergillus fumigatus. *PLoS Pathog* **9,** e1003716 (2013).
83. Dufrêne, Y. F. *et al.* Five challenges to bringing single-molecule force spectroscopy into living cells. *Nat. Methods* **8,** 123–127 (2011).

84. Müller, D. J., Helenius, J., Alsteens, D. & Dufrêne, Y. F. Force probing surfaces of living cells to molecular resolution. *Nat. Chem. Biol.* **5,** 383–390 (2009).
85. Baumgartner, W. *et al.* Cadherin interaction probed by atomic force microscopy. *Proc. Natl. Acad. Sci.* **97,** 4005–4010 (2000).
86. Rief, M., Oesterhelt, F., Heymann, B. & Gaub, H. E. Single Molecule Force Spectroscopy on Polysaccharides by Atomic Force Microscopy. *Science* **275,** 1295–1297 (1997).
87. Zocher, M., Zhang, C., Rasmussen, S. G. F., Kobilka, B. K. & Müller, D. J. Cholesterol increases kinetic, energetic, and mechanical stability of the human β2-adrenergic receptor. *Proc. Natl. Acad. Sci.* **109,** E3463–E3472 (2012).
88. Lipke, P. N. & Ovalle, R. Cell Wall Architecture in Yeast: New Structure and New Challenges. *J. Bacteriol.* **180,** 3735–3740 (1998).
89. Florin, E. L., Moy, V. T. & Gaub, H. E. Adhesion forces between individual ligand-receptor pairs. *Science* **264,** 415–417 (1994).
90. Lee, G. U., Chrisey, L. A. & Colton, R. J. Direct measurement of the forces between complementary strands of DNA. *Science* **266,** 771–773 (1994).
91. Bustanji, Y. *et al.* Dynamics of the interaction between a fibronectin molecule and a living bacterium under mechanical force. *Proc. Natl. Acad. Sci.* **100,** 13292–13297 (2003).
92. Hinterdorfer, P., Baumgartner, W., Gruber, H. J., Schilcher, K. & Schindler, H. Detection and localization of individual antibody-antigen recognition events by atomic force microscopy. *Proc. Natl. Acad. Sci.* **93,** 3477–3481 (1996).
93. Ros, R. *et al.* Antigen binding forces of individually addressed single-chain Fv antibody molecules. *Proc. Natl. Acad. Sci.* **95,** 7402–7405 (1998).
94. Ebner, A. *et al.* Functionalization of probe tips and supports for single-molecule recognition force microscopy. *Top. Curr. Chem.* **285,** 29–76 (2008).
95. Wildling, L. *et al.* Linking of Sensor Molecules with Amino Groups to Amino-Functionalized AFM Tips. *Bioconjug. Chem.* **22,** 1239–1248 (2011).
96. Kamruzzahan, A. S. M. *et al.* Antibody Linking to Atomic Force Microscope Tips via Disulfide Bond Formation. *Bioconjug. Chem.* **17,** 1473–1481 (2006).
97. Chaffin, W. L. Candida albicans Cell Wall Proteins. *Microbiol. Mol. Biol. Rev.* **72,** 495 – 544 (2008).
98. Free, S. J. in *Adv. Genet.* (Theodore Friedmann, J. C. D. and S. F. G.) **Volume 81,** 33–82 (Academic Press, 2013).
99. Orlean, P. Architecture and biosynthesis of the Saccharomyces cerevisiae cell wall. *Genetics* **192,** 775–818 (2012).
100. Dague, E. *et al.* Towards a nanoscale view of fungal surfaces. *Yeast* **24,** 229–237 (2007).
101. Dufrêne, Y. F. Atomic force microscopy of fungal cell walls: an update. *Yeast* **27,** 465–471 (2010).
102. Naglik, J. R., Moyes, D. L., Wächtler, B. & Hube, B. Candida albicans interactions with epithelial cells and mucosal immunity. *Microbes Infect.* **13,** 963–976 (2011).
103. Hoyer, L. L. The ALS gene family of Candida albicans. *Trends Microbiol.* **9,** 176–180 (2001).
104. Hoyer, L. L., Green, C. B., Oh, S.-H. & Zhao, X. Discovering the secrets of the Candida albicans agglutinin-like sequence (ALS) gene family – a sticky pursuit. *Med Mycol* **46,** 1–15 (2008).
105. Ramsook, C. B. *et al.* Yeast Cell Adhesion Molecules Have Functional Amyloid-Forming Sequences. *Eukaryot. Cell* **9,** 393 –404 (2010).

106. Sawaya, M. R. *et al.* Atomic structures of amyloid cross-β spines reveal varied steric zippers. *Nature* **447,** 453–457 (2007).
107. Garcia, M. C. *et al.* A Role for Amyloid in Cell Aggregation and Biofilm Formation. *PLoS ONE* **6,** e17632 (2011).
108. Rauceo, J. M. *et al.* Global Cell Surface Conformational Shift Mediated by a Candida albicans Adhesin. *Infect. Immun.* **72,** 4948–4955 (2004).
109. Alsteens, D., Garcia, M. C., Lipke, P. N. & Dufrêne, Y. F. Force-induced formation and propagation of adhesion nanodomains in living fungal cells. *Proc. Natl. Acad. Sci.* **107,** 20744 –20749 (2010).
110. Beaussart, A. *et al.* Single-Molecule Imaging and Functional Analysis of Als Adhesins and Mannans during Candida albicans Morphogenesis. *ACS Nano* **6,** 10950–10964 (2012).
111. Alsteens, D. *et al.* Unfolding Individual Als5p Adhesion Proteins on Live Cells. *ACS Nano* **3,** 1677–1682 (2009).
112. Alsteens, D., Ramsook, C. B., Lipke, P. N. & Dufrêne, Y. F. Unzipping a Functional Microbial Amyloid. *ACS Nano* **6,** 7703–7711 (2012).
113. Dufrêne, Y. F., Martínez-Martín, D., Medalsy, I., Alsteens, D. & Müller, D. J. Multiparametric imaging of biological systems by force-distance curve-based AFM. *Nat. Methods* **10,** 847–854 (2013).
114. Gow, N. A. R., van de Veerdonk, F. L., Brown, A. J. P. & Netea, M. G. Candida albicans morphogenesis and host defence: discriminating invasion from colonization. *Nat Rev Micro* **10,** 112–122 (2012).
115. Heinisch, J. J. Baker's yeast as a tool for the development of antifungal kinase inhibitors--targeting protein kinase C and the cell integrity pathway. *Biochim. Biophys. Acta* **1754,** 171–182 (2005).
116. Carrillo-Muñoz, A. J., Giusiano, G., Ezkurra, P. A. & Quindós, G. Antifungal agents: mode of action in yeast cells. *Rev. Esp. Quimioter. Publ. Of. Soc. Esp. Quimioter.* **19,** 130–139 (2006).
117. Levin, D. E. Regulation of cell wall biogenesis in Saccharomyces cerevisiae: the cell wall integrity signaling pathway. *Genetics* **189,** 1145–1175 (2011).
118. Dallies, N., François, J. & Paquet, V. A new method for quantitative determination of polysaccharides in the yeast cell wall. Application to the cell wall defective mutants of Saccharomyces cerevisiae. *Yeast* **14,** 1297–1306 (1998).
119. Adya, A. K., Canetta, E. & Walker, G. M. Atomic force microscopic study of the influence of physical stresses on Saccharomyces cerevisiae and Schizosaccharomyces pombe. *FEMS Yeast Res.* **6,** 120–128 (2006).
120. Canetta, E., Adya, A. K. & Walker, G. M. Atomic force microscopic study of the effects of ethanol on yeast cell surface morphology. *FEMS Microbiol. Lett.* **255,** 308–315 (2006).
121. Canetta, E., Walker, G. M. & Adya, A. K. Nanoscopic morphological changes in yeast cell surfaces caused by oxidative stress: an atomic force microscopic study. *J. Microbiol. Biotechnol.* **19,** 547–555 (2009).
122. Pillet, F. *et al.* Uncovering by Atomic Force Microscopy of an original circular structure at the yeast cell surface in response to heat shock. *BMC Biol.* **12,** 6 (2014).
123. Silhavy, T. J., Kahne, D. & Walker, S. The Bacterial Cell Envelope. *Cold Spring Harb. Perspect. Biol.* **2,** a000414 (2010).
124. Egan, A. J. F. & Vollmer, W. The physiology of bacterial cell division. *Ann. N. Y. Acad. Sci.* **1277,** 8–28 (2013).

125. Raetz, C. R. H. & Whitfield, C. Lipopolysaccharide endotoxins. *Annu. Rev. Biochem.* **71,** 635–700 (2002).
126. Braun, V. Covalent lipoprotein from the outer membrane of Escherichia coli. *Biochim. Biophys. Acta* **415,** 335–377 (1975).
127. Vollmer, W., Blanot, D. & de Pedro, M. A. Peptidoglycan structure and architecture. *FEMS Microbiol. Rev.* **32,** 149–167 (2008).
128. Mullineaux, C. W., Nenninger, A., Ray, N. & Robinson, C. Diffusion of green fluorescent protein in three cell environments in Escherichia coli. *J. Bacteriol.* **188,** 3442–3448 (2006).
129. De Duve, C. & Wattiaux, R. Functions of Lysosomes. *Annu. Rev. Physiol.* **28,** 435–492 (1966).
130. Raetz, C. R. & Dowhan, W. Biosynthesis and function of phospholipids in Escherichia coli. *J. Biol. Chem.* **265,** 1235–1238 (1990).
131. Skiada, A., Markogiannakis, A., Plachouras, D. & Daikos, G. L. Adaptive resistance to cationic compounds in Pseudomonas aeruginosa. *Int. J. Antimicrob. Agents* **37,** 187–193 (2011).
132. Lister, P. D., Wolter, D. J. & Hanson, N. D. Antibacterial-resistant Pseudomonas aeruginosa: clinical impact and complex regulation of chromosomally encoded resistance mechanisms. *Clin. Microbiol. Rev.* **22,** 582–610 (2009).
133. Morita, Y., Tomida, J. & Kawamura, Y. Responses of Pseudomonas aeruginosa to antimicrobials. *Front. Microbiol.* **4,** 422 (2014).
134. Tan, J. S. & File, T. M., Jr. Antipseudomonal penicillins. *Med. Clin. North Am.* **79,** 679–693 (1995).
135. Prior, R. B. & Warner, J. F. Morphological alterations of Pseudomonas aeruginosa by ticarcillin: a scanning electron microscope study. *Antimicrob. Agents Chemother.* **6,** 853–855 (1974).
136. Schlacher, K. & Goodman, M. F. Lessons from 50 years of SOS DNA-damage-induced mutagenesis. *Nat. Rev. Mol. Cell Biol.* **8,** 587–594 (2007).
137. Jacoby, G. A. & Sutton, L. Properties of plasmids responsible for production of extended-spectrum beta-lactamases. *Antimicrob. Agents Chemother.* **35,** 164–169 (1991).
138. Pasteran, F., Veliz, O., Rapoport, M., Guerriero, L. & Corso, A. Sensitive and Specific Modified Hodge Test for KPC and Metallo-Beta- Lactamase Detection in Pseudomonas aeruginosa by Use of a Novel Indicator Strain, Klebsiella pneumoniae ATCC 700603. *J. Clin. Microbiol.* **49,** 4301–4303 (2011).
139. Vaara, M. Novel derivatives of polymyxins. *J. Antimicrob. Chemother.* **68,** 1213–1219 (2013).
140. Koch-Weser, J. *et al.* Adverse effects of sodium colistimethate. Manifestations and specific reaction rates during 317 courses of therapy. *Ann. Intern. Med.* **72,** 857–868 (1970).
141. Yahav, D., Farbman, L., Leibovici, L. & Paul, M. Colistin: new lessons on an old antibiotic. *Clin. Microbiol. Infect.* **18,** 18–29 (2012).
142. Velkov, T., Thompson, P. E., Nation, R. L. & Li, J. Structure--activity relationships of polymyxin antibiotics. *J. Med. Chem.* **53,** 1898–1916 (2010).
143. Zhang, L., Dhillon, P., Yan, H., Farmer, S. & Hancock, R. E. Interactions of bacterial cationic peptide antibiotics with outer and cytoplasmic membranes of Pseudomonas aeruginosa. *Antimicrob. Agents Chemother.* **44,** 3317–3321 (2000).
144. Velkov, T., Roberts, K. D., Nation, R. L., Thompson, P. E. & Li, J. Pharmacology of polymyxins: new insights into an ‘old’ class of antibiotics. *Future Microbiol.* **8,** 711–724 (2013).

145. Vidaillac, C., Benichou, L. & Duval, R. E. In Vitro Synergy of Colistin Combinations against Colistin-Resistant Acinetobacter baumannii, Pseudomonas aeruginosa, and Klebsiella pneumoniae Isolates. *Antimicrob. Agents Chemother.* **56,** 4856–4861 (2012).
146. Soon, R. L. *et al.* Effect of colistin exposure and growth phase on the surface properties of live Acinetobacter baumannii cells examined by atomic force microscopy. *Int. J. Antimicrob. Agents* **38,** 493–501 (2011).
147. Soon, R. L., Nation, R. L., Hartley, P. G., Larson, I. & Li, J. Atomic Force Microscopy Investigation of the Morphology and Topography of Colistin-Heteroresistant Acinetobacter baumannii Strains as a Function of Growth Phase and in Response to Colistin Treatment. *Antimicrob. Agents Chemother.* **53,** 4979–4986 (2009).
148. Mortensen, N. P. *et al.* Effects of Colistin on Surface Ultrastructure and Nanomechanics of Pseudomonas aeruginosa Cells. *Langmuir* **25,** 3728–3733 (2009).
149. Niederl, J. B. & Vogel, H. J. Aldehyde—Resorcinol Condensations1. *J. Am. Chem. Soc.* **62,** 2512–2514 (1940).
150. Ostenson, C. G. Effects of the biguanide synthalin A on the pancreatic A2-cell of the guinea pig. *Exp. Clin. Endocrinol.* **81,** 255–262 (1983).
151. Mourer, M., Duval, R. E., Finance, C. & Regnouf-de-Vains, J.-B. Functional organisation and gain of activity: The case of the antibacterial tetra-para-guanidinoethyl-calix[4]arene. *Bioorg. Med. Chem. Lett.* **16,** 2960–2963 (2006).
152. Grare, M., Mourer, M., Regnouf de Vains, J.-B., Finance, C. & Duval, R.-E. [Towards new antibacterial drugs. Interest of para-guanidinoethylcalix[4]arene]. *Pathol. Biol. (Paris)* **54,** 470–476 (2006).
153. Hayhurst, E. J., Kailas, L., Hobbs, J. K. & Foster, S. J. Cell wall peptidoglycan architecture in Bacillus subtilis. *Proc. Natl. Acad. Sci.* **105,** 14603–14608 (2008).
154. Andre, G. *et al.* Imaging the nanoscale organization of peptidoglycan in living Lactococcus lactis cells. *Nat. Commun.* **1,** 1–8 (2010).
155. Fournier, P.-E. *et al.* Modern clinical microbiology: new challenges and solutions. *Nat. Rev. Microbiol.* **11,** 574–585 (2013).
156. Alsteens, D., Beaussart, A., El-Kirat-Chatel, S., Sullan, R. M. A. & Dufrêne, Y. F. Atomic Force Microscopy: A New Look at Pathogens. *PLoS Pathog* **9,** e1003516 (2013).
157. Dufrene, Y. F. Using nanotechniques to explore microbial surfaces. *Nat Rev Micro* **2,** 451–460 (2004).
158. Dufrêne, Y. F. Towards nanomicrobiology using atomic force microscopy. *Nat. Rev. Microbiol.* **6,** 674–680 (2008).
159. Dorobantu, L. S., Goss, G. G. & Burrell, R. E. Atomic force microscopy: A nanoscopic view of microbial cell surfaces. *Micron* **43,** 1312–1322 (2012).
160. Dorobantu, L. S. & Gray, M. R. Application of atomic force microscopy in bacterial research. *Scanning* **32,** 74–96 (2010).
161. Allison, D. P., Mortensen, N. P., Sullivan, C. J. & Doktycz, M. J. Atomic force microscopy of biological samples. *Wiley Interdiscip. Rev. Nanomed. Nanobiotechnol.* **2,** 618–634 (2010).
162. Lipke, P. N. *et al.* Strengthening relationships: amyloids create adhesion nanodomains in yeasts. *Trends Microbiol.* **20,** 59–65 (2012).
163. Rust, M. J., Bates, M. & Zhuang, X. Sub-diffraction-limit imaging by stochastic optical reconstruction microscopy (STORM). *Nat. Methods* **3,** 793–796 (2006).
164. Hess, S. T., Girirajan, T. P. K. & Mason, M. D. Ultra-high resolution imaging by fluorescence photoactivation localization microscopy. *Biophys. J.* **91,** 4258–4272 (2006).

165. Kamiyama, D. & Huang, B. Development in the STORM. *Dev. Cell* **23,** 1103–1110 (2012).
166. Gahlmann, A. & Moerner, W. E. Exploring bacterial cell biology with single-molecule tracking and super-resolution imaging. *Nat. Rev. Microbiol.* **12,** 9–22 (2014).
167. Betzig, E. *et al.* Imaging Intracellular Fluorescent Proteins at Nanometer Resolution. *Science* **313,** 1642–1645 (2006).
168. Manley, S. *et al.* High-density mapping of single-molecule trajectories with photoactivated localization microscopy. *Nat. Methods* **5,** 155–157 (2008).
169. Uphoff, S., Reyes-Lamothe, R., Leon, F. G. de, Sherratt, D. J. & Kapanidis, A. N. Single-molecule DNA repair in live bacteria. *Proc. Natl. Acad. Sci.* **110,** 8063–8068 (2013).
170. El-Kirat-Chatel, S. *et al.* Nanoscale analysis of caspofungin-induced cell surface remodelling in Candida albicans. *Nanoscale* **5,** 1105–1115 (2013).
171. Zhao, X., Oh, S.-H., Yeater, K. M. & Hoyer, L. L. Analysis of the Candida albicans Als2p and Als4p adhesins suggests the potential for compensatory function within the Als family. *Microbiology* **151,** 1619 –1630 (2005).
172. Zhao, X. *et al.* ALS3 and ALS8 represent a single locus that encodes a Candida albicans adhesin; functional comparisons between Als3p and Als1p. *Microbiology* **150,** 2415–2428 (2004).
173. Chang, T.-W. & Weinstein, L. Morphological changes in Gram-negative bacilli exposed to cephalothin. *J. Bacteriol.* **88,** 1790–1797 (1964).
174. Ellis, L. F., Herron, D. K., Preston, D. A., Simmons, L. K. & Schlegel, R. A. Evaluation of Antibiotic Efficacy Using Electron Microscopy: Morphological Effects of Guanylureido Cephalosporin, Chlorobenzoylureido Cephalosporin, BL-P1654, and Carbenicillin on Pseudomonas aeruginosa. *Antimicrob. Agents Chemother.* **9,** 334–342 (1976).
175. Hocquet, D. & Bertrand, X. Metronidazole increases the emergence of ciprofloxacin- and amikacin-resistant Pseudomonas aeruginosa by inducing the SOS response. *J. Antimicrob. Chemother.* **69,** 852–854 (2014).
176. Janion, C. Inducible SOS response system of DNA repair and mutagenesis in Escherichia coli. *Int. J. Biol. Sci.* **4,** 338–344 (2008).
177. Patel, M., Jiang, Q., Woodgate, R., Cox, M. M. & Goodman, M. F. A new model for SOS-induced mutagenesis: how RecA protein activates DNA polymerase V. *Crit. Rev. Biochem. Mol. Biol.* **45,** 171–184 (2010).
178. Miller, C. *et al.* SOS Response Induction by ß-Lactams and Bacterial Defense Against Antibiotic Lethality. *Science* **305,** 1629–1631 (2004).
179. Ando, T. *et al.* High-speed AFM and nano-visualization of biomolecular processes. *Pflüg. Arch. Eur. J. Physiol.* **456,** 211–225 (2008).
180. Ando, T. High-speed atomic force. *Microscopy* **62,** 81–93 (2013).
181. Kodera, N., Yamamoto, D., Ishikawa, R. & Ando, T. Video imaging of walking myosin V by high-speed atomic force microscopy. *Nature* **468,** 72–76 (2010).
182. Igarashi, K. *et al.* Traffic Jams Reduce Hydrolytic Efficiency of Cellulase on Cellulose Surface. *Science* **333,** 1279–1282 (2011).
183. Fantner, G. E., Barbero, R. J., Gray, D. S. & Belcher, A. M. Kinetics of antimicrobial peptide activity measured on individual bacterial cells using high-speed atomic force microscopy. *Nat. Nanotechnol.* **5,** 280–285 (2010).
184. Suzuki, Y. *et al.* High-speed atomic force microscopy combined with inverted optical microscopy for studying cellular events. *Sci. Rep.* **3,** (2013).

185. Yamashita, H. *et al.* Single-Molecule Imaging on Living Bacterial Cell Surface by High-Speed AFM. *J. Mol. Biol.* **422,** 300–309 (2012).
186. Conrad, R. S. & Gilleland, H. E., Jr. Lipid alterations in cell envelopes of polymyxin-resistant Pseudomonas aeruginosa isolates. *J. Bacteriol.* **148,** 487–497 (1981).
187. Champlin, F. R., Gilleland, H. E., Jr & Conrad, R. S. Conversion of phospholipids to free fatty acids in response to acquisition of polymyxin resistance in Pseudomonas aeruginosa. *Antimicrob. Agents Chemother.* **24,** 5–9 (1983).
188. Hale, J. D. & Hancock, R. E. Alternative mechanisms of action of cationic antimicrobial peptides on bacteria. *Expert Rev. Anti Infect. Ther.* **5,** 951–959 (2007).
189. Mogi, T. & Kita, K. Gramicidin S and polymyxins: the revival of cationic cyclic peptide antibiotics. *Cell. Mol. Life Sci.* **66,** 3821–3826 (2009).
190. Brogden, K. A. Antimicrobial peptides: pore formers or metabolic inhibitors in bacteria? *Nat. Rev. Microbiol.* **3,** 238–250 (2005).
191. David, H. L. & Rastogi, N. Antibacterial action of colistin (polymyxin E) against Mycobacterium aurum. *Antimicrob. Agents Chemother.* **27,** 701–707 (1985).
192. Moffatt, J. H. *et al.* Colistin resistance in Acinetobacter baumannii is mediated by complete loss of lipopolysaccharide production. *Antimicrob. Agents Chemother.* **54,** 4971–4977 (2010).
193. Jayol, A. *et al.* Resistance to colistin associated to a single amino acid change in protein PmrB among Klebsiella pneumoniae of worldwide origin. *Antimicrob. Agents Chemother.* (2014). doi:10.1128/AAC.00084-14
194. Ah, Y.-M., Kim, A.-J. & Lee, J.-Y. Colistin resistance in Klebsiella pneumoniae. *Int. J. Antimicrob. Agents* doi:10.1016/j.ijantimicag.2014.02.016
195. El Kirat, K., Morandat, S. & Dufrêne, Y. F. Nanoscale analysis of supported lipid bilayers using atomic force microscopy. *Biochim. Biophys. Acta BBA - Biomembr.* **1798,** 750–765 (2010).
196. Mingeot-Leclercq, M.-P., Deleu, M., Brasseur, R. & Dufrêne, Y. F. Atomic force microscopy of supported lipid bilayers. *Nat. Protoc.* **3,** 1654–1659 (2008).
197. Domenech, O., Dufrêne, Y. F., Van Bambeke, F., Tukens, P. M. & Mingeot-Leclercq, M.-P. Interactions of oritavancin, a new semi-synthetic lipoglycopeptide, with lipids extracted from Staphylococcus aureus. *Biochim. Biophys. Acta BBA - Biomembr.* **1798,** 1876–1885 (2010).

Conclusions

Using Atomic Force Microscopy, and through technological developments, we have: (i) obtained fundamental knowledge on the cell wall of pathogens, (ii) we have evaluated the effects of two reference antibiotics on the cell wall of the bacteria *Pseudomonas aeruginosa*, (iii) we have gained comprehension of the mechanisms of action of two last chance molecules, colistin and caspofungin, on the cell wall of the fungus *Candida albicans* and the bacteria *Klebsiella pneumoniae*, and (iv) finally we have better understood the mechanism of action of a new innovative antibacterial molecule, CX1, on the cell wall of multidrug resistant strain of *Pseudomonas aeruginosa*. This work, although relevant in the field of clinical microbiology, has not been simple to perform. Indeed, someone told me once "the PhD is not a linear way", and it is true. AFM experiments are complicated because they involve two different scientific fields. The technique must be efficient, but the biological model chosen must also be relevant. A good technique without a good biological model is useless. The other way around, a good biological model is not sufficient to produce significant results; the technique must be adapted too. This is why we have made our own technological developments during this PhD, but not without difficulties. For example, the anti-HA tip was first sought to be also an anti-His tip. But due to time constraint, we focused only on the HA-tip. Indeed, adjusting the antibody and antigen concentrations to reach the single molecule scale is a hard and time-consuming work. We also developed the same technology with an anti-V5 antibody; however no relevant biological questions were answered using this system. Finally, through collaborations, we could work on two different and relevant biological models containing the HA tag.

But collaborations are the intrinsic difficulty of AFM experiments. Because biophysics is an interdisciplinary field, good collaborations between AFM specialists and biologists are essentials. In this context, I have well-chosen my supervisors, since my entire PhD is

collaboration between an AFM specialist and pharmacist, Etienne Dague, and microbiologists, Raphaël Duval, Jean-Marie François and Hélène Martin-Yken. Working between these two scientific fields and personalities, I have been able to understand the technological requirements needed to perform AFM experiments, but also the importance of choosing the right biological models, for the right applications. I also had the chance to enlarge this environment, and to use different biological models that were not directly linked to my PhD subject, such as spores of *Aspergillus fumigatus*, and higher eukaryotic CHO cells. Then, beyond the choice of the model that corresponds to the technology developed, the difficulty of interdisciplinary lies in the communication and expectations of the experiments. Communication, first, because a term in physics does not mean the same thing in biology. Sometimes, these communication problems can lead to misunderstandings, the vocabulary issues have first to be cleared before starting experiments. And then, the expectations, because, the biologist does not know what the AFM is able to do, and because the AFM specialist does not understand the entire complexity of biological models. Indeed, the AFM specialist will know exactly the problems that will be encountered during experiments, and thus will know the limits. But the biologist also has limits, of "its" model. Therefore, the two partners have to identify these limits, which can sometimes be difficult.

Finally, the last point of this conclusion will be focused on the interest the army has in a project like this one. Indeed, this PhD is partially funded by the Direction Générale de l'Armement, for particular reasons. These last years, the world has witnessed the rise of terrorism, and Chemical, Biological, Radiological and Nuclear (CBRN) weapons have become an important threat to the countries security. These weapons are classified as "weapons of mass destruction", because their effects are difficult to control, due to their power and ability to

disseminate into the environment. Therefore, in this context, multidrug-resistant bacteria and yeasts present a major risk for the security of both soldiers and civilians. In order to anticipate this threat, scientific research, already active in the protection, detection, and decontamination, has to develop and understand the mechanisms of action of new antimicrobials, with a broad-spectrum. This PhD being focused on the comprehension of microbial cell wall with the aim of identifying new targets for antimicrobials, and on the understanding of mechanisms of action of antimicrobials, it then meets the priorities of protection of soldiers and nations confronted to CBRN weapons threats.

Chapter 2

Bibliographic analysis: the use of AFM in microbiology

Chapter 2.1: Atomic Force Microscopy in pharmacology: from microbiology to cancerology

My contribution to this review has focused on the use of AFM in yeast studies and in bacteriology.

Chapter 2.2: Use of AFM to explore cell wall properties and response to stress in the yeast *Saccharomyces cerevisiae*

My contribution in this second publication has been to review immobilization methods, as well as providing figures.

Chapter 2.3: Imaging living yeast cells and quantifying their biophysical properties by Atomic Force Microscopy

I have written and provided figures for this last book chapter, dedicated to the use of AFM in mycology studies.

Chapter 2.1:

Atomic Force Microscopy and pharmacology: from microbiology to cancerology

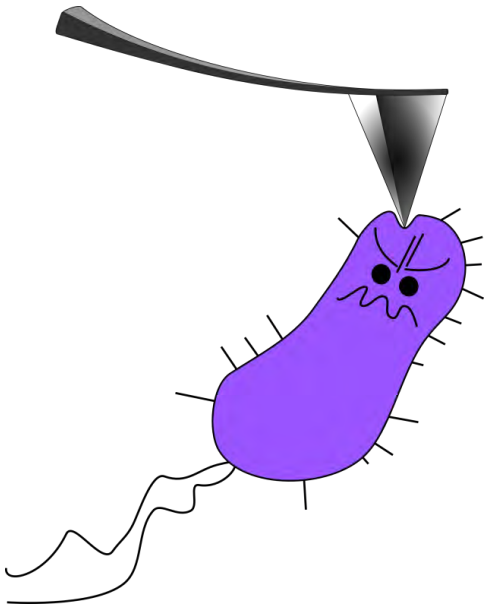

Pillet F., Chopinet L., Formosa C., and Dague E.

Biochimica et Biophysica Acta-General Subjects, **1840**, 1028-1050, 2014

Abstract

Background: Atomic Force Microscopy (AFM) has been extensively used to study biological samples. Researchers take advantage of its ability to image living samples to increase our fundamental knowledge (biophysical properties/ biochemical behavior) on living cell surface properties, at the nano-scale.

Scope of review: AFM, in the imaging modes, can probe cells morphological modifications induced by drugs. In the force spectroscopy mode, it is possible to follow the nanomechanical properties of a cell and to probe the mechanical modifications induced by drugs. AFM can be used to map single molecule distribution at the cell surface. We will focus on a collection of results aiming at evaluating the nano-scale effects of drugs, by AFM. Studies on yeast, bacteria and mammal cells will illustrate our discussion. Especially, we will show how AFM can help in getting a better understanding of drug mechanism of action.

Major conclusions: This review demonstrates that AFM is a versatile tool, useful in pharmacology. In microbiology, it has been used to study the drugs fighting Candida albicans or Pseudomonas aeruginosa. The major conclusions

are a better understanding of the microbes' cell wall and of the drugs mechanism of action. In cancerology, AFM has been used to explore the effects of cytotoxic drugs or as an innovative diagnostic technology. AFM has provided original results on cultured cells, cells extracted from patient and directly on patient biopsies.

General significance: This review enhances the interest of AFM technologies for pharmacology. The applications reviewed range from microbiology to cancerology.

Biochimica et Biophysica Acta 1840 (2014) 1028–1050

Contents lists available at ScienceDirect

Biochimica et Biophysica Acta

journal homepage: www.elsevier.com/locate/bbagen

Review

Atomic Force Microscopy and pharmacology: From microbiology to cancerology

Flavien Pillet [a,c], Louise Chopinet [b,c], Cécile Formosa [a,c,d,e], Étienne Dague [a,c,f,*]

[a] CNRS, LAAS, 7 avenue du colonel Roche, F-31077 Toulouse Cedex 4, France
[b] CNRS, IPBS—UMR 5089, BP64182, 205 route de Narbonne, F-31077 Toulouse Cedex 4, France
[c] Université de Toulouse, UPS, INSA, INP, ISAE, UT1, UTM, LAAS, ITAV, F-31077 Toulouse Cedex 4, France
[d] CNRS, UMR 7565, SRSMC, Vandoeuvre-lès-Nancy, France
[e] Université de Lorraine, UMR 7565, Faculté de Pharmacie, Nancy, France
[f] CNRS; ITAV-USR 3505; F31106 Toulouse, France

ARTICLE INFO

Article history:
Received 7 August 2013
Received in revised form 18 November 2013
Accepted 20 November 2013
Available online 27 November 2013

Keywords:
Atomic Force Microscopy
Pharmacology
Yeast
Bacterium
Cancer

ABSTRACT

Background: Atomic Force Microscopy (AFM) has been extensively used to study biological samples. Researchers take advantage of its ability to image living samples to increase our fundamental knowledge (biophysical properties/biochemical behavior) on living cell surface properties, at the nano-scale.
Scope of review: AFM, in the imaging modes, can probe cells morphological modifications induced by drugs. In the force spectroscopy mode, it is possible to follow the nanomechanical properties of a cell and to probe the mechanical modifications induced by drugs. AFM can be used to map single molecule distribution at the cell surface. We will focus on a collection of results aiming at evaluating the nano-scale effects of drugs, by AFM. Studies on yeast, bacteria and mammal cells will illustrate our discussion. Especially, we will show how AFM can help in getting a better understanding of drug mechanism of action.
Major conclusions: This review demonstrates that AFM is a versatile tool, useful in pharmacology. In microbiology, it has been used to study the drugs fighting *Candida albicans* or *Pseudomonas aeruginosa*. The major conclusions are a better understanding of the microbes' cell wall and of the drugs mechanism of action. In cancerology, AFM has been used to explore the effects of cytotoxic drugs or as an innovative diagnostic technology. AFM has provided original results on cultured cells, cells extracted from patient and directly on patient biopsies.
General significance: This review enhances the interest of AFM technologies for pharmacology. The applications reviewed range from microbiology to cancerology.

1. Introduction

Historically, imaging at high resolution is based on the optical microscope. However this technique suffers from the limitation of the photons wavelength, roughly 200 nm. To overcome this limitation the electron microscopes were developed by Ruska and Knoll. Here the resolution is limited by the electrons wavelength, which is much lower than for visible light (100 000 times shorter). Both technologies are based on lenses that focalize a photon or an electron beam on a sample. Scanning probe microscopes work in a completely different way. The principle relies on the measure of a parameter (*e.g.* the tunneling current [1] or the force [2]) between a sharp tip and a surface and to keep this parameter constant while scanning in order to get a three dimensional image of the sample. As stated by C. Gerber, one of the Atomic Force Microscope (AFM) pioneer, and P. Lang in a 2006 paper in Nature Nanotechnology [3]: the scanning probe microscopes (SPM) have opened the door to the nanoworld. SPM made it possible to explore and to manipulate it. Feynman had dreamed of "the room at the bottom" [4]; SPM had opened the doors (for example, Eigler and Schweizer wrote the acronym IBM with Xe atoms [5,6]). Particularly, AFM has contributed to major advances in very different fields from fundamental physic and chemistry to information technologies, molecular electronic and spintronic. Since 25 years [7–9] AFM has emerged as a first interest characterization technology in life science. The number of research articles, published each year, in which AFM is used has increased exponentially since 1981. Fig. 1A presents this evolution. It must be noticed that the increase of studies on living cells is slow. This is probably due to difficulties inherent to biology and living cells.

AFM can be used in imaging modes like contact mode or oscillation mode as described in Fig. 1B. In these modes a sharp tip mounted on a cantilever is scanned over the sample surface. In contact mode, the cantilever deflection is kept constant in order to apply a constant force and to generate isoforce images of the surface. In oscillation mode, the cantilever is oscillating near to its resonance frequency and the amplitude

* Corresponding author at: Université de Toulouse, UPS, INSA, INP, ISAE, UT1, UTM, LAAS, ITAV, F-31077 Toulouse Cedex 4, France.
E-mail address: edague@laas.fr (É. Dague).

0304-4165/$ – see front matter © 2013 Elsevier B.V. All rights reserved.
http://dx.doi.org/10.1016/j.bbagen.2013.11.019

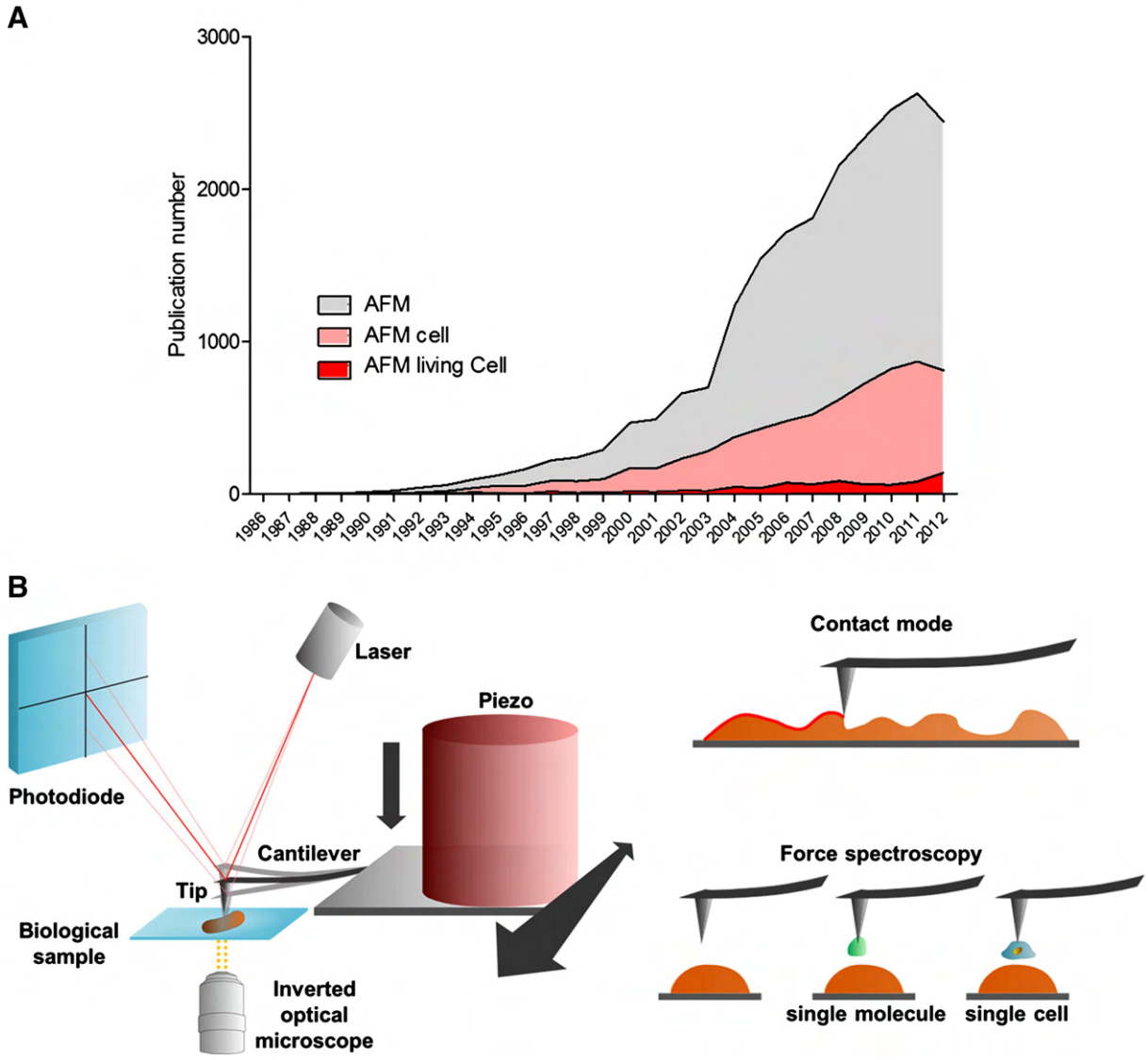

Fig. 1. (A) Evolution of the number of paper published each year, pubmed search using AFM or AFM and cell, or AFM and living and cell. (B) Schema introducing the AFM technology. A sharp tip is mounted on a cantilever that can be moved in the x, y, and z direction thanks to a piezo electric ceramic. The deflection of the cantilever is monitored on a 4 squares photodiode thanks to the reflection of a laser beam, aligned at the end of the, usually gold coated, cantielever. The AFM can be used to produce topographical images (like in contact mode) or to measure forces (in the force spectroscopy mode) between a bare or a functionnalized tip (with a biomolecule or a single cell) and the sample.

of the oscillation is kept constant while scanning, which creates isoamplitude images. However, AFM is not only an imaging technology. It is a highly sensitive force machine, able to measure forces as small as 10 to 20 pN. An AFM is therefore able to record force distance curves, which give measures and properties of the living material (this is sketched in Fig. 1). Nanomechanical properties and nano-adhesive properties of the samples can be measured using the AFM as a force machine. To make a link between the adhesive properties and a cell function it is possible to functionalize the AFM tip with a living cell. The results of such experiments create new paradigms in life science, and the interpretations in term of structure–function relationships are promising for pharmacologists. More and more articles are indeed dealing with the study of the effects of drugs on cells, studied by AFM.

The aim of our review is to give an overview of the AFM applications in biology (fungal cells, prokaryotic cells, mammal cells), with a special focus on the relevance in pharmacology. The first part is dedicated to fungal cells especially *Saccharomyces cerevisiae*, *Candida albicans* and *Aspergillus fumigatus*. The second part treats of bacteria. It gives an insight on the fundamental knowledge that AFM has provided on bacteria and then emphasizes on studies dedicated to the study of antimicrobial (antibiotics, antimicrobial peptides, innovative molecules) effects. Finally, the third part addresses mammal cells, exposed to external stress, like drugs, but also diseases and cancer.

2. AFM for fungal cell wall analysis, from fundamental knowledge to pharmacology

Atomic Force Microscopy is a polyvalent tool that allows biological and mechanical studies of entire living microorganisms, and therefore the comprehension of molecular mechanisms. This first section introduces the AFM modes, with yeast cells as a eukaryotic model to illustrate its potentialities, and their implications in pharmacology. We will first explore morphological and mechanical studies on various yeast cells. Then, we will present molecular mapping principle on cell-wall surface and the applications of this technique for biology. Finally, we will investigate the yeast pathogenicity in cellular invasion and we will give an overview of AFM pharmacology's studies on yeast.

2.1. Morphological and mechanical studies

Since its first development in 1986 by Binnig et al. [10], there have been an increasing number of AFM biological applications (Fig. 1). An

important part of publications corresponds to studies of cellular inner components and their mechanism of action. For example, different studies were dedicated to the visualization of nucleic acids like RNA or DNA with AFM [11,12] or protein oligomerization [13], but also biomolecular interactions such as Protein–DNA [14–16]. However, a major progress since 1995, made in AFM for biology offered the possibility to observe cells in liquid environment [17]. This first part will describe the AFM potentialities for high resolution imaging and probing the global nanomechanical properties of living cells.

2.1.1. Imaging fungal cells

As stated in the introduction, a main challenge is the gentle but firm immobilization of the biological sample required for any AFM experiment. Yeasts are round shaped cells of around 5 μm in diameter. The immobilization conditions have to maintain the yeasts in static position during AFM experiment. A solution described in the literature is to immobilize by drying the yeasts (Fig. 2A–B) [18,19]. This process causes cell death and the morphological properties of dead cells are different from living yeasts. To keep cells alive, AFM in liquid condition is required. And to this end, a rigorous, but non-denaturant immobilization method has to be used. A first AFM study in liquid condition was described by Gad and Ikai in 1995 [17]. The authors developed an immobilization method in agar surface to visualize living cells in native conditions; they observed bud scars for the first time by AFM. This example demonstrates the possibility to image living yeast, and thus structures at their surface that are directly linked to yeast-growth. More recently, porous membranes have been used to immobilize cells in liquid condition [20]. As shown in Fig. 2C, this method allows observation of bud scars on individual cells. In another study, the authors used this method to evaluate, at the nanoscale, the consequences of a defective cell wall in mutants yeasts, on the cell surface topography [21]. Finally, immobilization in PDMS stamps was developed. This method allows the immobilization of cells–yeasts (Fig. 2E) but also spores of *Aspergillus fumigatus* [22]. The mains advantages of this method are i) the transparency of the PDMS stamp which is therefore compatible with an inverted optical microscope, ii) the directed assembly of the cells, which result in predicted patterns of cells (no time is wasted to search for a cell), iii) the high number of cells trapped in the PDMS holes. The results presented in Fig. 2D shows the ultrastructure of the surface of spores of *A. fumigatus*; similar results were obtained with spores trapped in porous membranes [23]. Briefly, the spore is covered by a rodlet layer made of hydrophobins. These proteins self-organize at the spore surface, each rod being separated from its neighbor by 10 nm. During the spore germination, this nanostructure is disrupted.

Once immobilized, AFM experiments on yeasts can be conducted in different modes. The contact mode is an imaging mode. It consists in bringing a tip into contact with the surface, and scanning horizontally this surface with a constant applied force. An example of yeast imaged in contact mode was described in 1996 by Pereira et al. [24]. In this study, the authors observed different strains of *Saccharomyces cerevisiae*, the baker yeast, and showed that morphological aspects were different among strains. These observations revealed the high potential of contact mode to observe the morphological differences between yeasts strains. Another study performed in contact mode was dedicated to the visualization of different mutant yeasts defective in cell wall components; this study showed the involvement of cell wall architecture in the morphology of yeasts [21]. Finally, Kriznik et al. in 2005 characterized the morphological properties of the pathogen *Candida albicans* in its filamentous form but they used the taping mode [25].

In oscillation mode, stiff cantilevers are oscillated near their resonance frequency during the scan. The changes in the amplitude of oscillation report on the surface topography. Consequently, the lateral forces between the tip and the sample are reduced, which limits damaging of

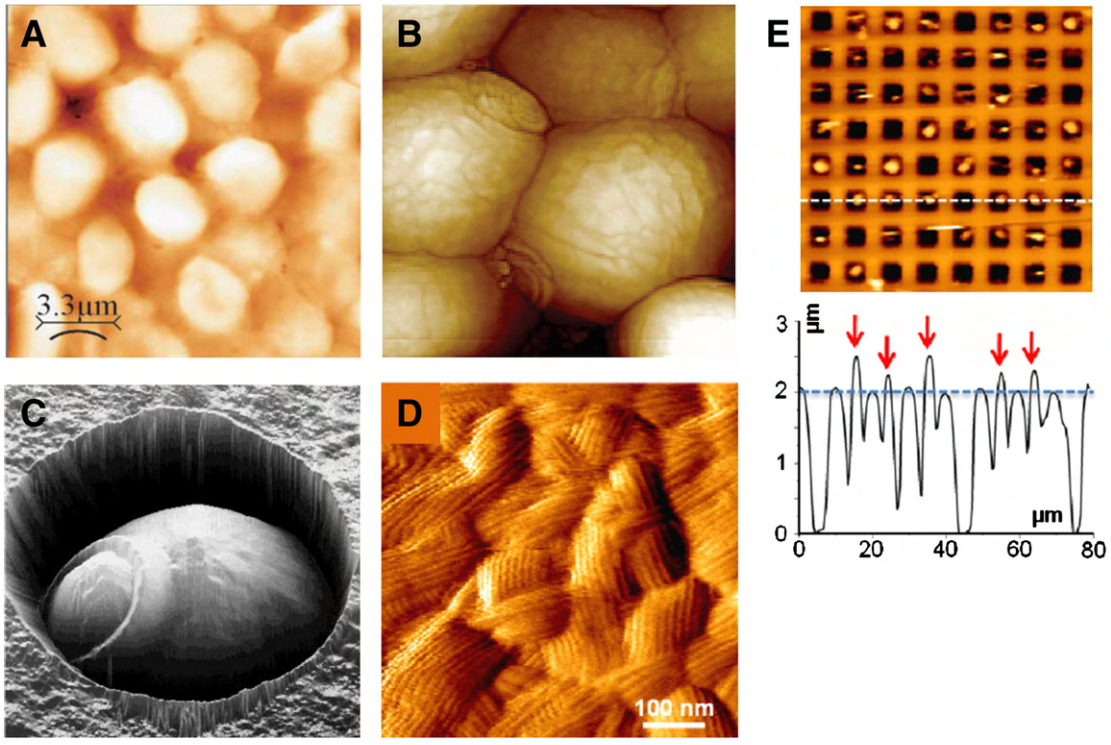

Fig. 2. High resolution imaging for yeast morphology studies. (A) Deflection image of dried *Saccharomyces cerevisiae*. The scale bar is 3.3 μm. (B) Height image of desiccated *S. cerevisiae*. The scan size image is 10 μm × 10 μm and the height scale is 0–4 μm. (C) Three-dimensional AFM height image (6 μm × 6 μm; z-range 1 μm), in aqueous solution, showing a single *S. cerevisiae* cell protruding from a porous membrane. (D) High-resolution AFM deflection image of the *A. fumigatus* spore surface. The scale bar is 100 nm. (E) AFM height images with associated sections of single *S. cerevisiae* yeasts trapped within the patterns of a PDMS stamp functionalized by ConA. Reprinted with permission from references [18–20] and [22] respectively.

the sample [26]. Several examples of oscillation mode images of yeasts can be found in the literature, to demonstrate morphological changes in cell-wall of *S. cerevisiae* according to various stresses [27] or to visualize rodlet structures on spores of *Aspergillus nidulans* [28].

2.1.2. Nanomechanical properties of yeast

In order to probe the nanomechanical properties of yeasts, such as spring constant, elasticity or turgor pressure, AFM is used in the force spectroscopy mode. In this mode the tip is continuously approached and retracted from the surface and force *versus* distance curves are recorded with spatial resolution. The approach curve describes the sample resistance to the applied force [29] and can be analyzed through theoretical physical models, giving access to mechanical parameters (Fig. 3A) [30]. When the tip is retracted from the sample, adhesion forces between the sample and the tip can be recorded, resulting in the measure of adhesion interactions. This will be described in the molecular mapping part.

To begin with, the spring constant of the sample can be deduced from an approach curve. To this end, the approach curve is fitted with the Hook model [31]. This spring constant describes the stiffness of the sample in N/m. Karreman et al., have for example measured the spring constant of yeasts grown with 0.8 M mannitol [32]. This induces an 8 time increase of the spring constant. The same behavior has been reported for yeast mutated for the gene HSP12. The defective cells also presented a high spring constant which has demonstrated the plasticizer role of the protein Hsp12.

However, the first nanometers of indentation, recorded on biological samples, are usually well fitted by the Hertz law [33]. By analyzing the data with this law, one can extract the Young Modulus value of the sample, meaning its elasticity in Pascal. The elasticity can reflect a cell state due to growth, environmental conditions or specific phenotype. Among others, it has been used to estimate the implication of certain genes in the yeast cell wall elasticity with different defective mutants [21,32], and to evaluate the influence of some molecules such as polyelectrolyte [34] or lithium [35] on the cell wall stiffness. However, it is to be noticed that living organism creates heterogeneous results. Indeed, differences can be observed on yeasts of the same strain in the same conditions (Fig. 3B) [22]. The important variations in YM reported on these five yeasts demonstrate a significant heterogeneity of cells coming from the same culture. Furthermore, YM values on the same cell are also heterogeneous, for example, the stiffness on a bud scar of *S. cerevisiae* is superior to the stiffness on another part of the cell wall, presumably due to an accumulation of chitin on the bud scar [36]. Similarly, Touhami et al. showed an increase of the stiffness in the regions of the yeast cell wall involved in the budding process [20]. Thus, one must be aware that repeatability is the key point to obtain values representing the whole sample elasticity. However, the resolution given by AFM allows measuring specific regions of interest and thus gives access to mechanical description of the surface of the cell.

Moreover, other mechanical properties than cell wall changes during growth-process can be described. An original work by Pelling et al. showed the change in the nanomechanical parameter of the cell-wall during motion of *S. cerevisiae* [29]. For this, the tip was put into contact with the cell wall and the cantilever oscillations were measured, translating cell-wall changes during motion. The authors were able to prove that a shift of temperature from 30 °C to 26 °C decreased the frequency of oscillation motion of cell-wall with similar amplitude. Furthermore, exposure of the cells to a metabolic inhibitor (sodium azide) caused the periodic motion to cease.

Altogether, nanomechanical measurements give new insights in the yeast cell wall organization and function.

2.1.3. Molecular mapping

Specific molecular interactions are the base of many biochemical processes. Recognition mechanisms involve several types of non-covalent bonds such as hydrogen bonds, Van der Waals forces, attractive/repulsive electrostatic and hydrophobic forces. The highly specific interactions between a ligand and its receptor for example, can be recorded by force spectroscopy during the retraction of the tip from the sample. To avoid the detection of non-specific events, the AFM tip can be functionalized with one of the actors of the interaction. These experiments, with functionalized AFM tips, are called Single Molecule Force Spectroscopy experiments, since they allow measuring specific interaction forces between only one molecule on the tip and one molecule at

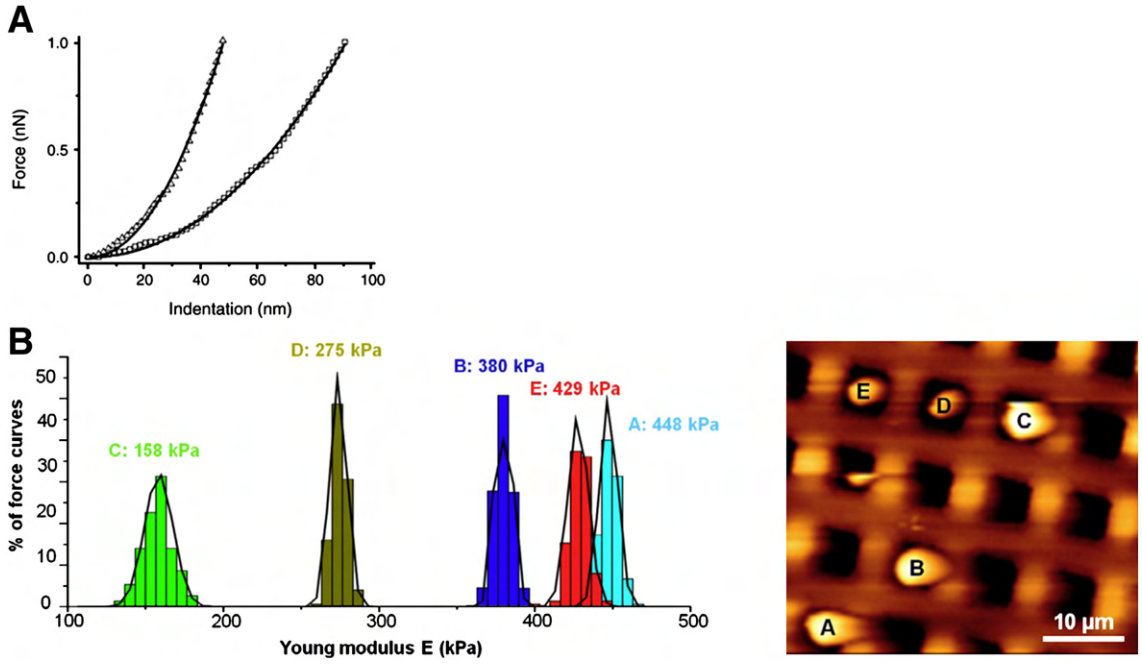

Fig. 3. Nanomechanical properties of living *S. cerevisiae* yeasts. (A) Force-indentation curves fitted by Hertzien model to extract a local Young modulus. The bud scar (triangles) has a modulus of 1.21 MPa, and the cell wall (circles) has a Young modulus of 0.54 MPa. (B) Young modulus determination on five *S. cerevisiae* yeasts. The histogram shows the Young modulus of each yeast trapped within the patterns of a PDMS stamp (AFM height image). Reprinted with permission from references [29,30] and [22] respectively.

the surface of the sample. In this part, we will first describe the molecular mapping principle. Then, different applications of molecular mapping on the yeast cell surface will be discussed.

2.1.4. Molecular mapping principle

As mentioned earlier, the tip functionalization is a prerequisite to measure specific interactions. Reviews of functionalization strategies can be found here [37–39]. A schematic representation of a tip functionalized with concanavalin A (protein that interacts with carbohydrates) is illustrated in Fig. 4A [40]. Adhesion forces were calculated from AFM retract force curves; an example of a retract force curve recorded during a single molecule force spectroscopy experiment is shown in Fig. 4B. The adhesion force was determined by measuring the piezo-retraction required to break the interaction between the lectin concanavalin A and the recognized carbohydrate. This process can be repeated several times, which enables, by moving the cantilever between each measurement, to obtain a map of the interactions. This indicates where the interaction is occurring, and thus how the probed molecule is distributed on the cell surface. In Fig. 4C, an adhesion map recorded with an AFM tip functionalized by concanavalin A, was obtained on a small region of a native yeast cell as indicated on the height image. Each pixel on the adhesion map represents a different force curve; the adhesion map gives therefore a global repartition of carbohydrates on the yeast-cell surface. The authors could conclude from these experiments that mannans were not uniformly distributed on the studied areas of the yeast cell wall [40].

2.1.5. Mapping and nanomechanical properties at the single molecule level

A recent example of molecular mapping study is the localization of Als3p on the yeast cell wall. Als3p is a protein (adhesin) involved in adhesion during host invasion. It was observed during the morphogenesis of *C. albicans* from yeast to hyphae [41]. This was performed with a tip functionalized by an antibody anti-Als3 (Fig. 5A). In the yeast form, adhesion maps show low rates of Als3 (Fig. 5B). However, during the hyphae transition, the Als3 rate is increased on the germinating yeast (Fig. 5C), and more specifically on the germ tube (Fig. 5D).

These changes were accompanied by a major increase of the hydrophobicity of the cell surface and confirmed the relationship between high adhesions in hyphae form and the pathogenicity of this form. In another study, the clustering of Wsc1, a transmembrane protein involved in stress response *via* the cell wall integrity pathway [42], was investigated on *S. cerevisiae* [43]. Molecular mapping was indirectly performed between Wsc1 modified by a Histidine tag, expressed by the yeast, and a tip functionalized by Ni^{2+}-nitriloacetate (NTA) groups. The authors proved that the clustering of Wsc1 was induced by stressing conditions, which suggested that this process was intimately connected to Cell Wall Integrity signaling pathway. This work confirmed that AFM was then a useful tool to understand molecular phenomena happening at the cell surface of yeast. Using the same methodology, another work demonstrated that cell wall thickness could be determined. To this end, different yeast mutants were generated, presenting increasing length of the Serine Threonine Rich (STR) region of the Wsc1 protein. This protein is anchored in the plasma membrane and is not detectable at the cell wall surface if the STR region is too short. The cell wall thickness was

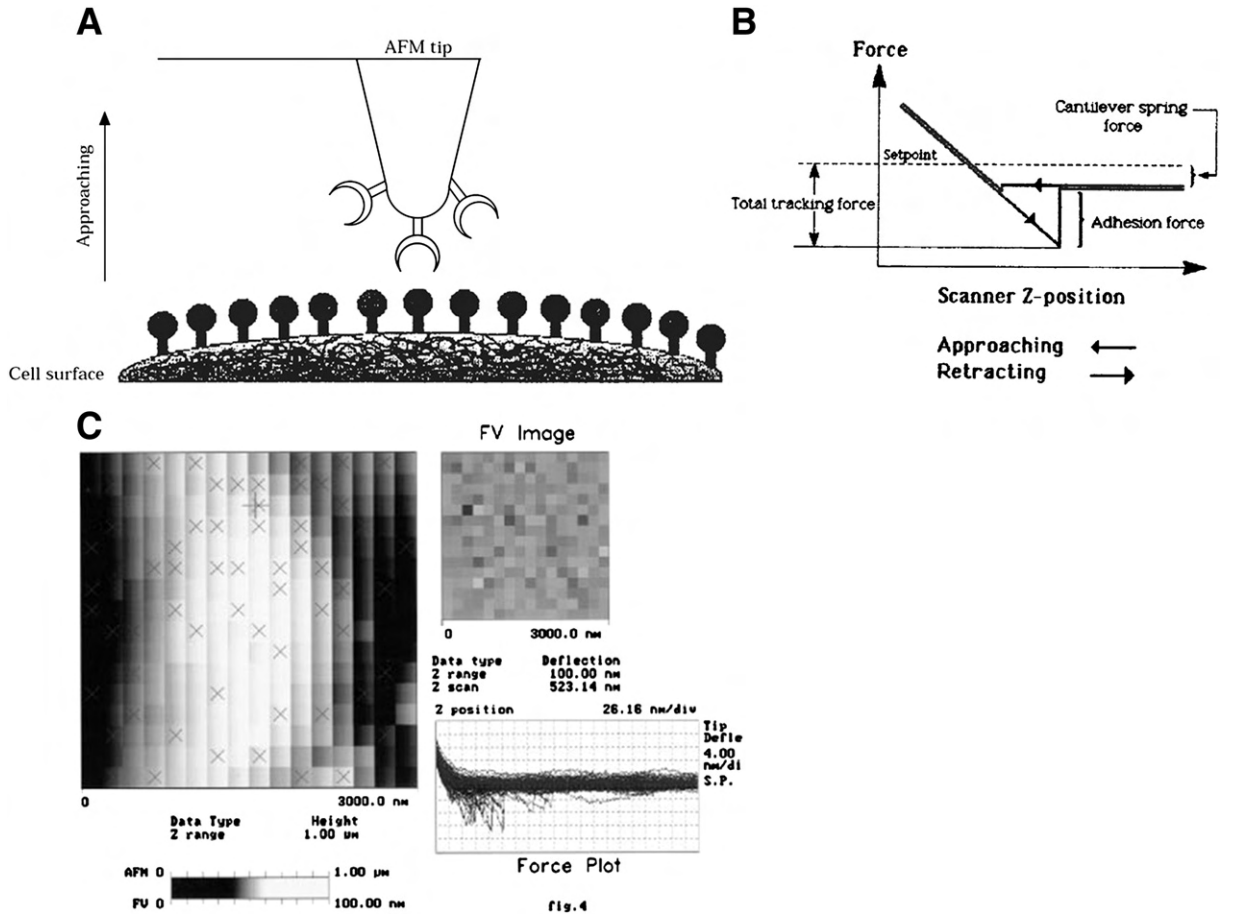

Fig. 4. Molecular mapping principle. (A) Model of experimental set-up configuration of molecular mapping by AFM. (B) Theoretical AFM force curve with adhesion force measurement during piezo retraction. (C) Typical force volume data frame showing different types of data that can be collected at the same time with this mode. Upper left is a height image, upper right is a force volume image, and lower right is a force curve display window. Reprinted with permission from Gad et al. [40].

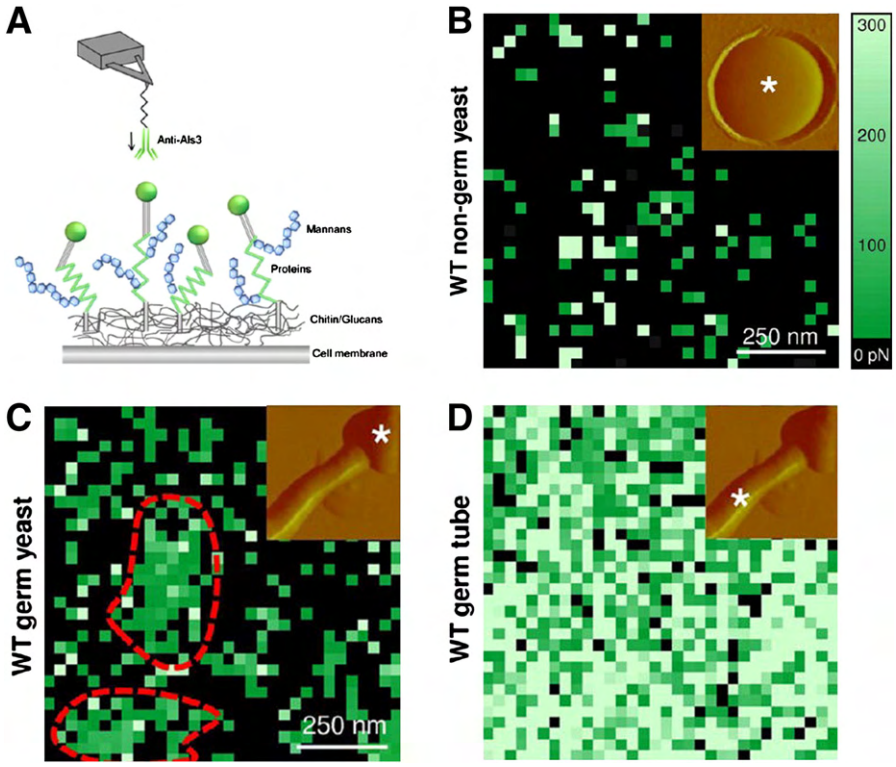

Fig. 5. Single molecular mapping according to *Candida albicans* morphology. (A) Schematic representation of interactions between Als adhesins (green) and anti-Als3 antibody immobilized on AFM tip. (B) Typical adhesion force map (1 μm × 1 μm, color scale: 300 pN) to probe Als3 proteins on yeast-form cell. Adhesion force maps for Als3 mapping on germinating yeast (C) and a germ tube (D). Reprinted with permission from Beaussart et al. [41].

thus deduced from the STR region length leading to the detection of Wsc1 at the cell wall surface [44]. AFM force spectroscopy measurements can also cause molecular re-organization at the surface of yeasts. For example, Alsteens et al. [45] demonstrated that the formation and propagation of the adhesin Als5 nanodomains in *C .albicans* was the consequence of localized delivery of piconewton force by the AFM tip functionalized with antibodies recognizing Als5. The same process was observed on dead cells, confirming that the process was not metabolic and indeed triggered by the AFM tip. The authors suggested that the functionalized tip could stretch, unfold Als5 and promote the aggregation and self-association of Als5. This process could be involved in cellular adhesion, in response to mechanical stimuli. In another study, with a tip functionalized with concanavalin A, difference in mannoproteins elongation was investigated between the cell wall surface of *S. cerevisiae* and *S. carlsbergensis* [36]. These experiments showed that only mannan chains were stretched from the surface of *S. carlsbergensis* whereas the entire mannoproteins were stretched from *S. cerevisiae*.

2.2. Yeast pathogenicity and pharmacologic studies by AFM

The number of fungal and yeast species on earth is around 611 000 [46]. Among them, only 600 species are human pathogens [47], like *A. fumigatus*, *Cryptococcus neoformans*, *Histoplasma capsulatum* or *C. albicans*. The last is one of the most common cause of hospital-acquired systemic infections, due to its adhesive and invasive properties, and its capability to form biofilms [48]. In order to fight against this pathogen, AFM has been used to study its virulence mechanisms, and to understand the effects induced by antifungal treatments on its cell wall [49,50]. This part will first focus on host–pathogen interactions involving *C. albicans*, studied by AFM. We will then describe the most recent studies on the effects of antifungal drugs on the cell wall of yeast.

2.2.1. Understanding yeast interactive behavior

For pathogens, adhesive properties are fundamental for host-invasion or biofilm formation. A first study by Götzinger et al. quantified the yeast *S. cerevisiae* adhesion to surface of silica particles by AFM [51]. The yeasts were immobilized on an AFM tip functionalized with concanavalin A, which interacts with the carbohydrates present at the surface of yeasts. Authors proved that adhesion of yeast to silica particles was very variable according to the pH solution and the roughness of silica particles.

More recently, interactions between *S. aureus* and *C. albicans* were investigated by AFM [52,53]. These pathogens are classically found in combination during human tissue infection. To understand their relationship during infection, the authors quantified the interactions between *S. aureus* immobilized on an AFM tip, and different regions of *C. albicans*, in yeast and hyphae form including three parts, the head, the middle and the tip (Fig. 6A). Adhesion forces were quantified during piezo retraction at the initial contact (0 s) or after 60 s of bond-maturation. The results in Fig. 6B demonstrate that *S. aureus* interacted preferentially on the hyphae form (tip and middle) and hardly on the head part or on the yeast form. Furthermore, the authors made the hypothesis that the 60 s of contact were required for adhesion because an active reorganization of the hyphae cell wall was used by the yeast to promote the adhesion of *S. aureus*. These observations confirmed that during infection *S. aureus* was interacting only with the hyphae form *of C. albicans*.

A direct AFM observation of the interaction between *C. albicans* and macrophages was presented by El Kirat et al. [54]. This study showed by differential interference contrast (DIC), fluorescence and AFM, the main steps of macrophage infection by *C. albicans*, including initial intercellular contact, internalization of yeast cells, intracellular hyphal growth and pathogen externalization from the macrophage. An example is given in Fig. 6C, where we can see yeast internalization into the macrophage. The ability to directly visualize these biological processes

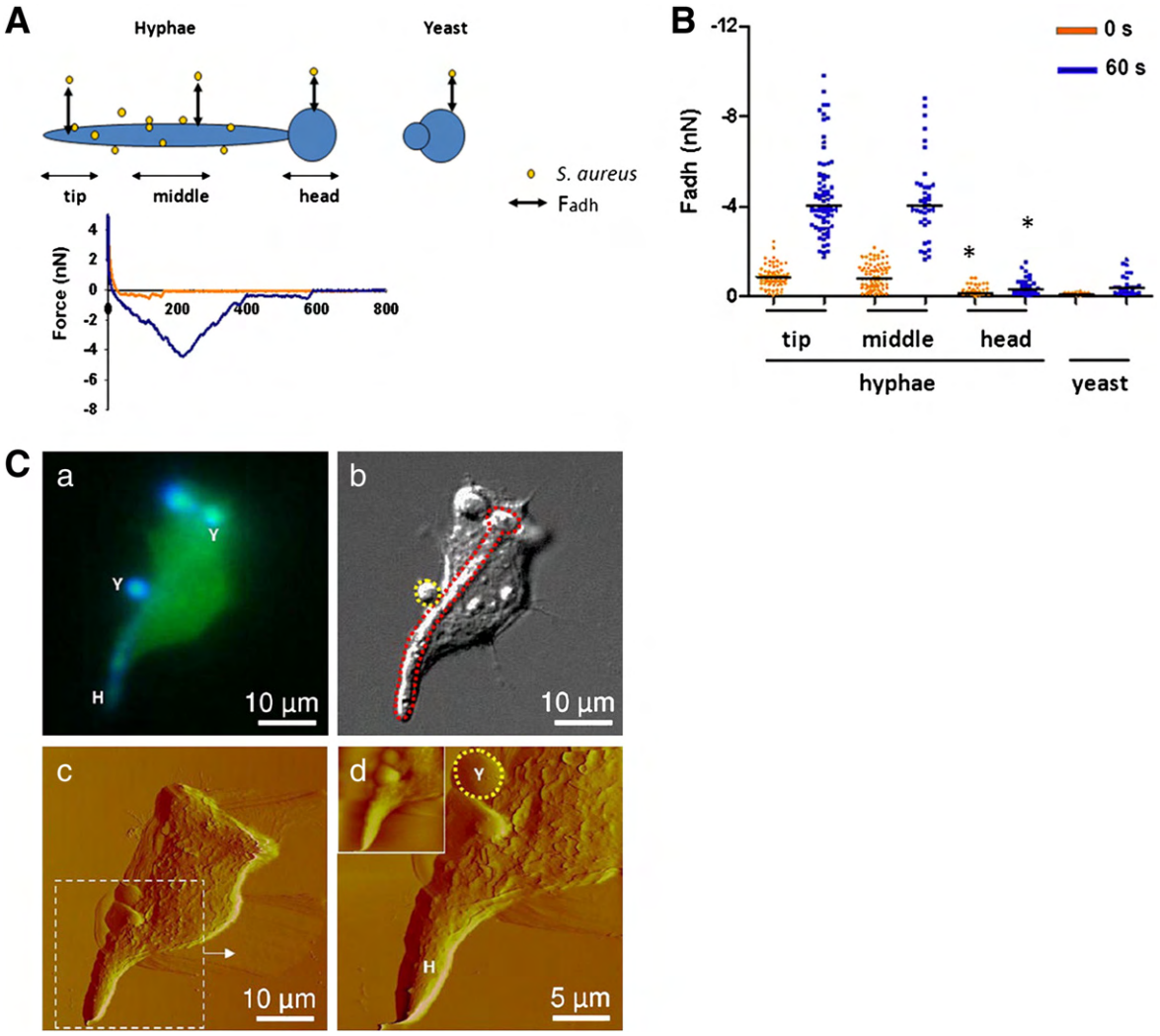

Fig. 6. Yeast–cells interactions. (A) At the top, schematic representation of the different hyphal regions defined for adhesion between *Staphylococcus aureus* and *Candida albicans hyphae*. At the bottom, example of force distance curves between *S. aureus* upon initial contact (orange curve) and after 60 s bond-maturation (blue curve) with *C. albicans* hyphal tip region. (B) Vertical scatter bars adhesion forces between *S. aureus* and different *C. albicans* morphologies. (C) Imaging of a single macrophage infected by *C. albicans* visualized by fluorescence (a), DIC (b) and AFM deflection images (c,d). Labels Y and H correspond to yeast and hyphal cells. The red and yellow dashed lines in (b) indicate an internalized hyphal cell and a free yeast cell, respectively. Reprinted with permission from references [52] and [54] respectively.

demonstrates how AFM can be used to understand infection mechanisms and help in anti-fungal investigation.

2.2.2. Pharmacology studies

AFM is also a promising tool to characterize the antifungal molecules effects on the morphology and the nanomechanical properties of the yeast cell wall. However, AFM pharmacology studies concerning yeast are very limited and only few studies were performed so far. For example, the ultrastructure alteration of the cell wall of *S. cerevisiae* by the tetrapisispora phaffii killer toxin (Kpkt) was characterized by AFM [55]. The authors demonstrated that Kpkt caused an alteration of the cell wall with a specific β-glucanase activity. In another study, AFM was used to evaluate the cell wall roughness of *C. albicans* after lemon grass oil (LGO) treatment in vapor phase [56]. The authors observed a decrease in the roughness of the cell wall. AFM was also used in another study to describe the biophysical properties associated with cell death

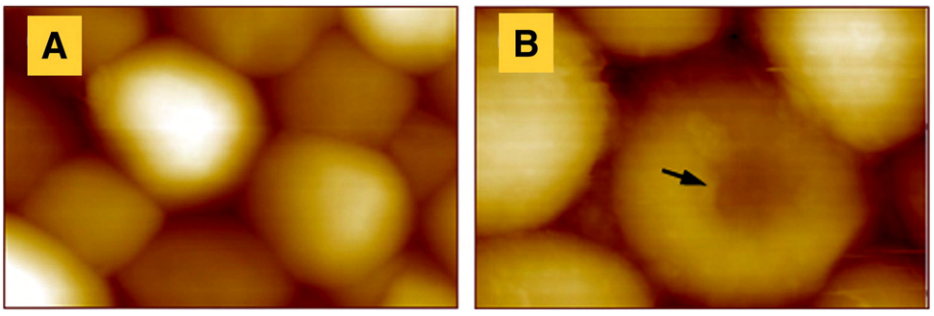

Fig. 7. Anti-fungal effect of allincin. AFM images of dried *C. albicans* untreated (A) or treated (B) during 24 h with allicin and amphotericin B. The arrow indicates a significant morphological change. Reprinted with permission from Kim et al. [50].

due to flucytosine (an analog of fluorinated pyrimidine, which mainly acts on RNA and DNA) and amphotericin B (acts on cell walls by an unknown mechanism). After drug treatment, the cell wall of *C. albicans* was perforated, deformed, and shrunken [49]. However, in contrary with LGO, the roughness of the cell wall was increased. In addition, a combination between drug treatment, such as allicin (organic compound harmful in yeast cell growth) and amphotericin B decreased the yeast viability and induced significant cell wall damages (burst or collapsed membranes) as shown in Fig. 7 [50].

These examples show how antifungal drugs induce cellular damages and death of pathogenic yeasts. Furthermore, they confirmed the potentiality of AFM for pharmacological studies. In addition, the AFM development during the last decades with others biological systems, such as bacterial and mammals cells, opens the way in pharmacology for microbiology and cancerology.

3. Atomic Force Microscopy in bacteriology

Atomic Force Microscopy has proven itself to be a powerful tool for the study of microbial systems. In this section, we will explore the applications of AFM to the bacterial field. In one hand, we will give an update of the studies dedicated to the morphology and behavior of bacteria alone, or interacting with their environment. Then, in another hand, we will focus on pharmacological studies that have been performed on bacteria, with antibiotics and antimicrobial peptides, as well as with innovative molecules.

3.1. Fundamental bacteriology

Bacteria are ubiquitous on earth, and have negative side effects in many fields such as food industry or human health. They can also be used to our benefit such as in waste water treatment plans or pharmacy (production of recombinant drugs). Bacteria interact with their environment through their surface and a lot of researches are therefore focused on the microorganism's surface. In this context, Atomic Force Microscopy has become more important, and an increasing number of researchers have exploited both imaging and force measurements capabilities to explore bacterial surface in terms of structure and function.

3.1.1. Imaging bacterial morphology

One of the most common applications of AFM in microbiology is to visualize the morphology of microorganisms. AFM provides the opportunity to image single bacterial cells; it can also be used to image several cells, as it is the case in biofilms for example, where aggregates of microorganisms adhere to each other on a surface [57]. Many bacteria are characterized by their shapes (coccus, bacilli or spores) and by their nanoscale ultrastrucutres, for example S-layers, capsular polysaccharides, flagella or fimbria. Fimbriae, also known as pili, are thin, hairlike appendages on the surface of gram-negative and gram-positive bacteria, that perform a variety of different functions such as genetic transfer *via* conjugation, movement across surfaces, and adherence to a variety of surfaces [58]. Scanning Electron Microscopy (SEM) has long been the only tool available for the direct observation of bacterial pili; however, this technique does not allow any quantitative analysis. With the recent progress made in biological application, it is then naturally that researchers interested in bacterial pili turned to AFM, such as for example Schäffer's team that investigated the geometric and elastic properties of the pili of different *Corynebacterium diphtheriae* strains, the etiological agent of diphtheria [59]. Their measurements showed that among mean-visible contour-length of the pili, there were significant strain-specific differences that could not be correlated to the efficiency of adhesion to substrates. In another study by Touhami et al., [58], the morphology of *Pseudomonas aeruginosa* pili were investigated using AFM, and the authors also studied the ability of pili to adhere to mica surfaces, highlighting the role of pili in bacterial adhesion. Finally in another study, Dufrêne's team successfully visualized self-assembled nanostructures that are formed by the pili of *Lactobacillus rhamnosus* GG [60].

Flagella differ from pili in their proteic composition. The bacterium flagella is a sophisticated molecular nanomachine composed of three substructures that provide motility, anchor the structure into the cell membrane, and a last one that acts as the rotary motor [61]. Flagella contribute to the virulence of pathogenic bacteria, and AFM imaging is a powerful tool to analyze the morphology of the flagellum. Different studies report on the morphology at high resolution of flagella; Gillis et al. have studied the expression of flagella in relation to its function, and showed that for different strains of *Bacillus thuringiensis* exhibiting different levels of flagellation, the amount of flagella observed at the nanoscale could be correlated with the motility behavior of the strains [62]. In another study conducted by Diaz et al., the authors used AFM imaging to determine if the growth of flagella was oriented during the early stages of biofilms formation [63]. The authors showed that it is indeed the case; the flagella are first oriented towards the neighboring cells, making contact and finally surrounding them. Chang et al. were more interested in the morphological modifications induced by pH on the flagella of *Escherichia coli*; they showed that both acidification and alkalization of the culture media was affecting the morphology of the flagella, by reducing theirs diameters [64].

Another nanoscopic ultrastructure that characterizes bacteria is the capsule, made of polysaccharides. Capsular polysaccharide has important functions for bacteria as for example nutrient uptake, protection against environmental stresses, adhesion to different surfaces, or survival against phagocytosis or antibiotics. This structure is therefore a virulence factor of the bacteria able to produce it, and AFM imaging has enable to study the morphology of this capsule and understand its surface characteristics. Among the studies dedicated to the capsule of bacteria [65,66], is the work conducted by Suo et al. in 2007. The authors show that HEPES, a buffer commonly used in biological experiments and presumed to have no effects on specimens, stabilizes the capsule formation of *E. coli* and *Salmonella typhimirium* [67]. An example on *S. typhimirium* is given in Fig. 8A; we can see on this amplitude image an aggregate of cells covered by capsular polysaccharide, after the cells were rinsed in HEPES buffer. Coldren et al. in 2009 worked on *S. aureus* capsule and could understand, using AFM, how the capsular polysaccharide is important for bacterial adhesion to surfaces, and therefore for biofilm formation [68].

Bacteria that do not display capsular polysaccharide can however display bacterial surface layers (S-layers). S-layers are 2D-cristalline arrays of glycoproteins; they represent the most common cell surface structures in bacteria [69]. As for capsular polysaccharide, S-layers are the frontier between the cell and the environment; they therefore play several roles such as protecting the cells from environmental stresses, or for nutrient uptake. Because of the particular self-assembly of S-layers proteins, it has been a good model for AFM imaging at high-resolution. S-layers proteins can either be recrystallized on surfaces such as silicon [70] or gold surface [71], or directly studied *in vivo* as Dupres et al. did [69]. In this study the authors imaged nanoarrays of S-layers on live *Corynebacterium glutamicum* and observed hexagonal unit cells with dimensions similar to those reported on isolated S-layers sheets. Their work also led to the discovering of a new inner layer composed of periodic nanogrooves, which could probably reflect the specificity of the *C. glutamicum* cell wall.

Bacteria can grow in bulk or form biofilms; some bacteria can also form endospores. Endospores are the disseminating agent of bacteria; their formation is triggered by conditions of limited nutrient availability and environmental stress. They are highly resistant to extreme temperatures or chemicals. The transformation of a dormant spore into a vegetative cell is an important step in the pathogenicity of the bacteria, and can be imaged using AFM. A few studies were dedicated to the germination of spores of *Bacillus anthracis* [72], or *Bacillus atrophaeus* [73,74]. One is a technical jewel since it shows the complete high-resolution imaging structural dynamics of single spores

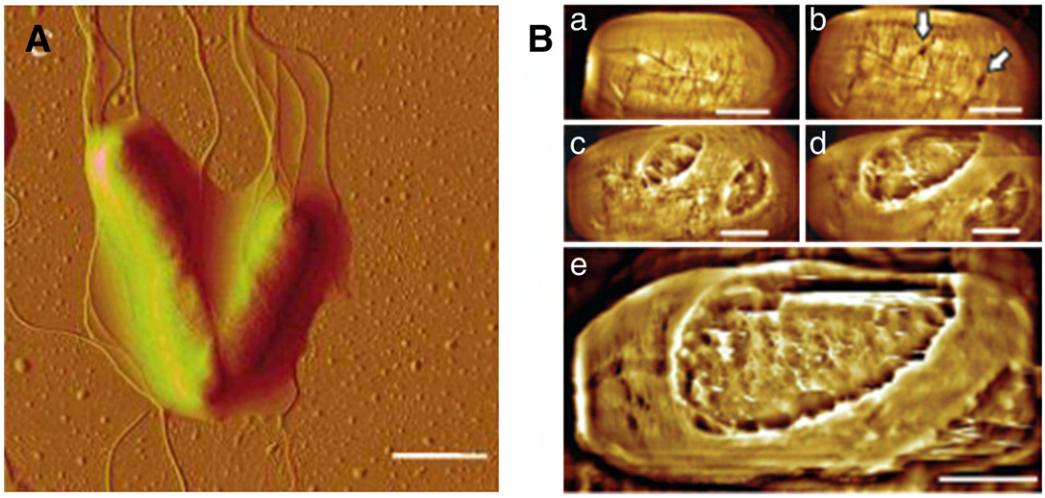

Fig. 8. High resolution imaging bacteria. (A) AFM amplitude image of aggregate of three *Salmonella typhimirium* cells covered by an EPS capsule. Note that part of the EPS is confined by the flagella. Scale bar = 2 μm. (B) Series of AFM height images showing the emergence of vegetative cells of *Bacillus atrophaeus*. The images show 60- to 70-nm-deep apertures in the rodlet layer (indicated with arrows in b), and subsequent eroded the entire spore coat (e). Images in a–e where recorded on the same spore; elapsed germination time (in hr:min) was as follows: (a) 3:40, (b) 5:45, (c) 7:05, (d) 7:30 and (e) 7:45. Scale bar = 500 nm. Reprinted with permission from references [67] and [75] respectively.

of *B. atrophaeus* [75]. In this study, the authors imaged the emergence of vegetative cells (Fig. 8B) trough rodlets apertures at the surface of the spore. These images are not only impressive for the phenomena they show, the also give new insights into the structure of native peptidoglycan; the fibrous network observed on Fig. 8B–C on the germ cell surface seems to represent nascent peptidoglycan architecture of newly formed cell wall. The authors then found a good experimental model for investigating the genesis of the bacterial peptidoglycan structure.

3.1.2. Nanomechanical properties of bacteria

The mechanical properties of bacterial cells, such as elastic moduli, spring constant or turgor pressure, can be investigated by AFM, *via* nanoindentations measurements. We will focus in this paragraph on elastic properties of bacterial cells that are expressed by Young's modulus. Understanding the elasticity of cells is important for elucidating the mechanisms underlying cells growth and behavior in different conditions. It is also known that, in many living organisms, the mechanical properties of the external membrane can indicate the state of the underlying system. In this frame, many studies using nanoindentations were used to study the bacterial cell wall. For example, Francius et al. found that the elastic properties of bacterial cells of *E. coli* were dependent on the expression of surface appendages such as fimbriae, and also on the ionic strength of the medium they are grown in [76]. Schaer-Zamaretti et al., however, could distinguish between different strains of *Lactobacillus* expressing or not S-layers by probing the elastic properties of such cells [77]. Gaboriaud et al. used nanoindentations measurements to understand the influence of a different pH on the nanomechanical properties of bacterial cells [78]. But a major concern in bacteriology is to determine whether a bacterium is dead or alive. That is the question that Cerf et al. answered with the nanoindentations measurements; as it is shown in Fig. 9A, live cells of *E. coli* show a Young modulus of

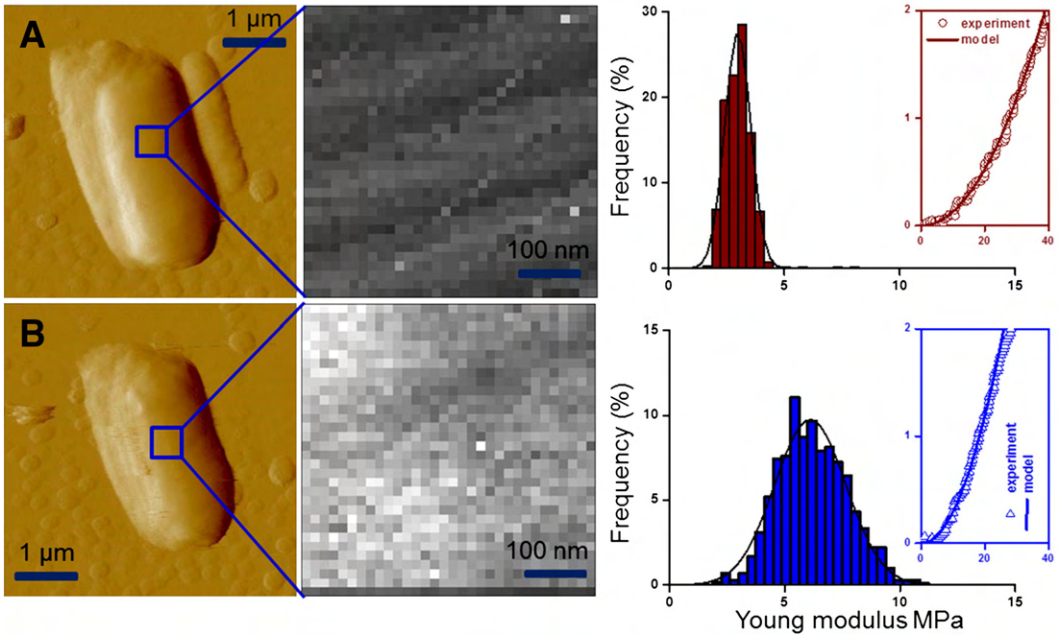

Fig. 9. Nanomechanical properties of bacterial cells. (A) Nanomechanical properties of alive *Escherichia coli* cells. AFM deflection images of single living *E. coli* bacterium and (B) of the same single bacteria killed by thermal treatment (20 min, 45 °C). The elasticity maps (z-range = 10 MPa) correspond to the images insets. The elasticity distribution is represented by the histograms, together with a typical force curve. Reprinted with permission from reference [79].

3.0 MPa, whereas heated (dead) cells (Fig. 9B) have a Young modulus increased to 6.1 MPa [79]. The authors then demonstrated that dead cells with a damaged membrane exhibit higher Young modulus values. A recent novel development in analysis of force curves generated in nanoindentations measurements allow now to extract the elastic modulus at the cell surface, but also in depths under the cell surface [80]. Longo et al. used this new analysis development to probe the nanomechanical properties of *E. coli* cells [81]. In this study, the authors found stiffer areas at the surface of the cells, and when they go deeper into the cells, they find these stiffer areas to have a complex form, that changes during time. This could be correlated to an accumulation of complex molecules underneath the cell membrane and reorganizing in the cell cytoplasm over time.

3.1.3. Probing molecules at the interface of bacteria

Besides imaging and probing nanomechanical properties of bacteria, it is also possible with AFM to study molecules at the surface of bacteria with bare or functionalized AFM tip. Understanding how complex molecules are assembled at the surface of bacteria under physiological conditions is of fundamental importance to elucidate their functions in different processes such as cell aggregation, adhesion to substrate, or interactions with external molecules or organisms. A first example is the interactions between bacteriophages and bacteria. Dubrovin et al. proposed two articles where the authors investigate the interactions between bacterial cells and bacteriophages [82,83]. While the first study focuses on the characterization of phages, and the effects of phages interactions with different strains of bacteria, the second study is dedicated to the investigation of the lytic cycle of the *Acinetobacter baumannii* bacteriophage AP22.

The results presented in Fig. 10A present AFM images of *A. baumannii* cells infected by AP22 bacteriophage over time. After 1 min of interaction between bacteria and phages (Fig. 10Aa), the phages have adsorbed on the surface of the cells; the high resolution image (Fig. 10Ab) clearly shows phage heads. However, after 3 min of incubation (Fig. 10Ac and d) the phages heads are empty, leading to the supposition that DNA release from the head takes place quite fast, and probably immediately upon phages adsorption on the cell's surface. And this phenomenon is even more visible after 6 min of incubation (Fig.10 Ae and f). Also others studies dedicated to bacteria/external molecule interactions were performed [84], and among them is one focusing on the interactions of different strains of *Lactococcus lactis* with mucins [85,86]. In this study, the authors, using cell probes, were able to measure the kinetic association/dissociation constants between the bacteria and the mucins.

The interactions with other microorganisms are mediated *via* surface molecules of bacteria. One of these molecules at the surface of gram-positive bacteria is peptidoglycan, a complex polymer made up of glycan strands of repeating disaccharides residues, cross-linked *via* peptide side chains. This molecule is a vital molecule for bacteria, as it is responsible for shape determination and cellular viability, and since it is a target for a lot of antibacterial treatments, it has been extensively studied. However few AFM studies report on the structure of peptidoglycan [87–89], and among them is the one of Hayhurst et al., [90], in which the authors propose an architectural model for the peptidoglycan of *Bacillus subtilis*. As it is shown in Fig. 10B, the authors claim that glycan strands form a "rope" that is coiled into a helix; this rope runs then all over the bacteria.

For gram-negative bacteria, the molecules that can be found on their surface are polysaccharides and lipopolysaccharides (LPS). Francius et al. in 2008 studied the localization and conformation of single polysaccharides at the surface of live *Lactobacillus rhamnosus* GG using functionalized AFM tips [91]. Using concanavaline A, a lectin that interacts with carbohydrates, he could pull off the surface individual mannose. As we can see on Fig. 10C, on a mutant strain impaired in adherence to epithelium, there is a dramatic decrease in adhesion

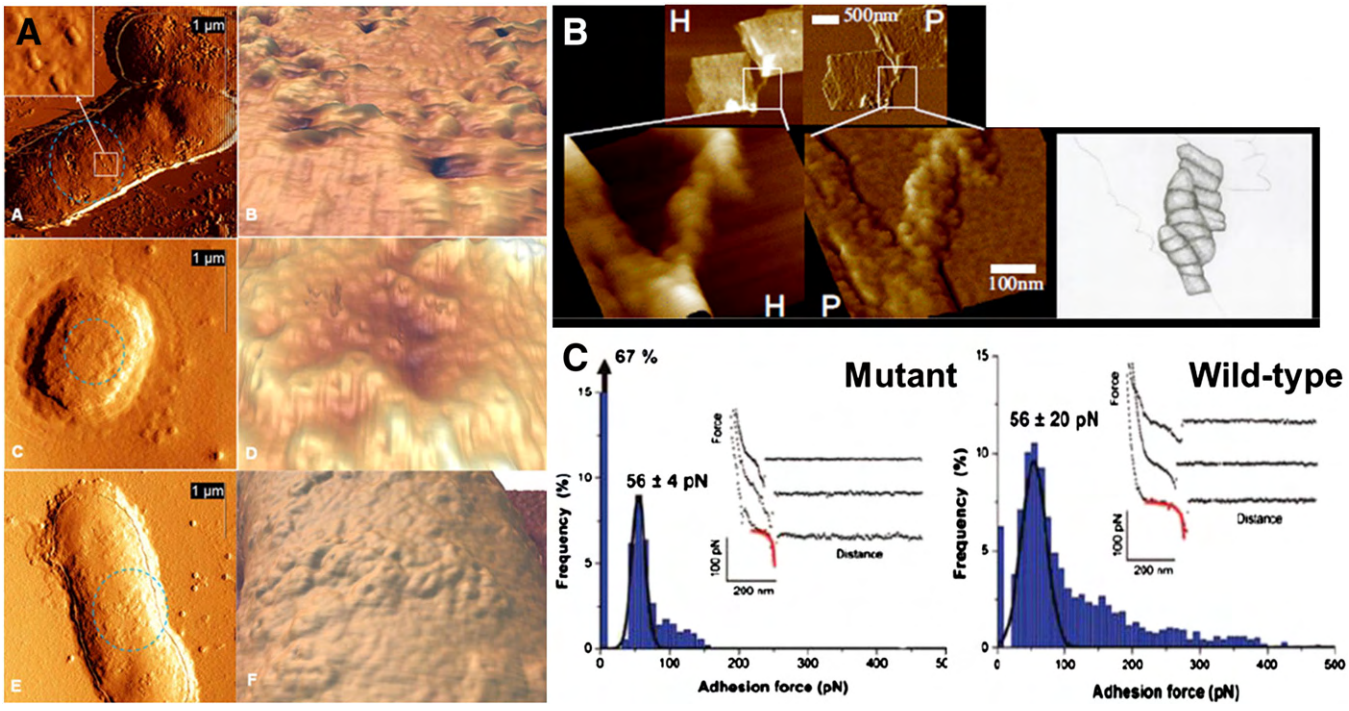

Fig. 10. Mapping and interactions with molecules at the interface. (A) Bacteriophage interactions with *Acinetobacter baumannii*. AFM images of *A. baumannii* cells infected for 1–6 min by the bacteriophage AP22. Left row: deflection AFM images of *A. baumannii* cells incubated with bacteriophages AP22 for 1 (a), 3(c), 6 (e) minutes. Right row: zoomed-in three dimensional reconstructions of bacterial surfaces depicted on the left (the zoomed regions are indicated by dotted circles in the height images). The inset in (a) demonstrates zoomed-in region, shown by the white square. (B) *Bacillus subtilis* sacculi architectural features revealed by AFM. The images show two cylinder fragments, from a purified sacculi from gently broken cells, joined by a twisted cable. H stands for Height image and P for Phase image. (C) Detecting individual mannose-rich polysaccharides on LGG bacteria. Adhesion force histograms are shown, (n = 1024) together with representative force curves recorded in buffered solution with a Con A tip on LGG wild-type and on the mutant CMPG5413 (impaired in adherence to gut epithelium, biofilm formation, and exopolysaccharide production). Reprinted with permission from references [83,90] and [91] respectively.

frequency compared to the native strain. Therefore, this technique of Single-Molecule Force Spectroscopy can be used to understand which molecules interacts with, in this case, the gut epithelium. Another study by Strauss et al., studied the role of LPS O-antigen on the adhesion of *E. coli* cells, using also AFM, with bare AFM tips [92], but there were also works performed on the coat proteins of spores of *Bacillus* [93,94], and on the adhesins at the surface of living mycobacteria [95].

3.2. Evaluating the effects of antibacterials molecules by AFM

Understanding the nanoscale behavior of bacteria under physiological conditions, or their interactions with other organisms in their native state is a first point; we need to know the "enemy" to efficiently fight against them. However, the common way to fight against bacteria is to use antibacterials. Among them, there are the antibiotics, used at home or in hospitals to treat infectious diseases, but there are also other kind of antibacterials, less used or under development, such as antibacterial peptides, and innovative molecules, that should be known about. This section will focus on how AFM techniques (imaging, force spectroscopy, single molecule force spectroscopy) can help understanding the nanoscale effects of antibiotics, or understanding the mechanism of action of new molecules not yet fully characterized.

3.2.1. Nanoscale effects of antibiotics on bacteria

Antibiotics have in most cases a well described mechanism of action on bacteria [96]. However, the effects on bacterial surface at the nanoscale are poorly understood, and for this purpose, the AFM technique is particularly well suited, since it allows imaging and probing nanomechanical properties on single living cells. Among antibiotics investigated by AFM, examples are β-lactams [97,98], aminoglycosides and their derivate molecules [99] and fluoroquinolones [100]. The results presented in Fig. 11A shows morphology modification of *P. aeruginosa* treated by ticarcillin (β-lactams) and tobramycin (aminoglycoside) [97]. As we can see, ticarcillin causes an elongation of the cells, whereas tobramycin alters the surface of the cell. But antibiotics cause also modifications of the cell wall nanomechanical properties, such as elasticity and spring constant. Francius et al. probed on living *S. aureus* cells the effects of lysostaphin, an enzyme that cleaves the peptidoglycan, over time [101]. The authors found that the lysostaphin treatment caused a decrease in the elasticity of the cell wall with the time of treatment, along with a decrease of the spring constant of the cells. These modifications could only be probed with force spectroscopy, and give precious information on the nanomechanical properties modification that antibiotics cause on bacterial cells.

Other authors were interested in vancomycin, a glycopeptide antibiotic, used in last chance in hospitals. This molecule binds with high affinity and specificity to the terminal D-Ala-D-Ala peptidoglycan precursors, leading eventually to cell lysis. In the study of Gilbert et al., AFM tips were functionalized with vancomycin, and used to perform single molecule force spectroscopy experiments on *L. lactis* during the course of division [102]. The results obtained (Fig. 11C) show that the D-Ala-D-Ala residues are located on the division septum of the cell, which suggest that the newly formed peptidoglycan is inserted in this region during the division process. This study demonstrates that AFM with antibiotic-modified AFM tip is a valuable tool to explore the dynamics of antibiotic–ligand interactions; it also gave new insights on the assembly process of peptidoglycan in gram-positive bacteria. Antimycobacterials have also been a subject of interest, and AFM investigations have been performed on *Mycobacterium JLS* [103] and *Mycobacterium bovis* BCG [104].

3.2.2. Antimicrobial peptides

However, bacteria becoming more and more resistant to antibiotics, new approaches have to be developed to find new ways of killing bacteria. Antimicrobial peptides have been developed for several years, but for now, their mechanism of action is not fully understood and need further studies. To this aim AFM can be used to evaluate the effects of such

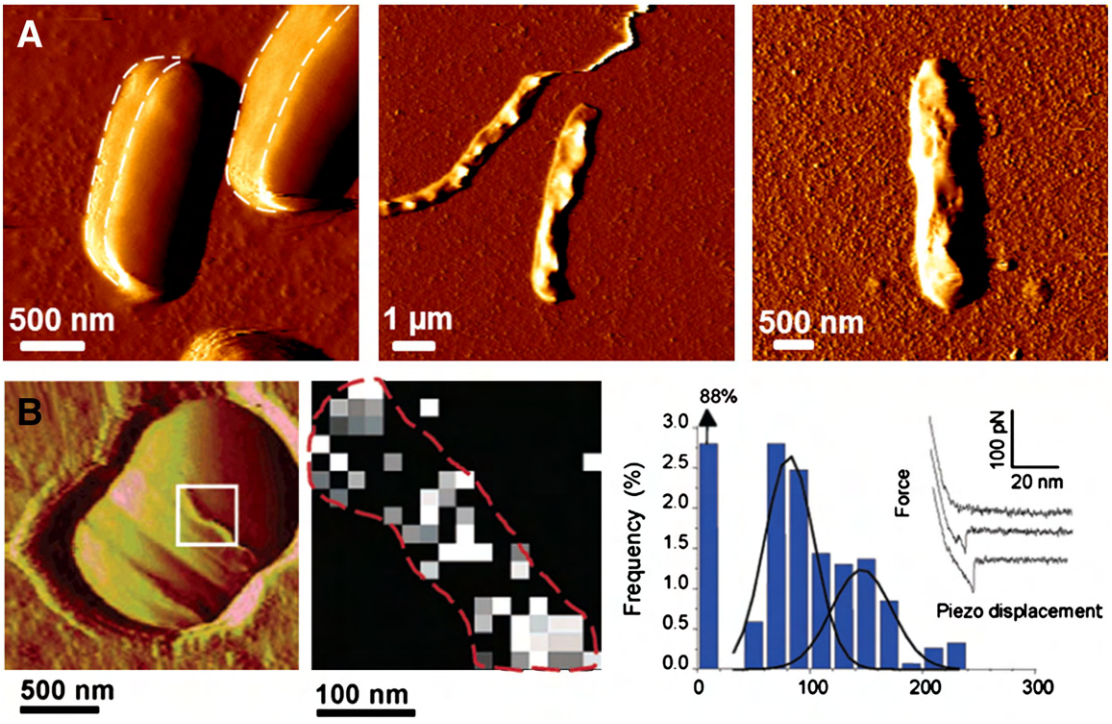

Fig. 11. Effects of antibiotics on bacteria. (A) Effects of ticarcillin and tobramycin on *Pseudomonas aeruginosa*. Vertical deflection images of native live cells of *Pseudomonas aeruginosa* (left image) treated by ticarcillin (middle image) and tobramycin (right image). (B) Imaging individual D-Ala-D-Ala sites on living *Lactococcus lactis*. The AFM image shows a single wild-type *Lactococcus lactis* cell during the course of the division process. The cell is located at the center of the image and trapped into a porous polymer membrane for noninvasive, *in-situ* imaging. The middle image represents the affinity map (gray scale: 100 pN), together with the adhesion force histogram (n = 1536), and representative force curves recorded with a vancomycin tip on the septum region (highlighted by the white box in the AFM image), using constant retraction speed (1000 nm/s) and interaction time (500 ms). Reprinted with permission from references [97] and [102] respectively.

molecules at the nanoscale, helping to the understanding on how these peptides interact with the bacterial cell wall. The most famous of antimicrobial peptide is colistin; this peptide is efficient against gram-negative bacteria, such as *Acinetobacter baumannii*, *P. aeruginosa* or *Klebsiella pneumoniae*, bacterial strains that are the cause of many cases of nosocomial infections. Very few AFM studies were dedicated to the study of the effects of colistin on gram-negative bacteria [105–107]; the main conclusions coming from these reports are that treated bacteria have an increased cell wall elasticity and spring constant, along with a decrease in the adhesive properties of the cells. These conclusions are consistent with the hypothesis that colistin acts as a detergent on the bacterial cell wall and removes the LPS from the surface. In fact, in these studies, results are also presented with colistin-resistant bacteria, that have cell wall structural differences compared to susceptible strains.

Research in the antimicrobial peptide field is actually emerging and many papers treat of the evaluation of the effects of various original peptides with AFM. The peptides studied have diverse origins; for example PGLa peptide comes from frog skin and its secretion and has been showed to remove the outer membrane of *E. coli* while decreasing the surface stiffness [108]. Meincken et al. compared the effects of three different peptides, melittin from the honeybee *Apis mellifera*, magainin and PGLa from frogs skin [109] on *E. coli*. While these peptides are close in terms of amino sequence, the authors could make the difference between the effects caused by each one of them on bacteria, thanks to AFM. Finally Li et al. evaluated the effects of sushi peptides S3 on *E. coli* cells [110]. The results presented in this paper show that after 1 h of treatment, bacteria are severely damaged and large amounts of cytoplasmic fluids are exuded. This indicates drastic permeabilization of the inner membrane, which would be the second step of the S3 mechanism of action. The first one is a damaging of the outer membrane; the second is the initiation of the permeabilization of the outer membrane, and finally the release of the cytoplasmic fluid from the bacteria. Therefore, the authors, thanks to AFM, could get a better understanding of the mechanism of action of a novel and still unknown antimicrobial peptide.

And since antimicrobial peptides are supposed to have a detergent-like action on the membranes of bacteria, many studies focused on characterizing the effects of peptides on phospholipidic layers that mimic these membranes. Roes et al. used reconstituted monolayers of LPS from *Salmonella enterica* to study the effects of polymyxin B; Francius et al. observed the interactions between supported bilayers of DOPC/DPPC and surfactins [111]. As a last example, Arseneault et al. made DPPG mono- and bilayers to understand the interactions with lactoferricin B, an antimicrobial peptide obtained from the pepsin cleavage of lactoferrin [112].

3.2.3. Innovative molecules and nanotechnologies

Whereas antimicrobial peptides have a mechanism of action different from antibiotics, still resistances to colistin, for example, have started to emerge. The research must therefore explore new possibilities for finding new antibacterial molecules that are different from both antibiotics and peptides, in order to avoid development of resistances. A new approach developed is the one of nanoparticles. Metallic nanoparticles are promising antibacterial agents since they are chemically stable, resistant to heat and have a long life. Currently a broad variety of metals and their compounds are used in microbiology research for their potential antimicrobial activity. There are already a few studies reporting on AFM investigations of the effects of nanoparticles on bacteria [113–115], and one of them is dedicated to copper iodide nanoparticles [116]. In this study, the authors have synthesized and evaluated the effects of this novel kind of nanoparticles on different bacterial strains, including multidrug resistant ones. The results of this study show that for *E. coli* (K12) cells treated with the nanoparticles, the membrane is totally disrupted compared to the native cells. In addition, the authors were also able to prove that copper iodide nanoparticles caused the generation of reactive oxygen species, therefore damaging the DNA of the bacterial cells.

Another new approach developed in the recent years is the one of calixarene molecules. An example of such molecule is the paraguanidinoethylcalix [4]arene (Cx1), that has been proven to be efficient on both gram-negative and gram-positive bacteria [117]. However the mechanism of action of this molecule was still unclear, and AFM techniques were used to get a better understanding of this molecule interaction with the cell wall of bacteria [118]. The results presented in Fig. 12A show that on a multidrug resistant strain of *P. aeruginosa*, Cx1 causes a dramatic decrease of the cell wall elasticity, from 517 to 75 kPa. This information shows that Cx1 is efficient on such a bacterial strain, and that its action destabilizes the cell wall of the gram-negative bacteria. To go further into the mechanism of actions, the authors probed the cell wall of treated and untreated bacteria with an AFM tip functionalized with concanavalin A, a lectin that binds to sugars. These single molecule force spectroscopy experiments revealed that the lectin could unfold a molecule only on Cx1 treated cells (Fig. 12B). This molecule could possibly be the peptidoglycan, which would be accessible because of the destabilization of the outer membrane caused by the interaction with Cx1. Research is still going on in this field, and new calixaneric molecules are under development [119–121].

Along with nanoparticles and calixarene, there are also approaches that involves carbon nanotubes which have been proven to be efficient against *E. coli* and *B. subtilis* [122], and chitosans, that were investigated using AFM on *B. cereus*, *E. coli* and *S. aureus* [123,124]. Eventually, emerging area of interest is the use of probiotics to cure infections. As the use of lactobacilli and staphylococci for the treatment of vaginal infection, that has been studied by cell–cell interaction [125] or cell–protein interaction as for lactococcus and mucin in the case of gastrointestinal infection [85,86] and probiotic action [126].

To conclude, we show in this section that Atomic Force Microscopy opens new perspectives for characterizing bacterial species, and understanding the molecular and nanomechanical processes underlying their behavior in physiological conditions. We have also seen that AFM techniques are very useful to study the nanoscale effects of antibiotics that have a known mechanism of action. However, since bacteria are becoming more and more resistant to the antibiotics, new approaches involving innovative molecules are developed and once again, AFM can be used to get a better understanding of the mechanism of action of these new molecules, with the hope that they will be used to treat nosocomial infections caused by multidrug-resistant bacteria.

4. AFM for mammal cells pharmacology's studies

This part focuses on the insights that Atomic Force Microscopy can give in the field of pharmacology for mammal's cells, from the general understanding of therapeutics treatment to special cases of diseases, with a whole part concerning cancer study. Most of the studies in this field are performed on cells lines or patient isolated cells *in vitro*, but recent progress have made possible to study entire biopsies, thus enlarging the use of AFM. It is to be noted that AFM studies of mammal cells are increasingly performed in combination with fluorescence microscopy. Coupling of these two techniques offers a wide range of possibility in studying biological phenomena. We will concentrate mainly on AFM results, but keep in mind that fluorescence microscopy and AFM are complementary in this type of studies.

4.1. General applications

The use of Atomic Force Microscopy for pharmacology's studies on mammalian cells have been led by 2 types of research field: 1) the understanding of cell response to an external stress (infection, injury) characterized by immune and differentiation or gene expression response; 2) the investigation of drug effect on cells, from internalization efficiency to affectation of cellular processes and active effect on pathogens. The following section will be then divided in 2 parts related to these concerns.

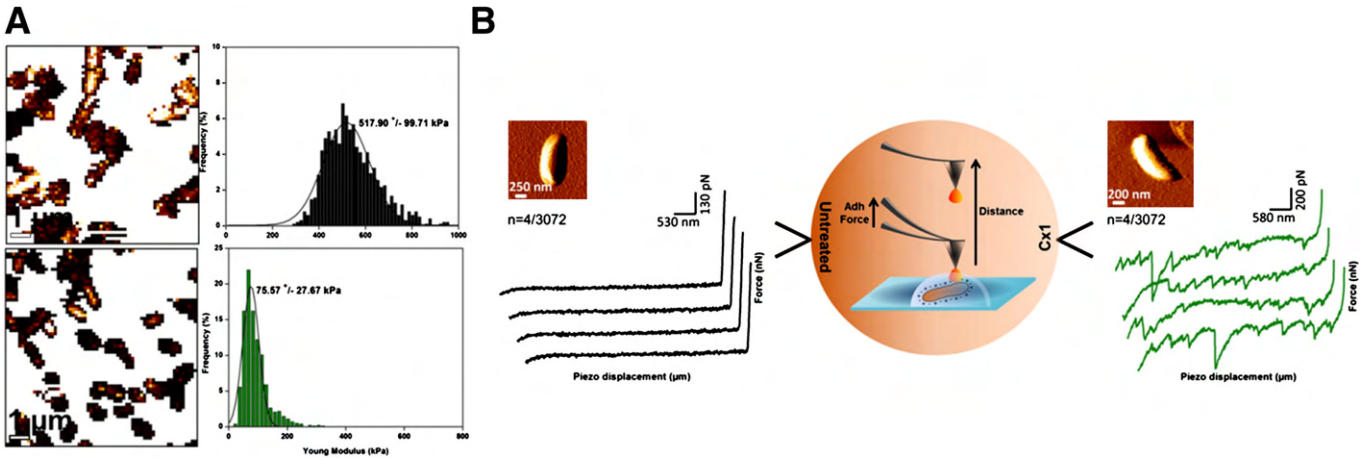

Fig. 12. Effects of innovative antibacterial molecules on bacteria. (A) Antibacterial effects of calixarene Cx1 on the elasticity of *Pseudomonas aeruginosa* multidrug resistant. Elasticity map (z-range = 1.5 MPa) of several cells of untreated *P. aeruginosa*, together with distribution of young modulus values (top images), and of cells treated with Cx1 (bottom images). (B) Effects of Cx1 on the architecture of the cell wall of *Pseudomonas aeruginosa* multidrug resistant. Schematic representation of the force curves (retract segment) obtained with ConcanavalinA functionalized AFM tips on untreated *P. aeruginosa* cells (left curves) and Cx1 treated cells (right curves). The 4 force curves (n) presented by conditions were chosen out of 3072 curves recorded on 3 different bacteria coming from 3 independent cultures. Reprinted with permission from reference [118].

4.1.1. Cell response to external stress

In the complex context of multicellular organisms, the cell response to an external stress is of interest to accurately target the dysfunction in case of disease. For example, the study of keratinocyte reaction to surfactant by AFM can help in the understanding of chemical stresses on the skin, showing that despite a morphological effect, no differences in stiffness are measured at non cytotoxic doses of sodium lauryl sulphate [127]. But AFM can also help in immune response characterization. Immune response is based on first, the detection of pathogen and then, their elimination. On one hand, lymphocytes B are involved in the humoral immune response, and recognize molecular component in extra cellular fluids that directly inform of the pathogen presence in the organism. These cells are responsible for antibody production. Their activation is a complex mechanism that appeared to change

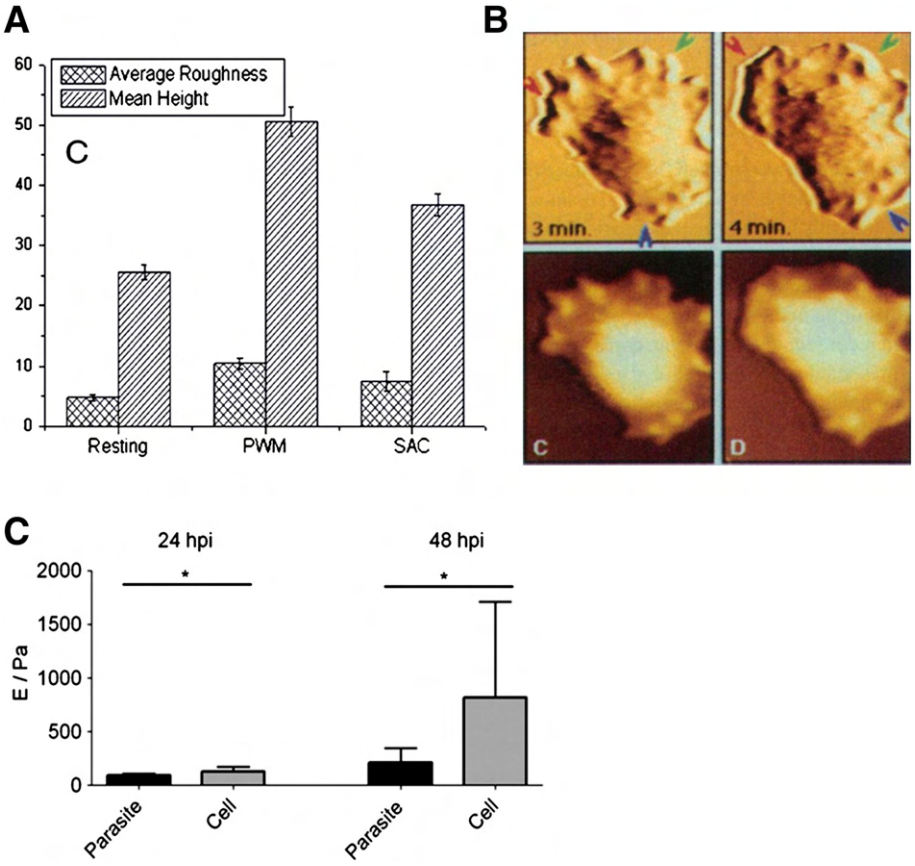

Fig. 13. AFM in pharmacology. (A) The average roughness and mean height particles of surface nanostructure of resting and B lymphocytes after their activation by pokeweed mitogen (PWM) or *Staphylococcus aureus Cowan I* (SAC). Mean ± SD. (B) AFM imaging of platelet activation along time, height image (z-range of 0–1.9 µm) and corrugation images (z-range of 0–280 nm). (C) Increase in stiffness of human hepatoma cells infected by *Plasmodium flaciparum*. ($P < 0.05$). Reprinted with permission from references [132,152,216].

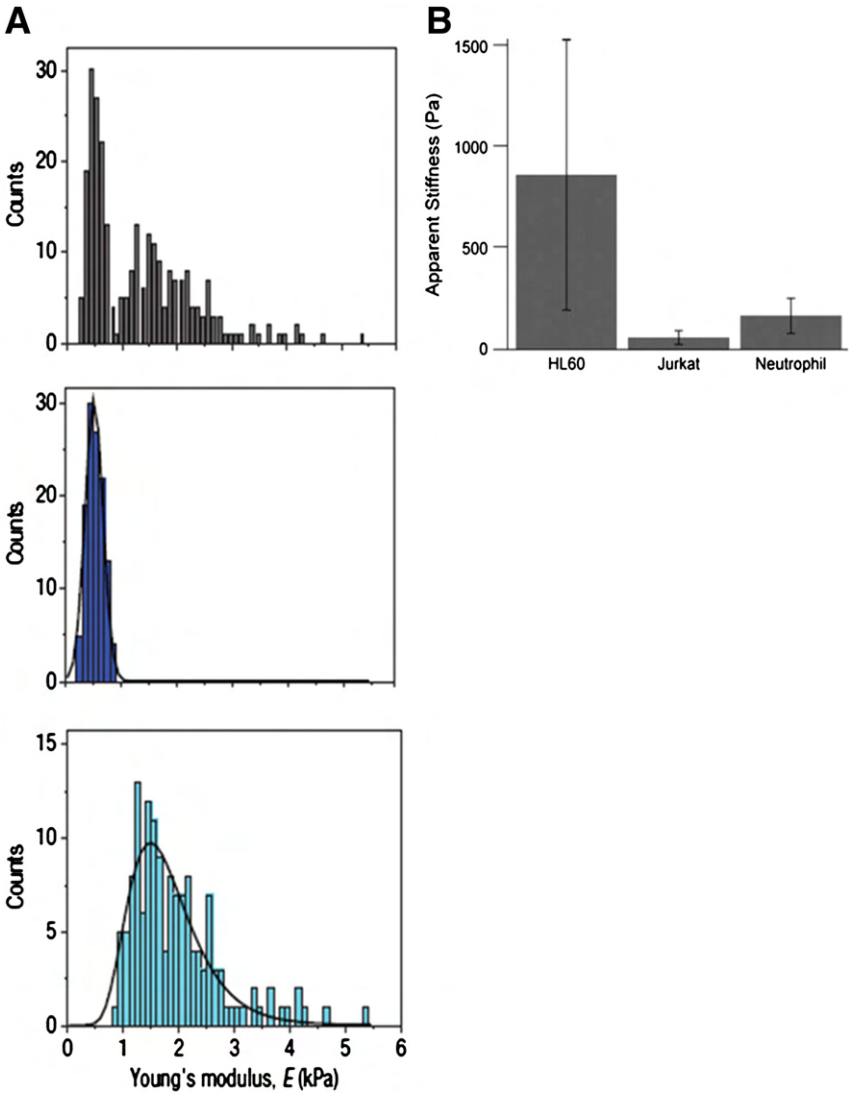

Fig. 14. Cancer cell characteristics. (A) Increase in cell elasticity of leukemic cells (HL60) leading to leukostasis. (B) Elasticity of cancer cells collected from patients with suspected metastatic cancer from seven different clinical samples. Grey: measurement for all cells together. Dark blue: cancer cells. Light blue: normal cells. Reprinted with permission from references [157,158].

their nanomechanics. Wang et al. have shown, using AFM, that activation of B cells by pokeweed mitogen (PWM) or *S. aureus* Cowan I (SAC) induces the clustering of B cell receptors at the cell surface, responsible for cytoplasm biochemical activation cascade and improvement of cell adhesion to antigen. This clustering is visible by topographic analysis such as roughness and particle (cluster) size (Fig. 14-A). Cell adhesion capacities have also been evaluated by force spectroscopy [128]. On the other hand, Lymphocyte T cells are responsible for cell-mediated immune response. To achieve their goals, these cells need to reach the site of infection (inflammation site), and then to cross endothelial barriers, which involves cell–cell adhesion, namely lymphocyte T–vascular endothelial cell adhesion. This crossing implies a change in adhesion protein expression pattern, like integrin and selectin, by endothelial cells. Zhang et al. have investigated the adhesion dynamics of the T-cell–endothelial interaction by force spectroscopy study between a functionalized tip where a lymphocyte cell is attached and endothelial cell on the substrate [129]. The adhesion forces have been measured and discriminated using antibodies against major adhesion proteins expressed by endothelial cells. These experiments lead to the conclusion that these proteins are the ones involved in lymphocyte B adhesion to endothelial cell. This inflammatory process involves also the increase of temperature, and thus heat stress. HSP60 protein (heat shock protein) production by endothelial cells has been studied by single molecule force spectroscopy and revealed the presence of this protein at the membrane surface of heat stressed cells and its possible implication in arthrogenesis [130]. Finally, macrophages phagocytosis plays an important role in the elimination of pathogens and dead cells following immune response [131].

As another stress that an organism is subjected to, injury is one of the most common one. In the process of maintaining blood vessel integrity, platelet activation is the first and key process. Topographical analysis of platelets activation has shown cytoskeleton reorganization at a resolution of 50 nm. A redistribution of the platelets granula and vesicles towards the lamellipodia of the cell has also been observed; this phenomenon leading to increase plasma membrane surface thus improving aggregation (Fig. 13B) [132].

We can see through these different examples that most of cellular responses involving different gene expression pattern are linked to cell membrane reorganization and changes in nanomechanical properties of the cell. These processes are observed for other mechanisms like cell differentiation or pathway activation. Han et al., in 2011 have validated the IGF-II (insulin-like growth factor) autocrine signaling pathway as a suitable target for the detection of muscle differentiation using AFM. They have been able to discriminate differentiated cells from others by

the detection of IGF-II at the cell surface thanks to anti-mouse IGF-II antibody immobilized on the AFM tip [133]. Using the same concept, Qiu et al. have characterized quantitatively the TRA-1–81 (un-differentiation marker) expression level on Human Embryonic stem cells surface to capture the "turn-on" signal and understand the mechanism of their early differentiation [134]. Another way to discriminate differentiated cell can be to measure their elasticity, as it is the case for the change from osteoblast (stiff) to osteocytes (soft) [135]. This stiffness is directly correlated to the capacity to adhere to substrate, and is accurate to test the biocompatibility of implant materials [136].

4.1.2. Drug effects and disease studies

Drug effect investigation can be done by the three classical measurements: adhesion force, elasticity or imaging, as for example this study about the effects of an anti-malaria compound on leukemic cells [137] or hormonal effects that have been widely studied and well documented by Hillebrand et al. [138]. i) Single molecule force spectroscopy has resolved at the molecular resolution the dynamics of AMPAR neuron receptors trafficking under NMDA stimulation [139]. ii) Effects of asthma drugs (aminophylline) on red blood cell elasticity have been correlated to their reduced capacity to transport oxygen in capillaries by increasing their stiffness and thus reverse the drug purpose [140]. iii) These elasticity changes are linked to a change in cell shape too. Imaging of cells leads to the understanding of molecule side effect, as for example chlorpromazine. Li et al. have shown that this schizophrenia drug affects endothelial cell morphologically [141]. $HgCl_2$ toxic effects have been also characterized by imaging cells in contact with the molecule [142]. Finally imaging can also be used to study the mechanism of drug internalization, as for example the study of the direct DNA insertion thanks to the AFM tip for nanomedicine [143].

We will now focus on the special case of cardio-vascular affections. Indeed, cardiac cells (cardiomyocytes) present the distinctive feature of being contractile, and AFM is nevertheless technically of interest to study them, as shown by Liu et al. This group has measured cell contractility with or without incubating them with Ibutilide, a classical drug used to treat arrhythmia, and started to determine its cellular target and mechanism of action [144]. The last development allows synchronizing AFM measurements with the contractility of the cells, providing the possibility to detect specific events [145]. The evaluation of recovery after infarct by elasticity measurements showed that stroma cell-derived factor 1α (SDF-1α) increases the elasticity of peri-infart mice tissue border zone and stiffening the scar, thus conducting to a better resistance to ventricular remodeling and infarct expansion [146]. The importance of the protein Ephrin B1 in the lateral membrane of cardiomyocytes has also been assessed by AFM. The deletion of Ephrin B1 makes the cardiomyocytes stiffer and progressively leads to the cardiac tissue disorganization. This protein is essential for the stability of cardiac tissue architecture cohesion [147]. Nevertheless, beyond the whole cell study, AFM can be run on organelles like mitochondria, which dysfunction is known to be implicated in the pathology of myocardial infarction. The release of cytochrome C by mitochondria was correlated to its swelling by fluorescence microscopy, thus not quantitatively. Lee et al. have shown that mitochondria indeed swell during apoptosis; the authors also gave quantitative morphological

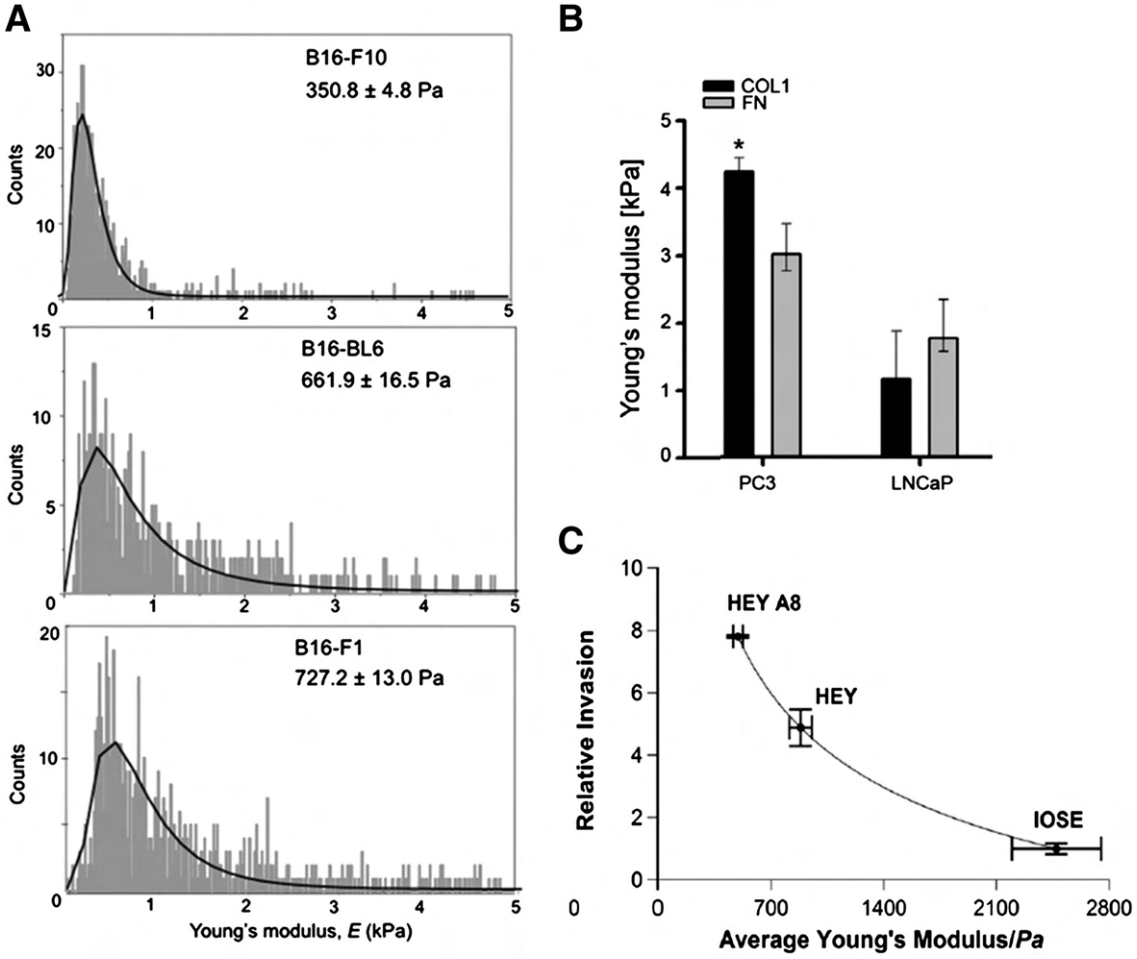

Fig. 15. Relation between stiffness and metastatic state. (A) Young's modulus distribution of murine melanoma cell of decreasing metastatic potential (B16-F10, B16-BL6 and B16-F1cells). (B) Substrate related elasticity of PC3 and LNCaP cell when culture on collagen (COL1) or fibronectin (FN). (C) Invasion *versus* average stiffness for ovarian surface epithelial cells (IOSE), and ovarian cancer (HEY and HEY A8 cells are HEY A8 cells that are more tumorigenic). Reprinted with permission from references [161,164,168].

analysis of rat heart mitochondria ischemic or not in native conditions. Furthermore, AFM allows them to detect nano-mechanical surface properties changes of ischemic cell mitochondria that are linked to their swelling [148].

Vascular diseases are also subjected to investigation by AFM. The inner part of blood vessel is responsible for blood pressure regulation through different mechanism like the release of vasoactive substance namely nitric oxide. The release of nitric oxide by the inner endothelial cells have been shown to be correlated with (and maybe regulated by) cell cortex stiffness changes [149]. Artherosclerosis lesions are affecting arterial cells stiffness too, specifically in branches and curved region of blood vessel, where endothelial cells appear to be stiffer than others endothelial cells [150]. This may be related to oxidized low-density lipoproteins (ox-LDL) cell exposure [151].

Furthermore, AFM can give answers to the questions raised by the pathogen infection process. For example the *Plasmodium falciparum* liver infection can be characterized by an increase in stiffness associated to a cell response to infection (and not the presence of the microorganism itself) (Fig. 13C), and may further enhance the understanding of this clinically silent step [152].

4.2. A tool for cancer-study development

Considered as the disease of the 20th century, cancer remains one of the most complicated and unsolved disease, meaning that no recovery treatment exists and only the eradication of tumor cells shows consistent results. In the following section accent will be put on the progress AFM allows for understanding this disease and the consequent medical applications that emerge with this nano-mechanical tool.

4.2.1. Nanomechanic of cancer cell

In 1999, Lekka et al. have for the first time compared the elasticity of cancerous cells *versus* "normal" ones [153]. They studied human epithelial bladder cells lines and show that cancerous cells present a lowest young modulus value than normal cells. This article was part of a set investigating several cancer types : prostate cancer cells [154], breast cancer cells [155] or cervical ones [156], all showing a decrease in stiffness for cancer cells, except in the case of leukemic cells where cell stiffness increase leading to leukostasis (Fig. 15A) [157]. In 2007, the same observations were published on cells directly taken from the body (pleural) fluids of patients with suspected lung, breast and pancreas cancer [158], validating the decrease of elasticity as a characteristic of cancerous cells, *in vitro* and *in vivo* (Fig. 15B).

These observations lead the authors to wonder why there was this particular change in elasticity and so to investigate the mechanics of the cancer cells. Rapidly the idea of the involvement of cytoskeleton in this measured softness was pointed out [159] and studied [160]. Moreover, the changes in elasticity of melanoma cell lines have shown that the decrease in stiffness was directly correlated to the metastatic potential of the cells [161], the stiffness being the lowest for melanoma B16-F10 cells that produce a large number of foci, and the highest with a reduce number of foci (Fig. 16A). The same relation has been shown for oesophageal cells lines in different phases of premalignancy [162].

All together, these data demonstrate that the nanomechanical properties of cancerous cells are linked to their condition, which enable them to change their elastic properties (deformability) in order to cross the cells barriers to create metastasis in the organism (leave the primary site, pass into circulation, stop at a secondary site and migrate again across the vascular barrier). Beyond this metastatic state, cancerous cells must be able to sense their environment to efficiently invade the right targeted-tissue. Firstly, the Young modulus of cancer cells was shown to change when cultured on different substrates, indicating a perception of their environment, and yet different capacities depending on their "function" [153]. For example elasticity of breast cancer cells decreases on fibronectin [163], which is related to the cancerous nature of the cells as shown on prostate cancer cells *versus* non-cancerous cells cultured on collagen (Fig. 16B) [164]. The extra cellular matrix is thus of

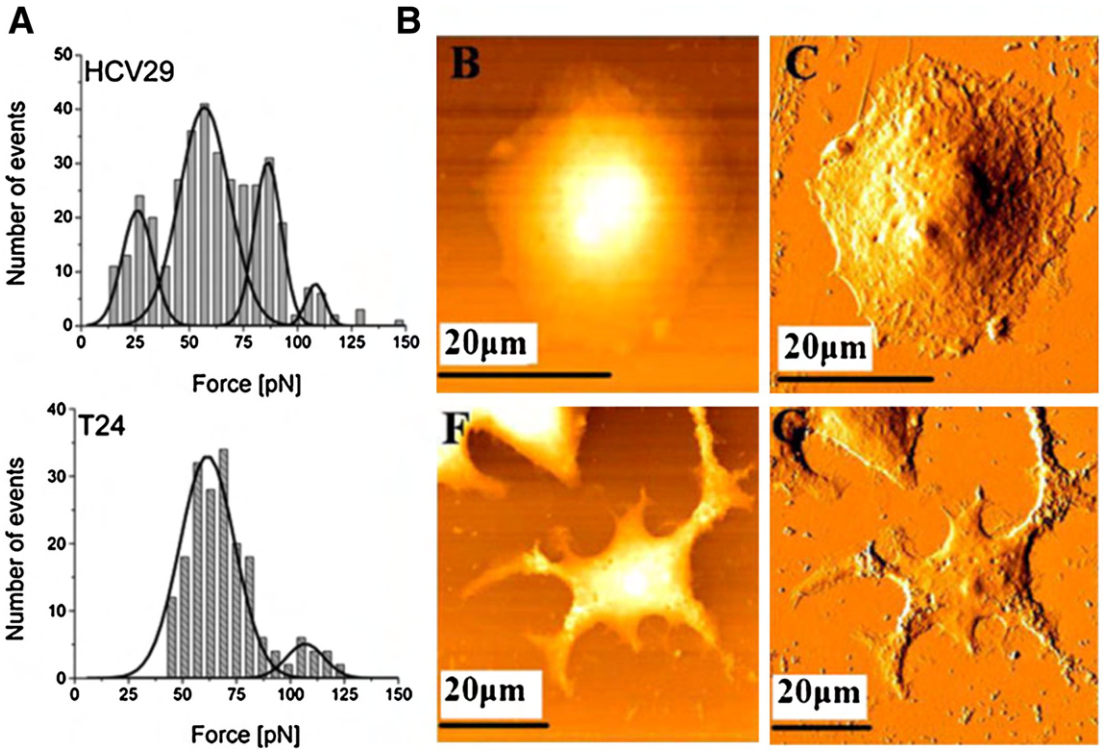

Fig. 16. Direct link between cancerous cell elasticity and their interaction with environment. (A) Distribution of the unbinding force for N-cadherin–GC4 complex in non-malignant HCV29 cells and malignant T24 bladder cells. (B) Morphological changes of MCF-7 cells treated without (B, C) or with (F, G) 30 µg/L BMP2 for 24 h. Reprinted with permission from references [173,174].

importance in cancer cell phenotypes [165–167]. Secondly, stiffness has been correlated to the capacity of invasion too as shown in Fig. 16C on ovarian cancer cells [168] or prostate cancer cells [169]. These invasive properties were also determined by the cells ability to adhere differently to the substrate depending on its nature [164,169]. Therefore, it was shown that the rigidity of the substrate influences the invasive cell response as the invasive mechanism implies the degradation of extracellular matrix: cells are then able to sense their environment and choose where to invade [170]. Likewise, during their invasion process, cancer cells can adhere to other cells, and this can be measured by direct cell–cell interactions for example between prostate metastatic cells known to form bone metastases and bone cells [171]. Reeves et al. have demonstrated the ability of prostate cancer cells fixed on the AFM tip to form contact with bone marrow endothelial cells fixed on the substrate [172]. By blocking extracellular part of trans-membrane protein such as integrin and selectin using specific antibodies, they observed a decrease in adhesion events between the two cell types. This result has demonstrated that cell–cell interaction in invasive process is performed through these specific proteins. Following the same idea, N-cadherin levels (calcium adhesion transmembrane proteins, that are characteristic of various cancers and involved in cell adhesive properties) have been measured on cancer and normal bladder cell surface with an antibody fixed on the AFM tip [173]. Results showed an enhanced level of the protein in cancer cells accompanied by higher unbinding forces, meaning that N-cadherin protein is more stable in cancerous cells (Fig. 17A). Furthermore, the presence of cell referenced as good secondary site for metastasis may enhance the invasion capacities of the cancer cells, as shown by Jin et al. on breast cancer cells that change their shape and make specialized migration structures in presence of the bone morphogenetic protein 2 (Fig. 17B) [174].

Cancerous cell changes in gene expression are directly related to the alteration of their function. The data presented above shows that morphological and force spectroscopy investigation help in resolving and understanding cancer cell mechanism and behavior.

4.2.2. Cancer treatment

After the determination of cancer cell characteristics and its subsequent link to their behavior, the treatment of patient by eradication of tumor is a second challenge for scientists. We will describe in this section the benefice of AFM for treatment efficiency and mode of action studies.

The first step regarding the efficiency of a therapeutic agent is the targeting of the cancer cells and its delivery. Indeed, most of the current chemical does not specifically affect the cancerous cells and thus need to be addressed. AFM can help in determining this targeting by the study of nanocarriers: nanoparticle interaction with melanoma cells [175] or nanoliposomes containing the well-known cisplatin drug intra cellular delivery in ovarian cancer cells [176]. These nanoliposomes have been shown to be well internalized in the cytoplasm in the size range of 100–300 nm (Fig. 18A). Adhesion specificity discrimination of chemical groups to enhance the targeting of cancerous cell by these

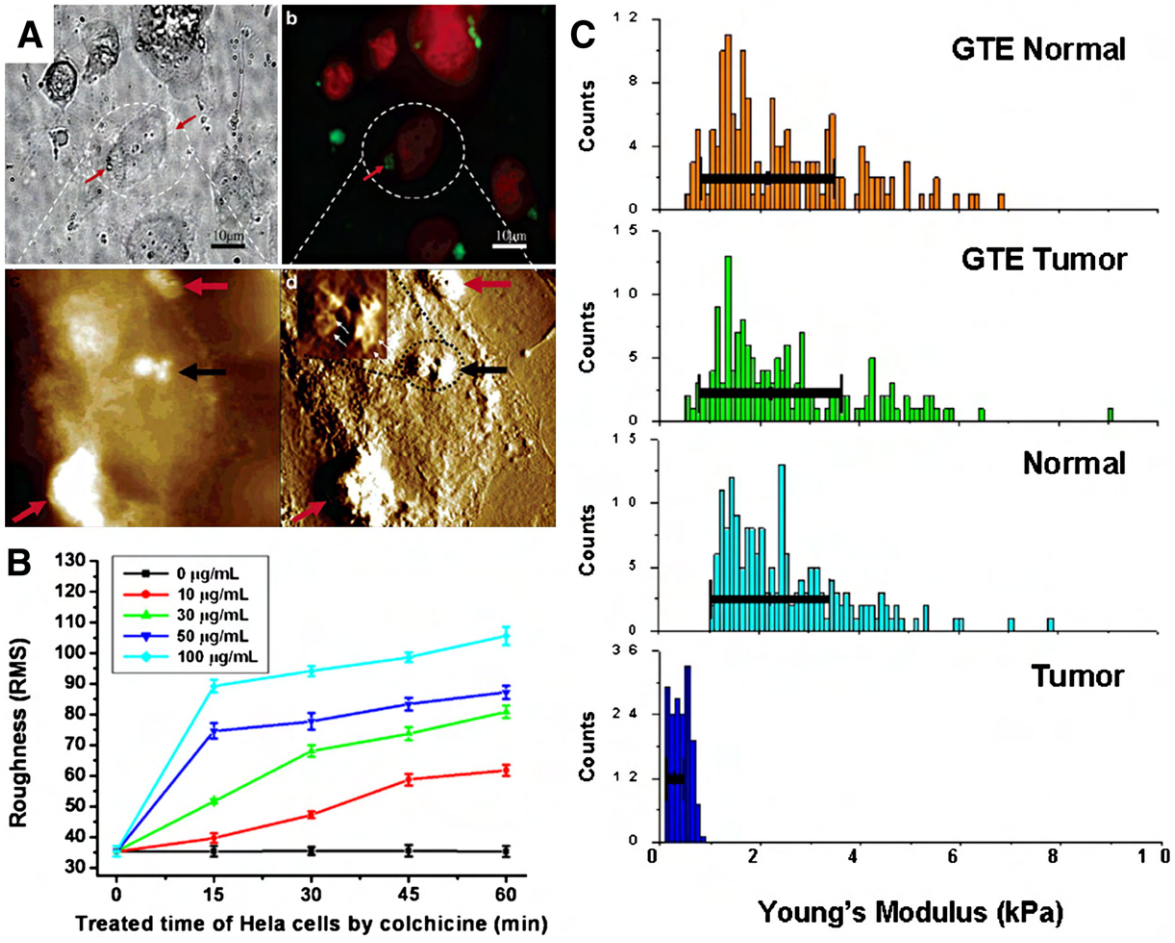

Fig. 17. Cancer treatment effects. (A) Internalization of small liposomes containing cisplatin in human ovarian cancer cell line (A2780) after 1 h incubation, top left: contrast phase image, top right: fluorescence images nucleus in red and liposomes in green, bottom left: height image, bottom right: error image. Black arrow: pointing at liposomes on cell surface, red arrows: in the cytoplasm. (B) Root–mean–square roughness variation of cell Hela cell membrane along time depending on colchicine dose. (C) Young's modulus of patient lung metastatic tumor and normal mesothelial cells before (ctrl) and after treatment with Green Tea Extract (GTE) for 24 h. Reprinted with permission from references [176,184,193].

nanocarriers can be measured directly on cells by functionalizing the AFM tip with the chemical itself [177]. The functionalization with these type of carriers can also be achieved through antibodies, for example against MUC-1, a cell surface marker for prostate, breast, and lung cancer [178]. Some antibodies are able, not only to target the cancer cells, but also to provoke apoptosis of the cell. This is the case of antibodies against epidermal growth factor receptor HER2, namely Trastzumab and Pertuzumab, which inhibit the dimerization of HER2 with other epidermal growth factor [179]. This method has also been used to study two cells interaction and helped to solve Zoledronic acid role on prostate cancer that reduced the adhesive interactions between cancer cells and bone marrow endothelial cells [172].

As stated in the previous section, interaction with their environment is of importance for cancerous cells. It is one of the effects of immune system on cancer cells, as shown by Braet et al. that demonstrated that natural killer cells affect the adhesion to substrate properties of colon carcinoma cells [180]. As membrane is the interface with cell's environment, it is one of the key actors that scientist look at when investigating anticancer treatment effects. For example, electropermeabilization treatment effect can be investigated by AFM [181]. Imaging cell surface after treating them with new drugs gives access to the way that drugs affect the cell and can help improving it. Some *ex-vivo* studies performed on lipid bilayers helped in defining the mechanism of action of anti-cancer compounds by imaging breast cancer cell native membrane rafts [182] or Latarcin2a peptide lytic activity on model membranes [183]. Several drug have been studied by imaging membrane on the complete cell: Colchicine on different organs carcinoma cells (dose dependent increase in roughness, Fig. 1) [184], Celecoxib on human colorectal cells [185], Paclitaxel on carcinoma cells [186,187], Alterporiol on breast cancer cells (dose dependent increase in membrane particule size) [188], lithium unexpected effect on carcinoma cells [189] and curcumin anti-cancer effect on liver cells [190]. Membrane is also the site where interactions with the environment occur, and the drug Celastrol affecting the invading capacity of endothelial cell in angiogenesis has been shown to reduce adhesion/affinity to fibronectin protein [191]. Ones must not forget that some drugs are affecting inner cell's components, like the bacterial protein Azurin that stabilize the p53 protein and thus enable apoptosis. The molecular details of this interaction have been assessed by AFM [192].

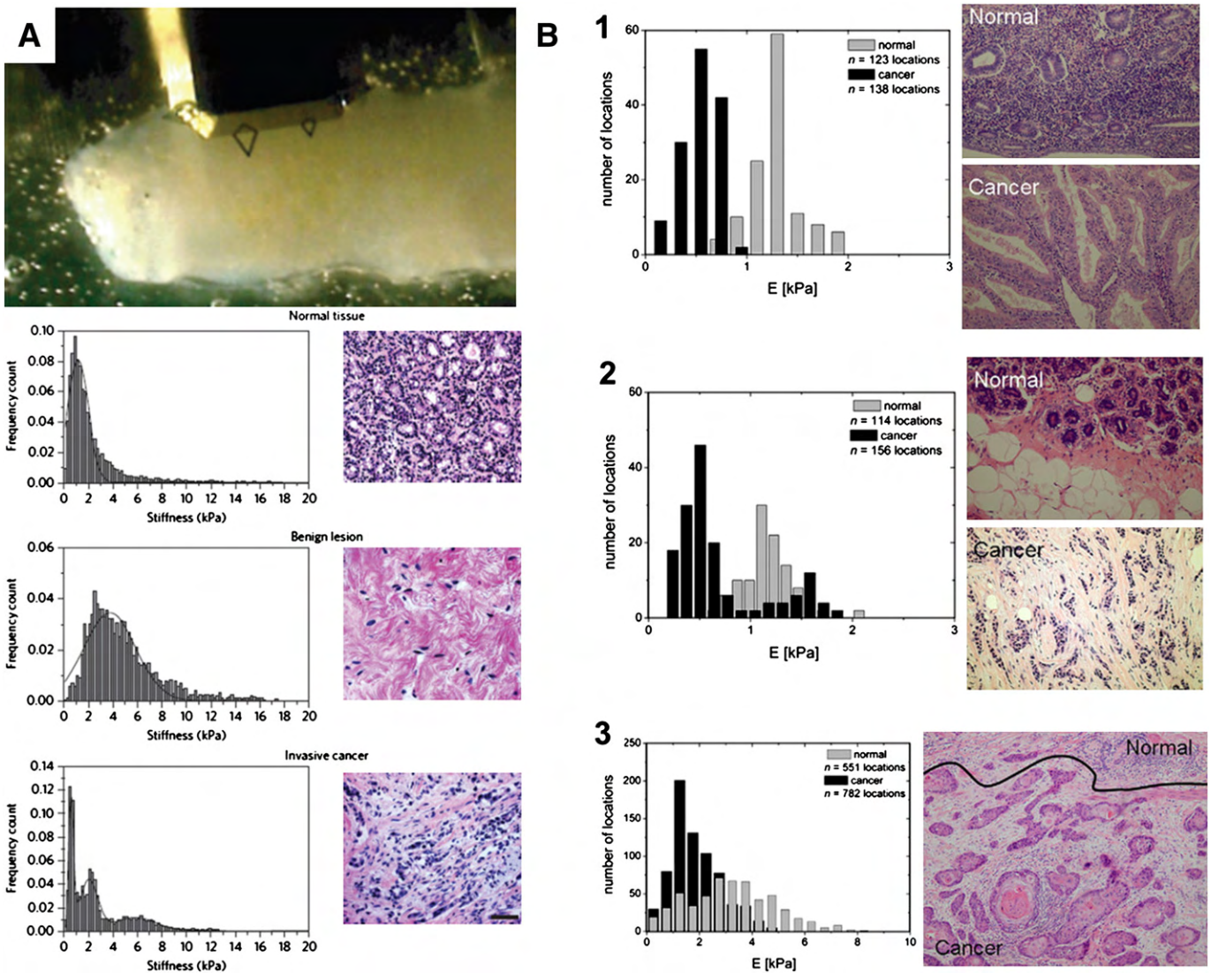

Fig. 18. Detection of cancerous cell from patient. (A) Top view of an oriented, immobilized biopsy with the cantilever positioned for AFM measurement. Scale bar, 500 μm. Elasticity of human breast tissue at different step of malignancy. (B) Stiffness distributions in tissues sections accompanied by the corresponding histological staining. (1) Nonneoplastic endometrium (gray columns) and well differentiated endometrioid carcinoma (black columns) of the uterine corpus. (2) Nonneoplastic breast tissue (gray columns) and infiltrating ductal carcinoma (black columns). (3) Vulvar cancer. Black columns denote cancer while gray ones, non-neoplastic parts of the tissue section separated by black line in the histological image. Reprinted with permission from references [198,210].

Of course the elasticity of the cell stays a good parameter to judge on the efficiency of a therapeutic molecule, as for example green tea extract that restores selectively the elasticity of cancerous cells thus confirming its anti-cancer non-destructive activity (Fig. 18C) [193]. However, depending on the effect or the cell, elasticity can show a different tendency. For example, elasticity can reflect the apoptotic effect of a drug, then ones must be looking at a decrease in Young modulus values as it is the case for Paclitaxel [186], and an increase in elasticity can label the resistance of tumor cells to an apoptotic agent like for the TRAIL (TNF-related apoptosis inducing ligand) [194].

4.2.3. Futures applications

We have described above the use of AFM for *in vitro* analysis of cancer cells, their properties, and their response to treatment. However the AFM can also be used as a diagnosis tool. *In vitro*, the discrimination between cancerous cells and healthy ones can be achieved by several assays. First, imaging cells can give answers to the question "are these cells cancerous?". The down-regulation of tumor suppressor protein as the matrix associated region protein SMAR1 has been studied by roughness measurement at the surface of cancer cells, and an increase in roughness was shown on cancer cells allowing the differentiation between cancer cell and healthy ones [195]. Secondly, adhesion measurements can inform on the glycosylation state of the cell, directly correlated to their cancer state [196]. As previously mentioned, the elasticity of the cell is a reliable measurement that undoubtedly makes the difference between cancer and non-cancer cells. Cross et al. have been the first to study cells from patients and thus gave the first diagnosis on lung, breast, pancreas cells (Fig. 15C) [158], and later adenocarcinoma [197]. The last improvements are turned to biopsies (Fig. 18) [173,198,210] and allow the correlation between cancer phenotypes and stiffness. These studies open up the use of AFM for bio-medical application of interest for clinical applications, and recent advances in force-curve analysis may help to finely tune these features [199,200].

5. Conclusion

Imaging cells at high resolution is of first importance in biology. The atomic force microscope cannot now be ignored because of its advantages. AFM works in liquid, thus potentially on living cells, with a resolution close to the nanometer (depending on the application). But, as exposed in the review, AFM is more than an imaging tool. It is able to measure forces, and gives access to the nanomechanical properties of cells, and/or to the localization of proteins, receptors, at the cell surface. We have reviewed the main domain of application of AFM on living cells: fungal cells, bacteria and mammal cells. However, AFM is also useful to study isolated proteins, DNA, and other biomolecules. We have shown, by reviewing the literature, that AFM experiments give an original vision of cells. It is of first interest to combine AFM analysis with other imaging techniques (MET, SEM, optical microscope, confocal microscope) to get a better understanding of the structure–function relationships. For example, by combining force measurements and transmission electronic microscope, it is possible to make a link between a stiffer structure and the underlying organelles that are present in the cell. The combination with chemical analysis like XPS or SIMS [201] also enlightens the relation between surface structures and chemical composition.

AFM technologies are continuously improving. Among others, we should cite high speed AFM [202,203], high speed force spectroscopies [204], multi-harmonic AFM [205], or the use of AFM as a microelectromechanical system [206]. These developments tend to increase our ability to track fast events occurring at the cell surface and contribute to redefine our understanding of the living cell surface. The next challenge is now to use AFM on living cells, in order to solve a biological problem, and not only to observe biological phenomena. This has been achieved, for example, for the early diagnosis of osteoarthritis [207], the determination of the cataract molecular mechanism [208,209], or for making the difference between normal and cancerous cells [210] (on cell lines, cells coming from patients and biopsis). Classical AFM has been combined with optical, confocal, fluorescence microscopy for several years now [211,212]. The next challenge is to combine these techniques with advanced AFM technologies as it has been recently done for optical microscopy and high speed AFM to observe single membrane proteins on eukaryotic cells [213,214]. The tracking of single molecules by FRET or TIRFF, on living cells, combined with AFM, is also an exciting perspective [215].

In this review we specially addressed the contribution of AFM in pharmacology. We exposed results obtained on fungal cells, bacteria and mammal cells exposed to drugs or encountering diseases. This particular point of view demonstrates that AFM is not providing only fundamental knowledge on cells but is now more and more contributing to studies with medical relevance.

References

[1] G. Binnig, H. Rohrer, C. Gerber, E. Weibel, Tunneling through a controllable vacuum gap, Appl. Phys. Lett. 40 (1982) 178–180.
[2] G. Binnig, C.F. Quate, Atomic force microscope, Phys. Rev. Lett. 56 (1986) 930–933.
[3] C. Gerber, H.P. Lang, How the doors of the nanoworld were opened, Nat. Nanotechnol. 1 (2006) 3–5.
[4] R.P. Feynman, Feynman's Talk, 1959.
[5] D.M. Eigler, E.K. Schweizer, Positioning single atoms with a scanning tunnelling microscope, Nature 344 (1990) 524–526.
[6] C. Toumey, 35 atoms that changed the nanoworld, Nat. Nanotechnol. 5 (2010) 239–241.
[7] P.K. Hansma, V.B. Elings, O. Marti, C.E. Bracker, Scanning tunneling microscopoy and atomic force microscopy : application to biology and technology, Science 247 (1988) 209–216.
[8] S. Liu, Y. Wang, Application of AFM in microbiology: a review, Scanning 32 (2010) 61–73.
[9] D.P. Allison, N.P. Mortensen, C.J. Sullivan, M.J. Doktycz, Atomic force microscopy of biological samples, Wiley Interdiscip. Rev. Nanomedicine Nanobiotechnol. 2 (2010) 618–634.
[10] G. Binnig, C.F. Quate, C. Gerber, Atomic Force Microscope, Phys. Rev. Lett. 56 (1986) 930–933.
[11] J.D. Ng, Y.G. Kuznetsov, A.J. Malkin, G. Keith, R. Giegé, A. McPherson, Visualization of RNA crystal growth by atomic force microscopy, Nucleic Acids Res. 25 (1997) 2582–2588.
[12] H.G. Hansma, K. Kasuya, E. Oroudjev, Atomic force microscopy imaging and pulling of nucleic acids, Curr. Opin. Struct. Biol. 14 (2004) 380–385.
[13] H. Seelert, A. Poetsch, N.A. Dencher, A. Engel, H. Stahlberg, D.J. Müller, Structural biology: proton-powered turbine of a plant motor, Nature 405 (2000) 418–419.
[14] L.I. Pietrasanta, D. Thrower, W. Hsieh, S. Rao, O. Stemmann, J. Lechner, et al., Probing the *Saccharomyces cerevisiae* centromeric DNA (CEN DNA)-binding factor 3 (CBF3) kinetochore complex by using atomic force microscopy, Proc. Natl. Acad. Sci. U. S. A. 96 (1999) 3757–3762.
[15] M. Gaczynska, P.A. Osmulski, Y. Jiang, J.-K. Lee, V. Bermudez, J. Hurwitz, Atomic force microscopic analysis of the binding of the *Schizosaccharomyces pombe* origin recognition complex and the spOrc4 protein with origin DNA, Proc. Natl. Acad. Sci. U. S. A. 101 (2004) 17952–17957.
[16] Y. Wu, J.S. Siino, T. Sugiyama, S.C. Kowalczykowski, The DNA binding preference of RAD52 and RAD59 proteins implications for RAD52 and RAD59 protein function in homologous recombination, J. Biol. Chem. 281 (2006) 40001–40009.
[17] M. Gad, A. Ikai, Method for immobilizing microbial cells on gel surface for dynamic AFM studies, Biophys. J. 69 (1995) 2226–2233.
[18] R. de Souza Pereira, M.I.N. da Silva, M.A. Cotta, Adhesion forces measured between a calcium blocker drug and its receptor in living cells using atomic force microscope, FEBS Lett. 552 (2003) 155–159.
[19] A.K. Adya, E. Canetta, G.M. Walker, Atomic force microscopic study of the influence of physical stresses on *Saccharomyces cerevisiae* and *Schizosaccharomyces pombe*, FEMS Yeast Res. 6 (2006) 120–128.
[20] A. Touhami, B. Nysten, Y.F. Dufrêne, Nanoscale mapping of the elasticity of microbial cells by Atomic Force Microscopy, Langmuir 19 (2003) 4539–4543.
[21] E. Dague, R. Bitar, H. Ranchon, F. Durand, H.M. Yken, J.M. François, An atomic force microscopy analysis of yeast mutants defective in cell wall architecture, Yeast 27 (2010) 673–684.
[22] E. Dague, E. Jauvert, L. Laplatine, B. Viallet, C. Thibault, L. Ressier, Assembly of live micro-organisms on microstructured PDMS stamps by convective/capillary deposition for AFM bio-experiments, Nanotechnology 22 (2011) 395102.
[23] E. Dague, D. Alsteens, J.-P. Latgé, Y.F. Dufrêne, High-resolution cell surface dynamics of germinating *Aspergillus fumigatus Conidia*, Biophys. J. 94 (2008) 656–660.
[24] R. De Souza Pereira, N.A. Parizotto, V. Baranauskas, Observation of baker's yeast strains used in biotransformation by atomic force microscopy, Appl. Biochem. Biotechnol. 59 (1996) 135–143.
[25] A. Kriznik, M. Bouillot, J. Coulon, F. Gaboriaud, Morphological specificity of yeast and filamentous *Candida albicans* forms on surface properties, C. R. Biol. 328 (2005) 928–935.

[26] D. Alsteens, V. Dupres, S. Yunus, J.-P. Latgé, J.J. Heinisch, Y.F. Dufrêne, High-resolution imaging of chemical and biological sites on living cells using peak force tapping atomic force microscopy, Langmuir 28 (2012) 16738–16744.

[27] E. Canetta, G.M. Walker, A.K. Adya, Correlating yeast cell stress physiology to changes in the cell surface morphology: atomic force microscopic studies, Sci. World J. 6 (2006) 777–780.

[28] L. Zhao, D. Schaefer, H. Xu, S.J. Modi, W.R. LaCourse, M.R. Marten, Elastic properties of the cell wall of *Aspergillus nidulans* studied with Atomic Force Microscopy, Biotechnol. Prog. 21 (2005) 292–299.

[29] A.E. Pelling, S. Sehati, E.B. Gralla, J.S. Valentine, J.K. Gimzewski, Local nanomechanical motion of the cell wall of *Saccharomyces cerevisiae*, Science 305 (2004) 1147–1150.

[30] A.E. Pelling, S. Sehati, E.B. Gralla, J.K. Gimzewski, Time dependence of the frequency and amplitude of the local nanomechanical motion of yeast, Nanomedicine: Nanotechnology Biol. Med. 1 (2005) 178–183.

[31] W.F. Heinz, J.H. Hoh, Spatially resolved force spectroscopy of biological surfaces using the atomic force microscope, Trends Biotechnol. 17 (1999) 143–150.

[32] R.J. Karreman, E. Dague, F. Gaboriaud, F. Quilès, J.F.L. Duval, G.G. Lindsey, The stress response protein Hsp12p increases the flexibility of the yeast *Saccharomyces cerevisiae* cell wall, Biochimica et Biophysica Acta (BBA)—Proteins and Proteomics 1774 (2007) 131–137.

[33] H. Hertz, Ueber die Berührung fester elastischer Körper, Journal Für Die Reine Und Angewandte Mathematik. 1882 (1881) 156–171.

[34] T. Svaldo-Lanero, S. Krol, R. Magrassi, A. Diaspro, R. Rolandi, A. Gliozzi, et al., Morphology, mechanical properties and viability of encapsulated cells, Ultramicroscopy 107 (2007) 913–921.

[35] P. Chen, H.-H. Liu, R. Cui, Z.-L. Zhang, D.-W. Pang, Z.-X. Xie, et al., Visualized investigation of yeast transformation induced with Li + and polyethylene glycol, Talanta 77 (2008) 262–268.

[36] D. Alsteens, V. Dupres, K. Mc Evoy, L. Wildling, H.J. Gruber, Y.F. Dufrêne, Structure, cell wall elasticity and polysaccharide properties of living yeast cells, as probed by AFM, Nanotechnology 19 (2008) 384005.

[37] P. Hinterdorfer, Y.F. Dufrêne, Detection and localization of single molecular recognition events using atomic force microscopy, Nat. Methods 3 (2006) 347–355.

[38] P. Hinterdorfer, M.F. Garcia-Parajo, Y.F. Dufrêne, Single-molecule imaging of cell surfaces using near-field nanoscopy, Acc. Chem. Res. 45 (2012) 327–336.

[39] Y.F. Dufrêne, P. Hinterdorfer, Recent progress in AFM molecular recognition studies, Pflugers Arch.—Eur. J. Physiol. 456 (2008) 237–245.

[40] M. Gad, Mapping cell wall polysaccharides of living microbial cells using atomic force microscopy, Cell Biol. Int. 21 (1997) 697–706.

[41] A. Beaussart, D. Alsteens, S. El-Kirat-Chatel, P.N. Lipke, S. Kucharíková, P. Van Dijck, et al., Single-molecule imaging and functional analysis of als adhesins and mannans during *Candida albicans* morphogenesis, ACS Nano 6 (2012) 10950–10964.

[42] D.E. Levin, Cell wall integrity signaling in *Saccharomyces cerevisiae*, Microbiol. Mol. Biol. Rev. 69 (2005) 262–291.

[43] J.J. Heinisch, V. Dupres, S. Wilk, A. Jendretzki, Y.F. Dufrêne, Single-molecule atomic force microscopy reveals clustering of the yeast plasma-membrane sensor Wsc1, PLoS One 5 (2010).

[44] V. Dupres, Y.F. Dufrêne, J.J. Heinisch, Measuring cell wall thickness in living yeast cells using single molecular rulers, ACS Nano 4 (2010) 5498–5504.

[45] D. Alsteens, M.C. Garcia, P.N. Lipke, Y.F. Dufrêne, Force-induced formation and propagation of adhesion nanodomains in living fungal cells, Proc. Natl. Acad. Sci. U. S. A. 107 (2010) 20744–20749.

[46] C. Mora, D.P. Tittensor, S. Adl, A.G.B. Simpson, B. Worm, How many species are there on earth and in the ocean? PLoS Biol. 9 (2011) e1001127.

[47] G.D. Brown, D.W. Denning, S.M. Levitz, Tackling human fungal infections, Science 336 (2012) 647.

[48] F.L. Mayer, D. Wilson, B. Hube, *Candida albicans* pathogenicity mechanisms, Virulence 4 (2013) 119–128.

[49] K.S. Kim, Y.-S. Kim, I. Han, M.-H. Kim, M.H. Jung, H.-K. Park, Quantitative and qualitative analyses of the cell death process in *Candida albicans* treated by antifungal agents, PLoS ONE 6 (2011) e28176.

[50] Y.-S. Kim, K.S. Kim, I. Han, M.-H. Kim, M.H. Jung, H.-K. Park, Quantitative and qualitative analysis of the antifungal activity of allicin alone and in combination with antifungal drugs, PLoS One 7 (2012).

[51] M. Götzinger, B. Weigl, W. Peukert, K. Sommer, Effect of roughness on particle adhesion in aqueous solutions: a study of *Saccharomyces cerevisiae* and a silica particle, Colloids Surf. B: Biointerfaces 55 (2007) 44–50.

[52] E.S. Ovchinnikova, B.P. Krom, H.J. Busscher, H.C. van der Mei, Evaluation of adhesion forces of *Staphylococcus aureus* along the length of *Candida albicans hyphae*, BMC Microbiol. 12 (2012) 281.

[53] A. Beaussart, P. Herman, S. El-Kirat-Chatel, P.N. Lipke, S. Kucharíková, P. Van Dijck, et al., Single-cell force spectroscopy of the medically important *Staphylococcus epidermidis–Candida albicans* interaction, Nanoscale (2013) 10894–10900.

[54] S. El-Kirat-Chatel, Y.F. Dufrêne, Nanoscale imaging of the *Candida*–Macrophage interaction using correlated fluorescence-atomic force microscopy, ACS Nano 6 (2012) 10792–10799.

[55] F. Comitini, I. Mannazzu, M. Ciani, Tetrapisispora phaffii killer toxin is a highly specific β-glucanase that disrupts the integrity of the yeast cell wall, Microb. Cell Factories 8 (2009) 55.

[56] A.K. Tyagi, A. Malik, In situ SEM, TEM and AFM studies of the antimicrobial activity of lemon grass oil in liquid and vapour phase against *Candida albicans*, Micron 41 (2010) 797–805.

[57] I.B. Beech, J.R. Smith, A.A. Steele, I. Penegar, S.A. Campbell, The use of atomic force microscopy for studying interactions of bacterial biofilms with surfaces, Colloids Surf. B: Biointerfaces 23 (2002) 231–247.

[58] A. Touhami, M.H. Jericho, J.M. Boyd, T.J. Beveridge, Nanoscale characterization and determination of adhesion forces of *Pseudomonas aeruginosa* pili by using atomic force microscopy, J. Bacteriol. 188 (2006) 370–377.

[59] J. Rheinlaender, A. Gräbner, L. Ott, A. Burkovski, T.E. Schäffer, Contour and persistence length of *Corynebacterium diphtheriae* pili by atomic force microscopy, Eur. Biophys. J. 41 (2012) 561–570.

[60] P. Tripathi, V. Dupres, A. Beaussart, S. Lebeer, I.J.J. Claes, J. Vanderleyden, et al., Deciphering the nanometer-scale organization and assembly of *Lactobacillus rhamnosus* GG pili using atomic force microscopy, Langmuir 28 (2012) 2211–2216.

[61] A. Gillis, V. Dupres, J. Mahillon, Y.F. Dufrêne, Atomic force microscopy: a powerful tool for studying bacterial swarming motility, Micron 43 (2012) 1304–1311.

[62] A. Gillis, V. Dupres, G. Delestrait, J. Mahillon, Y.F. Dufrêne, Nanoscale imaging of *Bacillus thuringiensis* flagella using atomic force microscopy, Nanoscale 4 (2012) 1585–1591.

[63] C. Díaz, P.L. Schilardi, R.C. Salvarezza, M. Fernández Lorenzo de Mele, Have flagella a preferred orientation during early stages of biofilm formation?: AFM study using patterned substrates, Colloids Surf. B: Biointerfaces 82 (2011) 536–542.

[64] K.-C. Chang, S.-J. Cheng, Y.-C. Chen, H.-R. Huang, J.-W. Liou, Nanoscopic analysis on pH induced morphological changes of flagella in *Escherichia coli*, J. Microbiol. Immunol. Infect. (2012), in press.

[65] H.-N. Su, Z.-H. Chen, S.-B. Liu, L.-P. Qiao, X.-L. Chen, H.-L. He, et al., Characterization of bacterial polysaccharide capsules and detection in the presence of deliquescent water by atomic force microscopy, Appl. Environ. Microbiol. 78 (2012) 3476–3479.

[66] O. Stukalov, A. Korenevsky, T.J. Beveridge, J.R. Dutcher, Use of atomic force microscopy and transmission electron microscopy for correlative studies of bacterial capsules, Appl. Environ. Microbiol. 74 (2008) 5457–5465.

[67] Z. Suo, X. Yang, R. Avci, L. Kellerman, D.W. Pascual, M. Fries, et al., HEPES-stabilized encapsulation of *Salmonella typhimurium*, Langmuir 23 (2007) 1365–1374.

[68] F.M. Coldren, E.L. Palavecino, N.H. Levi-Polyachenko, W.D. Wagner, T.L. Smith, B.P. Smith, et al., Encapsulated *Staphylococcus aureus* strains vary in adhesiveness assessed by atomic force microscopy, J. Biomed. Mater. Res. A 89A (2009) 402–410.

[69] V. Dupres, D. Alsteens, K. Pauwels, Y.F. Dufrêne, In vivo imaging of S-layer nanoarrays on *Corynebacterium glutamicum*, Langmuir 25 (2009) 9653–9655.

[70] J. Tang, A. Ebner, B. Kraxberger, M. Leitner, A. Hykollari, C. Kepplinger, et al., Detection of metal binding sites on functional S-layer nanoarrays using single molecule force spectroscopy, J. Struct. Biol. 168 (2009) 217–222.

[71] C. Horejs, R. Ristl, R. Tscheliessnig, U.B. Sleytr, D. Pum, Single-molecule force spectroscopy reveals the individual mechanical unfolding pathways of a surface layer protein, J. Biol. Chem. 286 (2011) 27416–27424.

[72] M. Saif Zaman, A. Goyal, G. Prakash Dubey, P.K. Gupta, H. Chandra, T.K. Das, et al., Imaging and analysis of *Bacillus anthracis* spore germination, Microsc. Res. Tech. 66 (2005) 307–311.

[73] M. Plomp, T.J. Leighton, K.E. Wheeler, M.E. Pitesky, A.J. Malkin, *Bacillus atrophaeus* outer spore coat assembly and ultrastructure, Langmuir 21 (2005) 10710–10716.

[74] P.A. Pinzón-Arango, G. Scholl, R. Nagarajan, C.M. Mello, T.A. Camesano, Atomic force microscopy study of germination and killing of Bacillusatrophaeus spores, J. Mol. Recognit. 22 (2009) 373–379.

[75] M. Plomp, T.J. Leighton, K.E. Wheeler, H.D. Hill, A.J. Malkin, In vitro high-resolution structural dynamics of single germinating bacterial spores, PNAS 104 (2007) 9644–9649.

[76] G. Francius, P. Polyakov, J. Merlin, Y. Abe, J.-M. Ghigo, C. Merlin, et al., Bacterial surface appendages strongly impact nanomechanical and electrokinetic properties of *Escherichia coli* cells subjected to osmotic stress, PLoS ONE 6 (2011) e20066.

[77] P. Schaer-Zammaretti, J. Ubbink, Imaging of lactic acid bacteria with AFM—elasticity and adhesion maps and their relationship to biological and structural data, Ultramicroscopy 97 (2003) 199–208.

[78] F. Gaboriaud, S. Bailet, E. Dague, F. Jorand, Surface structure and nanomechanical properties of *Shewanella putrefaciens* bacteria at two pH values (4 and 10) determined by atomic force microscopy, J. Bacteriol. 187 (2005) 3864–3868.

[79] A. Cerf, J.-C. Cau, C. Vieu, E. Dague, Nanomechanical properties of dead or alive single-patterned bacteria, Langmuir 25 (2009) 5731–5736.

[80] C. Roduit, B. Saha, L. Alonso-Sarduy, A. Volterra, G. Dietler, S. Kasas, OpenFovea: open-source AFM data processing software, Nat. Methods 9 (2012) 774–775.

[81] G. Longo, L.M. Rio, C. Roduit, A. Trampuz, A. Bizzini, G. Dietler, et al., Force volume and stiffness tomography investigation on the dynamics of stiff material under bacterial membranes, J. Mol. Recognit. 25 (2012) 278–284.

[82] E.V. Dubrovin, A.G. Voloshin, S.V. Kraevsky, T.E. Ignatyuk, S.S. Abramchuk, I.V. Yaminsky, et al., Atomic force microscopy investigation of phage infection of bacteria, Langmuir 24 (2008) 13068–13074.

[83] E.V. Dubrovin, A.V. Popova, S.V. Kraevskiy, S.G. Ignatov, T.E. Ignatyuk, I.V. Yaminsky, et al., Atomic force microscopy analysis of the *Acinetobacter baumannii* bacteriophage AP22 lytic cycle, PLoS ONE 7 (2012) e47348.

[84] C. Verbelen, Y.F. Dufrêne, Direct measurement of Mycobacterium–fibronectin interactions, Integr. Biol. 1 (2009) 296–300.

[85] E. Dague, D.T.L. Le, S. Zanna, P. Marcus, P. Loubière, M. Mercier-Bonin, Probing in vitro interactions between *Lactococcus lactis* and mucins using AFM, Langmuir 26 (2010) 11010–11017.

[86] D.T.L. Le, Y. Guérardel, P. Loubière, M. Mercier-Bonin, E. Dague, Measuring kinetic dissociation/association constants between *Lactococcus lactis* bacteria and mucins using living cell probes, Biophys. J. 101 (2011) 2843–2853.

[87] M. Firtel, G. Henderson, I. Sokolov, Nanosurgery: observation of peptidoglycan strands in *Lactobacillus helveticus* cell walls, Ultramicroscopy 101 (2004) 105–109.

[88] G. Andre, S. Kulakauskas, M.-P. Chapot-Chartier, B. Navet, M. Deghorain, E. Bernard, et al., Imaging the nanoscale organization of peptidoglycan in living *Lactococcus lactis* cells, Nat. Commun. 1 (2010) 27.

[89] R. Wheeler, S. Mesnage, I.G. Boneca, J.K. Hobbs, S.J. Foster, Super-resolution microscopy reveals cell wall dynamics and peptidoglycan architecture in ovococcal bacteria, Mol. Microbiol. 82 (2011) 1096–1109.
[90] E.J. Hayhurst, L. Kailas, J.K. Hobbs, S.J. Foster, Cell wall peptidoglycan architecture in *Bacillus subtilis*, PNAS 105 (2008) 14603–14608.
[91] G. Francius, S. Lebeer, D. Alsteens, L. Wildling, H.J. Gruber, P. Hols, et al., Detection, localization, and conformational analysis of single polysaccharide molecules on live bacteria, ACS Nano 2 (2008) 1921–1929.
[92] J. Strauss, N.A. Burnham, T.A. Camesano, Atomic force microscopy study of the role of LPS O-antigen on adhesion of *E. coli*, J. Mol. Recognit. 22 (2009) 347–355.
[93] J. Tang, D. Krajcikova, R. Zhu, A. Ebner, S. Cutting, H.J. Gruber, et al., Atomic force microscopy imaging and single molecule recognition force spectroscopy of coat proteins on the surface of *Bacillus subtilis* spore, J. Mol. Recognit. 20 (2007) 483–489.
[94] M. Plomp, A.J. Malkin, Mapping of proteomic composition on the surfaces of Bacillus spores by atomic force microscopy-based immunolabeling, Langmuir 25 (2009) 403–409.
[95] V. Dupres, F.D. Menozzi, C. Locht, B.H. Clare, N.L. Abbott, S. Cuenot, et al., Nanoscale mapping and functional analysis of individual adhesins on living bacteria, Nat. Methods 2 (2005) 515–520.
[96] M. Grare, De la génèse d'une nouvelle classe d'antibactériens à base de polyphénols cycliques de type calixarène. Etudes moléculaire(s), cellulaire(s), et structurale(s) en vue de l'identification des cibles d'action: le cas du para-guanidinoéthylcalix [4]arène, Université Henri Poincaré, Nancy-I, 2009.
[97] C. Formosa, M. Grare, R.E. Duval, E. Dague, Nanoscale effects of antibiotics on *P. aeruginosa*, Nanomed. Nanotechnol. Biol. Med. 8 (2012) 12–16.
[98] P.C. Braga, D. Ricci, Atomic force microscopy: application to investigation of *Escherichia coli* morphology before and after exposure to cefodizime, Antimicrob. Agents Chemother. 42 (1998) 18–22.
[99] M. Ouberai, F. El Garch, A. Bussiere, M. Riou, D. Alsteens, L. Lins, et al., The *Pseudomonas aeruginosa* membranes: a target for a new amphiphilic aminoglycoside derivative? Biochim. Biophys. Acta Biomembr. 1808 (2011) 1716–1727.
[100] M.T. Montero, M. Pijoan, S. Merino-Montero, T. Vinuesa, J. Hernández-Borrell, Interfacial membrane effects of fluoroquinolones as revealed by a combination of fluorescence binding experiments and atomic force microscopy observations, Langmuir 22 (2006) 7574–7578.
[101] G. Francius, O. Domenech, M.P. Mingeot-Leclercq, Y.F. Dufrêne, Direct observation of *Staphylococcus aureus* cell wall digestion by lysostaphin, J. Bacteriol. 190 (2008) 7904–7909.
[102] Y. Gilbert, M. Deghorain, L. Wang, B. Xu, P.D. Pollheimer, H.J. Gruber, et al., Single-molecule force spectroscopy and imaging of the vancomycin/d-Ala-d-Ala interaction, Nano Lett. 7 (2007) 796–801.
[103] Y. Wu, A. Zhou, In situ, real-time tracking of cell wall topography and nanomechanics of antimycobacterial drugs treated Mycobacterium JLS using atomic force microscopy, Chem. Commun. (2009) 7021–7023.
[104] C. Verbelen, V. Dupres, F.D. Menozzi, D. Raze, A.R. Baulard, P. Hols, et al., Ethambutol-induced alterations in *Mycobacterium bovis* BCG imaged by atomic force microscopy, FEMS Microbiol. Lett. 264 (2006) 192–197.
[105] R.L. Soon, R.L. Nation, M. Harper, B. Adler, J.D. Boyce, C.-H. Tan, et al., Effect of colistin exposure and growth phase on the surface properties of live *Acinetobacter baumannii* cells examined by atomic force microscopy, Int. J. Antimicrob. Agents 38 (2011) 493–501.
[106] R.L. Soon, R.L. Nation, P.G. Hartley, I. Larson, J. Li, Atomic force microscopy investigation of the morphology and topography of colistin-heteroresistant *Acinetobacter baumannii* strains as a function of growth phase and in response to colistin treatment, Antimicrob. Agents Chemother. 53 (2009) 4979–4986.
[107] N.P. Mortensen, J.D. Fowlkes, C.J. Sullivan, D.P. Allison, N.B. Larsen, S. Molin, et al., Effects of colistin on surface ultrastructure and nanomechanics of *Pseudomonas aeruginosa* cells, Langmuir 25 (2009) 3728–3733.
[108] A. da S. Junior, O. Teschke, Dynamics of the antimicrobial peptide PGLa action on *Escherichia coli* monitored by atomic force microscopy, World J. Microbiol. Biotechnol. 21 (2005) 1103–1110.
[109] M. Meincken, D.L. Holroyd, M. Rautenbach, Atomic force microscopy study of the effect of antimicrobial peptides on the cell envelope of *Escherichia coli*, Antimicrob. Agents Chemother. 49 (2005) 4085–4092.
[110] A. Li, P.Y. Lee, B. Ho, J.L. Ding, C.T. Lim, Atomic force microscopy study of the antimicrobial action of Sushi peptides on Gram negative bacteria, Biochim. Biophys. Acta Biomembr. 1768 (2007) 411–418.
[111] G. Francius, S. Dufour, M. Deleu, M. Paquot, M.-P. Mingeot-Leclercq, Y.F. Dufrêne, Nanoscale membrane activity of surfactins: influence of geometry, charge and hydrophobicity, Biochim. Biophys. Acta Biomembr. 1778 (2008) 2058–2068.
[112] M. Arseneault, S. Bédard, M. Boulet-Audet, M. Pézolet, Study of the interaction of lactoferricin B with phospholipid monolayers and bilayers, Langmuir 26 (2010) 3468–3478.
[113] C.Y. Flores, C. Diaz, A. Rubert, G.A. Benítez, M.S. Moreno, M.A. Fernández Lorenzo de Mele, et al., Spontaneous adsorption of silver nanoparticles on Ti/TiO2 surfaces. Antibacterial effect on *Pseudomonas aeruginosa*, J. Colloid Interface Sci. 350 (2010) 402–408.
[114] V. Gopinath, D. MubarakAli, S. Priyadarshini, N.M. Priyadharsshini, N. Thajuddin, P. Velusamy, Biosynthesis of silver nanoparticles from *Tribulus terrestris* and its antimicrobial activity: a novel biological approach, Colloids Surf. B: Biointerfaces 96 (2012) 69–74.
[115] A.K. Suresh, D.A. Pelletier, W. Wang, J.-W. Moon, B. Gu, N.P. Mortensen, et al., Silver nanocrystallites: biofabrication using *Shewanella oneidensis*, and an evaluation of their comparative toxicity on Gram-negative and Gram-positive bacteria, Environ. Sci. Technol. 44 (2010) 5210–5215.
[116] A. Pramanik, D. Laha, D. Bhattacharya, P. Pramanik, P. Karmakar, A novel study of antibacterial activity of copper iodide nanoparticle mediated by DNA and membrane damage, Colloids Surf. B: Biointerfaces 96 (2012) 50–55.
[117] M. Grare, M. Mourer, S. Fontanay, J.-B. Regnouf-de-Vains, C. Finance, R.E. Duval, In vitro activity of para-guanidinoethylcalix[4]arene against susceptible and antibiotic-resistant Gram-negative and Gram-positive bacteria, J. Antimicrob. Chemother. 60 (2007) 575–581.
[118] C. Formosa, M. Grare, E. Jauvert, A. Coutable, J.B. Regnouf-de-Vains, M. Mourer, et al., Nanoscale analysis of the effects of antibiotics and CX1 on a *Pseudomonas aeruginosa* multidrug-resistant strain, Sci. Rep. 2 (2012).
[119] M. Mourer, R.E. Duval, C. Finance, J.-B. Regnouf-de-Vains, Functional organisation and gain of activity: the case of the antibacterial tetra-para-guanidinoethyl-calix [4]arene, Bioorg. Med. Chem. Lett. 16 (2006) 2960–2963.
[120] M. Mourer, H. Massimba Dibama, P. Constant, M. Daffé, J.-B. Regnouf-de-Vains, Anti-mycobacterial activities of some cationic and anionic calix[4]arene derivatives, Bioorg. Med. Chem. 20 (2012) 2035–2041.
[121] M.B. Patel, N.R. Modi, J.P. Raval, S.K. Menon, Calix[4]arene based 1,3,4-oxadiazole and thiadiazole derivatives: design, synthesis, and biological evaluation, Org. Biomol. Chem. 10 (2012) 1785–1794.
[122] S. Liu, A.K. Ng, R. Xu, J. Wei, C.M. Tan, Y. Yang, et al., Antibacterial action of dispersed single-walled carbon nanotubes on *Escherichia coli* and *Bacillus subtilis* investigated by atomic force microscopy, Nanoscale 2 (2010) 2744–2750.
[123] P. Eaton, J.C. Fernandes, E. Pereira, M.E. Pintado, F. Xavier Malcata, Atomic force microscopy study of the antibacterial effects of chitosans on *Escherichia coli* and *Staphylococcus aureus*, Ultramicroscopy 108 (2008) 1128–1134.
[124] J.C. Fernandes, P. Eaton, A.M. Gomes, M.E. Pintado, F. Xavier Malcata, Study of the antibacterial effects of chitosans on *Bacillus cereus* (and its spores) by atomic force microscopy imaging and nanoindentation, Ultramicroscopy 109 (2009) 854–860.
[125] J.A. Younes, H.C. van der Mei, E. van den Heuvel, H.J. Busscher, G. Reid, Adhesion forces and coaggregation between vaginal staphylococci and lactobacilli, PLoS ONE 7 (2012) e36917.
[126] A. Beaussart, S. El-Kirat-Chatel, P. Herman, D. Alsteens, J. Mahillon, P. Hols, et al., Single-cell force spectroscopy of probiotic bacteria, Biophys. J. 104 (2013) 1886–1892.
[127] T. Kobiela, K. Lelen-Kaminska, M. Stepulak, M. Lekka, M. Malejczyk, J. Arct, et al., The influence of surfactants and hydrolyzed proteins on keratinocytes viability and elasticity, Skin Res. Technol. 19 (2013) e200–e208.
[128] J. Helenius, C.-P. Heisenberg, H.E. Gaub, D.J. Muller, Single-cell force spectroscopy, J. Cell Sci. 121 (2008) 1785–1791.
[129] X. Zhang, E.P. Wojcikiewicz, V.T. Moy, Dynamic adhesion of T lymphocytes to endothelial cells revealed by atomic force microscopy, Exp. Biol. Med. (Maywood) 231 (2006) 1306–1312.
[130] G. Pfister, C.M. Stroh, H. Perschinka, M. Kind, M. Knoflach, P. Hinterdorfer, et al., Detection of HSP60 on the membrane surface of stressed human endothelial cells by atomic force and confocal microscopy, J. Cell Sci. 118 (2005) 1587–1594.
[131] M. Beckmann, H.A. Kolb, F. Lang, Atomic force microscopy of peritoneal macrophages after particle phagocytosis, J. Membr. Biol. 140 (1994) 197–204.
[132] M. Fritz, M. Radmacher, H.E. Gaub, Granula motion and membrane spreading during activation of human platelets imaged by atomic force microscopy, Biophys. J. 66 (1994) 1328–1334.
[133] S.-W. Han, S. Mieda, C. Nakamura, T. Kihara, N. Nakamura, J. Miyake, Successive detection of insulin-like growth factor-II bound to receptors on a living cell surface using an AFM, J. Mol. Recognit. 24 (2011) 17–22.
[134] D. Qiu, J. Xiang, Z. Li, A. Krishnamoorthy, L. Chen, R. Wang, Profiling TRA-1–81 antigen distribution on a human embryonic stem cell, Biochem. Biophys. Res. Commun. 369 (2008) 735–740.
[135] Y. Sugawara, R. Ando, H. Kamioka, Y. Ishihara, S.A. Murshid, K. Hashimoto, et al., The alteration of a mechanical property of bone cells during the process of changing from osteoblasts to osteocytes, Bone 43 (2008) 19–24.
[136] Domke, Dannöhl, Parak, Müller, Aicher, Radmacher, Substrate dependent differences in morphology and elasticity of living osteoblasts investigated by atomic force microscopy, Colloids Surf. B: Biointerfaces 19 (2000) 367–379.
[137] X. Cai, S. Gao, J. Cai, Y. Wu, H. Deng, Artesunate induced morphological and mechanical changes of Jurkat cell studied by AFM, Scanning 31 (2009) 83–89.
[138] U. Hillebrand, M. Hausberg, D. Lang, C. Stock, C. Riethmüller, C. Callies, et al., How steroid hormones act on the endothelium—insights by atomic force microscopy, Pflugers Arch. 456 (2008) 51–60.
[139] A. Yersin, H. Hirling, S. Kasas, C. Roduit, K. Kulangara, G. Dietler, et al., Elastic properties of the cell surface and trafficking of single AMPA receptors in living hippocampal neurons, Biophys. J. 92 (2007) 4482–4489.
[140] A. Zuk, M. Targosz-Korecka, M. Szymonski, Effect of selected drugs used in asthma treatment on morphology and elastic properties of red blood cells, Int. J. Nanomedicine 6 (2011) 249–257.
[141] Y. Li, J. Zhang, B. Zhang, Atomic force microscopy study on chlorpromazine-induced morphological changes of living HeLa cells In Vitro, Scanning 31 (2009) 259–265.
[142] M. Lasalvia, G. Perna, E. Mezzenga, E. Migliorini, M. Lazzarino, N. L'abbate, et al., Atomic force microscopy investigation of morphological changes in living keratinocytes treated with HgCl(2) at not cytotoxic doses, J. Microsc. 243 (2011) 40–46.
[143] R. Afrin, U.S. Zohora, H. Uehara, T. Watanabe-Nakayama, A. Ikai, Atomic force microscopy for cellular level manipulation: imaging intracellular structures and DNA delivery through a membrane hole, J. Mol. Recognit. 22 (2009) 363–372.

[144] Y. Liu, J. Feng, L. Shi, R. Niu, Q. Sun, H. Liu, et al., In situ mechanical analysis of cardiomyocytes at nano scales, Nanoscale 4 (2012) 99–102.
[145] J.F. Saenz Cogollo, M. Tedesco, S. Martinoia, R. Raiteri, A new integrated system combining atomic force microscopy and micro-electrode array for measuring the mechanical properties of living cardiac myocytes, Biomed. Microdevices 13 (2011) 613–621.
[146] W. Hiesinger, M.J. Brukman, R.C. McCormick, J.R. Fitzpatrick III, J.R. Frederick, E.C. Yang, et al., Myocardial tissue elastic properties determined by atomic force microscopy after stromal cell-derived factor 1α angiogenic therapy for acute myocardial infarction in a murine model, J. Thorac. Cardiovasc. Surg. 143 (2012) 962–966.
[147] G. Genet, C. Guilbeau-Frugier, B. Honton, E. Dague, M.D. Schneider, C. Coatrieux, et al., Ephrin-B1 is a novel specific component of the lateral membrane of the cardiomyocyte and is essential for the stability of cardiac tissue architecture cohesion, Circ. Res. 110 (2012) 688–700.
[148] G.-J. Lee, S.-J. Chae, J.H. Jeong, S.-R. Lee, S.-J. Ha, Y.K. Pak, et al., Characterization of mitochondria isolated from normal and ischemic hearts in rats utilizing atomic force microscopy, Micron 42 (2011) 299–304.
[149] J. Fels, P. Jeggle, K. Kusche-Vihrog, H. Oberleithner, Cortical actin nanodynamics determines nitric oxide release in vascular endothelium, PLoS ONE 7 (2012) e41520.
[150] H. Miyazaki, K. Hayashi, Atomic force microscopic measurement of the mechanical properties of intact endothelial cells in fresh arteries, Med. Biol. Eng. Comput. 37 (1999) 530–536.
[151] J.A. Chouinard, G. Grenier, A. Khalil, P. Vermette, Oxidized-LDL induce morphological changes and increase stiffness of endothelial cells, Exp. Cell Res. 314 (2008) 3007–3016.
[152] P. Eaton, V. Zuzarte-Luis, M.M. Mota, N.C. Santos, M. Prudêncio, Infection by Plasmodium changes shape and stiffness of hepatic cells, Nanomedicine 8 (2012) 17–19.
[153] M. Lekka, P. Laidler, D. Gil, J. Lekki, Z. Stachura, A.Z. Hrynkiewicz, Elasticity of normal and cancerous human bladder cells studied by scanning force microscopy, Eur. Biophys. J. 28 (1999) 312–316.
[154] E.C. Faria, N. Ma, E. Gazi, P. Gardner, M. Brown, N.W. Clarke, et al., Measurement of elastic properties of prostate cancer cells using AFM, Analyst 133 (2008) 1498–1500.
[155] Q.S. Li, G.Y.H. Lee, C.N. Ong, C.T. Lim, AFM indentation study of breast cancer cells, Biochem. Biophys. Res. Commun. 374 (2008) 609–613.
[156] S. Iyer, R.M. Gaikwad, V. Subba-Rao, C.D. Woodworth, I. Sokolov, Atomic force microscopy detects differences in the surface brush of normal and cancerous cells, Nat. Nanotechnol. 4 (2009) 389–393.
[157] M.J. Rosenbluth, W.A. Lam, D.A. Fletcher, Force microscopy of nonadherent cells: a comparison of leukemia cell deformability, Biophys. J. 90 (2006) 2994–3003.
[158] S.E. Cross, Y.-S. Jin, J. Rao, J.K. Gimzewski, Nanomechanical analysis of cells from cancer patients, Nat. Nanotechnol. 2 (2007) 780–783.
[159] M. Lekka, P. Laidler, J. Ignacak, M. Łabedz, J. Lekki, H. Struszczyk, et al., The effect of chitosan on stiffness and glycolytic activity of human bladder cells, Biochim. Biophys. Acta 1540 (2001) 127–136.
[160] A. Mescola, S. Vella, M. Scotto, P. Gavazzo, C. Canale, A. Diaspro, et al., Probing cytoskeleton organisation of neuroblastoma cells with single-cell force spectroscopy, J. Mol. Recognit. 25 (2012) 270–277.
[161] T. Watanabe, H. Kuramochi, A. Takahashi, K. Imai, N. Katsuta, T. Nakayama, et al., Higher cell stiffness indicating lower metastatic potential in B16 melanoma cell variants and in (−)-epigallocatechin gallate-treated cells, J. Cancer Res. Clin. Oncol. (2012) 859–866.
[162] A. Fuhrmann, J.R. Staunton, V. Nandakumar, N. Banyai, P.C.W. Davies, R. Ros, AFM stiffness nanotomography of normal, metaplastic and dysplastic human esophageal cells, Phys. Biol. 8 (2011) 015007.
[163] S. Leporatti, D. Vergara, A. Zacheo, V. Vergaro, G. Maruccio, R. Cingolani, et al., Cytomechanical and topological investigation of MCF-7 cells by scanning force microscopy, Nanotechnology 20 (2009) 055103.
[164] D. Docheva, D. Padula, M. Schieker, H. Clausen-Schaumann, Effect of collagen I and fibronectin on the adhesion, elasticity and cytoskeletal organization of prostate cancer cells, Biochem. Biophys. Res. Commun. 402 (2010) 361–366.
[165] J. Alcaraz, R. Xu, H. Mori, C.M. Nelson, R. Mroue, V.A. Spencer, et al., Laminin and biomimetic extracellular elasticity enhance functional differentiation in mammary epithelia, EMBO J. 27 (2008) 2829–2838.
[166] G. Zhao, J. Cui, Q. Qin, J. Zhang, L. Liu, S. Deng, et al., Mechanical stiffness of liver tissues in relation to integrin β1 expression may influence the development of hepatic cirrhosis and hepatocellular carcinoma, J. Surg. Oncol. 102 (2010) 482–489.
[167] C.-A. Lamontagne, M. Grandbois, PKC-induced stiffening of hyaluronan/CD44 linkage; local force measurements on glioma cells, Exp. Cell Res. 314 (2008) 227–236.
[168] W. Xu, R. Mezencev, B. Kim, L. Wang, J. McDonald, T. Sulchek, Cell stiffness is a biomarker of the metastatic potential of ovarian cancer cells, PLoS ONE 7 (2012) e46609.
[169] L. Bastatas, D. Martinez-Marin, J. Matthews, J. Hashem, Y.J. Lee, S. Sennoune, et al., AFM nano-mechanics and calcium dynamics of prostate cancer cells with distinct metastatic potential, Biochim. Biophys. Acta 1820 (2012) 1111–1120.
[170] A. Parekh, N.S. Ruppender, K.M. Branch, M.K. Sewell-Loftin, J. Lin, P.D. Boyer, et al., Sensing and modulation of invadopodia across a wide range of rigidities, Biophys. J. 100 (2011) 573–582.
[171] P.-H. Puech, K. Poole, D. Knebel, D.J. Muller, A new technical approach to quantify cell–cell adhesion forces by AFM, Ultramicroscopy 106 (2006) 637–644.
[172] K.J. Reeves, J. Hou, S.E. Higham, Z. Sun, J.P. Trzeciakowski, G.A. Meininger, et al., Selective measurement and manipulation of adhesion forces between cancer cells and bone marrow endothelial cells using atomic force microscopy, Nanomedicine (London) (2012) 921–934.
[173] M. Lekka, D. Gil, W. Dąbroś, J. Jaczewska, A.J. Kulik, J. Lekki, et al., Characterization of N-cadherin unbinding properties in non-malignant (HCV29) and malignant (T24) bladder cells, J. Mol. Recognit. 24 (2011) 833–842.
[174] H. Jin, J. Pi, X. Huang, F. Huang, W. Shao, S. Li, et al., BMP2 promotes migration and invasion of breast cancer cells via cytoskeletal reorganization and adhesion decrease: an AFM investigation, Appl. Microbiol. Biotechnol. 93 (2012) 1715–1723.
[175] C.E. McNamee, S. Armini, S. Yamamoto, K. Higashitani, Determination of the binding of non-cross-linked and cross-linked gels to living cells by atomic force microscopy, Langmuir 25 (2009) 6977–6984.
[176] S. Ramachandran, A.P. Quist, S. Kumar, R. Lal, Cisplatin nanoliposomes for cancer therapy: AFM and fluorescence imaging of cisplatin encapsulation, stability, cellular uptake, and toxicity, Langmuir 22 (2006) 8156–8162.
[177] C.E. McNamee, Y. Aso, S. Yamamoto, Y. Fukumori, H. Ichikawa, K. Higashitani, Chemical groups that adhere to the surfaces of living malignant cells, Pharm. Res. 24 (2007) 2370–2380.
[178] T. Sulchek, R. Friddle, T. Ratto, H. Albrecht, S. DeNardo, A. Noy, Single-molecule approach to understanding multivalent binding kinetics, Ann. N. Y. Acad. Sci. 1161 (2009) 74–82.
[179] X. Zhang, X. Shi, L. Xu, J. Yuan, X. Fang, Atomic force microscopy study of the effect of HER 2 antibody on EGF mediated ErbB ligand–receptor interaction, Nanomedicine (2012) 627–635.
[180] F. Braet, D. Vermijlen, V. Bossuyt, R. De Zanger, E. Wisse, Early detection of cytotoxic events between hepatic natural killer cells and colon carcinoma cells as probed with the atomic force microscope, Ultramicroscopy 89 (2001) 265–273.
[181] L. Chopinet, C. Roduit, M.-P. Rols, E. Dague, Destabilization induced by electropermeabilization analyzed by atomic force microscopy, Biochim. Biophys. Acta Biomembr. 1828 (2013) 2223–2229.
[182] P.A. Corsetto, A. Cremona, G. Montorfano, I.E. Jovenitti, F. Orsini, P. Arosio, et al., Chemical–physical changes in cell membrane microdomains of breast cancer cells after omega-3 PUFA incorporation, Cell Biochem. Biophys. 64 (2012) 45–59.
[183] A. Won, A. Ruscito, A. Ianoul, Imaging the membrane lytic activity of bioactive peptide latarcin 2a, Biochim. Biophys. Acta 1818 (2012) 3072–3080.
[184] J. Wang, Z. Wan, W. Liu, L. Li, L. Ren, X. Wang, et al., Atomic force microscope study of tumor cell membranes following treatment with anti-cancer drugs, Biosens. Bioelectron. 25 (2009) 721–727.
[185] P. Venkatesan, S. Das, M.M.R. Krishnan, C. Chakraborty, K. Chaudhury, M. Mandal, Effect of AEE788 and/or Celecoxib on colon cancer cell morphology using advanced microscopic techniques, Micron 41 (2010) 247–256.
[186] K.S. Kim, C.H. Cho, E.K. Park, M.-H. Jung, K.-S. Yoon, H.-K. Park, AFM-detected apoptotic changes in morphology and biophysical property caused by paclitaxel in Ishikawa and HeLa cells, PLoS ONE 7 (2012) e30066.
[187] X.-P. Wang, T.-S. Chen, L. Sun, J.-Y. Cai, M.-Q. Wu, M. Mok, Live morphological analysis of taxol-induced cytoplasmic vacuolization [corrected] in human lung adenocarcinoma cells, Micron 39 (2008) 1216–1221.
[188] C. Huang, H. Jin, B. Song, X. Zhu, H. Zhao, J. Cai, et al., The cytotoxicity and anticancer mechanisms of alterporriol L, a marine bianthraquinone, against MCF-7 human breast cancer cells, Appl. Microbiol. Biotechnol. 93 (2012) 777–785.
[189] Z. Bai, H. Zhang, L. Zhu, W. Zuo, J. Ye, J. Feng, et al., Lithium inhibits cell volume regulation by acting on chloride channels and modifies ultrastructures of the cell membrane in nasopharyngeal carcinoma cells, Eur. J. Pharmacol. 641 (2010) 88–95.
[190] J. Jiang, H. Jin, L. Liu, J. Pi, F. Yang, J. Cai, Curcumin disturbed cell-cycle distribution of HepG2 cells via cytoskeletal arrangement, Scanning (2012) 256–260.
[191] C. Ke, H. Jin, J. Cai, AFM studied the effect of celastrol on β1 integrin-mediated HUVEC adhesion and migration, Scanning (2012) 316–326.
[192] M. Taranta, A.R. Bizzarri, S. Cannistraro, Probing the interaction between p53 and the bacterial protein azurin by single molecule force spectroscopy, J. Mol. Recognit. 21 (2008) 63–70.
[193] S.E. Cross, Y.-S. Jin, Q.-Y. Lu, J. Rao, J.K. Gimzewski, Green tea extract selectively targets nanomechanics of live metastatic cancer cells, Nanotechnology 22 (2011) 215101.
[194] M. Targosz-Korecka, R. Biedron, A.M. Szczygiel, G. Brzezinka, J. Szczerbinski, A. Zuk, Stiffness changes of tumor HEp2 cells correlates with the inhibition and release of TRAIL-induced apoptosis pathways, J. Mol. Recognit. 25 (2012) 299–308.
[195] R. Kaul-Ghanekar, S. Singh, H. Mamgain, A. Jalota-Badhwar, K.M. Paknikar, S. Chattopadhyay, Tumor suppressor protein SMAR1 modulates the roughness of cell surface: combined AFM and SEM study, BMC Cancer 9 (2009) 350.
[196] M. Lekka, P. Laidler, M. Labedź, A.J. Kulik, J. Lekki, W. Zajac, et al., Specific detection of glycans on a plasma membrane of living cells with atomic force microscopy, Chem. Biol. 13 (2006) 505–512.
[197] S.E. Cross, Y.-S. Jin, J. Tondre, R. Wong, J. Rao, J.K. Gimzewski, AFM-based analysis of human metastatic cancer cells, Nanotechnology 19 (2008) 384003.
[198] M. Lekka, Atomic force microscopy: a tip for diagnosing cancer, Nat. Nanotechnol. 7 (2012) 691–692.
[199] M.F. Murphy, F. Lilley, M.J. Lalor, S.R. Crosby, G. Madden, G. Johnston, et al., Evaluation of a nonlinear Hertzian-based model reveals prostate cancer cells respond differently to force than normal prostate cells, Microsc. Res. Tech. 76 (2013) 36–41.
[200] I. Sokolov, V. Kalaparthi, M. Kreshchuk, M.E. Dokukin, On averaging force curves over heterogeneous surfaces in atomic force microscopy, Ultramicroscopy 121 (2012) 16–24.
[201] E. Dague, A. Delcorte, J.-P. Latge, Y.F. Dufrene, Combined use of atomic force microscopy, X-ray photoelectron spectroscopy, and secondary ion mass spectrometry for cell surface analysis, Langmuir 24 (2008) 2955–2959.
[202] N. Kodera, D. Yamamoto, R. Ishikawa, T. Ando, Video imaging of walking myosin V by high-speed atomic force microscopy, Nature 468 (2010) 72–76.

[203] G.E. Fantner, R.J. Barbero, D.S. Gray, A.M. Belcher, Kinetics of antimicrobial peptide activity measured on individual bacterial cells using high-speed atomic force microscopy, Nat. Nanotechnol. 5 (2010) 280–285.
[204] Y.F. Dufrêne, D. Martínez-Martín, I. Medalsy, D. Alsteens, D.J. Müller, Multiparametric imaging of biological systems by force–distance curve-based AFM, Nat. Methods 10 (2013) 847–854.
[205] A. Raman, S. Trigueros, A. Cartagena, A.P.Z. Stevenson, M. Susilo, E. Nauman, et al., Mapping nanomechanical properties of live cells using multi-harmonic atomic force microscopy, Nat. Nanotechnol. 6 (2011) 809–814.
[206] G. Longo, L. Alonso-Sarduy, L.M. Rio, A. Bizzini, A. Trampuz, J. Notz, et al., Rapid detection of bacterial resistance to antibiotics using AFM cantilevers as nanomechanical sensors, Nat. Nanotechnol. 8 (2013) 522–526.
[207] M. Stolz, R. Gottardi, R. Raiteri, S. Miot, I. Martin, R. Imer, et al., Early detection of aging cartilage and osteoarthritis in mice and patient samples using atomic force microscopy, Nat. Nanotechnol. 4 (2009) 186–192.
[208] N. Buzhynskyy, J.-F. Girmens, W. Faigle, S. Scheuring, Human cataract lens membrane at subnanometer resolution, J. Mol. Biol. 374 (2007) 162–169.
[209] N. Buzhynskyy, R.K. Hite, T. Walz, S. Scheuring, The supramolecular architecture of junctional microdomains in native lens membranes, EMBO Rep. 8 (2007) 51–55.
[210] M. Plodinec, M. Loparic, C.A. Monnier, E.C. Obermann, R. Zanetti-Dallenbach, P. Oertle, et al., The nanomechanical signature of breast cancer, Nat. Nanotechnol. 7 (2012) 757–765.
[211] E. Henderson, D.S. Sakaguchi, Imaging F-actin in fixed glial cells with a combined optical fluorescence/atomic force microscope, NeuroImage 1 (1993) 145–150.
[212] J. Vesenka, C. Mosher, S. Schaus, L. Ambrosio, E. Henderson, Combining optical and atomic force microscopy for life sciences research, BioTechniques 19 (1995) 240–248(849, 852–853).
[213] S. Fukuda, T. Uchihashi, R. Iino, Y. Okazaki, M. Yoshida, K. Igarashi, et al., High-speed atomic force microscope combined with single-molecule fluorescence microscope, Rev. Sci. Instrum. 84 (2013) 073706.
[214] A. Colom, I. Casuso, F. Rico, S. Scheuring, A hybrid high-speed atomic force–optical microscope for visualizing single membrane proteins on eukaryotic cells, Nat. Commun. 4 (2013).
[215] Y. He, M. Lu, J. Cao, H.P. Lu, Manipulating protein conformations by single-molecule AFM-FRET nanoscopy, ACS Nano 6 (2012) 1221–1229.
[216] Q. Wang, M. Wang, S. Li, X. Xing, X. Liu, S. Dong, et al., AFM detection of mitogen-induced morphological changes in human B lymphocyte, Scanning 34 (2012) 60–67.

Chapter 2.2:

Use of Atomic Force Microscopy (AFM) to explore cell wall properties and response to stress in the yeast *Saccharomyces cerevisiae*

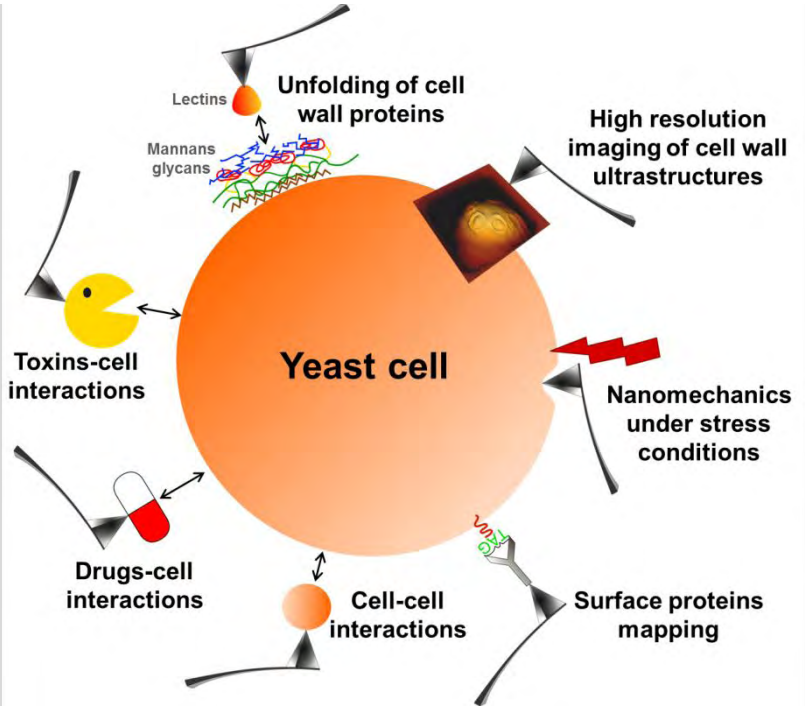

François J. M., Formosa C., Schiavone M., Pillet F., Martin-Yken H. and Dague E.

Current Genetics, **59**, 187-196, 2013

Abstract

0ver the past 20 years, the yeast cell wall has been thoroughly investigated by genetic and biochemical methods, leading to remarkable advances in the under- standing of its biogenesis and molecular architecture as well as to the mechanisms by which this organelle is remodeled in response to environmental stresses. Being a dynamic structure that constitutes the frontier between the cell interior and its immediate surroundings, imaging cell surface, measuring mechanical properties of cell wall or probing cell surface proteins for localization or interaction with external biomolecules are among the most burning questions that biologists wished to address in order to better understand the structure–function relationships of yeast cell wall in adhesion, flocculation, aggregation, bio- film formation, interaction with antifungal drugs or toxins, as well as response to environmental stresses, such as temperature changes, osmotic pressure, shearing stress, etc. The atomic force microscopy (AFM) is nowadays the most qualified and developed technique that offers the possibilities to address these questions since it allows working directly on living cells to explore and manipulate cell surface properties at nanometer resolution and to analyze cell wall proteins at the single molecule level. In this minireview, we will summarize the most recent contributions made by AFM in the analysis of the biomechanical and biochemical properties of the yeast cell wall and illustrate the power of this tool to unravel unexpected effects caused by environmental stresses and antifungal agents on the surface of living yeast cells.

Curr Genet (2013) 59:187–196
DOI 10.1007/s00294-013-0411-0

RESEARCH ARTICLE

Use of atomic force microscopy (AFM) to explore cell wall properties and response to stress in the yeast *Saccharomyces cerevisiae*

Jean Marie Francois · Cécile Formosa · Marion Schiavone · Flavien Pillet · Hélène Martin-Yken · Etienne Dague

Received: 10 June 2013 / Revised: 12 September 2013 / Accepted: 18 September 2013 / Published online: 27 September 2013

Abstract Over the past 20 years, the yeast cell wall has been thoroughly investigated by genetic and biochemical methods, leading to remarkable advances in the understanding of its biogenesis and molecular architecture as well as to the mechanisms by which this organelle is remodeled in response to environmental stresses. Being a dynamic structure that constitutes the frontier between the cell interior and its immediate surroundings, imaging cell surface, measuring mechanical properties of cell wall or probing cell surface proteins for localization or interaction with external biomolecules are among the most burning questions that biologists wished to address in order to better understand the structure–function relationships of yeast cell wall in adhesion, flocculation, aggregation, biofilm formation, interaction with antifungal drugs or toxins, as well as response to environmental stresses, such as temperature changes, osmotic pressure, shearing stress, etc. The atomic force microscopy (AFM) is nowadays the most qualified and developed technique that offers the possibilities to address these questions since it allows working directly on living cells to explore and manipulate cell surface properties at nanometer resolution and to analyze cell wall proteins at the single molecule level. In this minireview, we will summarize the most recent contributions made by AFM in the analysis of the biomechanical and biochemical properties of the yeast cell wall and illustrate the power of this tool to unravel unexpected effects caused by environmental stresses and antifungal agents on the surface of living yeast cells.

Keywords Atomic force microscopy (AFM) · *Saccharomyces cerevisiae* · Cell surface · Cell wall · Stress · Cellular sensors · Antifungal agents

Communicated by I. Hapala

Special issue: Yeast membranes and cell wall: From basics to applications

J. M. Francois (✉) · M. Schiavone · H. Martin-Yken
Université de Toulouse, INSA, UPS, INP, 135 avenue de Rangueil, 31077 Toulouse, France
e-mail: fran_jm@insa-toulouse.fr

J. M. Francois · M. Schiavone · H. Martin-Yken
INRA, UMR792 Ingénierie des Systèmes Biologiques et des Procédés, 31077 Toulouse, France

J. M. Francois · M. Schiavone · H. Martin-Yken
CNRS, UMR5504, 31400 Toulouse, France

C. Formosa · F. Pillet · E. Dague
CNRS, LAAS, 7 avenue du colonel Roche, 31077 Toulouse, France

C. Formosa · F. Pillet · E. Dague
Université de Toulouse, UPS, INSA, INP, ISAE, LAAS, 31077 Toulouse, France

Present Address:
F. Pillet
Institut de Pharmacologie et de Biologie Structurale, UMR 5089, 205 Route de Narbonne, 31077 Toulouse, France

Introduction

The yeast *Saccharomyces cerevisiae* has been used for millenniums in traditional biotechnology purposes such as making bread and ferment alcoholic beverages (Walker 1998). This yeast is nowadays employed as a microbial factory for the production of low-value/high-volume chemicals such as bioethanol (van Zyl et al. 2007) or high-value/low-volume chemicals such as artemisinin (Ro et al. 2006). During these biotechnological processes, yeast cells

have to cope with various environmental stresses that can be either physical (e.g. temperature and osmotic shock, dehydration, desiccation, shear/gravity stress, etc.); chemicals (e.g. ethanol toxicity, nutrient limitation, oxidation, pH shock) or biological (e.g. genotypic variation, cellular aging, competition with other microbes, etc.). The mechanisms involved in sensing these stresses and the resulting changes in cell physiology are crucial to understand how cells adapt and survive under these conditions. Investigation of these mechanisms has mainly relied on the use of molecular and biochemical approaches, which allowed demonstrating that cells can react to external cues by detecting environmental changes through cell sensors, embedded in the plasma membrane and then engaging signal transduction systems that trigger the appropriate intracellular responses (Zaman et al. 2008; Fuchs and Mylonakis 2009). A direct visualization and physical quantification of the response to these stresses would be quite relevant and complementary to these molecular and genetic studies. In particular, it would be interesting to visualize what is occurring at the cell surface and how much stresses impact on the biophysical properties of the cell wall. In addition, the cell surface of yeast cells is decorated with proteins that have a pivotal role in adhesion, communication and microbial infection (Jendretzki et al. 2011). How these cell surface proteins cope with the external cues and communicate the signal into the cell interior is still poorly understood. Answering these challenging questions is highly relevant for understanding several physiological and biotechnological processes, such as molecular recognition and cell adhesion, aggregation and flocculation, biofilm formation (Verstrepen and Klis 2006; Bauer et al. 2010), resistance to antifungal drugs (Mishra et al. 2007; Heinisch 2008) and barrier for mycotoxins compounds (Yiannikouris et al. 2006; Schatzmayr et al. 2006). In this context, atomic force microscopy (AFM) appears to be the complementary tool to tackle these crucial problems, because it allows manipulating at the single molecule or cell level and observing the cell surface at the nanometer resolution directly on living cells, which cannot be achieved with any other microscopy technologies including thin-section transmission electron microscopy (TEM). In this minireview, we will briefly explain the basic principles of AFM, discuss on the different methods that are employed to immobilize cells and provide an update of current works carried out using this tool to investigate biomechanical and biological properties of yeast cell wall. Finally, we will present an account of our recent works related to biophysical responses of yeast cells to some environmental stresses and antifungals. Due to limited space, this review will focus on researches carried out on the yeast *S. cerevisiae*, and when useful, other yeast species such as *Candida albicans* will be evoked.

Atomic force microscopy technology adapted to biological systems

Atomic force microscopy has been introduced as a high-resolution imaging technique in the eighties by Binnig and Quate (1986). Because this technique is based on the measure of the interaction force between a sharp tip and the sample, AFM belongs to the scanning probe microscopes family. These microscopes work by scanning a sample, while maintaining constant a given parameter. To achieve this goal, a cantilever terminated by a tip is mounted on a piezo-electric ceramic that is regulated by a control loop. AFM can operate in liquid, at a chosen temperature, providing high-resolution images of molecules or cells in a buffered solution by scanning the tip over the sample surface, which allows exploring the dynamic of cellular process under physiological conditions (Dufrene 2010). In addition this technology is also a force machine able to measure forces in the range of pico-Newtons. When the tip is approached to the surface sample and then retracted in the *Z* direction, forces versus distance (F-D) curves are recorded. On biological samples, the F-D curve consists in a non-contact and a deformation component (Fig. 1). Both the cantilever and the cell are deflected, and the true indentation of the cantilever in the soft sample can be obtained by subtracting this value to the one of cantilever deflection on a glass slide. This strategy has been used to investigate the nanomechanical properties of a large variety of microbial and mammals cells (Muller and Dufrene 2011). Moreover, the measure can be spatially resolved,

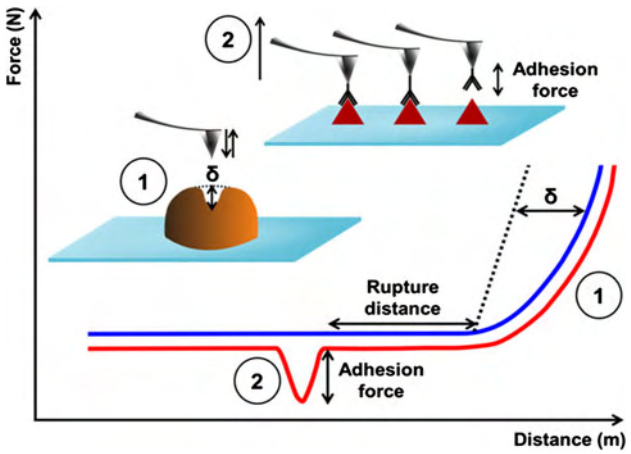

Fig. 1 Schematic representation of atomic force microscopy used in force spectroscopy mode. Force spectroscopy gives access to force curves that can be analyzed in two different ways. (1) Indentation (δ) is read on the force *curve* and represents the nanomechanical properties of the cell wall of yeasts. (2) single molecule force spectroscopy (SMFS) uses functionalized AFM tips with biomolecules or ligand; the interaction between a ligand chemically fixed on the AFM tip and the protein at the surface is given by the adhesion forces on the retracted force *curve* (*red curve*)

resulting in an elasticity map that can be related to some structural information about the cell surface. The retraction curve is also entailed of some relevant quantitative information on adhesion or interaction events. Indeed, when the AFM tip is in contact with a biological sample, a higher force is necessary to disrupt the interaction during the retraction of the tip from the sample, which results in the measurement of an adhesion force. In addition, the AFM tips can be functionalized with chemical groups, proteins or even with whole cells (Hinterdorfer and Dufrene 2006; Ebner et al. 2007; Jauvert et al. 2012), which allow to measure specific interactions or to manipulate single biomolecules. Accordingly, several force-distance curves, have to be recorded, giving rise to key insights into hydrophobicity of the surface when using CH3-functionalized tips (Dague et al. 2007; Alsteens et al. 2007), or to the localization and/or the binding strength of single proteins using functionalized tips with its corresponding antibody (Ebner et al. 2007).

Tools for immobilizing biological systems

A main advantage of AFM, compared to the scanning electron microscope (SEM), is the possibility to work in the buffer solution in which the biological systems like to be. Therefore, a major concern of AFM with these systems is to immobilize the cells, keeping them fully alive. The tip actually scans the surface and, therefore, induces lateral frictions that can move the biological sample. The paradox to be solved is to achieve a firm immobilization that does not damage this sample, while keeping it physiologically active. The quality of the results highly depends on the way to solve this paradox. Microbial cells immobilization on gel surface and on glass slides have been reviewed and criticized by Gad and Ikai 1995 and Dufrêne and coworkers (El Kirat et al. 2005). Briefly, these methods, as applied to yeast cells were (1) air drying or chemical fixation of a cells suspension on glass slide; (2) trapping yeast cells on soft material such agar or gelatin and (3) mechanical trapping in porous polycarbonate membranes. Air drying and chemical fixation are methods that very likely alter cell wall and cell vitality, while the use of soft material may contaminate the tips and thus can lead to erroneous results on the biophysical properties of the biological samples. Immobilization of yeast cells in a porous membrane requires a filtration through a polycarbonate membrane with pores of the size of the diameter of the cells. This is a very simple and very clean process. However, due to the low ratio between filled and unfilled pores, finding one cell under the AFM tip may take more than 15–30 min, even if the microscope is equipped with an inverted optical microscope because the membranes are impervious to light. Recently, we have proposed an alternative method that overcomes this limitation. It consists in a direct trapping of cells in micrometer-size chambers produced by soft lithography technology using an elastomer, such as polydimethylsulfoxane (PDMS) as the stamp (Whitesides et al. 2001) (Fig. 2). In this method, the filling rate can reach 80 %, using convective capillary deposition (Dague et al. 2011). This method allows the collection of data on several cells of different size in a reasonable time lapse. Using this technique, we showed heterogeneity of the Young's modulus (i.e. a measure of the elasticity) of yeast cells at the stationary phase on glucose (Dague et al. 2011). To summarize, trapping methods in porous membranes or in holes of PDMS stamps are the recommended immobilizing methods of biological cells as they are the best to preserve integrity and viability of the cells.

Biomechanical properties of cell wall

The yeast *S.cerevisiae* is surrounded by a thick, mechanically strong wall that is endowed of several key

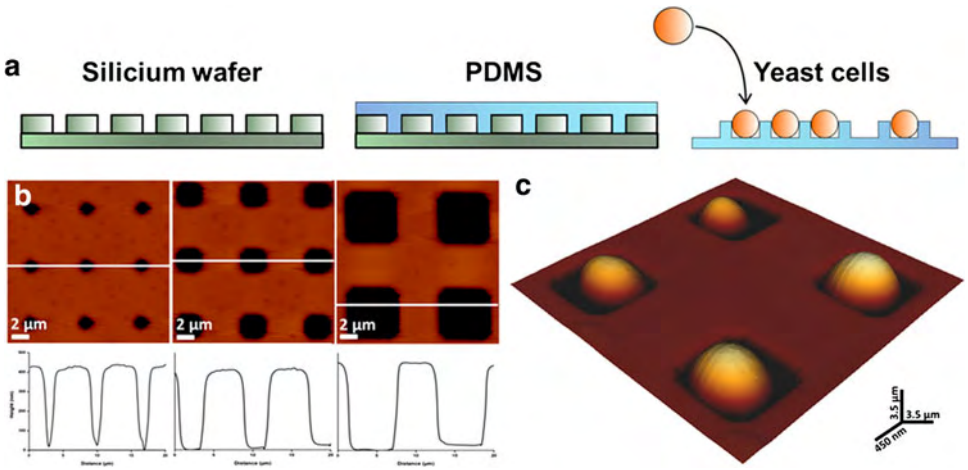

Fig. 2 Immobilization of living *Saccharomyces cerevisiae* cells. **a** Schematic representation of yeast cells in PDMS microstructured stamps. **b** Height AFM images and corresponding cross-sections of microstructured PDMS stamps. The structures ranged from 1.5 to 6.0 µm large and 2–3 µm depth. **c** *S. cerevisiae* cells trapped in the microstructured PDMS stamps as imaged by atomic force microscopy

physiological functions including maintaining cell shape, cell integrity and protecting cell interior of potentially harmful compounds from the environment. The cell wall also harbors several proteins that are implicated in molecular recognition and adhesion (Klis et al. 2006, 2009; Levin 2005). The chemical composition of yeast cell wall is well known. It consists in a microfibrillar network of β-glucans (β-1,3 and β-1,6-glucans) that represent 50–60 % of the cell wall mass, overlaid by highly glycosylated proteins decorated by long chains of mannose residues representing 40–50 % of the cell wall mass. Chitin, a linear polysaccharide of β-linked *N*-acetylglucosamine, is the third component of yeast cell wall. Though it is a minor component in term of quantity (1–3 %), it is indispensable for the yeast cell (Cabib et al. 2001). Over the last 15 years, the complexity of the cell wall architecture has emerged from detailed genetic, molecular and biochemical studies, which led to the discovery of several interconnections among these various wall components to form macromolecular complexes (see (Free 2013) and (Orlean 2012) for excellent and recent reviews on this subject). Although the precise assembly processes and proteins involved in these interconnections are not yet completely resolved, a modular concept of the cell wall has been proposed to account for its structural organization (Kollar et al. 1997; Smits et al. 1999; Klis et al. 2006). In addition, the molecular architecture of cell wall is not static but is constantly remodeled depending on growth conditions, morphological development as well as in response to cell surface stresses. This cell wall remodeling process is principally under the control of the cell wall integrity (CWI) signaling pathway that transmits the signals from the cell surface sensors to a MAP kinases cascade (Levin 2011), with the main consequence to reorganize cell wall architecture through changes in carbohydrate polymers of the cell wall, in the cross-links between these polymers and in a transient redistribution of the cell wall repair machinery to the site of the cell wall injuries (Klis et al. 2006; Lesage and Bussey 2006). These remarkable molecular and biochemical works have raised several new questions on the essential function of cell wall that requires innovative approaches and methods. Among them, AFM which allows directly visualizing and probing the ultrastructure of the cell wall is well dedicated to provide answers to several burning questions such as to know whether the mechanical strength of the cell that is largely attributed to its cell wall, is dependent on a specific component of this wall or not. In this context, and using various cell wall mutants altered in levels of β-glucan, mannans and chitin or in the cross-links between chitin and β-glucan, we found that the nanomechanical properties of the yeast cell wall could not be ascribed to a specific cell wall component but were mainly dependent on the intrinsic molecular organization of the cell wall, with cross-links of chitin to β-glucan playing an important role in the cell wall elasticity (Dague et al. 2010). These results were in frame with another report showing that the mechanical properties of the filamentous fungi *A. nidulans* were dependent on the change in the molecular structure of the hyphae cell walls rather than on the mere chemical composition of the wall (Zhao et al. 2005). However, this conclusion must be balanced by the fact that the elasticity, quantified by the Young's modulus in MPa units, is apparently 3–5 times higher at the bud scar than elsewhere on the mother cell (Touhami et al. 2003;Alsteens et al. 2008), suggesting that chitin, which is more abundant at this site, has a valuable role in the elasticity of the cell. A similar conclusion was recently reached from the study of the yeast *C. albicans* exposed to the antifungal drug caspofungin. It was found that chitin levels increased proportionally with the increase of caspofungin dose administrated to *C. albicans* cells, and this proportionality was reflected in an increase of the Young's modulus of this yeast cell (Formosa et al. 2013). This result corroborated an earlier AFM analysis of immobilized *Candida parapsilosis* on a glass slide that showed higher adhesion forces at the incipient bud, and also illustrated the heterogeneity at the cell surface that might have an impact on adhesion of these yeast cells (Mendez-Vilas et al. 2006). However, the importance of chitin in elasticity of a microbial cell is still an open question based on the finding that a *S. carlsbergensis* strain, which belongs to the *S. cerevisiae* species (Dunn and Sherlock 2008) and divides like this yeast species, shows comparable elasticity at the bud scar and on the rest of the mother cell surface (Alsteens et al. 2008).

Not solely cell wall remodeling but also cell wall thickness may vary depending on growth conditions, stress, mutations, etc., as indicated by the fact that the wall mass can fluctuate from 10 to 25 % of the total cell mass (Aguilar-Uscanga and Francois 2003; Backhaus et al. 2010). Thin-section transmission electron microscopy (TEM) has been the current method to determine cell wall thickness, but this method requires fixation and vacuum condition, precluding a dynamic investigation of wall thickness in living cells. An exquisite method to reach this goal was recently developed by Dupres et al. 2010. It is based on the genetic construction and expression of a molecular ruler from the His-tagged mechanosensor Wsc1, and its detection at the cell surface using AFM tips functionalized with Ni^{2+}-nitriloacetate groups. The rational of this idea came from a previous work of the same researchers, which showed that the Wsc1 membrane sensor that is required for sensing temperature, antifungal and pH stresses (Lodder et al. 1999; Reinoso-Martin et al. 2003; Serrano et al. 2006), is embedded in the plasma membrane by a single transmembrane domain and extends to 80-nm long in the cell wall by a large external serine/threonine domain

(STR). To reach the outermost cell surface, the Wsc1 sensor was elongated with a stepwise lengthening of a chimeric outer STR region of another sensor Mid2 and terminated with a His-tag. Plotting the amount of engineered Wsc1 sensors detected by the Ni^{2+}-NTA tip of AFM as a function of the sensor length resulted in a sharp increase of the curve at around 115 nm. This value of the cell wall thickness was about 10 % above the one determined by TEM (Backhaus et al. 2010). In addition, this molecular ruler method allows measuring the change in wall thickness in response to genetic intervention or environmental effects. For instance, these authors showed that the thickness of the cell wall was increased by 20 % in strains expressing mutant versions of the Wsc1 that prevent its endocytosis and internalization (Dupres et al. 2010). This result was explained by the generation of a permanent signal due to increased concentration of this sensor at the plasma membrane, which in turn triggers a more pronounced cell wall synthesis (Wilk et al. 2010). More intriguingly, the same authors found that the thickness of cell wall was hard to evaluate in yeast cells treated with the oxidative agent diamide, suggesting either that this stress strongly damaged the cell wall structure or that the expression and/or secretion of the Wsc1 sensor was impaired by the oxidative stress (Dupres et al. 2010).

Exploration of biochemical properties of cell surface using AFM

As already stated above, the yeast cell wall is a dynamic organelle that has to adapt to the changing environment. In respect to this dynamic notion, Pelling et al. (2004) reported nanomechanical motions of the *S. cerevisiae* cell wall with a periodicity in the range of 0.8–1.6 kHz and amplitudes of approximately 3 nm. These observations were obtained using AFM in a contact mode bearing cantilevers with a spring constant (k) much lower than that of the cell wall (k_{cell}) and by recording cantilever motion in contact with the cell as a function of time in an acoustically isolated environment with extremely low noise level. The fact that these nanomechanical motions were found to be temperature dependent, were inhibited by metabolic inhibitors known to impair ATP production, and that the force generated by the amplitude of these motions was in the range of 10 nN, led these authors to suggest that these nanoscale movements were of biological origins and could be driven by molecular motors, such as dynein, kinesin or myosin in a concerted and cooperative manner. It is thus tempting to associate these cell wall movements with the motion of the yeast actin cytoskeleton. This system is essential in critical processes such as endocytosis, cytokinesis, cell polarity, and cell morphogenesis that very likely have an impact on the remodeling of the cell surface (Guo et al. 2009; Lottersberger et al. 2006). Yeast cytoskeleton motility is driven by the coordinated activities of a set of 20–30 highly conserved actin-associated proteins. This actin network is known to rapidly assemble into patches, cables and rings, and disassemble in a spatially and temporally regulated manner in response to internal and external cues (reviewed in (Moseley and Goode 2006)). Investigating the cell wall motion using mutants of the actin skeleton or drugs such as latrunculine that inhibits actin polymerization should bring light into this potential role in the cell wall motion.

The outer layer of the yeast cell wall is made of highly mannosylated proteins decorated with large polysaccharides complex of 150 or more D-mannose units (mannan layers). Chemical and genetic studies pioneered by Ballou and collaborators have largely elucidated the structure of these polysaccharides attached to cell wall proteins (Ballou 1990). This mannoproteins coat bears important biochemical and biotechnological properties, such as adhesion, aggregation and flocculation (Caridi 2006; Verstrepen and Klis 2006) as well as virulence (de Groot et al. 2005; de Groot et al. 2008). Expression of these properties can be exerted through various types of interactions that can involve hydrophobic or electrostatic forces, or specific receptor-ligand binding forces. These forces can be measured using AFM tips that have been chemically or biochemically functionalized. For instance, Dague et al. (2007) showed that the hydrophobicity of bacterial surfaces could be quantified using hydrophobic, methyl-terminated tips. Using the same chemically-modified AFM tip, local hydrophobic character of two medically important microorganisms, *Aspergillus fumigatus* and *Mycobacterium bovis* were probed, revealing uniform distribution of hydrophobicity on the surface due to hydrophobin proteins for the filamentous fungus, and to the mycolic acid layer for the second microorganism (Dague et al. 2008). Conversely, Gotzinger et al. (2007) measured the adhesion force of *S. cerevisiae* to different types of silica surface using a single immobilized yeast cell at the apex of the AFM cantilever. Probing mannoproteins layer was made possible by functionalizing AFM tip with concanavalin A, a tetrameric protein of 102,300 kDa that shows strong affinity to mannose residues, with an unbinding force estimated around 60 pN (e.g. the force reflecting the rupture of a single ConA-mannose complex Alsteens et al. 2008). This technique was initiated by Gad et al. (1997) which have shown that the binding force between mannans and the ConA was comprised between 75 and 200 pN. More interestingly, they showed that the retraction curve of the functionalized tip with ConA could be very long, suggesting that the mannoproteins could be pulled out by the AFM tip via its

binding to the ligand. Recently, Alsteens et al. (2008) compared mannans properties of *S. carlsbergensis* and *S. cerevisiae* using a functionalized AFM tip with ConA. They showed that the polysaccharides were homogeneously distributed on both strains, but only the yeast *S. cerevisiae* species exhibited an adhesion force over a range of 0–400 nm, suggesting difference in the stretching of these macromolecules between the two yeast species. Based on these data, these authors suggested that the much longer rupture distances on *S. cerevisiae* may reflect the stretching of both mannans and the polypeptide chains of the mannoproteins. According to these authors, the different physical properties of the mannoproteins between the two species may explain why the surface of *S cerevisiae* is more hydrophobic than that of *S. carlsbergensis*, and hence why this former yeast species associated with CO_2 bubble and rise to the top of the fermented suspensions, whereas *S. carlsbergensis* is a bottom-fermenting brewing strain (Alsteens et al. 2008).

Exploring cell surface in response to stresses

Atomic force microscopy is the appropriate tool to directly visualize and quantify the physical, morphological and structural changes that can take place at the cell surface of yeast in response to various types of stresses. These biophysical data shall be pertinent for better understanding how cells adapt and survive to these adverse conditions, and also for many industrial processes under which yeasts are subjected to extreme culture conditions (high sugars or high ethanol concentration, high shearing force, high cell density, etc.). The group of Graeme Walker in Dundee (Scotland) has pioneered this research and published several papers on AFM study of the yeast *S. cerevisiae* and *S. pombe* in response to thermal and osmotic stresses (Adya et al. 2006), ethanol shock (Canetta et al. 2006) and oxidative stress (Canetta et al. 2009). In these studies, the mode of immobilizing cells was to spread a yeast suspension before and at different times after the stress on a glass slide and allow them to dry at room temperature for 5 h before AFM analysis. The obtained AFM images showed highly dense and compacted cells, the viability and cellular activity of which were uncertain, even though the authors evaluated these parameters before immobilizing cells. Roughness of the surface of yeast cells subjected to these different stresses as determined from the height images was shown to be dramatically increased with both the intensity (i.e. 40, 50 or 60°°C) and the duration of the stress. Eventually, these stresses caused shrinkage of the cells, likely by loss of cell turgor pressure, and causing rapid loss of cytoplasmic water. On the other hand, treatment of yeast cells with 1 % H_2O_2 for 10 min led to the formation of cavities, the size of which was much larger for *S. pombe* than *S. cerevisiae*. Upon longer incubation, this treatment caused a deterioration of the cell surface with appearance of very deep wrinkles. Altogether, these data, although only descriptive and subject to caution due to the immobilization techniques, were indicative that the cell wall structure is altered in response to harmful environmental stresses.

We have recently revisited the effects of heat stress and ethanol shock on the nanomechanical properties of *S. cerevisiae* cells by applying the method of immobilization described above and which consists in trapping the yeasts in micrometer square PDMS chambers by convective/capillarity method (Dague et al. 2011). The AFM images showed that a temperature shift of the yeast culture from 30 to 42 °C induced in less than 1 h the formation of a circular structure that takes its origin at a particular location on the cell surface and evolved as concentric rings at the cell surface (Fig. 3). These circular rings reached 2–3 µm diameter, which are larger than that of a normal bud scar. Concomitantly, the cell wall elasticity increased by twofold, which was accompanied by a twofold increase of chitin content of the heat stressed cells. This morphological process taking place at the cell surface was found to be dependent on genes required for the budding process such as *BNI1* and *CHS3,* and under the control of the CWI signaling pathway. From these genetic results, we came to the suggestion that the formation of these circular rings

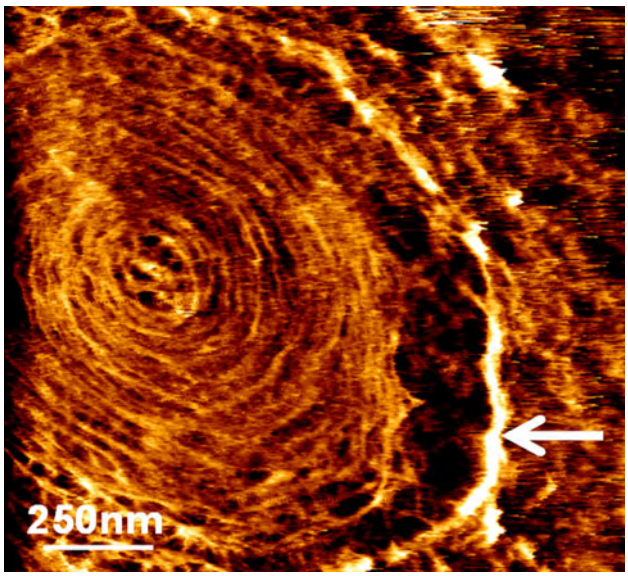

Fig. 3 Exploring the ultrastructure of yeast cell surface in response to a thermal stress by AFM Exponential growing yeast cells on YPD were subjected to temperature shift from 30 to 42 °C. After 1 h exposure, cells were immobilized in polycarbonate porous membranes and imaged by AFM in contact mode at very low applied force (<0.1 nN). High-resolution deflection image shows a succession of concentric rings, ended with a major ring (*white arrow*)

arise from a defective bud scar or bud emergence site during the temperature stress (Pillet et al. submitted for publication).

The other biotechnological relevant stress we recently explored was the response of yeast cells to ethanol shock. The tolerance of the yeast *S. cerevisiae* to its main fermentation product ethanol has been the concern of extensive researches for many years, with the aim to understand the mechanism of its toxicity (reviewed in Stanley et al. 2010; Ma and Liu 2010). In spite of a wealth of biochemical and molecular data on the response of yeast to ethanol stress, there is almost no physical data describing the biophysical effect that ethanol may exert at the single cell level. Using the same methodology as described above for heat shock, we explored the nanomechanical properties of the yeast BY4741 strain cultivated on a glucose medium exposed to 9 % ethanol for 0.5–5 h. This treatment resulted in a fivefold drop in the cell wall elasticity, in spite of the fact that the cell wall polysaccharides composition of the ethanol-treated yeast cells remained almost unchanged. These data suggested that one of the immediate effects of ethanol on the yeast cells is to inhibit cross-linking and remodeling systems that are essential in the construction of the molecular architecture of the yeast cell wall (Elzstein et al. submitted for publication).

Exploring cell surface in response to antifungal drugs

Cell wall is the target of choice for antifungal agents since it is a specific armor that does not exist in mammalian cells and its damaging leads to cell lysis and cell death (Heinisch 2005; Carrillo-Munoz et al. 2006). Due to the essential function of this organelle, exposure of yeast cells to antifungal agents such as caspofungin, a potent and specific inhibitor of β-glucan synthase (Deresinski and Stevens 2003) induces activation of the cell wall integrity pathway that eventually culminates into transcriptomic and metabolic responses aiming at counteracting the disastrous effects caused by this drug on cell wall (Lesage et al. 2004; Reinoso-Martin et al. 2003). These molecular data were recently complemented by two independent AFM studies of the caspofungin effects on the yeasts *C. albicans* and *S. cerevisiae* (Kirat-Chatel et al. 2013; Formosa et al. 2013). It was found that administration of this antifungal drug induced a deep cell wall remodeling in both yeast species, but quantitatively, the changes in cell wall composition were more pronounced in *C. albicans* cells, with notably a remarkable rise in chitin as a function of the caspofungin dose administrated to the *C. albicans* cells and with a concurrent increase in cell elasticity (Formosa et al. 2013). In addition, at low doses of caspofungin (i.e. at around 50 ng/ml or 0.5 MIC) the cell surface of *C. albicans* exhibited dramatic morphological changes that were accompanied by strong induction of cell surface adhesin Als1 and increased cell surface hydrophobicity (Kirat-Chatel et al. 2013). On the other hand, treatment of *S. cerevisiae* cells with high doses of caspofungin resulted in an impairment of cytokinesis (Formosa et al. 2013). Kim et al. (2011, 2012) also used AFM to investigate the effects of three other antifungal agents, namely flucytosine, amphotericin B and allicin on the changes of morphology and biophysics properties of *C. albicans*. Although the immobilizing technique may have impaired their analysis since the cells were fixed on glass slides using 0.5 % glutaraldehyde, these authors showed clearly that these drugs caused dramatic changes at the cell surface, which ended up by strong deformation and shrinkage. However, because of the mode of immobilization, it is difficult to further conclude on the effects of these drugs on the nanomechanical properties of the *C. albicans* wall. Notwithstanding these problems, AFM clearly unravels unexpected effects of antifungal agents on fungal adhesion and cell growth, which may help understanding the molecular basis of microbes–drugs interactions and opens new avenues for finding novel cellular targets and developing new therapeutic agents.

Concluding remarks and perspectives

The main purpose of this minireview was to emphasize how much the AFM technology can bring to the biologist for better understanding the cell wall biogenesis, for monitoring the cell surface dynamic in response to external cues and for answering some cell biology questions that cannot be seized by any other technical means. A typical example of these biological questions is illustrated by the discovery that the cell surface Wsc1 sensor protein behaves like a linear nanospring able to withstand high mechanical force and to respond to cell wall stress by modifying the spring constant (Dupres et al. 2009). As schematically illustrated in Fig. 4, combination of AFM with genetic and molecular manipulations is a powerful mean to address many cell biology questions of both fundamental and applied relevance, such as the precise role of cell wall remodeling enzymes in the nanomechanical properties of the yeast cell, the mechanism that is at the onset of cell adhesion, how cell surface proteins localize, assemble, and interact on the surface of living cells, as well as to extend the study of the budding process (Cabib and Arroyo 2013). These two latter questions are particularly relevant for understanding cell wall molecular organization and remodeling, since yeast has evolved by developing three different ways of attaching proteins to the polysaccharide moiety. A first class are proteins bound non covalently to

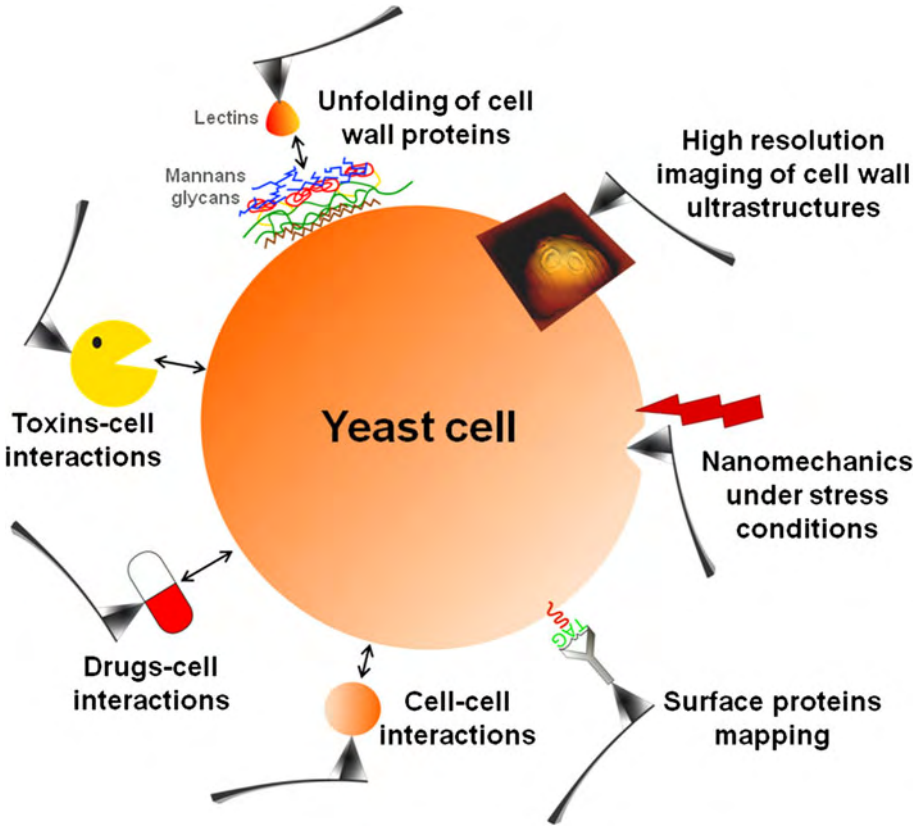

Fig. 4 Schematic illustration of the yeast cell biology questions that can be addressed by AFM

the β-1,3-glucan network (the SCWs family), a second category are proteins attached covalently through a remnant of the GPI anchor to β-1,6-glucans (the GPI-CWPs), while a third class are cell wall mannoproteins characterized by Protein Internal Repeat regions (PIR-CWPs or CCWs family) that are directly linked to β-1,3-glucans (Klis et al. 2006).

Despite its remarkable benefits in cell biology, AFM is still a technology under development that mainly suffers from a poor temporal resolution (typically registering an image takes 10–20 min), and bears artifacts linked to cell fixation, tips geometry and alteration, etc. (see (Heinisch et al. 2012) for a recent update on the advantages and limitations of AFM in cell biology). However, major breakthroughs in developing new quantitative-AFM based imaging techniques are appearing at a good pace. This includes the development of high-speed AFM, which allows operating at millisecond timescale and thus offers possibilities for exploring cellular dynamics (Casuso et al. 2011). Also, with the peak force tapping (PFT) or quantitative (Q) modes, the researcher is able to image the structure and physical properties of cells at high resolution (nm scale) and high speed. In addition, PFT using functionalized tips with biomolecules affords unprecedented possibilities for mapping biological sites on living cells at near molecular resolution in the range of 5 nm (Chopinet et al. 2013). This technology has been used to map the mechanosensor Mid2 at the yeast cell surface showing a higher density of this protein at the bud scar area than elsewhere on the mother cell (Alsteens et al. 2012). Combined with near-field scanning optical microscopy (NSOM) in which the tip is replaced by an optical fiber with a nanoscale aperture, topographic and optical images are simultaneously generated, revealing the spatial distribution of fluorescently labeled molecules at unprecedented nanometer spatial resolution (Hinterdorfer et al. 2012). Deciphering the nanoscale architecture of yeast cell walls, understanding how cell surface receptor assemble into nanodomains, modulate their functional state and communicate to confer efficient functional responses upon cell wall stress are some of the fundamental questions that can be addressed today by combining single-molecule imaging AFM with genetic tools, and thereby helping to answer several unresolved cell biology issues.

References

Adya AK, Canetta E, Walker GM (2006) Atomic force microscopic study of the influence of physical stresses on *Saccharomyces cerevisiae* and *Schizosaccharomyces pombe*. FEMS Yeast Res 6:120–128

Aguilar-Uscanga B, Francois JM (2003) A study of the yeast cell wall composition and structure in response to growth conditions and mode of cultivation. Lett Appl Microbiol 37:268–274

Alsteens D, Dague E, Rouxhet PG, Baulard AR, Dufrene YF (2007) Direct measurement of hydrophobic forces on cell surfaces using AFM. Langmuir 23:11977–11979

Alsteens D, Dupres V, Mc EK, Wildling L, Gruber HJ, Dufrene YF (2008) Structure, cell wall elasticity and polysaccharide properties of living yeast cells, as probed by AFM. Nanotechnology 19:384005

Alsteens D, Dupres V, Yunus S, Latge JP, Heinisch JJ, Dufrene YF (2012) High-resolution imaging of chemical and biological sites on living cells using peak force tapping atomic force microscopy. Langmuir 28:16738–16744

Backhaus K, Heilmann CJ, Sorgo AG, Purschke G, de Koster CG, Klis FM, Heinisch JJ (2010) A systematic study of the cell wall composition of *Kluyveromyces lactis*. Yeast 27:647–660

Ballou CE (1990) Isolation, characterization, and properties of *Saccharomyces cerevisiae mnn* mutants with nonconditional protein glycosylation defects. Methods Enzymol 185:440–470

Bauer FF, Govender P, Bester MC (2010) Yeast flocculation and its biotechnological relevance. Appl Microbiol Biotechnol 88:31–39

Binnig G, Quate CF (1986) Atomic force microscopy. Phys Rev Lett 56:930–933

Cabib E, Arroyo J (2013) How carbohydrates sculpt cells: chemical control of morphogenesis in the yeast cell wall. Nat Rev Microbiol 11:648–655

Cabib E, Roh DH, Schmidt M, Crotti LB, Varma A (2001) The yeast cell wall and septum as paradigms of cell growth and morphogenesis. J Biol Chem 276:19679–19682

Canetta E, Adya AK, Walker GM (2006) Atomic force microscopic study of the effects of ethanol on yeast cell surface morphology. FEMS Microbiol Lett 255:308–315

Canetta E, Walker GM, Adya AK (2009) Nanoscopic morphological changes in yeast cell surfaces caused by oxidative stress: an atomic force microscopic study. J Microbiol Biotechnol 19:547–555

Caridi A (2006) Enological functions of parietal yeast mannoproteins. Antonie Van Leeuwenhoek 89:417–422

Carrillo-Munoz AJ, Giusiano G, Ezkurra PA, Quindos G (2006) Antifungal agents: mode of action in yeast cells. Rev Esp Quimioter 19:130–139

Casuso I, Rico F, Scheuring S (2011) High-speed atomic force microscopy: structure and dynamics of single proteins. Curr Opin Chem Biol 15:704–709

Chopinet L, Formosa C, Rols MP, Duval RE, Dague E (2013) Imaging living cells surface and quantifying its properties at high resolution using AFM in QI mode. Micron 48:26–33

Dague E, Alsteens D, Latge JP, Verbelen C, Raze D, Baulard AR, Dufrene YF (2007) Chemical force microscopy of single live cells. Nano Lett 7:3026–3030

Dague E, Delcorte A, Latge JP, Dufrene YF (2008) Combined use of atomic force microscopy, X-ray photoelectron spectroscopy, and secondary ion mass spectrometry for cell surface analysis. Langmuir 24:2955–2959

Dague E, Bitar R, Ranchon H, Durand F, Yken HM, Francois JM (2010) An atomic force microscopy analysis of yeast mutants defective in cell wall architecture. Yeast 27:673–684

Dague E, Jauvert E, Laplatine L, Viallet B, Thibault C, Ressier L (2011) Assembly of live micro-organisms on microstructured PDMS stamps by convective/capillary deposition for AFM bioexperiments. Nanotechnology 22:395102

de Groot PW, Ram AF, Klis FM (2005) Features and functions of covalently linked proteins in fungal cell walls. Fungal Genet Biol 42:657–675

de Groot PW, Kraneveld EA, Yin QY, Dekker HL, Gross U, Crielaard W, de Koster CG, Bader O, Klis FM, Weig M (2008) The cell wall of the human pathogen *Candida glabrata*: differential incorporation of novel adhesin-like wall proteins. Eukaryot Cell 7:1951–1964

Deresinski SC, Stevens DA (2003) Caspofungin. Clin Infect Dis 36:1445–1457

Dufrene YF (2010) Atomic force microscopy of fungal cell walls: an update. Yeast 27:465–471

Dunn B, Sherlock G (2008) Reconstruction of the genome origins and evolution of the hybrid lager yeast *Saccharomyces pastorianus*. Genome Res 18:1610–1623

Dupres V, Alsteens D, Wilk S, Hansen B, Heinisch JJ, Dufrene YF (2009) The yeast Wsc1 cell surface sensor behaves like a nanospring in vivo. Nat Chem Biol 5:857–862

Dupres V, Dufrene YF, Heinisch JJ (2010) Measuring cell wall thickness in living yeast cells using single molecular rulers. ACS Nano 4:5498–5504

Ebner A, Hinterdorfer P, Gruber HJ (2007) Comparison of different aminofunctionalization strategies for attachment of single antibodies to AFM cantilevers. Ultramicroscopy 107:922–927

El Kirat K, Burton I, Dupres V, Dufrene YF (2005) Sample preparation procedures for biological atomic force microscopy. J Microsc 218:199–207

Formosa C, Schiavone M, Martin-Yken H, Francois JM, Duval RE, Dague E (2013) Nanoscale effects of Caspofungin against two yeast species; *Saccharomyces cerevisiae* and *Candida albicans*. Antimicrob Agents Chemother 57:3498–3506

Free SJ (2013) Fungal cell wall organization and biosynthesis. Adv Genet 81:33–82

Fuchs BB, Mylonakis E (2009) Our paths might cross: the role of the fungal cell wall integrity pathway in stress response and cross talk with other stress response pathways. Eukaryot Cell 8:1616–1625

Gad M, Ikai A (1995) Method for immobilizing microbial cells on gel surface for dynamic AFM studies. Biophys J 69:2226–2233

Gad M, Itoh A, Ikai A (1997) Mapping cell wall polysaccharides of living microbial cells using atomic force microscopy. Cell Biol Int 21:697–706

Gotzinger M, Weigl B, Peukert W, Sommer K (2007) Effect of roughness on particle adhesion in aqueous solutions: a study of *Saccharomyces cerevisiae* and a silica particle. Colloids Surf B Biointerfaces 55:44–50

Guo S, Shen X, Yan G, Ma D, Bai X, Li S, Jiang Y (2009) A MAP kinase dependent feedback mechanism controls Rho1 GTPase and actin distribution in yeast. PLoS ONE 4:e6089

Heinisch JJ (2005) Baker's yeast as a tool for the development of antifungal kinase inhibitors–targeting protein kinase C and the cell integrity pathway. Biochim Biophys Acta 1754:171–182

Heinisch JJ (2008) Baker's yeast as a tool for the development of antifungal drugs which target cell integrity—an update. Expert Opin Drug Discov 3:931–943

Heinisch JJ, Lipke PN, Beaussart A, El Kirat CS, Dupres V, Alsteens D, Dufrene YF (2012) Atomic force microscopy—looking at mechanosensors on the cell surface. J Cell Sci 125:4189–4195

Hinterdorfer P, Dufrene YF (2006) Detection and localization of single molecular recognition events using atomic force microscopy. Nat Methods 3:347–355

Hinterdorfer P, Garcia-Parajo MF, Dufrene YF (2012) Single-molecule imaging of cell surfaces using near-field nanoscopy. Acc Chem Res 45:327–336

Jauvert E, Dague E, Severac M, Caminade A, Ressier L, Majoral J, Trevisiol E (2012) Probing sungle molecule interactions by AFM using biofunctionalized dendritips. Sensor Actuators B Chem 168:436–441

Jendretzki A, Wittland J, Wilk S, Straede A, Heinisch JJ (2011) How do I begin? Sensing extracellular stress to maintain yeast cell wall integrity. Eur J Cell Biol 90:740–744

Kim KS, Kim YS, Han I, Kim MH, Jung MH, Park HK (2011) Quantitative and qualitative analyses of the cell death process in Candida albicans treated by antifungal agents. PLoS ONE 6:e28176

Kim YS, Kim KS, Han I, Kim MH, Jung MH, Park HK (2012) Quantitative and qualitative analysis of the antifungal activity of allicin alone and in combination with antifungal drugs. PLoS ONE 7:e38242

Kirat-Chatel S, Beaussart A, Alsteens D, Jackson DN, Lipke PN, Dufrene YF (2013) Nanoscale analysis of caspofungin-induced cell surface remodelling in *Candida albicans*. Nanoscale 5:1105–1115

Klis FM, Boorsma A, de Groot PW (2006) Cell wall construction in Saccharomyces cerevisiae. Yeast 23:185–202

Klis FM, Sosinska GJ, de Groot PW, Brul S (2009) Covalently linked cell wall proteins of Candida albicans and their role in fitness and virulence. FEMS Yeast Res 9:1013–1028

Kollar R, Reinhold BB, Petrakova E, Yeh HJ, Ashwell G, Drgonova J, Kapteyn JC, Klis FM, Cabib E (1997) Architecture of the yeast cell wall. Beta(1→6)-glucan interconnects mannoprotein, beta(1→)3-glucan, and chitin. J Biol Chem 272:17762–17775

Lesage G, Bussey H (2006) Cell wall assembly in *Saccharomyces cerevisiae*. Microbiol Mol Biol Rev 70:317–343

Lesage G, Sdicu AM, Menard P, Shapiro J, Hussein S, Bussey H (2004) Analysis of beta-1,3-glucan assembly in *Saccharomyces cerevisiae* using a synthetic interaction network and altered sensitivity to caspofungin. Genetics 167:35–49

Levin DE (2005) Cell wall integrity signaling in *Saccharomyces cerevisiae*. Microbiol Mol Biol Rev 69:262–291

Levin DE (2011) Regulation of cell wall biogenesis in *Saccharomyces cerevisiae*: the cell wall integrity signaling pathway. Genetics 189:1145–1175

Lodder AL, Lee TK, Ballester R (1999) Characterization of the wsc1 protein, a putative receptor in the stress response of *Saccharomyces cerevisiae*. Genetics 152:1487–1499

Lottersberger F, Panza A, Lucchini G, Piatti S, Longhese MP (2006) The *Saccharomyces cerevisiae* 14-3-3 proteins are required for the G1/S transition, actin cytoskeleton organization and cell wall integrity. Genetics 173:661–675

Ma M, Liu ZL (2010) Mechanisms of ethanol tolerance in *Saccharomyces cerevisiae*. Appl Microbiol Biotechnol 87:829–845

Mendez-Vilas A, Diaz J, Donoso MG, Gallardo-Moreno AM, Gonzalez-Martin ML (2006) Ultrastructural and physico-chemical heterogeneities of yeast surfaces revealed by mapping lateral-friction and normal-adhesion forces using an atomic force microscope. Antonie Van Leeuwenhoek 89:495–509

Mishra NN, Prasad T, Sharma N, Payasi A, Prasad R, Gupta DK, Singh R (2007) Pathogenicity and drug resistance in Candida albicans and other yeast species. A review. Acta Microbiol Immunol Hung 54:201–235

Moseley JB, Goode BL (2006) The yeast actin cytoskeleton: from cellular function to biochemical mechanism. Microbiol Mol Biol Rev 70:605–645

Muller DJ, Dufrene YF (2011) Atomic force microscopy: a nanoscopic window on the cell surface. Trends Cell Biol 21:461–469

Orlean P (2012) Architecture and biosynthesis of the *Saccharomyces cerevisiae* cell wall. Genetics 192:775–818

Pelling AE, Sehati S, Gralla EB, Valentine JS, Gimzewski JK (2004) Local nanomechanical motion of the cell wall of *Saccharomyces cerevisiae*. Science 305:1147–1150

Reinoso-Martin C, Schuller C, Schuetzer-Muehlbauer M, Kuchler K (2003) The yeast protein kinase C cell integrity pathway mediates tolerance to the antifungal drug caspofungin through activation of Slt2p mitogen-activated protein kinase signaling. Eukaryot Cell 2:1200–1210

Ro DK, Paradise EM, Ouellet M, Fisher KJ, Newman KL, Ndungu JM, Ho KA, Eachus RA, Ham TS, Kirby J, Chang MC, Withers ST, Shiba Y, Sarpong R, Keasling JD (2006) Production of the antimalarial drug precursor artemisinic acid in engineered yeast. Nature 440:940–943

Schatzmayr G, Zehner F, Taubel M, Schatzmayr D, Klimitsch A, Loibner AP, Binder EM (2006) Microbiologicals for deactivating mycotoxins. Mol Nutr Food Res 50:543–551

Serrano R, Martin H, Casamayor A, Arino J (2006) Signaling alkaline pH stress in the yeast *Saccharomyces cerevisiae* through the Wsc1 cell surface sensor and the Slt2 MAPK pathway. J Biol Chem 281:39785–39795

Smits GJ, Kapteyn JC, van den Ende H, Klis FM (1999) Cell wall dynamics in yeast. Curr Opin Microbiol 2:348–352

Stanley D, Bandara A, Fraser S, Chambers PJ, Stanley GA (2010) The ethanol stress response and ethanol tolerance of *Saccharomyces cerevisiae*. J Appl Microbiol 109:13–24

Touhami A, Nysten B, Dufrêne YF (2003) Nanoscale mapping of the elasticity of microbial cells by atomic force microscopy. Langmuir 19:4546

van Zyl WH, Lynd LR, den Haan R, McBride JE (2007) Consolidated bioprocessing for bioethanol production using *Saccharomyces cerevisiae*. Adv Biochem Eng Biotechnol 108:205–235

Verstrepen KJ, Klis FM (2006) Flocculation, adhesion and biofilm formation in yeasts. Mol Microbiol 60:5–15

Walker MA (1998) Yeast physiology and Biotechnology. Wiley, West Sussex

Whitesides GM, Ostuni E, Takayama S, Jiang X, Ingber DE (2001) Soft lithography in biology and biochemistry. Annu Rev Biomed Eng 3:335–373

Wilk S, Wittland J, Thywissen A, Schmitz HP, Heinisch JJ (2010) A block of endocytosis of the yeast cell wall integrity sensors Wsc1 and Wsc2 results in reduced fitness in vivo. Mol Genet Genomics 284:217–229

Yiannikouris A, Andre G, Poughon L, Francois J, Dussap CG, Jeminet G, Bertin G, Jouany JP (2006) Chemical and conformational study of the interactions involved in mycotoxin complexation with beta-d-Glucans. Biomacromolecules 7:1147–1155

Zaman S, Lippman SI, Zhao X, Broach JR (2008) How *Saccharomyces* responds to nutrients. Annu Rev Genet 42:27–81

Zhao L, Schaefer D, Xu H, Modi SJ, LaCourse WR, Marten MR (2005) Elastic properties of the cell wall of *Aspergillus nidulans* studied with atomic force microscopy. Biotechnol Prog 21:292–299

Chapter 2.3

Imaging living yeast cells and quantifying their biophysical properties by Atomic Force Microscopy

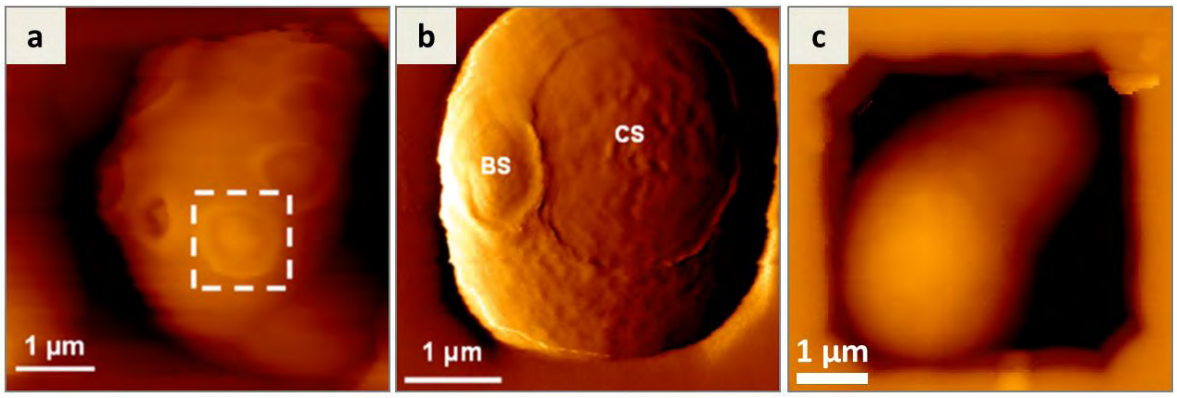

Formosa C. and Dague E.

Book Chapter submitted to Springer's Advanced Microscopy in Mycology

Abstract

As most of the studies performed on yeast cells focus on seeing the yeast from the “inside”, the aim of Atomic Force Microscopy (AFM) is to discover the yeast cell wall from the “outside”. This powerful technology has allowed researchers to ask new questions about yeasts cells, and to give new insights on the cell wall of yeasts, with not only a morphological point of view, but also a nanomechanical and functional point of view. Recent advances in AFM have made it possible to image yeast cells and to quantify their biophysical properties at the same time. In this chapter, we will first introduce the prerequisites needed for using AFM on yeast cells (*i. e.* immobilization methods). Then we will focus on the insights AFM has given on the morphology of the cell wall of yeasts. In a third part we will show how nanomechanical studies of the yeast cell wall can enlighten and give elements of response to complex biological phenomena. Finally we will discuss the possibility to functionalize the AFM tip in order to preform single molecule experiments or to measure cell-cell-surface interactions.

1. Introduction

Yeasts, like *Saccharomyces cerevisiae,* were used for thousands of years by humans to produce food and beverages and humans have also cohabited with harmful yeasts like *Candida albicans* for thousands of years. Both are surrounded by a thick, mechanically strong cell wall that plays several key physiological roles, such as maintaining cell shape and cell integrity, protecting the cell interior from harmful compounds in the environment. The cell wall also harbors several proteins that are implicated in molecular recognition and adhesion[1]. The chemical composition of the yeast cell wall is well known[2]. It consists in a microfibrillar network of β-glucans (β-1,3 and β-1,6-glucans) that represent 50 to 60 % of the cell wall mass, overlaid by highly glycosylated proteins decorated by long chains of mannose residues representing 40-50 % of the cell wall mass. Chitin, a linear polysaccharide of β-linked N-acetylglucosamine, is the third component of yeast cell wall and represents 1 to 3 % of the cell wall mass. The yeast cell wall is an essential organelle for the cell viability as it preserves the cell from osmotic pressure, heat shock, and it serves as a barrier and a filter against harmful molecules. Interestingly, amongst eukaryotes this cell wall is unique to fungi, and as it is essential for yeast viability, it represents an excellent target for antifungal drugs targeted against pathogenic yeasts. In addition, the molecular architecture of the yeast cell wall is not static, but constantly remodeled as a function of growth conditions, morphological development as well as in response to cell surface stresses[3]. Therefore, AFM, which visualizes and probes the ultrastructure of the cell wall, is perfectly suited for the study of its dynamic structure and its molecular modification under different conditions.

Since its invention in 1986[4], AFM has been used more and more to explore living cells at the nanoscale. AFM provides the unique opportunity to measure topography, nanomechanical properties and/or single molecule interactions, on living cells, with a nanoscale resolution. In the

basic contact imaging mode, a sharp tip, mounted on a flexible cantilever, is scanned, by a piezoelectric ceramic, over the sample surface (figure 1). The deflection of the cantilever is continuously monitored through a laser and photodiode system that records vertical and lateral deflection. In the constant force mode, a feedback loop acts on the piezoelectric ceramic to maintain a constant cantilever height and thus the applied force on the sample is kept constant. In tapping mode, the cantilever is oscillated near its resonant frequency while scanning over the surface. In this mode, the contact between the tip and the sample is defined as a decrease in the resonance amplitude, and the feedback loop adjusts the cantilever height in order to keep the amplitude constant. These two basic imaging modes result in topographic images of the samples recorded line by line, while raster scanning the sample with the tip. However, AFM is much more than a simple imaging tool as it is also able to detect forces as small as a few pN. In the force spectroscopy (FS) mode (figure 1), the tip is no longer scanned over the surface, but rather approaches and retracts from the surface. FS results in force *versus* distance curves that can be analyzed in terms of contact point, nanomechanical properties and adhesion forces. Moreover, it is also possible to record force curves according to a predefined matrix, resulting in height maps, nanomechanical maps or adhesion maps acquired point by point or force curve by force curve. This latter mode is named force volume and has now evolved towards modes that record force distance curves at a very high speed[5,6].

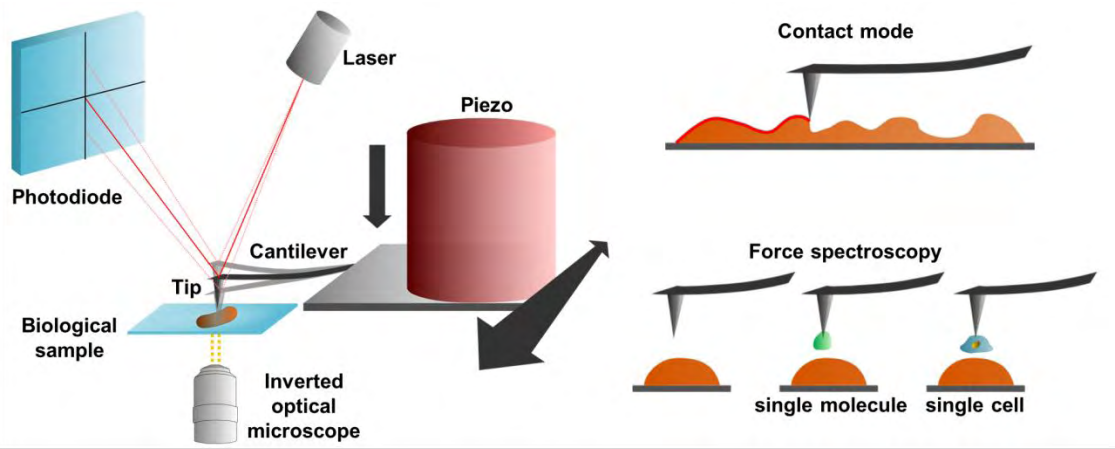

Figure 1. Schema introducing the AFM technology. A sharp tip is mounted on a cantilever that can be moved in the x, y, and z direction thanks to a piezo electric ceramic. The deflection of the cantilever is monitored on a 4 quadrant photodiode as the reflection of a laser beam, aligned at the end of the, usually gold coated, cantilever. The AFM can be used to produce topographical images (i.e. contact and tapping modes with raster scanning) or to measure forces (force spectroscopy mode) between a bare or a functionalized tip (with a biomolecule or a single cell) and the sample. Reprinted with permission from [7].

In this chapter we will see how AFM can refine our understanding of the yeast cell wall. First we will examine immobilization methods. Indeed, yeasts have to be immobilized in order to withstand the tip lateral forces induced during scanning but in such a way as not to modify the yeast cell wall. This was an essential question that needed to be solved properly before any AFM experiments could be pursued. Next we will focus on imaging data to demonstrate interest in live cell AFM. In particular, we will show that AFM is capable of recording cell growth, at the single cell level, as it can work in liquid (culture broth) and at a controlled temperature (microorganism growth temperature). Then we will examine the measurement of nanomechanical properties of the yeast cell wall, and attempt to make the link between the biochemical composition of the cell wall and its nanomechanical properties. We will also see how drugs modify the nanomechanical properties of the yeast cell wall. Finally, we will look at single molecule and single cell experiments. The prerequisite for such experiments is functionalization of the AFM tip with a molecule of interest, or with a cell. We will describe these functionalization methods followed by some interesting results of single molecule or cell force spectroscopy experiments.

2. Immobilization of yeasts cells

Atomic force microscopy is a scanning probe technique and therefore the tip, while scanning, induces lateral forces on the sample. If the sample, in our case, yeast cells, is not properly immobilized, no images and no force curves can be recorded. The first attempt to achieve a firm immobilization of microorganisms in general was to fix the cells by air drying[8] or by chemical fixation[9]. However these methods surely induce cell wall modifications. Other strategies were developed to overcome this difficulty: cells were immobilized in gelatin[10] or trapped into the pores of polycarbonate filters[11]. These techniques have been widely used over the recent years[12–15], although they can lead to tip pollution in the case of gelatin trapping, or it can submit cells to mechanical forces in the case of cells trapped in pores. Also both techniques are time-consuming since cells are spread all over the sample and can be quite difficult to find. To circumvent these problems, recent developments were dedicated to the fabrication of PolyDiMethylSiloxane (PDMS) stamps structured at the micro scale with wells of different sizes adapted to yeast cell diameter[16]. Then the cells are assembled into the micro wells using the convective/capillary deposition technique, as showed in figure 2a. This results in arrays of living cells, immobilized in a defined place. Figure 2b shows an arrangement of 16 cells organized in 16 holes. This innovative immobilization method makes it possible to analyze many more cells than in the past, which will result in an increase in the statistical meaning of the AFM results.

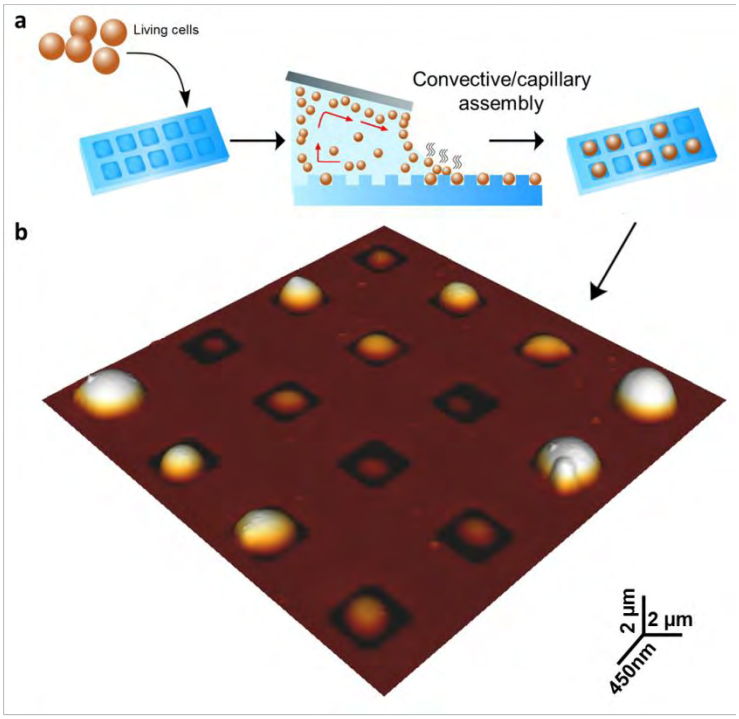

Figure 2. Assembling yeast cells in a PDMS stamp using convective capillary deposition. (a) Principle of convective capillary deposition used to organize the yeast cells in the holes of a PDMS stamp. A meniscus is created between a glass slide and the micro structured stamp. Evaporation at the meniscus creates a convective flux in the liquid that concentrates the cells in the meniscus. The slide is then pulled over the surface. When encountering a hole, the meniscus is caught and a single cell is immobilized in the hole. (b) AFM 3D height image of an array of 16 cells organized in a PDMS stamp.

3. Imaging living yeast cells by Atomic Force Microscopy

Having overcome the immobilization issue, live, unmodified cells could be imaged at high resolution using AFM. Imaging living microorganisms at high resolution is clearly a challenge. Light microscopy is diffraction limited, while electron microscopies usually require working in vacuum, and thus not live cells. In this context AFM provides the unique opportunity to observe yeasts, neither with photons nor electrons, but with a sharp tip in growth media with temperature control[17] and at high resolution imaging [18]. The first images of living *Saccharomyces cerevisiae* cells, immobilized in gelatin, showed bud and birth scars[19]. Figure 3a presents an example of a mother cell of *S. cerevisiae* with multiple bud scars, one of which is surrounded by

a dashed square[20]. Such features at the surface of yeasts cells have been described in multiple studies[11,21,22,23], by different authors. In figure 3b a bud scar (BS) can be seen next to a different larger structure, named by the authors of this study a circular structure (CS)[20], that appears on the *S. cerevisiae* surface after a 1 hour of heat shock at 42°C. This circular ring reaches 3 µm in diameter and is initiated on a bud scar. The authors showed that the formation of this structure required a functional budding process, as no CS were observed on yeasts in which genes involved in the budding process were deleted.

At the surface of fungal spores, such as spores of *Aspergillus fumigatus*, proteins named hydrophobins are auto-organized and confer hydrophobicity to the conidia (figure 3c). These proteins create a rodlet layer[24,25] that can be imaged by AFM at high resolution[26,27,2829]. Hydrophobins are amyloids proteins that are assembled into fibrils spaced from each other's with 10 nm. This rodlet layer is also described on spores of bacteria like *Bacillus atropheus*[30]or *Clostridiu*m *novyi*[31]. The disruption of this layer during spore germination has been followed in real-time[17], and demonstrated that AFM was able to image dynamic processes such as germination, on living cells. After 1 hour of germination, the rodlet layer is slightly disrupted. After 2 hours, the spore surface is heterogeneous; some regions still have an altered rodlet layer, whereas other regions are presenting an amorphous surface. Finally, after 3 hours the whole surface of the spore is amorphous. Unfortunately, it was impossible to image the emission of a germinative tube, probably because of the immobilization of the conidia in the pore of a polycarbonate filter made that impossible.

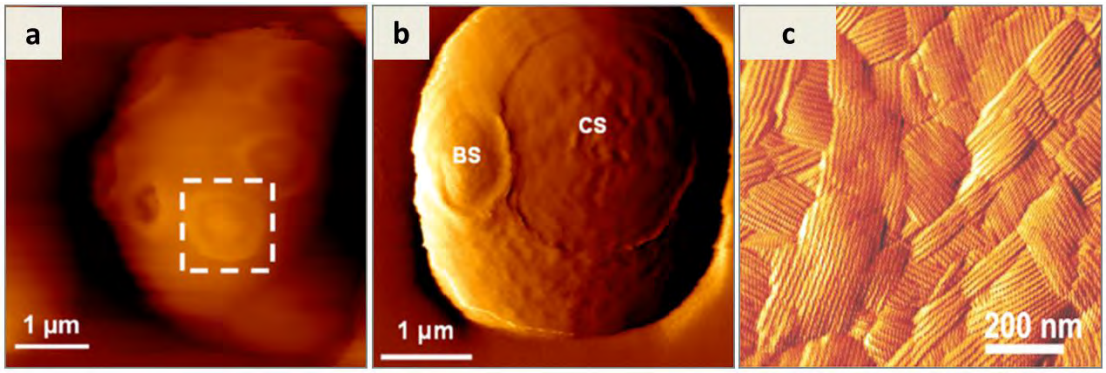

Figure 3. AFM high resolution imaging of (a) *Saccharomyces cerevisiae*. a ring made of 8 bud scars surrounded the cell. The dotted line square is centered on a BS, (b) the circular structure (CS) induced by heat shock on *S. cerevisiae*, next to a bud scar (BS) and (c) the rodlet layer made of hydrophobins of *Aspergillus fumigatus.*

Atomic Force Microscopy also allowed the direct imaging of of *Candida albicans* hyphal growth, as shown in figure 4a (Formosa *et al.*, personal communication). The hyphae growth were previously imaged, but in air after fixation and thus not on living cells[3229]. On figure 4a, the ramifications of the fungal hyphae are clearly observed. Another phenomenon that can be imaged, thanks this time to the immobilization method in PDMS stamps is the emission of matting projection by *S. cerevisiae* exposed to the α-factor (figure 4b). The α-factor, a yeast sexual hormone, triggers the formation of characteristic mating projections, also named "shmoos", by haploid yeast strains of **a** mating type[33]. This is an important processfacilitates contact between two partner cells so they can fuse to form a diploid zygote. The study of yeast mating has many implications for example in understanding analogous fundamental biological processes in higher eukaryotes, and its study by AFM could give new insights into the mechanisms underlying this process.

Finally it is also possible to image by AFM, the changes surface morphology induced by drugs, such as antifungals. Figure 4c and d shows a *Saccharomyces cerevisiae* cell treated with a high dose (4 × Minimal Inhibiting Concentration) of caspofungin, an antifungal drug used for fungal infections[34,35]. Upon treatment, the cell is no longer spherical but is elongated, resembling

Schizosaccharomyces pombe cells. The antifungal treated cell also presents a surprising feature on its surface, (figure 3d), with rings up to 15 nm high, indicating altered cell division likely associated with impairment of cytokinesis.

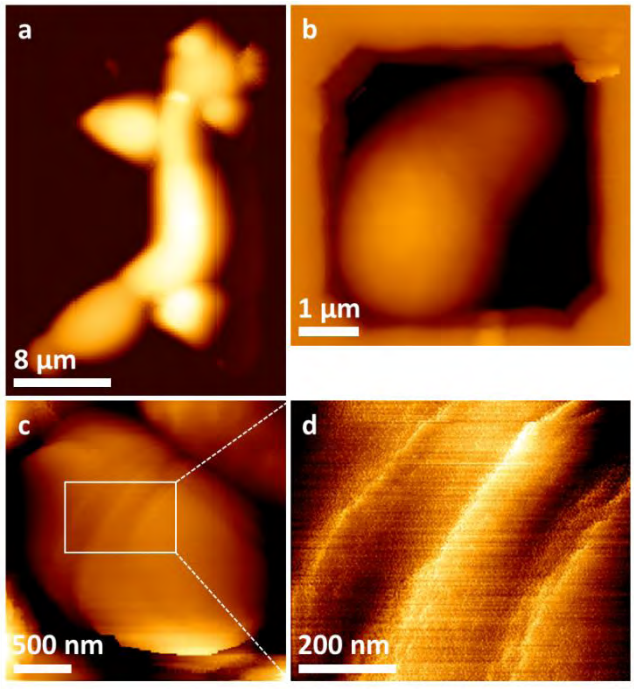

Figure 4. Imaging morphological changes in yeasts cells. High resolution imaging of (a) a *Candida albicans* hyphae immobilized on PDMS, (b) of a mating projection of *Saccharomyces cerevisiae* immobilized in a PDMS stamp, and (c) of a *Saccharomyces cerevisiae* cell submitted to a caspofungin treatment at 4 × MIC. The white square on (c) is imaged at higher resolution in (d).

Taken together, these examples show the importance of AFM, which offers the possibility to work in liquid conditions on live yeast cells. Indeed, AFM can be used to image at the nanoscale yeast cell morphologies, such as hyphae or shmoos, the ultrastructures naturally present at their surface (bud and birth scars, or those induced by a stress, such as the circular structure induced by thermal stress and rings induced by an antifungal treatment.

4. Probing the nanomechanical properties of yeasts cells

To probe the nanomechanical properties of living yeasts, such as elasticity, spring constant, or turgor pressure, AFM is used in the force spectroscopy mode. The nanomechanical property the most often used to describe the cell wall of yeasts is elasticity; therefore we will focus on this parameter in this chapter. The elasticity can be deduced from the approach force-distance curves obtained in the force spectroscopy mode. Force-distance curves can be converted into indentation curves, which are then fitted through the Hertz model, to extract the Young modulus value, meaning the elasticity, expressed in Pascals[36]. The elasticity of the cell wall reflects its composition, but also its molecular organization. In 2003, Touhami and coworkers[37] mapped the nanoscale elasticity of *S. cerevisiae*. Specifically, they compared the nanomechanical properties of a bud scar with the rest of the cell wall. They mapped a higher resistance on the bud scar than on the rest of the cell and correlated this result with the increased amount of chitin in the bud scar. A few years later, this result was reproduced on *S. cerevisiae* but not for another yeast species: *Saccharomyces carlbergensis*[22]. This result demonstrated that the correlation between nanomechanical data and the cell wall composition is not always straightforward.

Indeed, different components of the yeast cell wall are interconnected to form macromolecular complexes[3,38], that can be modified upon stress, or if genes involved in the cell wall synthesis are missing. A recent study showing the differences that can take place in the nanomechanical properties of yeasts cells focused on yeasts mutants of *Saccharomyces cerevisiae* defective in cell wall architecture[21]. In this work, the authors showed that native wild-type cells of *S. cerevisiae* had a global cell wall elasticity of 1.6 MPa, whereas its isogenic mutants defective in enzymes involved in cell wall crosslinking and assembly (*gas1, chr1chr2* mutants), or with a reduction of their chitin content (*chs3* mutant) had a Young's modulus reduced compared to wild-type cells. However, mutants with reduced contents of β-glucans (*fks1*),

mannans (*mnn9*), or defective in the regulation of the cell wall biosynthesis (*knr4*) presented higher Young's modulus values compared to wild-type cells. These results therefore show that the nanomechanical properties of yeasts cells are dependent not only on the composition of the cell wall, but also on the intrinsic molecular organization of the cell wall.

This relation between elasticity of the yeast cell wall and its composition/molecular organization has also been observed in a different context; thermal stress[20]. In this study, the authors showed that thermal stress induced an increase in the chitin content of the cell wall, which was accompanied by an increase in the Young's modulus values. When yeast cells are submitted to a parietal stress, one of the first defense mechanisms is the overproduction of chitin[39]. Chitin being a rigid polymer increases the elasticity of the cell wall when it is overproduced. Finally, previous studies on the effects of caspofungin on the yeast cell wall of *Saccharomyces cerevisiae* and *Candida albicans* also showed modification of the viscoelastic properties of cells upon treatment with this antifungal[35,40]. Figure 5 presents nanoindentation measurements performed on cells of *C. albicans* in native conditions, or treated by two different doses of caspofungin (0.5 and 4 × MIC). Figure 5a, b and c are elasticity maps of the whole cells immobilized in PDMS stamps, figure 5d, e and f are elasticity maps recorded on small areas of 1 µm² on top of the corresponding cells, and finally, figure 4g, h and i are the distributions of the young modulus values obtained for each pixel on the local elasticity maps. In these elasticity maps, the redder the pixel, the higher the Young's modulus. We can clearly see from this figure that treatment with caspofungin results in an increase of the Young's moduli. Remarkably, the higher the caspofungin dose, the higher the Young's moduli, which was correlated with higher chitin content in the cell wall of caspofungin treated yeasts. This work allowed correlating the elasticity of the yeast cell wall to its composition.

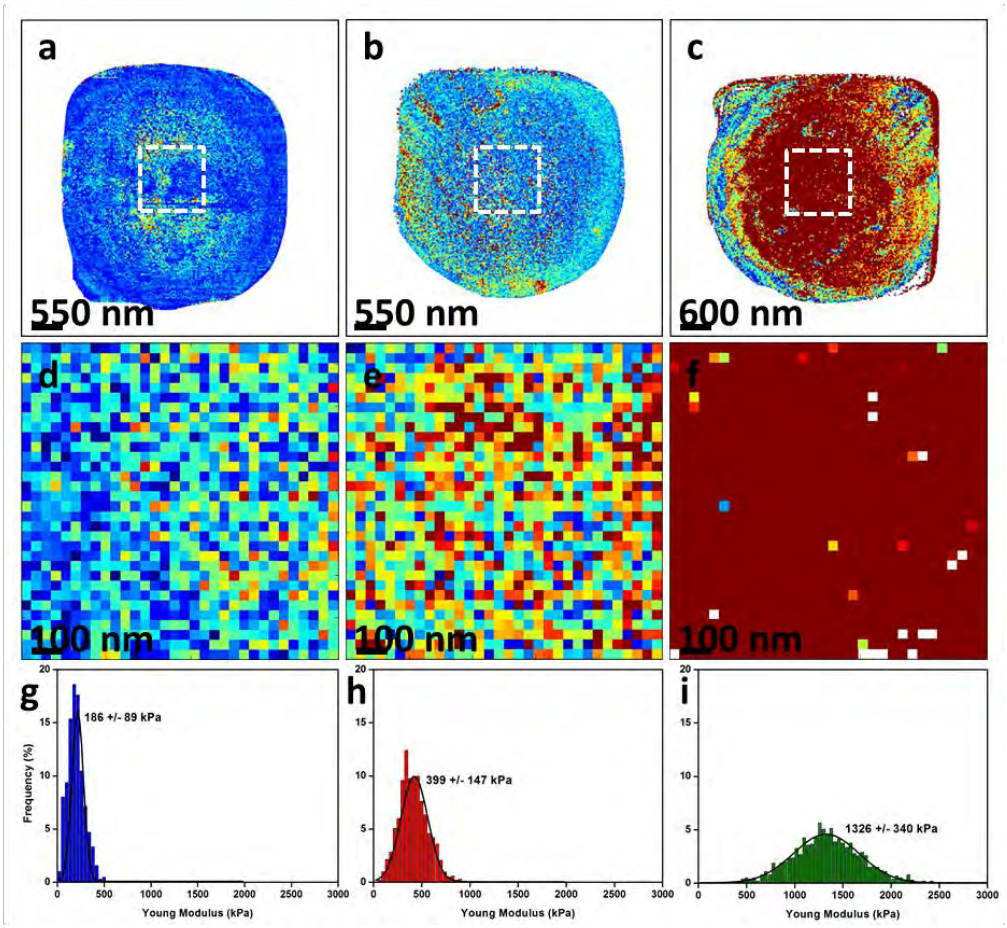

Figure 5. Mapping of *C. albicans* cell surface elasticity. (a to c) Elasticity maps (z range=0.5 MPa) of a native cell (a), of a cell treated with caspofungin at 0.5 × MIC (0.047 µg/ml) (b), and of a cell treated with caspofungin at 4 × MIC (0.376 µg/ml) (c). (d, e, and f) Local elasticity maps (z range=0.5 MPa) recorded on a 1 µm area (white dashed squares) on the tops of the cells in panels a to c, respectively. (g, h, and i) Distributions of Young's moduli (*n*=1024) corresponding to the local elasticity maps in panels d to f, respectively. Reprinted with permissions from [35].

These results therefore show how AFM can be used as a force machine, to probe the cell wall of yeasts cells, in their native state, submitted to genetic stress (mutants) or external stresses (heat shock and caspofungin treatment). Altogether, these nanomechanical data give new insights into the yeast cell wall organization and remodeling in response to different types of stresses.

5. Single cell and Molecule Force spectroscopy

Another property that can be probed by AFM is adhesion. Indeed, specific molecular interactions are the basis of various biochemical and biological processes. In order to gain significant data on these interactions, AFM tips can be functionalized with molecules that will interact specifically with target molecules at the surface of the cells. These experiments, performed with functionalized AFM tips, are called Single Molecule Force Spectroscopy (SMFS) experiments. Of the various strategies to functionalize AFM tips with biomolecules, some consist of nonspecific adsorption of proteins, for example BSA (Bovine Serum Albumin), to the silicon nitride surface of AFM tips[41], or the chemical fixation of biomolecules by sulfur-gold bonds to gold-coated AFM tips. This last strategy has been successfully used to functionalize AFM tips with methyl groups, CH_3, to probe the hydrophobic characteristics of the rodlet layer of *Aspergillus fumigatus*[42,43]. In this study, the authors showed that hydrophobic tips enable quantification of surface hydrophobicity on live cell surfaces, and how this hydrophobicity relatesd to a function such as surface adhesion or drug interaction.

It is also possible to covalently link a molecule containing amino groups directly to the silicon nitride AFM tip. Towards this end, AFM tips must be first amino-functionalized either by esterification with ethanolamine[44] or silanization with aminopropyl-triethoxysilane (APTES)[45]. Then, the amino-functionalized tip must be bridged to the biomolecule of interest, achieved through the use of heterobifunctionalized PolyEthylene Glycol (PEG)[46–48] or an aldehyde-phosphorus dendrimer as we previously described[49]. This second strategy has been used to map the polysaccharides at the surface of living yeast cells, with AFM tips functionalized with Concanavalin A, a protein that interacts specifically with carbohydrates[50]. In this study, the adhesive forces were calculated from the AFM retract portion of force curves, by measuring the piezoelectric retraction force required to break the interaction between the lectin and the

recognized carbohydrate. Such measurements allowed the authors to conclude that mannans were uniformly distributed on the cell wall surface.

This functionalization strategy has also been used to map the surface properties of the pathogenic yeast *Candida albicans*. This pathogenic yeast species has emerged as a major public health problem in the last two decades. This opportunistic pathogen causes a wide range of infections from surface, to mucosal and blood-stream infections[51]. In order to colonize and subsequently to disseminate in the blood stream, *C. albicans* first needs to adhere to different biotic substrates. This first stage of infection[52] is mediated by adhesins that are found on the surface of the yeast cell wall. Many of these adhesins are mannoproteins, and among them, the that identified as having a major role in host cell attachment is the Als (Agglutinin-like Sequences) family[53]. The Als were initially reported as having homology to the proteins responsible for auto-agglutination in the baker yeast *Saccharomyces cerevisiae*. Eight ALS have been identified, and they all are primarily involved in host-pathogen interactions[54]. In a recent study by Beaussart *et al.*, the authors have used SMFS experiments to map the localization of one of the proteins, Als3, on the surface of *Candida albicans* hyphae[55]. These experiments were performed with a tip functionalized with an anti-Als3 antibody, on different parts of the germinating tube; *i. e.* on the germinating yeast (figure 6a, b and c) and on the germ tube (figure 6d, e and f). The authors found the distribution of the Als3 proteins to be very different on the distinct hyphal regions. Indeed, the number and length of unfolding events was higher on the germ tube, indicating that the adhesin Als3 is much more exposed on the germ tube than on the germinating yeast. These results are consistent with the fact that the *ALS3* gene is specifically expressed during the yeast-hyphae transition[56].

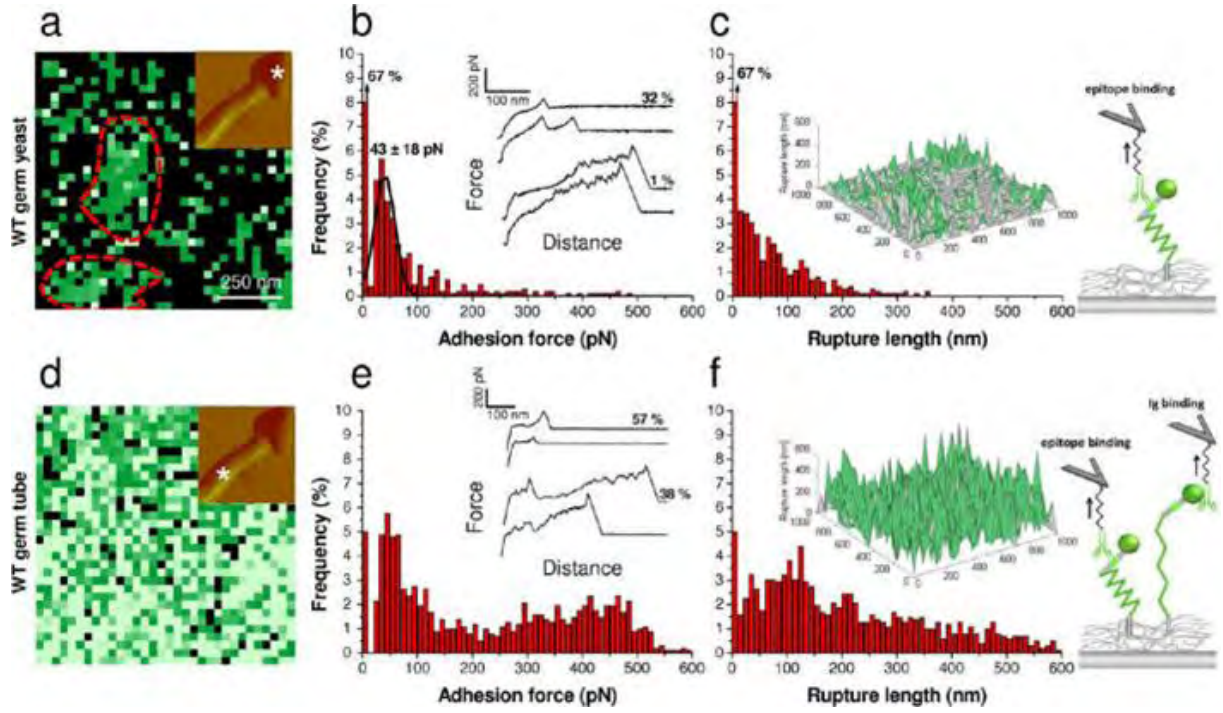

Figure 6. Cellular morphogenesis leads to a major increase in the distribution and extension of Als3 proteins. (a, d) Adhesion force maps (1 µm², z-range=300 pN) recorded in buffer on the yeast (a) and germ tube (d) of a germinating cell using an anti-Als3 tip. Insets: deflection images in which the * symbol indicate where the force maps were recorded. The dashed lines in (a) emphasize Als3 clusters. (b, e) Corresponding adhesion force histograms (n=1024) together with representative force curves. (c, f) Histograms of rupture distances (n=1024) and 3-D reconstructed polymer maps (false colors, adhesion forces in green). Similar data were obtained in several independent experiments using different tip preparations and cell cultures. Reprinted with permissions from [55].

Another characteristic of the Als proteins is that they contain an amyloid forming sequence, meaning that they are able to aggregate, under certain conditions, into amyloids at the surface of *Candida albicans* cells. A recent study by Alsteens *et al.* showed that the formation and propagation of nanodomains of the Als5 protein at the surface of *Saccharomyces cerevisiae* yeast cells overexpressing these proteins, was force-induced[57]. This study using functionalized AFM tips with an anti-Als5 antibodydemonstrated that a localized delivery of piconewton forces by the AFM tip could initiate the formation and propagation of the Als5 nanodomains over the cell. The authors therefore suggested that this process could be involved in cellular adhesion, in

response to mechanical stimuli, important processes for the early stages of infections by *Candida albicans*. With these two last examples, we show that FS in conjunction with functionalized AFM tips is a powerful tool to gain a better understanding of the molecular adhesive properties of living pathogenic yeasts cells. Such studies contribute to understanding how to prevent *Candida albicans* infections, as well as in the identification of new parietal targets for antifungal drugs.

As it is possible to functionalize an AFM tip with a molecule, it is also possible to functionalize an AFM tip with a living cell. This type of experiments is called Single Cell Force Spectroscopy experiments (SCFS). The principle is the same as for SMFS, but this time a living cell is immobilized onto the cantilever becoming the AFM tip which is engaged to interact with the surface or with another cell[58,59]. This strategy is re-emerging, and there are only few papers in which it is used for the study of living yeasts cells [58,59]. However, the Dufrêne lab has recently resurrected this idea, and published a study that aims to measure the adhesive forces between a yeast cell immobilized on a cantilever, and a hyphae of the same yeast species, *Candida albicans*[60]. This study allowed the authors to show that the *C. albicans* adhesin, Als3, present at the surface of hyphae, was responsible for adhesion between yeast cells. In the context of biofilm formation, these new data are of interest as they give new insights into the interactions between two morphotypes of the same yeast species. The same team also used SCFS to quantify adhesion between cells of *C. albicans*, and another type of pathogenic microorganism, *Staphylococcus epidermis*[61]. Indeed, these two types of microorganisms are often found together in the case of human infections[62]. The results of this study showed that the fungal molecules involved in the interactions with *S. epidermis* were adhesins, once again, as well as 0-mannosylations. It is interesting to note that, using the same cell probe strategy, the interactions between vaginal *Staphylococci* and *Lactococci* were probed[63]. This work, pioneering in the field of microbiology, opens doors to new questions about fungal adhesion, an important process involved in the first

stages of human yeast infections. Such studies could lead, for example, to the identification of anti-adhesion drugs that would prevent co-infections by *C. albicans* and *S. epidermis*. The lack of statistical data has been recently addressed and promising perspectives are evolving from the work of Potthoff[64] which aims at the serial quantification of adhesive forces using yeast probes.

6. Conclusions

AFM has emerged as a significant technology in the life sciences over the last 20 years. The number of publications utilizing AFM has grown exponentially [7] even if the number of studies dedicated to live cells is still slowly increasing. The latter is likely due to the difficulties associated with properly immobilizing live cells, which avoid damage to the cell membrane. For yeast cells, physical trapping in pores of polycarbonate membranes or in holes of microstructured PDMS stamps has solved this problem. As an imaging technology, AFM contributes to refine our understanding of the structures exposed on the yeast cell wall, such as, among others, bud scars and rodlet layers. Interestingly, AFM is also able to track morphological modifications occurring during cell growth in real time. More than an imaging technology, AFM probes the cell nanomechanical and adhesive properties. The data collected from force spectroscopy experiments have broadened our perception of the yeast cell wall. The well-known biochemical composition of the cell wall covers up the extremely complex and dynamic interplay of its organization and architecture. Therefore much more work is required to build a fully comprehensive description of the yeast cell wall and to fully understand these microorganisms.

References

1. Chaffin, W. L. Candida albicans Cell Wall Proteins. *Microbiol. Mol. Biol. Rev.* **72,** 495 – 544 (2008).
2. Lipke, P. N. & Ovalle, R. Cell Wall Architecture in Yeast: New Structure and New Challenges. *J. Bacteriol.* **180,** 3735–3740 (1998).
3. Orlean, P. Architecture and Biosynthesis of the Saccharomyces cerevisiae Cell Wall. *Genetics* **192,** 775–818 (2012).
4. Binnig, G. & Quate, C. F. Atomic force microscope. *Phys Rev Lett.* **56,** 930–933 (1986).
5. Dufrêne, Y. F., Martínez-Martín, D., Medalsy, I., Alsteens, D. & Müller, D. J. Multiparametric imaging of biological systems by force-distance curve-based AFM. *Nat. Methods* **10,** 847–854 (2013).
6. Chopinet, L., Formosa, C., Rols, M. P., Duval, R. E. & Dague, E. Imaging living cells surface and quantifying its properties at high resolution using AFM in QI^{TM} mode. *Micron* **48,** 26–33 (2013).
7. Pillet, F., Chopinet, L., Formosa, C. & Dague, É. Atomic Force Microscopy and pharmacology: From microbiology to cancerology. *Biochim. Biophys. Acta BBA - Gen. Subj.* **1840,** 1028–1050 (2014).
8. Canetta, E., Adya, A. K. & Walker, G. M. Atomic force microscopic study of the effects of ethanol on yeast cell surface morphology. *FEMS Microbiol. Lett.* **255,** 308–315 (2006).
9. Louise Meyer, R. *et al.* Immobilisation of living bacteria for AFM imaging under physiological conditions. *Ultramicroscopy* **110,** 1349–1357 (2010).
10. Gad, M. & Ikai, A. Method for immobilizing microbial cells on gel surface for dynamic AFM studies. *Biophys. J.* **69,** 2226–2233 (1995).
11. Touhami, A., Nysten, B. & Dufrêne, Y. F. Nanoscale mapping of the elasticity of microbial cells by atomic force microscopy. *Langmuir* **19,** 4539 (2003).
12. Francius, G., Domenech, O., Mingeot-Leclercq, M. P. & Dufrêne, Y. F. Direct Observation of Staphylococcus aureus Cell Wall Digestion by Lysostaphin. *J. Bacteriol.* **190,** 7904–7909 (2008).
13. Alsteens, D. *et al.* Structure, cell wall elasticity and polysaccharide properties of living yeasts cells, as probed by AFM. *Nanotechnology* 384005 (2008).
14. Dague, E., Alsteens, D., Latgé, J.-P. & Dufrêne, Y. F. High-Resolution Cell Surface Dynamics of Germinating Aspergillus fumigatus Conidia. *Biophys. J.* **94,** 656–660 (2008).
15. Gilbert, Y. *et al.* Single-Molecule Force Spectroscopy and Imaging of the Vancomycin/d-Ala-d-Ala Interaction. *Nano Lett.* **7,** 796–801 (2007).
16. Dague, E. *et al.* Assembly of live micro-organisms on microstructured PDMS stamps by convective/capillary deposition for AFM bio-experiments. *Nanotechnology* **22,** 395102 (2011).
17. Dague, E., Alsteens, D., Latge, J.-P. & Dufrene, Y. High-resolution cell surface dynamics of germinating Aspergillus fumigatus conidia. *Biophys J* **94,** 1–5 (2008).
18. Dupres, V., Alsteens, D., Pauwels, K. & Dufrêne, Y. F. In Vivo Imaging of S-Layer Nanoarrays on Corynebacterium glutamicum. *Langmuir* **25,** 9653–9655 (2009).
19. Kasas, S. & Ikai, A. A method for anchoring round shaped cells for atomic force microscope imaging. *Biophys. J.* **68,** 1678–1680 (1995).
20. Pillet, F. *et al.* Uncovering by Atomic Force Microscopy of an original circular structure at the yeast cell surface in response to heat shock. *BMC Biol.* **12,** 6 (2014).
21. Dague, E., Bittar, R., Durand, F., Martin-Hyken, H. & François, J. M. An Atomic Force Microscopy analysis of yeast mutants defective in cell wall architecture. *Yeast* **27,** 673–784

(2010).
22. Alsteens, D. *et al.* Structure, cell wall elasticity and polysaccharide properties of living yeast cells, as probed by AFM. *Nanotechnology* **19,** 384005 (2008).
23. Adya, A. K., Canetta, E. & Walker, G. M. Atomic force microscopic study of the influence of physical stresses on Saccharomyces cerevisiae and Schizosaccharomyces pombe. *FEMS Yeast Res.* **6,** 120–128 (2006).
24. Beever, R. E. & Dempsey, G. P. Function of rodlets on the surface of fungal spores. *Nature* **272,** 608–610 (1978).
25. Aimanianda, V. *et al.* Surface hydrophobin prevents immune recognition of airborne fungal spores. *Nature* **460,** 1117–1121 (2009).
26. Dufrêne, Y. F., Boonaert, C. J. P., Gerin, P. A., Asther, M. & Rouxhet, P. G. Direct probing of the surface ultrastructure and molecular interactions of dormant and germinating spores of Phanerochaete chrysosporium. *J Bacteriol* **181,** 5350–5354 (1999).
27. Dague, E., Delcorte, A., Latge, J. P. & Dufrene, Y. F. Combined use of atomic force microscopy, X-ray photoelectron spectroscopy, and secondary ion mass spectrometry for cell surface analysis. *Langmuir* **24,** 2955–2959 (2008).
28. Zykwinska, A., Pihet, M., Radji, S., Bouchara, J.-P. & Cuenot, S. Self-assembly of proteins into a three-dimensional multilayer system: Investigation of the surface of the human fungal pathogen Aspergillus fumigatus. *Biochim. Biophys. Acta BBA - Proteins Proteomics* doi:10.1016/j.bbapap.2014.03.001
29. Ma, H., Snook, L. A., Kaminskyj, S. G. W. & Dahms, T. E. S. Surface ultrastructure and elasticity in growing tips and mature regions of Aspergillus hyphae describe wall maturation. *Microbiology* **151,** 3679–3688 (2005).
30. Plomp, M., Leighton, T. J., Wheeler, K. E., Hill, H. D. & Malkin, A. J. In vitro high-resolution structural dynamics of single germinating bacterial spores. *PNAS* **104,** 9644–9649 (2007).
31. Plomp, M. *et al.* Spore coat architecture of Clostridium novyi NT spores. *J Bacteriol* **189,** 6457–6468 (2007).
32. Ma, H., Snook, L. A., Tian, C., Kaminskyj, S. G. W. & Dahms, T. E. S. Fungal surface remodelling visualized by atomic force microscopy. *Mycol. Res.* **110,** 879–886 (2006).
33. Merlini, L., Dudin, O. & Martin, S. G. Mate and fuse: how yeast cells do it. *Open Biol.* **3,** 130008 (2013).
34. Denning, D. W. Echinocandin antifungal drugs. *The Lancet* **362,** 1142–1151 (2003).
35. Formosa, C. *et al.* Nanoscale Effects of Caspofungin against Two Yeast Species, Saccharomyces cerevisiae and Candida albicans. *Antimicrob. Agents Chemother.* **57,** 3498–3506 (2013).
36. Hertz, H. Ueber die Berührung fester elastischer Körper. *J. Für Reine Angew. Math.* **92,** 156–171 (1881).
37. Touhami, A., Nysten, B. & Dufrêne, Y. F. Nanoscale Mapping of the Elasticity of Microbial Cells by Atomic Force Microscopy. *Langmuir* **19,** 4539–4543 (2003).
38. Free, S. J. in *Adv. Genet.* (Theodore Friedmann, J. C. D. and S. F. G.) **Volume 81,** 33–82 (Academic Press, 2013).
39. Ram, A. F. J. *et al.* Loss of the Plasma Membrane-Bound Protein Gas1p inSaccharomyces cerevisiae Results in the Release of β1,3-Glucan into the Medium and Induces a Compensation Mechanism To Ensure Cell Wall Integrity. *J. Bacteriol.* **180,** 1418–1424 (1998).
40. El-Kirat-Chatel, S. *et al.* Nanoscale analysis of caspofungin-induced cell surface remodelling in Candida albicans. *Nanoscale* **5,** 1105–1115 (2013).

41. Florin, E. L., Moy, V. T. & Gaub, H. E. Adhesion forces between individual ligand-receptor pairs. *Science* **264,** 415–417 (1994).
42. Alsteens, D., Dague, E., Rouxhet, P. G., Baulard, A. R. & Dufrêne, Y. F. Direct Measurement of Hydrophobic Forces on Cell Surfaces Using AFM. *Langmuir* **23,** 11977–11979 (2007).
43. Dague, E. *et al.* Chemical force microscopy of single live cells. *Nano Lett* **7,** 3026–3030 (2007).
44. Hinterdorfer, P., Baumgartner, W., Gruber, H. J., Schilcher, K. & Schindler, H. Detection and localization of individual antibody-antigen recognition events by atomic force microscopy. *Proc. Natl. Acad. Sci.* **93,** 3477–3481 (1996).
45. Ros, R. *et al.* Antigen binding forces of individually addressed single-chain Fv antibody molecules. *Proc. Natl. Acad. Sci.* **95,** 7402–7405 (1998).
46. Wildling, L. *et al.* Linking of Sensor Molecules with Amino Groups to Amino-Functionalized AFM Tips. *Bioconjug. Chem.* **22,** 1239–1248 (2011).
47. Ebner, A. *et al.* Functionalization of probe tips and supports for single-molecule recognition force microscopy. *Top. Curr. Chem.* **285,** 29–76 (2008).
48. Kamruzzahan, A. S. M. *et al.* Antibody Linking to Atomic Force Microscope Tips via Disulfide Bond Formation. *Bioconjug. Chem.* **17,** 1473–1481 (2006).
49. Jauvert, E. *et al.* Probing single molecule interactions by AFM using bio-functionalized dendritips. *Sens. Actuators B Chem.* **168,** 436–441 (2012).
50. Gad, M., Itoh, A. & Ikai, A. Mapping cell wall polysaccharides of living microbial cells using atomic force microscopy. *Cell Biol. Int.* **21,** 697–706 (1997).
51. Gow, N. A. & Hube, B. Importance of the Candida albicans cell wall during commensalism and infection. *Curr. Opin. Microbiol.* **15,** 406–412 (2012).
52. Naglik, J. R., Moyes, D. L., Wächtler, B. & Hube, B. Candida albicans interactions with epithelial cells and mucosal immunity. *Microbes Infect.* **13,** 963–976 (2011).
53. Hoyer, L. L. The ALS gene family of Candida albicans. *Trends Microbiol.* **9,** 176–180 (2001).
54. Hoyer, L. L., Green, C. B., Oh, S.-H. & Zhao, X. Discovering the secrets of the Candida albicans agglutinin-like sequence (ALS) gene family – a sticky pursuit. *Med Mycol* **46,** 1–15 (2008).
55. Beaussart, A. *et al.* Single-Molecule Imaging and Functional Analysis of Als Adhesins and Mannans during Candida albicans Morphogenesis. *ACS Nano* **6,** 10950–10964 (2012).
56. Liu, Y. & Filler, S. G. Candida albicans Als3, a Multifunctional Adhesin and Invasin. *Eukaryot. Cell* **10,** 168 –173 (2011).
57. Alsteens, D., Garcia, M. C., Lipke, P. N. & Dufrêne, Y. F. Force-induced formation and propagation of adhesion nanodomains in living fungal cells. *Proc. Natl. Acad. Sci.* **107,** 20744 – 20749 (2010).
58. Bowen, W. R., Lovitt, R. W. & Wright, C. J. Atomic force microscopy study of the adhesion of Saccharomyces cerevisiae. *J. Colloid Interface Sci.* **237,** 54–61 (2001).
59. Bowen, W. R., Lovitt, R. W. & Wright, C. J. Direct quantification of Aspergillus niger spore adhesion to mica in air using an atomic force microscope. *Colloids Surf. Physicochem. Eng. Asp.* **173,** 205–210 (2000).
60. Alsteens, D., Van Dijck, P., Lipke, P. N. & Dufrêne, Y. F. Quantifying the Forces Driving Cell–Cell Adhesion in a Fungal Pathogen. *Langmuir* **29,** 13473–13480 (2013).
61. Beaussart, A. *et al.* Single-cell force spectroscopy of the medically important Staphylococcus epidermidis-Candida albicans interaction. *Nanoscale* **5,** 10894–10900 (2013).

62. Peleg, A. Y., Hogan, D. A. & Mylonakis, E. Medically important bacterial–fungal interactions. *Nat Rev Micro* **8,** 340–349 (2010).
63. Younes, J. A., van der Mei, H. C., van den Heuvel, E., Busscher, H. J. & Reid, G. Adhesion Forces and Coaggregation between Vaginal Staphylococci and Lactobacilli. *PLoS ONE* **7,** e36917 (2012).
64. Potthoff, E. *et al.* Rapid and Serial Quantification of Adhesion Forces of Yeast and Mammalian Cells. *PLoS ONE* **7,** e52712 (2012).

Chapter 3

Detailed Results

Chapter 3.1: Technological developments to study the cell wall of microorganisms by AFM

3.1.1. A versatile tool to generate living cell arrays for AFM studies

3.1.2. Imaging living cells surface and quantifying its properties using AFM in QI™ mode

3.1.3. Mapping HA-tagged protein at the surface of living cells by AFM

Chapter 3.2: A nanoscale view of the yeast cell wall of *Candida albicans* and *Saccharomyces cerevisiae*

3.2.1. Multiparametric imaging of adhesive nanodomains at the surface of Candida albicans by AFM

3.2.2. Nanoscale effects of caspofungin on two yeast species; Saccharomyces cerevisiae and Candida albicans

Chapter 3.3: Nanoscale behavior of the bacterial cell wall exposed to antibacterials

3.3.1. Nanoscale effects of antibiotics on P. aeruginosa

3.3.2. Unravelling of the mechanism of resistance to colistin in Klebsiella pneumoniae

3.3.3. Nanoscale analysis of the effects of antibiotics and CX1 on a Pseudomonas aeruginosa multidrug resistant strain

<u>Chapter 3.1:</u> Technological developments to study the cell wall of microorganisms by AFM

3.1.1 Generating living cells arrays for Atomic Force Microscopy studies

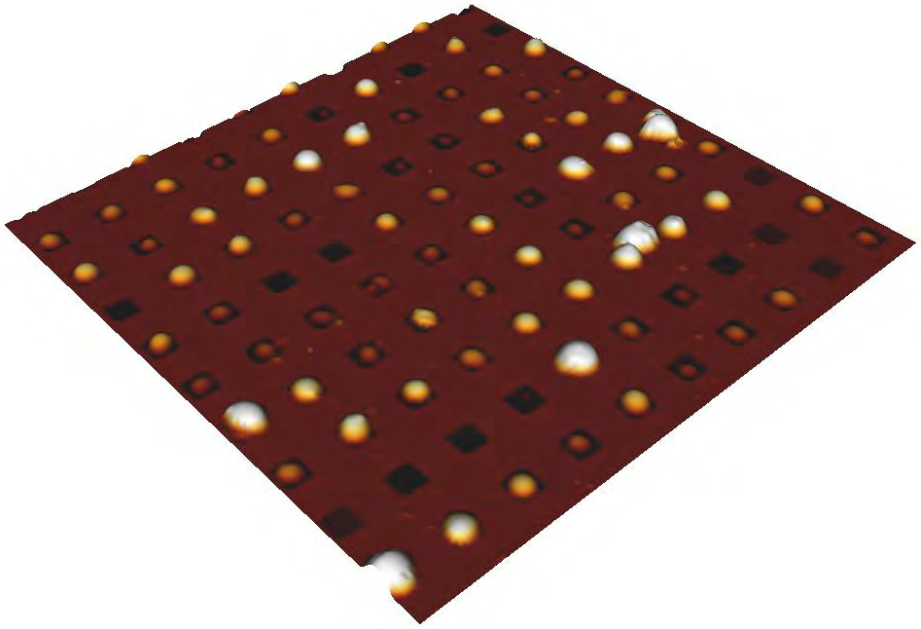

Formosa C., Pillet F., Schiavone M., Duval R. E., Ressier L., and Dague E.

Accepted in *Nature Protocols*

Abstract

Atomic Force Microscopy (AFM) is a useful tool to study the morphology, or the nanomechanical and adhesive properties of live microorganisms under physiological conditions. However, in order to perform AFM imaging, living cells must be immobilized; firmly enough to withstand the lateral forces exerted by the scanning tip, but without denaturing them. This protocol describes how to immobilize living cells, ranging from spores of bacteria to yeast cells, into polydimethylsiloxane (PDMS) stamps, with no chemical or physical denaturation. This protocol generates arrays of living cells, allowing statistically relevant measurements to be obtained from AFM measurements, which can increase the relevance of results. The first step of the protocol is to generate a microstructured silicon master, from which many microstructured PDMS stamps can be replicated. Living cells are finally assembled into the microstructures of these PDMS stamps using convective/capillary assembly. The complete procedure can be performed in one week, although the first step is done only once, thus repeats can be completed within one day.

De : protocols@nature.com
Objet : Update on manuscript NP-P140297C
Date : 16 octobre 2014 11:04:46 HAEC
À : edague@laas.fr
Répondre à : protocols@nature.com

Dear Dr Dague,

Thank you for your updated manuscript file. I am pleased to inform you that your protocol, "Generation of living cell arrays for Atomic Force Microscopy studies", is now in the process of being sent to our Production department and thus should soon be published in Nature Protocols. This message is intended to let you know what to expect from us over the next couple of months, and to let you know where to address any further questions.

Your protocol will now be copyedited to ensure that it conforms to Nature Protocols style. Assuming there are no major problems with the copy editing of your protocol you will be asked to view a set of proofs once your protocol has been laid out into the final pdf format your paper will be published in. Once proofs are generated, they will be sent to you electronically and you will be asked to send a corrected version within 24 hours. It is extremely important that you let us know now whether you will be difficult to contact over the next couple of months. If this is the case, we ask that you send us the contact information (email, phone and fax) of someone who will be able to check the proofs and deal with any last-minute problems.

Details of who to send proofs back to will be provided when you are sent your proofs. Please address any other correspondence about your proofs to protocols@nature.com.

Should you wish to purchase reprints of the pdf version of your protocol, please complete the reprint order form. This can be found at http://www.nature.com/reprints/reprints-forms/NProto-Auth-2014.pdf. Further details, such as answers to frequently asked questions, can be found at http://www.nature.com/reprints/index.html.

Once your article is published, please do encourage your colleagues to comment on your protocol on the website, as we hope regular commenting will keep our protocols up to date. We also welcome you to comment on the protocols already published. Shortly after your protocol has been published we will be in contact again with details of a code that will enable you to access the site free for a year, as a thank you for all your work in writing.

You can now use a single sign-on for all your accounts, view the status of all your manuscript submissions and reviews, access usage statistics for your published articles and download a record of your refereeing activity for the Nature journals.

In addition, NPG encourages all authors and reviewers to associate an Open Researcher and Contributor Identifier (ORCID) to their account. ORCID is a community-based initiative that provides an open, non-proprietary and transparent registry of unique identifiers to help disambiguate research contributions.

Please feel free to contact me at any time with any questions.

Best regards,
Katharine
****
Katharine Barnes, PhD
Managing Editor
Nature Protocols
4 Crinan Street, London N1 9XW, UK
http://www.natureprotocols.com
We invite you to read and comment on our content!

****

This email has been sent through the NPG Manuscript Tracking System NY-610A-NPG&MTS

INTRODUCTION

Since its first development in 1986[1], Atomic Force Microscopy has developed into a powerful tool that has opened the doors to the nanoworld[2]. AFM is particularly well suited for biology since it allows multiple characterizations (topography, mechanical and adhesive properties) of living cells in their physiological environment. However a prerequisite for such AFM experiments is the immobilization of the biological samples probed. This crucial step is often a challenge however as samples have to be immobilized individually and firmly enough to withstand the lateral forces exerted by the AFM tip, but without altering their cellular integrity.

Immobilizing cells for AFM experiments

Several techniques have been used to immobilize living cells. Living cells such as microorganisms can be chemically fixed on a solid substrate using glutaraldehyde or APTES[3], or immobilized on gelatin coated surfaces[4]. However these techniques can, respectively, modify the interface of the biological sample, or pollute the AFM tips, leading to artifacts. Another strategy is to trap round shaped cells such as bacterial coccus and yeast cells in the pores of polycarbonate membranes by filtration[5] or in lithographically patterned substrates by gentle drying[6]. The filtration technique has been widely used over recent years[7–10], although it is time-consuming and cells can be exposed to mechanical forces when trapped in the pores.

We therefore developed a new and versatile strategy in 2011[11–13], that consists in immobilizing round single living cells in microstructured polydimethylsiloxane (PDMS) stamps by convective/capillary deposition. We have demonstrated that this generic protocol can be used to immobilize different types of round shaped cells, ranging from small coccus bacteria, to yeasts cells and even algae, by tuning the geometry of the PDMS stamp patterns (supplementary data 1).

This approach was also exploited to immobilize yeasts cells of different species, *Saccharomyces cerevisiae* and *Candida albicans*[14–16], as well as spores of *Aspergillus fumigatus*[17].

Statistical significance of results obtained from AFM: the new challenge

Statistical analysis of results is desirable. As AFM is a tool adapted for single cell analysis, the significance of the data obtained with this technology requires analysis of multiple cells in order to achieve statistical confidence. This cannot be performed using techniques such as immobilization in pore filter, as the deposition of the cells on the surface is random and the rate of filled pores is low and not controlled. Using our method of immobilization, it is possible to generate arrays of cells; therefore, AFM results on an array of 100 cells can be performed using different AFM modes, such as multiparametric imaging, chemical force microscopy, single-molecule force spectroscopy, and single-cell force spectroscopy[18,14,19–21]. Such setups are effectively "lab chips" for AFM analysis. With the progress made in AFM data processing software[22], it is thus possible to take all the data acquired to analyze in a reasonable time lapse, so to generate relevant and significant results for biological studies.

Overview of the procedure

Immobilization of living cells in PDMS stamps involves 3 sequential stages. The first stage is the generation of a glass/chromium mask harboring microstructured patterns, and the transfer of these patterns onto a silicon wafer. The second stage consists of preparation of a corresponding PDMS stamp. Finally the third stage is the assembly of the living cells into the PDMS microstructured stamps. The generation of a silicon master is achieved by photolithography, followed by pattern transfer using deep reactive ion etching. The patterns of the silicon master are squares, ranging from 1.5 to 6 µm wide, with a pitch of 0.5 µm and a depth

ranging from 1 µm to 4 µm. The measurements of the silicon master should be verified using profilometry. These pattern geometries allow immobilization of a wide range of microorganisms of different sizes (Figure 1a). For example patterns with a width of 4 to 5 µm and a depth of 4 µm are best suited for yeast cells such as *Candida albicans* or *Saccharomyces cerevisiae*, whereas patterns 1.5 to 2 µm wide with a depth of 2 µm can be used to image smaller cells such as spores of fungi or round shaped bacteria. For the second stage of fabricating a PDMS stamp, a PDMS prepolymer solution is cured on the silicon master produced in stage one, and then demolded to obtain the microstructured PDMS stamps (Figure 1b). The deposition of cells into the microstructured PDMS stamps is accomplished using convective/capillary deposition. Adjustment of parameters such as temperature, humidity, translation speed and contact angle will ensure a high rate of cell trapping, and do not affect the cell interface since cells are put back into liquid right after the procedure. This stage can also be done manually if highly organized arrays of cells are not mandatory for the AFM experiments. The filling rate and the quality of the PDMS stamp can easily be verified by optical microscopy. PDMS, being a biocompatible and transparent polymer [23,24], does not induce any chemical modification of the cells in contact with it, and can be used with straight or inverted optical/fluorescence microscopes that are combined with AFMs.

Technical details of the procedure to generate a patterned glass/chromium mask and transfer the patterns to a silicon master, to fabricate PDMS stamps molded on the silicon master, and to assemble arrays of living cells into the microstructured PDMS stamps are described below. We demonstrate the type of AFM results obtained on living cells by showing results obtained from the medically important yeast pathogen *Candida albicans*, immobilized into PDMS microstructures. The versatility of this protocol has been demonstrated for other microorganisms[14–17]. We anticipate that this approach will be useful for researchers interested in

studying microorganisms with AFM at a population scale, as well as for biophysicists interested in generating cell arrays for applications in diagnostic or biodetection.

MATERIALS

REAGENTS

- AZ ECI 3012 photoresist (Microchemicals) **CAUTION** this reagent is flammable liquid and vapor, causes serious eye damage and may cause respiratory irritation. When handling, wear protective gloves, protective clothing, eye protection and face protection. Avoid breathing vapors or mists.
- Hexamethyldisilazane (Sigma-Aldrich) **CAUTION** this reagent is highly flammable liquid and vapor, harmful if inhaled or swallowed, and toxic in contact with skin. It also causes severe eye damage. When handling, wear protective gloves, protective clothing, eye protection and face protection.
- Microposit® MF® CD-26 developer (Shipley) **CAUTION** this reagent is toxic in contact with skin, causes eye damage and may cause respiratory irritation. When handling, wear protective gloves, protective clothing, eye protection and face protection. Avoid breathing vapor or mists.
- Octadecyltrichlorosilane (OTS) in liquid phase (Sigma-Aldrich) **CAUTION** this reagent causes severe skin burns and eye damage. When handling, wear protective gloves, protective clothing, eye protection and face protection.
- Polydimethylsiloxane elastomer Sylgard® 184 Silicone Elastomer (Dow Corning)
- *Candida albicans* (strain from ABC Platform®) or other cells of interest
- Yeast Peptone Dextrose (YPD) broth (Difco)

- Sodium acetate (Sigma-Aldrich)
- $CaCl_2$; $MnCl_2$ (Sigma-Aldrich)
- Glacial acetic acid (Sigma-Aldrich) **CAUTION** this reagent is flammable liquid and vapor, and causes skin burns and eye damage. When handling, wear protective gloves, protective clothing, eye protection and face protection.

EQUIPMENT

- CleWin Software for mask designing
- Mask writing Heidelberg DWL 200 (Heidelberg Instruments)
- Oxygen plasma Tepla 300 (PVA TePla America)
- Coating/Developing machine EVG 120 (EVG Group)
- Production mask aligner MA 150 (Suss Microtech)
- Inductively Coupled Plasma (ICP)-Reactive Ion Etching (RIE) Multiplex Alcatel AMS4200 (Alcatel Micro Machining Systems)
- Incubator (Memmert)
- Autoclave
- Incubator-shaker MAXQ4000 (Fisher scientific)
- Centrifuge Sorvall ST16R (Fisher Scientific)
- Shaker Vortex Top-Mix 1 (Fisher scientific)
- Nanowizard III BioScience atomic force microscope (JPK Instruments) mounted on an inverted optical microscope (Zeiss Axio Observer) equipped with FireWire CCD color camera (Imaging Source), with a 20×, 40× and 50× objectives.

REAGENT SETUP

Cell culture and cell treatment

From freshly plated cells, grow *C. albicans* yeasts cells in YPD broth at 30°C with agitation (180 rpm) for 18-20 hours. Collect the cells by centrifugation at 4500g, and rinse them two times in acetate buffer. CRITICAL Cell culture and cell treatment vary according to the type of microorganisms studied. Cell solutions should be prepared fresh prior to AFM experiments.

Sodium acetate buffer

For AFM experiments, prepare a sodium acetate buffer solution containing 18 mM sodium acetate, 1 mM $CaCl_2$, and 1 mM $MnCl_2$. Adjust the pH of the solution to 5.2 with glacial acetic acid. The solution can be stored at 4°C for two months.

PROCEDURE

Generation of the silicon wafer | TIMING ~ one week

1| Design the desired micropatterns of the silicon master using the CleWin software (See supplementary information for a CleWin file of the design used).

2| Write the patterns using laser lithography (Heidelberg DWL 200) to make a glass/chromium mask

PAUSE POINT The glass/chromium can be stored at room temperature (20°C) for several months in ambient conditions at 20°C and 40 % of humidity (no degradation with time).

3| Clean a virgin silicon wafer under oxygen (pressure of 1.7 mBar) plasma for 15 min at 800 W, using the Oxygen plasma Tepla 300. The temperature of the substrate during this step is 20°C at the beginning of the procedure, and 80°C at the end.

4| Deposit hexamethyldisilazane in solution on the clean silicon master to promote adherence of the photoresist

5| Deposit the photoresist AZ ECI 3012 on the silicon master using EVG 120 automatic coating/developing machine (5 seconds of deposition and 30 seconds of spinning), and bake it for 60 s at 90°C on a hot plate (baking is included in the EVG 120 coating recipe)

6| Expose the silicon master covered by the photoresist through the glass/chromium using the mask aligner MA 150 for 10 seconds

CRITICAL STEP During exposition, a critical parameter is the type of contact between the glass/chromium mask and the silicon master. This parameter is chosen on the mask aligner MA 150. The stronger the contact between the mask and the wafer is, the weaker the diffraction of the UV during exposition is, and better the resolution of the patterns is. For small patterns (under 5 µm), it is necessary to use the strongest mode of contact between the mask and the wafer, called Vacuum contact. In this mode, the wafer is pushed towards the mask, a joint is applied around the wafer, and the air between the mask and the wafer is pumped out to generate vacuum.

7| Post-Exposure-Bake the silicon master for 60 s at 110°C on a standard hot plate in ambient air (20°C and 40% of humidity) to complete polymerization of the exposed photoresist

8| Shape the patterns by dissolving the exposed photoresist in a solution of MF CD-26 developer for 20 s

CRITICAL STEP During development, a critical parameter is the time. Indeed, if the development is too long, the MF CD-26 solution starts to attack the photoresist patterns leading to the entire removal of the smallest ones.

9| Rinse both faces of the silicon master using DI H_2O, and dry under nitrogen

10| Perform Reactive Ion Etching on the silicon master using Multiplex Alcatel AMS 4200. This step must be realized under a plasma of sulfur hexafluoride (SF_6, 200 sccm) and octafluorocyclobutane (C_4F_8, 400 sccm) at a pressure of 0.07 mBar and a power of 2800 W (Inductive Coupled Plasma).

11| Remove remaining photoresist from the silicon master under oxygen (pressure of 1.7 mBar) plasma for 15 min at 800 W, using the Oxygen plasma Tepla 300. The temperature of the substrate during this step is 20°C at the beginning of the procedure, and 80°C at the end.

12| Put the silicon master in octadecyltrichlorosilane in liquid phase in order to render the silicon wafer anti-adhesive

PAUSE POINT The silicon master is generated only once, and can be used hundreds of times. It can be stored in ambient air (20°C and 40% of humidity) for several years when protected in an adapted plastic container.

Fabrication of the microstructured PDMS stamp | TIMING ~3 h

13| Prepare a PDMS prepolymer solution containing a mixture in a 10:1 mass ration of PDMS oligomers and a reticular agent (Sylgart® kit 184).

14| Degas the prepared solution under vacuum

15| Deposit the degased PDMS solution on the silicon master

CRITICAL STEP During this step, bubbles can form and may thus cause problem in the microstructures in the PDMS stamp. To avoid this, the silicon master with the PDMS can be degased again under vacuum.

16| Cure the PDMS solution on the silicon master for 1 h at 80°C, in ambient air (40% of humidity).

PAUSE POINT The PDMS cured on the silicon master can be stored at room temperature for several months. It is recommended to store the PDMS stamps, at room temperature, in ambient air, molded on the silicon master to avoid any contamination of it.

17| Cut with a scalpel and demold the microstructured PDMS motif

CRITICAL STEP Cutting a PDMS motif off the silicon master can be critical; the scalpel must be used gently in order to avoid scratching or splitting the silicon master.

Assembly of living cells in the microstructured PDMS stamps | TIMING ~20 min

18| Deposit a PDMS stamp bearing the microstructured motif on a freshly cleaned glass slide

19| Deposit a 60 µL droplet of the cell suspension on the PDMS stamp

CRITICAL STEP The PDMS stamp is hydrophobic, and the droplet of cells sometimes does not cover up the entire PDMS stamp. To avoid this problem, it is possible to render it hydrophilic by briefly activating it under oxygen plasma for 30 s at 200 W.

20| Assemble cells into the PDMS microstructure. This can be performed in two different ways: on a convective/capillary set up (option A) or manually (option B).

(A) On a capillary/convective setup

i) drag a droplet of the *C. albicans* cells onto the PDMS stamp at a given temperature (30°C), humidity (45%) and translation speed (2 µm/s) using a motorized linear stage.

(B) Manually.

i) Use a cover slip to drag the droplet of cells several times onto the PDMS stamp.

21| Use an atomic force microscope with an inverted optical microscope to verify the filling of the wells. If the filling is good, proceed to performing an AFM experiment with the whole PDMS stamp under liquid. Use an AFM procedure adapted to the types of measurements needed on the samples (imaging, probing of nanomechanical/adhesive properties, multiparametric imaging)[18,25]. If the wells are not filled, repeat steps 19 to 21.

TIMING

Steps 1-12, generation of the silicon wafer: ~1 week

Steps 13-17, fabrication of a microstructured PDMS stamp: ~3 h

Steps 18-21, assembly of living cells in the microstructured PDMS stamps: ~20 min

TROUBLESHOOTING

Cells have not filled the PDMS microstructures (step 20)

Filling of the microstructured wells is a crucial step, the success of which depends on the convective/capillary parameters, or on the type of microorganisms used. If after the convective/capillary assembly no cells or very few have filled the PDMS microstructured wells, it is possible that the convective/capillary assembly was too fast; hence reducing the speed can lead to better results. It can also be caused by too low concentration of cells in the droplet. In this case, the cell suspension can be concentrated by centrifugation, and resuspended in a smaller volume of the buffer used, in order to increase the probability of filling the wells. Finally, another possible reason is the surface hydrophobicity of cells. In the case of *C. albicans* cells, which are very adhesive, working with hydrophobic PDMS stamps is better. However, in the case of other yeast strains, such as *Saccharomyces cerevisiae*, that present less adhesins at their surface, a hydrophobic surface will keep them from filling the wells. In this case, we advise to work with hydrophilic stamps. Making the stamp hydrophilic can easily be achieved by UV-O_3 or O_2 plasma treatment.

ANTICIPATED RESULTS

The immobilization protocol described here (Figure 1) represents a versatile and non-denaturing method to immobilize living cells of different sizes (Figure 2), and therefore of

different types, without modifying their interfaces. Figure 2 shows PDMS stamps that have been characterized using AFM; cross-sections indicate the different sizes that can be obtained on the PDMS stamp. A key advantage of this protocol is that it allows the generation of cell arrays, which enables an increased sample size and hence statistical and gives access to population heterogeneity data.

Figure 3 shows results obtained using this protocol to generate a cell array of *Candida albicans*, with AFM imaging using Quantitative Imaging™ mode from JPK Instruments[14,26]. These data demonstrate that this protocol generates cell arrays, since all the 16 wells of 4.5 x 4.5 µm² (830 pixel per well), were filled with cells. It also shows the heterogeneity that exists between cells. Indeed, as we can see on this figure, some cells are higher than others, or present a bigger diameter, or are in a budding process. Force measurements can be performed on each of the cells present in this array, thus giving access to their mechanical or adhesive properties. Using multiparametric imaging (Quantitative Imaging™ mode in this case), one image of an entire cell array can lead to the quantification at the same time of the nanomechanical properties (i.e. Young modulus) and the adhesive properties of several cells. Figure 4 shows the result of such an experiment. Figure 4a shows a height image of a cell array of 10 × 10 wells of 5 x 5 µm² (165 pixels per well), presenting a filling rate of 85%. Figure 4b shows the elasticity map corresponding to the height image, and figure 3c presents the adhesion image corresponding to the height image. This set of data clearly demonstrates the power of such a protocol, used in combination with advanced AFM modes such as multiparametric imaging. Indeed, in one acquisition performed (165 pixels per well, 2.64 s of acquisition per wells), 85 cells were imaged, probed for their nanomechanical properties and for their surface adhesive properties. It is clearly visible on figure 4b and c that the same population of cells exhibits heterogeneity; this point was first evoked in our study in 2011[11]. Thus cells of *C. albicans* that have grown in the same culture

medium present different surface adhesive properties and cell wall Young modulus. If needed, high magnification and high resolution multiparametric data (height, adhesion, stiffness) can be recorded on single cells[27]. Due to the versatility of this protocol, similar results can be obtained for microorganisms of different sizes, such as coccus bacteria, other yeasts species, or algae.

This protocol opens the avenue to further developments that could lead to great advances in the field of microbiology. Indeed, the PDMS stamp could be coupled with a microfluidic system to add different substances (such as antifungals) to each well,. By probing at the same time the nanoscale characteristics of the cells present in these two wells, a direct comparison of the effects of the two different substances could be performed.

AUTHOR CONTRIBUTION

ED and LR developed the concept and designed the experiments. ED, LR, RED and CF conceived-designed the experiments and wrote the article. ED, CF, FP, MS made the experimental work and the data analysis work. CF, FP and MS worked on the experimental protocol. All the authors discussed the results and commented on the manuscript.

ACKNOLWDEGMENTS

We thank TEAM engineers and especially Adrian Laborde for technical support in silicon master fabrication. We thank Vincent Beges for art work on Figure 1. This work was supported by an ANR young scientist program (AFMYST project ANR-11-JSV5-001-01 n° SD 30024331) to ED. ED is researcher at the Centre National de Recherche Scientifique (CNRS). CF and MS are respectively supported by a grant from "Direction Générale de l'Armement" (DGA) and from Lallemand SAS.

COMPETING FINANCIAL INTERESTS

The authors declare that they have no competing financial interests.

REFERENCES

1. Binnig, G., Quate, C. F. & Gerber, C. Atomic Force Microscope. *Phys. Rev. Lett.* **56,** 930–934 (1986).
2. Gerber, C. & Lang, H. P. How the doors to the nanoworld were opened. *Nat. Nanotechnol.* **1,** 3–5 (2006).
3. Louise Meyer, R. *et al.* Immobilisation of living bacteria for AFM imaging under physiological conditions. *Ultramicroscopy* **110,** 1349–1357 (2010).
4. Doktycz, M. J. *et al.* AFM imaging of bacteria in liquid media immobilized on gelatin coated mica surfaces. *Ultramicroscopy* **97,** 209–216 (2003).
5. Kasas, S. & Ikai, A. A method for anchoring round shaped cells for atomic force microscope imaging. *Biophys. J.* **68,** 1678–1680 (1995).
6. Kailas, L. *et al.* Immobilizing live bacteria for AFM imaging of cellular processes. *Ultramicroscopy* **109,** 775–780 (2009).
7. Francius, G., Domenech, O., Mingeot-Leclercq, M. P. & Dufrêne, Y. F. Direct Observation of Staphylococcus aureus Cell Wall Digestion by Lysostaphin. *J. Bacteriol.* **190,** 7904–7909 (2008).
8. Alsteens, D. *et al.* Structure, cell wall elasticity and polysaccharide properties of living yeasts cells, as probed by AFM. *Nanotechnology* 384005 (2008).
9. Dague, E., Alsteens, D., Latgé, J.-P. & Dufrêne, Y. F. High-Resolution Cell Surface Dynamics of Germinating Aspergillus fumigatus Conidia. *Biophys. J.* **94,** 656–660 (2008).
10. Gilbert, Y. *et al.* Single-Molecule Force Spectroscopy and Imaging of the Vancomycin/d-Ala-d-Ala Interaction. *Nano Lett.* **7,** 796–801 (2007).
11. Dague, E. *et al.* Assembly of live micro-organisms on microstructured PDMS stamps by convective/capillary deposition for AFM bio-experiments. *Nanotechnology* **22,** 395102 (2011).
12. Francois, J. M. *et al.* Use of atomic force microscopy (AFM) to explore cell wall properties and response to stress in the yeast Saccharomyces cerevisiae. *Curr. Genet.* **59,** 187–196 (2013).
13. Pillet, F., Chopinet, L., Formosa, C. & Dague, É. Atomic Force Microscopy and pharmacology: From microbiology to cancerology. *Biochim. Biophys. Acta BBA - Gen. Subj.* **1840,** 1028–1050 (2014).
14. Chopinet, L., Formosa, C., Rols, M. P., Duval, R. E. & Dague, E. Imaging living cells surface and quantifying its properties at high resolution using AFM in QI^{TM} mode. *Micron* **48,** 26–33 (2013).
15. Formosa, C. *et al.* Nanoscale Effects of Caspofungin against Two Yeast Species, Saccharomyces cerevisiae and Candida albicans. *Antimicrob. Agents Chemother.* **57,** 3498–3506 (2013).
16. Pillet, F. *et al.* Uncovering by Atomic Force Microscopy of an original circular structure at the yeast cell surface in response to heat shock. *BMC Biol.* **12,** 6 (2014).
17. Beauvais, A. *et al.* Deletion of the α-(1,3)-Glucan Synthase Genes Induces a Restructuring of the Conidial Cell Wall Responsible for the Avirulence of Aspergillus fumigatus. *PLoS Pathog* **9,** e1003716 (2013).

18. Dufrêne, Y. F., Martínez-Martín, D., Medalsy, I., Alsteens, D. & Müller, D. J. Multiparametric imaging of biological systems by force-distance curve-based AFM. *Nat. Methods* **10,** 847–854 (2013).
19. Dufrêne, Y. F. Atomic force microscopy and chemical force microscopy of microbial cells. *Nat. Protoc.* **3,** 1132–1138 (2008).
20. Francius, G. *et al.* Stretching polysaccharides on live cells using single molecule force spectroscopy. *Nat. Protoc.* **4,** 939–946 (2009).
21. Beaussart, A. *et al.* Quantifying the forces guiding microbial cell adhesion using single-cell force spectroscopy. *Nat. Protoc.* **9,** 1049–1055 (2014).
22. Roduit, C. *et al.* OpenFovea: open-source AFM data processing software. *Nat. Methods* **9,** 774–775 (2012).
23. Cai, D. K., Neyer, A., Kuckuk, R. & Heise, H. M. Optical absorption in transparent PDMS materials applied for multimode waveguides fabrication. *Opt. Mater.* **30,** 1157–1161 (2008).
24. Chabinyc, M. L. *et al.* An Integrated Fluorescence Detection System in Poly(dimethylsiloxane) for Microfluidic Applications. *Anal. Chem.* **73,** 4491–4498 (2001).
25. Liu, S. & Wang, Y. Application of AFM in microbiology: a review. *Scanning* **32,** 61–73 (2010).
26. JPK Instruments. QITM mode- Quantitative Imaging with the Nanowizard 3 AFM. at <www.jpk.com>
27. Formosa, C. *et al.* Multiparametric imaging of adhesive nanodomains at the surface of Candida albicans by atomic force microscopy. *Nanomedicine Nanotechnol. Biol. Med.* doi:10.1016/j.nano.2014.07.008

FIGURES

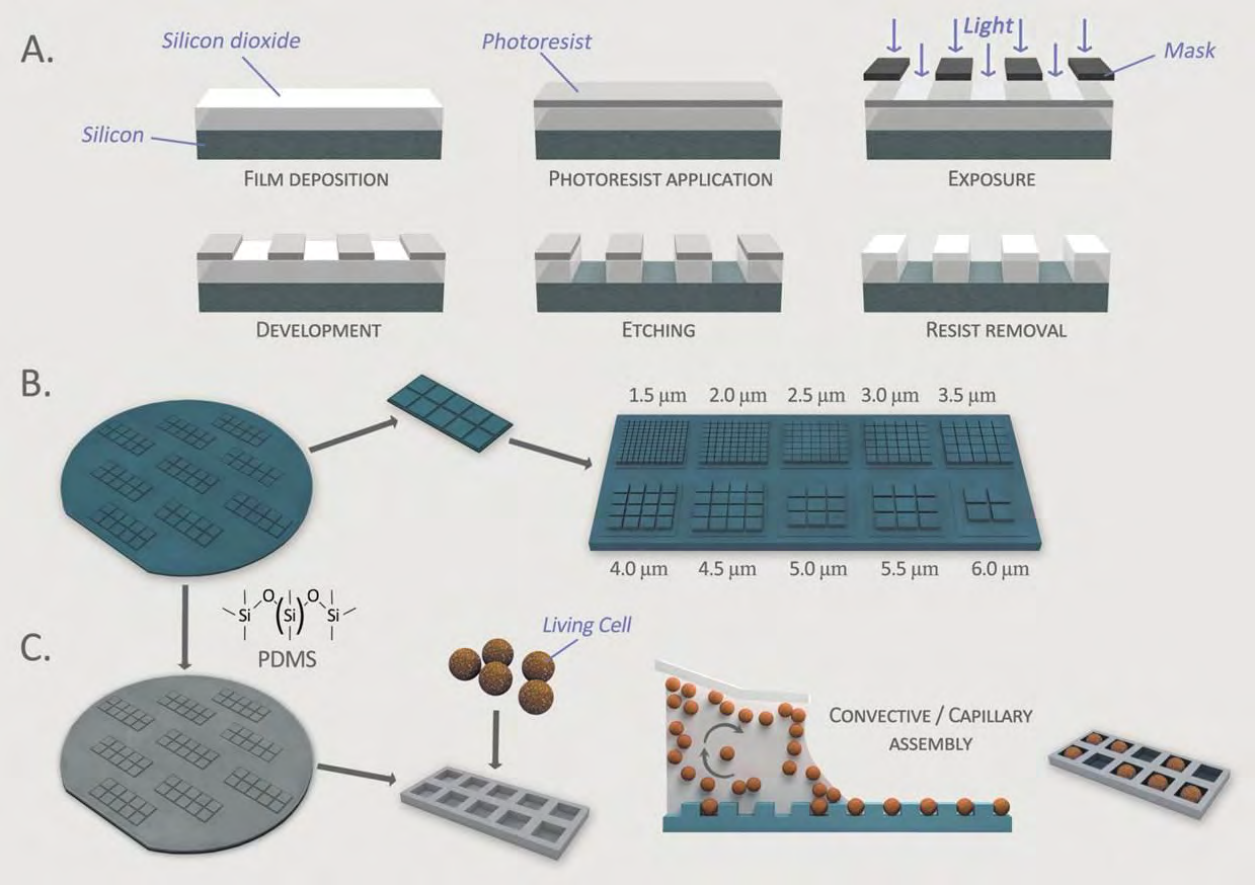

Figure 1. Schematics of the protocol of living cell immobilization. (A)The first stage consists of generation of a microstructured silicon master presenting the negative geometry desired for the PDMS stamps. (B) The second stage is dedicated to the PDMS stamp molding. Liquid PDMS is flowed over the silicon master and reticulated for 1h at 80°C. (C) Living cells are finally assembled inside the micro-patterns of the PDMS stamp by convective/capillary deposition forming a cell array.

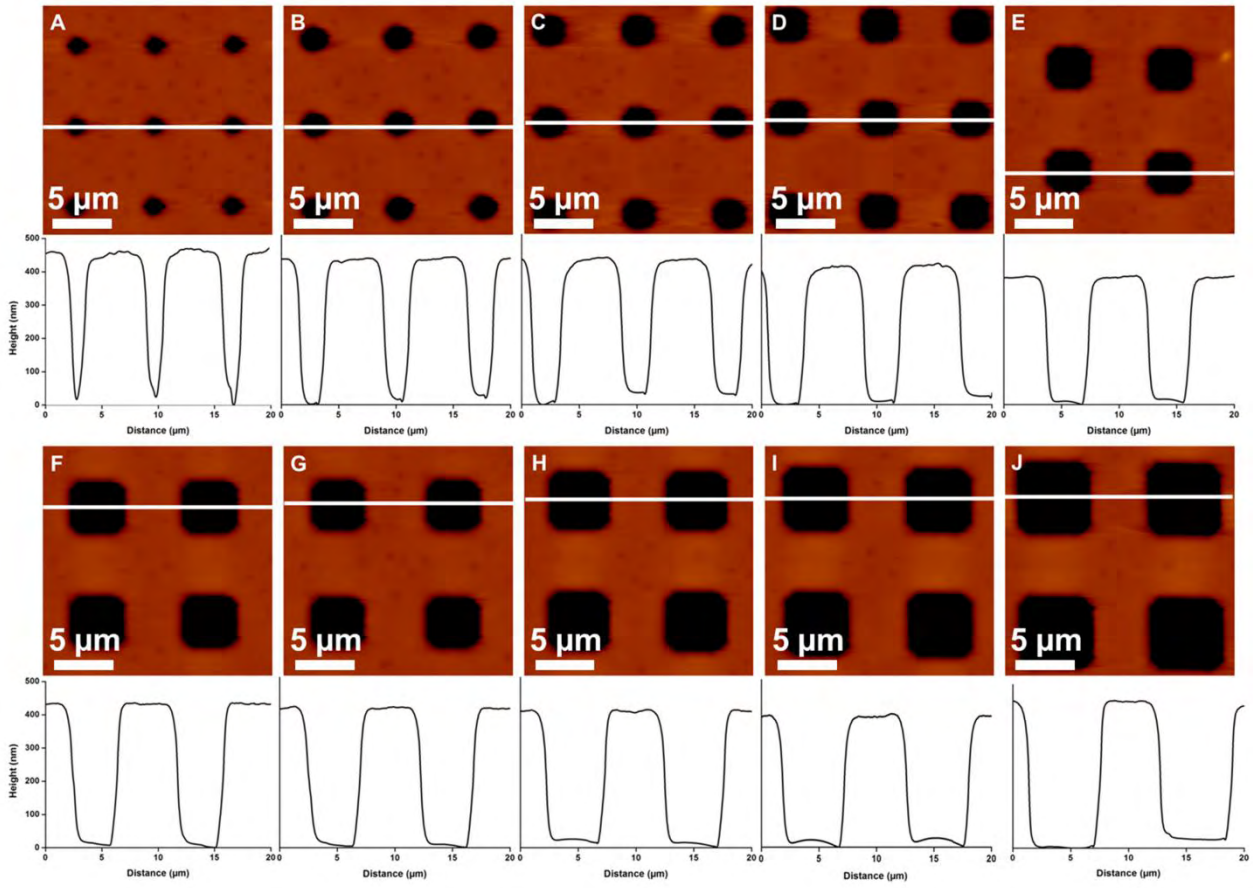

Figure 2. Characterization of the PDMS stamps obtained. AFM 2D Height images (scan-size = 20 µm, z-range = 0.5 µm) and corresponding cross-sections taken along the white lines on the height images. The structure sizes range from 1.5 µm (A), to 6 µm (J) with a pitch of 0.5 µm.

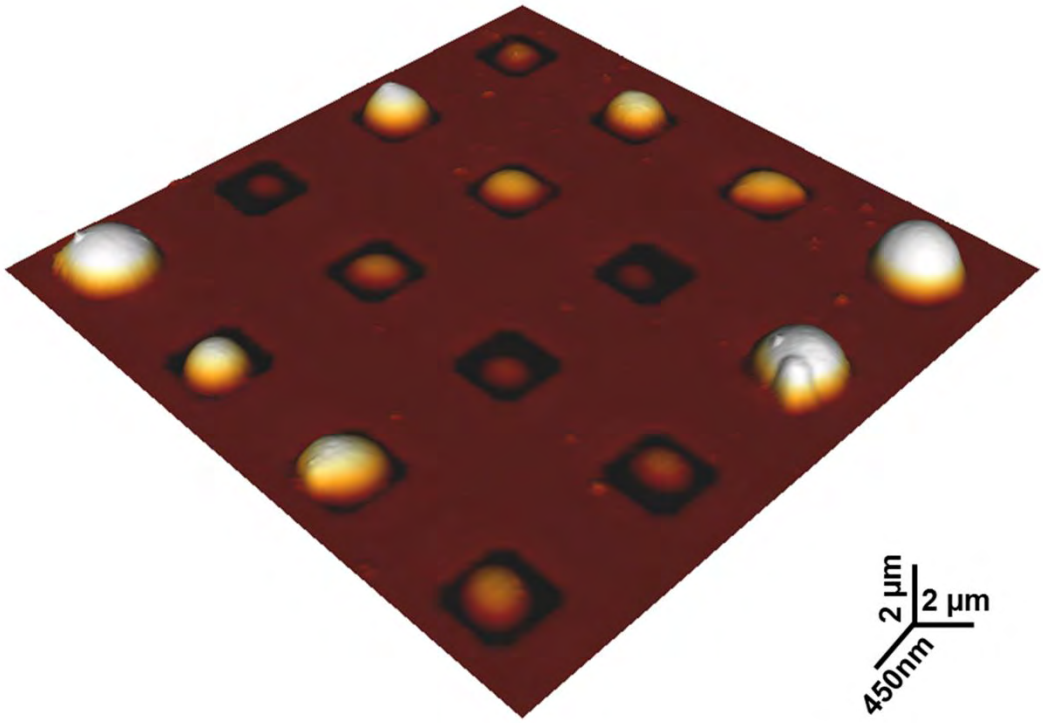

Figure 3. Imaging of a *C. albicans* cell array. AFM 3D height image (scan size = 40 µm, z-range = 2 µm) of an array of 4 × 4 microstructured PDMS wells, exhibiting a filling rate of 100%, in sodium acetate buffer.

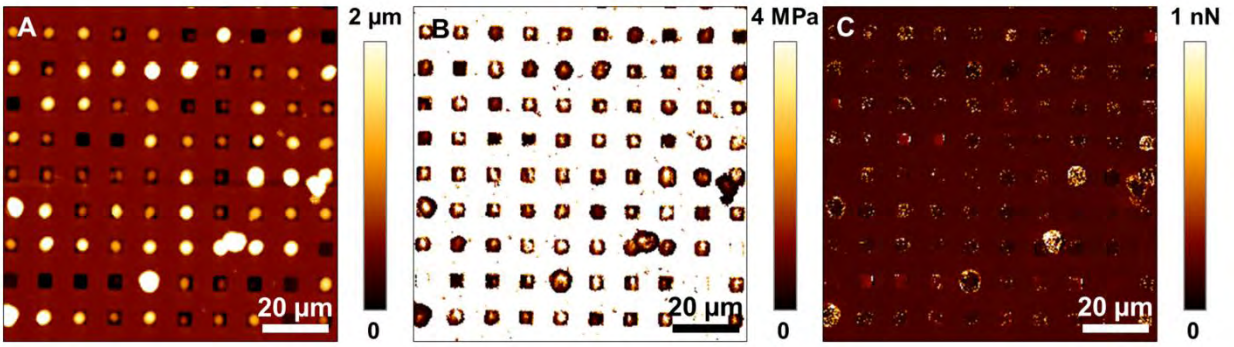

Figure 4. Multiparametric imaging of a *C. albicans* array. (A) AFM 2D height image (scan size = 100 µm) of an array of 10 × 10 microstructured PDMS wells, exhibiting a filling rate of 85%. (B) elasticity map and (C) adhesion map corresponding to the height image presented in (A).

Chapter 3.1: Technological developments to study the cell wall of microorganisms by AFM

3.1.2 Imaging living cells surface and quantifying its properties at high resolution using AFM in QI™ mode.

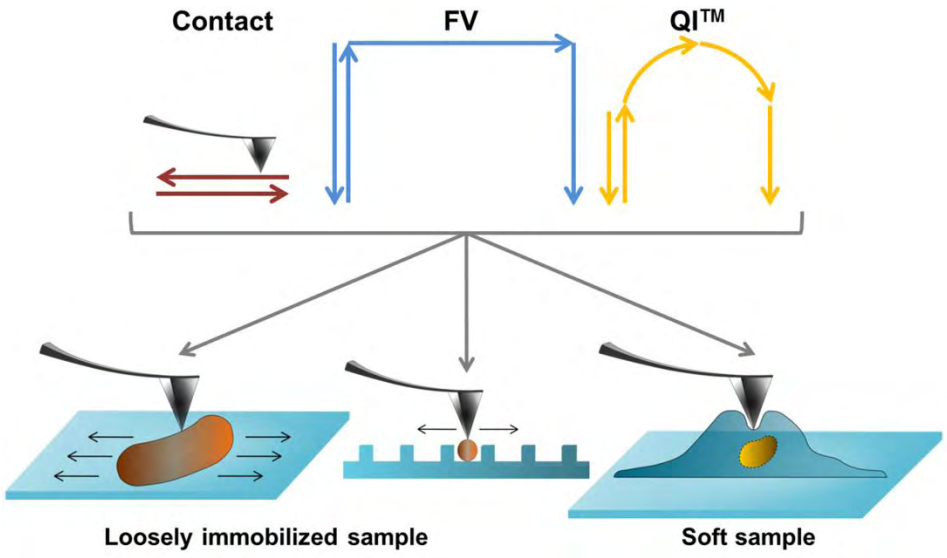

Chopinet L*., Formosa C*., Rols M. P., Duval R. E., and Dague E.

*These two authors equally contributed to the work

Micron, **48**, 26-33, 2013

Abstract

Since the last 10 years, AFM has become a powerful tool to study biological samples. However, the classical modes offered (imaging or tapping mode) often damage sample that are too soft or loosely immobilized. If imaging and mechanical properties are required, it requests long recording time as two different experiments must be conducted independently. In this study we compare the new QITM mode against contact imaging mode and force volume mode, and we point out its benefit in the new challenges in biology on six different models: *Escherichia coli*, *Candida albicans*, *Aspergillus fumigatus*, Chinese hamster ovary cells and their isolated nuclei, and human colorectal tumor cells.

Micron 48 (2013) 26–33

Contents lists available at SciVerse ScienceDirect

Micron

journal homepage: www.elsevier.com/locate/micron

Imaging living cells surface and quantifying its properties at high resolution using AFM in QI™ mode

L. Chopinet[a,b,c,1], C. Formosa[a,c,d,e,1], M.P. Rols[b,c], R.E. Duval[e,f,g], E. Dague[a,c,d,*]

[a] Centre National de la Recherche Scientifique, Laboratoire d'Analyse et d'Architecture des Systèmes (LAAS), Toulouse, France
[b] Centre National de la Recherche Scientifique, Institut de Pharmacologie et de Biologie Structurale, Toulouse, France
[c] Université de Toulouse, Toulouse, France
[d] Institut des Technologies Avancées en Sciences du Vivant, Toulouse, France
[e] CNRS, SRSMC (Structure et Réactivité des Systèmes Moléculaires Complexes), UMR 7565, Nancy, France
[f] Université de Lorraine, SRSMC, UMR 7565, Faculté de Pharmacie, Nancy, France
[g] ABC PlatformR, Nancy, France

ARTICLE INFO

Article history:
Received 13 December 2012
Received in revised form 6 February 2013
Accepted 7 February 2013

Keywords:
Atomic force microscopy
Quantitative imaging
Microorganisms
Eukaryotic cells
Imaging
Nanomechanical properties

ABSTRACT

Since the last 10 years, AFM has become a powerful tool to study biological samples. However, the classical modes offered (imaging or tapping mode) often damage sample that are too soft or loosely immobilized. If imaging and mechanical properties are required, it requests long recording time as two different experiments must be conducted independently. In this study we compare the new QI™ mode against contact imaging mode and force volume mode, and we point out its benefit in the new challenges in biology on six different models: *Escherichia coli*, *Candida albicans*, *Aspergillus fumigatus*, Chinese hamster ovary cells and their isolated nuclei, and human colorectal tumor cells.

1. Introduction

Since 25 years, Atomic Force Microscopy has emerged as a valuable tool in biology, to study the morphology of living cells, their surface roughness, and theirs nanomechanical properties (elasticity through Young modulus (YM) values, Single molecule force spectroscopy) (Müller and Dufrêne, 2011). Technological improvements were required to make this jump from physics to biology.

Classically, AFM provides two imaging modes to probe biological sample known as contact mode and tapping mode. In contact mode, the AFM tip raster scans over the sample to obtain high resolution images of sample surface in terms of height, the sample topography being measured by detecting changes in the deflection of the tip as a function of position on the surface (Liu and Wang, 2010). However, when applied to deformable soft samples, the resulting topographic images are poorly correlated with the variations in height across the sample since the AFM tip deforms the surface during the raster scan. As a second imaging mode, taping mode allows to image soft sample and with a very good resolution (Milhiet et al., 2011). In this mode, very stiff cantilever is used, and is oscillating near its resonance frequency during the scan, without being in contact with the sample. Change in the amplitude of oscillation during raster scanning report on the surface topography. Consequently, the lateral forces between the tip and the sample can be significantly reduced, which, in principle, avoid the deformation artifacts associated with contact-mode imaging. However, in a biological system where the electrolyte concentration is high, interactions with low-range surface forces affect the vibrating tip during its trajectory. These forces can influence the oscillation amplitude; therefore the contact between the tip and the sample becomes unavoidable, leading to a deformation of the sample.

Recent developments have conducted to high speed AFM (Kodera et al., 2010) or multi-frequency force spectroscopy (Garcia and Herruzo, 2012) in order to image sample faster. Those two modes overcome the time limitation by increasing the scan rate. However no biophysical properties can be extracted from the data, since these two advanced modes functions with oscillating tips. Indeed, besides topography imaging, AFM can also be used in force spectroscopy mode to measure biophysical properties of samples (such as elasticity and molecular organization of the sample surface) (Formosa et al., 2012b; Heinisch and Dufrene, 2010). A major

* Corresponding author at: Centre National de la Recherche Scientifique, Laboratoire d'Analyse et d'Architecture des Systèmes (LAAS), 7 avenue du colonel Roche, F-31400 Toulouse, France. Tel.: +33 561337841.
E-mail address: edague@laas.fr (E. Dague).
[1] These two authors contributed equally to the work.

0968-4328/$ – see front matter © 2013 Elsevier Ltd. All rights reserved.
http://dx.doi.org/10.1016/j.micron.2013.02.003

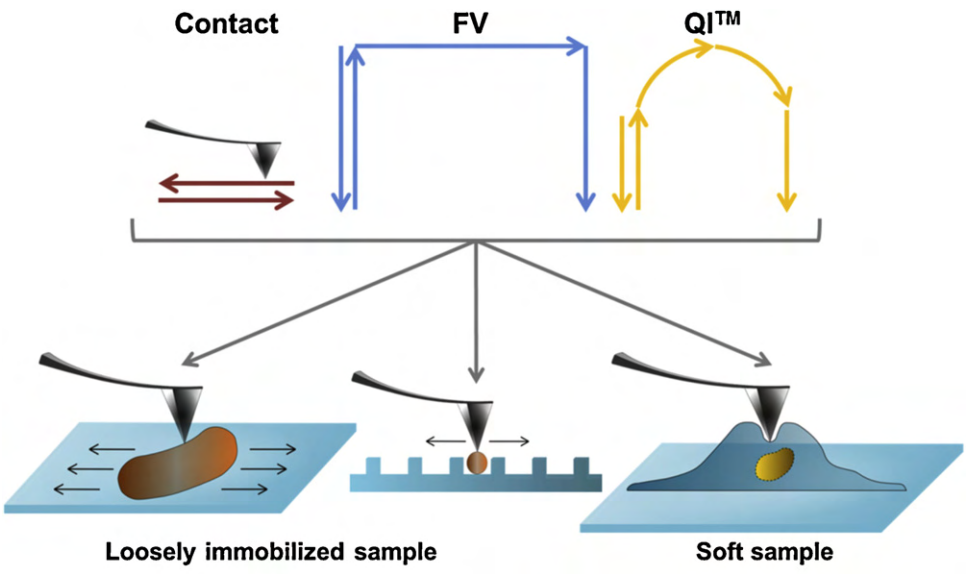

Fig. 1. Schematic outline representation. Contact, force volume (FV) and quantitative imaging™ (QI™) modes were applied to 3 different kinds of sample: loosely immobilized sample on PEI charged surface or on microstructured PDMS stamps, and soft sample.

interest of AFM is to combine imaging and force spectroscopy in order to make a link between structures and functions (Dufrene, 2004).

It was therefore needed to find a way to measure mechanical properties and image cells in liquid conditions, without altering their cell surface, or removing them from the substrate by lateral forces exerted by the scanning tip. A solution to this problem was to use a force-volume (FV) (also known as force mapping) mode. This mode, originally proposed by Radmacher et al. (1994), involves collecting a matrix of force curves across the sample surface that are individually analyzed, allowing spatial reconstruction of topographic maps. This avoids the problem of lateral forces associated with contact-imaging of soft surfaces, since the tip moves from point to point across the surface, the AFM tip being completely detached from the surface before moving to the next point. A particular interest of this mode is the possibility to extract the zero-force contact point from the fit to each force curve. From the zero-force contact points, an image that approximates the underformed ("true") sample topography can be reconstructed. However, there is still the main problem of using a FV mode: the time needed to acquire each force curve being too long, acquiring high resolution arrays can take hours, which is a problem while working on short term effects with living cells under physiological conditions. Moreover, the FV, because of its low resolution, does not give accurately precise images (Gaboriaud et al., 2008), leading to misinterpretations of the data collected. Therefore, if imaging data and mechanical properties want to be recorded, each will ask an individual acquisition with two different modes (contact/tapping imaging and FV), requiring for more and more time.

We present in this study a new advanced mode called quantitative imaging™ (QI™, ("QITM mode-quantitative imaging with the NanoWizard 3 AFM")), which allows acquiring high-resolution maps on challenging samples such as soft or loosely bound ones. We present a comparison of the mode with contact mode and force volume mode. In this quantitative imaging mode, force curves can be collected at the same speed and resolution as normal imaging. Thanks to the software OpenFovea developed by Kasas' team that analyzes the elasticity as a function of the indentation (Longo et al., 2012; Roduit et al., 2012b), we overcame the data treatment problem caused by the acquisition of thousands of force curves. The data can then be interpreted to provide information on elasticity or adhesion. This mode is based on force curve acquisition, processed quicker than a FV as the tip move laterally when retracted to be positioned above the next point measurement before approaching. The time to record a single force curve is up to 1.000 μm/s, and the resolution up to 512 px^2. As one force curve is recorded for each pixel, it allows having in a single acquisition both mechanical properties and topography data of the sample. We will demonstrate in this study that imaging and measuring soft sample or loosely immobilized ones in liquid is possible.

We applied this new imaging mode on four different biological samples (Fig. 1):

- living adherent mammalians cells (Chinese hamster ovary and human colorectal tumor cells), that are very soft and thus do not withstand forces exerted by a scanning tip,
- Chinese hamster ovary cell nuclei on PDMS without any fixation or PEI coated glass slides,
- yeasts cells and *Aspergillus fumigatus* spores immobilized in PDMS micro-structured stamps with no chemical fixation and are thus loosely bound to the substrate,
- *Escherichia coli* cells, immobilized on PEI coated glass slides under physiological conditions, meaning imaged in an ionic buffer that weaken the electrostatic interactions and make the bacterial cells loosely attached to the sample.

Through these different biological models and the data acquired with QI™ mode, we show how this imaging/spectroscopy mode is of interest for the challenges in biological sample characterization, and allows imaging of unexplored types of eukaryotic and prokaryotic cells.

2. Materials and methods

2.1. Atomic force microscopy

JPK NanoWizard 3 (JPK instrument, Berlin, Germany) coupled with an axiovert microscope from Zeiss was used for most of the experiment, with contact mode, force volume or QI™ mode and

cells imaging was done using the Petri Dish Heater. catalyst AFM from Bruker (Bruker, USA), coupled with Nikon fluorescence microscope was used for contact imaging of CHO cells with the Perfusing Stage Incubator. We used MLCT cantilevers (Bruker probes) with spring constant ranging from 0.028 to 0.042 N/m for mammals cells and from 0.011 to 0.019 for yeast and bacterial samples. QI™ and force mapping settings used are the following on mammals cells: *Z*-length: 5 μm; applied force: 4 nN; speed: 166 μm/s for QI™ imaging for slow imaging, 1000 μm/s for fast imaging; 24.98 μm/s for force mapping. QI™ mode has been described in this technical report ("QITM mode-quantitative imaging with the NanoWizard 3 AFM").

2.2. Bacterial sample preparation

E. coli (strain ATCC 22925; American type culture collection [ATCC]) were stocked at −80 °C, revivified on Mueller Hinton agar (Difco, 225250–500 g) and grown in Mueller Hinton broth (Difco, 275730–500 g) for 24 h at 35 °C under static conditions. *E. coli* cells were immobilized on polyethylenimine (PEI, Fluka P3124-100 mL) coated glass slides as described previously. Briefly, freshly oxygen plasma activated glass slides were covered by a 0.2% PEI solution in deionized water and left for incubation overnight. Then glass slides were rinsed with 20 mL of Milli-Q water and nitrogen dried. Bacterial cultures were harvested by centrifugation, washed two times in Milli-Q water, and resuspended to a concentration of $\sim 10^8$ cells/mL in phosphate buffered-saline 1X (10 mM) (PBS, Sigma, P2194-10PAK). A total of 1 mL of the suspension was applied to the PEI coated glass slide, allowed to stand for 1 h and rinsed with PBS 1X. AFM images and force-distance curves were recorded in PBS 1X in quantitative imaging mode with an AFM NanoWizard III (JPK Instruments, Berlin, Germany).

2.3. Yeast sample preparation

Candida albicans (from ABC© platform, Nancy, France) were stocked at −80 °C, revivified on standard YPD Agar (Difco, 225250–500 g) and grown in YPD Broth (Difco, 275730–500 g) for 24 h at 30 °C under static conditions. *C. albicans* cells were immobilized on microstructured PDMS stamps fabricated as described previously (Dague et al., 2011). Yeasts cultures were harvested by centrifugation, washed two times in acetate buffer (18 mM sodium acetate, 1 mM $MnCl_2$, 1 mM $CaCl_2$), and resuspended to a concentration of $\sim 10^8$ cells/mL in acetate buffer. A total of 100 μL of the suspension was deposited on the PDMS stamps by convective/capillary assembly. AFM images and force-distance curves were recorded in acetate buffer in quantitative imaging mode with an AFM Nanowizard III (JPK Instruments, Berlin, Germany).

2.4. Mammalian cell sample preparation

Chinese Hamster Ovary cells (wild type Toronto from ATCC) were grown in Minimum Eagle's Medium (MEM) supplemented with 8% fetal calf serum (Gibco), 1% peniciline (100 μmL^{-1})(Gibco)and 1% streptomycine (100 $mg\,mL^{-1}$) (Sigma), and incubated at 37 °C in humidified atmosphere with a 5% CO_2 incubator. Human Colorectal Tumor cells from ATCC, were grown in Dubelco modified Eagle's medium (DMEM; Gibco) without pyruvate supplemented with 8% fetal calf serum and 1% same antibiotics mixture as CHO cells. 75,000 cells for each type were grown in Petri dish during 24 h before measurement, and classical medium was replaced by MEM-HEPES medium (CM1MEM46-6U, Eurobio) supplemented with 8% fetal calf serum and cells were placed in the PetriDishHeater (JPK instrument, Berlin Germany) that maintained 37 °C during all the experiment. For experiment on catalyst (Bruker, USA), classical medium was used and 5% CO_2 gas was exposed trough the perfusing stage incubator.

2.5. Nucleus extraction

All the extraction process was run at 4 °C. 1 mL extraction buffer (15 mM Tris–HCl, pH 7.5, 0.15 M NaCl, 5 mM $MgCl_2$, 10 mM $CaCl_2$, 0.1% Tween 20, and a mixture of protease inhibitors (Roche Applied Science), 1 mM AEBSF (Euromedex 50985), 0.5% NP10) was added to −80 °C frozen culot of cells previously harvested and centrifugated in PBS (10 min 4 °C 500 × *g*). Cells were resuspended and homogeneizated gently by pipette 15 times. Then 3 × 15 s with 5 min between each at minimal speed of Thurax T25 basic homogenieizer were applied, and fractions were centrifuged 10 min at 800 × *g*, washed in PBS and centrifuged 3 min at 500 × *g* to obtain 70% extracted nuclei.

2.6. Data analysis

JPK data processing (JPK Instrument, Berlin, Germany) software was used for image processing. Images are flattened (order 1). OpenFovea 0.1a152 software was used for force curve analysis with the following settings: Model: cone; tip size: 0.62 rad; Poisson ratio: 0.5; method: raw: $F = ((2E\tan\alpha)/(\pi(1-\nu^2))\delta^2$. This Hertz model gives the force F as a function of the indentation (δ) and of the Young modulus (E). The opening angle (α) of this sort of tip is 35° and we arbitrary choose a Poisson ratio (ν) of 0.5. Size of indentation segment where Hertz fit was done is specified in figure legend.

3. Results

3.1. Imaging

3.1.1. Loosely immobilized micro-organisms and organelle

E. coli and *C. albicans* cells were scanned, both in contact mode and QI™ mode (Fig. 2a–d) under physiological conditions.

E. coli, a gram-negative bacterium, is the model bacteria. Moreover it is the bacteria the most frequently found in nosocomial infections (23%) and should therefore be highly investigated by AFM in order to explore therapeutic targets at the nanoscale (Formosa et al., 2012a). Nevertheless, few AFM studies are dedicated to *E coli* (Abu-Lail and Camesano, 2006; Cerf et al., 2009, 2008; Fantner et al., 2010; "Quantitative imaging of living biological samples by PeakForce QNM atomic force microscopy"), because of immobilization difficulties. The classical method using electrostatic interactions works poorly with this weakly negatively charged (De Kerchove and Elimelech, 2005) bacterium. The electrostatic interactions between the cell and the polycationic surface are not strong enough to immobilize the cell. When imaged in contact mode, we can see in Fig. 2a that the bacteria do not withstand the lateral forces exerted by the scanning tip, and are removed from the surface, even with the lowest applied force (0.5 nN). Any images of this microorganism are therefore impossible to record. Recent works by Longo et al. (2012) present nanoindentation images of *E. coli* cells. This is also a way to image this bacterial species, however, the lateral resolution shown by the authors is of 32 px^2, which is very low and does not allow a detailed observation of the bacterial cell wall. Here, we show height image (Fig. 2b) of *E. coli* cells, at a resolution of 256 px^2. Its dimensions can therefore be precisely determined since the height image obtained was calculated from the point of contact on each force curve recorded.

Candida albicans is also a dangerous microorganism. It is responsible for nosocomial infections, and causes a range of conditions including painful superficial infections, severe surface infections, and life-threatening blood-stream infections (Sudbery et al., 2004).

It is therefore a need to be able to image this yeast, in order to study its morphology, or the effects of antifungal molecules on its cell wall. Teams are already working on round cells of *C. albicans* with atomic force microscopy using porous membrane to trap them (Alsteens et al., 2008; Beaussart et al., 2012). But this technique causes mechanical stress on the cells. Here, we chose to refine a recent immobilizing method based on microstructured PDMS stamps (Dague et al., 2011). PDMS is a biocompatible polymer that does not affect the viability or the morphology of the yeasts cells. For these cells, we also used contact mode; as we can see on Fig. 2c, the beginning of the cell can be scanned, but very soon the scanning tip removes the cell from its hole, even with a very low applied force, as for *E. coli* samples. In QI™ mode, however, high resolution "zero-force" height image of the entire cells can be obtained (Fig. 2d).

As a last example of non-immobilized sample, we took isolated mammalian cell nuclei. Nucleus is one of the most important organelle of the mammalian cells as it contains genetic information. AFM on nuclei or other organelles studies are using flattened nuclear envelope on glass slide (Oberleithner et al., 1994), dried sample (Layton and Boyd, 2011) or only elasticity measurement through plasma membrane (McKee et al., 2011). As for bacteria and yeast, imaging isolated whole nucleus required its immobilization. We can see that contact image deformed nucleus, even if immobilized thanks to positive charge interaction on PEI glass slide with negative charge of nucleus envelope (Fig. 2e) (Layton and

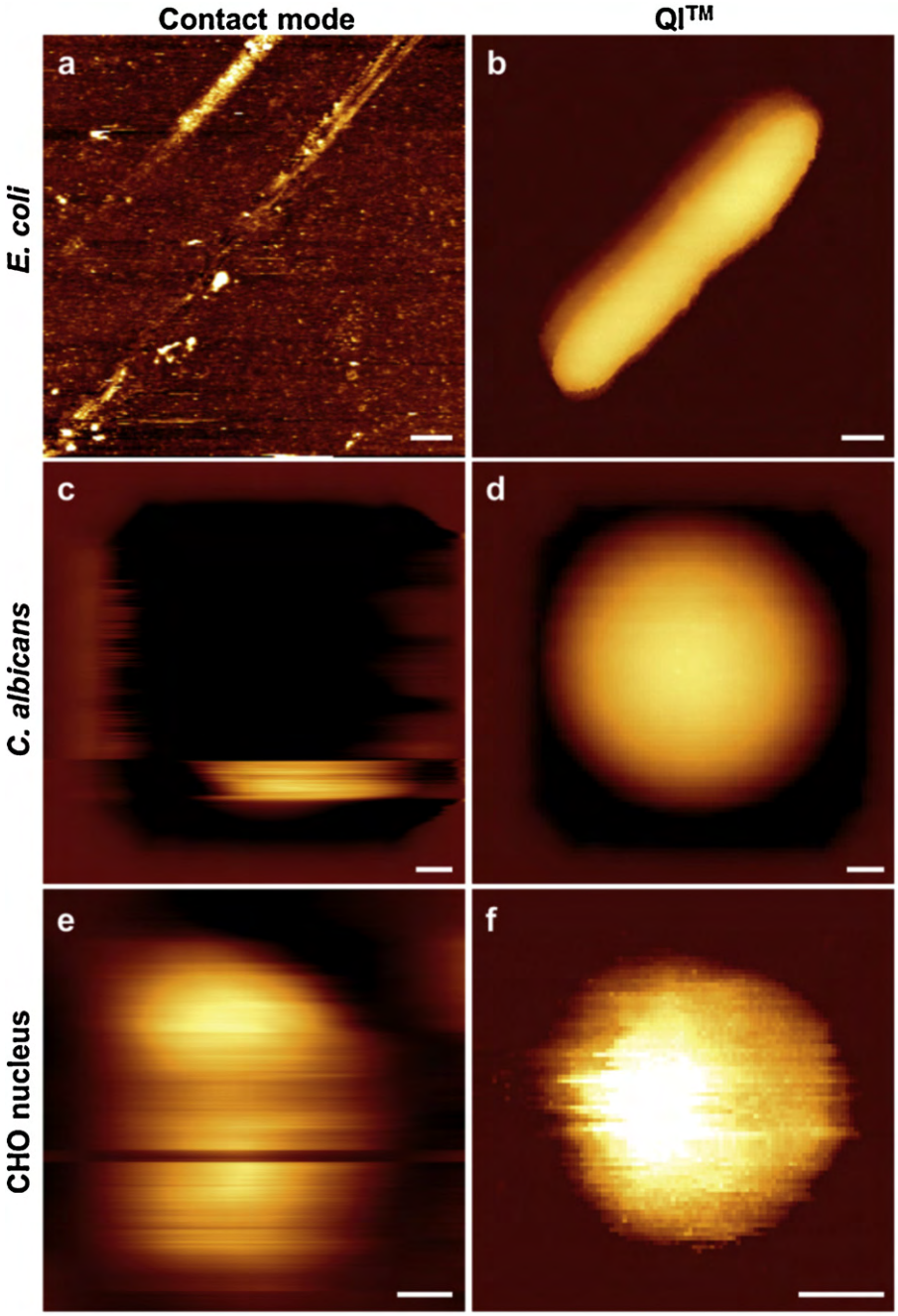

Fig. 2. Imaging of loosely immobilized samples. Contact height image (resolution: 512 lines) of (a) an *E. coli* cell (*z*-range = 1.2 μm, (c) a *C. albicans* cell (*z*-range = 2 μm) and (e) of a CHO nucleus (*z*-range = 1.8 μm). QI™ height image (256 px²) of (b) a *E. coli* cell (*z*-range = 20 nm), (d) a *C. albicans* cell (*z*-range = 2 μm) and (f) a CHO nucleus (*z*-range = 2 μm). The QI™ height images correspond to the contact height images. Scale bar a–d: 0.5 μm; e and f: 2 μm.

Boyd, 2011). With QI™ mode, imaging of nucleus can be achieved when nucleus is on PDMS without any electrostatic immobilization (Fig. 2f). Thanks to the non-destructive interaction between tip and sample, direct mechanical measurements in correlation with image acquisition can now be achieved on cells organelles.

3.1.2. Mammalian cells

Mammalian cell plasma membrane is very sensitive to tip when imaged in contact. Most of the time, their ability to adhere to the substrate they grow on allows the cells no to be removed by the scanning tip (Schulze et al., 2009). Though, this may not be sufficient, and different glass coating like poly-lysine, fibronectin or laminin must be used to enhance cell adhesion on substrate (Yokokawa et al., 2008). Despite these several immobilization techniques, the membrane/wall composition of eukaryotic cells is often a reason of unsuccessful AFM trials on living cells and incites to work on fixed cells. We studied living CHO cells that are a regular model for *in vitro* studies (Gamper et al., 2005) or, for example, membrane protein production (as ions channels) (Che Abdullah et al., 2011) and living HCT116 cells that are of interest for *in vitro* studies of cancer cell behavior and cancer treatment (Brattain et al., 1981). As shown in Fig. 3, one can managed to obtain good image of CHO or HCT116 cells after several try changing orientation of scanning not to disturb the cell (Fig. 3a and b), but most of the time some extensions related to tip/membrane interactions are visible (Fig. 3b) and do not give a good representation of the cell surface. Fig. 3c and d gives a good example of the quality obtained when imaging with QI™ mode at the same speed than classical contact imaging (Fig. 3c and d, 45 min required, 166 μm/s tip speed), or imaging faster (Fig. 3e, 15 min required, 1000 μm/s tip speed). QI™ mode images, because of their higher resolution, give more defined images of the cell surface (Fig. 3d), than FV image (Fig. 3f).

3.2. Mechanical properties

QI™ mode is not only useful for imaging difficult samples; it is also useful for nanomechanical measurements on those samples. Mechanical properties recording require a very well defined localization and thus a high resolution and correlation with the image of the sample. The correlation can be lost when switching from a mode to another. Here we present the direct correlation between height images (Fig. 4a and d) and elasticity maps for HCT116 (Fig. 4b and c) and *C. albicans* cells (Fig. 4e and f) showing the distribution of YM values on the sample. In each case, the same data were recorded using QI™ mode (Fig. 4c and e) and FV mode (Fig. 4d and f). When comparing the two methods using Fovea software (Roduit et al., 2012a, 2012b), we show that QI™ mode is more resolutive, due to the number of recorded force curves ($n = 65\,536$ at a resolution of 256 px^2) and allow a detailed view of the sample. For HCT116 cells, even if images show part of cytoskeleton network at cells membrane extremities either with QI™ mode or FV (Fig. 3d and f) by high YM value represented in yellow–red colors; in FV mode, the YM values seem to be homogeneously distributed all over the cell (Fig. 4b). When seen in QI™, cytoskeleton fibers stiffness (most likely actin fibers) at cells extremities are well detected as a higher YM is displayed (red lines underlying stress fiber underneath the membrane) (Fig. 4c). Beyond the abilities to record a well resolved map, a QI™ force measurement has a better intrinsic resolution too. We can clearly follow the stress fiber along the cell structure. On *C. albicans*, the curvature of the cell induces artificially soft force curves at the edge that must not be analyzed (outside of

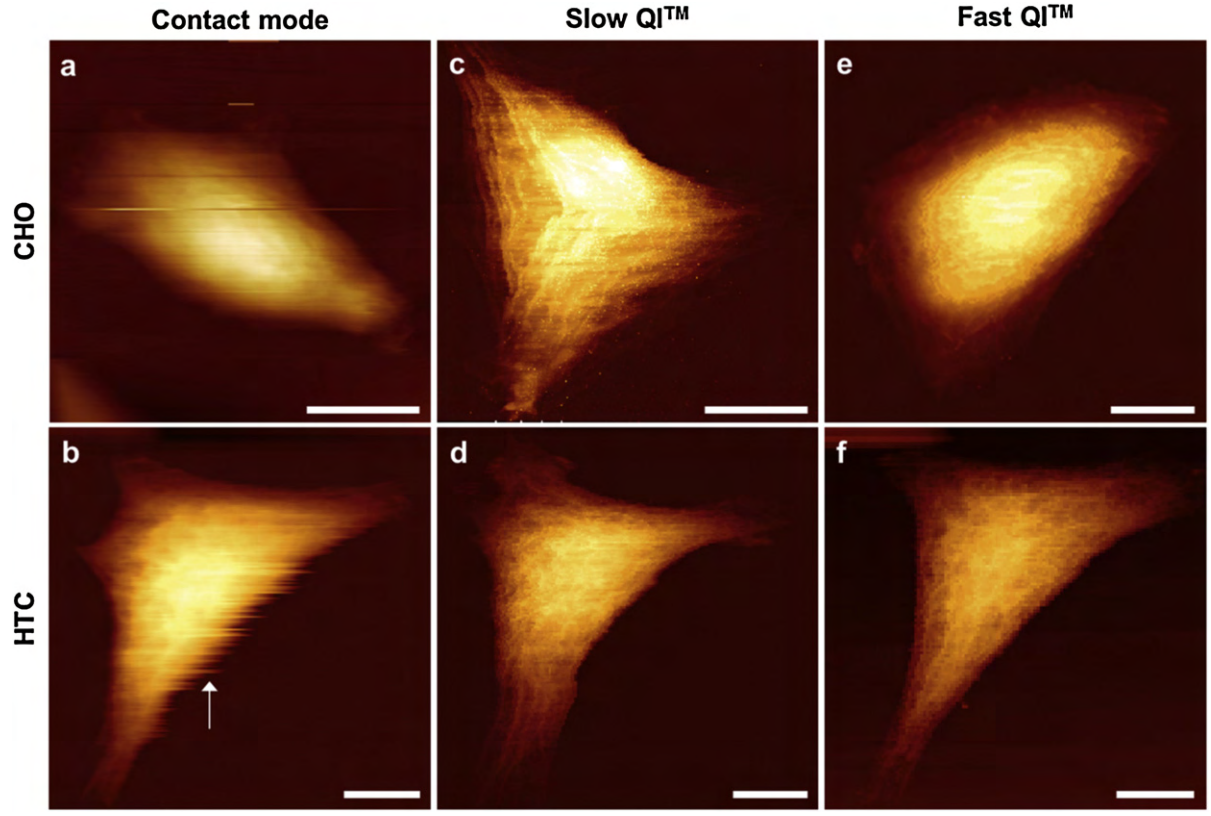

Fig. 3. Imaging of soft samples: mammals cells. Contact height image (resolution: 512 lines) of (a) a CHO cell (z-range = 4.5 μm) and (b) an HTC116 cell (z-range = 4.5 μm), the arrow point membrane extensions related to tip/membrane interactions. QI™ height image of (c) another CHO cell (256 px^2, speed = 45 min), and (d) the same HCT116 cell (256 px^2, speed = 45 min). (e) QI™ height image of (c) another CHO cell (256 px^2, speed = 15 min). (f) Force volume height image (128 px^2, speed = 15 min) of an HTC cell and. Scale bar: 10 μm. z-range for c–f: 7 μm.

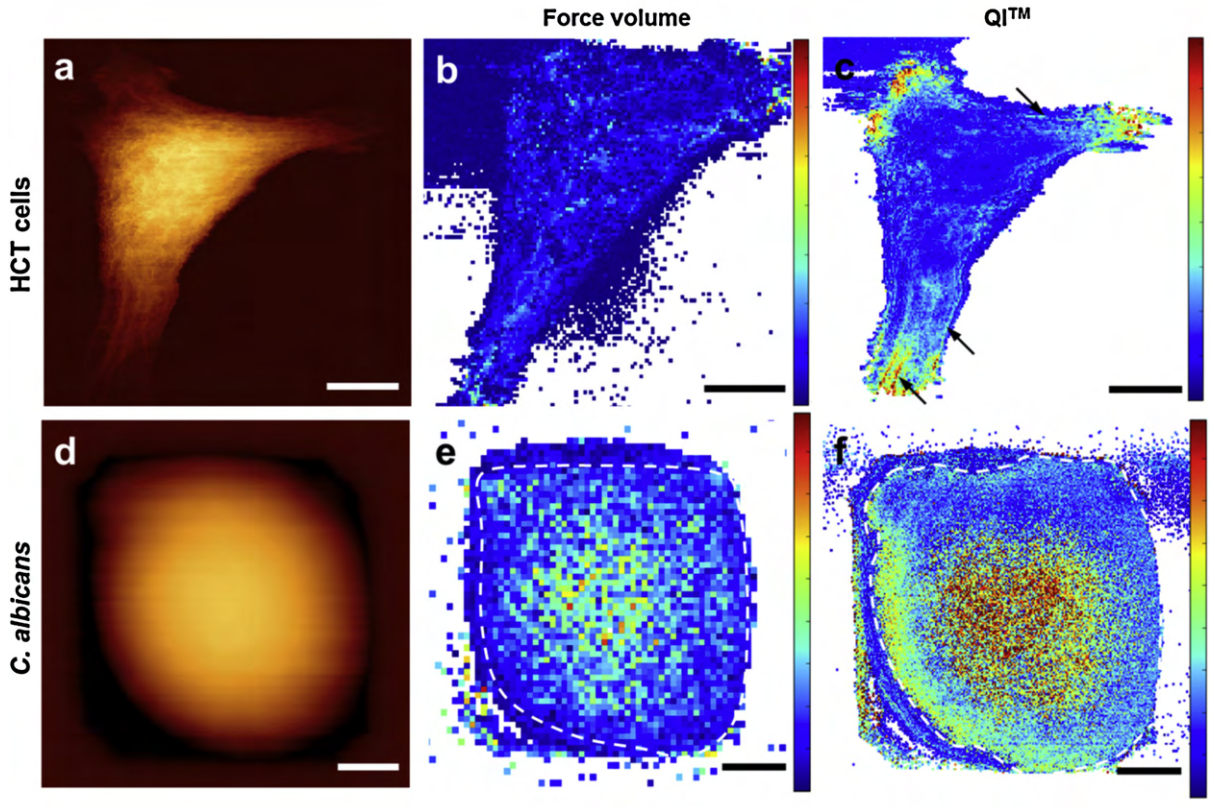

Fig. 4. Mechanical properties. QI™ height image (256 px²) of (a) an HCT116 cell (*z*-range = 7 μm). (b) Force volume elasticity map (128 px²) of the same HTC116 cell (YM-scale = 0–10 kPa). (c) QI™ elasticity map (256 px²) of the same HTC116 cell (YM-colorscale = 0–10 kPa). Arrows show the stress fibers revealed by QI™ measurement. (d) QI™ height image (256 px²) of a *C. albicans* cell (*z*-range = 2 μm). (e) Force volume elasticity map (64 px²) of the same *C. albicans* cell (YM-colorscale = 0–500 kPa). White dashed line circles the region of interest. (f) QI™ elasticity map (256 px²) of the same *C. albicans* cell (YM-colorscale = 500 kPa). White dashed line circles the region of interest. a–c: 10 μm, scale bar d–f: 1 μm.

the white region of interest drawn). In the FV mode only a small amount of force curves should finally be interpreted to extract relevant YM (250 force curves). As QI™ record more force curves, the amount of force curves that is not affected by *C. albicans* curvature is higher (4500 force curves) and the region of interest can be more accurately defined, which results in a better analysis.

If extent QI™ force curves can be analyzed for extracting YM values, retract force curves can also be analyzed. This gives access to nano-adhesive properties of entire cells, in the same time as recording the height image of the sample. This is indeed a powerful tool that can allow probing with high resolution, for example, the hydrophobic properties of cells (Alsteens et al., 2007). We present here, on Fig. 5a and d, images of spores of *A. fumigatus* trapped in PDMS microstructured stamps. On the adhesion image recorded in QI™ mode, we can directly see that the spores of the wild-type strain of *A. fumigatus* (KU strain) are adhesive, whereas the spores of the mutant strain (5T) do not show adhesion at all (Fig. 5b and e). This can be explained by the fact that wild-type spores present auto-organized hydrophobic proteins (rodlets) on their surface (Fig. 5c), whereas the mutant strain do not express these proteins (Fig. 5f), but present an hydrophilic polysaccharidic surface (Dague et al., 2008). So simply by imaging a sample, QI™ mode offers the possibility to directly visualize the adhesive properties of this sample. This gives the opportunity to ask new questions concerning the samples observed, questions that would not have been asked in the first place.

4. Discussion

This study of QI™ mode has been conducted in order to test the potentialities of this mode for biology (Table 1). (i) The first advantage of QI™ is to allow high resolution force measurements in the meantime of imaging. This point reduces drastically the time needed for each experiment and allows the direct correlation of image and mechanical/adhesion data on the same cell/sample (Fig. 4). (ii) Speed of recording can be increased to obtain images in short time; this allows accessing short time effect of component of interest (Fig. 3c). (iii) This mode allows imaging loosely bound samples; therefore there is no need to use chemical or denaturing immobilization in order to image the samples. The experiments can

Table 1
Comparative table of quantitative imaging™ mode (QI™), force volume mode (FV) and contact imaging mode.

	QI™	FV	Contact
Sample damage	++ (None)	++ (None)	−− Constant force is applied
Speed	++ (1000 μm/s)	− (2498 μm/s)	−− (≈10 μm/s, but large range)
Z-lenght	++ (8 μm)	++ (8 μm)	/
x–*y* resolution	++ (512 px²)	− (128 px²)	++ (1024 px²)
Force resolution	10 pN	10 pN	No force measurement
Analysis	++ (Any model)	++ (Any model)	No force measurement

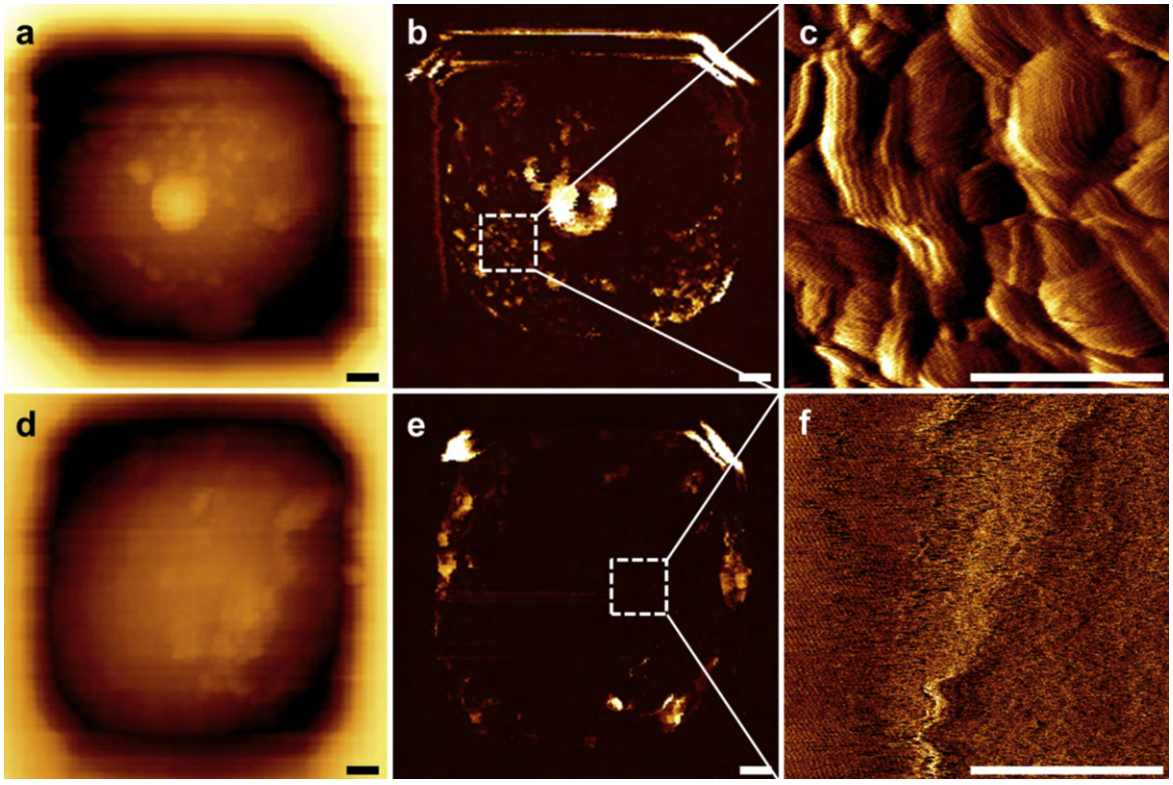

Fig. 5. Adhesive properties. QI™ height image (resolution: 256 px²) of (a) an *A. fumigatus* spore strain Ayg (wild-type) (*z*-range = 0.5 μm) and (d) an *A. fumigatus* strain 5T (*z*-range = 0.5 μm). (b and e) Adhesion image (*z*-range = 2 nN) corresponding to the height images. (c and f) Contact mode vertical deflection images of the white dashed squares on b and d. Scale bar: 0.25 μm.

then be performed in conditions of controlled temperature and in liquid, which is closer to the physiological reality of biology. (iv) The ramp size of the force curves benefit of half of the piezo length (7.5 μm). For adhesive samples like *A. fumigatus* spores, without a long enough ramp size, the interactions between the tip and the samples are never broken and prevent imaging of the spore. Such a ramp is accessible with QI™ mode, without any impact on the scan speed. (v) For mechanical/adhesive properties, the number of recorded force curves can be up to 512 × 512. For each pixel, a force curve is recorded and saved, allowing an analysis of each individual force curve (Fig. 4).

Other AFM constructers have designed modes similar to QI™ for imaging/mechanical/adhesive properties measurements at high speed and resolution. A few years ago Bruker proposed a solution named PeakForce QNM (Adamcik et al., 2012; Heu et al., 2012; Pittenger et al., 2010; Sweers et al., 2011). This mode is also a FV based mode, with a force exerted on the sample maintained constant. The force curves are recorded at a maximum speed of 2 kHz, with a maximum force curve ramp size of 300 nm. This produces a paradox: to image adhesive samples hard cantilevers must be used (and it works (Heu et al., 2012)). But in order to measure the nanomechanical properties of soft samples, soft cantilevers should be used. However, PeakForce QNM technique is able to measure YM of materials ranging from soft gels (1 MPa) to rigid polymers (20 GPa) (Young et al., 2011). In an application note the supplier claims that PeakForce QNM provides quantitative modulus results over the range of 700 kPa–700 GPa (Pittenger et al., 2010). In another application note ("Quantitative imaging of living biological samples by PeakForce QNM atomic force microscopy"), the authors were able to measure low Young modulus (ranging from 75 to 250 kPa) using softer cantilevers (Berquand, 2011). A recent study demonstrated that PFQNM is suitable for high resolution chemical force spectroscopy (Alsteens et al., 2012). The three different samples that we present in this study all have a low Young modulus; CHO cells are approximately of 30 kPa (Kuznetsova et al., 2007).

QI™ mode can also be used in Single Molecule Force Spectroscopy (SMFS), with functionalized AFM tips. It will then be possible to map the whole surface of the cell at high speed and resolution. Thus, complete cartography of proteins at the surface of cells will be possible, which is of great interest for the biologist community. Recent works by Alsteens et al. (2010) have showed the localization of Als5 at the surface of yeast over-expressing Als5p, using AFM tips functionalized by an antibody anti-Als5p. Their pioneering results are nevertheless of low resolution (roughly 16 nm), because of the limitations in terms of speed and resolution of the AFM they used. With QI™, the same kind of experiments could be performed at a higher resolution, and at the scale of the whole cell. Also QI™ retract force curves are real precise, so for example, an interaction of 50 pN can be measured, as well as in any other FV mode.

5. Conclusion

In conclusion, QI™ mode gives the opportunity to simultaneously image and measure soft or loosely immobilized samples, fast, at a good resolution, resulting in force-curve data that can be analyzed by any model. The versatility of this mode makes it the most appropriate for kinetic studies on difficult biological samples, if image data are required, or mechanical/adhesive properties, or both.

Acknowledgements

We thank Direction Générale de l'Armement (DGA) for Cécile Formosa and Louise Chopinet 3 years Ph.D. grants, ANR Young

Scientist Program “AFMyst” (#30024332) that provided financial support, Charles Roduit for providing us an updated Fovea software and, S.Roga for nucleus extraction protocole, and F. Pillet for its critical and careful reading of the manuscript.

References

Abu-Lail, N.I., Camesano, T.A., 2006. Specific and nonspecific interaction forces between *Escherichia coli* and silicon nitride, determined by Poisson statistical analysis. Langmuir 22, 7296–7301.

Adamcik, J., Lara, C., Usov, I., Jeong, J.S., Ruggeri, F.S., Dietler, G., Lashuel, H.A., Hamley, I.W., Mezzenga, R., 2012. Measurement of intrinsic properties of amyloid fibrils by the peak force QNM method. Nanoscale 4, 4426–4429.

Alsteens, D., Dague, E., Rouxhet, P.G., Baulard, A.R., Dufrêne, Y.F., 2007. Direct measurement of hydrophobic forces on cell surfaces using AFM. Langmuir 23, 11977–11979.

Alsteens, D., Dupres, V., Mc Evoy, K., Wildling, L., Gruber, H.J., Dufrene, Y.F., 2008. Structure, cell wall elasticity and polysaccharide properties of living yeasts cells, as probed by AFM. Nanotechnology, 384005.

Alsteens, D., Dupres, V., Yunus, S., Latgé, J.-P., Heinisch, J.J., Dufrêne, Y.F., 2012. High-resolution imaging of chemical and biological sites on living cells using peak force tapping atomic force microscopy. Langmuir 28, 16738–16744.

Alsteens, D., Garcia, M.C., Lipke, P.N., Dufrêne, Y.F., 2010. Force-induced formation and propagation of adhesion nanodomains in living fungal cells. Proceedings of the National Academy of Sciences USA 107, 20744–20749, http://dx.doi.org/10.1073/pnas.1013893107.

Beaussart, A., Alsteens, D., El-Kirat-Chatel, S., Lipke, P.N., Kucharíková, S., Van Dijck, P., Dufrêne, Y.F., 2012. Single-molecule imaging and functional analysis of als adhesins and mannans during candida albicans morphogenesis. ACS Nano 6, 10950–10964.

Brattain, M.G., Fine, W.D., Khaled, F.M., Thompson, J., Brattain, D.E., 1981. Heterogeneity of malignant cells from a human colonic carcinoma. Cancer Research 41, 1751–1756.

Cerf, A., Cau, J.-C., Vieu, C., 2008. Controlled assembly of bacteria on chemical patterns using soft lithography. Colloids and Surfaces B: Biointerfaces 65, 285–291.

Cerf, A., Cau, J.-C., Vieu, C., Dague, E., 2009. Nanomechanical properties of dead or alive single-patterned bacteria. Langmuir 25, 5731–5736.

Che Abdullah, C.A., Asanithi, P., Brunner, E.W., Jurewicz, I., Bo, C., Azad, C.L., Ovalle-Robles, R., Fang, S., Lima, M.D., Lepro, X., Collins, S., Baughman, R.H., Sear, R.P., Dalton, A.B., 2011. Aligned, isotropic and patterned carbon nanotube substrates that control the growth and alignment of Chinese hamster ovary cells. Nanotechnology 22, 205102, http://dx.doi.org/10.1088/0957-4484/22/20/205102.

Dague, E., Delcorte, A., Latge, J.-P., Dufrene, Y.F., 2008. Combined use of atomic force microscopy, X-ray photoelectron spectroscopy, and secondary ion mass spectrometry for cell surface analysis. Langmuir 24, 2955–2959.

Dague, E., Jauvert, E., Laplatine, L., Viallet, B., Thibault, C., Ressier, L., 2011. Assembly of live micro-organisms on microstructured PDMS stamps by convective/capillary deposition for AFM bio-experiments. Nanotechnology 22, 395102, http://dx.doi.org/10.1088/0957-4484/22/39/395102.

De Kerchove, A.J., Elimelech, M., 2005. Relevance of electrokinetic theory for soft particles to bacterial cells: implications for bacterial adhesion. Langmuir 21, 6462–6472.

Dufrene, Y.F., 2004. Using nanotechniques to explore microbial surfaces. Nature Reviews Microbiology 2, 451–460.

Fantner, G.E., Barbero, R.J., Gray, D.S., Belcher, A.M., 2010. Kinetics of antimicrobial peptide activity measured on individual bacterial cells using high-speed atomic force microscopy. Nature Nanotechnology 5, 280–285.

Formosa, C., Grare, M., Duval, R.E., Dague, E., 2012a. Nanoscale effects of antibiotics on *P. aeruginosa*. Nanomedicine: Nanotechnology, Biology and Medicine 8, 12–16.

Formosa, C., Grare, M., Jauvert, E., Coutable, A., Regnouf-de-Vains, J.B., Mourer, M., Duval, R.E., Dague, E., 2012b. Nanoscale analysis of the effects of antibiotics and CX1 on a Pseudomonas aeruginosa multidrug-resistant strain. Science Reports 2, 575, http://dx.doi.org/10.1038/srep00575.

Gaboriaud, F., Parcha, B.S., Gee, M.L., Holden, J.A., Strugnell, R.A., 2008. Spatially resolved force spectroscopy of bacterial surfaces using force–volume imaging. Colloids and Surfaces B: Biointerfaces 62, 206–213.

Gamper, N., Stockand, J.D., Shapiro, M.S., 2005. The use of Chinese hamster ovary (CHO) cells in the study of ion channels. Journal of Pharmacological and Toxicological Methods 51, 177–185.

Garcia, R., Herruzo, E.T., 2012. The emergence of multifrequency force microscopy. Nature Nanotechnology 7, 217–226.

Heinisch, J.J., Dufrene, Y.F., 2010. Is there anyone out there? Single-molecule atomic force microscopy meets yeast genetics to study sensor functions. Integr. Biol. 2, 408–415.

Heu, C., Berquand, A., Elie-Caille, C., Nicod, L., 2012. Glyphosate-induced stiffening of HaCaT keratinocytes, a peak force tapping study on living cells. Journal of Structural Biology 178, 1–7.

Kodera, N., Yamamoto, D., Ishikawa, R., Ando, T., 2010. Video imaging of walking myosin V by high-speed atomic force microscopy. Nature 468, 72–76.

Kuznetsova, T.G., Starodubtseva, M.N., Yegorenkov, N.I., Chizhik, S.A., Zhdanov, R.I., 2007. Atomic force microscopy probing of cell elasticity. Micron 38, 824–833.

Layton, B.E., Boyd, M.B., 2011. Atomic Force Microscopy of Isolated Mitochondria, in Atomic Force Microsocpy in Biomedical Research. Pier Carlo Braga, Davide Ricci.

Liu, S., Wang, Y., 2010. Application of AFM in microbiology: a review. Scanning 32, 61–73.

Longo, G., Rio, L.M., Roduit, C., Trampuz, A., Bizzini, A., Dietler, G., Kasas, S., 2012. Force volume and stiffness tomography investigation on the dynamics of stiff material under bacterial membranes. Journal of Molecular Recognition 25, 278–284.

McKee, C.T., Raghunathan, V.K., Nealey, P.F., Russell, P., Murphy, C.J., 2011. Topographic modulation of the orientation and shape of cell nuclei and their influence on the measured elastic modulus of epithelial cells. Biophysical Journal 101, 2139–2146.

Milhiet, P.-E., Dosset, P., Godefroy, C., Le Grimellec, C., Guigner, J.-M., Larquet, E., Ronzon, F., Manin, C., 2011. Nanoscale topography of hepatitis B antigen particles by atomic force microscopy. Biochimie 93, 254–259.

Müller, D.J., Dufrêne, Y.F., 2011. Atomic force microscopy: a nanoscopic window on the cell surface. Trends in Cell Biology 21, 461–469.

Oberleithner, H., Brinckmann, E., Schwab, A., Krohne, G., 1994. Imaging nuclear pores of aldosterone-sensitive kidney cells by atomic force microscopy. Proceedings of the National Academy of Sciences 91, 9784–9788.

Pittenger, B., Erina, N., Su, C., 2010. Quantitative mechanical property mapping at the nanoscale with PeakForce QNM. Bruker application note http://nanoscaleworld.bruker-axs.com/nanoscaleworld/media/p/418.aspx

JPK Instruments QI™ mode-Quantitative Imaging with the NanoWizard 3 AFM http://www.jpk.com/afm.230.en.html

Berquand, A., 2011. Quantitative imaging of living biological samples by PeakForce QNM atomic force microscopy Bruker application note http://nanoscaleworld.bruker-axs.com/nanoscaleworld/media/p/2028.aspx

Radmacher, M., Cleveland, J.P., Fritz, M., Hansma, H.G., Hansma, P.K., 1994. Mapping interaction forces with the atomic force microscope. Biophysical Journal 66, 2159–2165.

Roduit, C., Longo, G., Benmessaoud, I., Volterra, A., Saha, B., Dietler, G., Kasas, S., 2012a. Stiffness tomography exploration of living and fixed macrophages. Journal of Molecular Recognition 25, 241–246.

Roduit, C., Saha, B., Alonso-Sarduy, L., Volterra, A., Dietler, G., Kasas, S., 2012b. OpenFovea: open-source AFM data processing software. Nature Methods 9, 774–775.

Schulze, C., Müller, K., Käs, J.A., Gerdelmann, J.C., 2009. Compaction of cell shape occurs before decrease of elasticity in CHO-K1 cells treated with actin cytoskeleton disrupting drug cytochalasin D. Cell Motility and the Cytoskeleton 66, 193–201.

Sudbery, P., Gow, N., Berman, J., 2004. The distinct morphogenic states of *Candida albicans*. Trends in Microbiology 12, 317–324.

Sweers, K., Van der Werf, K., Bennink, M., Subramaniam, V., 2011. Nanomechanical properties of alpha-synuclein amyloid fibrils: a comparative study by nanoindentation, harmonic force microscopy, and Peakforce QNM. Nanoscale Research Letters 6, 270.

Yokokawa, M., Takeyasu, K., Yoshimura, S.H., 2008. Mechanical properties of plasma membrane and nuclear envelope measured by scanning probe microscope. Journal of Microscopy 232, 82–90.

Young, T.J., Monclus, M.A., Burnett, T.L., Broughton, W.R., Ogin, S.L., Smith, P.A., 2011. The use of the PeakForceTM quantitavive nanomechanical mapping AFM-based method for high-resolution Young's modulus measurments of polymers. Measurement Science and Technology, 22.

<u>Chapter 3.1</u>: Technological developments to study the cell wall of microorganisms by AFM

3.1.3 Mapping HA-tagged protein at the surface of living cells by Atomic Force Microscopy

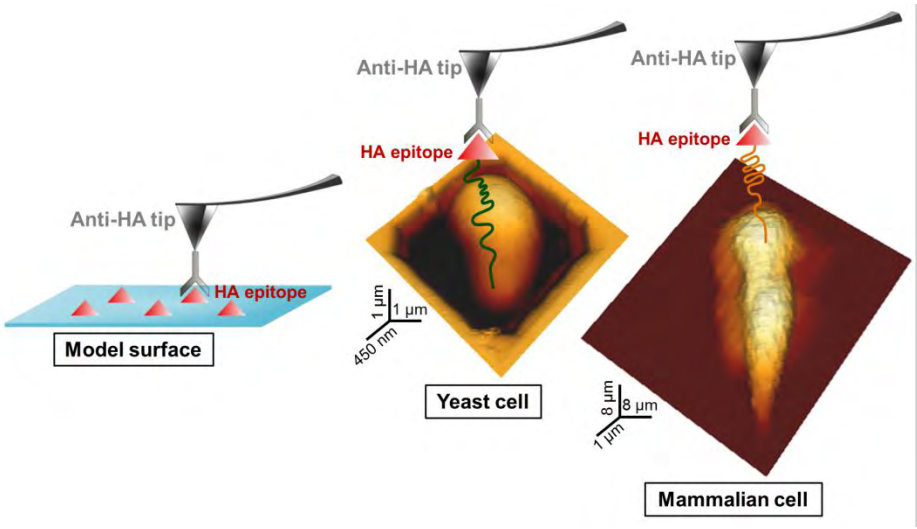

Formosa C., Lachaize V., Galés C., Rols M. P., Martin-Yken H., François J. M., Duval R. E. and Dague E.

Accepted in *Journal of Molecular Recognition*

Abstract

Single Molecule Force Spectroscopy (SMFS) using Atomic Force Microscopy (AFM) is more and more used to map and describe receptors, enzymes, adhesins, or other proteins at living cells surface. Nevertheless, this technique requires, to be specific, antibodies or other molecules directed against the protein of interest at the cell surface. Unfortunately, specific antibodies are usually lacking and/or are extremely expensive. To overcome this problem, a strategy is to tag the protein of interest with a small peptide against which specific antibodies exist. In this context, we chose to work with the Human influenza hemagglutinin (HA) tag (YPYDVPDYA), and labeled 2 proteins: Ccw12 responsible for cell wall remodeling in the yeast *Saccharomyces cerevisiae* and the β2 Adrenergic Receptor (β2AR), a G-protein coupled receptor (GPCR) in higher eukaryotes. We first described the interaction between HA antibodies, immobilized on AFM tips via dendrimers, and HA epitopes, immobilized on epoxy glass slides. Using our system we then investigated the distribution of Ccw12 proteins over the cell wall surface of the yeast *S. cerevisiae*. We were able to find the tagged protein on the surface of mating yeasts, at the tip of the mating projections. Finally, we were able to unfold multimers of β2AR from the membrane of living transfected Chinese Hamster Ovaries (CHO) cells. This result confirms that GPCR are oligomerized in cell membranes and opens the door to the study of the influences of agonist/antagonist on the receptor conformation, and of the influence of the cell membrane lipidic composition on the receptor organization.

De : h.hoerber@bristol.ac.uk
Objet : Journal of Molecular Recognition - Decision on Manuscript ID JMR-14-0062.R1
Date : 25 juin 2014 19:14:20 HAEC
À : edague@laas.fr

25-Jun-2014

Dear Dr. Dague,

It is a pleasure to accept your manuscript entitled "Mapping HA-tagged protein at the surface of living cells by Atomic Force Microscopy" in its current form for publication in Journal of Molecular Recognition. The comments of the referee(s) who reviewed your manuscript are included at the bottom of this letter.

A signed copyright transfer agreement is needed for publication. If you have not already provided us with one you can access the copyright transfer agreement at:

http://media.wiley.com/assets/1540/95/ctapsglobal.pdf

To enable the publisher to disseminate the author's work to the fullest extent, the author must sign a Copyright Transfer Agreement, transferring the copyright of the article from the author to the publisher.

If you have not yet uploaded a CTA, please ensure that you have identified the form with the manuscript ID number; scan your signed CTA and e-mail to ctaforms@wiley.com stating the manuscript ID number in the subject line of the e-mail.

Please note that this does not take away your rights to reuse your own article after publication, and that if the copyright belongs to your employing institution, they should sign the form instead of you.

If you have already provided us with the signed form, you do not need to do anything at this stage. You will be contacted by our typesetters/copyeditors shortly.

Thank you for your fine contribution.

Sincerely,

Prof. Heinrich Hoerber
Editor, Journal of Molecular Recognition
h.hoerber@bristol.ac.uk

Introduction

Since its invention in 1986 by Binnig *et al.* [1], Atomic Force Microscopy (AFM) has developed into a multifunctional toolbox that opened the door to the nanoworld [2]. The basic principle of this technique relies on the measurement of a force between a sharp tip and a surface sample, and to keep this force constant while scanning in order to get a three dimensional image of the sample. An advantage of AFM is the possibility to work with living cells in their physiological environment. However, AFM is not only an imaging technology; it is also a highly sensitive force machine. Indeed, AFM is also able to record force distance curves, thus giving access to nanomechanical and adhesive properties of the living material probed. In this context, an AFM-based technique, Single Molecule Force Spectroscopy (SMFS), has recently emerged in the field. In this technique, AFM tips interact with biomolecules immobilized on innate substrates or artificial biomembranes *(in vitro* studies), or present at the surface of living cells so to understand the intra- and inter-molecular interactions of biomolecular systems [3,4]. SMFS techniques have been widely used *in vitro*, to monitor, for example, the interaction of cellular adhesion molecules, such as cadherins [5] or oligosaccharides [6], or to characterize the anchoring forces of peptides in lipid membranes [7]. These *in vitro* studies generally do not need specific probes as they involve only one molecule, inserted in a membrane or linked to a surface, that can be picked up by the AFM tip [8,9]. However, they use purified biological molecules that have been removed from their native biological context, and the results obtained cannot be directly linked to biological processes happening *in vivo* [10]. Nevertheless, it is possible to study more accurately molecular interactions and recognition as they happen in their natural environment, by performing SMFS experiments directly on living cells [11,12].

However such experiments are often challenging, because of the heterogeneity of the cellular surfaces. In lower eukaryotic cells, such as yeast cells, the cell wall is composed of

heterogeneous components (mannans, mannoproteins, glucans, chitin), that are structurally organized among the cell wall depth. This heterogeneity and complex molecular organization is essential for maintaining a functional cell wall that protects the cells from the environment, and allows morphogenic events to take place [13,14]. In the case of higher eukaryotes, the key feature of cell surface heterogeneity refers to the spatiotemporal confinement of proteins and lipids in defined and dynamic microscale regions of the plasma membrane [15,16]. Association between lipids and proteins can modulate their biological functions, and therefore cellular bioprocesses such as cell adhesion, or cell-cell interactions [17,18]. During SMFS experiments, all these different components at the surface of living cells can cause non-specific interactions with the AFM tip (hydrophobic interactions, electrostatic…).

In this context, it is necessary to functionalize AFM tips with specific antibodies targeting only one specific protein at the surface of the cells. However, the difficulty to obtain antibodies recognizing native membrane proteins with high specificity and affinity prevents the use of functionalized AFM tips to explore the behavior of these proteins at the cell surface. As an alternative strategy, biologists have developed a genetic strategy consisting in labelling proteins to their amino (N-) or carboxy (C-) terminus with specific small tags and then expressing these tagged-proteins in living cells. Several and general epitope tags such as Human influenza hemagglutinin (HA) tag (YPYDVPDYA), FLAG tags (DYKDDDDK) or myc tags (EQKLISEEDL) and corresponding high specific and affine antibodies recognizing these epitopes have been thus developed and are commonly used by the biology community, therefore offering the possibility to follow the protein of interest with high accuracy with a specific antibody against the epitope tag. We took advantage of these specific antibodies and decided to functionalize an AFM tip with an antibody targeted against the HA epitope-tag. Different strategies to functionalize AFM tips with biomolecules have been described so far. Some of them

consist in the nonspecific adsorption of proteins, for example BSA (Bovine Serum Albumin), to the silicon nitride surface of AFM tips [19], or in the chemical fixation of biomolecules by sulfur-gold bonds to gold-coated AFM tips. This last strategy has been successfully used for measuring interactions forces between complementary DNA strands [20], or between fibronectin and bacterial cells [21]. However, in the first case, the adsorption is nonspecific, and in the second case, the gold-coating of AFM tips modifies the spring constant of the cantilevers where the tips are fixed. To avoid these problems, it is possible to covalently link a molecule containing amino groups directly to the silicon nitride AFM tip. To this end, AFM tips must be first amino-functionalized either by esterification with ethanolamine [22] or silanization with aminopropyl-triethoxysilane (APTES) [23]. Then, the amino-functionalized tip has to be bridged to the biomolecule of interest. This can be achieved through the use of heterobifunctionalized PolyEthylene Glycol (PEG) [24–26], or, as we decided in our study, through the use of an aldehyde-phosphorus dendrimer, as we previously described [27]. This strategy developed in our team in 2012, and already used for probing the surface of live bacteria [28], consists in making "dendritips" by reacting amino-functionalized AFM tips with dendrimers, therefore leading to dendrimer-activated tips. Then, the free aldehydes functions at the surface of the dendrimers are available to react with amino-functions present on every protein and on many biomolecules. Using this strategy we are able to measure specific interactions between a biomolecule immobilized on the AFM tip and a biomolecule immobilized on an abiotic surface, or at the surface of living cells, without modifying the spring constant of the cantilever. Single molecule events can be detected using this strategy using appropriate concentrations in the biomolecules grafted on the AFM tip. Finally, another advantage of this strategy, compared to PEG linkers for example, is that the interaction detected takes place at the exact position of the AFM tip, which allows precise mapping of proteins.

In this study, we developed an AFM tip functionalized with an anti-HA (peptide YPYDVPDYA) antibody, and validated our system on model surfaces functionalized with HA epitopes. Our system was used to probe two transmembrane proteins of two different biological models. The yeast *S. cerevisiae* Ccw12 protein is a covalently linked mannoprotein, and is considered as a crucial structural cell wall component, as mutant strains deleted for this protein present cell wall damages [29]. The other investigated protein is the β2-adrenergic receptor (β2-AR) which is the hallmark of the mammalian G-protein-coupled receptor (GPCR). These proteins constitute the largest class of cell-surface receptors that are involved in signal transduction [30], and mediate complex cellular responses to highly diverse extracellular signals [31]. To probe these proteins at the surface of the corresponding model systems, a HA-epitope tag was fused at their N-terminus. These fusion proteins were then transiently over-expressed in yeast and mammalian cells and probed using functionalized AFM tips with anti-HA antibodies. Although this strategy has been used in recent papers with HA tagged bacterial proteins, of V5 tagged yeast proteins [32–34], via the use of heterobifunctionalized PEG linkers, we show here for the first time that such experiments are possible using a dendrimer-based functionalization strategy, with yeasts proteins but also with human molecules, such as β2-AR, at the surface of mammalian cells.

Material and Methods

Yeast growth conditions and transformation

Saccharomyces cerevisiae strain BY4741 (MATa his3Δ1 leu2Δ10 met15Δ0 ura3Δ0) ΔCCW12 was stocked at -80°C, revivified on Yeast Peptone Dextrose agar (Difco, 242720-500g) and grown in Yeast Peptone Dextrose broth (Difco, 242820-500g) for 20 hours at 30°C under agitation (180 rpm). Yeast transformation were conducted using LiAc, according to [35]. Strain

Δccw12 + p*CCW12-GFP-HA* was grown in YNB Leu- for 20 hours at 30°C under agitation (180 rpm). For mating projections, strain *Δccw12* + p*CCW12-GFP-HA* was put into fresh media for 2 hours at 30°C under agitation (180 rpm), and α-factor (Sigma T6901) was added at a concentration of 0.01 mg/mL for another 2 hours at 30°C under agitation (180 rpm) before AFM experiments.

CHO cells growth conditions and transfection

Chinese Hamster Ovary cells (Wild Type Toronto, WTT, from ATCC) were grown in Minimum Eagle's Medium (MEM) supplemented with 10% fetal calf serum (Gibco), 1% Peniciline/Streptomycine mixture (100 $u.mL^{-1}$) (Gibco), and incubated at 37°C in humidified atmosphere with a 5% CO_2 incubator. Transient transfections were performed 24 h after cell seeding using X-tremeGENE 9 DNA transfection reagent (Roche) according to the manufacturer's protocol. In all cases, cells were co-transfected with a fluorescent marker encoding vector (pGFP2-N1, Perkin Elmer) so to identify transfected cells.

Sample preparation and AFM experiments

Yeast cells were concentrated by centrifugation, washed two times in acetate buffer (18 mM CH_3COONa, 1 mM $CaCl_2$, 1 mM $MnCl_2$, pH = 5.2), resuspended in acetate buffer, and immobilized on polydimethylsiloxane (PDMS) stamps prepared as described by Dague *et al* [36]. Briefly, freshly oxygen activated microstructured PDMS stamps were covered by a total of 100 µL of the solution of cells and allowed to stand for 15 minutes at room temperature. The cells were deposited into the microstructures of the stamp by convective/capillary assembly. The stamp was then immerged in a Petri dish containing acetate buffer (+ α-factor at 0.01 mg/mL for mating projection experiments), and placed in the PetriDishHeater (JPK) that maintained the device at 30°C during the whole experiment. For CHO cells, 75,000 cells for each conditions were grown in Petri dishes during 24h before measurement, and classical medium was replaced by DMEM-HEPES

medium (HEPES 15 mM) and cells were placed in the PetriDishHeater (JPK) that maintained the Petri dish at 37°C during the whole experiment. Images were recorded in acetate buffer in Quantitative Imaging^{TM} mode [37], with MLCT AUWH cantilevers (nominal spring constant of 0.01 N/m). For Single Molecule Force Spectroscopy (SFMS) experiments, the applied force was kept constant at 0.5 nN, for all experiments.

AFM tip functionalization

Functionalized tips were produced according to a French patent [38] of the authors described in sensors and actuators [27]. Briefly, AFM tips were functionalized with dendrimers presenting CHO functions able to covalently link with NH_2 functions of proteins. Those dendritips were then incubated with the HA antibody at a concentration of 0.01 mg/mL (LifeProTein, LT0422, HA.C5 clone monoclonal antibody) for 1 hour, before being used for force spectroscopy experiments.

Glass slides functionalization

A drop of HA epitopes YPYDVPDYA (synthesized, LifeProTein) at a concentration of 5 mg/mL was deposited on epoxy glass slides and incubated overnight. The following day, glass slides were rinsed with acetate buffer (18 mM CH_3COONa, 1 mM $CaCl_2$, 1 mM $MnCl_2$, pH = 5.2) and further used for SMFS experiments.

Results

In order to probe HA-tagged protein at the surface of living cells, the first step was to functionalize AFM tips with HA antibodies, and verify that they can specifically interact with synthetic HA peptides immobilized on epoxy glass slides. The results presented in figure 1a show interaction forces at a loading rate of 70 000 pN/s. The forces measured are of 61.7 ± 18.9 pN, which is in the range of specific molecular interactions such as antigen-antibody interactions [39]. We also fixed the non-adhesive curves percentage to 80%, by adjusting the antibody and

epitope concentrations, with the aim of measuring only single molecule interactions. To examine whether these interactions were specific, we performed blocking experiments by saturating the epitopes on the glass slide with anti-HA antibodies (figure 1b). The resulting measures indicated that the tip was not able anymore to interact with the epitopes at the surface thus confirming the specificity of the interaction. Next, we characterized the interactions between HA epitopes and HA-tip, by performing force spectroscopy experiments with varying loading rates and contact time. The rupture force for a specific biological interaction is expected to be a function of the loading rate [5,40]. This loading rate dependence comes from the molecular link that exists in biological interactions such as antigen-antibody. Figure 1c shows the variation of the adhesion force for loading rates between 10 000 and 100 000 pN/s. The direct relation between the adhesion force and the loading rate is clear, with an increase from 30.6 ± 4.8 pN for a loading rate of 20 000 pN/s, to 62.5 ± 24.8 pN/s for a loading rate of 100 000 pN/s. Based on these results, we have been able to estimate the kinetic dissociation constant ($Koff$) on the HA-HA antibody interaction according to the following equation 1 [40]:

$$F = f\beta \times \ln\left(\frac{r}{f\beta Koff}\right)$$

where F is the measured adhesion force, $f\beta$ is defined as the ratio between the thermal energy scale (K_BT, where K_B is Boltzmann's constant and T is temperature) and the length of the interaction at a transition state, and r the loading rate. At zero force, equation 1 can be rewritten as follows (equation 2):

$$Koff = \frac{r0}{f\beta}$$

The values $f\beta$ (slope) and r0 (loading rate at zero force) were deduced from data presented in Figure 1b. The *Koff* parameter, estimated using the second equation, was equal to 1.4×10^{-5} s^{-1}.

In parallel, we studied the variation of the adhesion probability with the contact time between the HA epitopes and the HA-tip, while keeping the loading rate (LR) constant to 70 000 pN/s. As showed in Figure 1d, the adhesion probability increased with the contact time, from 20% to 80% for a contact time ranging from 0 to 2 s, until reaching a plateau. This dependence of the probability of adhesion to the contact time confirms that we are probing a specific recognition that could be described by an association kinetic constant (*Kon*). The calculation needed to provide a *Kon*, would nevertheless require many approximations. Especially, the number of binding partners and the effective volume they're in. We therefore decided not to estimate the *Kon*, but to provide $t_{0.5}$ (contact time needed to reach 50 % of adhesive events) = 0.05 s. All together, we have an adhesion force (61.7 ± 18.9 pN; LR = 70 000 $pN.s^{-1}$) typical for epitope-antibody recognition, the adhesion force is a function of the loading rate (*Koff* = 1.4×10^{-5} s^{-1}) and the adhesion probability increases with the contact time according to a log ($t_{0.5}$ = 0.05 s, plateau 80%).

Once this validation step with our anti-HA tip on a model surface bearing HA epitopes accomplished, we then further used our HA functionalized AFM tip first on living yeast cells, immobilized in microstructured PDMS stamps [41,42]. To this end, we labeled the plasmidic Ccw12 parietal yeast protein to HA-tag, and transformed yeast cells *Δccw12* deleted for the genomic allele of the gene encoding this protein with this plasmid. The first experiments consisted in probing the surface of *Δccw12* (control strain, figure 2a) so to control that no unspecific interactions were observed between the surface and the HA tip. Figure 2b presents the adhesion map obtained while representative force curves and histogram of the adhesion forces are presented in figure 2c and d. In this case, 78.1% of the force curves presented no retract adhesions, and the few adhesions measured (Figure 1d) were not specific as their distance on the

force curve is far from the contact point (more than 100 nm). Then we probed the surface of the same strain but overexpressing HA-tagged Ccw12 protein (Figure 2e). Unexpectedly, the results showed that there were no interactions between the tip and the sample, with a percentage of force curves with no retract adhesions reaching 96.7%. Since Ccw12 is a protein expressed at the tip of mating projections [43], we then incubated this same strain in the presence of α-factor, a yeast sexual pheromone triggering the formation of these characteristic mating projections by haploid yeast strains of **a** mating type [44]. We were able to image the formation of mating projections or "shmoos", for the first time (to our knowledge) under liquid conditions with an AFM (figure 2i). When we probed the surface of these shmoos using the anti-HA tip, we could clearly see interactions between the tip and the sample on the adhesion map (figure 2j); 67.4% of the force curves in this case exhibited retract adhesions, with adhesion forces of 69.3 ± 31.4 pN at a loading rate of 70 000 pN/s (figure 2k and l). This adhesion force value is consistent with similar data obtained on yeasts cells using anti-V5 functionalized AFM tips and V5-tagged protein [32]. Therefore we can conclude that in this particular morphogenic state, the cell wall is modified so that the protein becomes accessible to the AFM tip, at the surface of the cells.

To show the versatility of our system, we used the anti-HA tips on a different biological system, so to extend the versatility and power of the functionalized tip. For that purpose, we used mammalian CHO cells overexpressing the human G-protein-coupled receptor β2-AR. In these experiments, cells were transiently co-transfected with a GFP encoding vector (Green Fluorescent Protein) together with a plasmid coding for the HA-β2-AR, thus allowing us to probe only transfected cells. Figure 3a and b present optical images of the cells under the AFM tips; on the dark-field image white arrows indicate fluorescent cells, *i. e.* transfected cells. Cells were maintained at 37°C during all experiments in a 15 mM HEPES buffer, in order to keep them alive during the AFM experiment. Figure 3c presents a height image of a CHO cell imaged under these

conditions. As we did for yeast cells, we first used anti-HA tips to probe the surface of untransfected cells (control cells) to control for unspecific interactions that would mask/interfere with the specific ones on transfected cells. The adhesion map and representative force curves (Figure 3d and g) showed that such interactions were indeed undetectable; 83.8 % of the recorded force curves presented no retract adhesions (n=1024 on 4 cells coming from two independent cultures) A second control consisted in probing the surface of cells transfected with a non-coding vector, so to verify that the transfection process would not destabilize the plasma membrane, which could lead to unspecific interactions. Figures 3e and h show comparable results as the one obtained on untransfected cells, since we did not detect retract adhesions on 86.8 % of the force curves recorded (n=1280 on 5 cells coming from 2 independent cultures). However, when cells were transfected with the HA-β2-AR encoding plasmid, the receptors were expressed at the surface of the cells, and could be unfolded using the anti-HA tip, as showed in figure 3f and i. In these conditions, we found 65.2% of adhesive force curves, the average in adhesion force being of 63.4 +/- 25.7 pN (n=1280, on five different cells coming from 2 independent cultures), at a loading rats of 100 000 pN/s. A detailed analysis of the force curves obtained on this sample is presented in figure 4. On this figure, we presented 26 force curves obtained on different cells transfected with the plasmid coding for the HA-β2-AR, with a functionalized AFM tip. We can clearly see on this figure that the unfoldings are of different sizes, and are distributed in a range going from 170 nm to 3.5 µm. The β2-AR is composed of 413 amino acids (protein database, GenBank: AAN01267.1) organized in 7 transmembrane (TM) domains [45]. Assuming that 1 amino acid is, on average, 0.4 nm long [8], we expect a single β2-AR receptor unfolding around $413 \times 0.4 = 165.2$ nm. Based on our AFM results, it thus follows that we did not stretch a single β2-AR receptor unit, or maybe in the case of the top force curve presented in figure 4, but this is too much uncertain to be confirmed. The more general force curves patterns obtained in these

experiments, with long unfoldings, could thus represent the stretching of several receptors. In agreement with this hypothesis, the β2-AR is well-known to oligomerize at the cell surface [46,47]. In our conditions of receptor overexpression, it is likely possible that several receptors oligomerized at different orders were stretched at the cell surface by the functionalized AFM tip over varying lengths. If we take a closer look at the force curves, we can see that some of them present two distinct unfolding patterns (last one from the bottom for example on figure 4), *i.e.* with a return to the base line between two unfoldings on the same force curve. This can be explained by the fact that the AFM tip starts stretching one group of oligomerized receptors, then the interaction is broken, but since the tip is still close to the surface, it interacts with a second group of oligomerized receptors.

Discussion

Loading rate experiments allowed us to determine the dissociation kinetic constant $Koff$ for the couple HA-antiHA, equal, in our case, to 1.4×10^{-5} s^{-1}. Such constants were previously determined with the same technic for other antigen-antibody couples; for example Hinterdorfer's team found a $Koff$ of 6.7×10^{-4} s^{-1} for the couple HSA-antiHSA (Human Serum Albumin) [22]. Our result is consistent with this literature data, as our $Koff$ is in the same range of values. When varying the contact time during force spectroscopy experiments, we reached a plateau at 80% of probability of adhesion. This dependence of the probability of adhesion to the contact time is a proof that the interaction probed is specific, and that the HA-antiHA complex formed via multiple bonds [48]. However, the Kon (association kinetic constant) was not calculated in this study, due to uncertainties in the effective concentration (number of binding partners and effective volume) in epitopes at the surface of the area probed. These approximations are

probably responsible for the large heterogeneity in the *Kon* values that can be found in the literature [49]. However, it is important to measure the relationship between the adhesion probability and the contact time for at least 2 reasons; firstly, it is a proof that a specific recognition is probed; secondly, it gives an idea of a reasonable contact time that could be used on living cells.

We then used our HA-antiHA system to probe the protein Ccw12 at the surface of living cells of the budding yeast *S. cerevisiae*. Yeast cells are surrounded by a thick cell wall, composed of β1,3- and β1,6-glucans, chitin, mannans and proteins [13]. Cell wall proteins are mannoproteins that play important roles, both as structural components and as enzymes involved in cell-cell interaction and cell wall assembly [50]. The Ccw12p, the protein studied, is one of these ***C***ovalently linked ***C***ell ***W***all proteins (***CCW*** proteins) that belongs to the family of cell wall protein attached by a modified GPI (GlycosylPhosphatidylInositol) anchor to β-glucans [14] and that can be released by β-1,3-glucanases [51]. Loss of Ccw12p results in reduced growth rate, increased sensitivity to cell wall perturbing agents Calcofluor White (CW) and Congo Red (CR), and increased amount of cell wall chitin, suggesting that Ccw12p is required for the maintenance of the cell wall stability [29,51]. Furthermore, it has been showed by electron microscopy that Ccw12p is playing a role in the formation of a tightly packed outer mannan layer protecting the inner glucans networks [29]. The results that we obtained on the *ccw12Δ* mutant are consistent with these data. Indeed, retract adhesions obtained on the force curves recorded on this mutant are not specific, as they occur far away from the contact point. These retract adhesions can be compared to sugar adhesions, as it has been previously seen at the surface of live yeasts cells [52,53]. This would be consistent with the role of Ccw12p in maintaining cell wall stability by forming a tight mannan layer; when the protein is not present the cell wall architecture is

modified so that polysaccharides can be stretched off the surface. We then probed the surface of the same strain, but complemented with a plasmid expressing the HA- Ccw12 protein. In this case, there were no more retract adhesions on force curves, suggesting that in this strain, the protein has been reintroduced, and has played its native function in the remodeling of the cell wall, as no polysaccharides were stretched. However, it was expected in this case to probe Ccw12 protein thanks to our functionalized AFM tip. We could not stretch it, meaning that the protein was either not there, or not accessible to the functionalized probe. The first hypothesis could be quickly evacuated. Compared to the mutant *ΔCcw12*, the outer layer of polysaccharides could not be stretched, meaning that the phenotype caused by the loss of Ccw12 was restored upon expression of the HA-Ccw12 protein. Therefore the fusion protein exerted the same function as the wild-type protein. To test the second hypothesis and knowing that Ccw12 role is also to preserve the cell wall integrity at sites of active growth [54], we decided to look for Ccw12 on mating projections (shmoos) where active cell wall synthesis occurs. Indeed, it has been previously showed that GPI-anchored proteins in *Candida albicans*, another yeast species, could be embedded into the glucan layers deep enough to be hidden from the surface of round cells [55]. However the same proteins have been shown to be exposed on hyphal forms of *C. albicans* [56], meaning that changes in the cell wall organization between two morphological types of the same species could expose the proteins. Such a phenomenon could happen in *S. cerevisiae*, since Ccw12p is also embedded in the glucans layer of the cell wall, and could be exposed on a different morphological type, such as mating projections. When we probed the surface of a mating projection of this strain complemented, at the tip of the shmoo, the anti-HA tip could, indeed, interact specifically with HA epitopes, meaning that the protein, accumulated at this particular area on the shmoo tip, was accessible. The results are in agreement with different studies [43,54] and especially the one of Ragni *et al*. in which the genetic interaction network of

CCW12 is studied. The authors demonstrate that Ccw12 is required for cell wall integrity during active cell wall synthesis (budding and shmoos formation) and accumulate in these regions. Indeed, they use Ccw12 protein marked with GFP (Green Fluorescent Protein) in order to localize it in the cell; their results show that this protein strongly accumulates in areas of active cell wall synthesis, meaning at the budding site on the cell surface of mother cells, at the periphery of small buds, at the septum after cytokinesis, and at the tip of mating projections. This would explain why we could not unfold it from exponential phase yeasts cells; the protein is perhaps embedded into the cell wall of round cells, and therefore not accessible with the AFM tip. This localization of the protein confirms an essential function of this protein in ensuring cell wall stability during mating processes.

Finally in the last part of our study, we used the anti-HA tip on CHO cells over-expressing the human β2 adrenergic G protein-coupled receptor. Only one study, by Zocher *et al*., has focused on the unfolding of this specific receptor [9]. In this pioneering work, the authors have reconstituted single units of the β2-AR into phospholipid bilayers and used SMFS to characterize it. For that, an AFM tip was pushed onto the membrane at a force of 0.7 nN, which promotes the adhesion of single proteins polypeptides to the bare AFM tip, and retracted while recording the cantilever deflection (force). This allows therefore the unfolding of only one receptor, out of a membrane containing only this receptor, in 0.5 % of the force curves recorded. They found that the force required to unfold the different domains of the β2-AR was ranging between 30 and 220 pN, depending on the domain considered, the loading rate but also the lipidic environment (presence or absence of cholesteryl hemisuccinate mimicking cholesterol). In our experiments, CHO cells not only expressed β2-AR receptors, but also other plasma membrane components. This is why we needed to find a way to specifically probe the β2-AR, and thus we tagged the receptor with an extracellular HA epitope. This allowed the specific unfolding of β2-

AR receptors at the surface of living cells, which is, as far as we know, the first time this phenomenon was recorded in living cells. However, unlike Zocher's work, we were not able to measure single receptor unfolding. Indeed, it has been showed that G-coupled proteins receptors, like other transmembrane receptors, can form dimers and higher-order oligomers at the surface of living cells [57]. Indeed, despite fully functional GPCRs monomers were described in reconstituted nanodiscs [58,59], large amounts of studies reported GPCRs oligomers can spontaneously form in living cells (GPCR Oligomerization Knowledge Base, http://www.gpcr-okb.org, [60]). More recently, the receptor oligomer size was directly correlated with the receptor expression level [61]. Consistent with this notion, in our conditions, the β2-ARs are overexpressed, meaning that number of them is expressed at the cell surface, which could this force the oligomerization process and lead to subsequent formation of higher order oligomers. It seems therefore difficult to conclude directly from our results whether β2-AR monomers are really a rare event in living cells which could explain why we could not unfold single receptors, or if high order oligomers is a general feature of this receptor in agreement with our results showing that we were more generally able to unfold only oligomerized receptors at different orders. These unfoldings represented in figure 4, are ranging from 170 nm for the smallest (estimation of one β2-AR protomer), to 3.5 µm for the longest (~ 20 receptor clusters). The size of GPCR oligomer complexes is really a matter of debate and its estimation seems most likely relying on the technological approach [62]. However, AFM analysis of native disk membranes isolated from mice led to the visualization of rhodopsin arrangement in arrays of dimers [63], which could be consistent with large unfoldings presented in our study. Despite the fact that our data strongly support the concept of GPCR oligomerization at the plasma membrane of cultured cells [47], we cannot however completely rule out that longer receptor unfoldings could also

reflect heterodimerization of the β2-AR with other transmembrane proteins (other endogenously expressed GPCRs, tyrosine kinases receptors or accessory proteins), as previously described [64]. These data are of first interest and will allow, in the future, answering new questions about the organization of GPCRs at the surface of living cells or about their behavior to different stimuli in their native environment.

Conclusions

In this study we developed a functionalized AFM tip with antibodies targeting the widely used HA epitope. The anti-HA tips, first validated on a model surface, was used on two biological systems, the yeast *Saccharomyces cerevisiae* and higher eukaryotic CHO cells. In the first case, we mapped the Ccw12 protein, essential for maintaining of the cell wall stability, only at the tip of mating projections. In the second case, the anti-HA tip allowed us for the first time to unfold the β2-AR receptor from the surface of living cells. Our anti-HA tip is therefore a versatile tool, that can be used in all types of molecular systems as long as they involve an HA epitope tag, at the surface of living cells, both microorganisms and mammalian cells.

References

1. Binnig G, Quate CF, Gerber C (1986) Atomic Force Microscope. *Phys Rev Lett* **56**: 930–934.
2. Gerber C, Lang HP (2006) How the doors to the nanoworld were opened. *Nat Nanotechnol* **1**: 3–5.
3. Dufrêne YF, Evans E, Engel A, Helenius J, Gaub HE, Müller DJ (2011) Five challenges to bringing single-molecule force spectroscopy into living cells. *Nat Methods* **8**: 123–127.
4. Müller DJ, Helenius J, Alsteens D, Dufrêne YF (2009) Force probing surfaces of living cells to molecular resolution. *Nat Chem Biol* **5**: 383–390.
5. Baumgartner W, Hinterdorfer P, Ness W, Raab A, Vestweber D, Schindler H, Drenckhahn D (2000) Cadherin interaction probed by atomic force microscopy. *Proc Natl Acad Sci* **97**: 4005–4010.
6. Rief M, Oesterhelt F, Heymann B, Gaub HE (1997) Single Molecule Force Spectroscopy on Polysaccharides by Atomic Force Microscopy. *Science* **275**: 1295–1297.
7. Ganchev DN, Rijkers DTS, Snel MME, Killian JA, de Kruijff B (2004) Strength of Integration of Transmembrane α-Helical Peptides in Lipid Bilayers As Determined by Atomic Force Spectroscopy†. *Biochemistry (Mosc)* **43**: 14987–14993.
8. Rief M, Gautel M, Oesterhelt F, Fernandez JM, Gaub HE (1997) Reversible Unfolding of Individual Titin Immunoglobulin Domains by AFM. *Science* **276**: 1109–1112.
9. Zocher M, Zhang C, Rasmussen SGF, Kobilka BK, Müller DJ (2012) Cholesterol increases kinetic, energetic, and mechanical stability of the human β2-adrenergic receptor. *Proc Natl Acad Sci* **109**: E3463–E3472.
10. Robinson CV, Sali A, Baumeister W (2007) The molecular sociology of the cell. *Nature* **450**: 973–982.
11. Zhang X, Shi X, Xu L, Yuan J, Fang X (2013) Atomic force microscopy study of the effect of HER 2 antibody on EGF mediated ErbB ligand–receptor interaction. *Nanomedicine Nanotechnol Biol Med* **9**: 627–635.
12. Lama G, Papi M, Angelucci C, Maulucci G, Sica G, De Spirito M (2013) Leuprorelin Acetate Long-Lasting Effects on GnRH Receptors of Prostate Cancer Cells: An Atomic Force Microscopy Study of Agonist/Receptor Interaction. *PLoS ONE* **8**: e52530.
13. Lipke PN, Ovalle R (1998) Cell Wall Architecture in Yeast: New Structure and New Challenges. *J Bacteriol* **180**: 3735–3740.
14. Orlean P (2012) Architecture and Biosynthesis of the Saccharomyces cerevisiae Cell Wall. *Genetics* **192**: 775–818.
15. Sonnino S, Prinetti A (2012) Membrane Domains and the Lipid Raft Concept. *Curr Med Chem* **20**: 4–21.
16. Maxfield FR (2002) Plasma membrane microdomains. *Curr Opin Cell Biol* **14**: 483–487.
17. Phillips R, Ursell T, Wiggins P, Sens P (2009) Emerging roles for lipids in shaping membrane-protein function. *Nature* **459**: 379–385.
18. Lee AG (2004) How lipids affect the activities of integral membrane proteins. *Biochim Biophys Acta BBA - Biomembr* **1666**: 62–87.
19. Florin EL, Moy VT, Gaub HE (1994) Adhesion forces between individual ligand-receptor pairs. *Science* **264**: 415–417.
20. Lee GU, Chrisey LA, Colton RJ (1994) Direct measurement of the forces between complementary strands of DNA. *Science* **266**: 771–773.

21. Bustanji Y, Arciola CR, Conti M, Mandello E, Montanaro L, Samorí B (2003) Dynamics of the interaction between a fibronectin molecule and a living bacterium under mechanical force. *Proc Natl Acad Sci* **100**: 13292–13297.
22. Hinterdorfer P, Baumgartner W, Gruber HJ, Schilcher K, Schindler H (1996) Detection and localization of individual antibody-antigen recognition events by atomic force microscopy. *Proc Natl Acad Sci* **93**: 3477–3481.
23. Ros R, Schwesinger F, Anselmetti D, Kubon M, Schäfer R, Plückthun A, Tiefenauer L (1998) Antigen binding forces of individually addressed single-chain Fv antibody molecules. *Proc Natl Acad Sci* **95**: 7402–7405.
24. Wildling L, Unterauer B, Zhu R, Rupprecht A, Haselgrübler T, Rankl C, Ebner A, Vater D, Pollheimer P, Pohl EE, et al. (2011) Linking of Sensor Molecules with Amino Groups to Amino-Functionalized AFM Tips. *Bioconjug Chem* **22**: 1239–1248.
25. Ebner A, Wildling L, Zhu R, Rankl C, Haselgrübler T, Hinterdorfer P, Gruber HJ (2008) Functionalization of probe tips and supports for single-molecule recognition force microscopy. *Top Curr Chem* **285**: 29–76.
26. Kamruzzahan ASM, Ebner A, Wildling L, Kienberger F, Riener CK, Hahn CD, Pollheimer PD, Winklehner P, Hölzl M, Lackner B, et al. (2006) Antibody Linking to Atomic Force Microscope Tips via Disulfide Bond Formation. *Bioconjug Chem* **17**: 1473–1481.
27. Jauvert E, Dague E, Séverac M, Ressier L, Caminade A-M, Majoral J-P, Trévisiol E (2012) Probing single molecule interactions by AFM using bio-functionalized dendritips. *Sens Actuators B Chem* **168**: 436–441.
28. Formosa C, Grare M, Jauvert E, Coutable A, Regnouf-de-Vains JB, Mourer M, Duval RE, Dague E (2012) Nanoscale analysis of the effects of antibiotics and CX1 on a Pseudomonas aeruginosa multidrug-resistant strain. *Sci Rep* **2**:
29. Ragni E, Sipiczki M, Strahl S (2007) Characterization of Ccw12p, a major key player in cell wall stability of Saccharomyces cerevisiae. *Yeast* **24**: 309–319.
30. Galés C, Van Durm JJJ, Schaak S, Pontier S, Percherancier Y, Audet M, Paris H, Bouvier M (2006) Probing the activation-promoted structural rearrangements in preassembled receptor–G protein complexes. *Nat Struct Mol Biol* **13**: 778–786.
31. Manglik A, Kobilka B (2014) The role of protein dynamics in GPCR function: insights from the β2AR and rhodopsin. *Curr Opin Cell Biol* **27C**: 136–143.
32. Alsteens D, Garcia MC, Lipke PN, Dufrêne YF (2010) Force-induced formation and propagation of adhesion nanodomains in living fungal cells. *Proc Natl Acad Sci* **107**: 20744 – 20749.
33. El-Kirat-Chatel S, Beaussart A, Boyd CD, O'Toole GA, Dufrêne YF (2014) Single-Cell and Single-Molecule Analysis Deciphers the Localization, Adhesion, and Mechanics of the Biofilm Adhesin LapA. *ACS Chem Biol* **9**: 485–494.
34. El-Kirat-Chatel S, Boyd CD, O'Toole GA, Dufrêne YF (2014) Single-Molecule Analysis of Pseudomonas fluorescens Footprints. *ACS Nano* **8**: 1690–1698.
35. Gietz RD, Schiestl RH (2007) High-efficiency yeast transformation using the LiAc/SS carrier DNA/PEG method. *Nat Protoc* **2**: 31–34.
36. Dague E, Jauvert E, Laplatine L, Viallet B, Thibault C, Ressier L (2011) Assembly of live micro-organisms on microstructured PDMS stamps by convective/capillary deposition for AFM bio-experiments. *Nanotechnology* **22**:
37. Chopinet L, Formosa C, Rols MP, Duval RE, Dague E (2013) Imaging living cells surface and quantifying its properties at high resolution using AFM in QI™ mode. *Micron* **48**: 26–33.

38. Dague E, Trevisiol E, Jauvert E Pointes de microscope à force atomique modifiées et biomodifiées.
39. Kienberger F, Kada G, Mueller H, Hinterdorfer P (2005) Single Molecule Studies of Antibody–Antigen Interaction Strength Versus Intra-molecular Antigen Stability. *J Mol Biol* **347**: 597–606.
40. Evans E, Ritchie K (1997) Dynamic strength of molecular adhesion bonds. *Biophys J* **72**: 1541–1555.
41. Formosa C, Schiavone M, Martin-Yken H, François JM, Duval RE, Dague E (2013) Nanoscale Effects of Caspofungin against Two Yeast Species, Saccharomyces cerevisiae and Candida albicans. *Antimicrob Agents Chemother* **57**: 3498–3506.
42. Francois JM, Formosa C, Schiavone M, Pillet F, Martin-Yken H, Dague E (2013) Use of atomic force microscopy (AFM) to explore cell wall properties and response to stress in the yeast Saccharomyces cerevisiae. *Curr Genet* **59**: 187–196.
43. Seidel J, Tanner W (1997) Characterization of two new genes down-regulated by alpha-factor. *Yeast Chichester Engl* **13**: 809–817.
44. Merlini L, Dudin O, Martin SG (2013) Mate and fuse: how yeast cells do it. *Open Biol* **3**: 130008.
45. Rasmussen SGF, Choi H-J, Rosenbaum DM, Kobilka TS, Thian FS, Edwards PC, Burghammer M, Ratnala VRP, Sanishvili R, Fischetti RF, et al. (2007) Crystal structure of the human β2 adrenergic G-protein-coupled receptor. *Nature* **450**: 383–387.
46. George SR, O'Dowd BF, Lee SP (2002) G-Protein-coupled receptor oligomerization and its potential for drug discovery. *Nat Rev Drug Discov* **1**: 808–820.
47. Bulenger S, Marullo S, Bouvier M (2005) Emerging role of homo- and heterodimerization in G-protein-coupled receptor biosynthesis and maturation. *Trends Pharmacol Sci* **26**: 131–137.
48. Benoit M, Gabriel D, Gerisch G, Gaub HE (2000) Discrete interactions in cell adhesion measured by single-molecule force spectroscopy. *Nat Cell Biol* **2**: 313–317.
49. Le DTL, Guérardel Y, Loubière P, Mercier-Bonin M, Dague E (2011) Measuring Kinetic Dissociation/Association Constants Between Lactococcus lactis Bacteria and Mucins Using Living Cell Probes. *Biophys J* **101**: 2843–2853.
50. Hagen I, Ecker M, Lagorce A, Francois JM, Sestak S, Rachel R, Grossmann G, Hauser NC, Hoheisel JD, Tanner W, et al. (2004) Sed1p and Srl1p are required to compensate for cell wall instability in Saccharomyces cerevisiae mutants defective in multiple GPI-anchored mannoproteins. *Mol Microbiol* **52**: 1413–1425.
51. Mrsa V, Ecker M, Strahl-Bolsinger S, Nimtz M, Lehle L, Tanner W (1999) Deletion of New Covalently Linked Cell Wall Glycoproteins Alters the Electrophoretic Mobility of Phosphorylated Wall Components of Saccharomyces cerevisiae. *J Bacteriol* **181**: 3076–3086.
52. Francius G, Lebeer S, Alsteens D, Wildling L, Gruber HJ, Hols P, Keersmaecker SD, Vanderleyden J, Dufrêne YF (2008) Detection, Localization, and Conformational Analysis of Single Polysaccharide Molecules on Live Bacteria. *ACS Nano* **2**: 1921–1929.
53. Alsteens D, Dupres V, Mc Evoy K, Wildling L, Gruber HJ, Dufrene YF (2008) Structure, cell wall elasticity and polysaccharide properties of living yeasts cells, as probed by AFM. *Nanotechnology* 384005.
54. Ragni E, Piberger H, Neupert C, García-Cantalejo J, Popolo L, Arroyo J, Aebi M, Strahl S (2011) The genetic interaction network of CCW12, a Saccharomyces cerevisiae gene required for cell wall integrity during budding and formation of mating projections. *BMC Genomics* **12**: 107.

55. Boisramé A, Cornu A, Costa GD, Richard ML (2011) Unexpected Role for a Serine/Threonine-Rich Domain in the Candida albicans Iff Protein Family. *Eukaryot Cell* **10**: 1317–1330.
56. Monniot C, Boisramé A, Da Costa G, Chauvel M, Sautour M, Bougnoux M-E, Bellon-Fontaine M-N, Dalle F, d' Enfert C, Richard ML (2013) Rbt1 Protein Domains Analysis in Candida albicans Brings Insights into Hyphal Surface Modifications and Rbt1 Potential Role during Adhesion and Biofilm Formation. *PLoS ONE* **8**: e82395.
57. Bouvier M (2001) Oligomerization of G-protein-coupled transmitter receptors. *Nat Rev Neurosci* **2**: 274–286.
58. El Moustaine D, Granier S, Doumazane E, Scholler P, Rahmeh R, Bron P, Mouillac B, Banères J-L, Rondard P, Pin J-P (2012) Distinct roles of metabotropic glutamate receptor dimerization in agonist activation and G-protein coupling. *Proc Natl Acad Sci U S A* **109**: 16342–16347.
59. Whorton MR, Bokoch MP, Rasmussen SGF, Huang B, Zare RN, Kobilka B, Sunahara RK (2007) A monomeric G protein-coupled receptor isolated in a high-density lipoprotein particle efficiently activates its G protein. *Proc Natl Acad Sci U S A* **104**: 7682–7687.
60. Khelashvili G, Dorff K, Shan J, Camacho-Artacho M, Skrabanek L, Vroling B, Bouvier M, Devi LA, George SR, Javitch JA, et al. (2010) GPCR-OKB: the G Protein Coupled Receptor Oligomer Knowledge Base. *Bioinforma Oxf Engl* **26**: 1804–1805.
61. Calebiro D, Rieken F, Wagner J, Sungkaworn T, Zabel U, Borzi A, Cocucci E, Zürn A, Lohse MJ (2013) Single-molecule analysis of fluorescently labeled G-protein-coupled receptors reveals complexes with distinct dynamics and organization. *Proc Natl Acad Sci U S A* **110**: 743–748.
62. Ferré S, Casadó V, Devi LA, Filizola M, Jockers R, Lohse MJ, Milligan G, Pin J-P, Guitart X (2014) G Protein–Coupled Receptor Oligomerization Revisited: Functional and Pharmacological Perspectives. *Pharmacol Rev* **66**: 413–434.
63. Fotiadis D, Liang Y, Filipek S, Saperstein DA, Engel A, Palczewski K (2003) Atomic-force microscopy: Rhodopsin dimers in native disc membranes. *Nature* **421**: 127–128.
64. Achour L, Labbé-Jullié C, Scott MGH, Marullo S (2008) An escort for GPCRs: implications for regulation of receptor density at the cell surface. *Trends Pharmacol Sci* **29**: 528–535.

Figures

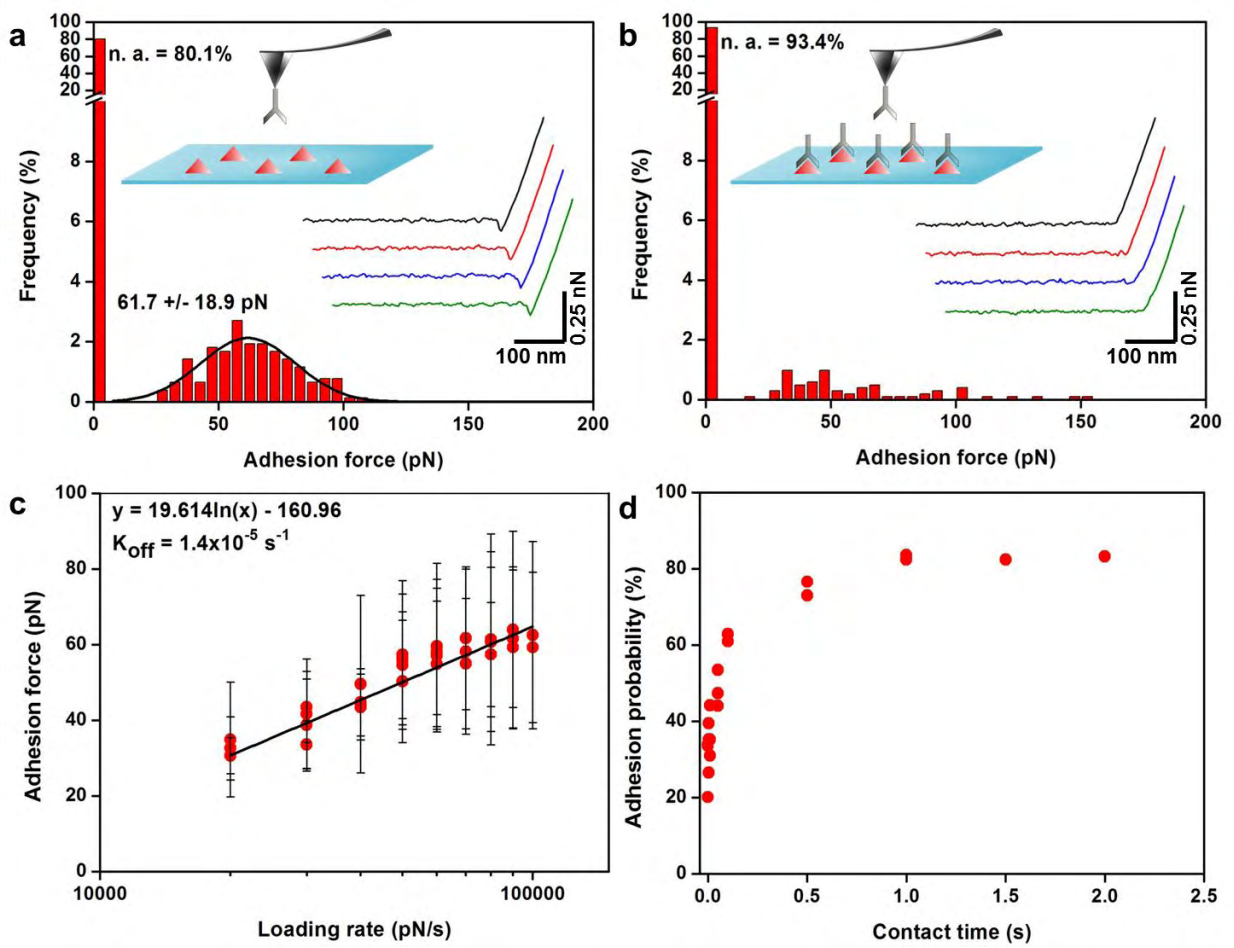

Figure 1. Single Molecule Force Spectroscopy with HA and HA antibody-functionalized AFM tips (HA-tip). (a) single molecule interactions between HA peptide immobilized on epoxy glass slide, and HA-antibodies immobilized on an AFM tip, at a loading rate of 70 000 pN/s. (b) blocking of HA specific sites by HA-antibodies and single-molecule force spectroscopy with HA antibody AFM tips. (c) Loading-rate dependence of interaction forces between HA and HA antibodies, and (d) contact-time dependence of the adhesion probability.

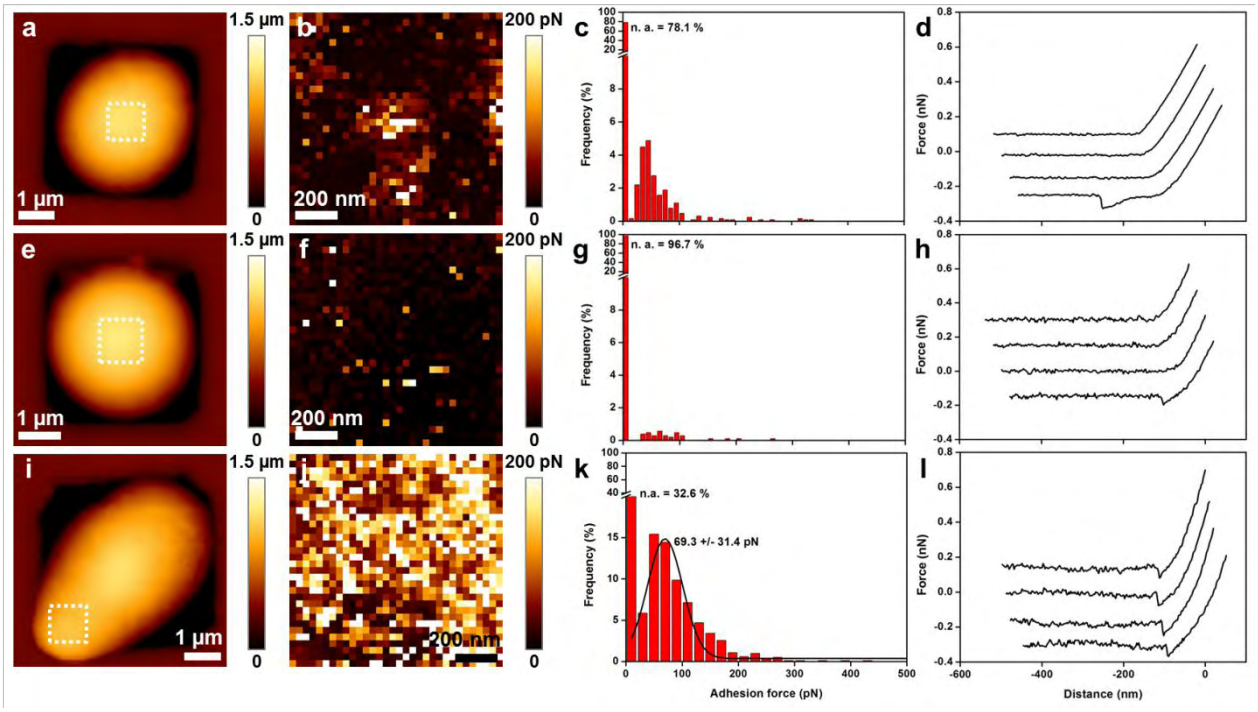

Figure 2. Mapping of HA-tagged protein CCW12 at the surface of living *Saccharomyces cerevisiae* cells immobilized in PDMS stamps. (a) AFM height image of a *S. cerevisiae* cell lacking CCW12 protein (strain ΔCCW12), (b) of a *S. cerevisiae* cell lacking CCW12 protein and complemented by a plasmid coding for CCW12-HA (strain ΔCCW12+p), and (c) of the same strain during mating projection process. (b, f and j) adhesions maps recorded with HA-tips on small areas on top of the cells, delimited by whites squares on a, e and i. (c, g, and k) Representative histograms of interaction forces and (d, h and l) representative force curves recorded on top of the cells.

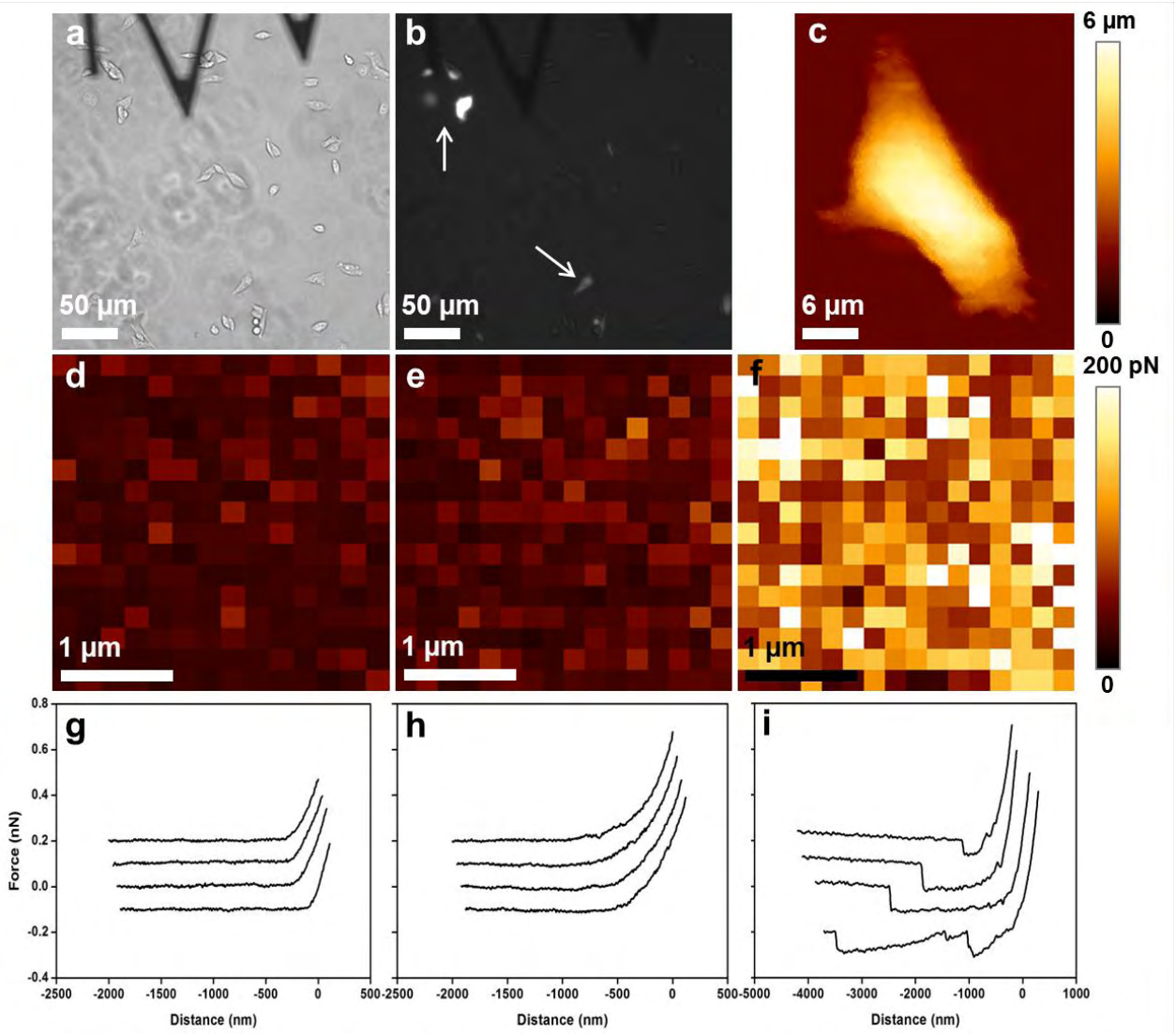

Figure 3. Mapping of HA-tagged β2-adrenergic receptors at the surface of living CHO cells. (a) Optical image of CHO cells immobilized on TPP coated petri dishes during AFM experiments, and (b) fluorescent CHO cells (transfected cells). (c) AFM height image of a single CHO cell. (d) Adhesion map of a small area recorded with HA-tips on top of a control CHO cell, (e) of a CHO cell transfected with an empty plasmid, and (f) of a CHO cell transfected with a plasmid coding for HA-tagged β2-adrenergic receptors. (g, h and i) Representative force curves on top of the cells.

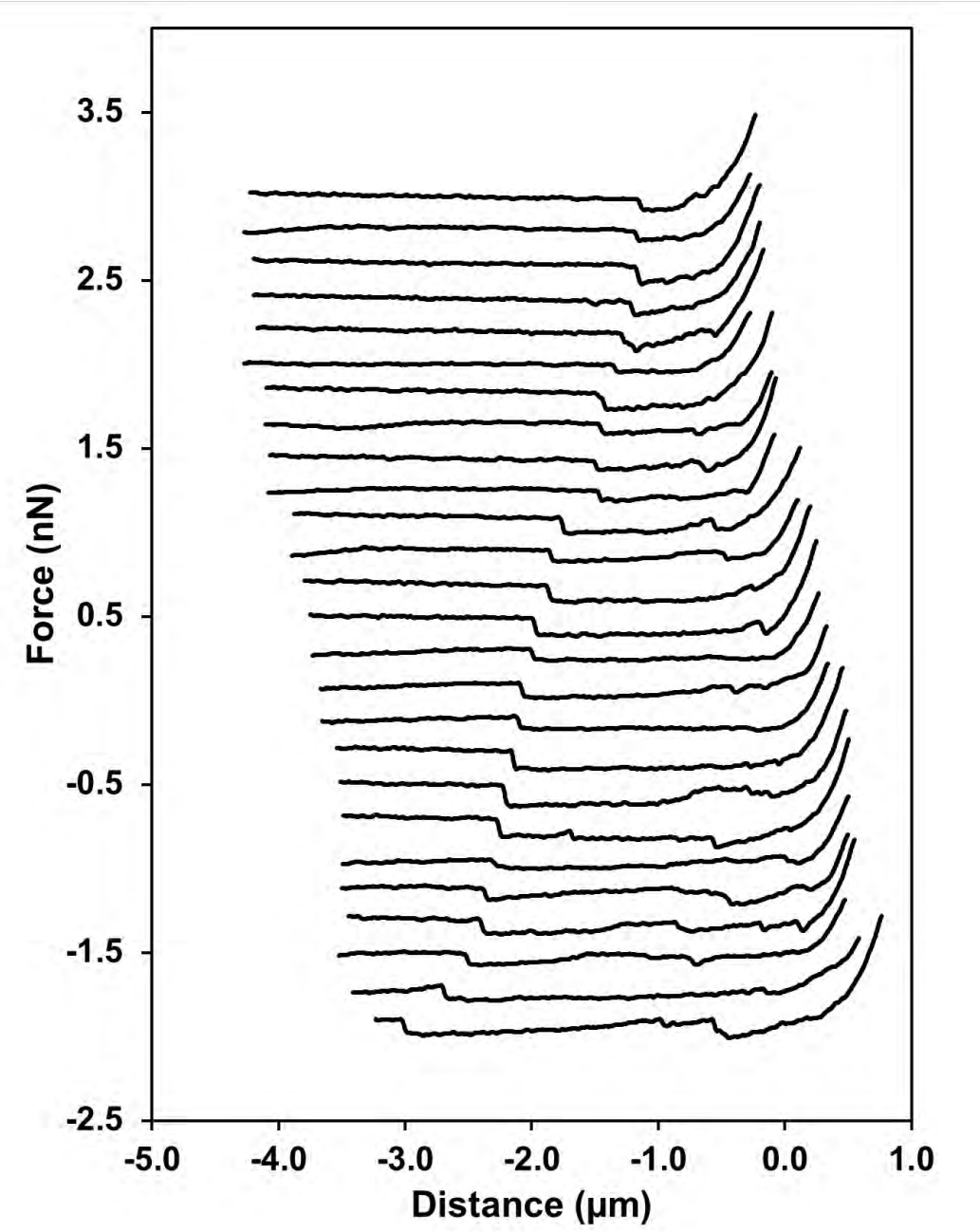

Figure 4. Detail of the force curves obtained on CHO cells transfected with a plasmid coding for HA-tagged β2-adrenergic receptors.

<u>Chapter 3.2</u>: A nanoscale view of the yeast cell wall of *Candida albicans* and *Saccharomyces cerevisiae*

3.2.1 Multiparametric imaging of adhesive nanodomains at the surface of *Candida albicans* by Atomic Force Microscopy

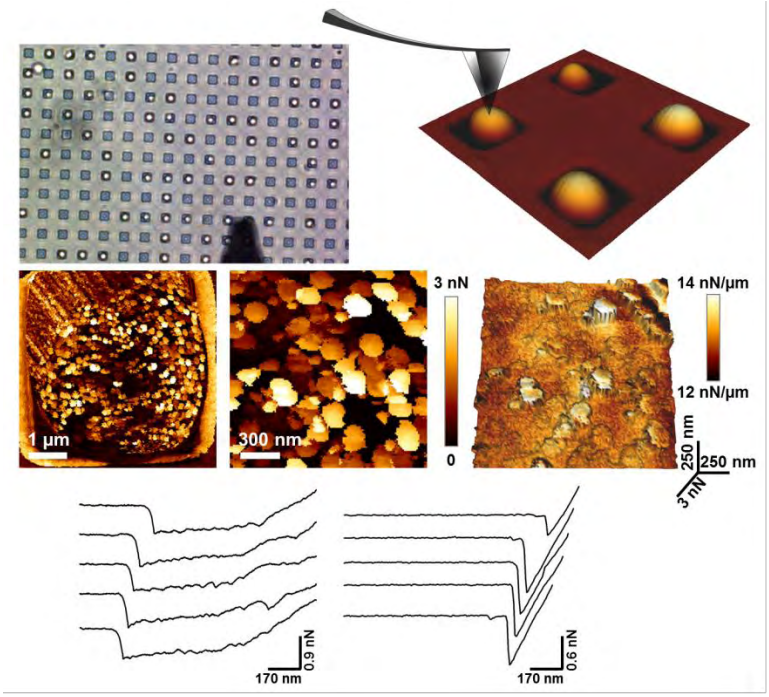

Formosa C., Schiavone M., Boisrame A., Richard M. L., Duval R. E., and Dague E.

In press in *Nanomedicine NBM*

Abstract

Candida albicans is an opportunistic pathogen. It adheres to mammalian cells through a variety of adhesins that interact with hosts ligands. The spatial organization of these adhesins on the cellular interface is however poorly understood, mainly because of the lack of instrument able to tract single molecules on single cells. In this context, the Atomic Force Microscope (AFM) makes it possible to analyze the force signature of single proteins on single cells. The present study is dedicated to the mapping of the adhesive properties of *C. albicans* cells. We observed that the adhesins at the cell surface were organized in nanodomains composed of free or aggregated mannoproteins. This was demonstrated by the use of functionalized AFM tips and synthetic amyloid forming/disrupting peptides. This direct visualization of amyloids nanodomains will help in understanding the virulence factors of *C. albicans*.

Nanomedicine: Nanotechnology, Biology, and Medicine
xx (2014) xxx–xxx

nanomedicine
Nanotechnology, Biology, and Medicine

nanomedjournal.com

Multiparametric imaging of adhesive nanodomains at the surface of *Candida albicans* by atomic force microscopy

Cécile Formosa, MS[a,b,c,d], Marion Schiavone, MS[a,b], Anita Boisrame, PhD[e,f], Mathias L. Richard, PhD[e,f], Raphaël E. Duval, PhD[c,d,g], Etienne Dague, PhD[a,b,*]

[a]*CNRS, LAAS, F-31400 Toulouse, France*
[b]*Université de Toulouse, LAAS, F-31400 Toulouse, France*
[c]*CNRS, UMR 7565, SRSMC, Vandœuvre-lès-Nancy, France*
[d]*Université de Lorraine, UMR 7565, Faculté de Pharmacie, Nancy, France*
[e]*INRA, UMR1319 Micalis, F-78352 Jouy-en-Josas, France*
[f]*AgroParisTech, UMR Micalis, F-78850 Thiverval Grignon, France*
[g]*ABC Platform®, Nancy, France*

Received 26 March 2014; accepted 21 July 2014

Abstract

Candida albicans is an opportunistic pathogen. It adheres to mammalian cells through a variety of adhesins that interact with host ligands. The spatial organization of these adhesins on the cellular interface is however poorly understood, mainly because of the lack of an instrument able to track single molecules on single cells. In this context, the atomic force microscope (AFM) makes it possible to analyze the force signature of single proteins on single cells. The present study is dedicated to the mapping of the adhesive properties of *C. albicans* cells. We observed that the adhesins at the cell surface were organized in nanodomains composed of free or aggregated mannoproteins. This was demonstrated by the use of functionalized AFM tips and synthetic amyloid forming/disrupting peptides. This direct visualization of amyloids nanodomains will help in understanding the virulence factors of *C. albicans*.

Key words: *Candida albicans*; Adhesins; Nanodomains; Atomic force microscopy; Multiparametric AFM

Background

The yeast *Candida albicans* has emerged as a major public health problem these last two decades. This opportunistic pathogen causes a wide range of infections from surface infections, to mucosal and blood-stream infections.[1] Whereas mucosal infections are common and occur in healthy organisms, blood-stream infections are observed only in immunocompromised patients and are life-threatening. This type of infection, also known as candidaemia, can develop into disseminated candidiasis when the infection spreads to internal organs, leading to high mortality rates.[2] In order to colonize and subsequently to disseminate in the blood stream *C. albicans* needs to adhere to different substrates. This first stage of infection[3] is mediated by adhesins that are found on the surface of the yeast cell wall. Many of these adhesins are mannoproteins, and among them, the adhesin family identified as having a major role in host cell attachment is the Als (agglutinin-like sequences) family.[4]

The Als were initially reported as having homologies with the proteins responsible for auto-agglutination in the baker yeast *Saccharomyces cerevisiae*. Eight Als have been identified, they all are primarily involved in host–pathogen interactions.[5] It was found that there were amyloid-forming sequences in the Als adhesins of *Candida albicans*.[6] Amyloids are insoluble fibrillar protein aggregates whose core consists in crystalline arrays of identical sequence in many molecules of the amyloid protein.[7,8]

This work was supported by an ANR young scientist program (AFMYST project ANR-11-JSV5-001-01 n°SD 30024331) to ED. CF and MS are respectively supported by a grant from "Direction Générale de l'Armement" (DGA) and from Lallemand SAS. ED is a researcher at Centre National de la Recherche Scientifique. We are grateful to "Association Lorraine pour la Recherche et le Développement de Composés Bioactifs", for its financial support.

*Corresponding author at: LAAS-CNRS, 7 avenue du Colonel Roche, 31400 Toulouse, France.
E-mail address: edague@laas.fr (E. Dague).

http://dx.doi.org/10.1016/j.nano.2014.07.008
1549-9634/

Cells expressing the Als proteins can rapidly aggregate, and the aggregation has amyloid-like properties. Like amyloid formation, aggregation ability propagates through the adherent cell population and depends on conformational changes of the Als protein. This transition of the conformational state to an aggregative state of the proteins is characterized by the formation of hydrophobic nanodomains on the entire surface of the cell.[9]

A few papers written by Lipke's team were dedicated to the direct visualization of these nanodomains using fluorescent dyes such as thioflavin T or 8-anilino-1-naphtalene-sulfonic acid (ANS).[6,8,9] Another technique that can be used to visualize these nanodomains is atomic force microscopy (AFM). AFM has recently emerged as a valuable tool to study the surface of living cells,[10] and especially pathogenic cells.[11] This technology has been used by Alsteens et al to image the formation and propagation of nanodomains in living yeast cells[12] and also to unfold amyloid proteins from the yeasts surface using single molecule force spectroscopy.[13-15] To this end, the authors functionalized AFM tips with antibodies targeted against the Als protein directly or against an epitope tag present in the Als protein. These studies allowed the authors to localize the adhesive nanodomains caused by the aggregation of Als proteins at the surface of living yeast cells, and to unravel the structure of the Als proteins studied by stretching.

In our study, we used AFM as an imaging tool to visualize and localize adhesins nanodomains at the surface of living wild-type *Candida albicans* cells. Using recent developments in the AFM technology, we and others have imaged and quantified at the same time the nanomechanical properties, the adhesiveness (force and nature of the interaction), the size and the thickness of the nanodomains,[16,17] at high resolution. The data collected showed that these nanodomains are localized differently at the surface of the cell, depending on the structures featured by the cells (bud scars, buds). We also showed that there were degrees of adhesiveness, depending on whether the amyloid proteins had totally aggregated (hydrophobic nanodomains) or not, and that these degrees of aggregation were directly correlated to the stiffness of the yeast cell wall. Finally, using force measurements and amyloid forming or inhibiting peptides, we showed that Als proteins (probably among others) were participating to these nanodomains.

Methods

Yeasts growth conditions

Candida albicans (from ABC Platform® Bugs Bank, Nancy, France) was stocked at −80 °C, revivified on Yeast Peptone Dextrose agar (Difco, 242720-500g) and grown in Yeast Peptone Dextrose broth (Difco, 242820-500g) for 20 hours at 30 °C under static conditions.

Sample preparation for AFM experiments

Yeast cells were concentrated by centrifugation, washed two times in acetate buffer (18 mM CH_3COONa, 1 mM $CaCl_2$, 1 mM $MnCl_2$, pH = 5.2), resuspended in acetate buffer, and immobilized on polydimethylsiloxane (PDMS) stamps prepared as described by Dague et al.[18] Briefly, freshly oxygen activated microstructured PDMS stamps were covered by a total of 100 μL of the solution of cells and allowed to stand for 15 min at room temperature. The cells were then deposited into the microstructures of the stamp by convective/capillary assembly. Images were recorded in acetate buffer in Quantitative Imaging ™ mode with MLCT AUWH (Bruker) cantilevers (nominal spring constant of 0.01 N/m). The applied force was kept at 1.5 nN for imaging and at 0.5 nN for force spectroscopy experiments. The loading rate for imaging was of 2 500 000 pN/s (acquisition frequency of the force curves is of 25 Hz) and for force spectroscopy of 75 000 pN/s (acquisition frequency of the force curves is of 1.25 Hz). For imaging and force spectroscopy, we used an AFM Nanowizard III (JPK Instruments, Berlin, Germany). The cantilevers spring constants were determined by the thermal noise method.[19] For all the results presented in this study, silicon nitride AFM tips were bare, except in the case of Figure 4, *G* (lower panel), where a functionalized AFM tip has been used.

AFM tips functionalization

The functionalized tips were produced according to a French patent of the authors described later in sensors and actuators.[20] Briefly, AFM tips were functionalized with dendrimers presenting CHO functions able to covalently link with NH_2 functions of proteins. These dendritips were then incubated with the lectin Concanavalin A (Sigma, L7647-100MG, 100 μg/mL) for 1 hour, before being used for force spectroscopy experiments.

Results analysis

All results were analyzed using the data processing software from JPK Instruments. The stiffness values measured on cells were determined from the slope of the linear portion of the raw deflections versus piezo displacement curves, according to:

$$kcell = k\left(\frac{s}{1-s}\right)$$

with s the experimentally accessible slope of the compliance region reached for sufficient loading forces. In this model, the experimental setup can be represented by two linear springs, one is the AFM's cantilever, and the other is the cell envelope exhibiting an effective spring constant. It is then possible to calculate the effective spring constant *kcell* of the cell envelope from the observed slope s of the force curve and the known spring constant k of the cantilever.[21]

Results

Candida albicans cells display localized adhesiveness

Thanks to our innovative method to immobilize cells into PDMS stamps,[18] and using Quantitative Imaging™ mode,[16] we were able to image and quantify the adhesive properties of single *C. albicans* cells at the same time. Figure 1, *A*, shows a budding yeast cell; on the corresponding adhesion image (Figure 1, *B*), we can see that only the bud, and not the mother-cell, presents adhesives patches. This original result is

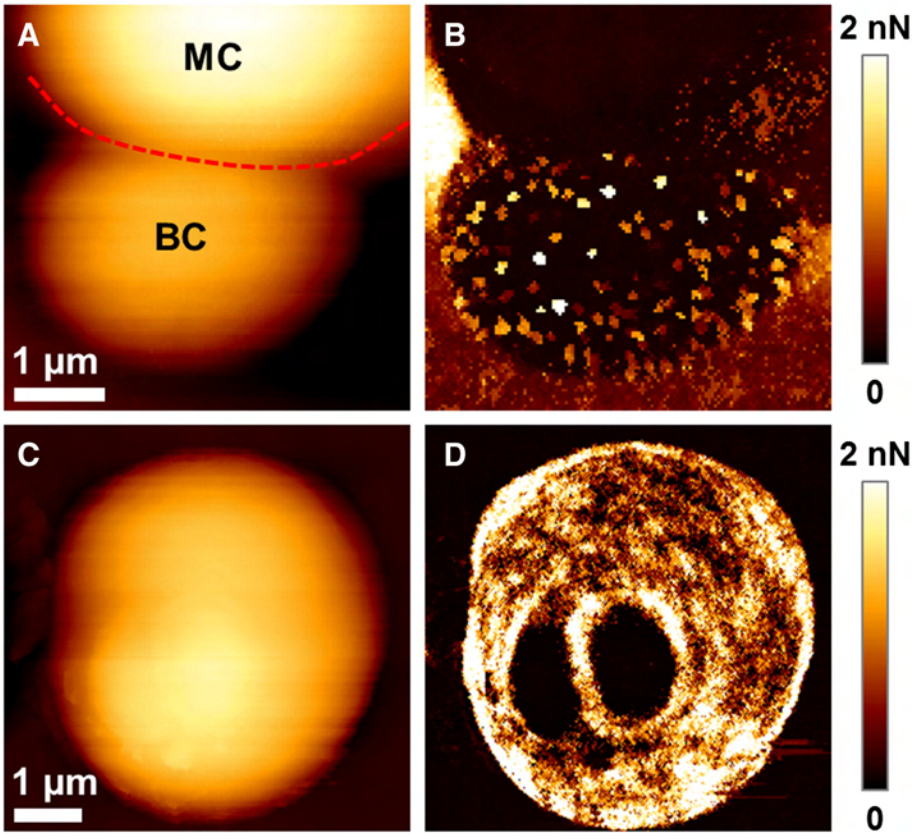

Figure 1. Localization of the adhesive properties of *C. albicans* cells. **(A)** Height image (z-range, 1.5 μm) of a budding *C. albicans* cell in a PDMS stamp, and **(B)** adhesion image corresponding to the height image. On **(A)**, MC stands for mother cell, BC stands for budding cell, and the red dotted line represents the demarcation between the two different cells. **(C)** Height image (z-range, 3.5 μm) of a single *C. albicans* cell exhibiting two bud scars, and **(D)** adhesion image corresponding to the height image.

surprising as non-budding cells are highly adhesive (see below). This result seems to indicate that the mother-cell cell wall changes during the budding process. As for the cell in Figure 1, *C*, this cell displays two bud scars, a common feature at the surface of yeast cells, which are not adhesive whereas the rest of the cell is. This type of distribution of the adhesion on yeast cells has already been seen using immunofluorescence with antibodies targeted against surface proteins of *C. albicans*. Coleman et al for example showed that the Als1 protein was expressed all over *C. albicans* cells, with the exception of bud scars.[22] The comparison of our results to these data suggests then that the adhesions probed by AFM might be due to surface proteins, such as Als1 in the case of the cell presenting bud scars, but perhaps also others adhesins.

C. albicans cell wall adhesins are able to aggregate into nanodomains

As showed before,[9,12] the proteins expressed at the surface of *C. albicans* cell wall are able to aggregate, and to form nanodomains. However, these nanodomains have not been yet characterized at the nanoscale, nor were imaged at high resolution. In fact, these nanodomains have specific adhesive properties that can be mapped using AFM in the Quantitative Imaging™ mode. High resolution (256 pixels^2) adhesive images are presented in Figure 2. It shows adhesive nanodomains, at the surface of a living wild-type *C. albicans* cell. On the cell presented in this figure (Figure 2, *A*), the corresponding adhesion image shows very distinct adhesive nanodomains that were probed with bare AFM tips. These nanodomains are homogeneously distributed all over the cell here, which does not present any morphological features such as buds or bud scars. When zooming into small areas on top of the cell (white squares on Figure 2, *B*), we could measure the area of each nanodomain. On this cell and on another one showed in Figure 3, *A*, 60 nanodomain areas were measured; the values obtained plotted on Figure 2, *E* shows that nanodomains have an average area of 0.09 ± 0.03 μm^2. This corresponds to an average diameter of 170 nm, which confirms the nanoscale of these nanodomains. Some of the nanodomains are also higher than the rest of the cell wall. When the whole cell is imaged, it is not visible; however, specific analysis of the Figure 3, *D* and the graphic Figure 3, *H* representing the topography of the cell surface revealed nanodomains that had a different height compared to the rest of the cell. The cross-sections taken along the blue line showed the height of a nanodomain of 20 nm. Once again, this confirmed the nanoscale of the nanodomains at the surface of *C. albicans*.

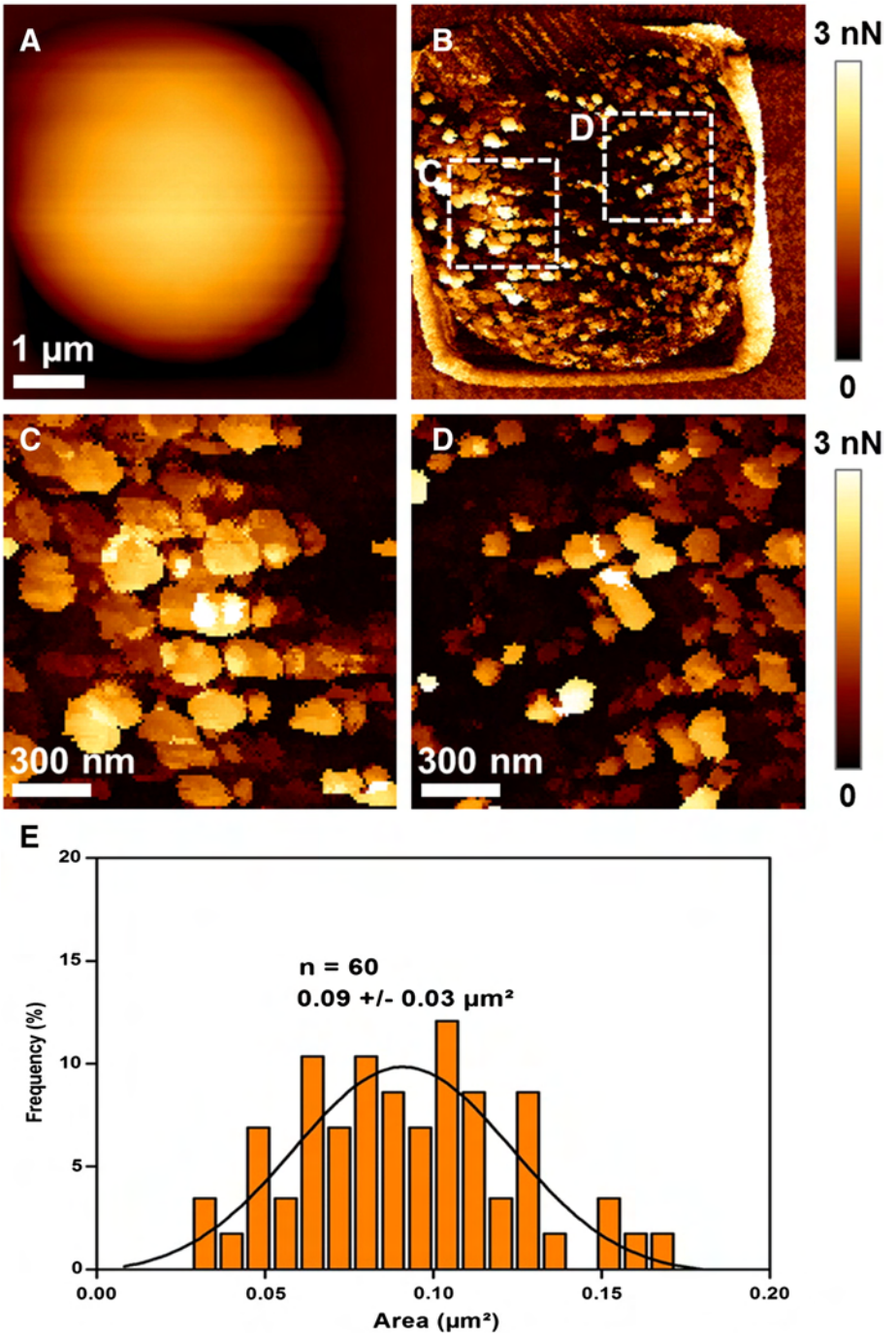

Figure 2. Imaging of the adhesive domains of *C. albicans* cells in acetate buffer, at 25 °C for 2 hours. **(A)** Height image (z-range, 2.5 µm) of a single *C. albicans* cell in a polydimethylsiloxane (PDMS) stamp, and **(B)** adhesion images corresponding to the height images. **(C and D)** Adhesion images of small areas on top of the cell, represented by the white squares in **(B)**. **(E)** Distribution of the areas values of the domains in **(C)** and **(D)**.

Different nanodomains have different nanomechanical properties

Adhesion is measured as the rupture force recorded when retracting the tip from the surface, when approaching and pulling with the tip on the cell wall, thus AFM makes it possible to measure nanomechanical properties of living cells. Here we choose to use an analysis based on the Hooke model which considers the coupled cantilever/cell wall as a spring. The stiffness values measured on cells were determined from the slope of the linear portion of the raw deflections versus piezo displacement curves, according to:

$$kcell = k\left(\frac{s}{1-s}\right)$$

with s the experimentally accessible slope of the compliance region reached for sufficient loading forces. Indeed, the most interesting

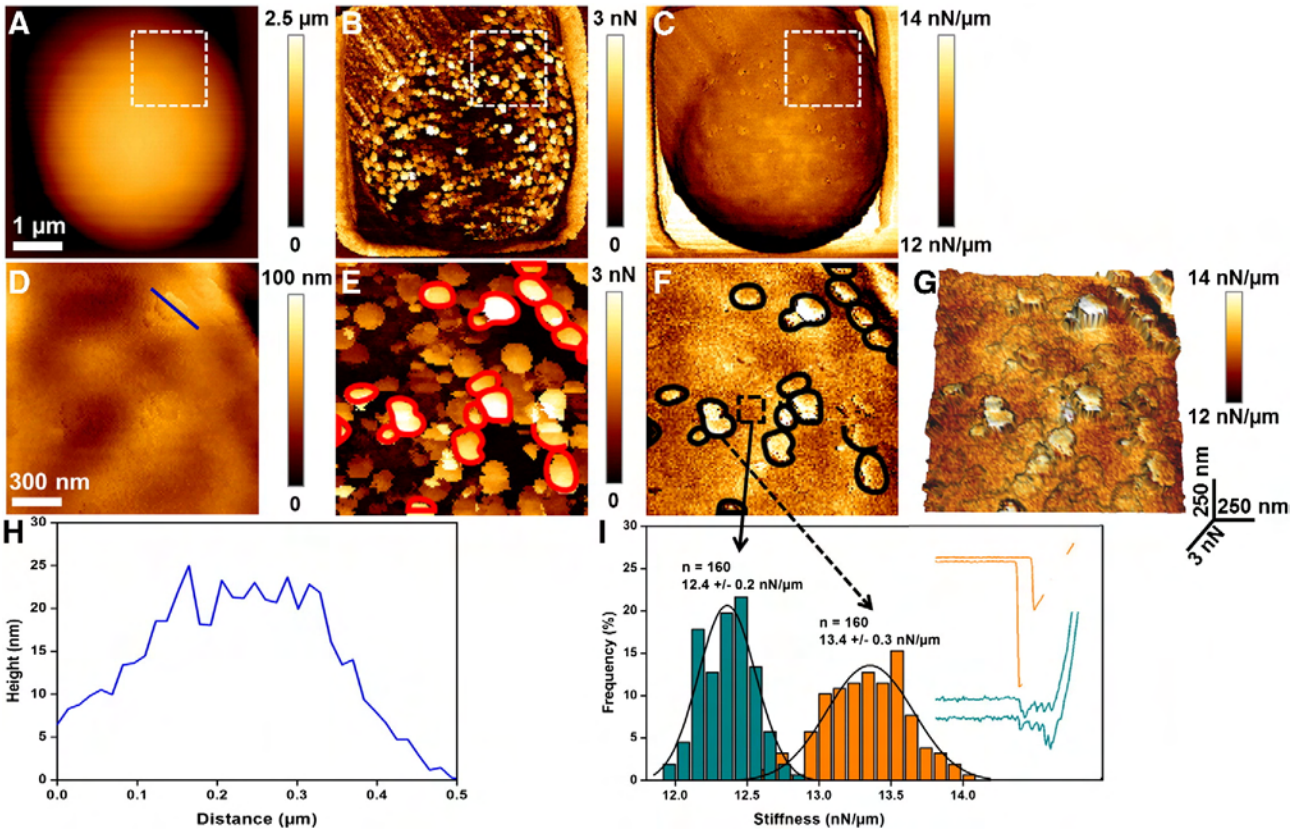

Figure 3. Nanomechanics of the adhesive domains of *C. albicans* cells. **(A)** Height image (z-range, 2.5 µm) of a *C. albicans* cell in a PDMS stamp, **(B)** corresponding adhesion image, and **(C)** corresponding stiffness image. **(D)** Height image (z-range, 100 nm) of a small area on top of the cell, represented by the white square on **(A)**, **(E)** corresponding adhesion image and **(F)** corresponding stiffness image. Note that the adhesive nanodomains circled in red on **(E)** are also found on the stiffness image (black circles on **F**). **(G)** is a 3D-image of the adhesion mapped with the stiffness. **(H)** Cross-section taken along the blue line on **(D)**, and **(I)**, distribution of the stiffness values corresponding to the yeast cell wall and the less adhesive domains (blue columns) or to the most adhesive domains (yellow columns).

result in this study is the correlation that can be directly made between the adhesiveness of the nanodomain, and its stiffness. Nanodomains on Figure 3, *E* (adhesion map), circled in red were found on the stiffness image (Figure 3, *F*) circled in black; they correspond to the zones where the stiffness of the cell wall is increased, to 13.4 ± 0.3 nN/µm. As for less adhesive nanodomains, they do not present any difference in stiffness from the rest of the cell, and are 12.4 ± 0.2 nN/µm. The 3D-view of the adhesion, mapped with the stiffness (Figure 3, *G*) illustrates this clear correlation; the more adhesive the nanodomain is, the stiffer it is.

Another fascinating point is that for the more adhesive nanodomains, the retract force curves present typical hydrophobic adhesions,[23-25] with adhesions occurring when the tip is retracted from the surface, *i. e.* 26.7 ± 9.7 nm far from the contact point (Figure S1, values measured on 300 force curves recorded on 3 different cells). Force curves from the other, less adhesive, nanodomains presented retract adhesions resembling to proteins unfolding, occurring 520.0 ± 153.9 nm after the tip withdrawal (Figure S1, values measured on 300 force curves recorded on 3 different cells). Therefore it seems that the nanodomains are of 2 different natures. There is a class of nanodomains, hydrophobic, higher and stiff, and another class displaying proteins unfolding properties, as soft as the rest of the cell wall. What is the molecular nature of these 2 types of nanodomains, and are they correlated?

Understanding the adhesive properties of the 2 nanodomains classes

To answer the previous question, we monitored the retract force curves recorded on the nanodomains (Figure 4). We found the same correlation as in Figure 3; the force curves recorded on an adhesive nanodomains presented hydrophobic retract adhesions, whereas the force curves recorded on a less adhesive nanodomain presented protein, unfolding like, profiles. In order to determine the nature of these last unfoldings, we probed the surface of *C. albicans* cells with an AFM tip functionalized with Concanavalin A (ConA), a protein that interacts with yeast mannoproteins, such as surface adhesins.[26] The resulting force curves (Figure 4, *I*) showed retract adhesions displaying unfoldings of different lengths, but with a similar profile. We also observed condensed spikes with adhesion forces of 40.9 ± 12.1 pN (Figure S1, values measured on 300 force curves recorded on 3 different cells). This value was measured on force curves thanks to the worm-like-chain (WLC) model using the highest point of each individual small spikes to adjust the baseline.

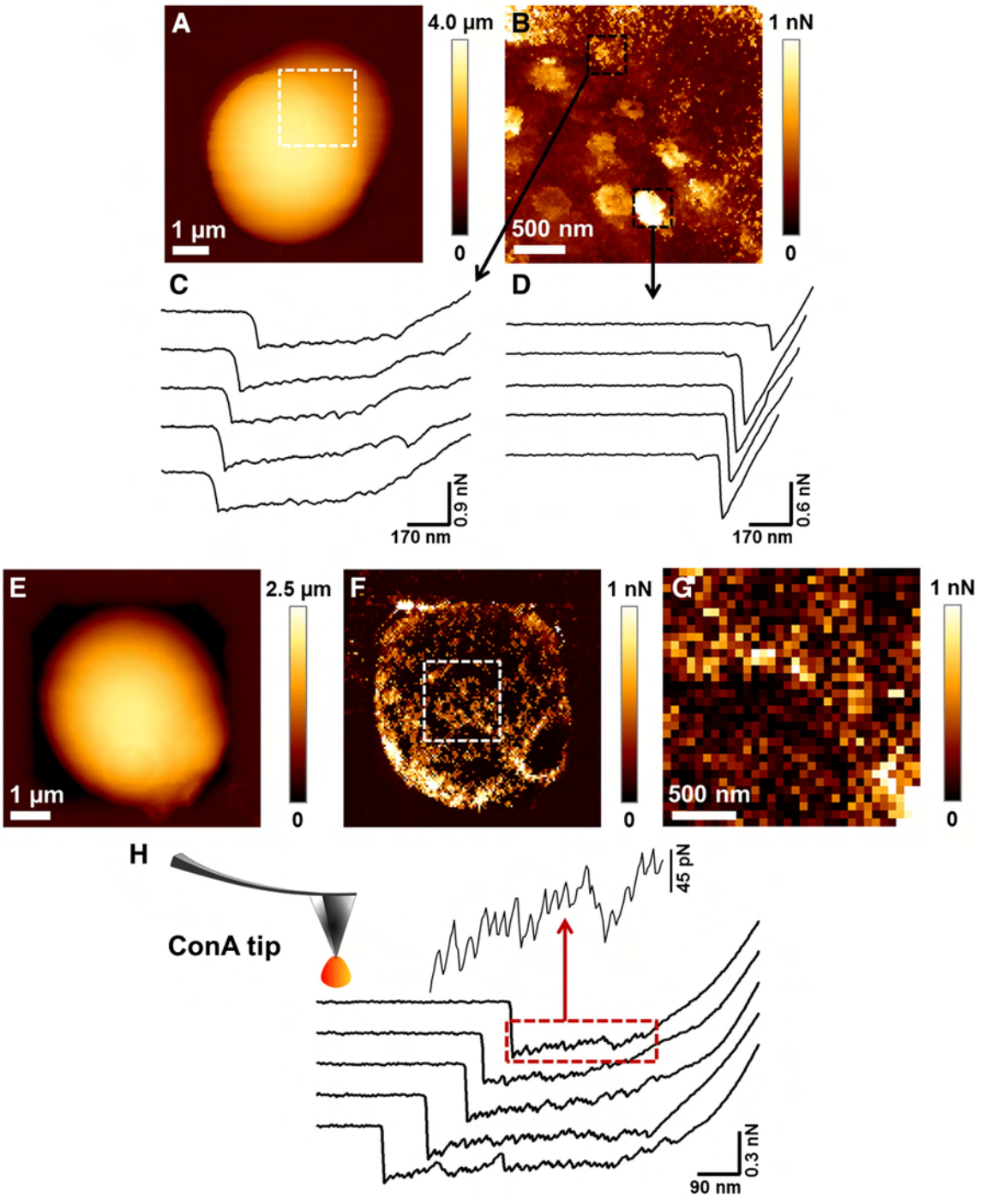

Figure 4. Adhesion force curves of *C. albicans* adhesive domains. **(A)** Height image (z-range, 4.0 µm) of a *C. albicans* cell in a PDMS stamp. **(B)** Adhesion image of a small area on top of the cell, represented by the white square on **(A)**. **(C and D)** representative force curves obtained on the zones indicated by the arrows on **(B)**. **(E)** Height image (z-range, 2.5 µm) of a *C. albicans* cell in a PDMS stamp, **(F)** corresponding adhesion image recorded with a bare tip, and **(G)** adhesion image of a 2 μm^2 area on top of the cell, represented by the white square on **(F)**, recorded with the Con A tip. **(H)** Representative force curves obtained in **(G)** with the Con A tip.

In a previous study conducted in 2009[14] by Alsteens et al, adhesins (Als5) were unfolded from the surface of live *S. cerevisiae* cells overexpressing this protein. The retract force curves obtained in this study show high similarity with the ones we obtain here with functionalized AFM tips, with the presence of serin-threonin rich segments unfolded with a force consistent with the one obtained in our case, *i. e.* 40.9 ± 12.1 pN, (condensed pikes on Figure 4, *H*). We can therefore, based on this comparison with the data of the literature, conclude that the less adhesive nanodomains at the surface of live *C. albicans* are composed of

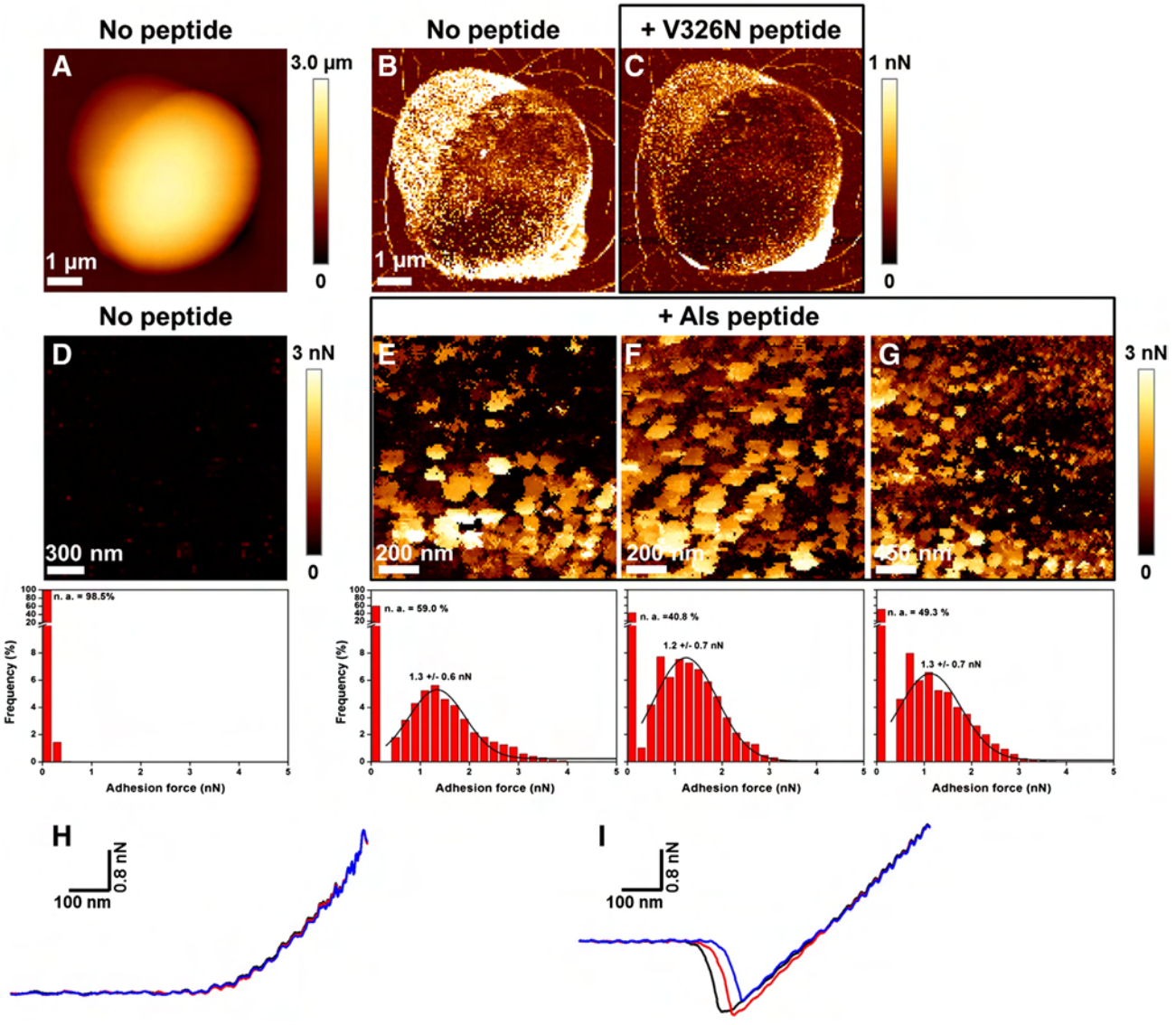

Figure 5. Imaging of the adhesive domains of *C. albicans* cells treated with Als1, 3, 5p amyloid disrupting peptide (V326N peptide) or Als1, 3, 5p amyloid forming peptide (Als peptide). **(A)** Height image of a single *C. albicans* cell in a PDMS stamp, **(B)** corresponding adhesion image, and **(C)** corresponding adhesion image after adding V326N peptide. **(D)** Adhesion image of small area on top of a *C. albicans* cell before adding the Als peptide, and **(E-G)** adhesion images of small areas on top of the same *C. albicans* cell after adding the Als peptide. For **(D-G)** histograms represent the distribution of the adhesion forces measured on the force curves obtained on the corresponding images. **(H)** representative force curves obtained on **(D)** and **(I)** representative force curves obtained on **(E-G)**.

free adhesins, and maybe of Als proteins. However, since all adhesins (like Als, Hwp1, Eap1, Rbt1 etc) are mannoproteins, we cannot, at this stage, make a statement on which adhesins are unfolded here.

As for the second type of nanodomains, the hydrophobic ones, our hypothesis is that they are composed of the same proteins as the less adhesive ones. In fact, adhesins (like Als) display amyloid sequences located on a domain of the protein called T, that enable them to change their conformation[6] and to aggregate into amyloid nanodomains. And when this phenomenon is started, it propagates to the whole cell.[9] We therefore made the hypothesis that the adhesive nanodomains are in fact amyloid nanodomains, made of Als proteins.

From adhesins to amyloid nanodomains: the role of Als proteins

To verify this hypothesis, and according to the literature on Als proteins, we synthesized a peptide exhibiting the same sequence as the one of the T domain of the Als1/3/5 proteins. We then put this peptide in the presence of the cells in order to trigger the amyloid formation. We also synthesized the same peptide, but with a mutation on one amino acid (V326N peptide), in order to obtain a peptide that inhibits the formation of the amyloid nanodomains.[8] Since Als3 is only expressed on the surface of hyphae, we will only be able to generate or destroy the amyloid formation of Als1 and Als5. The results presented in Figure 5 showed a cell before and after adding the mutated

peptide. We can clearly see on these adhesion images the loss of general adhesion and of two nanodomains at the center of the cell. It seems like the mutated peptide disrupted the amyloids at the surface of the cell. And the other way around, when cells were incubated with the amyloid forming peptide, we could observe the formation of the nanodomains at the surface of the cells, as it is showed on the adhesion images on local areas on top of *C. albicans* cells in Figure 5, *E*, *F* and *G*. Indeed, 98.5% of the force curves recorded on cells without treatment with the Als peptide presented no retract adhesions (Figure 5, *H*) whereas on treated cells, ~ 50% of the force curves presented hydrophobic retract adhesions (Figure 5, *I*). These results allow us to conclude that the proteins at the origin of the nanodomains are then mannoproteins, more specifically Als1 or Als5, or both, that form amyloids.

Discussion

We show in this study that wild-type live *C. albicans* cells exhibit extraordinary adhesive properties. In the case of budding cells, placed in acetate buffer at 25 °C for 2 hours, we observed that the mother cell is not adhesive and that only the bud presents adhesive nanodomains. On the contrary, we show that non budding cells are covered by adhesive nanodomains, in the same experimental conditions. This illustrates the amazing plasticity of this species[2,27] able to grow as a commensal or as a pathogen,[1,28] in all the parts of the intestinal track, but also on the vaginal mucosa, as unicellular budding cells or as filamentous hyphae. Moreover its cell wall is permanently remodeled as a reaction to its environment (temperature, pH, dissolved O_2, ions, interacting surface/cells/bacteria) what makes it challenging to reproduce the experimental conditions inducing a certain cell wall phenotype. We then demonstrate that the molecules at the origin of these adhesions could aggregate into nanodomains, which can be probed at high resolution using a suited AFM mode, QI™. These nanodomains are different in terms of level of adhesiveness, which is a property directly correlated to their stiffness and to the hydrophobic state or not of the molecule at the origin of these nanodomains. We then went further in the study, using functionalized AFM tips, and were able to determine that the less adhesive nanodomains were formed by mannoproteins that can interact specifically with Concanavalin A. These mannoproteins are able to aggregate to form the adhesive nanodomains because they have amyloid properties as we showed in Figure 5.

Amyloid aggregation is a primitive[29] and very stable[30] protein folding and a common structural motif. It is a cross β-sheet quaternary structure that usually auto-aggregates as fibrils. It has been, first, associated with neurodegenerative diseases like Alzheimer, Parkinson, or Creutzfeldt-Jakob diseases. However it is more and more unclear if the amyloid lesions are the cause or a consequence of the disease. Amyloid aggregates are now described as functional proteins assembly and can be found from bacteria to humans.[31] In microorganisms, amyloid has been described as a functional coat.[32] It consists in curli (*E. coli*), chaperons (*Streptomyces)* or hydrophobins (*Aspergillus etc)*; all of these proteins are implicated in adhesion to the host and in the invasion, infection process. It is now well known that adhesins (and especially *Als*) of *C. albicans* have amyloid-forming sequences[6,33] and that these proteins form domains involved in cell aggregation or biofilm formation.[8] Nevertheless the characterization, structure and properties of the amyloids adhesive nanodomains remain unclear.

In this work we measured for the first time the nanoscale size of amyloid domains (average area of 0.09 μm^2) at the surface of live *C. albicans* cells. The domains are of 2 different classes. Some present the characteristic of individual proteins whereas the others are hydrophobic, stiffer than the rest of the cell (13.4 ± 0.3 nN/μm compared to 12.4 ± 0.2 nN/μm), and are slightly protruding. It means that there is a state modification from soluble proteins into insoluble proteins, which is a characteristic of amyloid structures. This transformation is dependent on the proteins concentration and can only occur when the protein density exceeds a threshold. The roles of the two classes of domains are probably different. On one hand we could hypothesize that the hydrophobic nanodomains were involved in the cell adhesion to abiotic hydrophobic surfaces or to cell membrane as it is known that membrane binding is an inherent property of amyloid aggregates.[34,35] Amyloid aggregation is also a way to store proteins, in a limited space and to sort them when required. This has been demonstrated for hormones in secretory granules.[36,37] Thus *C. albicans* may store some adhesins for the subsequent invasion phases. On the other hand the protein like domains may be responsible for specific adhesion to fibronectin and other extra cellular proteins of the matrix. It seems rational that several adhesins, brought together, would be more efficient in a binding process than a single adhesion. This finding has to be added to *C. albicans* plasticity[2] and participate to explain its remarkable adaptation and pathogenicity.

However, there are still many things to explore on the cell wall of *C. albicans*, and future work will be dedicated to exploring the changes appearing on the mother cell during the budding process.

Appendix A. Supplementary data

Supplementary data to this article can be found online at http://dx.doi.org/10.1016/j.nano.2014.07.008.

References

1. Gow NA, Hube B. Importance of the Candida albicans cell wall during commensalism and infection. *Curr Opin Microbiol* 2012;**15**:406-12.
2. Poulain D. *Candida albicans*, plasticity and pathogenesis. *Crit Rev Microbiol* 2013:1-10.
3. Naglik JR, Moyes DL, Wächtler B, Hube B. Candida albicans interactions with epithelial cells and mucosal immunity. *Microbes Infect* 2011;**13**:963-76.
4. Hoyer LL. The ALS, gene family of Candida albicans. *Trends Microbiol* 2001;**9**:176-80.
5. Hoyer LL, Green CB, Oh S-H, Zhao X. Discovering the secrets of the Candida albicans agglutinin-like sequence (ALS) gene family – a sticky pursuit. *Med Mycol* 2008;**46**:1-15.

6. Ramsook CB, Tan C, Garcia MC, Fung R, Soybelman G, Henry R, et al. Yeast cell adhesion molecules have functional amyloid-forming sequences. *Eukaryot Cell* 2010;**9**:393-404.
7. Sawaya MR, Sambashivan S, Nelson R, Ivanova MI, Sievers SA, Apostol MI, et al. Atomic structures of amyloid cross-β spines reveal varied steric zippers. *Nature* 2007;**447**:453-7.
8. Garcia MC, Lee JT, Ramsook CB, Alsteens D, Dufrêne YF, Lipke PN. A role for amyloid in cell aggregation and biofilm formation. *PLoS ONE* 2011;**6**:e17632.
9. Rauceo JM, Gaur NK, Lee K-G, Edwards JE, Klotz SA, Lipke PN. Global cell surface conformational shift mediated by a candida albicans adhesin. *Infect Immun* 2004;**72**:4948-55.
10. Müller DJ, Dufrêne YF. Atomic force microscopy: a nanoscopic window on the cell surface. *Trends Cell Biol* 2011;**21**:461-9.
11. Alsteens D, Beaussart A, El-Kirat-Chatel S, Sullan RMA, Dufrêne YF. Atomic force microscopy: a new look at pathogens. *PLoS Pathog* 2013;**9**:e1003516.
12. Alsteens D, Garcia MC, Lipke PN, Dufrêne YF. Force-induced formation and propagation of adhesion nanodomains in living fungal cells. *Proc Natl Acad Sci* 2010;**107**:20744-9.
13. Beaussart A, Alsteens D, El-Kirat-Chatel S, Lipke PN, Kucharíková S, Van Dijck P, et al. Single-molecule imaging and functional analysis of Als adhesins and mannans during Candida albicans morphogenesis. *ACS Nano* 2012;**6**:10950-64.
14. Alsteens D, Dupres V, Klotz SA, Gaur NK, Lipke PN, Dufrêne YF. Unfolding individual Als5p adhesion proteins on live cells. *ACS Nano* 2009;**3**:1677-82.
15. Alsteens D, Ramsook CB, Lipke PN, Dufrêne YF. Unzipping a functional microbial amyloid. *ACS Nano* 2012;**6**:7703-11.
16. Chopinet L, Formosa C, Rols MP, Duval RE, Dague E. Imaging living cells surface and quantifying its properties at high resolution using AFM in QI™ mode. *Micron* 2013;**48**:26-33.
17. Dufrêne YF, Martínez-Martín D, Medalsy I, Alsteens D, Müller DJ. Multiparametric imaging of biological systems by force-distance curve-based AFM. *Nat Methods* 2013;**10**:847-54.
18. Dague E, Jauvert E, Laplatine L, Viallet B, Thibault C, Ressier L. Assembly of live micro-organisms on microstructured PDMS stamps by convective/capillary deposition for AFM bio-experiments. *Nanotechnology* 2011;**22**:395102.
19. Hutter JL, Bechhoefer J. Calibration of atomic-force microscope tips. *Rev Sci Instrum* 1993;**64**:1868-73.
20. Jauvert E, Dague E, Séverac M, Ressier L, Caminade A-M, Majoral J-P, et al. Probing single molecule interactions by AFM using bio-functionalized dendritips. *Sensors Actuators B Chem* 2012;**168**:436-41.
21. Arnoldi M, Fritz M, Bäuerlein E, Radmacher M, Sackmann M, Boulbitch A. Bacterial turgor pressure can be leasured by atomic force microscopy. *Phys Rev E* 1999;**62**:1034-44.
22. Coleman DA, Oh S-H, Zhao X, Hoyer LL. Heterogeneous distribution of Candida albicans cell-surface antigens demonstrated with an Als1-specific monoclonal antibody. *Microbiology* 2010;**156**:3645-59.
23. Dague E, Alsteens D, Latge JP, Verbelen C, Raze D, Baulard AR, et al. Chemical force microscopy of single live cells. *Nano Lett* 2007;**7**:3026-30.
24. Alsteens D, Dague E, Rouxhet PG, Baulard AR, Dufrene YF. Direct measurement of hydrophobic forces on cell surfaces using AFM. *Langmuir* 2007;**23**:11977-9.
25. Dague E, Alsteens D, Latgé J-P, Dufrêne YF. High-resolution cell surface dynamics of germinating Aspergillus fumigatus conidia. *Biophys J* 2008;**94**:656-60.
26. Alsteens D, Dupres V, Evoy KM, Wildling L, Gruber HJ, Dufrêne YF. Structure, cell wall elasticity and polysaccharide properties of living yeast cells, as probed by AFM. *Nanotechnology* 2008;**19**:384005.
27. Odds F. *Candida and candidiosis. A review and bibliography. 2nd edition*. London: Bailliere Tindall; 1988.
28. Gow NAR, van de Veerdonk FL, Brown AJP, Netea MG. Candida albicans morphogenesis and host defence: Discriminating invasion from colonization. *Nat Rev Microbiol* 2012;**10**:112-22.
29. Greenwald J, Riek R. Biology of amyloid: Structure, function, and regulation. *Structure* 2010;**18**:1244-60.
30. Perczel A, Hudáky P, Pálfi VK. Dead-End Street of Protein Folding: Thermodynamic Rationale of Amyloid Fibril Formation. *J Am Chem Soc 2007*;129:14959–14965.
31. Fowler DM, Koulov AV, Balch WE, Kelly JW. Functional amyloid–from bacteria to humans. *Trends Biochem Sci* 2007;**32**:217-24.
32. Gebbink MFBG, Claessen D, Bouma B, Dijkhuizen L, Wösten HAB. Amyloids—a functional coat for microorganisms. *Nat Rev Microbiol* 2005;**3**:333-41.
33. Otoo HN, Lee KG, Qiu W, Lipke PN. Candida albicans Als adhesins have conserved amyloid-forming sequences. *Eukaryot Cell* 2008;**7**:776-82.
34. Sparr E, Engel MFM, Sakharov DV, Sprong M, Jacobs J, de Kruijff B, et al. Islet amyloid polypeptide-induced membrane leakage involves uptake of lipids by forming amyloid fibers. *FEBS Lett* 2004;**577**:117-20.
35. Gellermann GP, Appel TR, Tannert A, Radestock A, Hortschansky P, Schroeckh V, et al. Raft lipids as common components of human extracellular amyloid fibrils. *Proc Natl Acad Sci U S A* 2005;**102**:6297-302.
36. Maji SK, Perrin MH, Sawaya MR, Jessberger S, Vadodaria K, Rissman RA, et al. Functional amyloids as natural storage of peptide hormones in pituitary secretory granules. *Science* 2009;**325**:328-32.
37. Dannies PS. Concentrating hormones into secretory granules: Layers of control. *Mol Cell Endocrinol* 2001;**177**:87-93.

<u>Chapter 3.2</u>: A nanoscale view of the yeast cell wall of *Candida albicans* and *Saccharomyces cerevisiae*

3.3.2 Nanoscale effects of caspofungin against two yeasts species,

Saccharomyces cerevisiae and *Candida albicans*

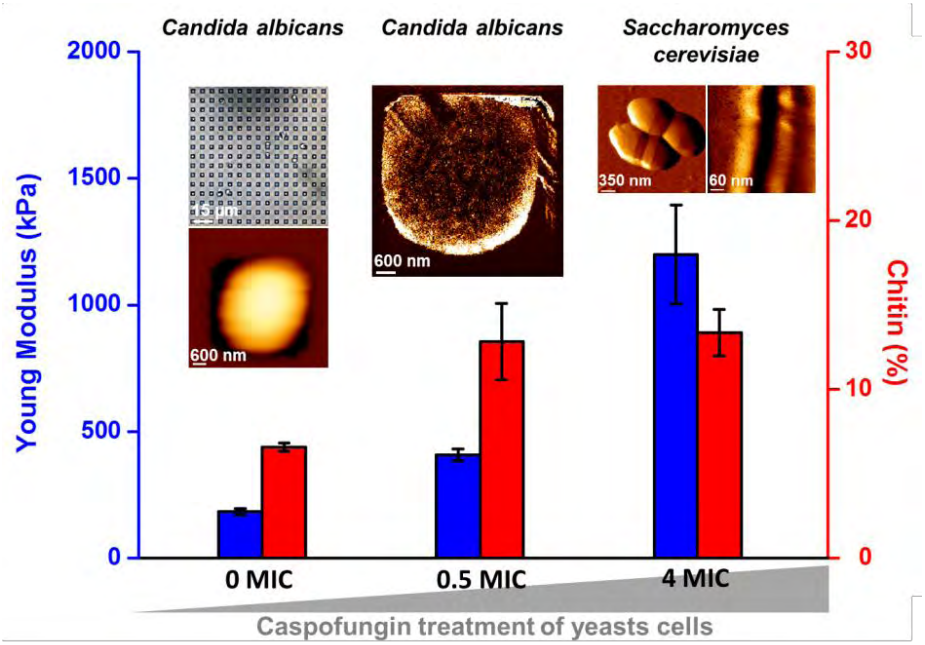

Formosa C., Schiavone M., Martin-Yken H., François J. M., Duval R. E., and Dague E.

Antimicrobial Agents and Chemotherapy, **57**, 2498-3506, 2013

Abstract

Saccharomyces cerevisiae and *Candida albicans* are model yeasts for biotechnology and human health, respectively. We used atomic force microscopy (AFM) to explore the effects of caspofungin, an antifungal drug used in hospitals, on these two species. Our nanoscale investigation revealed similar, but also different, behaviors of the two yeasts in response to treatment with the drug. While administration of caspofungin induced deep cell wall remodeling in both yeast species, as evidenced by a dramatic increase in chitin and decrease in β-glucan content, changes in cell wall composition were more pronounced with *C. albicans* cells. Notably, the increase of chitin was proportional to the increase in the caspofungin dose. In addition, the Young modulus of the cell was three times lower for *C. albicans* cells than for *S. cerevisiae* cells and increased proportionally with the increase of chitin, suggesting differences in the molecular organization of the cell wall between the two yeast species. Also, at a low dose of caspofungin (i.e., 0.5×MIC), the cell surface of *C. albicans* exhibited a morphology that was reminiscent of cells expressing adhesion proteins. Interestingly, this morphology was lost at high doses of the drug (i.e., 4×MIC). However, the treatment of *S. cerevisiae* cells with high doses of caspofungin resulted in impairment of cytokinesis. Altogether, the use of AFM for investigating the effects of antifungal drugs is relevant in nanomedicine, as it should help in understanding their mechanisms of action on fungal cells, as well as unraveling unexpected effects on cell division and fungal adhesion.

Nanoscale Effects of Caspofungin against Two Yeast Species, Saccharomyces cerevisiae and Candida albicans

C. Formosa, M. Schiavone, H. Martin-Yken, J. M. François, R. E. Duval and E. Dague

Antimicrob. Agents Chemother. **2013, 57(8):3498. DOI: 10.1128/AAC.00105-13.**
Published Ahead of Print 13 May 2013.

AAC Journals.ASM.org

Nanoscale Effects of Caspofungin against Two Yeast Species, *Saccharomyces cerevisiae* and *Candida albicans*

C. Formosa,[a,b,c,d] M. Schiavone,[a,b,e] H. Martin-Yken,[b,e] J. M. François,[b,e] R. E. Duval,[c,d,f] E. Dague[a,b]

CNRS, LAAS, Toulouse, France[a]; Université de Toulouse, LAAS, Toulouse, France[b]; CNRS, SRSMC, UMR 7565, Vandœuvre-lès-Nancy, France[c]; Université de Lorraine, SRSMC, UMR 7565, Nancy, France[d]; INRA, UMR 972 LISBP, Toulouse, France[e]; ABC Platform, Nancy, France[f]

***Saccharomyces cerevisiae* and *Candida albicans* are model yeasts for biotechnology and human health, respectively. We used atomic force microscopy (AFM) to explore the effects of caspofungin, an antifungal drug used in hospitals, on these two species. Our nanoscale investigation revealed similar, but also different, behaviors of the two yeasts in response to treatment with the drug. While administration of caspofungin induced deep cell wall remodeling in both yeast species, as evidenced by a dramatic increase in chitin and decrease in β-glucan content, changes in cell wall composition were more pronounced with *C. albicans* cells. Notably, the increase of chitin was proportional to the increase in the caspofungin dose. In addition, the Young modulus of the cell was three times lower for *C. albicans* cells than for *S. cerevisiae* cells and increased proportionally with the increase of chitin, suggesting differences in the molecular organization of the cell wall between the two yeast species. Also, at a low dose of caspofungin (i.e., 0.5× MIC), the cell surface of *C. albicans* exhibited a morphology that was reminiscent of cells expressing adhesion proteins. Interestingly, this morphology was lost at high doses of the drug (i.e., 4× MIC). However, the treatment of *S. cerevisiae* cells with high doses of caspofungin resulted in impairment of cytokinesis. Altogether, the use of AFM for investigating the effects of antifungal drugs is relevant in nanomedicine, as it should help in understanding their mechanisms of action on fungal cells, as well as unraveling unexpected effects on cell division and fungal adhesion.**

The yeast cell wall is composed of 50 to 60% β-glucans (glucose residues attached by 1,3-β- and 1,6-β-linkages), 40 to 50% mannoproteins (highly glycosylated polypeptides), and 1 to 3% chitin (1, 2). It is an essential dynamic structure playing roles in maintaining cell shape and integrity, sensing the surrounding environment, and interacting with surfaces and other cells (3). The cell wall represents 15 to 25% of the cell dry mass, the chemical composition of which is well established. *Saccharomyces cerevisiae*, also called baker's yeast, is the best-characterized eukaryotic model for scientific and biomedical research. Although the chemical composition of the yeast cell wall is well known, its molecular ultrastructure (organization or assembly) has not been extensively studied at nanoscale (4, 5), although there are a few reports on the nanomechanical and adhesive properties of the yeast cell wall under native conditions or under stress conditions (6–8). As for *Candida albicans*, it is by far the most common human-pathogenic fungal species. It can cause a range of pathogenic effects, including painful superficial infections, severe surface infections, and life-threatening bloodstream infections (9). It is a major cause of morbidity and mortality in immunocompromised patients as a result of AIDS, cancer chemotherapy, or organ transplantation (10).

Given its medical relevance, *C. albicans* has been the subject of extensive research to find new antifungal drugs to fight it. To date, only three classes of antifungal drugs are available for systemic *C. albicans* infections: the polyenes (such as amphotericin B), the azoles (ketoconazole, itraconazole, fluconazole, and voriconazole), and flucytosine. Although many of these drugs have advanced the management of fungal infections, failure rates remain high (11), and the emergence of resistant fungal strains is a growing problem (12). In this context, a new class of antifungal drugs, the echinocandins, was very welcome in the biomedical domain (13). There are currently three drugs belonging to the class that are available for clinical use: caspofungin, micafungin, and anidulafungin. The echinocandins are large polypeptide molecules that inhibit β-1,3-glucan synthase, an enzyme involved in cell wall synthesis. The disruption of this polysaccharide results in the loss of cell wall integrity. The activity of echinocandins is generally opposite to that of the azoles in that they are fungicidal against yeasts and fungistatic against molds (13). As echinocandins have been used only recently in the clinic, the mechanism of resistance to the drugs is still poorly documented, although a few cases of resistant isolates from patients treated with the antifungal implicating mutations in the *FKS1* gene encoding β1,3-glucan synthase (14–17) have been reported.

Whereas the target of echinocandins (i.e., β-1,3-glucan synthase) is well characterized, the global effects of this antifungal drug class on the cell wall of yeasts at nanoscale have not been studied. Such a study is now becoming feasible with the recent advances in atomic force microscopy (AFM) under liquid conditions. Since its invention in 1986 (18), AFM has proven to be a powerful tool in biology (19) for evaluating the effects of antimicrobial drugs against live bacteria or fungi (20, 21). In this study, we used AFM under liquid conditions to investigate nanomechanical effects caused by caspofungin on *S. cerevisiae* and *C. albicans*. Furthermore, we used biochemical methods to determine the cell wall composition in order to evaluate a potential correlation between these biophysical properties and cell wall modifications in response to caspofungin for the two yeast species.

Received 15 January 2013 **Returned for modification** 27 February 2013
Accepted 4 May 2013
Published ahead of print 13 May 2013
Address correspondence to E. Dague, edague@laas.fr.
C.F and M.S. contributed equally to the work.

doi:10.1128/AAC.00105-13

MATERIALS AND METHODS

Yeast growth conditions. *S. cerevisiae* strain BY4741 (MAT**a** *his3Δ1 leu2Δ10 met15Δ0 ura3Δ0*) (22) and *C. albicans* (from ABC Platform Bugs Bank, Nancy, France) were stocked at −80°C, revivified on yeast extract-peptone-dextrose (YPD) agar (Difco; 242720-500g), and grown in yeast extract-peptone-dextrose broth (Difco; 242820-500g) for 20 h at 30°C under static conditions. For caspofungin treatment, caspofungin was added for 20 h before the experiments. Before AFM experiments were conducted, the yeasts were grown in yeast extract-peptone-dextrose broth containing caspofungin at a concentration of 0.063 μg/ml (0.5× MIC) and 0.5 μg/ml (4× MIC) for *S. cerevisiae* and 0.047 μg/ml (0.5× MIC) and 0.37 μg/ml (4× MIC) for *C. albicans*.

MIC determination for caspofungin. The MIC values for caspofungin were determined using commercially available Etest strips containing a gradient of caspofungin (bioMérieux; 532400). For the diffusion test, a yeast solution (optical density at 590 nm [OD_{590}] = 0.150) was applied to the yeast extract-peptone-dextrose agar plates. The plates were allowed to dry for 15 min before the Etest stripes were applied in a radial fashion onto the agar surface. The MIC was determined after 24 h at 30°C by the intersection of the lower part of the elliptical growth inhibition area with the Etest strip.

We chose to use Etest from bioMérieux, as it gave repeatable results compared to the EUCAST (23) or CLSI (24) method. It must be noted that EUCAST does not publish clinical breakpoints for caspofungin for *C. albicans* "due to significant interlaboratory variation in MIC ranges for caspofungin."

We used yeast extract-peptone-dextrose agar (Difco; 242720-500g) and incubation at 30°C in order to determine the caspofungin MIC for the conditions under which we performed the AFM and biochemical experiments of the study. However, we also performed the Etest at 35°C for 24 h, and we found the same results for both *S. cerevisiae* and *C. albicans* as with incubation at 30°C. The common applications for the caspofungin Etest would be to use agar containing RPMI 1640, glucose, and MOPS (morpholinepropanesulfonic acid). However, under these conditions in liquid, the cells of *C. albicans* behave differently, since they form hyphae. In our study, we focused on cells with a spherical shape, the one that *C. albicans* assumes in bloodstream infections. This is why we performed all the experiments in YPD, and thus, we made the choice to determine the MICs in YPD also.

Sample preparation for AFM experiments. Yeast cells were concentrated by centrifugation, washed two times in acetate buffer (18 mM CH_3COONa, 1 mM $CaCl_2$, 1 mM $MnCl_2$, pH 5.2), resuspended in acetate buffer, and immobilized on polydimethylsiloxane (PDMS) stamps prepared as described by Dague et al. (25). Briefly, freshly oxygen-activated microstructured PDMS stamps were covered with a total of 100 μl of the solution of cells and allowed to stand for 15 min at room temperature. The cells were then deposited into the microstructures of the stamp by convective/capillary assembly. For *S. cerevisiae* cells treated with caspofungin at 4.0× MIC, polyethylenimine (PEI)-coated glass slides were used to immobilize the cells, as described previously (26). Briefly, freshly oxygen-activated glass slides were covered with a 0.2% PEI solution in deionized water and left for incubation overnight. Then, the glass slides were rinsed with 20 ml of Milli-Q water and nitrogen dried. A total of 1 ml of the yeast suspension was then applied to the PEI-coated glass slide, allowed to stand for 1 h, and rinsed with acetate buffer. Images were recorded in acetate buffer in quantitative-imaging mode (27, 28) with MLCT AUWH cantilevers (nominal spring constants, 0.01, 0.1, and 0.5 N/m). For imaging, cantilevers with a spring constant of 0.01 N/m were used. For force spectroscopy experiments, cantilevers with spring constants of 0.1 and 0.5 N/m were used. The applied force was kept at 0.5 nN for both imaging and force spectroscopy. For imaging and force spectroscopy, we used an AFM Nanowizard III (JPK Instruments, Berlin, Germany). The cantilevers' spring constants were determined by the thermal-noise method (29). For elasticity measurements, force maps of 32-by-32 force curves were recorded on a small area on top of the cells. The force-distance curves recorded were transformed into force-indentation curves by subtracting the cantilever deflection on a solid surface. The indentation curves were then fitted to the Hertz model, which links force (F) as a function of the Young modulus (E) and the square of the indentation (δ) for a conical indenter according to the following equation: $F = [2E \tan\alpha/\pi(1 - \nu^2)]\delta^2$, where α is the tip opening angle (17.5°) and ν is the Poisson ratio, assumed to be 0.5.

Isolation of cell walls for acid hydrolysis and chitinase assays. Cells from three independent cultures were collected at the exponential phase, harvested by centrifugation (5 min; 4,500 × *g*; 4°C), and washed two times with sterilized water. The pellet was resuspended in 0.5 ml of cold water and transferred to lysing matrix tubes (MPBio; 6960-500) containing 0.5-mm glass beads. The cells were disrupted by 8 cycles of 20 s at 6.5 m/s using a Fastprep system (Mp Biomedicals). Cell walls were isolated by centrifugation and extensive washing, as described by Francois (2), and then lyophilized.

Determination of cell wall polysaccharides by acid hydrolysis and quantification by HPAEC-pulsed amperometric detection. Sulfuric acid hydrolysis of the cell wall and quantification of glucosamine, glucose, and mannose residues released after chitin, β-glucan, and mannan hydrolysis were determined as described by Dallies et al. (30) with modifications according to the method of Francois (2). High-performance anionic chromatography (HPAEC) was carried out on an ICS 5000 system (Thermofisher Scientific, Courtaboeuf, France). Separation and quantification of the released monosaccharides were performed on a CarboPac PA10 analytical column (250 by 4 mm), with a CarboPac PA10 guard column, by isocratic elution of 18 mM NaOH at 25°C and a flow rate of 1 ml/min. Detection was performed on a pulsed amperometric system equipped with a gold electrode.

Chitin determination. A solution of 200 μl of 50 mM potassium acetate, pH 5.0, was added to purify cell walls (10 mg dry mass). After incubation at 65°C for 5 min, 1 U of chitinase from *Streptomyces griseus* (Sigma-Aldrich; C6137) was added. The enzymatic mixture was then incubated for 16 h at 37°C. Chitin levels from yeast cell walls were determined by the colorimetric method, as described by Reissig et al. (31) and adapted for the micromethod (a method performed in a microtiter plate, i.e., 96-well plate), using *N*-acetylglucosamine (Sigma-Aldrich; A8625) as a standard. A volume of 125 μl of the enzymatic mixture was heated with 25 μl of 0.8 M potassium tetraborate, pH 9.0 (Sigma-Aldrich; P1463), at 100°C for 8 min. After cooling at room temperature, 750 μl of Reissig reagent diluted 10 times was added, and tubes were incubated for 40 min at 37°C. The absorbance was read at 585 nm.

RESULTS

Caspofungin affects the morphology and cell division of *S. cerevisiae*. Our innovative method of cell trapping and immobilization in microstructured PDMS stamps (25) allowed us to image yeast cells and obtain morphological and mechanical properties at nanoscale (Fig. 1a and b). For each condition, five cells from three independent cultures were analyzed. The MIC determined with the Etest was 0.125 $\mu g \cdot ml^{-1}$. As shown in Fig. 1c, native cells of *S. cerevisiae* are roughly ovoid, with a mean diameter of 4.5 ± 0.2 μm (Fig. 1e). Upon treatment for 16 h with caspofungin at 0.5× MIC, the cells keep their round shape (Fig. 1b and d), and their mean size is decreased by about 25% ± 2.5% (Fig. 1f). A small dose of caspofungin, therefore, reduces the size of cells, apparently without any other modifications. When yeast cells were treated for 16 h with a high dose of caspofungin (4× MIC), the *S. cerevisiae* cells were no longer spherical but elongated, resembling *Schizosaccharomyces pombe* cells. The cross section taken along the line in Fig. 2b indicated a length of about 2.3 μm (Fig. 2f), which is 50% shorter than the untreated cells. However, two cells that remained connected are distinctly seen in Fig. 2d; they present a surprising feature on their surfaces, at the center of each one.

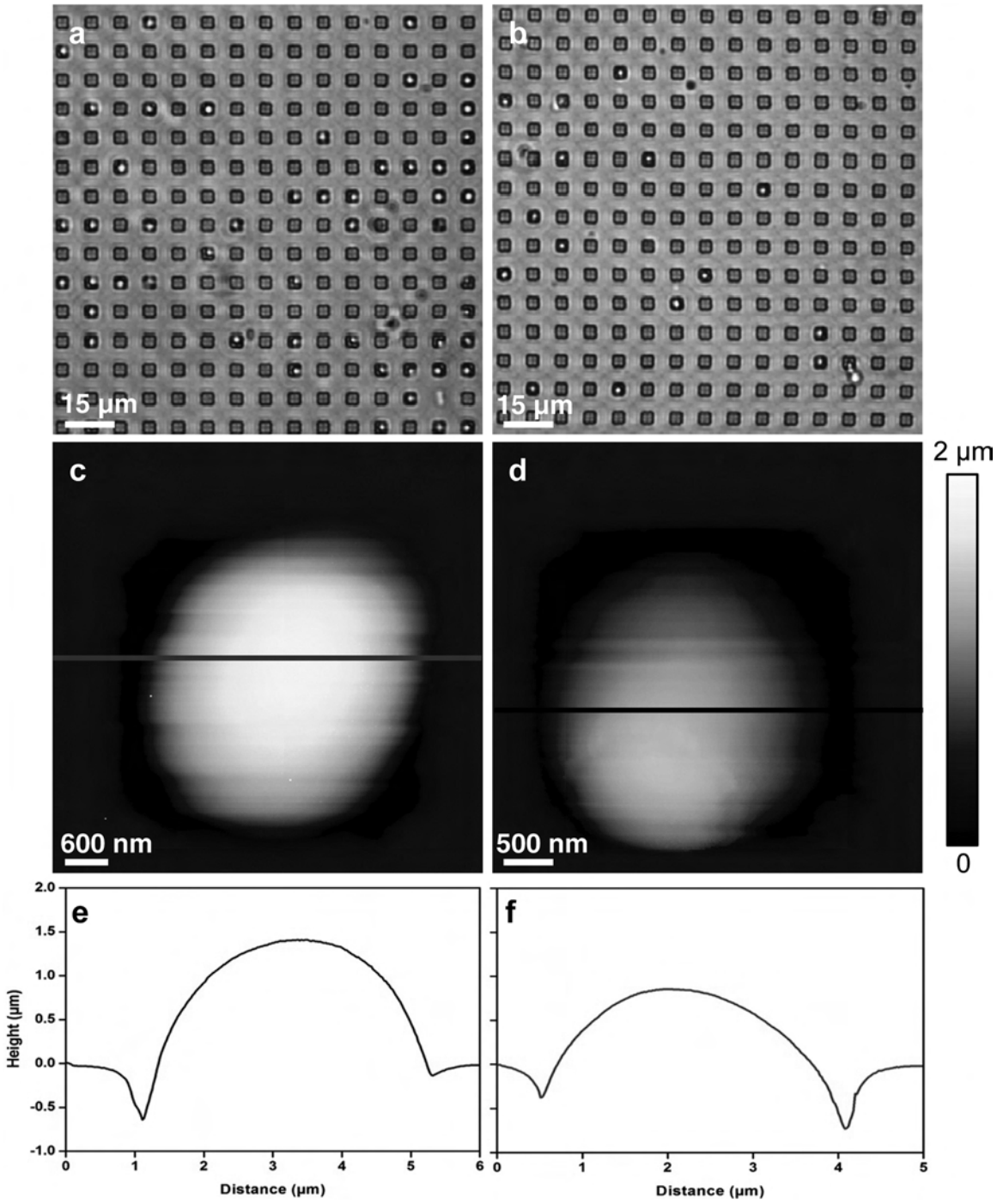

FIG 1 Images of *S. cerevisiae* cells (strain BY4147) trapped in microstructured PDMS stamps. (a and b) Optical images of live native cells (a) and of cells treated with caspofungin at 0.5× MIC (0.063 μg/ml) (b). (c and d) AFM height images of a native cell (c) and of a cell treated with caspofungin at 0.5× MIC (0.063 μg/ml) (d). (e and f) Cross sections taken along the lines on the height images.

When we took a closer look at this feature (Fig. 2e and g), we could visualize two rings that were 15 nm high and that were separated by a groove of approximately 200 nm. These results suggest that the morphology and cell division process of *S. cerevisiae* are altered at high doses of caspofungin. How can we explain such an effect?

It is known that caspofungin is an inhibitor of β-1,3-glucan synthase (13). Thus, cells treated with this antifungal drug should present a reduced percentage of the cell wall polysaccharide. Accordingly, we found a reduction in the β-glucan content, from 54% of cell dry mass in untreated *S. cerevisiae* cells to 49 and 45% in cells treated with caspofungin concentrations of 0.5× and 4× MIC, respectively (Table 1). The reduction of glucans was compensated for by an increase of mannans, from 45% of dry mass in untreated cells to 50 and 53% in cells treated at 0.5× and 4× MIC,

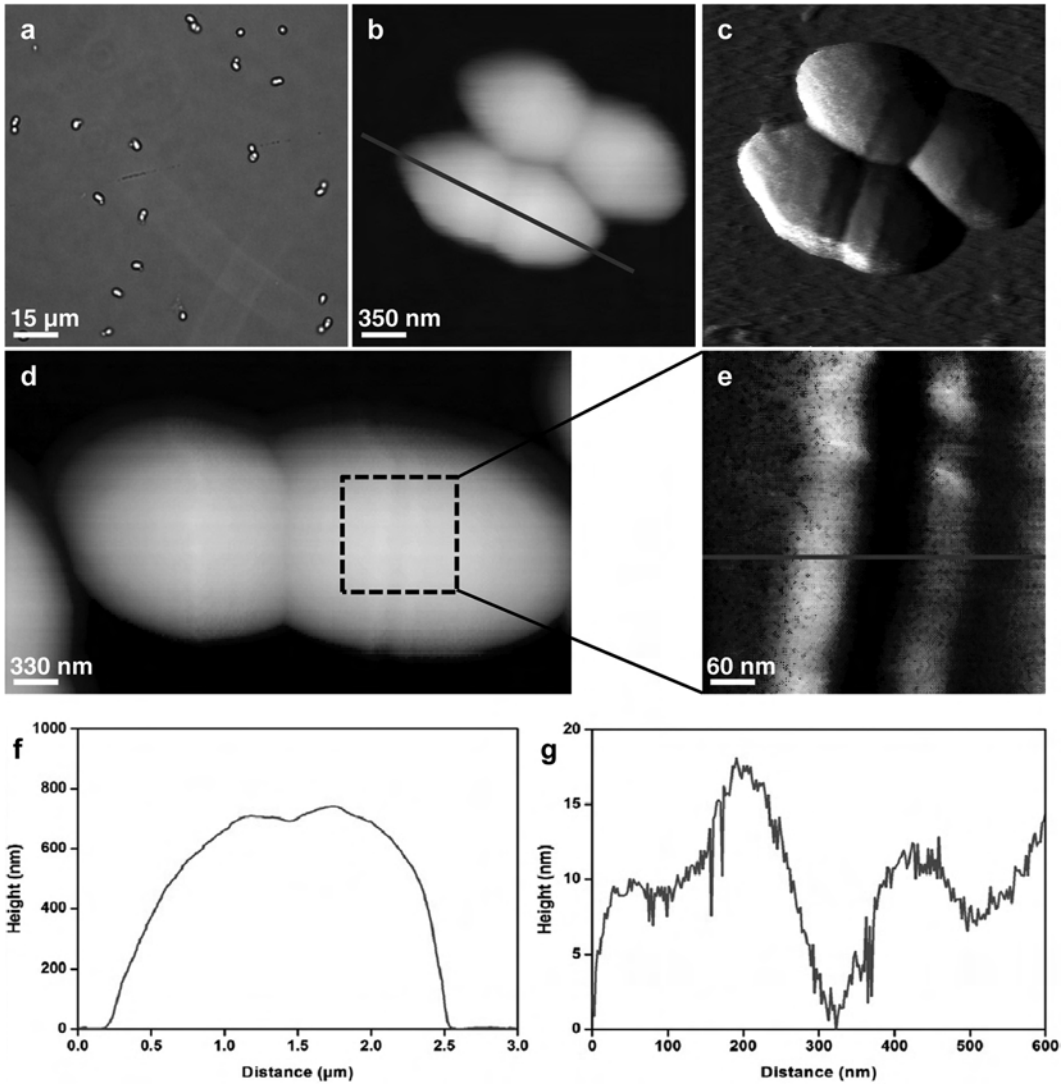

FIG 2 Images of *S. cerevisiae* (strain BY4741) cells treated with caspofungin at 4× MIC (0.5 μg/ml). (a) Optical image of living cells immobilized on a PEI-coated glass slide. (b) AFM height image (z range = 1.2 μm) of two cells. (c) Vertical-deflection image corresponding to the height image in panel b. (d) AFM height image of a single cell (z range = 1.2 μm). (e) Height image of the boxed area in panel d (z range = 20 nm). (f and g) Cross-sections taken along the lines in panels b (f) and e (g).

respectively (Table 1). This cell wall remodeling in response to caspofungin treatment was also accompanied by changes in chitin. However, only at high doses of caspofungin (4× MIC) was an increase in chitin content found, from 5% in untreated cells or cells treated with 0.5× MIC of caspofungin to 14% of cell wall mass with a caspofungin dose of 4× MIC (Table 1). These results are in agreement with previous works of Juchimiuk et al. (32), who showed that *S. cerevisiae* cells treated with 3.0 μg/ml caspofungin had their contents of β-1,3-glucans reduced by 50% and their chitin contents increased by 3- to 5-fold. These data are in agreement with the general view that the response of *S. cerevisiae* cells to cell wall stress results in a deep reorganization of the cell wall as a

TABLE 1 Biochemical analysis of glucans and mannans of the cell wall of yeasts by acid hydrolysis and of chitin by the Reissig method[a]

	Content (% dry mass ± SD) in cells treated with caspofungin at:					
	S. cerevisiae			*C. albicans*		
Component	0× MIC	0.5× MIC	4× MIC	0× MIC	0.5× MIC	4× MIC
Glucans	54.1 ± 4.9	48.5 ± 6.5	45.0 ± 7.6	52.0 ± 3.2	48.5 ± 5.5	30.9 ± 8.6
Mannans	45.3 ± 2.9	50.4 ± 6.2	53.7 ± 7.1	46.5 ± 3.3	44.2 ± 3.0	59.3 ± 7.5
Chitin	4.8 ± 0.2	5.1 ± 0.8	13.8 ± 5.2	6.6 ± 2.6	12.8 ± 4.1	17.9 ± 5.3

[a] For each species and set of conditions, cells from 3 independent cultures were analyzed.

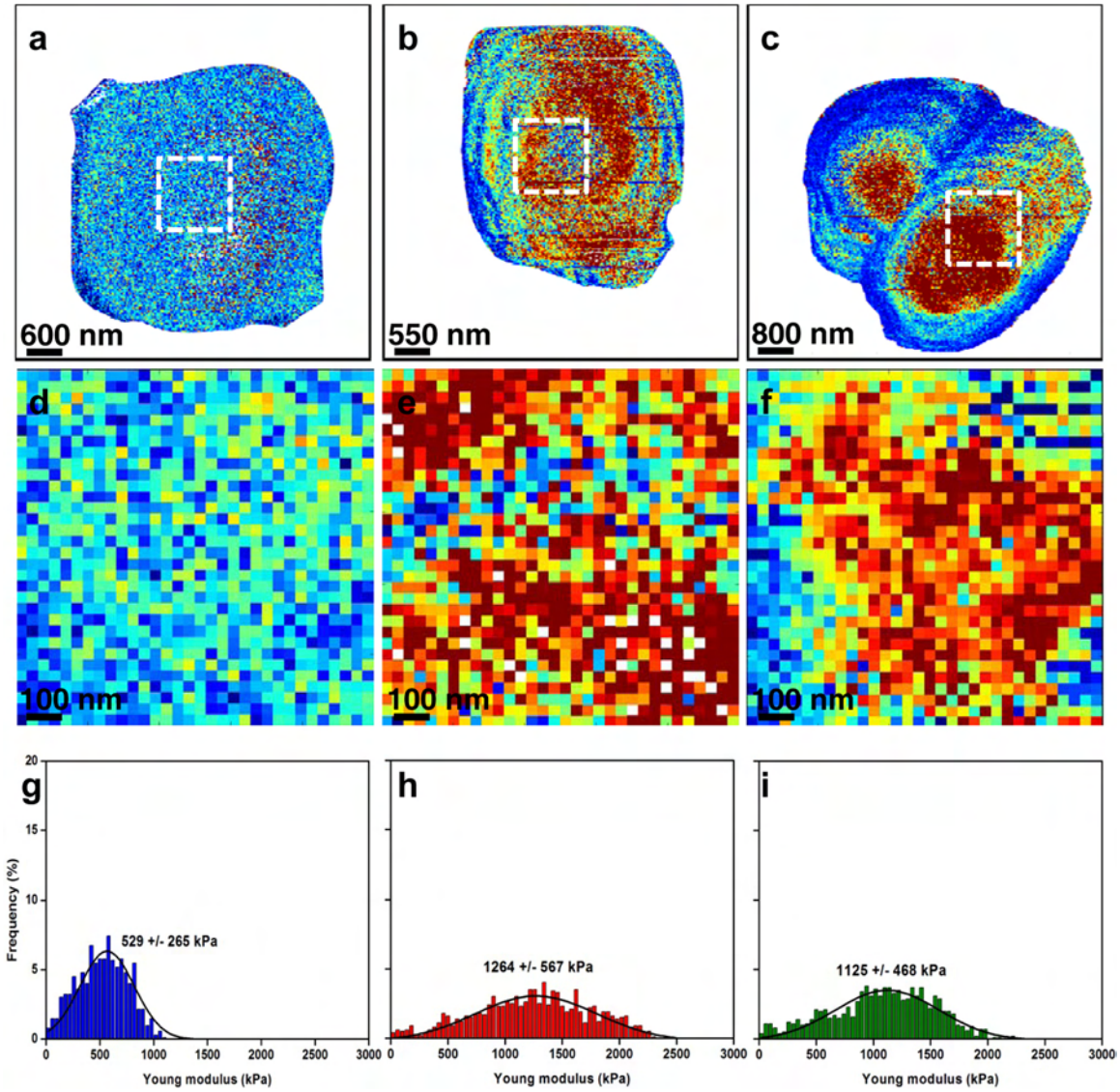

FIG 3 Mapping of *S. cerevisiae* (strain BY4741) cell surface elasticity. (a to c) Elasticity maps (z range = 1.5 MPa) of a native cell (a), of a cell treated with caspofungin at 0.5× MIC (0.063 μg/ml) (b), and of a cell treated with caspofungin at 4× MIC (0.5 μg/ml) (c). (d, e, and f) Local elasticity maps (z range = 1.5 MPa) recorded on a 1-μm area (white dashed squares) on the tops of cells in panels a to c, respectively. (g, h, and i) Distributions of Young modulus values (n = 1,024) corresponding to the local elasticity maps in panels d to f, respectively.

means to rescue cell wall integrity (33) and, in the case of antifungal stress, in the overproduction of mannans and reduction of β-glucans.

Nanomechanical properties of *S. cerevisiae*. In view of the role of the cell wall in conferring rigidity and protection on the yeast cell, we next addressed the pertinent question of whether the observed changes in cell morphology and chitin content were correlated with modifications in cell wall mechanical properties. To this end, *S. cerevisiae* cells exposed to two different concentrations of caspofungin were probed using nanoindentation measurements. The results of this experiment are shown in Fig. 3. The images of the cells recorded in quantitative-imaging mode (27, 28) allow analysis of all the force curves recorded in a single image (n = 65,536). By applying a mask, thanks to the analysis software (OpenFovea [34, 35]), only the force curves corresponding to the cells are extracted, leading to the elasticity maps presented in Fig. 3a, b, and c. In all the elasticity maps presented in this study, each pixel corresponds to a force curve that has been converted into an indentation curve and fitted with a Hertz model, from which a Young modulus (YM) value was extracted. The redder the pixel, the higher the YM value. These elasticity maps showed artifacts due to the spherical shape of the cells; the edges of the cells seem to have decreased YM values compared to the centers of the cells. However, these elasticity maps give a global view of the elasticity of the whole cells, with untreated cells that appear to be softer than caspofungin-treated cells. These observations were confirmed by local nanoindentation measurements performed on a 1-μm^2 area on the surface of each cell (Fig. 3d, e, and f). These areas on the tops of the cells are flatter, so the YM artifacts are avoided. Untreated cells had a YM value of 529 ± 265 kPa (Fig. 3g), whereas

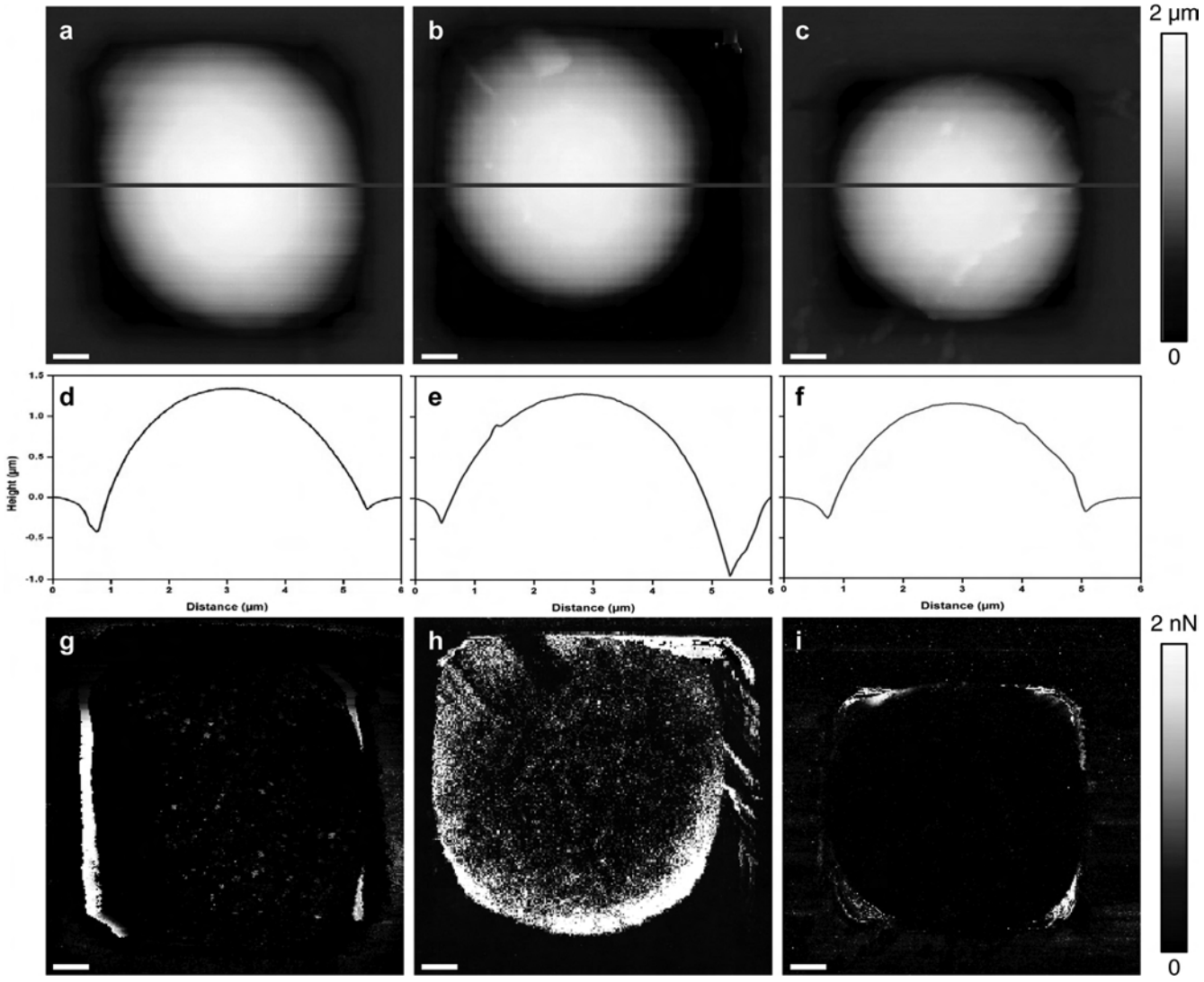

FIG 4 Imaging of *C. albicans* cells trapped in microstructured PDMS stamps. (a to c) AFM height images of a native cell (a), of a cell treated with caspofungin at 0.5× MIC (0.047 μg/ml) (b), and of a cell treated with caspofungin at 4× MIC (0.376 μg/ml) (c). (d, e, and f) Cross sections taken along the lines on the images in panels a to c, respectively. (g, h, and i) adhesion images corresponding to the height images in panels a to c, respectively.

cells treated with caspofungin at 0.5× MIC and 4× MIC (Fig. 3h and i) had YM values that increased to 1,264 ± 567 and to 1,125 ± 468 kPa, respectively.

Effects of caspofungin treatment on *C. albicans*. Using the Etest assay, we determined a MIC of about 0.094 $\mu g \cdot ml^{-1}$. The doses that were used in this study (0.5× MIC and 4× MIC) were therefore lower than the one reported to induce paradoxical growth effects (36). Caspofungin treatment does not cause morphology modification in *C. albicans*; the cells are spherical, with a mean diameter of 4.1 ± 0.2 μm, as shown in Fig. 4a, b, and c. However, caspofungin treatment induced other modifications of the surfaces of *C. albicans* cells. The results presented in Fig. 4g, h, and i are adhesion images of the cells. Native cells are not adhesive, whereas cells treated with caspofungin at 0.5× MIC present adhesions homogeneously distributed over the surface of the cell, as indicated in the adhesion map presented Fig. 4h. However, cells treated with caspofungin at 4× MIC do not show adhesion at all, like native cells.

Probing the cell surface of *C. albicans* using nanoindentation measurements (Fig. 5), we unexpectedly found a YM value for the untreated *C. albicans* cells of 186 ± 89 kPa, which is three times lower than that of *S. cerevisiae* cells. Taking into account that the proportions of mannans, β-glucans, and chitin in the cell wall are very similar for the two yeast species (1, 37), a likely explanation for the difference in YM values may reside in a difference in the molecular architectures of the cell wall between the two yeast species, notably in cross-linking between the components. Treatment of *C. albicans* cells with caspofungin at 0.5× MIC or 4× MIC for 16 h resulted in an increase of the YM value to 399 ± 147 kPa and 1,326 ± 340 kPa, respectively (Fig. 5h and i). Quite remarkably, this increase in YM values was correlated with the increase in the chitin level in *C. albicans* cells upon treatment with caspofungin (Fig. 6b and Table 1). In addition, the rise of chitin in the walls of *C. albicans* cells treated with caspofungin was accompanied by a decrease in β-glucans and an increase of mannans, as already noticed for *S. cerevisiae* cells, but the effects of caspofungin were

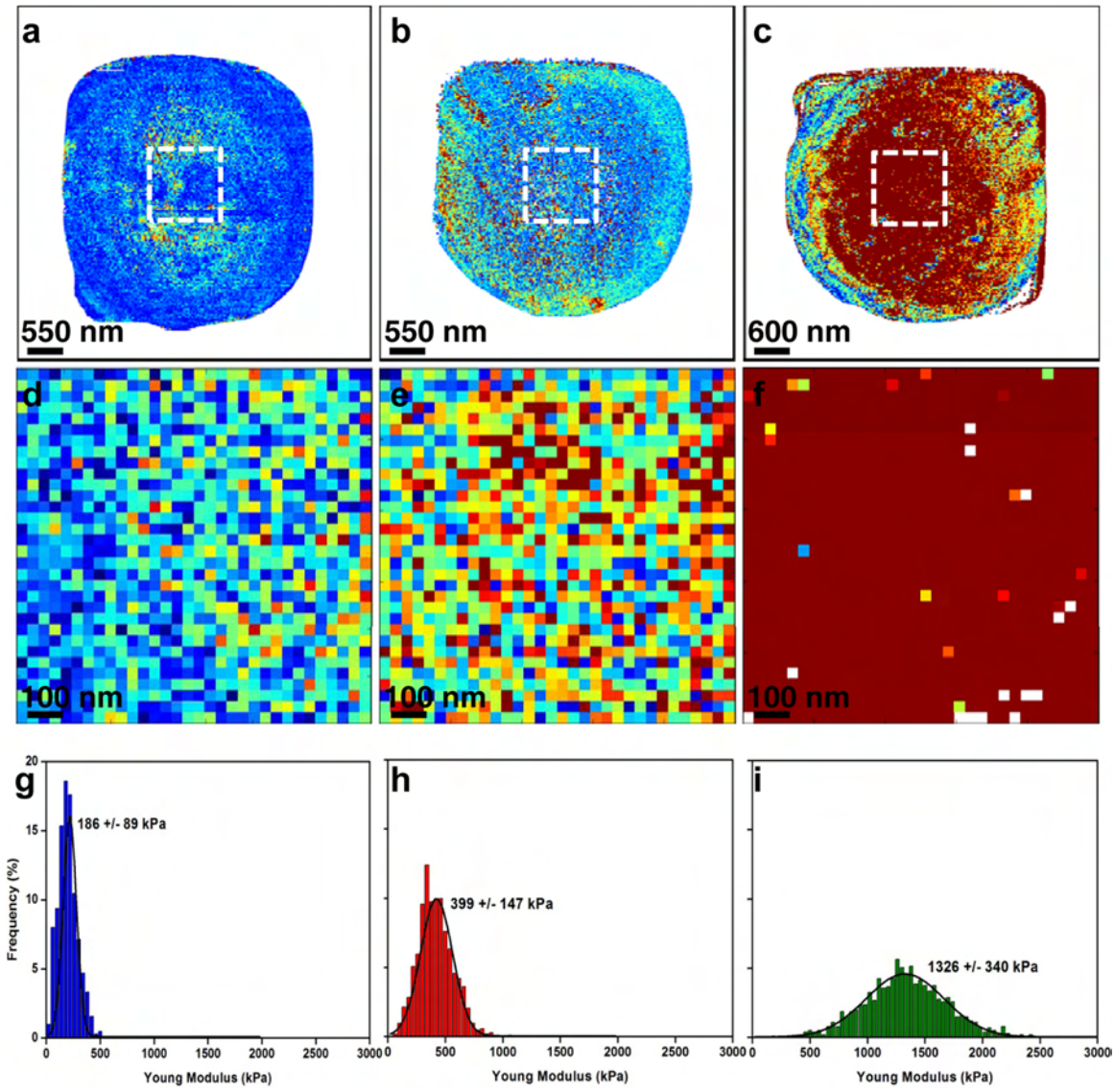

FIG 5 Mapping of *C. albicans* cell surface elasticity. (a to c) Elasticity maps (z range = 0.5 MPa) of a native cell (a), of a cell treated with caspofungin at 0.5× MIC (0.047 μg/ml) (b), and of a cell treated with caspofungin at 4× MIC (0.376 μg/ml) (c). (d, e, and f) Local elasticity maps (z range = 0.5 MPa) recorded on a 1-μm area (white dashed squares) on the tops of the cells in panels a to c, respectively. (g, h, and i) Distributions of Young modulus values (n = 1,024) corresponding to the local elasticity maps in panels d to f, respectively.

apparently more prominent. Notably, untreated cells displayed a β-glucan content of 52% of the cell wall mass. This proportion was reduced to 49% upon treatment with 0.5× MIC and to 31% when the cells were treated with 4× MIC of caspofungin. As for mannans, the proportion in untreated cells was close to 46% and increased to 59% when the cells were cultivated in the presence of a dose of 4× MIC of caspofungin.

DISCUSSION

We used AFM to investigate the effects of caspofungin on the morphology and nanomechanical properties of two yeast species, *S. cerevisiae* and *C. albicans*. With respect to *S. cerevisiae*, our results indicated that caspofungin at high doses alters the cell division process by perturbing cytokinesis. These modifications were observed along with a diminution of the β-1,3-glucan content and an increase in the chitin content. Studies by Cabib and coworkers have shown the importance of chitin and β-1,3-glucans during the cell division of yeasts (38–40). Their work focused on the remodeling of the cell wall during cell division, and particularly on the neck at the mother-bud interface. This crucial region is the site where cytokinesis and septation take place (41). Cabib et al. showed that control of growth at the neck is exerted by a septin ring and a chitin ring present at the location. A defect in either one of the rings leads to only minor morphological abnormalities. However, when both are faulty, control of growth is lost, the neck widens, and cytokinesis does not take place (38). They also showed that the chitin ring at the neck is specifically bound to β-1,3-glucans (42) and that this linkage is necessary for the control of growth at the mother-daughter neck. As indicated in Fig. 2, the apparent impairment in cytokinesis in yeast treated with a high

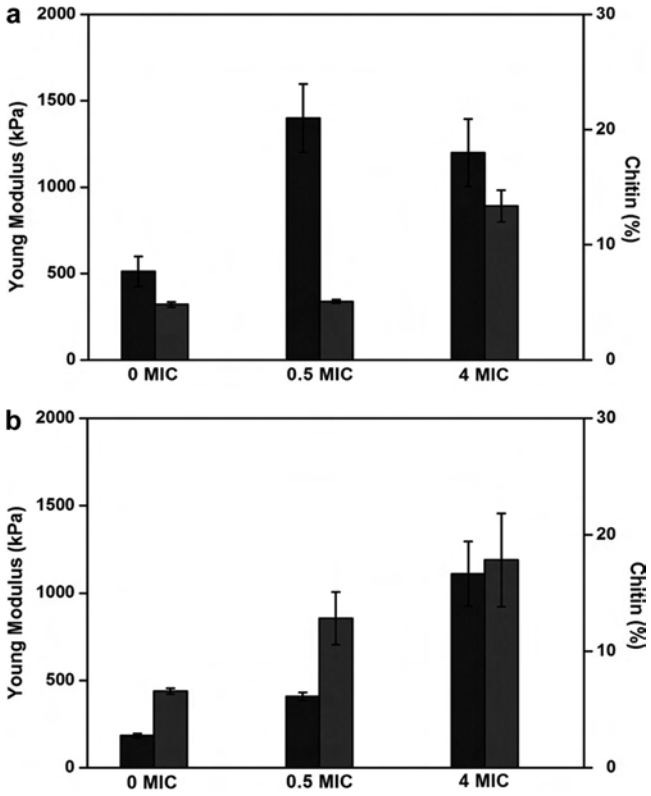

FIG 6 Quantitative analysis of chitin compositions of the yeast cell wall, correlated with Young modulus values. The histograms show Young modulus values (black bars) and chitin (gray bars) for *S. cerevisiae* (strain BY4741) (a) and for *C. albicans* (b) under different caspofungin conditions. The analyses for Young modulus values were performed on five cells from 3 independent cultures.

dose of caspofungin might be due to excess chitin that is present at the bud neck and that is not linked to β-1,3-glucans, as the content of the latter is reduced.

While the increase in the YM value of the cell wall of *S. cerevisiae* could be correlated with the increase in chitin induced at a high dose of caspofungin, this was not the case for a lower dose of caspofungin, for which the YM value was already the same as at the higher dose of the antifungal drug. These results suggest that the force measurements performed with atomic force microscopy are not solely linked to changes in the cell wall composition but may unravel deep reorganization of the cell wall architecture without significant change in its cell wall components (43). A recent study conducted by our team (43) focused on *S. cerevisiae* mutants defective in, among other things, β-glucan elongation (*gas1*Δ), chitin synthesis (*chs3*Δ), and cross-linkages between chitin and β-glucans (*chr1chr2*Δ). This AFM study showed that cell wall elasticity was mainly dependent on the architecture and molecular composition of the cell wall. Moreover, chitin was identified as playing an important role in the nanomechanical properties of the cell wall. Our results are therefore in line with this previous study, and the amount of chitin in the cell wall could be directly correlated with the increase in the YM values. The difference in the nanomechanical properties of the two yeast species suggests a difference in the molecular architectures of their cell walls, even though the cell wall compositions were seemingly comparable.

With respect to *C. albicans* cells, global morphology and cell division do not appear to be affected, even at high doses of caspofungin. The modifications induced by the treatment concern the adhesive properties of the cells. As we saw, cells treated with a low dose of caspofungin present adhesions on their surfaces. *C. albicans* cells display adhesion proteins on their surfaces when cultivated under particular conditions (44). A key adhesin family identified is the Als (for agglutinin-like sequence) family (45, 46), which includes eight large cell surface glycoproteins. Als proteins play major roles in the processes of infection and colonization of the host. Since their discovery, many studies have been dedicated to understanding their functions and localization on the surfaces of cells. A recent study by Alsteens et al. (47) has characterized the localization of Als5 at the surface of mutant strains of *S. cerevisiae* using atomic force microcopy; in 2012, Beaussart et al. (48) characterized the localization of Als3 on the surfaces of *C. albicans* cells during morphogenesis. Their work provides confirmation that Als proteins can be mapped at the surfaces of living cells. Among these proteins is Als1p, which is involved in different processes, such as adherence to endothelial cells, flocculation, and filamentation (49). Gregori et al. (50) showed that Als1 is a critical factor required for caspofungin-induced flocculation. The authors show that cells treated by caspofungin present levels of *ALS1* mRNA that are strongly upregulated. Following these sets of data, we could hypothesize that the adhesion shown in Fig. 3h is due to expression of Als1. However, at high doses, the expression of the gene could be inhibited, leading us to think that the expression of Als1 under antifungal stress is a complex dynamic process that needs further study. Perhaps, at high doses of caspofungin, either the cells are dying or the transcriptional and translational machinery at this level of drug is strongly impaired, so that synthesis of new components at the cell wall, such as adhesion proteins, is inhibited. This hypothesis awaits further work, for instance, by measuring the expression of genes encoding some of these adhesion proteins in *C. albicans* cells challenged at different concentrations of caspofungin. These results were recorded on living cells of wild-type *C. albicans*, which gives us an insight into the physiological localization of the protein. Further work must be done to probe these adhesions with functionalized AFM tips under different conditions of growth and stress.

ACKNOWLEDGMENTS

E.D. is a researcher of the Centre National de la Recherche Scientifique (CNRS). This work was supported by a grant from the Young Scientist Program of ANR (Agence Nationale de la Recherche), project ANR-11-JSV5-001-01, no. (SD) 30 02 43 31, and by a grant from Region Midi Pyrenees (project no. 10051296) to J.M.F. C.F. is supported by a grant from Direction Générale de l'Armement (DGA) for her 3-year Ph.D. study and M.S. by Lallemand SAS.

We thank Charles Roduit for providing us with updated Fovea software. We thank Merck for providing caspofungin and Claire Murzeau for her help in the experiments.

C.F., R.E.D., J.M.F, and E.D. designed the experiments. C.F., M.S., H.M.-Y., and E.D. performed the experiments. C.F. and E.D. wrote the paper. Critical analysis and discussion of the results were carried out by all the authors, who also helped in critical reading of the manuscript and approved its final version.

REFERENCES

1. **Lipke PN, Ovalle R.** 1998. Cell wall architecture in yeast: new structure and new challenges. J. Bacteriol. **180:**3735–3740.

2. **Francois JM.** 2006. A simple method for quantitative determination of polysaccharides in fungal cell walls. Nat. Protoc. **1:**2995–3000.
3. **Chaffin WL.** 2008. Candida albicans cell wall proteins. Microbiol. Mol. Biol. Rev. **72:**495–544.
4. **Dague E, Gilbert Y, Verbelen C, Andre G, Alsteens D, Dufrêne YF.** 2007. Towards a nanoscale view of fungal surfaces. Yeast **24:**229–237.
5. **Dufrêne YF.** 2010. Atomic force microscopy of fungal cell walls: an update. Yeast **27:**465–471.
6. **Alsteens D, Dupres V, McEvoy K, Wildling L, Gruber HJ, Dufrene YF.** 2008. Structure, cell wall elasticity and polysaccharide properties of living yeasts cells, as probed by AFM. Nanotechnology **19:**384005. doi:10.1088/0957-4484/19/38/384005.
7. **Adya AK, Canetta E, Walker GM.** 2006. Atomic force microscopic study of the influence of physical stresses on Saccharomyces cerevisiae and Schizosaccharomyces pombe. FEMS Yeast Res. **6:**120–128.
8. **Canetta E, Adya AK, Walker GM.** 2006. Atomic force microscopic study of the effects of ethanol on yeast cell surface morphology. FEMS Microbiol. Lett. **255:**308–315.
9. **Sudbery P, Gow N, Berman J.** 2004. The distinct morphogenic states of Candida albicans. Trends Microbiol. **12:**317–324.
10. **Gow NA, Hube B.** 2012. Importance of the Candida albicans cell wall during commensalism and infection. Curr. Opin. Microbiol. **15:**406–412.
11. **Denning DW.** 1998. Invasive aspergillosis. Clin. Infect. Dis. **26:**781–803.
12. **Sanglard D, Odds FC.** 2002. Resistance of Candida species to antifungal agents: molecular mechanisms and clinical consequences. Lancet Infect. Dis. **2:**73–85.
13. **Denning DW.** 2003. Echinocandin antifungal drugs. Lancet **362:**1142–1151.
14. **Park S, Kelly R, Kahn JN, Robles J, Hsu M-J, Register E, Li W, Vyas V, Fan H, Abruzzo G, Flattery A, Gill C, Chrebet G, Parent SA, Kurtz M, Teppler H, Douglas CM, Perlin DS.** 2005. Specific substitutions in the echinocandin target Fks1p account for reduced susceptibility of rare laboratory and clinical Candida sp. isolates. Antimicrob. Agents Chemother. **49:**3264–3273.
15. **Balashov SV, Park S, Perlin DS.** 2006. Assessing resistance to the echinocandin antifungal drug caspofungin in Candida albicans by profiling mutations in FKS1. Antimicrob. Agents Chemother. **50:**2058–2063.
16. **Garcia-Effron G, Park S, Perlin DS.** 2009. Correlating echinocandin MIC and kinetic inhibition of fks1 mutant glucan synthases for Candida albicans: implications for interpretive breakpoints. Antimicrob. Agents Chemother. **53:**112–122.
17. **Garcia-Effron G, Lee S, Park S, Cleary JD, Perlin DS.** 2009. Effect of Candida glabrata FKS1 and FKS2 mutations on echinocandin sensitivity and kinetics of 1,3-β-D-glucan synthase: implication for the existing susceptibility breakpoint. Antimicrob. Agents Chemother. **53:**3690–3699.
18. **Binnig G, Quate CF, Gerber C.** 1986. Atomic force microscope. Phys. Rev. Lett. **56:**930–934.
19. **Müller DJ, Dufrêne YF.** 2011. Atomic force microscopy: a nanoscopic window on the cell surface. Trends Cell Biol. **21:**461–469.
20. **Formosa C, Grare M, Jauvert E, Coutable A, Regnouf-de-Vains JB, Mourer M, Duval RE, Dague E.** 2012. Nanoscale analysis of the effects of antibiotics and CX1 on a Pseudomonas aeruginosa multidrug-resistant strain. Sci. Rep. **2:**575.
21. **Formosa C, Grare M, Duval RE, Dague E.** 2012. Nanoscale effects of antibiotics on P. aeruginosa. Nanomedicine **8:**12–16.
22. **Baker Brachmann C, Davies A, Cost GJ, Caputo E, Li J, Hieter P, Boeke JD.** 1998. Designer deletion strains derived from Saccharomyces cerevisiae S288C: a useful set of strains and plasmids for PCR-mediated gene disruption and other applications. Yeast **14:**115–132.
23. **EUCAST.** 18 February 2012. Document E.DEF 7.2. Method for the determination of broth dilution of antifungal agents for fermentative yeasts; revised March 2012. EUCAST, Basel, Switzerland.
24. **CLSI.**2008. Reference method for broth dilution antifungal susceptibility. Testing of yeasts. Approved standard, 3rd ed. CLSI document M27-A3, vol. 28, no. 14. CLSI, Wayne, PA.
25. **Dague E, Jauvert E, Laplatine L, Viallet B, Thibault C, Ressier L.** 2011. Assembly of live micro-organisms on microstructured PDMS stamps by convective/capillary deposition for AFM bio-experiments. Nanotechnology **22:**395102. doi:10.1088/0957-4484/22/39/395102.
26. **Francius G, Tesson B, Dague E, Martin-Jézéquel Dufrêne VYF.** 2008. Nanostructure and nanomechanics of live Phaeodactylum tricornutum morphotypes. Environ. Microbiol. **10:**1344–1356.
27. **JPK Instruments.** 2011. QI™ mode-quantitative imaging with the NanoWizard 3 AFM. http://www.jpk.com/afm.230.en.html.
28. **Chopinet L, Formosa C, Rols MP, Duval RE, Dague E.** 2013. Imaging living cells surface and quantifying its properties at high resolution using AFM in QI™ mode. Micron **48:**26–33.
29. **Hutter JL, Bechhoefer J.** 1993. Calibration of atomic-force microscope tips. Rev. Sci. Instruments **64:**1868–1873.
30. **Dallies N, François J, Paquet V.** 1998. A new method for quantitative determination of polysaccharides in the yeast cell wall. Application to the cell wall defective mutants of Saccharomyces cerevisiae. Yeast **14:**1297–1306.
31. **Reissig JL, Strominger JL, Leloir LF.** 1955. A modified colorimetric method for the estimation of N-acetylamino sugars. J. Biol. Chem. **217:**959–966.
32. **Juchimiuk M, Pasikowska M, Zatorska E, Laudy AE, Smoleńska-Sym G, Palamarczyk G.** 2010. Defect in dolichol-dependent glycosylation increases sensitivity of Saccharomyces cerevisiae towards anti-fungal drugs. Yeast **27:**637–645.
33. **Ram AFJ, Kapteyn JC, Montijn RC, Caro LHP, Douwes JE, Baginsky W, Mazur P, Van den Ende H, Klis FM.** 1998. Loss of the plasma membrane-bound protein Gas1p in Saccharomyces cerevisiae results in the release of β1,3-glucan into the medium and induces a compensation mechanism to ensure cell wall integrity. J. Bacteriol. **180:**1418–1424.
34. **Radotić K, Roduit C, Simonović J, Hornitschek P, Fankhauser C, Mutavdžić D, Steinbach G, Dietler G, Kasas S.** 2012. Atomic force microscopy stiffness tomography on living Arabidopsis thaliana cells reveals the mechanical properties of surface and deep cell-wall layers during growth. Biophys. J. **103:**386–394.
35. **Roduit C, Saha B, Alonso-Sarduy L, Volterra A, Dietler G, Kasas S.** 2012. OpenFovea: open-source AFM data processing software. Nat. Methods **9:**774–775.
36. **Bizerra FC, Melo ASA, Katchburian E, Freymüller E, Straus AH, Takahashi HK, Colombo AL.** 2011. Changes in cell wall synthesis and ultrastructure during paradoxical growth effect of caspofungin on four different Candida species. Antimicrob. Agents Chemother. **55:**302–310.
37. **Chaffin WL, López-Ribot JL, Casanova M, Gozalbo D, Martínez JP.** 1998. Cell wall and secreted proteins of Candida albicans: identification, function, and expression. Microbiol. Mol. Biol. Rev. **62:**130–180.
38. **Schmidt M, Varma A, Drgon T, Bowers B, Cabib E.** 2003. Septins, under Cla4p regulation, and the chitin ring are required for neck integrity in budding yeast. Mol. Biol. Cell **14:**2128–2141.
39. **Cabib E, Blanco N, Arroyo J.** 2012. Presence of a large β(1–3)glucan linked to chitin at the Saccharomyces cerevisiae mother-bud neck suggests involvement in localized growth control. Eukaryot. Cell **11:**388–400.
40. **Blanco N, Reidy M, Arroyo J, Cabib E.** 2012. Cross-links in the cell wall of budding yeast control morphogenesis at the mother-bud neck. J. Cell Sci. **125:**5781–5789.
41. **Lippincott J, Li R.** 1998. Sequential assembly of myosin II, an IQGAP-like protein, and filamentous actin to a ring structure involved in budding yeast cytokinesis. J. Cell Biol. **140:**355–366.
42. **Cabib E, Durán A.** 2005. Synthase III-dependent chitin is bound to different acceptors depending on location on the cell wall of budding yeast. J. Biol. Chem. **280:**9170–9179.
43. **Dague E, Bitar R, Ranchon H, Durand F, Yken HM, François JM.** 2010. An atomic force microscopy analysis of yeast mutants defective in cell wall architecture. Yeast **27:**673–684.
44. **Sundstrom P.** 2002. Adhesion in Candida spp. Cell. Microbiol. **4:**461–469.
45. **Hoyer LL, Green CB, Oh S-H, Zhao X.** 2008. Discovering the secrets of the Candida albicans agglutinin-like sequence (ALS) gene family—a sticky pursuit. Med. Mycol. **46:**1–15.
46. **Hoyer LL.** 2001. The ALS gene family of Candida albicans. Trends Microbiol. **9:**176–180.
47. **Alsteens D, Garcia MC, Lipke PN, Dufrêne YF.** 2010. Force-induced formation and propagation of adhesion nanodomains in living fungal cells. Proc. Natl. Acad. Sci. U. S. A. **107:**20744–20749.
48. **Beaussart A, Alsteens D, El-Kirat-Chatel S, Lipke PN, Kucharíková S, Van Dijck P, Dufrêne YF.** 2012. Single-molecule imaging and functional analysis of Als adhesins and mannans during Candida albicans morphogenesis. ACS Nano. **6:**10950–10964.
49. **Coleman DA, Oh S-H, Zhao X, Hoyer LL.** 2010. Heterogeneous distribution of Candida albicans cell-surface antigens demonstrated with an Als1-specific monoclonal antibody. Microbiology **156:**3645–3659.
50. **Gregori C, Glaser W, Frohner IE, Reinoso-Martín C, Rupp S, Schüller C, Kuchler K.** 2011. Efg1 controls caspofungin-induced cell aggregation of Candida albicans through the adhesin Als1. Eukaryot. Cell **10:**1694–1704.

Chapter 3.3: Nanoscale behavior of the bacterial cell wall exposed to antibacterials

3.3.1 Nanoscale effects of antibiotics on *P. aeruginosa*

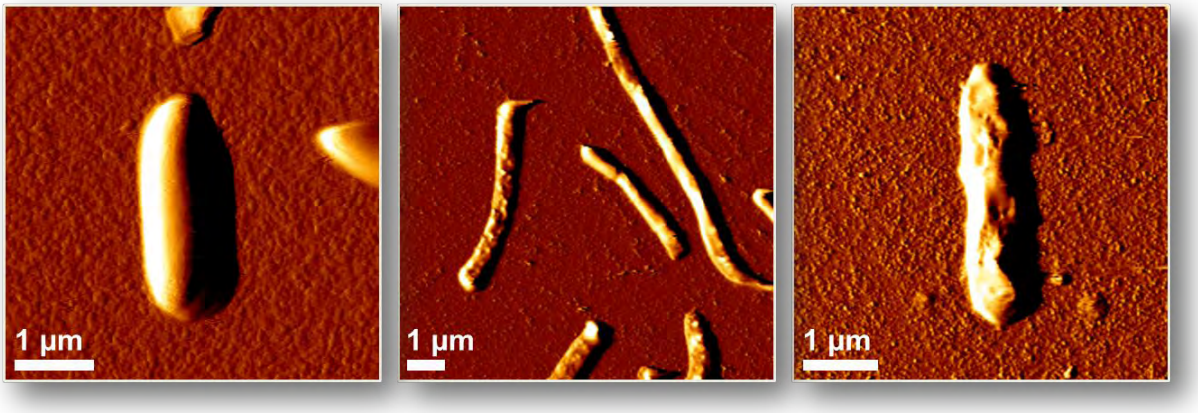

Formosa C., Grare M., Duval R. E., and Dague E.

Nanomedicine NMB, **8**, 12-16, 2012

Abstract

Studying living bacteria at the nanoscale in their native liquid environment opens an unexplored landscape. We focus on *Pseudomonas aeruginosa* and demonstrate how the cell wall is biophysically affected at the nanoscale by two reference antibiotics (ticarcillin and tobramycin). The elasticity of the cells drops dramatically after treatment (from 263 ± 70 kPa to 50 ± 18 and 24 ± 4 kPa, respectively on ticarcillin- and tobramycin-treated bacteria) and major micro- and nano-morphological modifications are observed (the surface roughness of native, ticarcillin- and tobramycin-treated bacteria are respectively 2.5, 0.8, and 4.4 nm for a surface area of 40,000 nm^2). Thus the nanoscale approach in liquid is valid and can be extended.

BASIC SCIENCE

Nanomedicine: Nanotechnology, Biology, and Medicine
8 (2012) 12–16

Short Communication

nanomedjournal.com

Nanoscale effects of antibiotics on *P. aeruginosa*

Cecile Formosa, MS[a,b,c], Marion Grare, PhD[e], Raphaël E. Duval, PhD[d], Etienne Dague, PhD[a,b,c,*]

[a]*Centre National de la Recherche Scientifique, Laboratoire d'Analyse et d'Architecture des Systèmes (LAAS), Toulouse, France*
[b]*Centre National de la Recherche Scientifique, Toulouse, France*
[c]*Université de Toulouse, Toulouse, France*
[d]*SRSMC, Nancy-University, CNRS, Faculty of Pharmacy, Nancy, France*
[e]*Laboratoire de Bactériologie Hygiène, Institut Fédératif de Biologie, Toulouse, France*

Received 28 June 2011; accepted 20 September 2011

Abstract

Studying living bacteria at the nanoscale in their native liquid environment opens an unexplored landscape. We focus on *Pseudomonas aeruginosa* and demonstrate how the cell wall is biophysically affected at the nanoscale by two reference antibiotics (ticarcillin and tobramycin). The elasticity of the cells drops dramatically after treatment (from 263 ± 70 kPa to 50 ± 18 and 24 ± 4 kPa, respectively on ticarcillin- and tobramycin-treated bacteria) and major micro- and nano-morphological modifications are observed (the surface roughness of native, ticarcillin- and tobramycin-treated bacteria are respectively 2.5, 0.8, and 4.4 nm for a surface area of 40,000 nm²). Thus the nanoscale approach in liquid is valid and can be extended.

From the Clinical Editor: *Pseudomonas aeruginosa* cell wall was demonstrated to be biophysically affected at the nanoscale by two reference antibiotics, ticarcillin, and tobramycin, with the elasticity dropping dramatically after treatment.

Key words: *Pseudomonas aeruginosa*; Atomic Force Microscopy; Ticarcillin; Tobramycin; Elasticity; Bacterial cell wall

For 25 years, Atomic Force Microscopy (AFM) has emerged as a valuable tool in microbiology.[1] Recently it has been used to study the effects of antimicrobial drugs on living microorganisms.[2] An advantage of AFM is the possibility to work in liquid on living cells. Nevertheless, sample immobilization is a challenge[3] and explains why in most publications the bacteria were air dried. Here, we focused on the dreadful bacteria *Pseudomonas aeruginosa*[4] and overcome the immobilization problem by taking advantage of electrostatic interactions between a positively charged surface and the negatively charged bacteria. *P. aeruginosa,* is implicated in 10% of nosocomial infections in France. This pathogen, resistant to several antibiotics and antiseptics, has a great capacity for acquiring new resistance mechanisms under selective antibiotic pressure.[5] Therefore, understanding the effects of antibiotics on these bacteria has become a necessity. We studied two reference antibiotics, ticarcillin and tobramycin, which are highly active on *P. aeruginosa*. They have known action mechanisms and are widely used in terapeutics, unlike other molecules, e.g. colistin wihch effects were recently studied.[6] Ticarcillin is a β-lactamin which inhibits the bacterial transpeptidases and transglycosylases responsible for the assembly of the cell wall peptidoglycan.[6] Tobramycin is an aminoglycoside that works by binding to the 30S and 50S bacterial ribosome to prevent formation of the 70S complex. As a result, mRNA cannot be translated into protein.[7] These two different mechanisms of action should therefore produce different effects on the bacterial cells. In this study, our purpose was to understand better the antibiotics' effects on the cell wall of *P. aeruginosa* at the nanoscale.

We chose to explore the effects of tobramycin and ticarcillin on *P. aeruginosa* ATCC 27853. We used AFM (details appear in Supplementary Material 1) to explore bacterial cell wall modifications. We recorded images of single bacteria (Figure 1) and images at higher resolution on the top of the cells to qualitatively explore the impact of tobramycin and ticarcillin on

Financial support (for Marion Grare, Raphaël E. Duval) was provided by the French Ministry of Further Education and Research and the French National Scientific Research Center (CNRS). Etienne Dague is a researcher from LAAS-CNRS UPR 8001, Centre National de la Recherche Scientifique, hosted in Centre Pierre Potier ITAV, UMS 3039. Cecile Formosa is funded by LAAS-CNRS UPR 8001, hosted in Centre Pierre Potier ITAV, UMS 3039.

No conflict of interest was reported by the authors of this article.

*Corresponding author: LAAS-CNRS, Groupe NBS, 31000 Toulouse, France.
E-mail address: edague@laas.fr (E. Dague).

1549-9634/$ – see front matter © 2012 Elsevier Inc. All rights reserved.
doi:10.1016/j.nano.2011.09.009

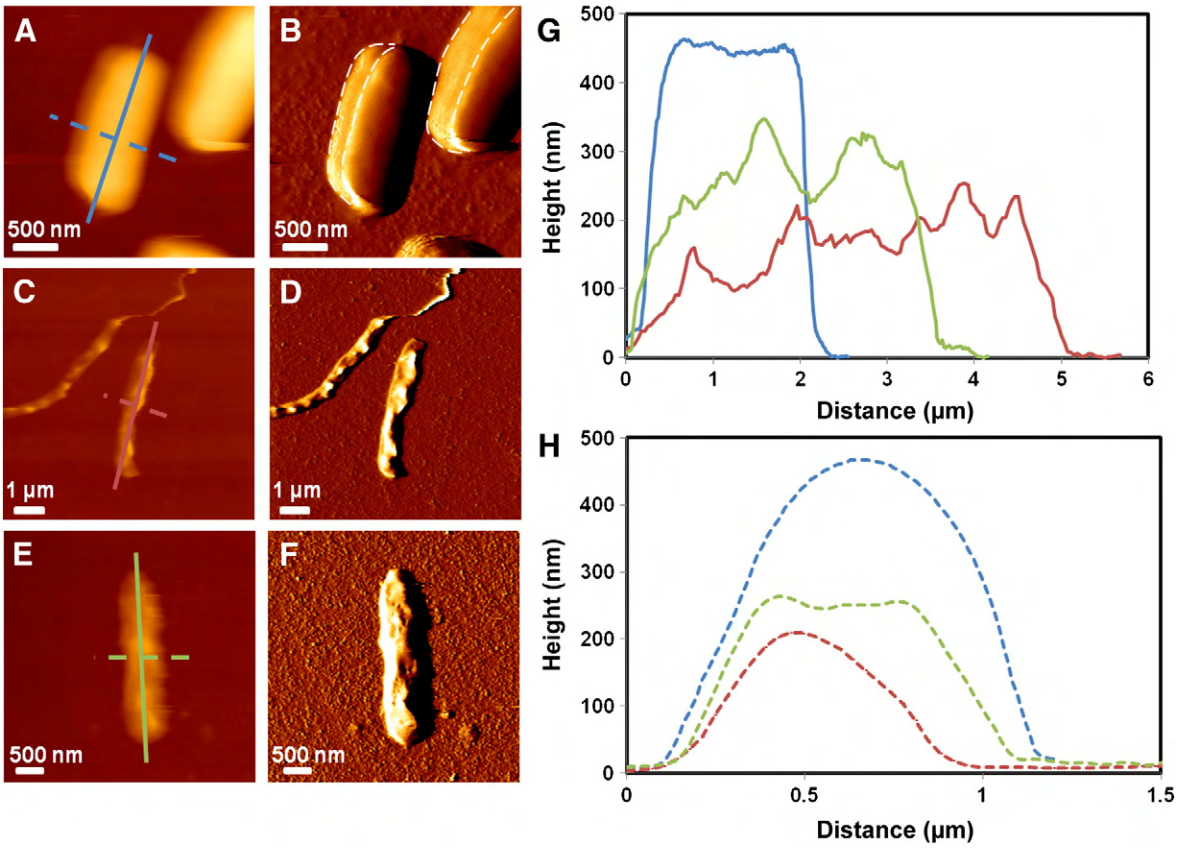

Figure 1. Imaging of bacteria. Height images (z range = 1µm) recorded on **(A)** native, **(C)** ticarcillin- and **(E)** tobramycin- treated cell. **(B, D and F)** Vertical deflection images correspond to the height images. **(G)** Vertical cross-sections taken along the solid lines of native (*blue*), ticarcillin- (*green*) and tobramycin-treated cell (*red*). **(H)** Horizontal cross-sections taken along the dashed lines.

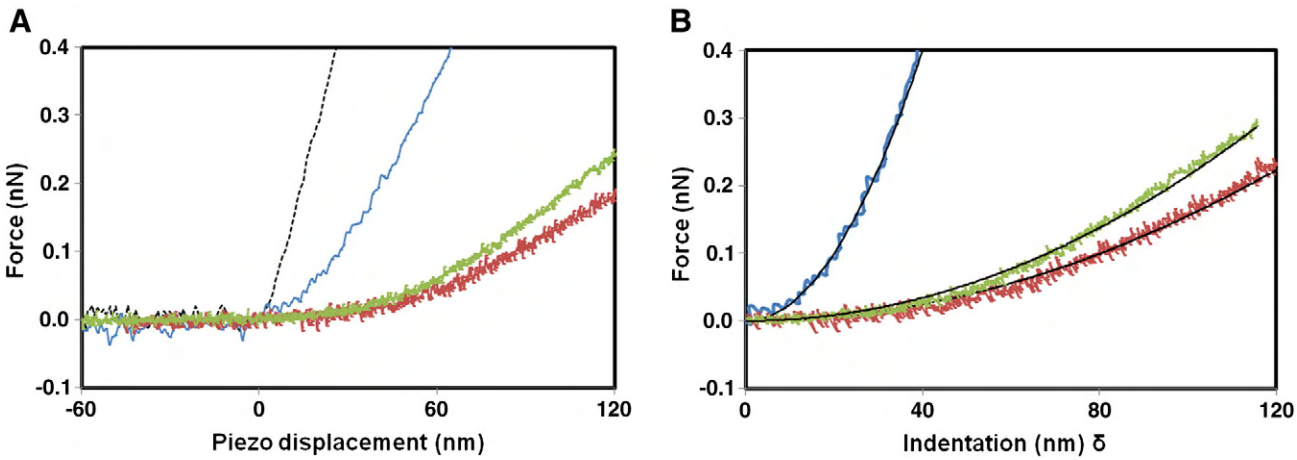

Figure 2. Mechanical properties of native (*blue*), ticarcillin- (*green*) and tobramycin-treated (*red*) bacteria. **(A)** Representative force-displacement curves recorded on the glass slide (*dashed line*) and on single cells. The lines between the dashed lines and the colored lines represent the indentation (δ). **(B)** Force-indentation curves obtained from the curves showed in panel A. Colored lines show the data, whereas the black lines show the theoretical fits (Hertz model) used to extract Young modulus values.

P. aeruginosa surface topology. We then recorded force maps of 20 × 20 force curves on the same area of the cells. The force curves were recorded in the same conditions with calibrated cantilevers. The force-distance curves recorded on the bacteria were treated to subtract the cantilever deflection on a solid surface (see Figure 2). The distance difference, at a given force, between a curve recorded on glass and on the bacteria is called indentation (δ). The indentation curves were then fitted to the Hertz model,

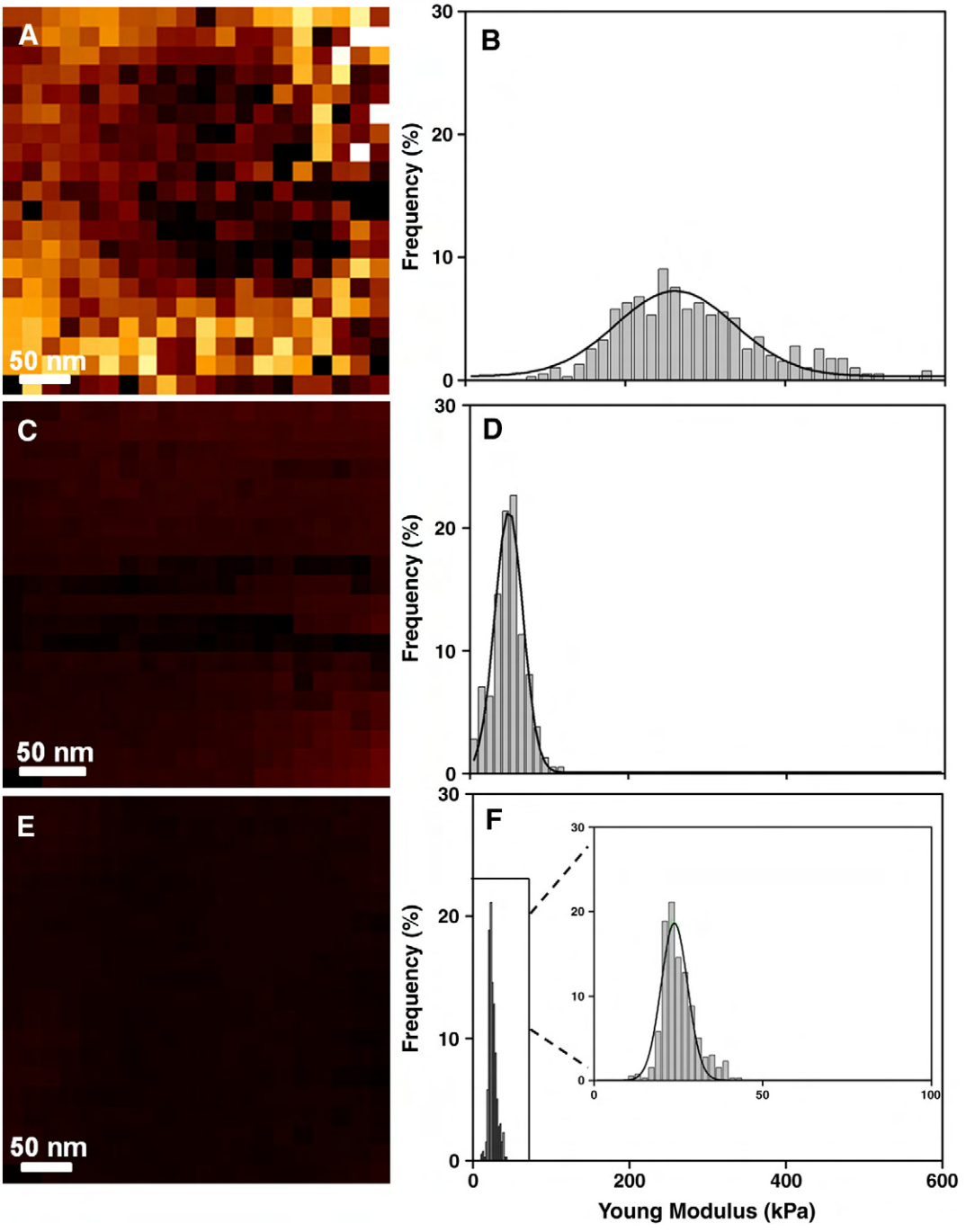

Figure 3. Mapping of bacteria surface elasticity. **(A)** elasticity map (z-range = 600 kPa) recorded on a native, **(C)** ticarcillin- and **(E)** tobramycin-treated cell. **(B, D and F)** Distribution of Young Modulus values (n = 399 force curves) corresponding to the elasticity maps. In **F** the insert presents more clearly the E repartition.

which links force (F) as a function of the elastic modulus (E) and the square of the indentation (δ) for a conical indenter.

$$F = \frac{2E \tan \alpha}{\pi(1 - \nu^2)} \delta^2 \quad (1)$$

In equation (1), α is the tip opening angle (36°) and ν the Poisson ratio assumed to be 0.5.

Figure 1 presents height and deflection AFM images of *P. aeruginosa* in (A) native condition, after (C) ticarcillin and (E) tobramycin treatment. The native cell shows a smooth surface. The cells are 2 μm long (blue line, Figure 1, *G*), 1.2 μm large (blue dashed line, Figure 1, *H*) and 450 nm high (blue lines, Figure 1, *G* and *H*). Due to this relatively higher height, convolution artifacts can be seen on the deflection image in Figure 1, *B* (white dashed lines). Figure 2 is a comparison of the

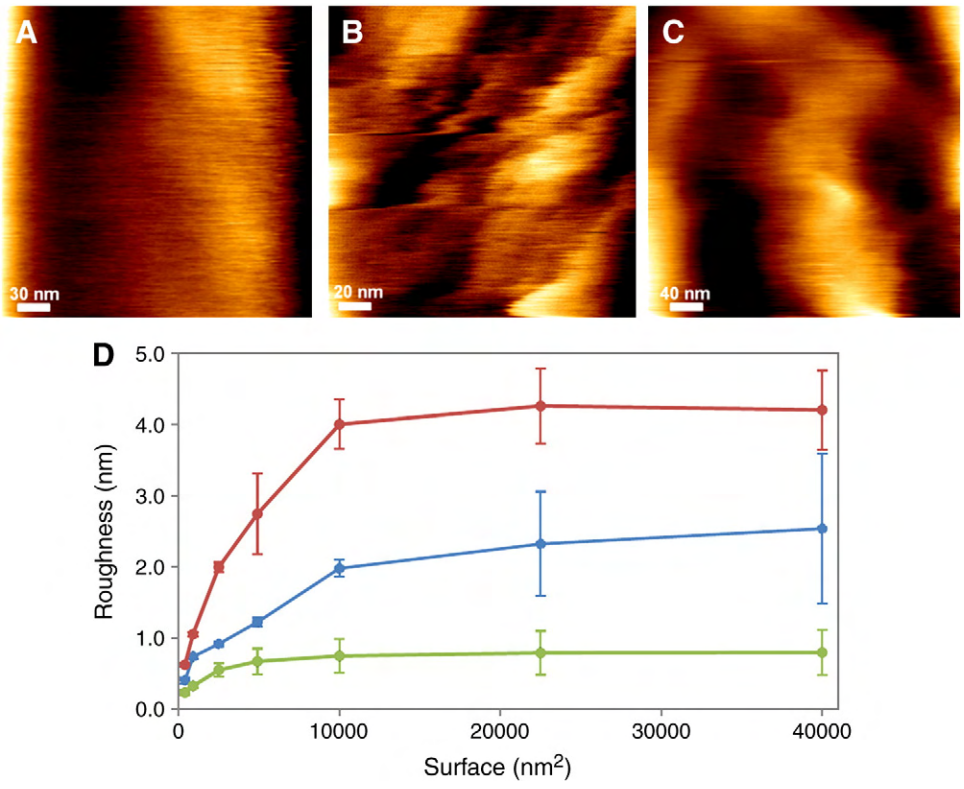

Figure 4. Imaging of bacteria cells. Height images recorded on **(A)** native, **(B)** ticarcillin- **(C)** tobramycin-treated cell. **D** shows the roughness measured on the height images of native (blue), ticarcillin- (green) and tobramycin-treated cells (red).

elastic properties of native and treated cells. Figure 2, *A* shows representative raw data, whereas Figure 2, *B* shows the force versus indentation curve. In Figure 2 the plain black lines are the Hertz model fitted to the indentation curves. On those curves it is clear that both ticarcillin and tobramycin induce a dramatic decrease of the bacterial cell wall elasticity. In Figure 3 this obvious observation is quantified with force volume. Native cells have a Young modulus of 261 ± 70 kPa (Figure 3, *B*), whereas for ticarcillin- and tobramycin-treated cells, the histograms (Figure 3, *D* and *F*) show that the modulus drops, respectively, to 24 ± 4 kPa and 50 ± 18 kPa (for statistic see Supplementary Material 2). On the elasticity maps in Figure 3, *A*, *C* and *E*, each pixel represents an elastic modulus. The brighter the pixel is, the higher the Young modulus is. The maps are homogeneous and confirm that the elasticity decreases between the native and treated cells. From Figure 4, high-resolution height images of the cells' surface and a roughness analysis, we learn that the native cells are smooth, homogeneous, and bulging whereas the tobramycin-treated cells are rougher. Surprisingly, the Power Spectral Density (PSD) analysis of ticarcillin-treated cells show a decrease of the surface roughness. Moreover, bacteria growing in presence of ticarcillin form filaments. This morphology, already observed by Scanning Electron Microscopy,[8] can be explained by the fact that β-lactamins, like ticarcillin, activates the SOS system of the bacteria, therefore inhibiting the cell division.[9,10] The Young modulus of ticarcillin-treated cells is reduced to 50 ± 18 kPa (Figure 3), which indicates that ticarcillin affects the bacterial cell wall. This observation is consistent with the mechanism of action of the antibiotic that inhibits the biosynthesis of the peptidoglycan. Therefore the bacteria are not able to yield a rigid cell wall, leading to the decrease of the Young modulus.

Tobramycin binds to the bacterial ribosome, which leads to the synthesis of abnormal proteins. These proteins are then incorporated to the bacterial cell wall, which loses its integrity. We show that tobramycin-treated cells have a deformed cell wall (Figure 1), and a Young modulus highly reduced in comparison with native cells (Figure 3).

This set of data demonstrates that looking at the nanobiophysical properties of bacteria treated by antibiotics is rich in information. A straightforward extension of this study will be (i) to work with *P. aeruginosa* strains resistant to ticarcillin or/and tobramycin; and (ii) to analyze the effects of innovative antimicrobial agents. Because of the method and data presented here, we are confident that real and major advances in both fundamental and applied microbiology could be done.

Appendix A. Supplementary data

Supplementary data to this article can be found online at doi:10.1016/j.nano.2011.09.009.

References

1. Dufrêne YF, Müller DJ. Atomic Force Microscopy as a multifunctional molecular toolbox in nanobiotechnology. Nat Nanotech 2008;3:261-9.
2. Dorobantu LS, Gray MR. Application of atomic force microscopy in bacterial research. Scanning 2010;32:74-96.
3. El Kirat K, Burton I, Duprès V, Dufrêne YF. Sample preparation procedures for biological atomic force microscopy. J Microscopy 2005;218:199-207.
4. Hauser AR, Ozer EA. *Pseudomonas aeruginosa*. Nat Rev Microbiol 2011;9 [Poster].
5. Strateva T, Yordanov D. *Pseudomonas aeruginosa*: a phenomenon of bacterial resistance. J Med Microbiol 2009;58:133-48.
6. Mortensen NP, Fowlkes JD, Sullivan CJ, Allison DP, Larsen NB, Molin S, et al. Effects of colistin on surface ultrastructure and nanomechanics of *Pseudomonas aeruginosa* cells. Langmuir 2009;25: 3728-33.
7. Jehl F, Chomarat M, Weber M, Gérard A. De l'antibiogramme à la p. rescription. Edition Biomérieux. France: Marcy L'étoile; 2004.
8. Prior RB, Warner JF. Morphological alterations of *Pseudomonas aeruginosa* by ticarcillin: a scanning electron microscope study. Antimicrob Agents Chemother 1974;6:853-5.
9. Schlacher K, Goodman M. Lessons from 50 years of SOS DNA-damage-induced mutagenesis. Nat Rev Mol Cell Biol 2007;8:587-94.
10. Blaquez J, Gomez-Gomez JM, Oliver A, Juan C, Kapur V, Martin S. PBP3 inhibition elicits adaptative responses in *Pseudomnoas aeruginosa*. Mol Microbiol 2006;62:84-99.

<u>Chapter 3.3:</u> Nanoscale behavior of the bacterial cell wall exposed to antibacterials

3.3.2 Unraveling of a mechanism of resistance to colistin in *Klebsiella pneumoniae* thanks to Atomic Force Microscopy

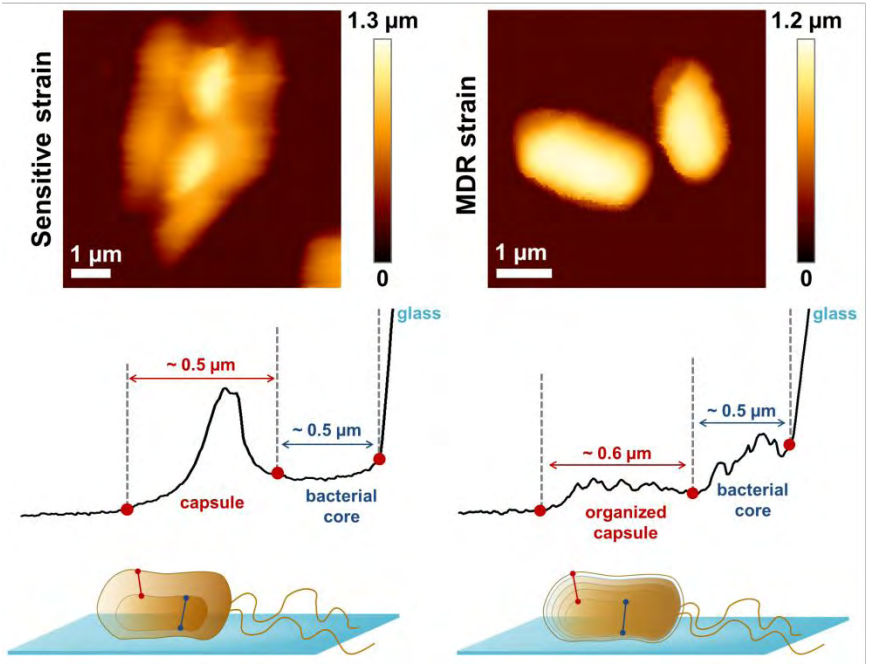

Formosa C., Vidaillac C., Duval R. E., and Dague E.

In revision in *Journal of Antimicrobial and Chemotherapy*

Abstract

Objectives: We focused on polymyxin E (colistin), and studied its effects at the nanoscale on the morphology and nanomechanical properties of *Klebsiella pneumoniae* ATCC 700603, and of its colistin resistant derivate called Kp ATCCm, using Atomic Force Microscopy (AFM).

Methods: *Klebsiella pneumoniae* cells were immobilized on polyethylenimine coated glass slides. All images and force curves were recorded in Phosphate Buffered Saline, with calibrated cantilevers and controlled applied force, on an AFM Nanowizard III (JPK Instruments, Berlin, Germany). Young modulus was extracted from force curves fitted through the Hertz model, and stiffness values were extracted from force curves fitted through the Hooke model. In each case, bacteria coming from three independent cultures were analyzed.

Results: Morphology results showed that colistin removed the capsule from the sensitive strain, but not from the resistant strain. Nanomechanical data on the resistant strain showed that colistin increased the Young modulus of the capsule. Extend force curves recorded on top of the cells allowed to hypothesize on the nanoarchitecture of the capsule of the two strains: Kp ATCC 700603 has a soft capsule in one layer whereas Kp ATCCm capsule is harder and organized in several layers.

Conclusions: In this study, we could show for the first time the effects of colistin at the nanoscale on the cell wall of *K. pneumoniae* using AFM in liquid conditions. This led us to hypothesize a new mechanism of resistance to colistin based on a multilayered organization of the capsular polysaccharides.

Introduction

K. pneumoniae, a member of the *Enterobacteriaceae* family, has been recognized over 100 years ago as a cause of community-acquired pneumonia[1]. However, the vast majority of *Klebsiella* infections are associated with hospitalizations; urinary tract, bloodstream, lungs as well as abdominal cavity infections have now became common. Numerous virulence factors have been described for *K. pneumoniae*, such as extracellular capsules. These are essential for the species' virulence, since the capsular material forms thick bundles of fibrillous structures that cover the bacterial surface in massive layers[2]. This protects the bacteria from phagocytosis and prevents killing by bactericidal serum factors[3]. Another important feature of *K. pneumoniae* is its ability to resist to a large number of antibiotics, through multiple mechanisms (efflux pumps, lack of permeability, and production of enzymes). For example, within a few years after the introduction of cephalosporins, *K. pneumoniae* strains within hospitals were showed to produce β-lactamases able to inactivate these agents. These β-lactamases were in fact ESBL (Extended-Spectrum β-Lactamases), and are plasmid mediated enzymes that hydrolyze oxymino-β-lactamins agents. Because these plasmids are mobile genetic elements, they spread and evolve rapidly[4]; they now also carry resistance genes to other antibiotics, including aminoglycosides, chloramphenicol and sulfonamides. Therefore, *K. pneumoniae* strains containing these plasmids are multidrug resistant[2,3,5]. However, many ESBLs are readily inhibited by the commercially available β-lactamases inhibitors (clavulanic acid, tazobactam and sulbactam)[6], which serve as an important phenotypic test to identify ESBLs. In this study, we have specifically worked on the well-characterized *K. pneumoniae* ATCC 700603 strain, a clinical isolate obtained from a patient in the USA in 1994, which produces an ESBL called SHV-18[7–9]. Because this ESBL is sensitive to clavulanic acid, it has been used as a reference strain for quality control in ESBL detection.

Management and treatment of ESBL-producing *K. pneumoniae* infections can be challenging. Currently, carbapenems are the only class of antibiotics that have consistently been effective against ESBL-producing *K. pneumoniae*. However, bacteria have developed cabapenemases (KPC), which are ESBL-like enzymes that confer resistance to extended-spectrum cephalosporins and carbapenems[1,6,10]. Therefore, clinicians had to turn back to an old antibiotic of the polymyxin class, colistin, as a last resort agent for the treatment of infections caused by multidrug resistant *Klebsiella pneumoniae*[11]. Polymyxins are cyclic lipodecapeptides that are strongly cationic. They were discovered as early as 1947[12], and widely used at that time. But, following reports on nephrotoxicity and neurotoxicity in the 1970s, they were largely replaced by other less-toxic antibiotics[13,14]. Polymyxin B and polymyxin E (colistin) are the main antibiotics of this group, and the only ones used clinically. They are bactericidal, and act rapidly and specifically on Gram-negative bacteria. Here we have focused on colistin that, as for polymyxin B, has for initial target, the LPS (LipoPolySaccharide) of the outer membrane of Gram-negative bacteria. Thanks to its positive charges, colistin interacts electrostatically with LPS, and competitively displaces divalent cations from the phosphate groups of lipid A of LPS[15]. This results in a change in the permeability of the cell wall, leakage of cell contents, and subsequently, cell death[15,16]. However, some authors argue that interaction with membranes is a part of the polymyxin activity, but not actually the lethal event[17]. Therefore the precise mechanism of action of colistin still remains contentious[18], and especially on capsulated bacterial species such as *Klebsiella pneumoniae*. In a similar way, mechanisms resulting in a decreased susceptibility to colistin are also unclear, and only two mechanisms of resistance, involving the extracellular capsule, or the modification of the initial target of colistin, LPS, are currently recognized[11].

In this study, we have used a technology coming from physics, and adapted to biological conditions, Atomic Force Microscopy (AFM), to probe the effects at the nanoscale of colistin on *K. pneumoniae* ATCC 700603, and on its colistin-resistant derivate named Kp ATCCm[19], in order to better understand the mechanism of resistance to colistin. Since its invention in 1986[20], AFM has developed into a powerful technology in biology[21] and especially to probe the effects of antimicrobial drugs against live bacteria or fungi[22–25]. Although the effects of colistin have already been showed by AFM on cells of *Pseudomonas aeruginosa* and *Acinetobacter baumannii*[26–28], no work have been performed on live cells of *Klebsiella pneumoniae,* using AFM in liquid conditions. The results of this original study enlighten the mechanism of resistance of Kp ATCCm to colistin.

Materials and Methods

Bacteria growth conditions

The bacteria *Klebsiella pneumoniae* ATCC 700603 and Kp ATCCm (resistant derivative of *K. pneumoniae* ATCC 700603, ABC Platform® Bugs Bank) were stocked at -80 °C, revivified on Mueller Hinton Agar (Difco, 225250-500 g) and grown in Mueller Hinton Broth (Difco, 275730-500 g) for 24 hours at 37°C under static conditions. Antibiograms of the two strains are presented in Supplementary data 1 and 2.

Antibiotic treatments

Minimal Inhibitory Concentrations (MICs) of colistin sulfate salt (Sigma Aldrich, C4461-1G) were calculated for each strain according to the macro-dilution method provided by the Clinical and Laboratory Standards Institute[29] (CLSI). For Kp ATCC 700603, the MIC of colistin was found to be 0.5 mg/L, and for Kp ATCCm, it was found to be 16 mg/L. These results were confirmed by antibiograms performed with automated Vitek2 system, BioMérieux, France

(Supplementary data 1 and 2). Then, before AFM experiments, bacteria were grown in Mueller Hinton broth containing colistin at a concentration of 0.5×MIC (0.25 mg/L for Kp ATCC 700603 and 8 mg/mL for Kp ATCCm) or 0.75×MIC (0.375 mg/L for Kp ATCC 700603 and 12 mg/L for Kp ATCCm), during 18 to 20 hours, at 37°C under static conditions.

Sample preparation for AFM experiments

Bacterial cells were concentrated by centrifugation (4500g, 3 min), washed 2 times in PBS (Phosphate Buffered Saline) 1X (Sigma, P3813-10PAK, filtered on 0.22 µm filters), re-suspended in PBS 1X to a concentration of ~ 10^8 cells/mL, and immobilized on PolyEthylenImine (PEI, Fluka P3142-100 mL) coated glass slides (prepared as described elsewhere[30]). Briefly, freshly oxygen activated glass slides were covered by a 0.2% PEI solution in deionized water and left for incubation overnight. Then the glass slides were rinsed with 20 mL of Milli-Q water and nitrogen dried. A total of 1 mL of the bacterial suspension was then applied to the PEI coated glass slide, allowed to stand for one hour and rinsed with PBS 1X.

AFM experiments

Images were recorded in PBS 1X, in Quantitative Imaging™ mode available on a Nanowizard III AFM (JPK Instruments, Berlin, Germany), with MLCT AUWH cantilevers (nominal spring constant of 0.01 N/m, Bruker, USA) at an applied force of 1 nN, with a z-length between 2 and 3 µm and an approach-retract speed between 130 and 250 µm/s. Cantilevers spring constant were measured prior to each experiments using the thermal noise method[31]. Force curves were recorded in Force Volume mode at an applied force of 2.0 nN. Data were processed using the JPK Data processing software (JPK Instruments, berlin, Germany). For nanomechanical data, Hertz model was used to extract Young modulus values, and Hooke model to extract stiffness values. The Hertz model gives the force F as a function of the indentation (δ), and of the Young modulus (E) according to the equation $F = ((2.E.\tan\alpha)/(\pi.(1-\nu^2).\delta^2$, where α is the tip opening

angle (35°) and v the Poisson ratio (arbitrarily assumed to be 0.5)[32]. The Hooke model considers the couple cantilever/cell wall as a spring. The stiffness of the cell wall (k_{cell}) is therefore determined from the slope of the linear portion of the raw force curves, according to $k_{cell} = k(s/1-s)$, where s is the experimentally accessible slope of the compliance region reached for sufficient loading forces, and k the cantilever spring constant[33].

Results

Colistin removes the capsule from the sensitive strain

K. pneumoniae ATCC 700603 was first probed in native conditions or under colistin treatment, thanks to AFM used in the Quantitative Imaging™ mode[34]. Figure 1 presents the morphology modifications of the bacteria submitted to colistin treatment. The height image in Figure 1a shows two bacterial cells surrounded by their capsule in absence of colistin; the cross-sections data show that bacteria are 0.88 ± 0.11 µm high and 1.12 ± 0.15 µm large, whereas the capsule is 0.56 ± 0.09 µm high but covers a surface of 3.46 ± 0.28 µm in width (Figure 1b, values measured on five cells coming from three independent cultures). As for the extend force curves obtained on untreated cells, at a high applied force (2 nN), 81.3% of them (n = 5120) show a spike that could correspond to the moment where the tip touches the capsule and moves through it, then through the bacterial cell, before reaching the glass slide (linear portion of the force curve) (Figure 1c). When cells are treated with colistin, at either 0.5×MIC (0.25 mg/L, Figure 1d, e, and f), or 0.75×MIC (0.375 mg/L, Figure 1g, h and i), the capsule is no longer visible around the cells, which is confirmed by the cross-sections showing only the bacterial profile, with a height of 0.88 ± 0.06 µm and a width of 1.13 ± 0.11 µm (values measured on ten cells coming from six independent cultures). As for the extend force curves recorded on these cells, they do not display

a spike anymore, allowing us to hypothesize that these spikes correspond indeed to the rupture of the capsule by the AFM tip.

Colistin resistant strain Kp ATCCm displays a different capsular organization

In the case of the colistin resistant derivative of *K. pneumoniae* ATCC 700603 (i.e. Kp ATCCm), as it can be seen on the height images in Figure 2a, d and g, this strain does not morphologically suffer from the colistin treatment. Indeed, the cross-sections in Figure 2b, e and h, show the same profile in the three different conditions, native, or colistin treatment at 0.5×MIC (8 mg/L) or at 0.75×MIC (12 mg/L).. The bacteria are 0.83 ± 0.06 µm high and 1.50 ± 0.11 µm large, thus larger than the sensitive strain (values measured on fifteen cells coming from nine independent cultures). At this stage, first differences can be observed between the two strains. Even in native conditions, Kp ATCCm does not have a capsule covering a large surface like Kp ATCC. However since Kp ATCCm cells are wider than sensitive strains cells, we can conclude that its capsule has a different morphology, and is tightly bound to the bacterial cell wall. But the most interesting data obtained on Kp ATCCm cells are the extend force curves, presented in Figure 2c, f and i. In native conditions, force curves display two spikes. After the first one on the left of the force curve (the further away from the contact point), small condensed spikes are visible, suggesting that successive layers are ruptured by the AFM tip. When cells are treated by colistin, the force curves present the same profile, except that the small condensed spikes are not observed anymore after the first spike, meaning that the several layers observed in native conditions are not present anymore. In the three cases, the linear portions of the force curves correspond to the contact of the tip with the glass slide, as force curves recorded on the glass slide with the same tip present the same slope (data not shown). At this stage, the morphology data and the extend force curves recorded on cells of the sensitive and resistant strains of *K. pneumoniae*, demonstrate that

colistin is able to remove the capsule from the bacteria only in the case of the sensitive strain, and that the two strains present a different capsular organization that can be probed thanks to force spectroscopy. However the force curves of treated Kp ATCCm cells indicate that this capsular organization is lost upon treatment. The next question is then: what are the effects of colistin on the nanomechanical properties of the cells?

Colistin modifies the nanomechanical properties of Kp ATCC and Kp ATCCm

Figure 3 presents the nanomechanical results obtained on the sensitive strain of *K. pneumoniae*. In native conditions, extend force curves obtained on cells, converted into indentation curves (Figure 3b, grey line), and fitted through the Hertz model (Figure 3b, empty circles) give access, according a first interpretation of the force curves, to the stiffness of the capsule. Stiffness values measured on five cells coming from 3 independent cultures are in average of 3.6 ± 1.0 kPa (Figure 3a). However, when cells are treated with colistin, whatever the dose, force curves present only a few nanometers of indentation, and cannot be fitted through the Hertz model anymore. After verifying that the slope of these force curves was different from the ones of force curves recorded on glass slides (Supplementary data 3), we chose to analyze them with the Hooke model, which considers the couple cantilever/cell wall as a spring. This model gives access to the bacterial spring constant, expressed in N/m. Figure 3c shows the force curves obtained for cells treated with colistin at 0.5×MIC (0.25 mg/L, blue line) and at 0.75×MIC (0.375 mg/L, orange line), fitted with the Hooke model (empty circles). The results obtained on five cells coming from three independent cultures in each case, are of 12.6 ± 0.7 nN/µm for a treatment at 0.5×MIC, and of 11.5 ± 0.6 nN/µm at 0.75×MIC. The difference between these two conditions is therefore not significant. These results allow us to conclude that in native conditions, cells are covered by the capsule, and only the stiffness of this capsule can be

measured. However, when cells are treated with colistin, the capsule is removed from the surface, giving access to the tip to the bacterial cell wall. The cell wall is not soft enough for the tip to indent into it; as we cannot compare spring constant values with the untreated cells, where the cell wall is not accessible, it is impossible to conclude whether the cell wall is naturally stiff, or if it is a result of the colistin treatment.

In the case of the colistin resistant strain, Kp ATCCm, the situation is different, since colistin seems to have no effect on the morphology of the cells (Figure 2). However, extend force curves acquired on cells treated with colistin suggested that the organization of the capsule visible in native conditions, was lost upon treatment. In native conditions, we could fit the first spike of the indentation curve, likely corresponding to the capsule of the cells, through the Hertz model (Figure 4b). The values obtained on five cells coming from three independent cultures were of 21.3 ± 4.2 kPa (Figure 4a). This value, 5 times higher than the one measured on the capsule of the sensitive strain, confirms the previous observation in the differences of the capsular organization between the two strains. Then, since the capsule is still present when cells are treated with colistin, we could fit the indentation curves obtained on treated cells also through the Hertz model (Figure 4b), and found an increase in the average stiffness values to 74.4 ± 19.7 kPa when cells are treated by colistin at 0.5×MIC (8 mg/L), and to 88.5 ± 19.4 kPa when cells are treated by colistin at 0.75×MIC (12 mg/L, Figure 4a). Therefore, along with the apparent loss of the capsule organization on the force extend force curves (Figure 2) recorded on treated Kp ATCCm cells, the nanomechanical data also show that the stiffness of the capsule of the colistin resistant strain increases upon treatment by colistin.

Discussion

As it has been introduced earlier, the described mechanism of action of colistin is to interact thanks to its strong positive charge to LPS molecules present on the outer membrane of Gram-negative bacteria, inducing changes in the membrane permeability, therefore leading to cell death[15,35]. However, the exact mechanism by which colistin induces bacterial death is still unknown. Some studies have showed that multiple cell targets might be involved, as the polymyxin-mediated killing takes place prior to an increase in the membrane permeability[36,37]. Also, colistin has been shown to be efficient on mycobacterial species, which have mycolic acid-based cell wall instead of LPS[38]. Thus LPS might not be the only target of colistin; phospholipids might also be a target of colistin. But in the case of capsulated bacteria, colistin has to interact first with capsular polysaccharides, before it can go through the capsule, to reach LPS on the outer membrane, and then the phospholipids of the cytoplasmic membrane. Finally the killing of bacteria occurs either because of the formation of ions channels, transmembrane pores or membrane ruptures of the cytoplasmic membrane[36,39].

In our case, we have worked with *Klebsiella pneumoniae*, a capsulated bacterial species. It has been postulated that polymyxin triggers *in vivo* the release of capsular polysaccharides from the bacteria[40]. This is in line with the results we obtained on the colistin sensitive strain, since the capsule was removed from the bacteria upon colistin treatment (Figure 1). The same authors have also showed that capsular polysaccharides in *Klebsiella pneumoniae* were involved in polymyxin resistance, providing a protective shield against polymyxin interactions with the cell surface[41], or by binding colistin therefore reducing the amount of colistin reaching the cell surface[40]. However, the amount of capsule polysaccharides must reach a certain threshold in order to confer the resistance to colistin. Other colistin resistance mechanisms have also been

described, such as modification of the LPS, changes in the negative charge of the outer membrane, or efflux pumps systems[42].

In this study, we observe an undescribed resistance mechanism to colistin. Indeed, as it can be seen on Figure 5, force curves recorded on the sensitive strain present a spike, corresponding to the contact and indentation of the AFM tip into the capsular polysaccharide. As the applied force is high, the AFM tip goes through the capsule (0.5 µm), then the bacterial core (0.5 µm), before reaching the PEI layer coated on the glass slide. Similar experiments conducted on bacteria and eukaryotic cells have proved the possibility to read from the force curves obtained from such experiments the architecture of the different compartments of the cells traversed[43–45]. In the case of the colistin resistant strain, the extend force curves present a first spike followed by several condensed spikes on a distance of 0.6 µm, before reaching a second spike. Figure 5b presents the interpretation that we made of such force curves. The tip first touches and indent into the capsule, but soon meets another layer of polysaccharides, that is broken with a less important force (small spike), and another layer, and so on before reaching the bacterial cell. Then the bacterial core is traversed on 0.5 µm by the AFM tip before it reaches the glass slide again. The fact that we obtained on the force curves these several ruptures after the first spike allowed us to hypothesize that the capsule was in fact multilayered. To reinforce this hypothesis, an indentation curve recorded on top of a single live cell in native conditions was analyzed (graphic in Figure 5b). Every spikes observed on this indentation curve have been fitted through the Hertz model (empty circles). For every fit, approximately the same stiffness values are extracted (20 kPa), letting us postulate that each small spikes corresponds to the rupture of a layer of polysaccharide. Since Kp ATCCm is resistant to colistin (MIC = 16 mg/L) compared to Kp ATCC 700603 (MIC = 0.5 mg/L), then this multilayered structure of the capsule could be a key for colistin resistance in Kp ATCCm. But colistin still interacts with the capsular

polysaccharides of the Kp ATCCm strain. Indeed, studies have showed that capsular polysaccharides could be of different chemical composition. Colistin being positively charged, it binds to anionic capsule, but not with cationic or uncharged ones[40]. In our case, the nanomechanical data indicate that the capsule of Kp ATCCm becomes harder (the stiffness increases), along with the dose of colistin and loses its organization in several superposed layers. Therefore, colistin has an effect on the nanomechanical properties of the capsule, leading us to think that colistin still interacts with the capsule, but because of its organization, cannot go through it to reach the cytoplasmic membrane of the bacteria.

To conclude, this study allowed imaging by Atomic Force Microscopy the capsule of living cells of *Klebsiella pneumoniae*, which is, as far as we know, a first time happening. It also allowed us to show that colistin was able to remove the capsule of a sensitive-colistin strain, but not of a resistant strain. We finally hypothesized, thanks to force spectroscopy experiments, a model for colistin resistance, which is based on the nanoarchitecture of the capsule. Indeed, the colistin resistant strain presents a well-organized multilayered capsule that interacts with colistin but without letting the molecule go through to the cell wall to reach its targets. Now, additional AFM experiments on clinical isolates of colistin susceptible and resistant *K. pneumoniae* are needed to further investigate the morphology of the capsule, the impact of colistin exposure on these isolates, and ultimately, the mechanisms of colistin resistance during therapy.

Acknowledgements

ED is a researcher of Centre National de la Recherche Scientifique (CNRS). We thank Dr. Marion Grare for performing antibiograms on the two strains used.

Funding

This work has been supported by grant from "Young Scientist Program" of ANR (Agence Nationale de la Recherche), project ANR-11-JSV5-001-01, n° (SD) 30 02 43 31. CF is supported by a grant from "Direction Générale de l'Armement" (DGA) for her 3 years PhD study.

Transparency declarations

None to declare

References

1. Keynan Y, Rubinstein E. The changing face of Klebsiella pneumoniae infections in the community. *Int J Antimicrob Agents* 2007; **30**: 385–9.
2. Podschun R, Ullmann U. Klebsiella spp. as nosocomial pathogens: epidemiology, taxonomy, typing methods, and pathogenicity factors. *Clin Microbiol Rev* 1998; **11**: 589–603.
3. Gupta A, Ampofo K, Rubenstein D, Saiman L. Extended spectrum beta lactamase-producing Klebsiella pneumoniae infections: a review of the literature. *J Perinatol Off J Calif Perinat Assoc* 2003; **23**: 439–43.
4. Livermore DM. Current epidemiology and growing resistance of gram-negative pathogens. *Korean J Intern Med* 2012; **27**: 128–42.
5. Jacoby GA, Sutton L. Properties of plasmids responsible for production of extended-spectrum beta-lactamases. *Antimicrob Agents Chemother* 1991; **35**: 164–9.
6. Perez F, Endimiani A, Hujer KM, Bonomo RA. The continuing challenge of ESBLs. *Curr Opin Pharmacol* 2007; **7**: 459–69.
7. Rasheed JK, Anderson GJ, Yigit H, *et al.* Characterization of the Extended-Spectrum β-Lactamase Reference Strain, Klebsiella pneumoniae K6 (ATCC 700603), Which Produces the Novel Enzyme SHV-18. *Antimicrob Agents Chemother* 2000; **44**: 2382–8.
8. Pasteran F, Veliz O, Rapoport M, Guerriero L, Corso A. Sensitive and Specific Modified Hodge Test for KPC and Metallo-Beta- Lactamase Detection in Pseudomonas aeruginosa by Use of a Novel Indicator Strain, Klebsiella pneumoniae ATCC 700603. *J Clin Microbiol* 2011; **49**: 4301–3.
9. Bush K, Jacoby GA. Updated Functional Classification of ?-Lactamases. *Antimicrob Agents Chemother* 2010; **54**: 969–76.
10. Munoz-Price LS, Poirel L, Bonomo RA, *et al.* Clinical epidemiology of the global expansion of Klebsiella pneumoniae carbapenemases. *Lancet Infect Dis* 2013; **13**: 785–96.
11. Ah Y-M, Kim A-J, Lee J-Y. Colistin resistance in Klebsiella pneumoniae. *Int J Antimicrob Agents* 2014; **44**: 8–15.
12. Vaara M. Novel derivatives of polymyxins. *J Antimicrob Chemother* 2013; **68**: 1213–9.
13. Koch-Weser J, Sidel VW, Federman EB, Kanarek P, Finer DC, Eaton AE. Adverse effects of sodium colistimethate. Manifestations and specific reaction rates during 317 courses of therapy. *Ann Intern Med* 1970; **72**: 857–68.
14. Nation RL, Li J. Colistin in the 21st Century. *Curr Opin Infect Dis* 2009; **22**: 535–43.
15. Yahav D, Farbman L, Leibovici L, Paul M. Colistin: new lessons on an old antibiotic. *Clin Microbiol Infect* 2012; **18**: 18–29.
16. Velkov T, Thompson PE, Nation RL, Li J. Structure--activity relationships of polymyxin antibiotics. *J Med Chem* 2010; **53**: 1898–916.
17. Zhang L, Dhillon P, Yan H, Farmer S, Hancock RE. Interactions of bacterial cationic peptide antibiotics with outer and cytoplasmic membranes of Pseudomonas aeruginosa. *Antimicrob Agents Chemother* 2000; **44**: 3317–21.
18. Velkov T, Roberts KD, Nation RL, Thompson PE, Li J. Pharmacology of polymyxins: new insights into an 'old' class of antibiotics. *Future Microbiol* 2013; **8**: 711–24.
19. Vidaillac C, Benichou L, Duval RE. In Vitro Synergy of Colistin Combinations against Colistin-Resistant Acinetobacter baumannii, Pseudomonas aeruginosa, and Klebsiella pneumoniae Isolates. *Antimicrob Agents Chemother* 2012; **56**: 4856–61.
20. Binnig G, Quate CF, Gerber C. Atomic Force Microscope. *Phys Rev Lett* 1986; **56**: 930–4.

21. Müller DJ, Dufrêne YF. Atomic force microscopy: a nanoscopic window on the cell surface. *Trends Cell Biol* 2011; **21**: 461–9.
22. Formosa C, Grare M, Duval RE, Dague E. Nanoscale effects of antibiotics on P. aeruginosa. *Nanomedicine Nanotechnol Biol Med* 2012; **8**: 12–6.
23. Formosa C, Grare M, Jauvert E, *et al.* Nanoscale analysis of the effects of antibiotics and CX1 on a Pseudomonas aeruginosa multidrug-resistant strain. *Sci Rep* 2012; **2**. Available at: http://dx.doi.org/10.1038/srep00575.
24. Formosa C, Schiavone M, Martin-Yken H, François JM, Duval RE, Dague E. Nanoscale Effects of Caspofungin against Two Yeast Species, Saccharomyces cerevisiae and Candida albicans. *Antimicrob Agents Chemother* 2013; **57**: 3498–506.
25. El-Kirat-Chatel S, Beaussart A, Alsteens D, Jackson DN, Lipke PN, Dufrêne YF. Nanoscale analysis of caspofungin-induced cell surface remodelling in Candida albicans. *Nanoscale* 2013; **5**: 1105–15.
26. Soon RL, Nation RL, Harper M, *et al.* Effect of colistin exposure and growth phase on the surface properties of live Acinetobacter baumannii cells examined by atomic force microscopy. *Int J Antimicrob Agents* 2011; **38**: 493–501.
27. Soon RL, Nation RL, Hartley PG, Larson I, Li J. Atomic Force Microscopy Investigation of the Morphology and Topography of Colistin-Heteroresistant Acinetobacter baumannii Strains as a Function of Growth Phase and in Response to Colistin Treatment. *Antimicrob Agents Chemother* 2009; **53**: 4979–86.
28. Mortensen NP, Fowlkes JD, Sullivan CJ, *et al.* Effects of Colistin on Surface Ultrastructure and Nanomechanics of Pseudomonas aeruginosa Cells. *Langmuir* 2009; **25**: 3728–33.
29. Clinical and Laboratory Standards Institute. *Methods for dilution antimicrobial susceptibility tests for bacteria that grow aerobically; approved standards*. Wayne, PA; 2009.
30. Francius G, Tesson B, Dague E, Martin-Jézéquel V, Dufrêne YF. Nanostructure and nanomechanics of live Phaeodactylum tricornutum morphotypes. *Environ Microbiol* 2008; **10**: 1344–56.
31. Hutter JL, Bechhoefer J. Calibration of atomic-force microscope tips. *Rev Sci Instrum* 1993; **64**: 1868–73.
32. Hertz H. Ueber die beruhrung fester elastischer korper. *J Reine Angew Math* 1881: 156–71.
33. Arnoldi M, Fritz M, Bäuerlein E, Radmacher M, Sackmann E, Boulbitch A. Bacterial turgor pressure can be measured by atomic force microscopy. *Phys Rev E* 2000; **62**: 1034–44.
34. Chopinet L, Formosa C, Rols MP, Duval RE, Dague E. Imaging living cells surface and quantifying its properties at high resolution using AFM in QI^{TM} mode. *Micron* 2013; **48**: 26–33.
35. Bergen PJ, Landersdorfer CB, Zhang J, *et al.* Pharmacokinetics and pharmacodynamics of 'old' polymyxins: what is new? *Diagn Microbiol Infect Dis* 2012; **74**: 213–23.
36. Mogi T, Kita K. Gramicidin S and polymyxins: the revival of cationic cyclic peptide antibiotics. *Cell Mol Life Sci* 2009; **66**: 3821–6.
37. Hale JD, Hancock RE. Alternative mechanisms of action of cationic antimicrobial peptides on bacteria. *Expert Rev Anti Infect Ther* 2007; **5**: 951–9.
38. David HL, Rastogi N. Antibacterial action of colistin (polymyxin E) against Mycobacterium aurum. *Antimicrob Agents Chemother* 1985; **27**: 701–7.
39. Brogden KA. Antimicrobial peptides: pore formers or metabolic inhibitors in bacteria? *Nat Rev Microbiol* 2005; **3**: 238–50.
40. Llobet E, Tomás JM, Bengoechea JA. Capsule polysaccharide is a bacterial decoy for antimicrobial peptides. *Microbiology* 2008; **154**: 3877–86.

41. Campos MA, Vargas MA, Regueiro V, Llompart CM, Albertí S, Bengoechea JA. Capsule Polysaccharide Mediates Bacterial Resistance to Antimicrobial Peptides. *Infect Immun* 2004; **72**: 7107–14.
42. Ah Y-M, Kim A-J, Lee J-Y. Colistin resistance in Klebsiella pneumoniae. *Int J Antimicrob Agents*. Available at: http://www.sciencedirect.com/science/article/pii/S0924857914000880. Accessed June 11, 2014.
43. Liu H, Wen J, Xiao Y, *et al*. In situ mechanical characterization of the cell nucleus by atomic force microscopy. *ACS Nano* 2014; **8**: 3821–8.
44. Obataya I, Nakamura C, Han S, Nakamura N, Miyake J. Nanoscale operation of a living cell using an atomic force microscope with a nanoneedle. *Nano Lett* 2005; **5**: 27–30.
45. Suo Z, Avci R, Deliorman M, Yang X, Pascual DW. Bacteria survive multiple puncturings of their cell walls. *Langmuir ACS J Surf Colloids* 2009; **25**: 4588–94.

Figures

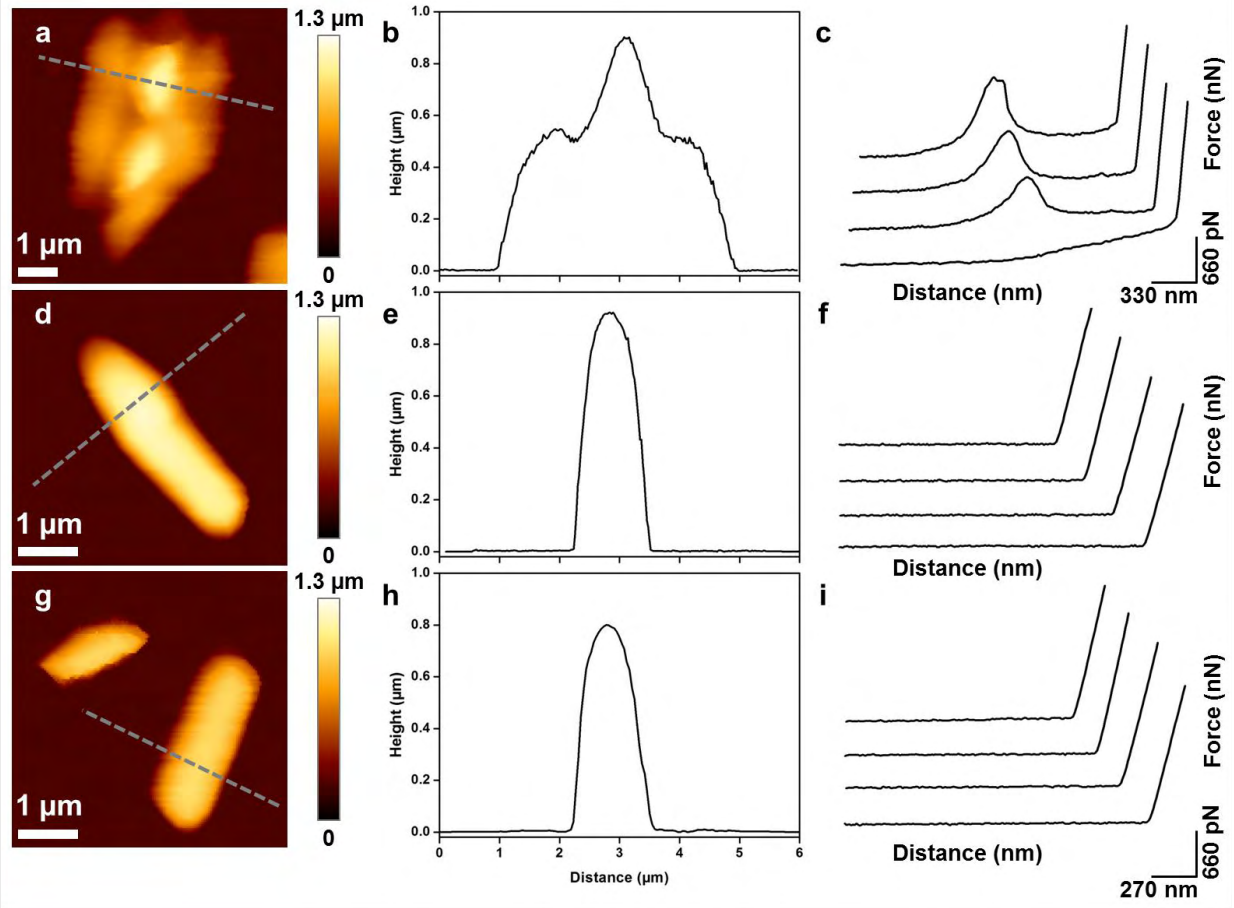

Figure 1. Imaging of *K. pneumoniae* ATCC 700603 cells. (a) Height image of *K. pneumoniae* ATCC 700603 cells under native conditions, (d) treated with colistin at 0.5×MIC (0.25 mg/L) or (g) treated with colistin at 0.75×MIC (0.375 mg/L). (b, e and h) cross-sections recorded along the dashed lines respectively on a, d and g. (c, f and i) representative extend force curves recorded on small areas on top of cells presented respectively in a, d and g. In each condition, force curves were recorded on 5 cells coming from 3 independent cultures (total of 5120 force curves per condition).

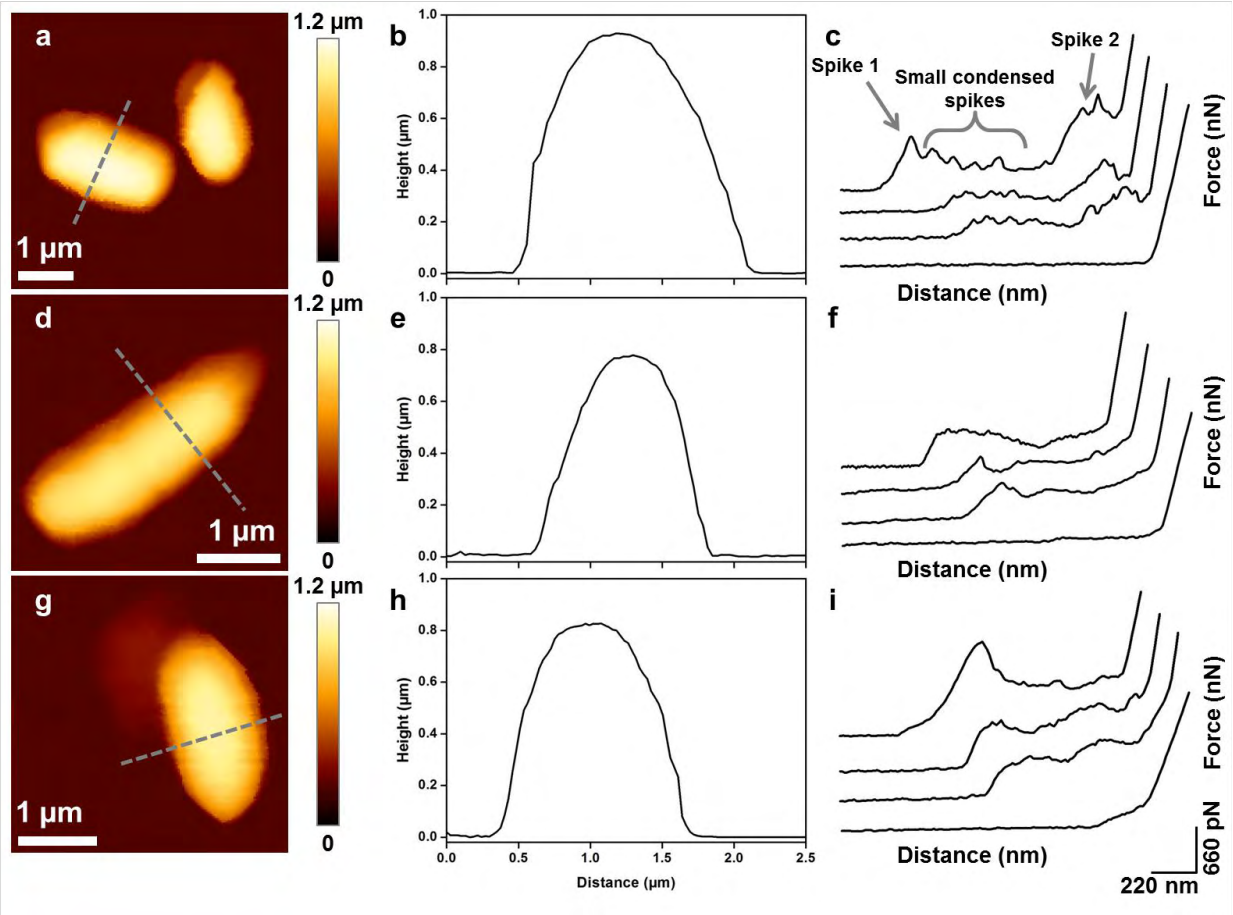

Figure 2. Imaging of *K. pneumoniae* colistin resistant (Kpm) cells. (a) Height image of Kpm cells under native conditions, (d) treated with colistin at 0.5×MIC (8 mg/L) or (g) treated with colistin at 0.75×MIC (12 mg/L). (b, e and h) cross-sections recorded along the dashed lines respectively on a, d and g. (c, f and i) representative extend force curves recorded on small areas on top of cells presented respectively in a, d and g. In each condition, force curves were recorded on 5 cells coming from 3 independent cultures (total of 5120 force curves per condition).

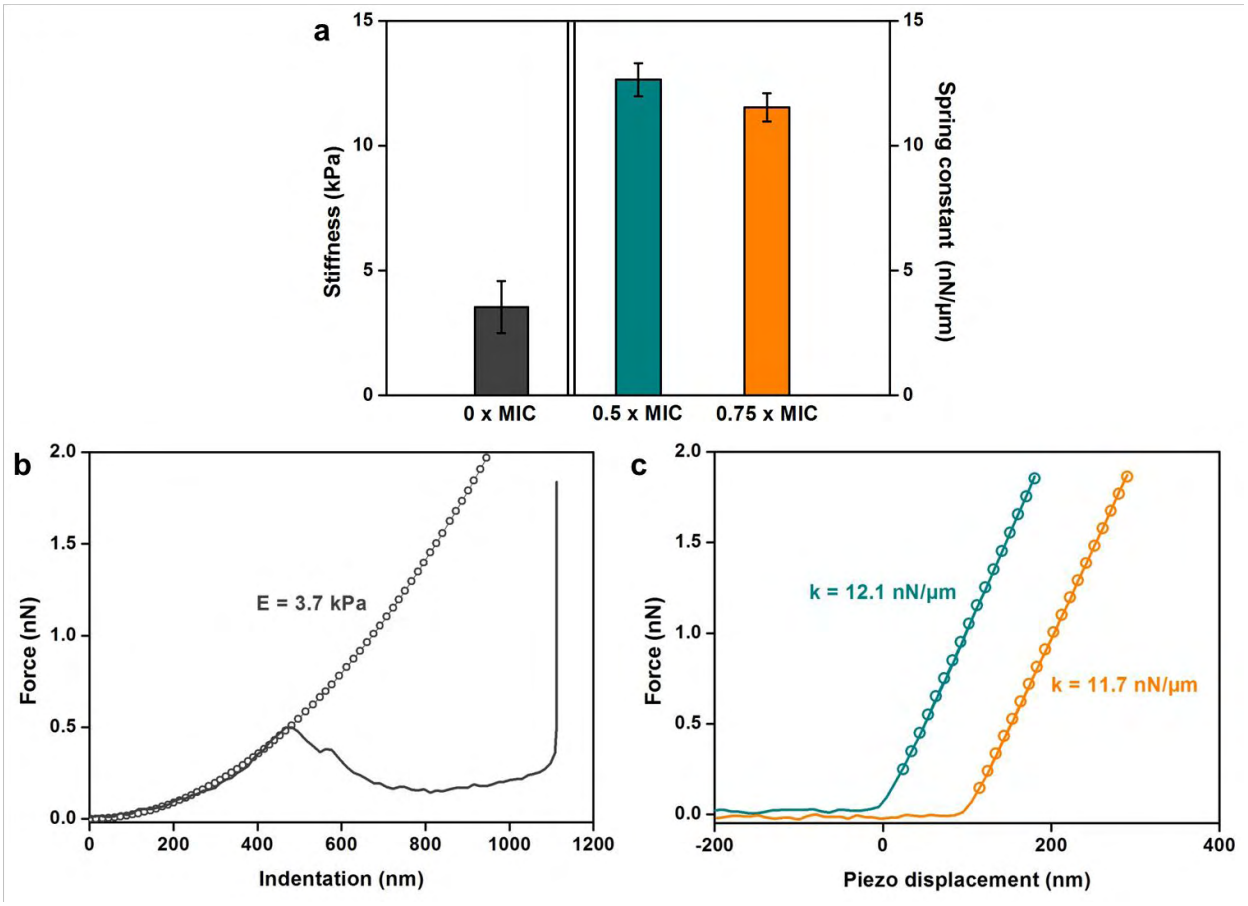

Figure 3. Nanomechanical properties of *K. pneumoniae* ATCC 700603 cells. (a) Histogram presenting the stiffness values measured on cells in native conditions (grey bar) or the bacterial spring constants measured on cells treated with colistin at 0.5×MIC (0.25 mg/L, blue bar) or treated with colistin at 0.75×MIC (0.375 mg/L, orange bar). In each case, values were measured on three cells coming from three independent cultures. (b) Representative indentation curve obtained on top of a cell in native conditions (grey line), fitted through the Hertz model (empty circles). (c) Representative force curves obtained on cells treated with colistin at 0.5×MIC (0.25 mg/L, blue line) or treated with colistin at 0.75×MIC (0.375 mg/L, orange line), fitted through the Hooke model (empty circles).

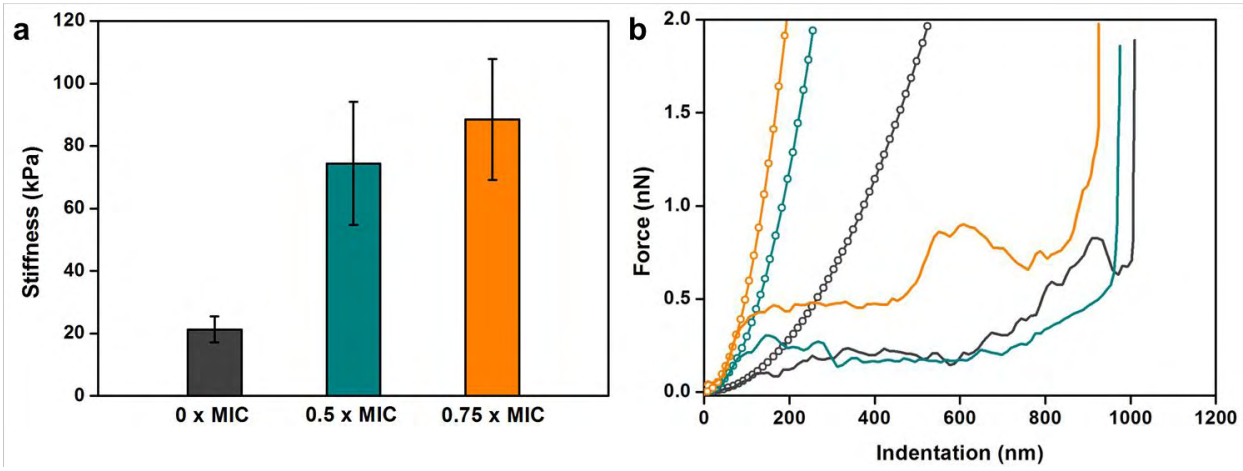

Figure 4. Nanomechanical properties of *K. pneumoniae* colistin resistant (Kpm) cells. (a) Histogram presenting the stiffness values measured on cells in native conditions (grey bar), treated with colistin at 0.5×MIC (8 mg/L, blue bar) or treated with colistin at 0.75×MIC (12 mg/L, orange bar). In each case, values were measured on three cells coming from three independent cultures. (b) Representative indentation curves obtained on top of a cell in native conditions (grey line), treated with colistin at 0.5×MIC (8 mg/L, blue line) or treated with colistin at 0.75×MIC (12 mg/L, orange line), fitted through the Hertz model (empty circles).

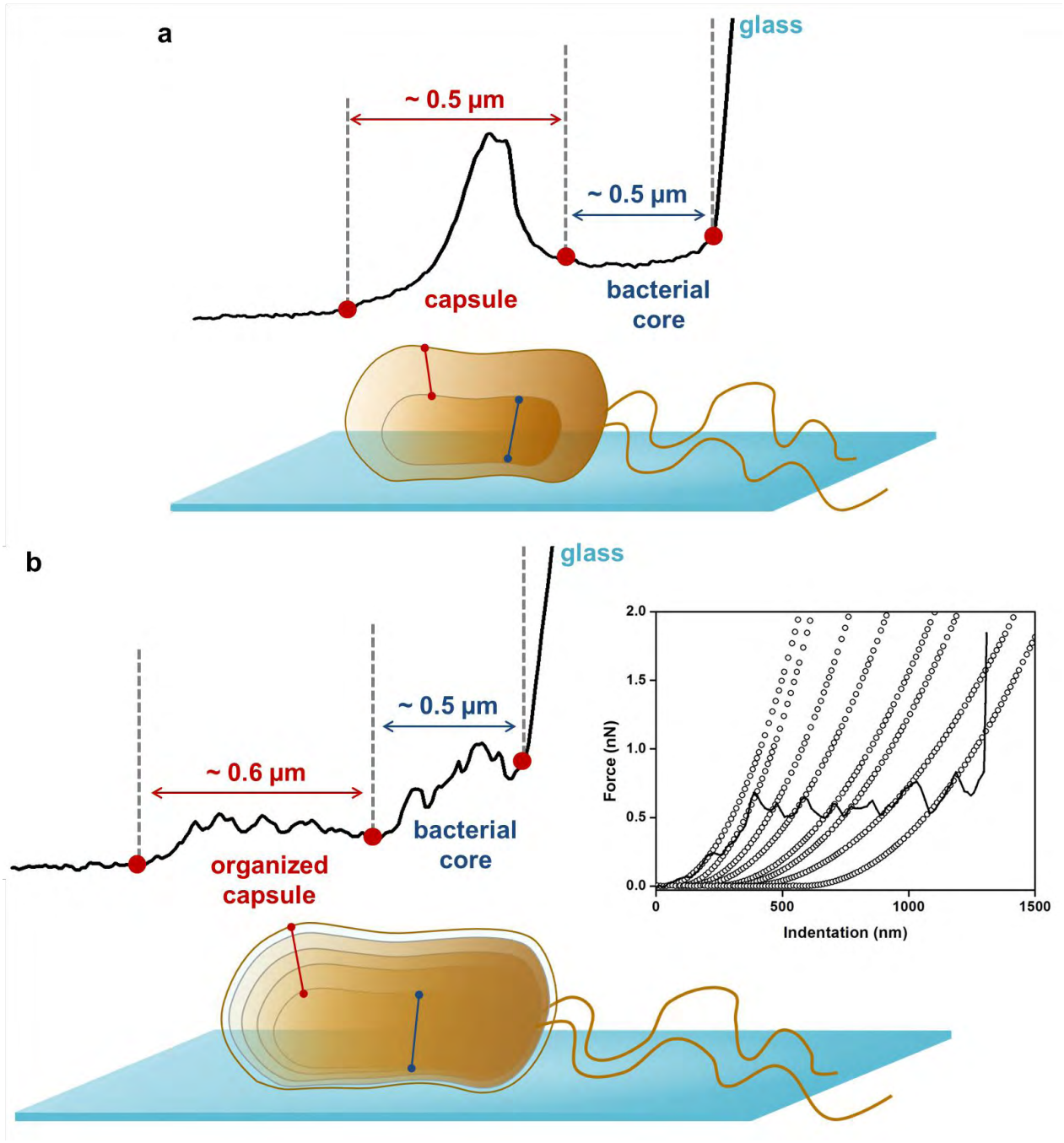

Figure 5. Schematic representation of the hypothesis formulated on the capsular architecture. (a) capsule organization of *K. pneumoniae* ATCC 700603, and (b) capsule organization of *K. pneumoniae* colistin resistant (Kpm). The graphic in (b) shows an indentation curve recorded on top of a Kpm cell in native conditions (grey line), which each spikes have been fitted through the Hertz model.

Chapter 3.3: Nanoscale behavior of the bacterial cell wall exposed to antibacterials

3.3.3 Nanoscale analysis of the effects of antibiotics and CX1 on a *Pseudomonas aeruginosa* multidrug-resistant strain

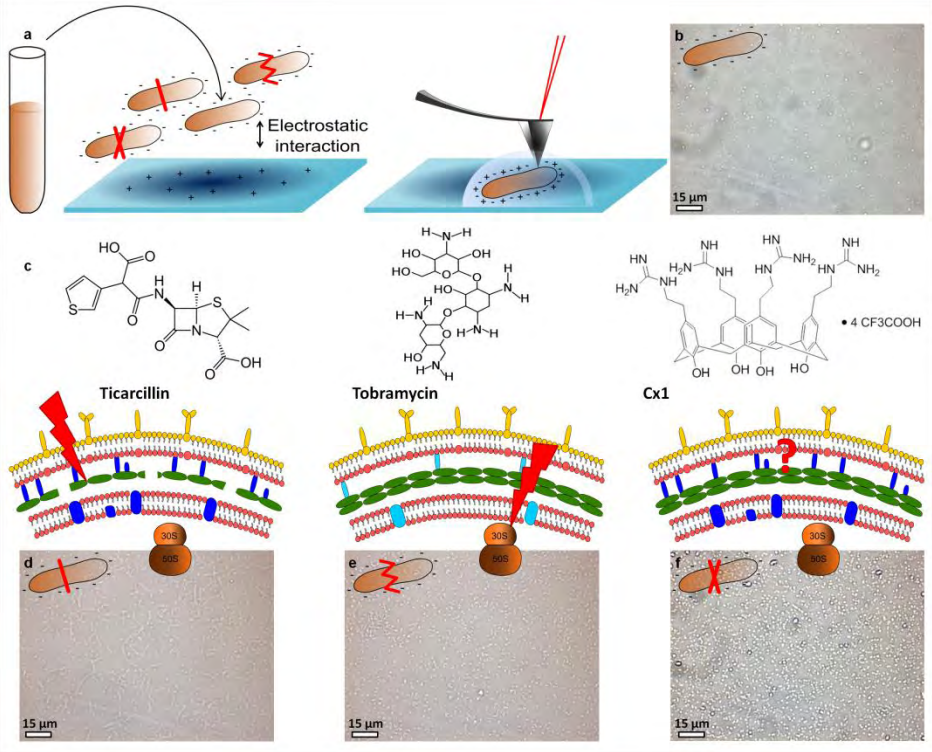

Formosa C., Grare M., Jauvert E., Coutable A., Regnouf-de-Vains J. B., Mourer M., Duval R. E., and Dague E.

Scientific Reports, **2**, 575, 2012

Abstract

Drug resistance is a challenge that can be addressed using nanotechnology. We focused on the resistance of the bacteria *Pseudomonas aeruginosa* and investigated, using Atomic Force Microscopy (AFM), the behavior of a reference strain and of a multidrug resistant clinical strain, submitted to two antibiotics and to an innovative antibacterial drug (CX1). We measured the morphology, surface roughness and elasticity of the bacteria under physiological conditions and exposed to the antibacterial molecules. To go further in the molecules action mechanism, we explored the bacterial cell wall nanoscale organization using functionalized AFM tips. We have demonstrated that affected cells have a molecularly disorganized cell wall; surprisingly long molecules being pulled off from the cell wall by a lectin probe. Finally, we have elucidated the mechanism of action of CX1: it destroys the outer membrane of the bacteria as demonstrated by the results on artificial phospholipidic membranes and on the resistant strain.

SCIENTIFIC REPORTS

OPEN

SUBJECT AREAS:
ANTIMICROBIALS
NANOBIOTECHNOLOGY
BIOPHYSICS
CHEMISTRY

Received
8 June 2012

Accepted
30 July 2012

Published
14 August 2012

Correspondence and requests for materials should be addressed to E.D. (edague@laas.fr)

Nanoscale analysis of the effects of antibiotics and CX1 on a *Pseudomonas aeruginosa* multidrug-resistant strain

C. Formosa[1,2,3,4], M. Grare[6], E. Jauvert[1,2,3], A. Coutable[1,2,3], J. B. Regnouf-de-Vains[4], M. Mourer[4], R. E. Duval[4,5] & E. Dague[1,2,3]

[1]Centre National de la Recherche Scientifique, Laboratoire d'Analyse et d'Architecture des systèmes (LAAS), Toulouse, France, [2]Centre National de la Recherche Scientifique, Toulouse, France, [3]Université de Toulouse, Toulouse, France, [4]SRSMC, Université de Lorraine - CNRS, Nancy, France, [5]ABC Platform®, Nancy, France, [6]Laboratoire de Bactériologie Hygiène, Institut Fédératif de Biologie, Toulouse, France.

Drug resistance is a challenge that can be addressed using nanotechnology. We focused on the resistance of the bacteria *Pseudomonas aeruginosa* and investigated, using Atomic Force Microscopy (AFM), the behavior of a reference strain and of a multidrug resistant clinical strain, submitted to two antibiotics and to an innovative antibacterial drug (CX1). We measured the morphology, surface roughness and elasticity of the bacteria under physiological conditions and exposed to the antibacterial molecules. To go further in the molecules action mechanism, we explored the bacterial cell wall nanoscale organization using functionalized AFM tips. We have demonstrated that affected cells have a molecularly disorganized cell wall; surprisingly long molecules being pulled off from the cell wall by a lectin probe. Finally, we have elucidated the mechanism of action of CX1: it destroys the outer membrane of the bacteria as demonstrated by the results on artificial phospholipidic membranes and on the resistant strain.

During the last three decades, the resistance to antibiotics has increased and disseminated all over the world. Bacteria have developed several ways to resist against almost all antibiotics used and few new effective antibiotics have been discovered so far[1,2]. The return in the pre-antibiotic era[3] seems to be a reality for some infections with multidrug-resistant (MDR) or extremely-drug resistant (XDR) bacteria[4]. *Pseudomonas aeruginosa* is one of these "superbugs"; and infections associated with multidrug-resistant *P. aeruginosa* are having a substantial impact on hospital costs and mortality rates. *P. aeruginosa* is an invasive, Gram negative opportunistic pathogen that causes a wide range of severe infections including bacteraemia, pneumonia, meningitis, urinary tract and wound infections[5]. Moreover, *P. aeruginosa* is naturally resistant to multiple antibiotics; this is due to its natural low outer membrane permeability and to many adaptive resistance mechanisms (loss of porins, surexpression of efflux pumps, presence of many beta-lactamases or carbapenemases…)[5–9]. Most frequently pandrug-resistant *P. aeruginosa* are isolated from wound or respiratory tract infections: resistance including third-generation cephalosporin, carbapenems, fluoroquinolones and aminosides. The last effective antibiotic was often colistin, an old and highly toxic molecule[10,11]. There is therefore, an urgent need for new antibacterials, with an innovative mechanism of action.

Among various approaches to develop new antibacterial agents is one dedicated to cationic compounds[12]. In this work we focused on a polycationic calixarene-based guanidinium compound. Calixarenes are rigid oligomeric phenol macrocycles spatially organized, purely synthetic, with a structure completely different from antibiotics currently used in therapy[13]. Pioneer works demonstrated that our lead compound, the tetra *para*-guanidinoethylcalix[4]arene[13] (named CX1) has a real antibacterial activity with a broad spectrum, including MDR bacteria[14]. The main interest of this new drug is that because of an innovative structure, it will take bacteria some time to find a mechanism of resistance. Moreover we have demonstrated *in vitro* that this compound is not able to select resistant mutant[15]. However the mechanism of action of this new cationic antibacterial drug has not yet been extensively studied. The initial hypothesis is that the introduction of positive charges on the calixarene core (i.e. guanidinium functions) leads to a constrained tetra cation able to disorganize the bacterial cell wall. *P. aeruginosa* possesses a highly negatively charged outer membrane and so is a good candidate to study the interaction with CX1.

Since it's invention in 1986, Atomic Force Microscopy (AFM)[16,17] has created new paradigms in life nanoscience. It gives access to the ultrastructural (imaging, Single Molecule Force Spectroscopy (SMFS)) and nanomechanical (force spectroscopy) properties of single living cells[18–22]. For the study of live bacteria, AFM provides the opportunity to investigate the surface nanostructure under controlled aqueous conditions[23,24]. Therefore it is ideal to study the nanoscale effects of anti-infective drugs on bacteria[25,26].

Results

The approach that we have developed includes several technical aspects of the AFM (imaging living cells, supported bilayers, SMFS, nanomechanical measurements). The experimental components and principle of our approach are described in Fig. 1. *P. aeruginosa* cells were immobilized[27] by taking advantage of the electrostatic interaction between the bacteria's negative charges and a positively charged surface. To this end, glass slides were coated with PolyEthylenImine (PEI), a polycation. Bacteria were then incubated on the PEI coated glass slides for an hour at room temperature[28].

In the first part of this study, we characterized the effects of ticarcillin and tobramycin on the structure and the nanomechanical properties of *P. aeruginosa* ATCC 27853 (reference strain) and PaR3 (clinical strain resistant to almost all antibiotics, antibiogram in Supplemantary data 1). In a second part, by comparing the nano-effects (cell shape alteration, elasticity modifications, cell wall disorganization) caused by them with the ones caused by CX1, we get a better understanding of the mechanism of action of CX1 (Fig.1).

Morphology and surface roughness. The morphological effects, of ticarcillin and tobramycin on the reference strain are presented in Table 1. Supplementary data 2 and 3 present the raw data of respectively morphology and surface roughness. The results show only one analysis, these features were observed on at least 5 bacteria coming from 3 independent cultures. Bacteria in native conditions (without treatment) show a smooth surface. They are 2.2 µm long, 1.1 µm large and 453.5 nm high. We confirmed at the nanoscale, that bacteria growing in the presence of ticarcillin formed filaments of 6 to 18 µm long. For tobramycin, we showed that treated bacteria have a deformed cell wall. These effects of the antibiotics are not observed on the multidrug resistant strain PaR3, demonstrating that these two molecules have no effect on the morphology of the bacteria. Concerning our lead compound, CX1,

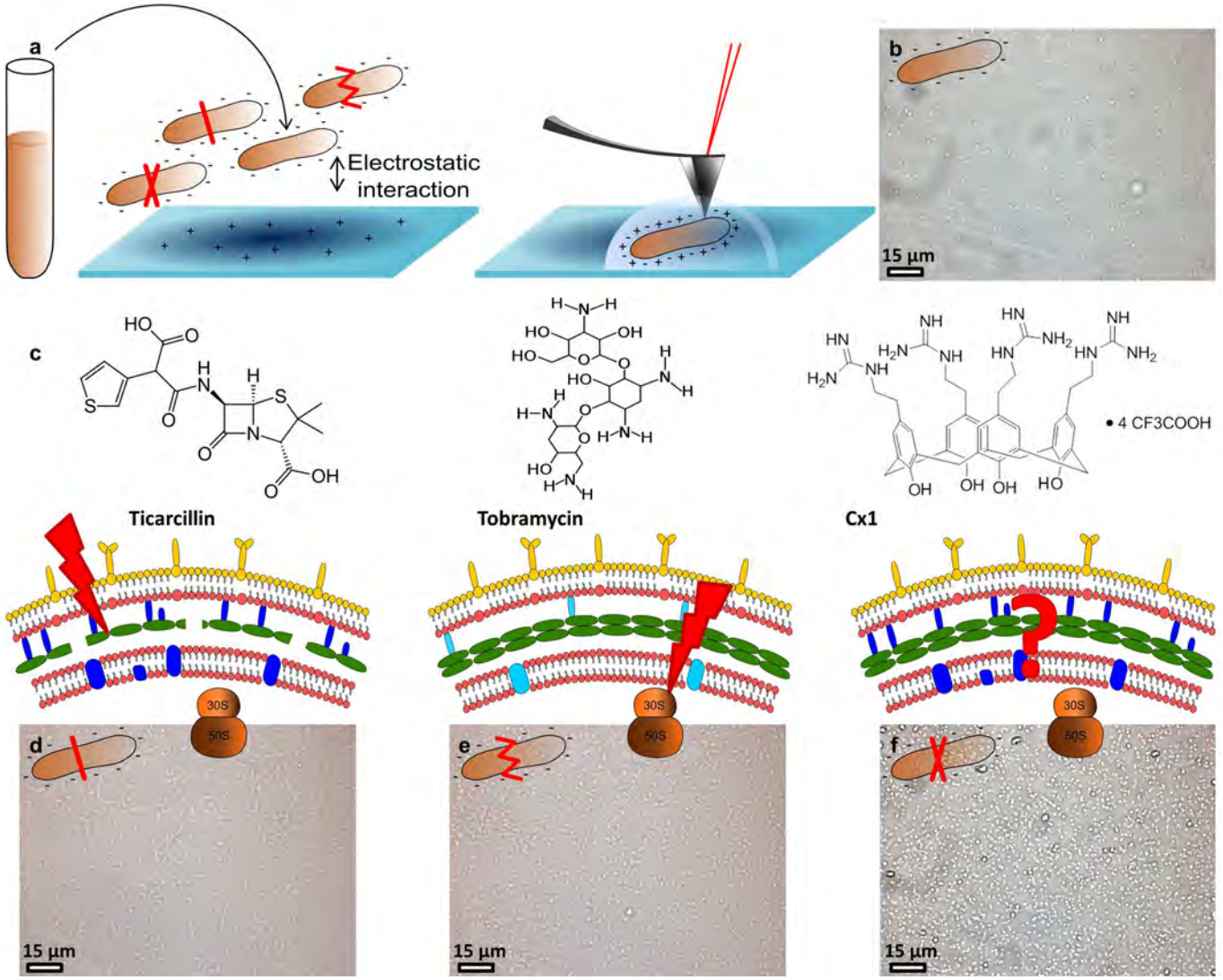

Figure 1 | Schematic representation of the strategy used. (a) cells cultivated in Mueller Hinton broth for 20 hours at 35°C are immobilized on a polyethylenimine coated glass slide for AFM experiments. (b) optical image of the surface covered with immobilized untreated *P. aeruginosa* ATCC 27853. (c) molecules used in the study and their targets. (d) optical images of *P. aeruginosa* ATCC 27853 treated by ticarcillin (4 µg/mL), (e) by tobramycin (0.25 µg/mL) and (f) by CX1 (32 µg/mL).

Table 1 | Recapitulative table of the morphology and roughness results obtained on *P. aeruginosa* ATCC 27853 and PaR3. L stands for length, W stands for width and H stands for height. The analyses were performed on at least 5 different bacteria coming from 3 independent cultures

	ATCC 27853			PaR3		
	Size	Aspect	Roughness	Size	Aspect	Roughness
Native	L: 2.2 ± 0.3 μm W:1.1 ± 0.1 μm H: 453.5 ± 9.5 nm	Smooth	0.2 ± 0.04 nm	L: 1.6 ± 0.2 μm W: 0.6 ± 0.1 μm H: 350.4 ± 14.4 nm	Smooth	0.6 ± 0.1 nm
Ticarcillin	L: Variable W: 1.0 ± 0.3 μm H: 251.1 ± 17.9 nm	Filament	0.6 ± 0.1 nm	L: 1.6 ± 0.1 μm W: 0.6 ± 0.1 μm H: 352.8 ± 33.3 nm	Smooth	0.6 ± 0.1 nm
Tobramycin	L: 3.2 ± 0.8 μm W: 1.1 ± 0.2 μm H: 205.2 ± 30.6 nm	Altered surface	0.6 ± 0.1 nm	L: 1.6 ± 0.1 μm W: 0.6 ± 0.1 μm H: 355.4 ± 37.2 nm	Smooth	0.6 ± 0.1 nm
CX1	L: 2.0 ± 0.2 μm W: 1.3 ± 0.2 μm H: 458.6 ± 51.5 nm	Altered surface	1.0 ± 0.2 nm	L: 1.8 ± 0.1 μm W: 0.6 ± 0.1 μm H: 355.9 ± 36.9 nm	Altered surface	1.5 ± 0.2 nm

we showed that it causes an alteration of the bacterial cell wall on the two different strains, without size modifications. We also focused on the surface roughness as it is a feature that characterizes a bacterial species[25,26,29] (Table 1 and Supplementary Data 3) and showed that the surface of the reference strain was modified by the three molecules: the roughness is increased from 0.2 nm to 0.6 nm in presence of ticarcillin or tobramycin, and to 1.0 nm in presence of CX1. PaR3 presented a smooth surface with no modification of the roughness when grown with antibiotics. When treated by CX1, the surface aspect is modified, showing perforations, and the roughness is increased from 0.6 to 1.5 nm.

Nanomechanical properties. In view of the role of the bacterial cell wall conferring rigidity and protection, we then addressed the pertinent question as to whether the observed structural changes were correlated with differences in the cell wall mechanical properties. To this end, PaR3 treated with ticarcillin, tobramycin or CX1 were probed using nanoindentation measurements (Fig. 2). Several bacteria were probed (global effect) and then local measurements (surface elasticity) were performed on each bacterium present on the global force map (n=5). These experiments were also conducted on *P. aeruginosa* ATCC 27853 (Supplementary data 4). To this end, arrays of 32 by 32 force curves were recorded on each bacterium. All the force curves were then converted into indentation curves and fitted with the Hertz model $F = ((2.E.\tan\alpha)/(\pi.(1-\nu^2)).\delta^2$, where F is the force (experimentally measured), E the Young modulus, α the opening angle of the tip (measured using MEB 35°, data not shown), ν the Poisson ratio (arbitrarily assumed to be 0.5) and δ the indentation (experimentally measured). This procedure gives access to the Young Modulus values that are represented on the histograms on Fig. 2. For each experiment, AFM tips were calibrated using the thermal noise method[30], the spring constant values ranged from 0.012 to 0.019 N/m. The global force maps give information about the multidrug resistant bacterial population behavior towards the different molecules; it seems that only CX1 treated cells have an affected cell wall with a global decreased elasticity compared to antibiotics treated cells. These information were then confirmed with the local nanoindentation measurements that show that untreated PaR3 cells have a Young Modulus of 520 ± 100 kPa, whereas ticarcillin or tobramycin-treated bacteria had a Young Modulus respectively of 300 ± 66 kPa and 252 ± 61 kPa. After treatment by CX1, bacteria presented a Young modulus that drops to 76 ± 28 kPa. These results showed that interestingly, treatment by ticarcillin and tobramycin decreases the cell wall elasticity, but in a reasonable range. CX1, however, dramatically decreases the cell wall elasticity.

Single molecule force spectroscopy. At this stage of the work, we know that CX1 disorganizes the cell wall of *P. aeruginosa*, but we still do not know how. To go further, dendritips[31,32] were functionalized with lectin ConcanavalinA (ConA). ConA binding structure and specificity have been well determined for mannose-containing structures[33–35], including recognition of biantennary, complex N-glycans[36], and for terminal glucose[35]. These lectin tips were then used to perform adhesion force maps on bacteria in their native environment, or after treatment by the three molecules. Fig. 3 shows the force curves recorded on the two strains in the different conditions. We can see that force curves recorded on both untreated strains showed no adhesions (Fig. 3b). After ticarcillin or tobramycin treatment, the reference strain showed force curves presenting many adhesions, and PaR3 showed nothing but flat curves (Fig. 3c and 3e). In Fig. 4, the distributions of the breaking forces and the ruptures distances (as sketched in Fig. 4g) were represented in histograms, for the conditions for which force curves showed adhesions. First, for the reference strain, with ticarcillin (Fig. 4a and 4b), the adhesion forces reached 98 ± 56 pN. Only a small fraction of these adhesions happened between 0 and 1 μm (3%), the major part ranging from 2 to 6 μm. With tobramycin (Fig. 4c) the force curves showed multiple adhesions. The adhesion force histogram (Fig. 4d) shows that forces only reach 37 ± 1 pN which is more or less three times less than with ticarcillin. Similar results were obtained with CX1; adhesions were ranging from 0 to 5 μm (Fig. 4e), and forces reached 186 ± 206 pN (Fig. 4f). For PaR3, we have previously showed that only CX1 conducted to a decrease in the elasticity of the cell wall. On the force curves recorded on PaR3 with a lectin probe, we observed adhesions ranging from 0 to 6 μm (Fig. 4j), and that reached 135 ±127 pN (Fig. 4k). The pulled out molecules are surprisingly long (up to 6 μm), much longer than the bacteria itself.

Effects of CX1 on supported bilayers. In order to mimic the effect of CX1 on the outer membrane of *P. aeruginosa*, we created phospholipidic bilayers supported on mica leaves with lipids widely found in bacterial outer membranes; POPE (1-Palmitoyl-2-oleoyl-sn-glycero-3-phosophoethanolamine) and POPG (1-Palmitoyl-2-oleoyl-sn-glycero-3-phosphatidylglycerol) (2:1)[37]. The method was previously described and has proven useful for the understanding of surfactin effect on lipid bilayer[38]. The results showed in Fig. 5 present these bilayers treated by CX1 at a concentration of 10 μg/mL. We have seen that in 1 hour, holes were created in the synthetic membrane. Those holes could be compared to the one observed in the cell wall of PaR3 treated by CX1 (Fig. 5e and 5f), which allowed us to think that CX1, with its spatial organization and its charges, is able to create perforations in the bacterial outer membrane.

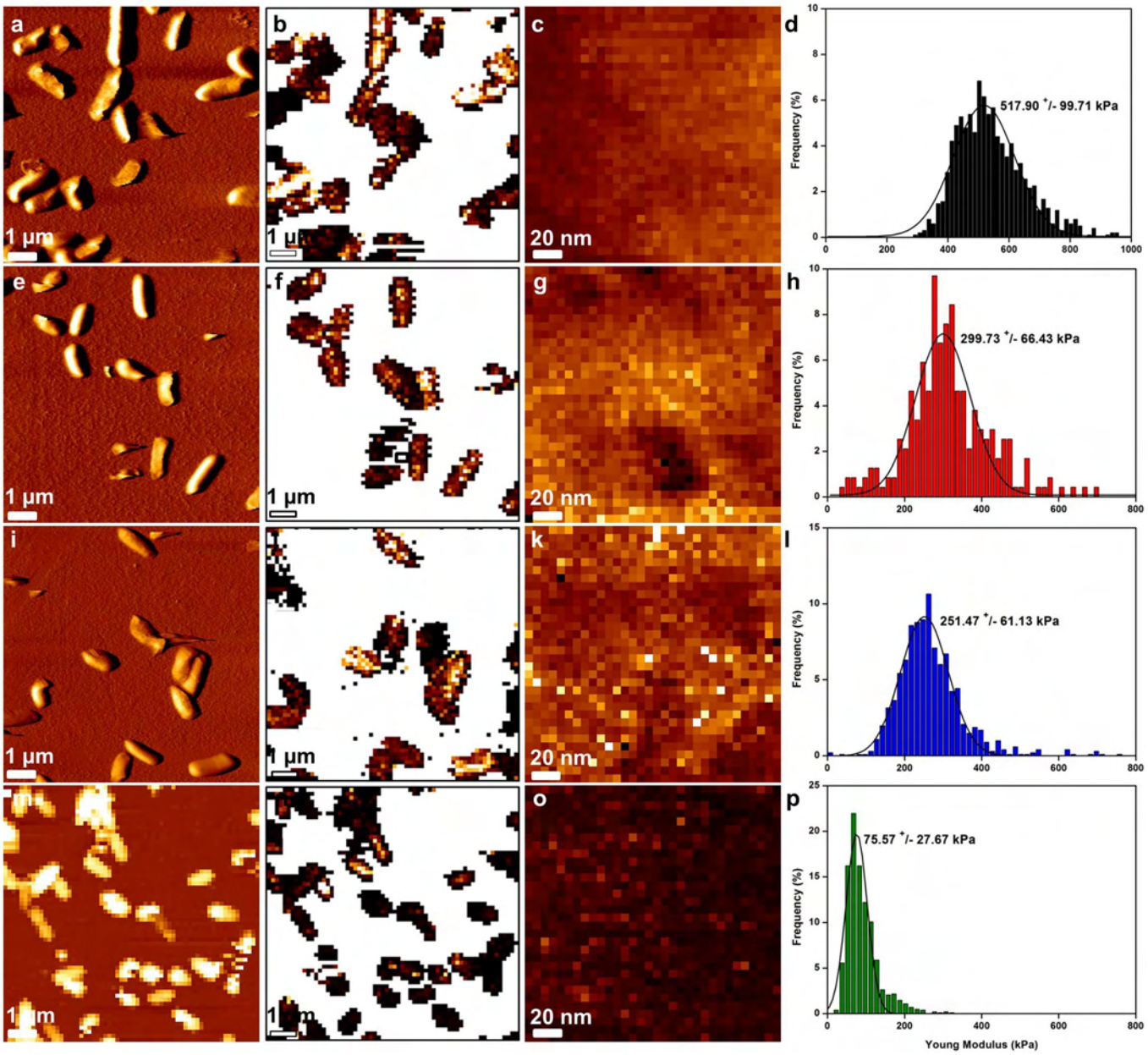

Figure 2 | Mapping of *P. aeruginosa* R3 cell surface elasticity. (a) vertical deflection image of native cells, (e) ticarcillin-treated cells (4 µg/mL), (i) tobramycin-treated cells (0.25 µg/mL). (m) height image (z-range = 800 nm) of CX1-treated cells (32 µg/mL). (b), (f), (j) and (n), elasticity maps (z-range = 1.5 MPa) corresponding to the vertical deflection images. (c), (g), (k) and (o), local elasticity maps (z-range = 800 kPa) recorded on one bacterium from the corresponding vertical deflection images. (d), (h), (l) and (p), distributions of Young Modulus values corresponding to the local elasticity maps.

Discussion

We choose to work with two strains of *P. aeruginosa*; a reference strain susceptible to antibiotics (ATCC 27853), and a clinical isolate (PaR3, ABC Platform® Bugs Bank) collected from a respiratory sample, resistant to almost all antibiotics (antibiotic susceptibility profile is given in Supplementary data 1). This isolate is resistant to ticarcillin and tobramycin, two antibiotics widely used in *P. aeruginosa* infections. The first one belongs to the β-lactams family, and inhibits the peptidoglycan synthesis by interacting with the Penicillin Binding Proteins (PBP). After treatment by ticarcillin, filamentous forms of *P. aeruginosa* are described[28,39]. This is caused by the fact that β-lactams like ticarcillin activate the SOS system of bacteria, therefore inhibiting the cell division[39]. Tobramycin belongs to the aminoglycosides family and interacts with the 30S ribosomal sub-unit. This leads to the synthesis of abnormal proteins which are then incorporated to the cell wall, which loses its integrity.

The results of surface roughness, consistent with the morphology analysis, showed that only CX1 is able to alter the cell wall of PaR3 and this is our first clue; thus, we have originally emphasized the fact that PaR3 is resistant to ticarcillin and tobramycin. However, we can hypothesize that the resistance mechanism must either have an energy cost, or result in a cell wall modification since the elasticity is a little decreased by classical antibiotics. So after 24 hours of growing in the presence of the antibiotics, PaR3 cell wall seems to be affected in an insignificant way. With CX1, the elasticity decreased, indicating that the integrity of the wall is compromised. PaR3 is unable to resist to the disorganization of the cell wall induced by CX1, whereas it resists to the one induced by ticarcillin and tobramycin. So, we showed that an innovative molecule, like CX1, is able

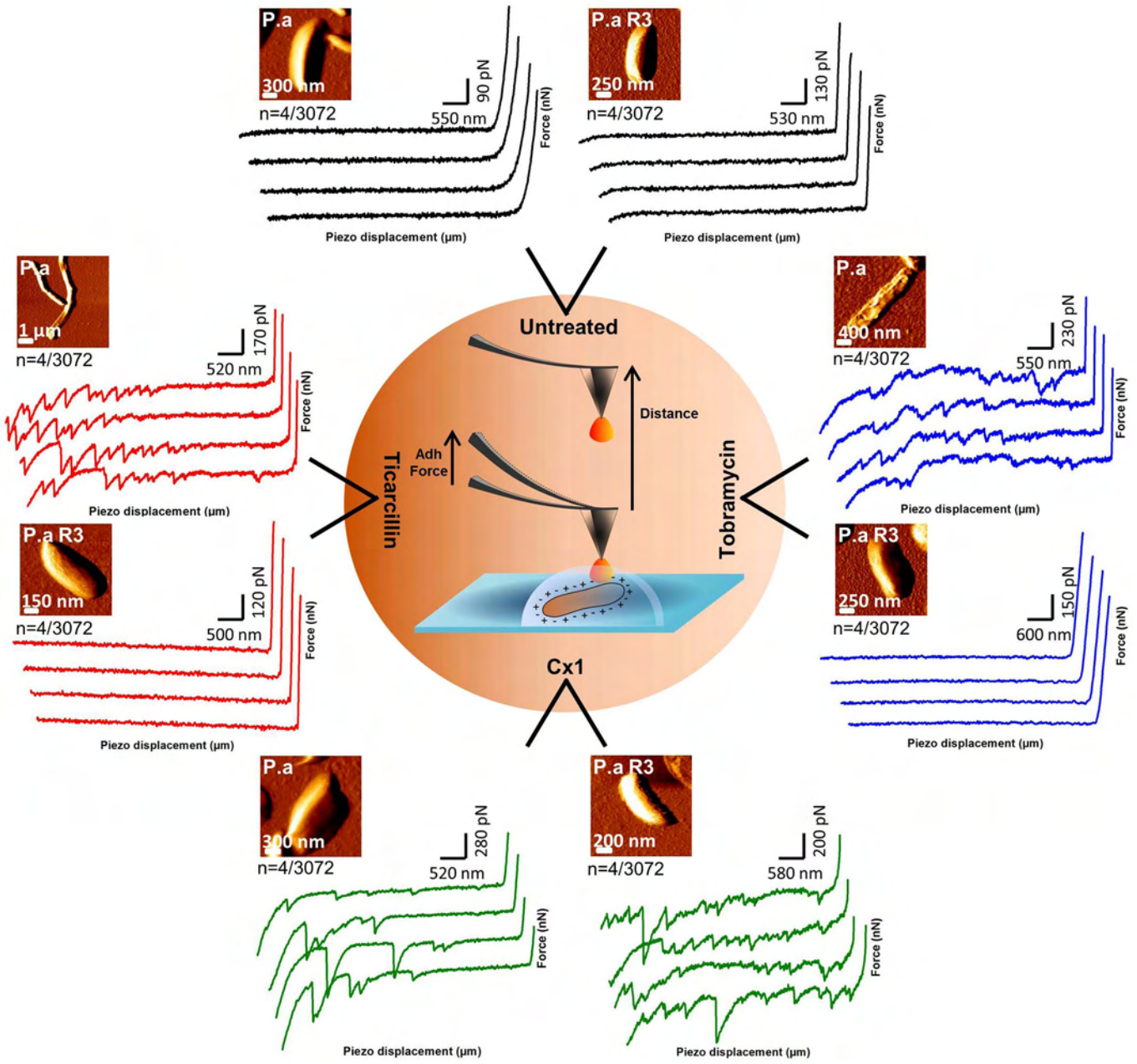

Figure 3 | Force spectroscopy of the ConA-tip interactions. Schematic representation of the force curves (retract segment) obtained with ConcanavalinA functionalized tips on *P. aeruginosa* ATCC 27853 and PaR3 in native conditions, treated by ticarcillin (4 µg/mL), tobramycin (0.25 µg/mL) and CX1 (32 µg/mL). The 4 force curves (n) presented by conditions were chosen out of 3072 curves recorded on 3 different bacteria coming from 3 independent cultures.

to disorganize the cell wall of a MDR *P. aeruginosa*. The bacterial cell wall plays several roles, it is a barrier that withstands the osmotic pressure, it gives shape to the cells, ensures communication with the environment. Thus the cell wall disorganization is another proof showing that CX1 is an efficient antimicrobial molecule against a resistant strain of *P. aeruginosa*.

The next step in this investigation has been to explore at the molecular level, the effects of the antibiotics and of CX1. To this end we used lectin functionalized AFM probes and looked at what could be pulled out from the surface (fig. 3 and 4). PaR3 showed nothing but flat curves with ticarcillin and tobramycin. This can be explained by the fact that PaR3 cell wall was not disorganized and no molecules could be pulled out from the surface by the functionalized AFM tip. But interestingly, when CX1 was used to treat the different bacterial strains, multiple adhesions could be seen on the force curves (Fig. 3d). These new results are consistent with the nanomechanical evidence. CX1 disorganizes the bacterial cell at the molecular level. On the reference strain, antibiotics and CX1 disorganized the cell wall leading to a dramatic decrease of the elasticity (Supplementary data 4) and to the stretching of surprisingly long glycans (lectin recognition) molecules. We must, therefore, have unfolded a super coiled molecule. Recently, Andre *et al* studied the architecture of peptidoglycan in *Bacillus subtilis*[40], and showed that glycan strands could be polymerized and crosslinked to form a peptidoglycan rope, which would then be coiled into a helical cable. Hayhurst *et al*[41] worked on the same bacteria and showed that glycan strands were up to 5 µm, so way longer than the cell itself. The authors also proposed a coiled-coil model for peptidoglycan architecture. Following these ideas, our AFM tips could pull the peptidoglycan and uncoil it on large distances, consistently with the force curves

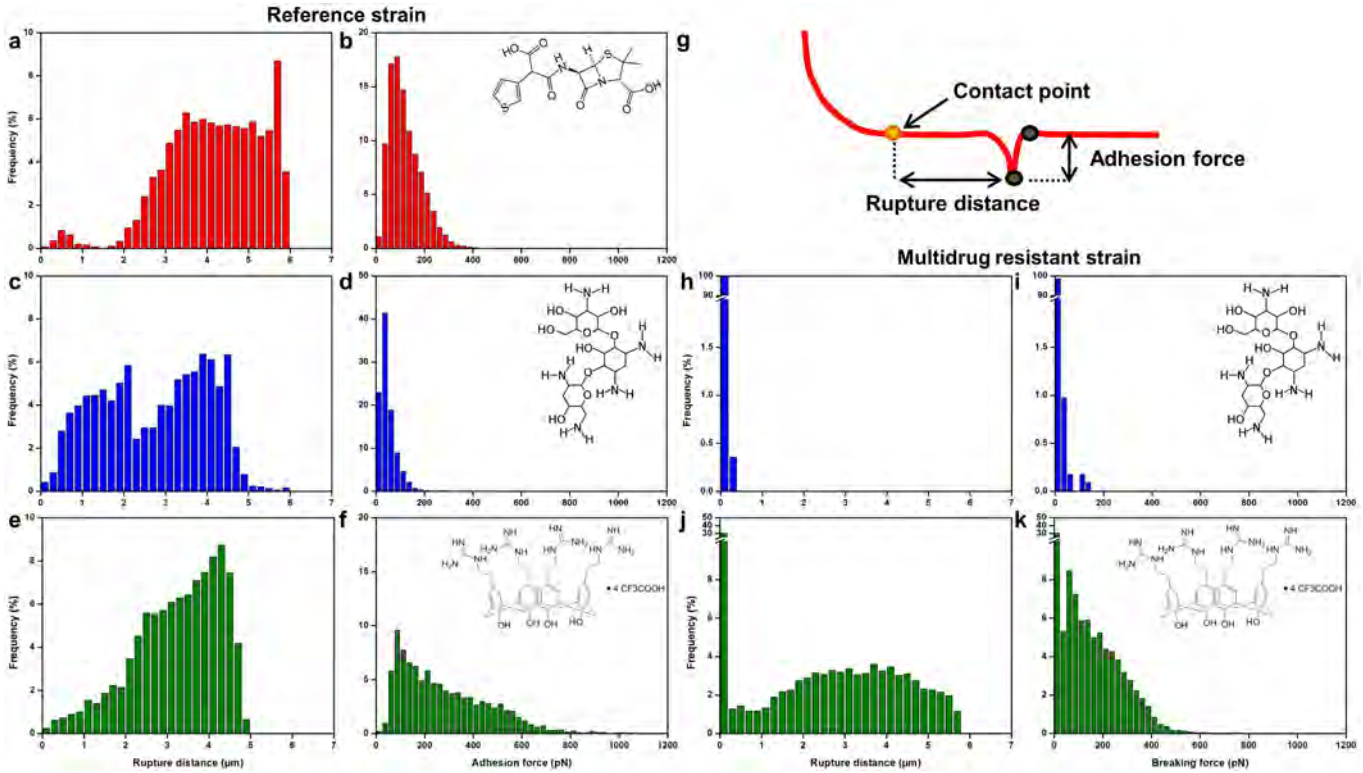

Figure 4 | Force spectroscopy of the ConA-tips interactions. (a), adhesion force histograms (n = 1024 force curves) obtained on *P. aeruginosa* ATCC 27853 ticarcillin-treated cells (4 µg/mL), (c), tobramycin-treated cells (0.25 µg/mL) and (e), CX1-treated cells (32 µg/mL). (b), (d) and (f), corresponding rupture distance histograms. (g), schematic representation of how the retract segment of the force curves were analyzed. (h), adhesion force histograms (n = 1024 force curves) obtained on *P. aeruginosa* R3 tobramycin-treated cells (0.25 µg/mL) and (j), CX1-treated cells (32 µg/mL). (i) and (k), corresponding rupture distance histograms.

observed in Fig. 3. In Gram-negative bacteria, a thin peptidoglycan layer is overlaid by a bilayers of phospholipids and lipopolysaccharids containing membrane proteins (for example porins, Braun lipoproteins)[40]. When bacteria are in native conditions, the peptidoglycan is very well organized and covered by the outer membrane, thus inaccessible for the lectin probe, resulting in no adhesive behavior when probed with a lectin tip. But when the ATCC strain is treated by ticarcillin, the landscape is different. Ticarcillin binds to transmembrane enzymes: carboxypeptidase and transpeptidase respectively responsible for the cleavage of the DAla-DAla motif and the assembly of the cleaved pentapeptides. The bacteria are thus unable to grow normally which leads to the activation of their SOS system. This results in extraordinary long bacteria (sometimes longer than 10 µm). Nevertheless, at the extremity of these "spaghetti"-like bacteria, a 2 µm long part of normal peptidoglycan remains. So when pulling with the lectin probe on the first 2 µm at the extremity of the bacteria, nothing happens. Then, new abnormal peptidoglycan is pulled out, which results in the force curves presented in Fig. 3.

With tobramycin, it is the protein synthesis of the ATCC 27853 strain that is altered. Braun lipoproteins and porins are essential components of the outer membrane structure. It is therefore not surprising that we can access to the peptidoglycan through the altered membrane. As the Young modulus is highly affected by tobramycin, it is also straight that the peptidoglycan is affected, but this is not yet described. However tobramycin inhibits the synthesis of all proteins among which the enzymes involved in the peptidoglycan synthesis. It is therefore not surprising that the peptidoglycan of tobramycin treated cells is abnormal and could lead to the force curves profile presented in Fig. 3c.

Finally, with CX1, it is even clearer that the peptidoglycan is affected for both the ATCC and the multidrug resistant strain PaR3; the Young modulus drops, indeed, dramatically. However, it must be noticed that for the ATCC strain; the force curves in Fig. 3d show less adhesive events with CX1 treatment than with ticarcillin or tobramycin treatment. This is not true with PaR3 which seems very affected by CX1.

A keen analyze conducted on the force curves presented on Fig. 3 shows that the distance between each adhesive event, when occurring, is of 280 ± 155 nm ($277 > n > 290$ according to the condition). As Vollmer *et al.*[42] proposed in a recent work, the glycan strands of *P. aeruginosa* are 17 nm long. In line with this data, and consistently with the architectural model of the peptidoglycan proposed by Dufrêne and Foster's teams, it seems like our functionalized AFM tip pulls out from the damaged bacteria the peptidoglycan by "packs" of glycans strands. In Gram-negative bacteria, the peptidoglycan layer is encored to the outer membrane by the Braun lipoproteins. These "packs" of glycan strands could then correspond to the distances between the Braun lipoproteins all along the bacteria. Ticarcillin, tobramycin and CX1 treatments induce, indeed, the same distance rupture between the adhesive events. This means that although the 3 molecules have completely different mechanism of action, they induce somehow the same disorder. Therefore the hypothesis of the distance between the Braun lipoproteins is consolidated. Braun lipoproteins synthesis is inhibited by tobramycin and they make the link between the peptidoglycan (ticarcillin inhibits its synthesis) and the outer membrane (CX1 deeply alter phospholipid bilayers as it will be demonstrated in the next paragraph). If these new data gives light on the architecture of Gram negative bacteria cell wall, the fundamental mechanism of action of CX1 still remains unclear. We suppose that, when the positively charged calixarene, interacts with the negatively charged ultrastructures of the bacterial surface (i.e. phospholipids and lipopolysaccharides), its particular three-dimensional organization causes disruptions of the outer membrane of the cell wall as suggested by the increased surface

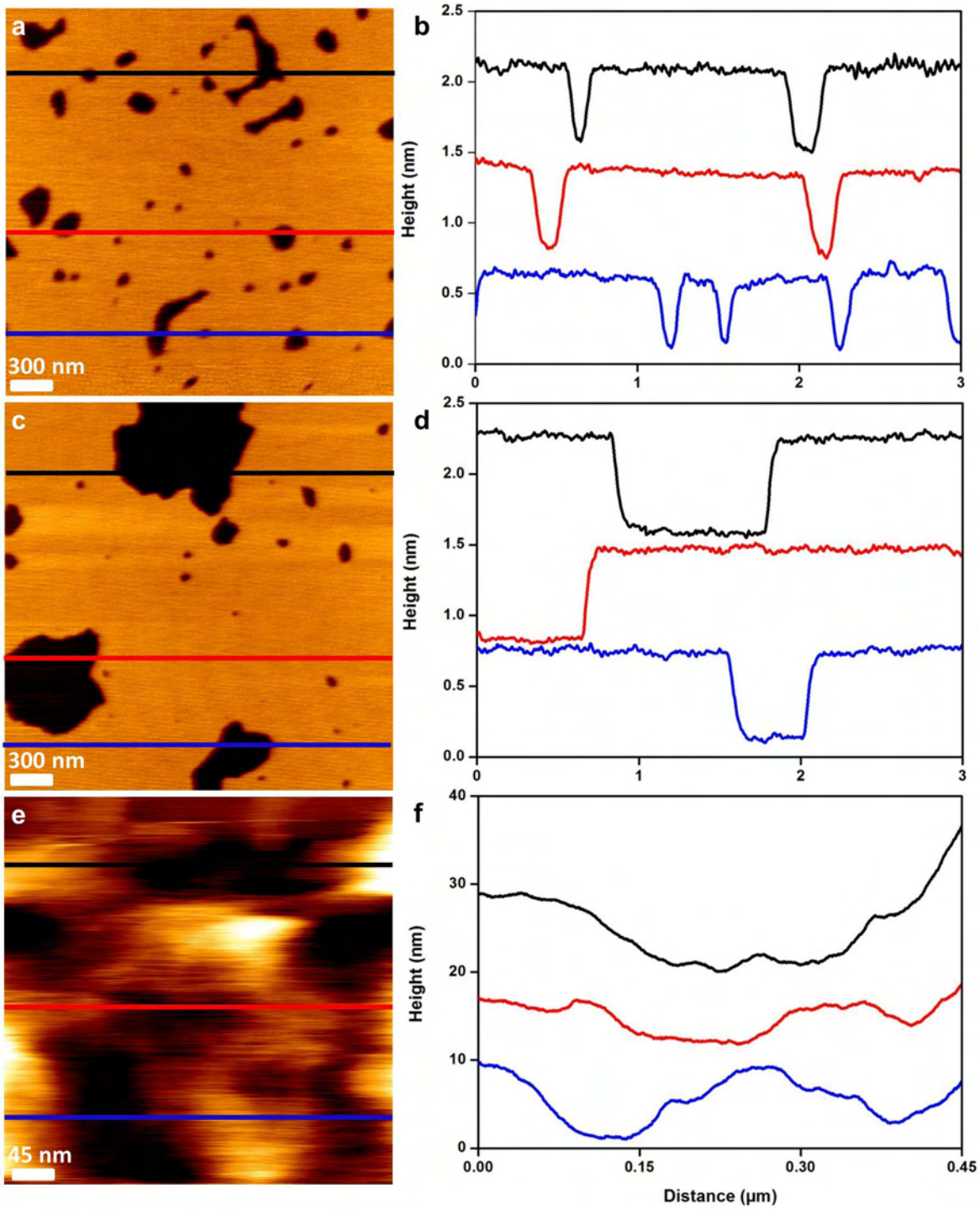

Figure 5 | POPE:POPG (2:1) supported bilayers. (a), height images (z-range = 1.5 nm) of POPE:POPG (2:1) supported bilayers at t=0 minutes after treatment by CX1 (0.01 mg/mL), and (c), 1 hour after treatment. (e), height images (z-range = 600 nm) of PaR3 treated by CX1 (32 μg/mL). (b), (d) and (f), cross sections taken along the colored lines on the images.

roughness (Supplementary data 4) which is in line with the mechanism of action described for cationic antimicrobial peptides[43–46].

These AFM experiments, conducted on two *P. aeruginosa* strains, a susceptible one (ATCC 27853) and a resistant one (PaR3), has allowed us to evaluate the effects of three different antibacterial molecules. The in depth analysis of AFM raw data collected on treated bacteria is an original way to get fundamental knowledge on the bacterial cell wall organization. These results confirm that CX1 is efficient on resistant bacteria and has a different mechanism of action as tobramycin and or ticarcillin. Also, these very new results allowed us to make an hypothesis on the potential mechanism of action of the CX1; it interacts with the surface of the Gram-negative bacteria and creates holes in the outer membrane. This hypothesis was then confirmed by the experiments conducted on the supported biomembranes that showed destruction by creation of holes. Interestingly it has been demonstrated that CX1 has no side effects on eukaryotic HaCaT cells[14] or on membranes made of zwiterrionic phospholipids (DMPC, DMPS)[47].

It is also obvious that CX1 damage the peptidoglycan as we saw on the nanoindentations results, and therefore there is no reason why

CX1 could not reach and damage the inner membrane. The next step is now to determine if CX1 has also an intracellular target, which has not been explored yet.

Methods

Bacteria growth conditions. The bacteria (ATCC 27853) (reference strain for the Comité de l'Antibiogramme de la Société Française de Microbiologie, CA-SFM, the European Committee on Antimicrobial Susceptibility Testing, EUCAST, and the Clinical and Laboratory Standards Institute, CLSI) and Pa R3 (isolated from a respiratory sample, ABC platform® Bugs Bank) were stocked at −80 °C, revivified on Mueller Hinton Agar (Difco, 225250-500 g) and grown in Mueller Hinton Broth (Difco, 275730-500 g) for 24 hours at 35°C under static conditions.

Antibiotic treatments. The antibiotics were added during the 18 to 24 hours before the experiments.

Before AFM measurements were conducted, bacteria were grown in Mueller Hinton broth containing the antibiotics at a concentration of 4 µg/mL for ticarcillin (Sigma, T5639-1 g), 0.25 µg/mL for tobramycin (Sigma, T4014-100 mg), and 32 µg/mL for CX1 for 24 hours at 35°C.

Sample preparation for AFM experiments. Cells were concentrated by centrifugation, washed 2 times in Milli-Q water, re-suspended in PBS 1X (Sigma, P2194-10PAK) to a concentration of ~ 10^8 cells/mL, and immobilized on PEI (Fluka P3142-100 mL) coated glass slides (prepared as described elsewhere e.g.[48]). Briefly, freshly oxygen activated glass slides were covered by a 0.2% PEI solution in deionized water and left for incubation overnight. Then the glass slides were rinsed with 20 mL of Milli-Q water and nitrogen dried. A total of 1 mL of the bacterial suspension was then applied to the PEI coated glass slide, allowed to stand for one hour and rinsed with PBS 1X. Images were recorded in PBS 1x in contact mode with MLCT AUHW cantilever (nominal spring constant 0.01 N/m). The applied force was kept as low as possible around 200 pN. For imaging and force spectroscopy we used an AFM Nanowizard II and III (JPK instruments, Berlin, Germany). The cantilevers spring constant were measured by the thermal noise methods[30,49] ranging 14.56 to 15.20 mN/m. The functionalized tips were produced according to a french patent of the authors[31] described later in sensors and actuators[32]. Briefly, AFM tips are functionalized with dendrimers presenting CHO functions able to covalently link with NH2 functions of proteins. Those dendritips are then incubated with the lectin concanavalin A (Sigma, L7647-100MG, 100µg/mL) for 1 hour, before being used for force spectroscopy experiments.

Phospholipid bilayers. POPE (1-Palmitoyl-2-oleoyl-sn-glycero-3-phosophoethanolamine) and POPG (1-Palmitoyl-2-oleoyl-sn-glycero-3-phosphatidylglycerol) (Avanti Polar Lipids) were dissolved in $CHCl_3$ (2:1) and mixed in glass tubes to obtain the desired concentration. The solvent was evaporated with nitrogen and dried in a dessicator. Dried films were maintained under reduced pressure overnight and thereafter rehydrated using PBS 10 mM, 1 mM $CaCl_2$, 1 mM $MnCl_2$, pH 7.4. To obtain small unilamellar vesicles (SUVs), the suspension was sonicated to clarity (3 cycles of 3 min) using a 500W probe sonicator (Fisher Bioblock Scientific, France; 35% of the maximal power) while keeping the suspension in an ice bath. The suspension was finally centrifuged (5 min, 15000 g). The SUV solution was then put into contact with freshly cleaved mica substrates for 45 min at room temperature. Then samples were imaged using hyperdrive mode from Nanowizard III JPK instrument and PPP-NCHAuD-10 probes provided by Nanosensors.

1. Taubes, G. The Bacteria fight back. *Science* **321**, 356–361 (2008).
2. Payne, D. J. Desperately seeking new antibiotics. *Science* **321**, 1644–1645 (2008).
3. Paterson, D. L. & Lipman, J. Returning to the pre-antibiotic era in the critically ill: The XDR problem. *Crit. Care Med.* **35**, 1789–1791 (2007).
4. Lipsitch, M., Bergstrom, C. T. & Levin, B. R. The epidemiology of antibiotic resistance in hospitals: Paradoxes and prescriptions. *Proc. Natl. Acad. Sci. USA* **97**, 1938–1943 (2000).
5. Hauser, A. R. & Ozer, E. A. *Pseudomonas aeruginosa. Nat. rev. Microbiol.* **9**, Poster (2011).
6. Skiada, A., Markogiannakis, A., Plachouras, D. & Daikos, G. L. Adaptive resistance to cationic compounds in *Pseudomonas aeruginosa*. *Int. J. Antimicrob. Agents* **37**, 187–193 (2011).
7. Lister, P. D., Wolter, D. J. & Hanson, N. D. Antibacterial-Resistant Pseudomonas aeruginosa: Clinical Impact and Complex Regulation of Chromosomally Encoded Resistance Mechanisms. *Clin. Microbiol. Rev.* **22**, 582–610 (2009).
8. Strateva, T. & Yordanov, D. *Pseudomonas aeruginosa*: a phenomenon of bacterial resistance. *J. Med. Microbiol.* **59** (2009).
9. Breidenstein, E. B. M., de la Fuente-Núñez, C. & Hancock, R. E. *Pseudomonas aeruginosa: all roads lead to resistance. Trends Microbiol.* **19**, 419–426 (2011).
10. Mortensen, N. P. *et al.* Effects of colistin on surface ultrastructure and nanomechanics of *Pseudomonas aeruginosa* cells. *Langmuir* **25**, 3728-3733 (2009).
11. Soon, R. L. *et al.* Effect of colistin exposure and growth phase on the surface properties of live *Acinetobacter baumannii* cells examined by atomic force microscopy. *Int. J. Antimicrob. Agents* **38**, 493–501 (2011).
12. Yin, L. M., Edwards, M. A., Li, J., Yip, C. M. & Deber, C. M. Roles of hydrophobicity and charge distribution of cationic antimicrobial peptides in peptide-membrane interactions. *J. Biol. Chem.* **287**, 7738–7745 (2012).
13. Mourer, M., Duval, R. E., Finance, C. & Regnouf-de-Vains, J.-B. Functional organisation and gain of activity: The case of the antibacterial tetra-para-guanidinoethyl-calix[4]arene. *Bioorg. Med. Chem. Lett.* **16**, 2960–2963 (2006).
14. Grare, M. *et al.* In vitro activity of para-guanidinoethylcalix[4]arene against susceptible and antibiotic-resistant Gram-negative and Gram-positive bacteria. *J. Antimicrob. Chemother.* **60**, 575–581 (2007).
15. Grare, M. *et al.* In vitro mutation studies with a new promising compound, the para-guanidinoethylcalix[4]arene. *Abstr. 48th Intersci. Conf. Antimicrob. Agents Chemother., abstr. F1-3951* (2008).
16. Binnig, G., Rohrer, H., Gerber, C. & Weibel, E. Tunneling through a controllable vacuum gap. *Appl. Phys. Lett.* **40**, 178–180 (1982).
17. Binnig, G. & Quate, C. F. Atomic force microscope. *Phys. rev. lett.* **56**, 930–933 (1986).
18. Muller, D. J., Helenius, J., Alsteens, D. & Dufrene, Y. F. Force probing surfaces of living cells to molecular resolution. *Nat. Chem. Biol.* **5**, 383–390 (2009).
19. Dufrêne, Y. F. & Müller, D. J. Atomic Force Microscopy as a multifunctional molecular toolbox in nanobiotechnology. *Nat. Nanotechnol.* **3**, 261–269 (2008).
20. Cross, S. E., Jin, Y.-S., Rao, J. & Gimzewski, J. K. Nanomechanical analysis of cells from cancer patients. *Nat. Nanotechnol.* **2**, 780–783 (2007).
21. Buzhynskyy, N., Girmens, J.-F., Faigle, W. & Scheuring, S. Human cataract lens membrane at subnanometer resolution. *J. Mol. Biol.* **374**, 162–169 (2007).
22. Stolz, M. *et al.* Early detection of aging cartilage and osteoarthritis in mice and patient samples using atomic force microscopy. *Nat. Nanotechnol.* **4**, 186–192 (2009).
23. Liu, S. & Wang, Y. Application of AFM in microbiology: a review. *Scanning* **32**, 61–73 (2010).
24. Dorobantu, L. S. & Gray, M. R. Application of atomic force microscopy in bacterial research. *Scanning* **32**, 74–96 (2010).
25. Alsteens, D. *et al.* Organization of the mycobacterial cell wall: a nanoscale view. *Pflugers Arch.* **456**, 117–125 (2008).
26. Francius, G., Domenech, O., Mingeot-Leclercq, M. P. & Dufrêne, Y. F. Direct observation of *Staphylococcus aureus* cell wall digestion by lysostaphin. *J. Bact.* **190**, 7904–7909 (2008).
27. El Kirat, K., Burton, I., Dupres, V. & Dufrene, Y. F. Sample preparation procedures for biological atomic force microscopy. *J. Microsc.* **218**, 199–207 (2005).
28. Formosa, C., Grare, M., Duval, R. E. & Dague, E. Nanoscale effects of antibiotics on *P. aeruginosa*. *Nanomed. Nanotechnol. Biol. Med.* **8**, 12–16 (2012).
29. Francius, G. *et al.* Conformational analysis of single polysaccharide molecule on live bacteria. *ACS Nano* **2**, 1921–1929 (2008).
30. Emerson Iv, R. J. & Camesano, T. A. On the importance of precise calibration techniques for an atomic force microscope. *Ultramicroscopy* **106**, 413–422 (2006).
31. Dague, E., Jauvert, E. & Trevisiol, E. France Pointe de microscope à force atomique modifiée et biomodifiée, 2010 n° dépôt 10 57932, 30/09/2010
32. Jauvert, E. *et al.* Probing single molecule interactions by AFM using bio-functionalized dendritips. *Sens. Actuators B Chem.* **168**, 436–441 (2012).
33. Hardman, K. D. & Ainsworth, C. F. Structure of concanavalin A at 2.4-A resolution. *Biochem.* **11**, 4910–4919 (1972).
34. Naismith, J. H. & Field, R. A. Structural Basis of Trimannoside Recognition by Concanavalin A. *J. Biol. Chem.* **271**, 972–976 (1996).
35. Gupta, D., Dam, T. K., Oscarson, S. & Brewer, C. F. Thermodynamics of lectin-carbohydrate interactions. *J. Biol. Chem.* **272**, 6388–6392 (1997).
36. Moothoo, D. N. & Naismith, J. H. Concanavalin A distorts the beta-GlcNAc-(1-2)-Man linkage of beta-GlcNAc-(1-2)-alpha-Man-(1-3)-[beta-GlcNAc-(1-2)-alpha-Man-(1-6)]-Man upon binding. *Glycobiol.* **8**, 173–181 (1998).
37. Fotiadis, D. Atomic force microscopy for the study of membrane proteins. *Curr. Opin. Biotechnol.* (In Press).
38. Francius, G. *et al.* Nanoscale membrane activity of surfactins: Influence of geometry, charge and hydrophobicity. *Biochim. Biophys. Acta* **1778**, 2058–2068 (2008).
39. Prior, R. B. & Warner, J. F. Morphological alterations of *Pseudomonas aeruginosa* by ticarcillin: a scanning electron microscope study. *Antimicrob. Agents Chemother.* **6**, 853–855 (1974).
40. Andre, G. *et al.* Imaging the nanoscale organization of peptidoglycan in living Lactococcus lactis cells. *Nat. Commun.* **1**, 27 (2010).
41. Hayhurst, E. J., Kailas, L., Hobbs, J. K. & Foster, S. J. Cell wall peptidoglycan architecture in *Bacillus subtilis*. *Proc. Natl. Acad. Sci.* **105**, 14603–14608 (2008).
42. Vollmer, W. & Seligman, S. J. Architecture of peptidoglycan: more data and more models. *Trends Microbiol.* **18**, 59–66 (2010).
43. Jenssen, H., Hamill, P. & Hancock, R. E. W. Peptide antimicrobial agents. *Clin. Microbiol. Rev.* **19**, 491–511 (2006).
44. Finlay, B. B. & Hancock, R. E. W. Can innate immunity be enhanced to treat microbial infections? *Nat. Rev. Microbiol.* **2**, 497–504 (2004).
45. McPhee, J. B., Lewenza, S. & Hancock, R. E. W. Cationic antimicrobial peptides activate a two-component regulatory system, PmrA-PmrB, that regulates resistance to polymyxin B and cationic antimicrobial peptides in Pseudomonas aeruginosa. *Mol. Microbiol.* **50**, 205–217 (2003).

46. Hancock, R. E. W. & Patrzykat, A. Clinical development of cationic antimicrobial peptides: from natural to novel antibiotics. *Curr. Drug Targets Infect. Disord.* **2**, 79–83 (2002).
47. Sautrey, G. *et al*. Membrane activity of tetra-*p*-guanidinoethylcalix[4]arene as a possible reason for its antibacterial properties.*J. Phys. Chem. B* **115**, 15002–15012 (2011).
48. Francius, G., Tesson, B., Dague, E., Martin-Jézéquel, V. & Dufrêne, Y. F. Nanostructure and nanomechanics of live *Phaeodactylum tricornutum* morphotypes. *Environ. Microbiol.* **10**, 1344–1356 (2008).
49. Hutter, J. L. & Bechhoefer, J. Calibration of Atomic Force Microscope tips. *Rev. Sci. Instrum.* **64**, 1868 (1993).

Acknowledgements

ED is a researcher of Centre National de la Recherche Scientifique (CNRS). CF received funding from Direction Générale de l'Armement (DGA) and Agence Nationale pour la Recherche (ANR). We thank the program Young Scientist from ANR and especially the AFMYST project. The authors thank UMS 3039 ITAV for the use of the AFM facilities.

Authors contribution

ED and RED are the leads author of the paper. ED, RED, MG and CF conceived-designed the experiments and wrote the article. CF made the experimental work and the data analysis work. EJ and AC worked on the experimental protocols and prepared respectively dendritips and phospholipid bilayers. MM and JBRdV conceived CX1 as a possible antibacterial agent and furnished batch used in this study. All the authors discussed the results and commented on the manuscript.

Additional information

Supplementary information accompanies this paper at http://www.nature.com/scientificreports

Competing financial interests: The authors declare no competing financial interests.

How to cite this article: Formosa, C. *et al*. Nanoscale analysis of the effects of antibiotics and CX1 on a *Pseudomonas aeruginosa* multidrug-resistant strain. *Sci. Rep.* **2**, 575; DOI:10.1038/srep00575 (2012).

Chapitre 4

Résumé de la thèse en français

Chapitre 4.1. Introduction

Chapitre 4.2. Développements technologiques pour étudier la paroi des microorganismes par AFM.

Chapitre 4.3. Etude à l'échelle nanométrique de la paroi *de Saccharomyces cerevisiae* et *Candida albicans.*

Chapitre 4.4. Comportement nanométrique de la paroi bactérienne en réponse au traitement par des antibiotiques

Chapitre 4.5. L'AFM pour comprendre le mécanisme d'action d'une nouvelle molécule antibactérienne

Cette partie décrit les résultats obtenus au cours de ma thèse de façon résumée. L'analyse bibliographique se trouve dans le Chapitre 1.

Chapitre 4.1 : Introduction

Ce travail consiste à utiliser les techniques de Microscopie à Force Atomique (AFM) pour étudier la paroi de microorganismes pathogènes, et pour évaluer leurs interactions avec des antimicrobiens. Ces trois dernières décennies, la résistance microbienne a augmenté de façon drastique et s'est propagée dans le monde. Les bactéries et levures pathogènes ont développé différents moyens pour résister à presque tous les antimicrobiens utilisés. Ces pathogènes peuvent être à l'origine de nombreuses infections superficielles, mais sont aussi la cause d'infections mettant en jeu la vie de patients immunodéprimés. Il y a donc deux urgences : la première est de trouver de nouvelles molécules antimicrobiennes, avec une structure chimique innovante, et si possible, un mécanisme d'action innovant. Cependant, pour atteindre cet objectif, il est essentiel d'acquérir de nouvelles données fondamentales sur la paroi microbienne, afin d'identifier des cibles originales à leur surface pour de nouvelles molécules. La deuxième urgence est donc de développer des techniques pour explorer les surfaces microbiennes depuis un angle différent, ce qui nécessite une approche expérimentale originale. Dans ce contexte, les approches biophysiques restent sous-exploitées en microbiologie clinique. Au cours de cette thèse, nous avons tiré avantage d'une technologie provenant de la physique, et adaptée aux conditions biologiques ; la Microscopie à Force Atomique. Le principe de cette technologie consiste à mesurer la force entre une pointe et une surface, et de garder cette force constante pendant l'acquisition afin d'obtenir une image tridimensionnelle de l'échantillon[1] (mode contact, figure 1.) L'AFM peut aussi être utilisé en mode spectroscopie de force (FS), où la pointe AFM est appuyée vers la surface, jusqu'à l'atteindre et indenter dans l'échantillon, avant d'être retirée de la surface, pour obtenir des courbes de force (figure 1 et 2).

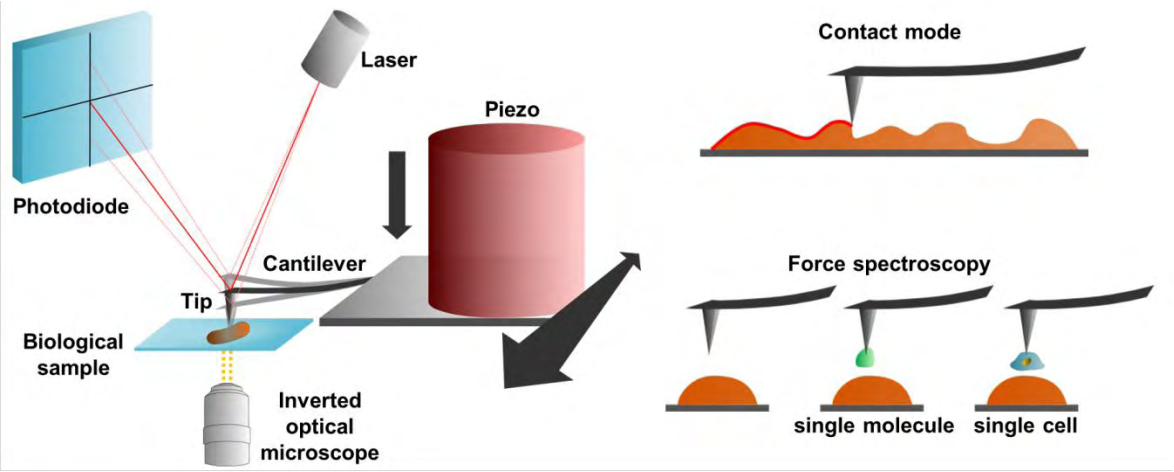

Figure 4. Schéma introduisant la technologie AFM. Une pointe est placée sur un levier qui peut être déplacé dans les directions x, y et z grâce à une céramique piézo-électrique. La déflection du levier est enregistrée sur une photodiode à quatre quadrants grâce à la réflexion d'un laser, aligné au bout du levier, habituellement recouvert d'or. L'AFM peut être utilisé pour produire des images topographiques (mode contact par exemple), ou bien pour mesurer des forces (en mode spectroscopie de force), entre une pointe nue ou fonctionnalisée (avec une molécule ou une cellule) et l'échantillon. Reproduit depuis [1].

Un avantage de l'AFM est la possibilité de travailler en liquide sur des cellules vivantes, ce qui nous a permis par exemple d'imager l'élongation de cellules vivantes de *Pseudomonas aeruginosa* traitées avec de la ticarcilline, un antibiotique à cible pariétale[2]. Nous avons également pu imager la disparition de la capsule de la bactérie *Klebsiella pneumoniae* traitée avec de la colistine, un antibactérien de la « dernière chance », avec un mécanisme d'action très mal connu. Cependant, l'immobilisation des échantillons est très souvent un challenge, qui doit être adressé pour chaque microorganisme étudié. En effet, les échantillons doivent être suffisamment immobilisés pour supporter les forces latérales exercées par la pointe, mais sans qu'ils soient dénaturés. L'immobilisation des échantillons représente un domaine de recherche à part entière, et nous a amené à fabriquer un timbre de polydimethylsiloxane (PDMS) microstructuré, avec des puits de différentes tailles, pour immobiliser des cellules rondes de différentes tailles telles que les levures. Une fois cette étape réalisée, l'AFM peut ensuite être utilisé dans les modes

d'imagerie et de spectroscopie de force classiques (figure 1, mode contact, mode oscillant, mode force volume), mais également dans des modes avancés afin d'obtenir des set de données de très haute résolution, ou multiparamétriques sur des cellules vivantes[3]. Nous avons par exemple utilisé le mode multiparamétrique, appelé Quantitative Imaging mode (QI™), de JPK Instruments, pour imager et quantifier les propriétés nanomécaniques/adhésives de microorganismes (*Candida albicans*, *Escherichia coli*, *Aspergillus fumigatus*), aussi bien que de cellules de mammifères (Chinese Hamster Ovaries) et de leur noyaux isolés.

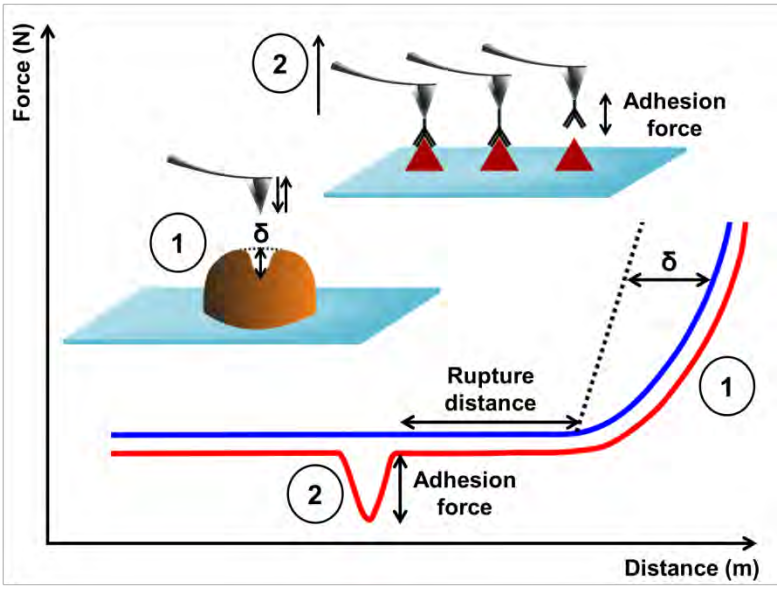

Figure 5. Représentation schématiques de l'AFM utilisé en mode spectroscopie de force. La spectroscopie de force donne accès à des courbes de force qui peuvent être analysées de deux façons différentes. (1) l'indentation (δ) est lue sur la courbe de force et représente les propriétés nanomécaniques de la paroi des levures. (2) la spectroscopie de force à l'échelle de la molécule unique (Single Molecule Force Spectroscopy, SMFS) utilise des pointes AFM fonctionnalisées avec des biomolécules ou ligands ; l'interaction entre un ligand chimiquement immobilisé sur la pointe AFM et une protéine à la surface est donnée par les force d'adhésions présentes sur la courbe de retrait (courbe rouge). Reproduit depuis [4].

Mais l'AFM n'est pas seulement une technologie d'imagerie ; c'est également une machine de force très sensible. Un AFM est donc capable d'enregistrer des courbes force-distance, qui donnent accès aux propriétés nanomécaniques et adhésives des matériaux vivants sondés (Figure 2). Grâce à cette possibilité, nous avons pu étudier les propriétés adhésives de la levure pathogène

Candida albicans et montrer à sa surface la présence de protéines capables d'agréger en nanodomaines et de former des plaques amyloïdes. Nous avons également pu observer les modifications de ces propriétés adhésives lors d'un traitement des cellules avec la caspofongine[5], un antifongique utilisé uniquement en dernière intention lors d'infections mettant en jeu la vie du patient. Finalement, pour aller plus loin dans l'architecture de la paroi des microorganismes, il est possible de fonctionnaliser des pointes AFM avec des biomolécules (Figure 1 et 2). Nous avons utilisé cette stratégie pour fonctionnaliser des pointes avec de la Concanavalin A, une lectine qui se lie de façon spécifique aux sucres présents à la surface des bactéries[6]. Ces expériences nous ont permis de démontrer la résistance d'une souche multirésistante de *Pseudomonas aeruginosa* aux antibiotiques classiques, mais aussi de comprendre le mécanisme d'action d'une molécule antibactérienne innovante, le CX1, sur cette espèce, grâce à l'étude de la structure de son peptidoglycane[7]. Nous avons ensuite utilisé cette même technique de fonctionnalisation de pointe pour localiser les protéines spécifiques exprimées au bout des projections de conjugaison de *Saccharomyces cerevisiae*. Pour cela, nous avons créé un système de reconnaissance basé sur les interactions antigènes-anticorps, en fonctionnalisant les pointes AFM avec un anticorps dirigé contre un peptide utilisé pour marquer les protéines d'intérêt. La validité de ce système a été vérifiée sur surface modèles ; sa versatilité a été confirmée sur des cellules vivantes de mammifères CHO.

Chapitre 4.2 : Développements technologiques pour étudier la paroi des microorganismes par AFM

Un prérequis pour les expériences AFM est l'immobilisation des échantillons biologiques étudiés. Cependant, immobiliser des microorganismes vivants est souvent un challenge ; les échantillons doivent être immobilisés suffisamment pour supporter les forces latérales exercées par la pointe AFM, sans qu'ils ne soient dénaturés. Nous avons développé dans notre équipe en 2011 une technique consistant à piéger des cellules sphériques telles que des levures ou des spores d'*Aspergillus fumigatus* dans des timbres de PDMS microstructurés. Cette stratégie est composée de 3 étapes. La première étape est de générer un masque verre/chrome présentant les motifs microstructurés, et de transférer ces motifs sur un moule en silicium par photolithographie et gravure réactive à ions. La deuxième étape est ensuite de fabriquer les timbres de PDMS ; pour cela, une solution de prépolymère de PDMS, contenant une mixture d'oligomères de PDMS et d'un agent réticulant (ration massique 10 :1), est réticulée sur le moule en silicium pendant 1 heure à 80°C. Le PDMS peut ensuite être démoulé afin d'obtenir un timbre de PDMS microstructuré. L'étape finale est enfin d'assembler les cellules dans les puits microstructurés du timbre de PDMS par dépôt capillaire/convectif. Cela consiste à étaler une goutte de suspension cellulaire sur le timbre de PDMS à une température, un taux d'humidité, une vitesse de translation et un angle de contact donné. Cette procédure peut également être faite de façon manuelle si l'obtention de matrices organisées de cellules n'est pas essentielle. Une présentation générale de cette technique est présentée en figure 3.

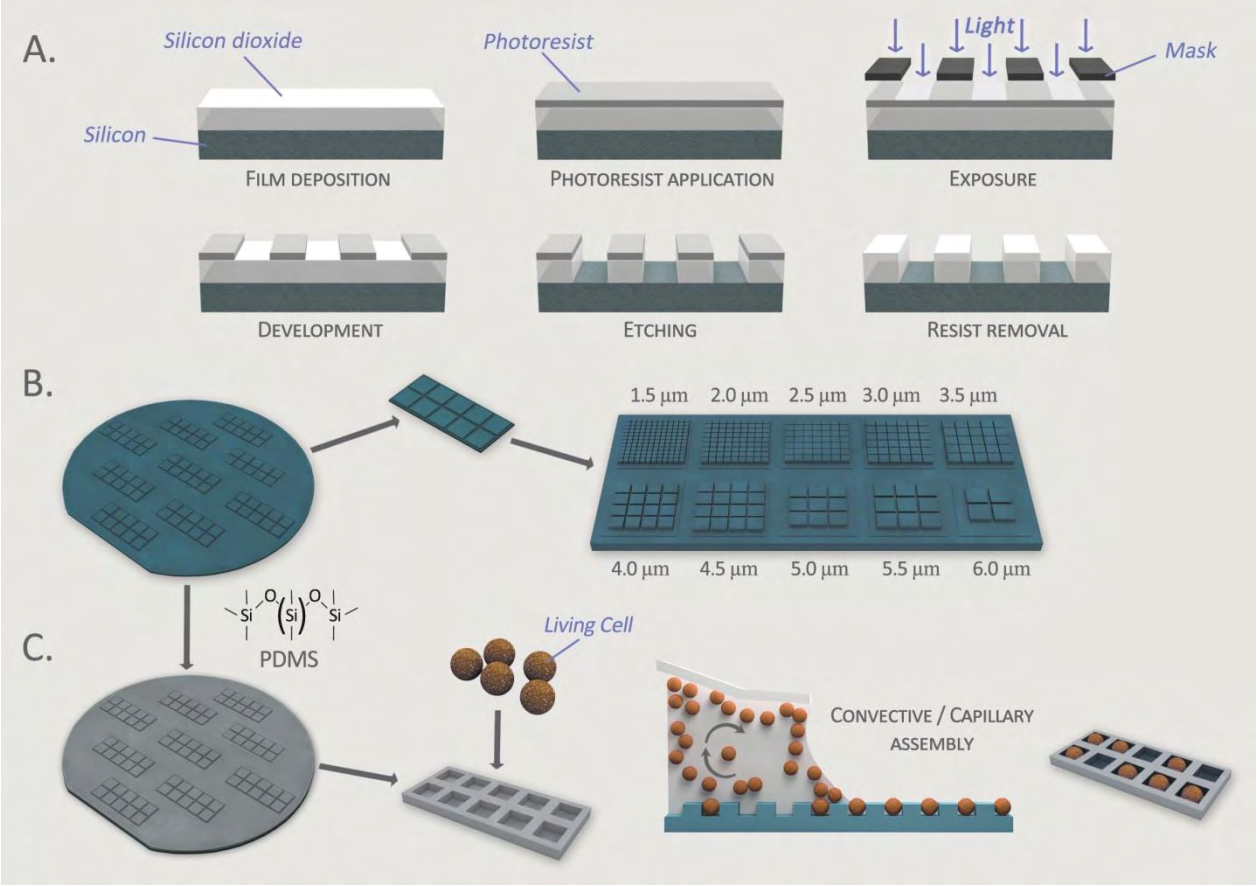

Figure 6. Représentation schématique de la procédure d'immobilisation des cellules dans les timbres de PDMS. La première étape (a) consiste à générer un moule en silicium présentant la géométrie négative désirée pour le timbre de PDMS. La seconde étape (b) est dédiée au moulage du timbre. Le PDMS liquide est délayé sur le moule en silicium et réticulé pendant 1 heure à 80°C. Finalement (c) les cellules sont assemblées dans les timbres de PDMS microstructurés par dépôt capillaire/convectif, afin de former des matrices de cellules.

Le premier timbre de PDMS, développé dans notre équipe en 2011[8], présentait des motifs carrés de 5 µm de côté. Son utilisation était donc limitée à l'immobilisation de microorganismes de 5 µm de diamètre approximativement. Au cours de ma thèse, nous avons développé un nouveau timbre de PDMS, avec des motifs carrés allant de 1,5 à 6 µm de côté, et avec des profondeurs allant de 1 à 4 µm. Cette nouvelle géométrie permet d'immobiliser une large gamme de microorganismes de différentes tailles, sans les dénaturer puisqu'aucuns produits chimiques ne

sont utilisés. Nous avons utilisé cette méthode pour immobiliser des cellules de *Candida albicans*, de *Saccharomyces cerevisiae* et d'*Aspergillus fumigatus*.

Une fois cette étape d'immobilisation franchie, le prochain challenge est de trouver un mode d'imagerie où les forces latérales sont réduites, qui permette de faire des images de haute résolution, et idéalement qui permette d'obtenir des données quantitatives. Etant donné nos besoins, nous nous sommes intéressés au nouveau mode avancé proposé par JPK Instruments, appelé Quantitative Imaging (QI™) mode. Ce mode est basé sur la mesure de courbes de force sur toute la surface de l'échantillon, comme un force volume, mais dont l'acquisition est plus rapide. Dans ce mode, le temps pour enregistrer une courbe de force unique est de 1,0 ms, et la résolution peut aller jusqu'à 512 pixel², ce qui est adapté aux études cinétiques sur des échantillons biologiques. Une comparaison du mode QI™ avec le mode force volume (FV) et le mode contact est présentée en figure 4.

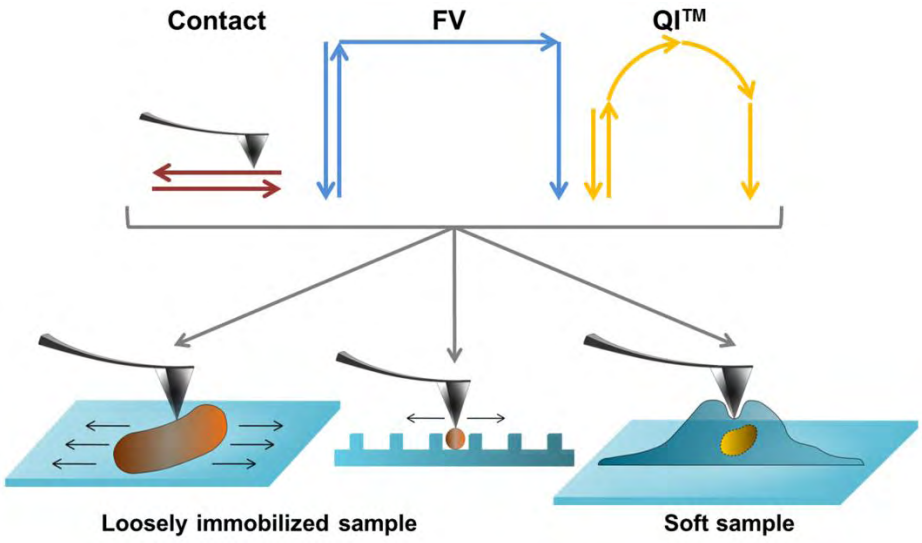

Figure 8. Comparaison des modes AFM. Pour chaque mode, contact, force volume et QI™, le mouvement de la pointe AFM est représenté. Ces modes ont été utilisés sur différents échantillons, mous et mal immobilisés. QI™ est le plus adapté pour ces types d'échantillons. Reproduit depuis [3].

Dans ce mode, pendant l'acquisition, une courbe de force est enregistrée pour chaque pixel, donnant alors accès à la « vraie » topographie de surface de l'échantillon, en extrayant le point de contact à force zéro de chaque courbe. Chaque courbe à l'approche peut être analysée individuellement avec des modèles théoriques, donnant accès aux propriétés nanomécaniques de l'échantillon, comme l'élasticité et la rigidité. Finalement, chaque courbe au retrait peut être extraite pour mesurer les forces d'adhésions entre la pointe, biofontionnalisée ou non, et l'échantillon biologique. Nous avons démontré dans ce travail que ce mode AFM était utilisé pour imager des échantillons mal immobilisés et mous puisque peu de forces latérales sont exercées par la pointe pendant l'acquisition. De plus, nous avons montré qu'il était possible grâce à ce mode de cartographier à haute résolution les propriétés nanomécaniques et adhésives des échantillons. Ces résultats sont publiés dans le journal Micron. Nous avons utilisé cette technologie pendant ma thèse pour imager et quantifier les propriétés nanomécaniques/adhésives de différents microorganismes, tels que *Candida albicans*, *Saccharomyces cerevisiae*, *Aspergillus fumigatus*, et *Klebsiella pneumoniae*.

Afin d'accéder à des données adhésives significatives sur des cellules vivantes, l'AFM peut être utilisé en mode QI^{TM} ou FV avec de pointes fonctionnalisées ; cette technique est appelée spectroscopie de force à l'échelle de la molécule unique. Dans cette technique, les pointes AFM sont mises en interaction avec des biomolécules immobilisées sur des substrat ou des biomembranes artificielles (études *in vitro*), ou présentes à la surface de cellules vivantes (études *in vivo*), afin de comprendre les interactions intra- et intermoléculaires des systèmes biomoléculaires[9,10]. Au cours de ma thèse, nous avons choisi de fonctionnaliser des pointes AFM avec un anticorps spécifique du peptide Human influenza (HA) dont la séquence peptidique est YPYDVPDYA. Pour cela, nous avons utilisé une stratégie développée dans notre équipe en

2012[6], qui consiste à fabriquer des « dendritips » en faisant réagir des pointes AFM fonctionnalisées avec une amine, avec des dendrimères. Cela conduit à l'obtention de pointes dendrimères, comme décrit dans la figure 5. Ensuite, les fonctions aldéhydes libres présentes à la surface du dendrimère sont disponibles et peuvent réagir avec les fonctions amines présentes sur toutes les protéines et sur de nombreuses biomolécules. En utilisant cette stratégie de fonctionnalisation, nous sommes capables de mesurer des interactions spécifiques entre une biomolécule immobilisée sur la pointe AFM et une biomolécules immobilisée sur une surface, ou présente à la surface de cellules vivantes.

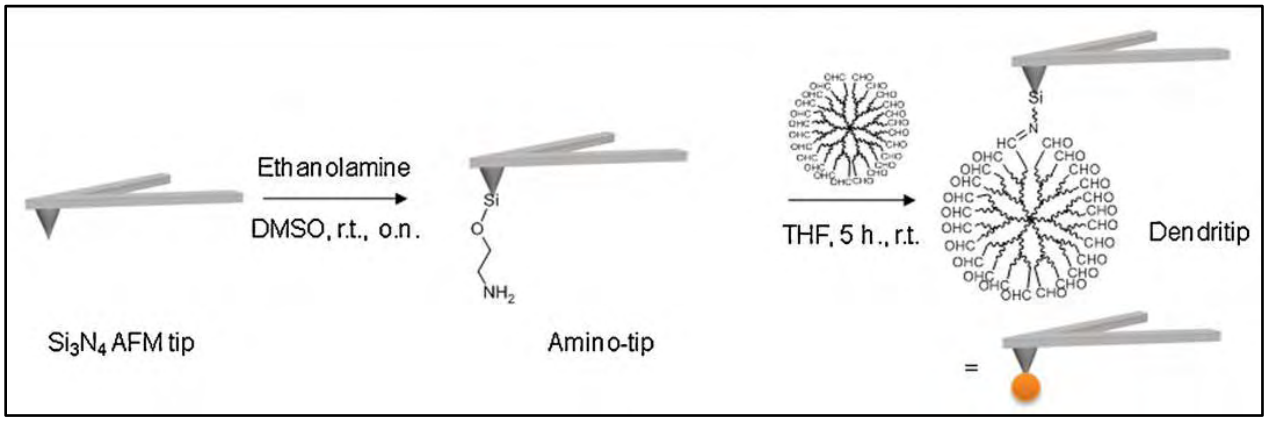

Figure 9. Représentation schématique de la fabrication de dendritips. Les groupes amines sont introduits sur la pointe AFM, et le dendrimère présentant 96 groupements aldéhydes est attaché via la formation d'une liaison imine. Reproduit depuis [6].

La première étape pour fabriquer notre système HA-anti HA a été de valider notre pointe AFM fonctionnalisée avec l'anticorps anti-HA sur surface modèle fonctionnalisée avec les épitopes HA. Pour cela, nous avons effectué des expériences de blocage, de loading rate et de temps de contact, afin de montrer la spécificité de l'interaction entre l'anticorps et l'épitope, et de caractériser cette interaction thermodynamiquement (calcul de la constante cinétique de dissociation *Koff*). Puis, après cette étape de validation, nous avons utilisé notre système sur des

cellules de levures surexprimant la protéine pariétale Ccw12 marquée avec l'épitope HA. Cette protéine, impliquée dans le remodelage de la paroi, n'a pu être cartographiée qu'à la surface des cellules en projections de conjugaison. Cela nous a permis d'imager pour la première fois ces projections de conjugaisons par AFM ; de plus, les résultats obtenus avec la pointe anti-HA ont permis d'ouvrir de nouvelles perspectives sur l'étude du remodelage de la paroi des levures. Finalement, pour montrer la versatilité de notre système, nous avons utilisé des cellules de mammifères CHO, et avons déplié depuis leur surface un récepteur couplé aux protéines G ; le récepteur β2 adrénergique, marqué avec l'épitope HA. Ces résultats sont publiés dans le Journal of Molecular Recognition.

Chapitre 4.3 : Etude à l'échelle nanométrique de la paroi de *Saccharomyces cerevisiae* et *Candida albicans*

Le premier type de microorganisme que nous avons étudié au cours de ma thèse est la levure, et particulièrement l'espèce *Candida albicans*, le pathogène fongique humain le plus commun, et *Saccharomyces cerevisiae*, mieux connue comme la levure de boulanger. Les levures sont entourées d'une paroi épaisse, mécaniquement forte, qui joue plusieurs rôles physiologiques, comme maintenir la forme de la cellule et son intégrité et protéger l'intérieur de la cellule de l'environnement extérieur. La paroi de la levure présente aussi différentes protéines impliquées dans la reconnaissance moléculaire et l'adhésion[11]. La composition chimique de la paroi de la levure est bien connue, et consiste en un réseau microfibrillaire de β-glucanes (50-60% de la masse de la paroi), recouvert par des protéines hautement glycosylées décorées de longues chaines de résidus mannoses (40-50% de la masse pariétale). La chitine, un polysaccharide

linéaire, est le troisième composant de la paroi et représente 1 à 3% de la masse de la paroi. Ces 15 dernières années, la complexité de l'architecture de la paroi a émergé d'études biochimiques, moléculaires et génétiques, ce qui a permis de découvrir plusieurs interconnections entre ces différents composant pour former des complexes macromoléculaires[12]. De plus, l'architecture moléculaire de la paroi n'est pas statique, mais est en constant remodelage dépendant des conditions de culture, des développements morphologiques en réponse à des stress de surface. Dans ce contexte, l'AFM, qui permet une visualisation et une étude directe de l'ultrastructure de la paroi des levures, est parfaitement adapté pour l'étude de cette structure dynamique dans différentes conditions[13,14].

La levure *Candida albicans* est devenue un problème de santé publique majeur ces 20 dernières années. Elle est en effet la cause de différentes infections, allant des infections de la peau, jusqu'aux infections du système sanguin, observées chez les patients immunodéprimés, et mettant en jeu leur vie. La première étape de l'infection par *Candida albicans* est l'adhésion, permise par les adhésines présentes à la surface des levures. Beaucoup de ces adhésines sont des mannoprotéines, et parmi elles, la famille des Als (Agglutinin-like Sequences) a été identifiée comme ayant un rôle majeur dans l'attachement aux cellules hôtes. Il existe 8 Als différentes chez *Candida albicans* ; toutes présentent des séquences de formation amyloïdes. Les amyloïdes sont des agrégats fibrillaires de protéines insolubles ; les cellules exprimant ce type de protéine peuvent rapidement s'agréger. Afin d'observer ces plaques amyloïdes à la surface des cellules, nous avons utilisé la Microscopie à Force Atomique, en mode Quantitative Imaging. Nous avons ainsi pu imager et quantifier en même temps les propriétés nanomécaniques, l'adhésivité, la taille et l'épaisseur des nanodomaines amyloïdes observés à la surface de *Candida albicans*, à haute résolution. L'imagerie de ces nanodomaines amyloïdes est présentée en Figure 6.

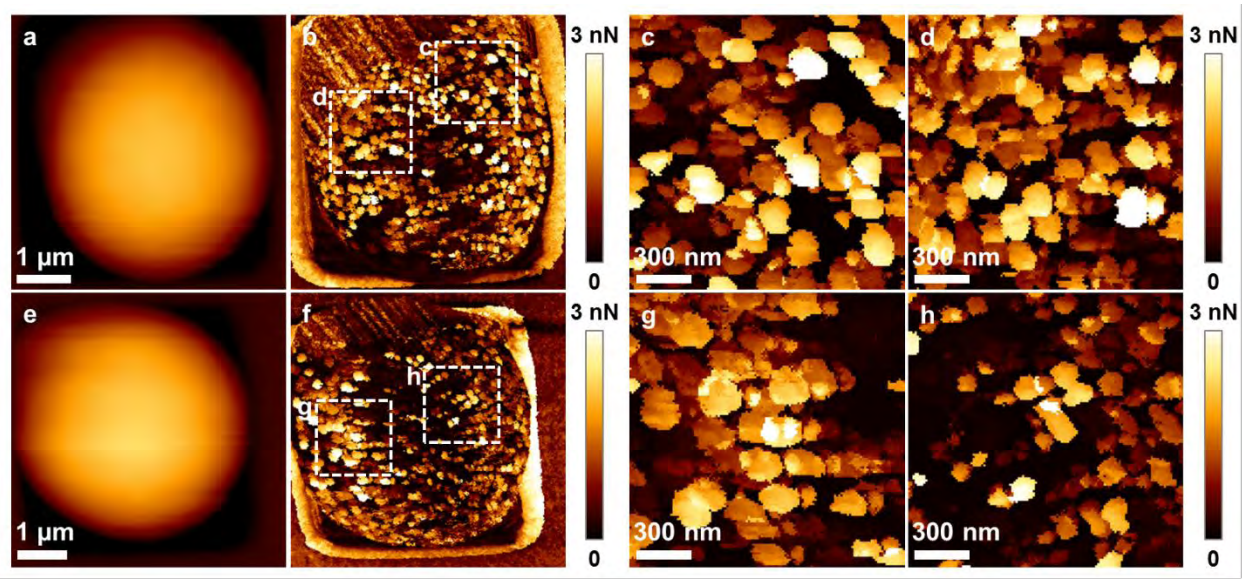

Figure 12. Imagerie des nanodomaines adhésifs de *Candida albicans*. (a et e) images de hauteur (échelle à 2.5 µm) de deux cellules de Candida albicans dans des timbres de PDMS, et (b et f) images d'adhésion correspondant aux images de hauteur. (c, d, g et h) Images d'adhésion de petites zones enregistrées au sommet des cellules, représentées par les carrés blancs en b et f. Résultats en cours de publication.

Les données collectées ont permis de montrer que ces nanodomaines sont localisés différemment à la surface des cellules, en fonction des structures exhibées par les cellules (cicatrices de bourgeonnement, bourgeons). Cela illustre la plasticité de cette espèce, capable de pousser en tant qu'espèce commensale ou pathogène[15], dans différentes parties de l'hôte (tube digestif, muqueuse vaginale), sous forme de cellule ronde ou d'hyphes[16]. Nous avons également montré qu'il y avait des degrés d'adhésivité, en fonction de l'état d'agrégation des protéines amyloïdes, et qu'ils étaient directement corrélables à la rigidité de la paroi. Pour aller plus loin, nous avons utilisé des pointes AFM fonctionnalisées, et avons ainsi pu déterminer que certains nanodomaines moins adhésifs étaient composés de mannoprotéines libres. Grâce à des mesures de force et des peptides spécifiques activant ou inhibant la formation des plaques amyloïdes, nous avons montré que ces mannoprotéines étaient capables de s'agréger et de former des nanodomaines adhésifs, grâce à leurs séquences amyloïdes. Ces résultats, bientôt publiés dans le

journal Nanomedicine NBM, sont à rajouter à la spécificité de *Candida albicans*, et participent à expliquer sa remarquable adaptation et pathogénicité.

La paroi de la levure est également la cible de choix pour les agents antifongiques, puisqu'elle représente une armure spécifique qui n'existe pas chez les cellules de mammifères, et dont l'endommagement conduit à la mort des cellules[17]. Au cours de ma thèse, nous nous sommes intéressés à la caspofongine, un antifongique ciblant la synthèse des β-glucanes, et avons étudié ses effets à l'échelle nanométrique sur les espèces de levures *Candida albicans*, et *Saccharomyces cerevisiae* (levure modèle). Pour cela, nous avons utilisé l'AFM en mode Quantitative Imaging™, combiné à notre méthode d'immobilisation en timbre de PDMS. En parallèle, nous avons également quantifié les différents composants de la paroi des cellules grâce à une méthode d'hydrolyse acide[18]. Nos résultats ont montré que l'administration de caspofongine provoquait un remodelage de la paroi des cellules des deux espèces, dépendant de la dose de caspofongine. Les changements dans la composition de la paroi étaient cependant plus prononcés pour *Candida albicans*, avec notamment une augmentation de chitine plus élevée en fonction de la dose de caspofongine, parallèlement à l'augmentation de l'élasticité de la paroi. De plus, à de faibles doses de caspofongine, la surface des cellules de *Candida albicans* présentent des adhésions, qui pourraient potentiellement être dues à la présence de mannoprotéines comme des adhésines de la famille des Als. Le traitement de *Saccharomyces cerevisiae* avec des fortes doses de caspofongine, lui, a donné lieu à une inhibition de la cytokinèse. La figure 7 présente de façon résumée ces résultats, publiés dans le journal Antimicrobial Agents and Chemotherapy.

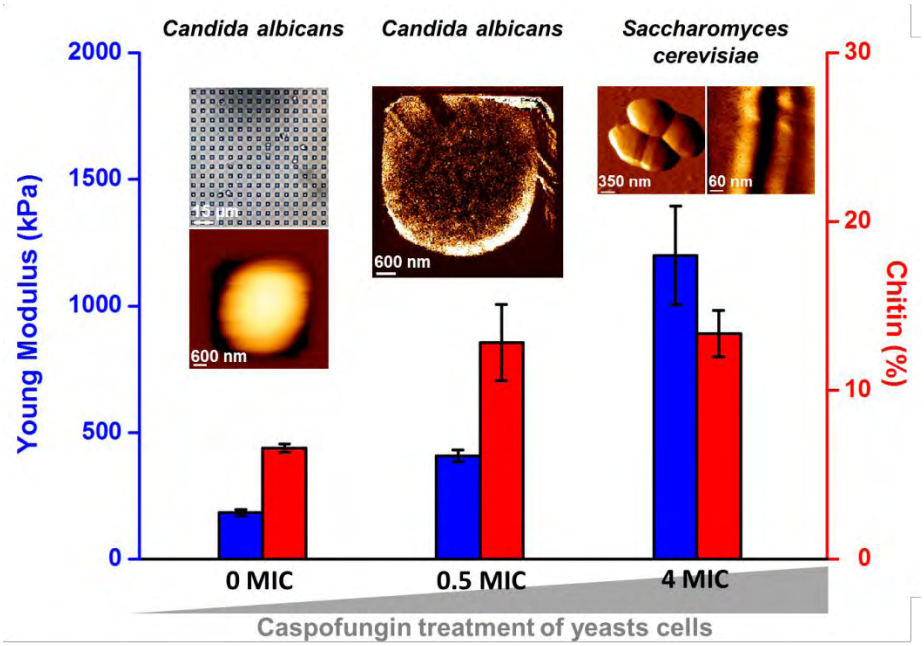

Figure 13. Résumé des effets de la caspofongine sur *Candida albicans* et *Saccharomyces cerevisiae*. Les valeurs de module de Young des cellules de *Candida albicans* augmentent avec la dose de caspofongine ; cette augmentation peut être directement corrélée à l'augmentation de la quantité de chitine dans la paroi. Les cellules de *Candida albicans* ont des propriétés adhésives modifiées par le traitement caspofongine à 0.5 CMI, alors que la morphologie de *Saccharomyces cerevisiae* est modifiée à de fortes doses de caspofongine. Reproduit depuis [5].

L'utilisation de l'AFM a permis de montrer des effets inattendus de la caspofongine sur les propriétés adhésives et la croissance de deux espèces de levures différentes. Ces résultats aident à la compréhension des bases moléculaires des interactions microbes-drogues, et ouvrent de nouvelles voies pour développer de nouveaux agents thérapeutiques. De façon globale, les résultats obtenus par AFM sur la levure montrent comment l'AFM permet d'amener de nouvelles données fondamentales sur la paroi des levures, et met en lumière la complexité des mécanismes moléculaires qui assurent le maintien de la paroi et de son assemblement.

Chapitre 4.4 : Comportement nanométrique de la paroi bactérienne en réponse au traitement par des antibiotiques

Nous avons dans une deuxième partie étudié la paroi des bactéries, et plus particulièrement des bactéries à Gram-négatif. La paroi bactérienne est une structure complexe composée de plusieurs couches, qui a plusieurs rôles, dans la protection des cellules de leur environnement, dans la division cellulaire, et dans le passage des nutriments depuis l'extérieur vers l'intérieur de la cellule, et des déchets dans l'autre sens. Les bactéries à Gram-négatif sont entourées d'une membrane interne, puis d'une fine couche de peptidoglycane, et enfin d'une membrane externe contenant des lipopolysaccharides (LPS). La paroi bactérienne est unique car certains de ses composants, comme le peptidoglycane et le LPS ne sont retrouvés dans aucunes autres cellules. C'est également un constituant essentiel pour la survie des bactéries ; il représente alors une cible parfaite pour des antibactériens. Il devient donc particulièrement intéressant de sonder cette paroi bactérienne avec l'AFM, afin d'obtenir de nouvelles données fondamentales sur cette structure dynamique complexe, pour comprendre son comportement à l'échelle nanométrique, en interaction avec des antibactériens, et ainsi identifier de nouvelles cibles pour des antibactériens innovants.

La première espèce utilisée accours de ma thèse est *Pseudomonas aeruginosa*. Cette espèce bactérienne est une espère Gram-négative, pathogène opportuniste, qui cause de nombreuses infections. De plus, cette espèce est naturellement résistante aux antibactériens grâce à sa perméabilité de membrane naturellement basse, et grâce à de nombreux mécanismes de résistances adaptatifs. La manière la plus simple de lutter contre ce type de bactérie est d'utiliser des antibiotiques. Nous avons alors étudié les effets de deux antibiotiques de référence, la

ticarcilline et la tobramycine, sur la paroi de *Pseudomonas aeruginosa*. Ces antibiotiques, actifs sur cette espèce bactérienne, et largement utilisés en milieu clinique, inhibent respectivement la synthèse du peptidoglycane et des protéines. Les résultats que nous avons obtenu ont montré que les bactéries cultivées en présence de ticarcilline présentaient des modifications significatives de la morphologie en formant des filaments ; cette morphologie peut être expliquée par le fait que les β-lactamines comme la ticarcilline activent le système SOS, conduisant à l'inhibition de la division cellulaire[19]. Les cellules traitées avec la tobramycine ne présentaient pas d'élongation mais une surface déformée, due au fait que le traitement tobramycine conduit à la synthèse de protéines anormales incorporées dans la paroi, ce qui provoque la perte de son intégrité. Ces résultats, présentés dans la figure 8, sont publiés dans le journal Nanomedicine NBM.

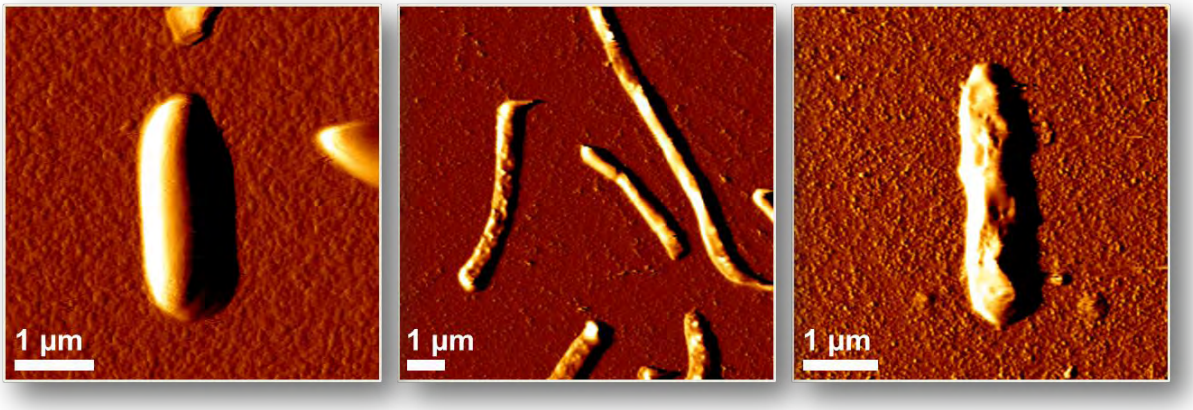

Figure 16. Modifications morphologiques des cellules de *Pseudomonas aeruginosa* induites par les traitements par des antibiotiques. Images de déflection vertical des cellules en condition témoin (image de gauche), traité par la ticarcilline (image centrale), et traitée par de la tobramycine (image de droite). Adapté de [2].

Ce premier set de données nous a permis de démontrer que étudier les propriétés biophysiques des bactéries pendant un traitement avec un antibactérien était riche en information ; cette

méthode peut alors être utilisée pour étudier les effets d'autres antibactériens sur la paroi de cellules multirésistantes.

Nous avons ensuite étudié les effets d'une autre molécule antibactérienne, la polymyxine E ou colistine, sur la paroi de souches multirésistantes de l'espère bactérienne Gram-négatif *Klebsiella pneumoniae*. Cette espèce bactérienne est à l'origine de nombreuses infections du système urinaire, des poumons, de la cavité abdominale et du sang lors d'hospitalisations. De nombreux facteurs de virulence ont été décrits pour cette espèce bactérienne. Parmi eux, les capsules extracellulaires sont essentielles à la pathogénicité des cellules ; en effet, elles protègent les cellules de la phagocytose et empêchent leur destruction par les facteurs sériques. Un autre facteur de virulence est la capacité de *Klebsiella pneumoniae* de résister à un grand nombre d'antibiotiques. Cela est dû au fait que les cellules produisent des enzymes qui hydrolysent les oxymino-β-lacatamines ; ces enzymes sont appelées ESBL pour β-lactamases à large spectre. Même si ces enzymes sont inhibées par des inhibiteurs de β-lactamases, les souches les possédant possèdent également d'autres gènes de résistance, et sont donc multirésistantes. Au cours de cette thèse, nous nous sommes intéressés à la souche connue ATCC 700603 de *Klebsiella pneumoniae*, qui est utilisé comme contrôle de qualité dans la détection des β-lactamases à large spectre en milieu hospitalier. Nous avons cherché à évaluer les effets de la colistine sur cette souche, ainsi que sur une souche dérivée résistante à la colistine, appelée Kpm, à l'échelle nanométrique. La cible première de la colistine est le lipide A du lipopolysaccharide présent à la surface des bactéries Gram-négatives. L'interaction entre la colistine est le lipide A conduit alors à la déstabilisation de la membrane, à l'augmentation de sa perméabilité, et donc à la mort des cellules[20]. Cependant ce mécanisme d'action fait toujours l'objet de controverses, et le mécanisme d'action précis de la colistine est toujours inconnu[21]. Notre étude nous a permis

d'imager pour la première fois la capsule de *Klebsiella pneumoniae*, à l'échelle nanométrique, et de la caractériser du point de vue nanomécanique. Sur la souche sensible, nous avons montré que la colistine avait un effet « détergent » en enlevant la capsule des bactéries. Sur la souche résistante à la colistine, les données d'imagerie ont montré que la capsule était différente de celle de la souche sensible, en apparaissant étroitement liée à la paroi de la cellule, au lieu d'être étendue sur une large surface autour des cellules, comme c'est le cas pour la souche sensible. Avec le traitement colistine, même à des doses hautes, la capsule n'est pas enlevée des cellules. Ces résultats nous ont alors permis de formuler l'hypothèse selon laquelle la souche résistante à une capsule modifiée, qui lui confère la résistance à la colistine. Une analyse plus poussée des courbes de force obtenues sur les deux souches a montré que dans le cas de la souche sensible, la pointe AFM passe d'abord à travers une couche de polysaccharide capsulaire, avant d'atteindre la bactérie, puis la lame de verre. Sur la souche résistante, la pointe pénètre d'abord de multiples couches de polysaccharides, avant d'atteindre la bactérie puis la lame de verre. La souche résistante à la colistine présente alors une nanoarchitecture de capsule en couches superposées. Cependant malgré cette organisation, et le fait que les cellules résistent à la colistine, leur capsule est quand même affectée par la molécule. En effet, les données nanomécaniques montrent que le module de Young de la capsule des cellules résistantes augmente avec la dose de colistine. La figure 9 présente l'hypothèse qui a pu être formulée grâce aux données globales de cette étude, sur l'architecture de la capsule de la souche sensible (a) et de la souche résistante à la colistine (b).

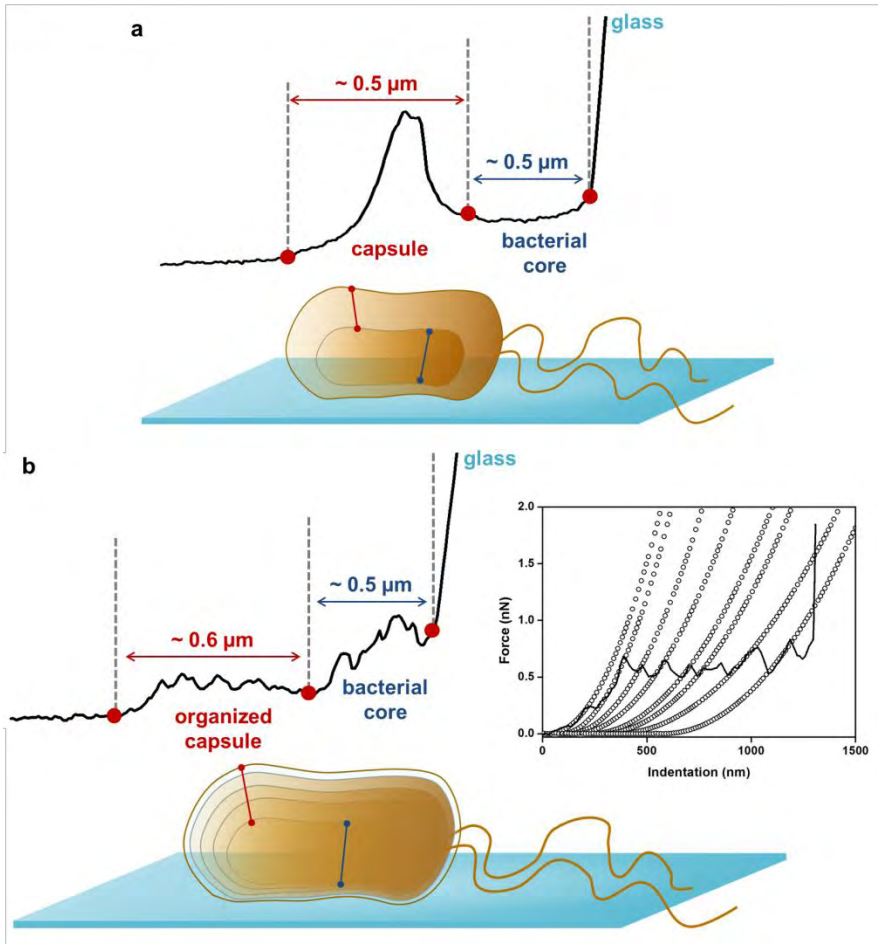

Figure 17. Représentation schématique de l'hypothèse formulée sur l'architecture capsulaire de *Klebsiella pneumoniae*. (a) organisation de la capsule de *K. pneumoniae* ATCC 700603, et (b) organisation de la capsule de *K. pneumoniae* résistante à la ticarcilline (Kpm). Le graphique en (b) montre une courbe d'indentation enregistrée au sommet d'une cellule de la souche Kpm en condition normales (ligne grise), et dont chaque pic a été fitté avec le modèle d'Hertz. Résultats en cours de publication.

De façon générale, ces résultats nous ont permis d'amener de nouvelles données sur le mécanisme de résistance de la souche Kpm à la colistine. En effet, la souche Kpm résiste probablement aux effets de la colistine grâce à l'architecture particulière de sa capsule, en couches superposées, qui empêchent la colistine d'atteindre sa cible, c'est-à-dire le lipopolysaccharide présent sur la membrane externe. Ces résultats sont en cours de publication dans le Journal of Antimicrobial Chemotherapy.

Chapitre 4.5 : L'AFM pour comprendre le mécanisme d'action d'une nouvelle molécule antibactérienne

Cependant la colistine étant une molécule toxique, notamment pour les reins et les neurones, et les bactéries Gram-négatives étant de plus en plus résistantes, il devient urgent de trouver de nouveau antibactériens avec un mécanisme d'action innovant. Parmi différentes approches pour développer des nouveaux agents antibactériens, une est dédiée aux calixarènes polycationiques, et notamment à un calixarène en particulier, appelé CX1, dont l'efficace pour lutter *in vitro* contre les bactéries aussi bien à Gram-négatif que positif a été montrée récement[22]. L'hypothèse initiale concernant son mécanisme d'action est que l'introduction de charges positives sur le calixarène déstabilise et désorganise la paroi bactérienne. Nous avons choisi d'évaluer les effets de cette molécule sur la bactérie *Pseudomonas aeruginosa* ; en effet, la paroi de cette souche étant hautement chargée négativement, il s'agit d'un bon candidat pour tester l'interaction avec le CX1. Nous avons alors développé une stratégie pour évaluer les effets à l'échelle nanométrique du CX1 sur cette souche, et ainsi comprendre son mécanisme d'action. Pour cela, nous avons choisi de travailler avec une souche sensible de *P. aeruginosa* (ATCC 27853), mais également avec une souche multirésistante de *P. aeruginosa*, notamment à la ticarcilline et à la tobramycine. Etant donné que les mécanismes d'action de ces deux antibiotiques sont bien décrits, en comparant les effets causés par ces molécules à ceux causés par le CX1, nous pourrons mieux comprendre le mécanisme d'action du CX1 et déterminer sa cible bactérienne. Cette stratégie est résumée dans la figure 10.

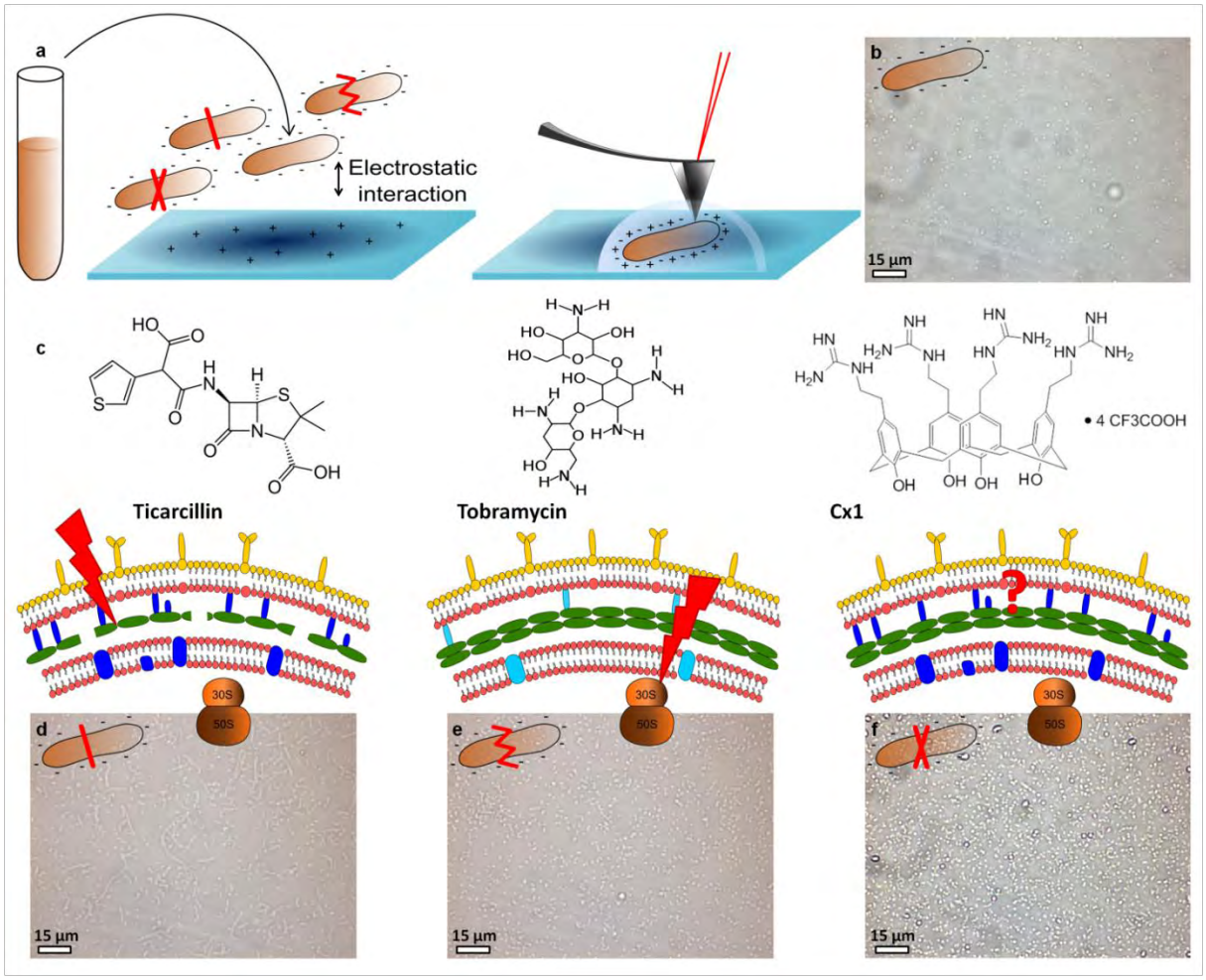

Figure 19. Représentation schématique de la stratégie utilisée pour étudier le mécanisme d'action du CX1. (a) les cellules cultivées en bouillon de culture Mueller Hinton pendant 20 heures à 35°C sont immobilisées sur une lame de verre fonctionnalisée avec du polyéthylénimine pour les expériences AFM. (b) image optique de la surface couverte par des cellules non traitées et immobilisées de P. aeruginosa. (c) molécules utilisés dans cette étude et leurs cibles. (d) images optiques de cellules de P. aeruginosa traitées avec de la ticarcilline (4 mg/mL), € de la tobramycine (0.25 mg/mL) et f du Cx1 (32 mg/mL). Reproduit depuis [7].

Les résultats obtenus ont montré que sur la souche multirésistante de *Pseudomonas aeruginosa*, le CX1 avait des effets dramatiques sur le module de Young de la paroi, ce qui n'était pas le cas avec un traitement ticarcilline et tobramycine. CX1 est donc efficace sur cette souche, et son action déstabilise la paroi de la bactérie. Pour aller plus loin dans la compréhension du mécanisme d'action de la molécule, nous avons sondé la paroi de cellules traitées et non traitées avec des pointes AFM fonctionnalisées avec la Concanavaline A, une lectine qui se lie aux sucres

présents à la surface des bactéries. Ces expériences à l'échelle de la molécule unique ont révélé que la lectine était capable de déplier une molécule de 6 µm de long, seulement depuis la surface de cellules traitées avec du CX1. D'autres expériences faites sur des bicouches phospholipidiques soumises à un traitement par le CX1 pendant une heure ont montré que l'antibactérien créait des perforations dans les bicouches. Des perforations similaires ont d'ailleurs également été observées à la surface de cellule traitées avec du CX1. Nous savons donc que CX1 cause une déstabilisation importante de la paroi des bactéries (diminution du module de Young, déploiement de longues molécules, perforations observées à la surface des cellules), et est capable de perforer des membranes phospholipidiques de même composition que la membrane externe des bactéries Gram-négatives. Nous pouvons alors formuler l'hypothèse suivante concernant le mécanisme d'action du CX1 : cette molécule interagit avec la membrane externe des bactéries Gram-négative et la perfore. Ces perforations donnent alors accès à la pointe fonctionnalisée à une molécule longue située sous la membrane externe ; cette molécule peut possiblement être le peptidoglycane, dont la structure en « corde » superenroulée a été démontrée récement[23,24], ce qui pourrait expliquer le fait que cette molécule soit déployée sur de si longues distances. L'ensemble de ces résultats est publié dans le journal Scientific Reports.

L'étape suivante à une telle étude, est maintenant de comprendre comment cette molécule peut être utilisée en synergie avec d'autres antibiotiques, et si la combinaison de molécules peut permettre de restaurer l'action des antibiotiques sur des souches multirésistantes.

Références bilbiographiques

1. Pillet, F., Chopinet, L., Formosa, C. & Dague, É. Atomic Force Microscopy and pharmacology: From microbiology to cancerology. *Biochim. Biophys. Acta BBA - Gen. Subj.* **1840,** 1028–1050 (2014).
2. Formosa, C., Grare, M., Duval, R. E. & Dague, E. Nanoscale effects of antibiotics on P. aeruginosa. *Nanomedicine Nanotechnol. Biol. Med.* **8,** 12–16 (2012).
3. Chopinet, L., Formosa, C., Rols, M. P., Duval, R. E. & Dague, E. Imaging living cells surface and quantifying its properties at high resolution using AFM in QI^{TM} mode. *Micron* **48,** 26–33 (2013).
4. Francois, J. M. *et al.* Use of atomic force microscopy (AFM) to explore cell wall properties and response to stress in the yeast Saccharomyces cerevisiae. *Curr. Genet.* **59,** 187–196 (2013).
5. Formosa, C. *et al.* Nanoscale Effects of Caspofungin against Two Yeast Species, Saccharomyces cerevisiae and Candida albicans. *Antimicrob. Agents Chemother.* **57,** 3498–3506 (2013).
6. Jauvert, E. *et al.* Probing single molecule interactions by AFM using bio-functionalized dendritips. *Sens. Actuators B Chem.* **168,** 436–441 (2012).
7. Formosa, C. *et al.* Nanoscale analysis of the effects of antibiotics and CX1 on a Pseudomonas aeruginosa multidrug-resistant strain. *Sci Rep* **2,** (2012).
8. Dague, E. *et al.* Assembly of live micro-organisms on microstructured PDMS stamps by convective/capillary deposition for AFM bio-experiments. *Nanotechnology* **22,** (2011).
9. Dufrêne, Y. F. *et al.* Five challenges to bringing single-molecule force spectroscopy into living cells. *Nat. Methods* **8,** 123–127 (2011).
10. Müller, D. J., Helenius, J., Alsteens, D. & Dufrêne, Y. F. Force probing surfaces of living cells to molecular resolution. *Nat. Chem. Biol.* **5,** 383–390 (2009).
11. Chaffin, W. L. Candida albicans Cell Wall Proteins. *Microbiol. Mol. Biol. Rev.* **72,** 495 – 544 (2008).
12. Orlean, P. Architecture and Biosynthesis of the Saccharomyces cerevisiae Cell Wall. *Genetics* **192,** 775–818 (2012).
13. Dague, E. *et al.* Towards a nanoscale view of fungal surfaces. *Yeast* **24,** 229–237 (2007).
14. Dufrêne, Y. F. Atomic force microscopy of fungal cell walls: an update. *Yeast* **27,** 465–471 (2010).
15. Gow, N. A. & Hube, B. Importance of the Candida albicans cell wall during commensalism and infection. *Curr. Opin. Microbiol.* **15,** 406–412 (2012).
16. Poulain, D. *Candida albicans* , plasticity and pathogenesis. *Crit. Rev. Microbiol.* 1–10 (2013). doi:10.3109/1040841X.2013.813904
17. Carrillo-Muñoz, A. J., Giusiano, G., Ezkurra, P. A. & Quindós, G. Antifungal agents: mode of action in yeast cells. *Rev. Esp. Quimioter. Publ. Of. Soc. Esp. Quimioter.* **19,** 130–139 (2006).
18. Dallies, N., François, J. & Paquet, V. A new method for quantitative determination of polysaccharides in the yeast cell wall. Application to the cell wall defective mutants of Saccharomyces cerevisiae. *Yeast* **14,** 1297–1306 (1998).
19. Schlacher, K. & Goodman, M. F. Lessons from 50 years of SOS DNA-damage-induced mutagenesis. *Nat. Rev. Mol. Cell Biol.* **8,** 587–594 (2007).

20. Yahav, D., Farbman, L., Leibovici, L. & Paul, M. Colistin: new lessons on an old antibiotic. *Clin. Microbiol. Infect.* **18,** 18–29 (2012).
21. Velkov, T., Roberts, K. D., Nation, R. L., Thompson, P. E. & Li, J. Pharmacology of polymyxins: new insights into an 'old' class of antibiotics. *Future Microbiol.* **8,** 711–724 (2013).
22. Grare, M. *et al.* In vitro activity of para-guanidinoethylcalix[4]arene against susceptible and antibiotic-resistant Gram-negative and Gram-positive bacteria. *J. Antimicrob. Chemother.* **60,** 575–581 (2007).
23. Hayhurst, E. J., Kailas, L., Hobbs, J. K. & Foster, S. J. Cell wall peptidoglycan architecture in Bacillus subtilis. *Proc. Natl. Acad. Sci.* **105,** 14603–14608 (2008).
24. Andre, G. *et al.* Imaging the nanoscale organization of peptidoglycan in living Lactococcus lactis cells. *Nat. Commun.* **1,** 27 (2010).

Appendices

Appendix 1: Uncovering by Atomic Force Microscopy of an original circular structure at the yeast cell surface in response to heat shock

I have contributed in this publication in AFM experiments on yeasts cells, along with Flavien Pillet and Marion Schiavone

Appendix 2: Deletion of the α-(1,3)-glucan synthase genes induces a restructuring of the conidial cell wall responsible for the avirulence of *Aspergillus fumigatus*

In this publication I have, with Etienne Dague, performed AFM experiments to show the adhesive properties of spores of Aspergillus fumigatus.

Appendix 1:

Uncovering by Atomic Force Microscopy of an original circular structure at the yeast cell surface in response to heat shock

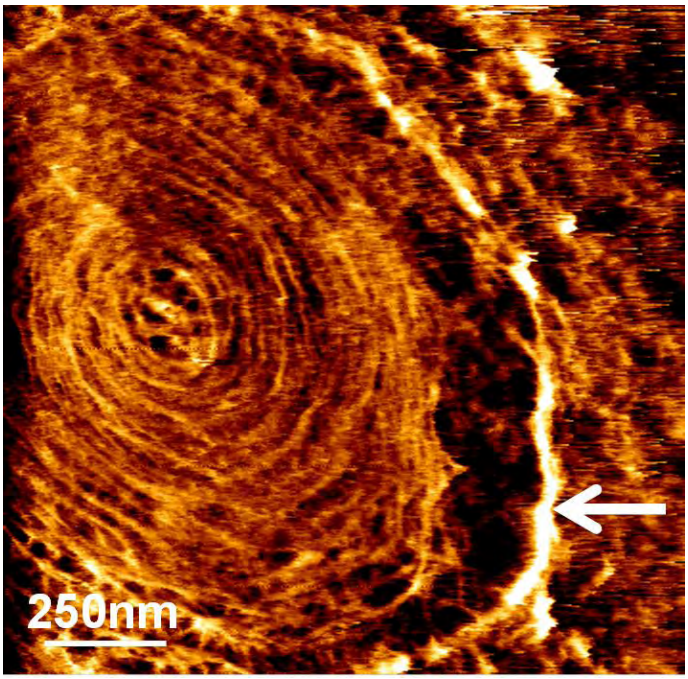

Pillet F., Lemonier S., Schiavone M., Formosa C., Martin-Yken H., François J. M., and Dague E.

BMC Biology, **12**, 2014

Abstract

Background: Atomic Force Microscopy (AFM) is a polyvalent tool that allows biological and mechanical studies of full living microorganisms, and therefore the comprehension of molecular mechanisms at the nanoscale level. By combining AFM with genetical and biochemical methods, we explored the biophysical response of the yeast Saccharomyces cerevisiae to a temperature stress from 30°C to 42°C during 1 h.

Results: We report for the first time the formation of an unprecedented circular structure at the cell surface that takes its origin at a single punctuate source and propagates in a concentric manner to reach a diameter of 2–3 μm at least, thus significantly greater than a bud scar. Concomitantly, the cell wall stiffness determined by the Young's Modulus of heat stressed cells increased two fold with a concurrent increase of chitin. This heat-induced circular structure was not found either in wsc1Δ or bck1Δ mutants that are defective in the CWI signaling pathway, nor in chs1Δ, chs3Δ and bni1Δ mutant cells, reported to be deficient in the proper budding process. It was also abolished in the presence of latrunculin A, a toxin known to destabilize actin cytoskeleton.

Conclusions: Our results suggest that this singular morphological event occurring at the cell surface is due to a dysfunction in the budding machinery caused by the heat shock and that this phenomenon is under the control of the CWI pathway.

BMC Biology

RESEARCH ARTICLE Open Access

Uncovering by Atomic Force Microscopy of an original circular structure at the yeast cell surface in response to heat shock

Flavien Pillet[1,2†], Stéphane Lemonier[1,2,3†], Marion Schiavone[1,2,4,5,6], Cécile Formosa[1,2,7,8], Hélène Martin-Yken[4,5,6], Jean Marie Francois[4,5,6*] and Etienne Dague[1,2,3*]

Abstract

Background: Atomic Force Microscopy (AFM) is a polyvalent tool that allows biological and mechanical studies of full living microorganisms, and therefore the comprehension of molecular mechanisms at the nanoscale level. By combining AFM with genetical and biochemical methods, we explored the biophysical response of the yeast *Saccharomyces cerevisiae* to a temperature stress from 30°C to 42°C during 1 h.

Results: We report for the first time the formation of an unprecedented circular structure at the cell surface that takes its origin at a single punctuate source and propagates in a concentric manner to reach a diameter of 2–3 μm at least, thus significantly greater than a bud scar. Concomitantly, the cell wall stiffness determined by the Young's Modulus of heat stressed cells increased two fold with a concurrent increase of chitin. This heat-induced circular structure was not found either in *wsc1*Δ or *bck1*Δ mutants that are defective in the CWI signaling pathway, nor in *chs1*Δ, *chs3*Δ and *bni1*Δ mutant cells, reported to be deficient in the proper budding process. It was also abolished in the presence of latrunculin A, a toxin known to destabilize actin cytoskeleton.

Conclusions: Our results suggest that this singular morphological event occurring at the cell surface is due to a dysfunction in the budding machinery caused by the heat shock and that this phenomenon is under the control of the CWI pathway.

Keywords: Atomic Force Microscopy (AFM), *Saccharomyces cerevisiae*, Heat-shock, Cell wall, Chitin, Budding

Background

The yeast *Saccharomyces cerevisiae* is a unicellular eukaryotic microorganism surrounded by a 100–120 nm thick cell wall [1]. The fungal cell wall is an essential structure that maintains cell shape and cell integrity, ensures resistance to internal turgor pressure and thereby prevents cell lysis [2]. The cell wall of *Saccharomyces cerevisiae*, which represents 10 - 25% of the cell dry mass according to the culture and process conditions [3], consists of three types of polymers that are interconnected to produce a modular complex structure [4]. The inner layer of the cell wall is composed of a β-1,3-glucan network (80 - 90% of the total β-glucan) branched with chitin (1–2% of the cell wall). Together, they form a structure that is largely responsible for the mechanical strength of the whole cell wall [5,6]. In addition, β-1,6-linked glucans (8 - 18% of total β-glucans) are branched on the β-1,3-glucan network, and also linked to the mannoproteins that compose the outer layer [7,8]. The yeast cell wall is a dynamic structure, the molecular architecture of which is continuously remodeled during morphogenetic processes and growth [9]. It also undergoes remodeling in response to environmental stresses, such as ethanol and oxidative stress [10,11], thermal and osmotic stress [12-14], and in response to antifungal drugs such as allicin or caspofungin [15,16]. These

* Correspondence: fran_jm@insa-toulouse.fr; edague@laas.fr
†Equal contributors
[4]Université de Toulouse, INSA, UPS, INP, 135 avenue de Rangueil, F-31077 Toulouse, France
[1]CNRS, LAAS, 7 avenue du colonel Roche, F-31077 Toulouse, France
Full list of author information is available at the end of the article

remodeling processes are organized by a "cell wall rescue-mechanism" that relies on a combination of several signaling pathways, with a major role played by the PKC1-dependent cell wall integrity (CWI) pathway (reviewed in [9,17]). Important biochemical modifications identified so far during stresses were i) massive deposition of chitin that takes place in the lateral walls of both the mother cells and the growing buds, ii) an increased cross-linkage between chitin and β-1,3-glucan and iii) the appearance of novel linkages between cell wall proteins and chitin through β-1,6-glucan [18,19]. Altogether, these cell wall repair mechanisms have been considered as a mean to combat cell wall weakening caused by these stresses [4,20]. However, a direct visualization of the topography and nanomechanical changes associated to these biochemical and molecular changes induced by stresses was still missing to better understand the cell wall biogenesis and remodeling mechanism. The remarkable development of the Atomic Force Microscopy (AFM) technology, combined with genetical and molecular tools, is therefore powerful to fulfil this gap and investigate the dynamics of microbial cell surfaces in response to external cues [21,22].

In this study, we have investigated the effects of heat shock on the nanomechanical properties of the yeast cell wall. We chose this stress condition because of the large body of data available on the heat shock response in the yeast *Saccharomyces cerevisiae* (reviewed in [23]). In brief, this response is characterized at the genome level by an intense program of changes in gene expression leading to repression of protein biosynthetic machinery and the induction of a battery of genes encoding heat shock proteins (HSPs). The main metabolic and physiological changes reported in response to heat stress are an accumulation of trehalose and an inhibition of glycolysis [24,25], associated with a transient arrest of cell division. Heat shock also triggers the activation of the CWI pathway, resulting in a global transcriptomic change including the overexpression of genes encoding cell wall remodeling enzymes [26]. Although AFM analysis of temperature stress on yeast cells has been previously addressed by Adya *et al.* [27], we have revisited this stress because of two major technical concerns in the study reported by the latter authors. Firstly, the immobilization procedure they used could likely alter the cell viability and integrity since yeast cells were immobilized on glass slides by air-drying for more than 5 hr. Secondly, the stress was carried out at temperature ranging from 50 to 90°C, which is incompatible with yeast life and irrelevant in a biotechnological viewpoint.

Using a recent immobilization method that ensures the viability and integrity of the yeast cells [28], we showed that a temperature shift from 30 to 42°C induced the singular formation of circular rings that initiate at a single point on the yeast cell surface and expanded in a concentric manner to reach a diameter of 2 to 3 μm after 1 h of incubation. Appearance of this circular structure was accompanied by a twofold increase of chitin and by a raise of the cell wall stiffness. Furthermore, we showed that the formation of this unique circular structure was dependent on the budding process and was regulated by the CWI pathway.

Results

Heat shock induces the formation of a circular structure at the yeast cell surface

To explore the heat shock effects on the yeast cell surface by AFM, a culture sample from exponentially growing yeast cells on YPD cultivated at 30°C was shifted at 42°C for 1 h. Both unstressed and heat shocked cells were then trapped in polycarbonate porous membrane (Figure 1, top panel) or immobilized in holes of a PDMS stamp (Figure 1; lower panel). The presence of two typical bud scars on the unstressed yeast cell was clearly identified on AFM deflection images (Figure 1A & A'). In contrast, the heat-shocked yeast cell presented beside a bud scar, a circular structure (CS) that had a size larger than the bud scar on its cell surface. This CS was not an epiphenomenon since it was observed over 20–25 individual heat shocked cells analyzed from three independent experiments. In addition, the formation of this unique CS was time dependent, since small concentric rings started to be observed after 20 min incubation at 42°C, and their number and size increased with time to finally covered the whole observable cell surface after 2 hr (data not shown). Also, we always observed only one CS per cell, although it could not be excluded that another circular structure was formed underside, since this side of the cells was not accessible to AFM study. This singular event was clearly associated with the heat shock response as witnessed by a rapid and huge accumulation of trehalose (Additional file 1: Figure S1), a key marker of the response of yeast to a thermal stress [24,29]. Also, the viability of heat shocked yeast cells after 1 h of treatment at 42°C was more than 99% as evaluated by methylene blue staining method (Additional file 2: Table S1).

Ultrastructure of the cell surface CS using high resolution AFM imaging

To show that bud scar and CS were morphologically different, we carried out a detailed analysis of AFM height images on unstressed and heat shocked cells. A first difference was in the diameter of the two features, which was around 1 μm maximum for the bud scar but exceeded 2.5 μm for the cell surface CS (Figure 2). Also, the cross section taken on the AFM height image of the

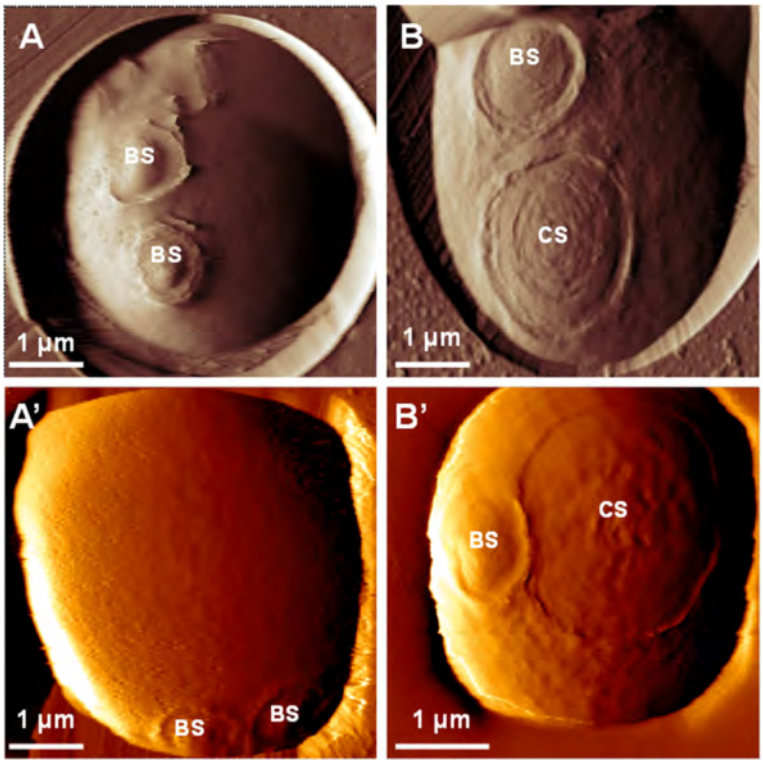

Figure 1 Heat-shock exposition of yeast cells leads to the formation of an unexpected circular structure. AFM deflection images of surface topology of a living yeast cell at 30°C (unstressed) **(A, A')** or exposed to heat shock during 1 h at 42°C (heat-shocked) **(B, B')**. Yeast cells were trapped in polycarbonate porous membrane (top panel) or within the patterns of a PDMS stamp (back panel). Bud scar (BS) and circular structure (CS) are indicated on AFM images.

unstressed yeast cell confirmed the typical convex structure of the bud scar (Figure 2B & C), followed by a depression and terminated by an apparent rigid ring which corresponds to a local accumulation of chitin [30]. In contrast, the cell surface CS identified on the heat shocked cells showed a different morphology, being relatively smooth inside the structure and terminated by a sharp ring. At a higher resolution, the AFM deflection image allowed identifying a succession of circular rings that originated from a single point and expanded in a concentric manner to end up by one last sharp ring (Figure 3).

Heat shock increases the yeast cell wall stiffness

Quantitative data on the effects of heat shock were obtained by scanning a given area of the cell surface with the AFM tip. To this end, we choose an area on the cell that was elsewhere from bud and CS. Thousands of Force Volume (FV) measurements were recorded, translated into pixel units to yield an elasticity map from which Young's Modulus (YM) values (expression of cell wall stiffness) could be calculated (Figure 4A & B). Qualitatively, the elasticity map of an unstressed yeast cell was homogeneous, while for the heat shocked cells, there was clearly a central region on the chosen area exhibiting higher pixel intensities, suggesting a difference in the elasticity or stiffness between the unstressed and the heat shocked cells. The YM values were extracted from all the force curves (*e.g.* 19443 FV curves from 19 unstressed cells, and 15307 FV curves from 15 heat-shocked yeast cells) and expressed as histograms that followed a Gauss distribution (Figure 4C and C'). The median values of the Gauss model fitting curve were used to determine YM from unstressed and heat-shocked cells. An unpaired *t*-test applied on the obtained YMs data (Additional file 3: Figure S2) allowed concluding that the YM from heat shocked was statistically two-fold higher than that of unstressed yeast cells (p value < 0.0001). The same methodology was used to evaluate the YM at the CS vicinity of the heat shocked cells. As shown in Figure 5, the YM was even higher at the CS, reaching more than 2 MPa inside this structure. Taking into account that cell wall stiffness is generally correlated with changes in chitin level, this finding raised the question whether this increase of stiffness at the CS is linked to increase of chitin or to some other cell wall remodeling events.

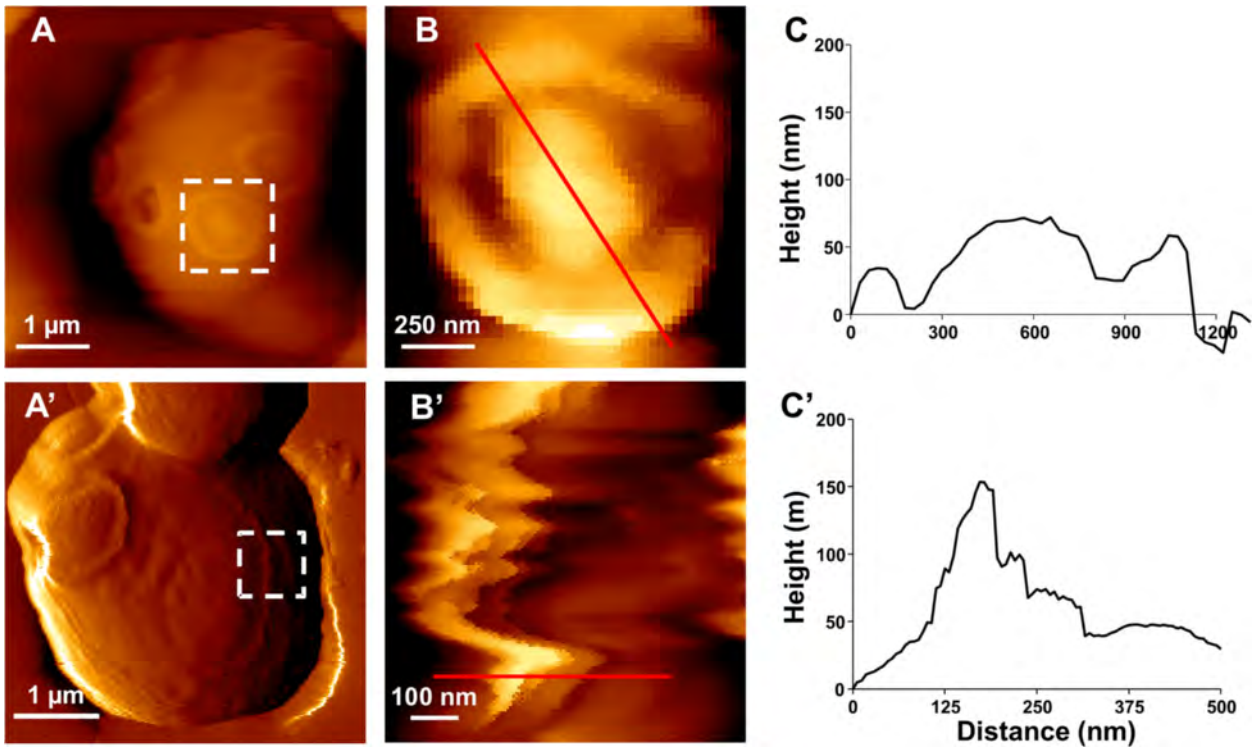

Figure 2 Morphological differences between a bud scar (BS) and circular structure (CS) at the cell surface. In **(A, A')**, AFM deflection image of an unstressed and of a heat-shocked yeast cell after 1 hr at 42°C at a z range of 2.5 µm. The white dotted squares indicated AFM height image analysis for the BS **(A)** and for part of the CS **(A')**. In **(B & B')** are zoomed height images of these squares area (at z range of 200 nm). In **(C & C')** are cross sections taken across the red lines, respectively in **B** and **B'** respectively.

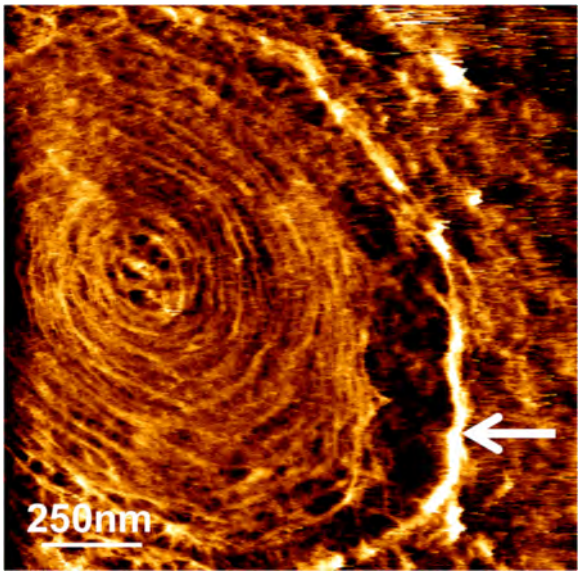

Figure 3 Exploring the ultrastructure of a CS by AFM. High-resolution deflection image shows a succession of concentric rings, followed by 1 major ring (white arrow).

Chitin content in cell wall and link with cell wall stiffness

The formation of a cell surface CS and the increased stiffness suggested that the biochemical composition of the cell wall could have been modified in response to heat shock. To explore this hypothesis, we performed biochemical measurements of carbohydrate composition of the cell wall. As reported in Table 1, levels of β-glucan and mannans were not different between unstressed yeast cells and cells incubated at 42°C for 1 h. In contrast, the heat shock treatment clearly induced a 45% increase in the chitin content (from 46.2 µg/mg in unstressed cells to 68.3 µg/mg in cells after 1 h incubation at 42°C). To verify that this increase of chitin was preferentially associated with the formation of the CS, we visualized this polymer after staining it with calcofluor white (CFW). As expected, the presence of bud scars with a diameter around 1 µm was clearly visible on a yeast cell cultivated at 30°C (Figure 6A). However, it was interesting to notice that a ring of chitin with a diameter above 2 µm roughly co-localized with the CS in a heat shocked cell for 1 hr at 42°C (Figure 6B & C). Taken together, these result suggested that the increase of cells stiffness in response to heat shock may be linked to chitin levels.

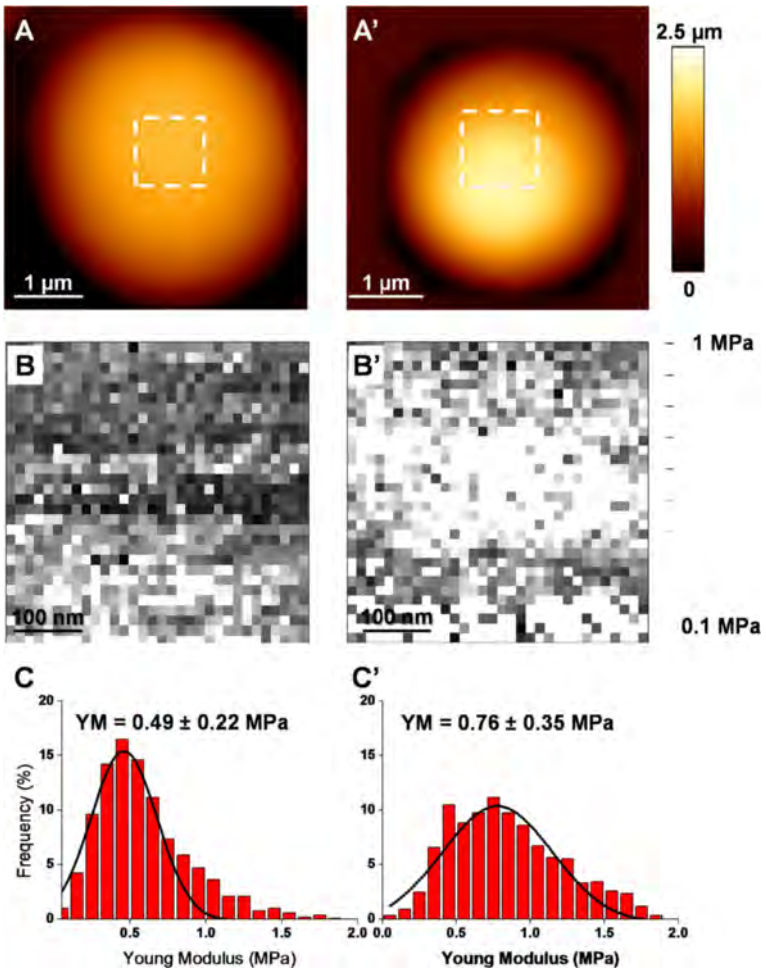

Figure 4 Yeast stiffness is increased by heat-shock at 42 °C. Young's Modulus (YM) determinations on an unstressed **(A–C)** and a heat-shocked cells **(A'-C')**. The white squares showed in the height images, (z range = 2 µm) **(A, A'),** indicate the localization of the elasticity maps shown in **(B, B')**. Histograms of the YM distributions **(C, C')** associated with the elasticity maps. YM medians were calculated by fitting a Gauss model (indicated by the black curves).

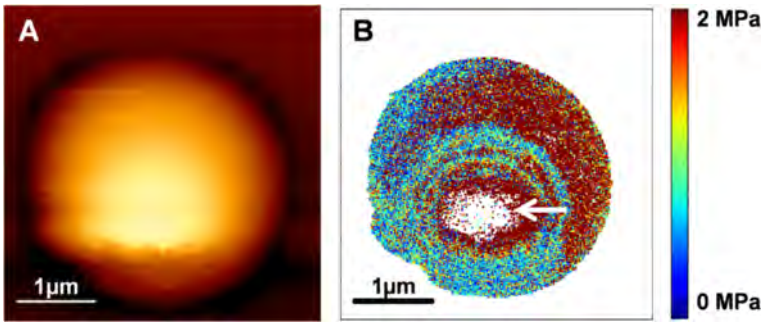

Figure 5 Stiffness map of a heat-shocked yeast cell. Height image (z range of 2.5 µm) **(A)**, with the corresponding elasticity map in quantitative mode, **(B)** at the z range of 2 MPa. A higher young modulus was characterized in the central part of CS (white arrow).

Table 1 The chitin content in cell wall is increased upon heat-shock

	Chitin	β-glucans	Mannans
30°C	46.2 ± 9.5	440 ± 115	293 ± 24
42°C	68.3 ± 3.3	408 ± 99	301 ± 17

Carbohydrate composition of cell wall from unstressed (30°C) and heat-shocked cells during 1 h at 42°C were determined by acid hydrolysis for β-glucans and mannans and by enzymatic digestion for chitin. Values reported in μg per mg of dry cell wall are the mean ± SD of 3 biological independent experiments technically repeated 2 times.

The formation of the cellular surface CS is dependent on the budding process

The finding that this singular CS was found on about 40% of the heat-shocked cells, showing some morphological signs of a bud, and produced at the vicinity of a previous bud, raised the hypothesis that this structure might be dependent upon the budding machinery system. The process of budding has been thoroughly investigated at the biological, genetic and molecular levels, and showed the implication of many genes and many structural and regulatory networks that encompass cell polarity, cytoskeleton, secretory pathway, cell signaling, etc. [31]. To provide a first biological evidence that the CS formation is dependent on the budding process, we used latrunculin A (LatA), a toxin known to destabilize the actin cytoskeleton [32] that is implicated in the budding process. Exponentially growing cells were subjected to a heat shock at 42°C for 1 hr in the presence of 200 μM LatA. On a sampling of 10 independent yeast cells, we were unable to observe any CS at the cell surface, as compared to results with heat-shocked cells not treated with LatA (Additional file 4: Figure S3A). Furthermore, in the absence of heat shock, the perturbation of the actin cytoskeleton by LatA did not lead to the formation of CS (Additional file 4: Figure S3BC). To get additional biological evidence that the CS involves the budding process, we performed heat shock experiments with exponentially growing yeast cells that were incubated in a nitrogen-depleted medium for 72 hr. This condition results in growth arrest in G1 phase of the cell cycle with virtually all the cells unbudded [33] They were then subjected to heat shock at 42°C for one hour and AFM analysis was carried out on 10 starved cells before and 1 hr after heat-shock. In none of the heat-shocked cells, could we find any CS at the cell surface (Additional file 5: Figure S4). This result can be taken as indirect evidence that CS is depending on the budding process, because of the inability of the nitrogen-starved yeast cells to bud both at 30 and 42°C. Thus, the circular structure only forms during active cell growth and this cannot be separated from a cell-cycle phase specific defect.

At the genetic level, we addressed this question using targeted mutants such as *chs3Δ* that is defective in chitin ring formation during bud emergence [34], *chs1Δ* since the loss of this gene impairs septum reparation during cytokinesis [35] as well as a mutant deleted for *BNI1* because this gene encodes a formin protein that is required for the proper initiation of bud growth and the proper shape of vegetative buds through formation of actin cables [36]. High resolution AFM imaging carried out on 15 cells from 3 independent experiments did not reveal any formation of singular cell surface CS in these different mutants after a heat shock at 42°C for 1 h (Additional file 6: Figure S5).

The formation of the cellular surface CS is regulated by CWI pathway

Heat shock is known to activate the CWI pathway, and the surface sensor Wsc1 is one of the sensors that detect and transmit this cell wall stress to the signaling cascade [37]. To evaluate whether the formation of the cell surface CS was under the control of the CWI signaling and whether Wsc1 could be implicated in this response, both *bck1Δ* mutant defective in the MAP kinase of the CWI pathway [38] and *wsc1Δ* mutant cells were analyzed by

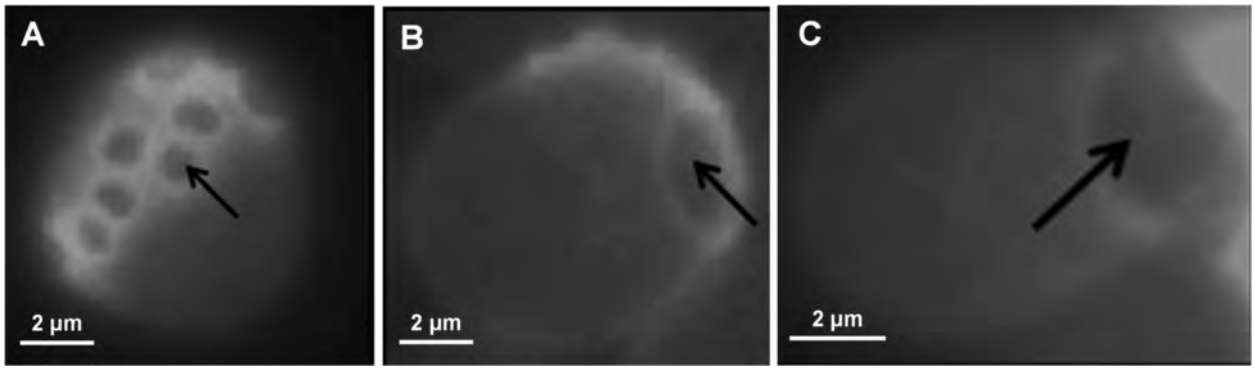

Figure 6 Fluorescence images of calcofluor white stained yeast cells. In **(A),** BY4741 cells cultivated at 30 °C showing bud scars. **(B & C),** BY4741 cells after 1 h of heat shock showing the circular structure **B** and **C**.

AFM before and after 1 hr heat shock at 42°C. As compared to the wild type cells, which under this heat stress condition exhibited a large cell surface CS, neither the *bck1Δ* nor *wsc1Δ* cells imaged by AFM presented this singular structure (Additional file 7: Figure S6). The failure to identify any CS formation on these mutants upon 1 hr incubation at 42°C could not be due to cell death nor loss of heat shock response, since loss of viability of *wsc1Δ* and *bck1Δ* mutants was only 1 and 25% respectively (Additional file 2: Table S1), and both mutants readily accumulated trehalose in response to the thermal stress as wild type cells (Additional file 1: Figure S1). In addition, we failed to identify this structure on more than 20 independent analyzed *wsc1Δ* and *bck1Δ* mutant cells. Therefore, these results support an implication of CWI pathway in the formation of the cell surface CS. We also noticed that the YM of the unstressed *wsc1Δ* was comparable to the one determined on heat-shocked wild type cells (Additional file 8: Figure S7). Also, these unstressed *wsc1Δ* cells exhibited a chitin content twofold higher than the wild type cells (Additional file 9: Table S2), arguing in favor of a correlation between chitin content and stiffness of the cell wall. After exposure to 42°C for 1 h, the YM values and the chitin content in the *wsc1Δ* mutant were not significantly affected (Additional files 8 and 9: Figure S7 and Table S2).

Discussion

The Atomic Force Microscopy (AFM) is nowadays the most powerful scanning microscopy tool used to visualize and to explore the dynamics of living cells at the nanometer resolution under physiological conditions. Being also a force machine, it allows force spectroscopy measurements of the cell mechanics [39]. Therefore, it is a superb method for investigating the biomechanical consequences of a heat shock on the yeast cell, with the eventual aim to correlate the putative biophysical changes observed using this methodology to the largely documented molecular and metabolic responses to heat shock [23]. In this study, we reported for the first time the formation of a circular structure (CS) that is induced upon exposure of yeast cell to 42°C. The high resolution AFM imaging clearly indicated that this singular feature takes its origin from a single point and propagates in concentric rings during the time of incubation at 42°C. In addition, this singular CS was observed in yeast cells immobilized by two different methods, which further supports the idea that the formation of this feature is a true morphological event induced by heat shock. The reason why Adya *et al.* [27] did not find this morphological event in their heat shock study by AFM could be explained by the immobilisation technique these authors used, which likely destroyed the integrity of the cell surface.

The discovery of only one singular CS per cell (although we could not preclude that another one was formed underside of the cell since this was not accessible to the AFM analysis), together with the close vicinity of this structure to a previous bud and with the fact that it appeared on about 40% of the heat shocked cells were indications that this amazing structure may be related to a failure in the budding emergence and/or in the budding process. This suggestion is supported by the inability of a mutant defective in *BNI1* encoding a formin protein that is needed for proper bud pattern formation to produce the CS in response to heat shock. The function of this protein is to assemble linear actin cables along the mother daughter axis and at the bud neck [40]. The polarization of the actin cytoskeleton is an essential process for cell expansion and budding in the yeast *S. cerevisiae*, and a defect in this process results in abnormal morphology characterized either by elongated buds or spherical buds [36]. Delley & Hall [41] have reported that a mild heat shock from 24 to 37°C induces a transient depolarization of the actin cytoskeleton that is accompanied by a transient depolarized distribution of the β-glucan synthase complex, composed of the catalytic subunits Fks1 or Fks2 and the regulatory subunit Rho1. They further showed that this depolarization of the actin cytoskeleton and β-glucan synthase was mediated by the plasma membrane protein Wsc1. Interestingly, we found that heat-induced formation of CS was abolished when latrunculin A, a toxin molecule known to disrupt actin cystokeleton [32], was added prior to the thermal stress, as well as in *wsc1Δ* mutant cells. In addition, the use of Calcofluor white staining method highlighted the presence of chitin rings at the vicinity of the CS outer ring. This finding is reminiscent of the presence of the chitin ring that delimitate the bud scars on the yeast cell surface [30]. Taken together, these results support the idea that the heat-induced formation of CS is a morphological consequence at the cell surface of a defective budding process due to perturbation of the actin cytoskeleton depolarization process.

It is known that the CWI pathway is activated under heat stress and although the cell surface mechanosensor Wsc1 is important in detecting this cell wall stress and to transmit the signal to the Pkc1 MAP kinase cascade [42], it is not the sole sensor implicated in the heat stress response [43]. Therefore, the finding that *bck1Δ* mutant cells, defective in the MAP kinase of the CWI pathway, could not produce this structure in response to the thermal stress indicates that the morphological process that leads to CS formation is indeed under the control of the CWI pathway.

The nanomechanical properties of yeast cells obtained from the AFM force volume curves showed that the heat stress caused a twofold increase in the Young's Modulus

values, indicating that the stiffness of the cell wall was increased (or its elasticity decreased). Interestingly, the measurement of cell wall β-glucans, mannans and chitin in yeast cells exposed to 42°C only showed an increase of approximately twofold of the chitin content. Moreover, the loss of *WSC1* resulted also in a twofold increase of both the chitin content and the Young's Modulus. Taken together, these results suggest that the cell wall elasticity is mainly linked to the relative changes in the chitin content as described recently by Formosa *et* al. [44]. This result does not contradict our previous work showing that the cell wall elasticity was merely dependent on cross-linkages between chitin and β-glucans rather than on a particular cell wall component [6], since chitin content is in fact the most critical component that ensures strength of the cell wall through the covalent connection that it makes with the other cell wall components.

Conclusions

The powerful technology AFM allowed identifying and precisely describing an unexpected morphological phenomenon occurring at the cell surface, which may explain physically how yeast cells are damaged by temperature stress and could eventually lead to cell death. Our results are also relevant in regards to the rough industrial growth conditions and processes which the yeast *S. cerevisiae* has to cope with, and which may cause comparable morphological defects at the cell surface.

Materials and methods

Yeast strains and growth conditions

Yeast strain BY4741 (MATa *his3Δ1 leu2Δ10 met15Δ0 ura3Δ0*) [45] and its isogenic deletion mutants *wsc1Δ*, *bck1Δ*, *chs1Δ*, *chs3Δ* and *bni1Δ* obtained from Open Biosystem (USA) were used in this study. Yeast cells were routinely cultivated at 30°C in a standard rich YEPD (Yeast Extract Peptone Dextrose) medium containing 10 g/l of yeast extract, 20 g/l of peptone and 20 g/l of dextrose. Heat shock experiments were carried out with exponentially growing cells (OD_{600} at 1–2 unit) by putting part of the yeast culture (10 mL in 50 mL Erlen flask) in a water bath set at 42°C during 1 h.

Latrunculin A and nitrogen starvation experiments

Latrunculin [32] was added at 200 μM to exponentially growing cells cultivated at 30°C or just before transferring yeast culture cells at 42°C. For nitrogen starvation experiment, exponentially growing cells in YEPD (collected at OD_{600} at 1.0 unit) were washed 3 times in nitrogen-depleted medium (50 mM of phosphate without nitrogen, 2% of glucose, pH 6.2) and resuspended at OD_{600} of 1.0 unit in this medium for 72 h at 30°C before heat shock as described above.

AFM sample preparation

Yeast cells were immobilized according to two different protocols. The first method consisted in filtering a small volume of yeast culture (1 to 5 mL) through a polycarbonate membrane pore sizes of 5 μm in order to trap cells into the micrometer size pores of the nylon filter (Merck Millipore, Darmstadt, Germany). After filtration, the filter was washed once with 4 mL of acetate buffer 20 mM, pH 5.5. In the second method, the cells were captured in microstructured polydimethylsiloxane (PDMS) stamps according to [28]. Briefly, 1 mL of the cell culture were washed quickly 3 times with 1 mL of AFM buffer (18 mM CH_3COONa, 1 mM $CaCl_2$ and 1 mM $MnCl_2$, pH 5.2), resuspended in 1 mL of the same buffer, and 100 μl of this cell suspension was deposited on a freshly oxygen activated microstructured PDMS stamp. The cells were allowed to stand for 15 min at room temperature and then forced to enter the microstructures of the stamp by convective/capillary assembly [28]. A typical example of cells immobilized in holes of a PDMS stamp is given in Additional file 10: Figure S8. To get statistical significance of the AFM data, about 10–12 cells have been analyzed from three independent experiments. In addition, three independent investigators performed AFM experiments. Each investigator has analyzed 10–12 cells.

AFM imaging and Force spectroscopy experiments

AFM images of yeast cells trapped in polycarbonate membrane were recorded with a Nanowizard II form JPK (JPK Instruments, Berlin, Germany), in contact mode, using OTR4 (Olympus provided by Bruker) cantilevers. AFM experiments on yeasts immobilized on PDMS stamps were performed with a Nanowizard III form JPK (JPK Instruments, Berlin, Germany) in contact mode, Quantitative Imaging mode (QI) [46] and Force Volume mode (FV). The cantilevers used (OTR4 and MLCT) had a spring constant measured by the thermal noise method [47] ranging from 0.01 to 0.5 N/m. Cell wall elasticity was deduced from the Young's modulus which was calculated from FV measurement using the Hertz model [48].

Extraction of cell wall and determination of β-glucan and mannan polysaccharides

Yeast cells (about 50 mg dry mass or 10^9 cells) were collected by centrifugation (5 min, 3000 g), washed once with 10 mL of cold sterilized water, and after a second centrifugation, cell pellet was resuspended in cold water. The cell walls (about 10 mg dry mass) obtained from control and heat shocked yeast cells were extracted

according to the protocol described by Dallies *et al*. [49]. The content of β-glucans and mannans in the *S. cerevisiae* cell walls were determined by acid sulfuric hydrolysis method as described by François [50]. The released monosaccharides (glucose and mannose) were quantified by HPAEC-PAD on a Dionex-ICS 5000 system (Thermofisher Scientific, France). Separation was performed on a CarboPac PA10 analytical column (250 × 4 mm) with a guard column CarboPac PA10, by an isocratic elution of NaOH 18 mM at 25°C and a flow rate of 1 mL/min. Detection was performed by pulsed amperometric system equipped with a gold electrode.

Analytical methods

Intracellular trehalose level was determined as previously described [51]. For accurate chitin determination in the yeast cell wall, an enzyme assay has been used as follows. Lyophilized cell walls (about 10 mg) were suspended in 200 μl of 50 mM potassium acetate buffer, pH 5.0 and boiled at 65°C for 5 min. After mixing and cooling to ambient temperature, the cell wall suspension was treated with 1U of chitinase from *Streptomyces griseus* (Sigma-Aldrich, France) for 24 h at 37°C. The *N*-acetyl glucosamine released by the chitinase action was then determined using a colorimetric method as described by Reissig *et al*. [52] and adapted for a micro method. Briefly, 125 μl of the enzymatic mixture was heated with 25 μl of 0.8 M potassium tetraborate pH 9.0 at 100°C for 8 minutes. After cooling at room temperature, 750 μl of Reissig reagent (10 g of 4-dimethylaminobenzaydedyde dissolve in 12.5 mL 10 N HCl and 87.5 mL of glacial acetic acid) diluted ten times in deionized water was added, and the tubes were incubated 40 minutes at 37°C. The absorbance was read at 585 nm. The chitin content was obtained from N-acetylglucosamine standard curve (from 0 to 100 μg/mL) made in the same condition.

Miscellaneous methods

Calcofluor white treatment of yeast cells before and 1 hr after heat shock was carried out as following the procedure described in [53]. Cell viability was performed using methylene blue according to [54].

Additional files

Additional file 1: Figure S1. The accumulation of trehalose is correlated with survival of cells under heat stress condition. Comparison of trehalose accumulation in the wild-type yeast BY4741 and the defective mutants *wsc1*Δ and *bck1*Δ. Control (full bar) and heat-shocked condition (hachured bar) are represented.

Additional file 2: Table S1. Evaluation of viability by blue methylene test. The percentage of mortality was evaluated before and after heat shock with the defective mutants *wsc1* and *bck1*, and the wild-type yeast with or without nitrogen starvation during 72 h.

Additional file 3: Figure S2. Young modulus increase with heat-shock. Distribution of Young modulus values calculate with 19 elasticity maps (n_{curves} = 19443) from individual yeasts unstressed **(A)**, in comparison with 15 elasticity maps (n_{curves} = 15307) from individual yeasts heat-shocked at 42°C **(B)**. YM medians were indicated on diagrams and calculated from fits in gauss model (red curves). **(C)** Statistic unpaired t test between averages and standard deviations calculated from young modulus values. The 3 asterisks shown significant differences between elasticity of unstressed yeasts (full bar) and heat-shock yeasts (hachured bar) at the P value < 0.0001.

Additional file 4: Figure S3. The absence of F-Actin prevent the formation CS. AFM high resolution images of wild-type cells after heat shock in absence **(A)** or in presence of 200 μM Latrunculin A **(B)**. Cells incubated 1 hr at 30°C with 200 μM of Latrunculin A **(C)**.

Additional file 5: Figure S4. The formation of CS require budding process. High-resolution deflection images of wild-type incubate 72 h at 30°C in nitrogen starvation, without **(A)** or with heat shock 1 hr at 42°C **(B)**.

Additional file 6: Figure S5. The heat-induced formation of the cell surface circular structure is abolished in mutants defective in the budding process. High-resolution AFM deflection images of *bni1*Δ **(A)**, *chs3*Δ **(B)** and *chs1*Δ **(C)** mutants after heat shock.

Additional file 7: Figure S6. The CWI controls the stiffness of the cell wall and the formation of the cell surface circular structure in response to heat shock. High-resolution AFM deflection images of wild-type cell **(A)**, *wsc1*Δ **(B)** and *bck1*Δ **(C)** cell defective in the CWI pathway imaged after 1 hr of incubation at 42°C.

Additional file 8: Figure S7. The stiffness of *wsc1*Δ unstressed was similar to wild-type yeast exposed at 42°C during 1 h. Distribution of Young modulus values calculate with 4 elasticity maps (n = 4096) from individual *wsc1*Δ yeasts unstressed.

Additional file 9: Table S2. Chitin rate was similar in *wsc1*Δ mutant with or without heat-shock at 42°C. Carbohydrate composition of *wsc1*Δ mutant was determinated by acid hydrolysis and enzymatic method and expressed in μg/mg of cell wall dry mass.

Additional file 10: Figure S8. Yeast immobilization on PDMS stamp. **(A)** AFM height image of a PDMS stamp containing some immobilized yeasts. The z range is 2.5 μm. **(B)** 3D projection associated to the height image.

Competing interests

We declare that we have no competing interest.

Authors' contributions

ED and JMF are the lead authors of the paper. FP and SL carried out the most of the AFM experiments. MS performed extraction and analysis of carbohydrates contents in yeast. CF worked on complementary AFM experiments. HMY participated in writing the paper and performed the biological part of the experiments. All authors read and approved the final manuscript.

Acknowledgement

We thank the team of J.M François for fruitful discussions and experimental help. We are grateful to Louise Chopinet for collaboration in statistical analysis. This work was supported by an ANR young scientist program (AFMYST project ANR-11-JSV5-001-01 n° SD 30024331) to ED and by a grant n°10051296 from Region Midi Pyrénées to JMF. ED is researcher at the Centre National de Recherche Scientifique (CNRS). CF and MS are respectively supported by a grant from "Direction Générale de l'Armement" (DGA) and from Lallemand SAS.

Author details

[1]CNRS, LAAS, 7 avenue du colonel Roche, F-31077 Toulouse, France. [2]Université de Toulouse, UPS, INSA, INP, ISAE, LAAS, F-31077 Toulouse, France. [3]CNRS, ITAV-USR 3505, F31106 Toulouse, France. [4]Université de Toulouse, INSA, UPS, INP, 135 avenue de Rangueil, F-31077 Toulouse, France. [5]INRA, UMR792 Ingénierie des Systèmes Biologiques et des Procédés, F-31077 Toulouse, France. [6]CNRS, UMR5504, F-31400 Toulouse, France. [7]CNRS, UMR 7565, SRSMC, Vandoeuvre-lès-Nancy, France. [8]Université de Lorraine, UMR 7565, Faculté de Pharmacie, Nancy, France.

Received: 9 December 2013 Accepted: 10 January 2014
Published: 27 January 2014

References

1. Dupres V, Dufrêne YF, Heinisch JJ: **Measuring Cell Wall Thickness in Living Yeast Cells Using Single Molecular Rulers.** *ACS Nano* 2010, **4:**5498–5504.
2. Klis FM, Mol P, Hellingwerf K, Brul S: **Dynamics of cell wall structure in Saccharomyces cerevisiae.** *FEMS Microbiology Reviews* 2002, **26:**239–256.
3. Aguilar-Uscanga B, François J m: **A study of the yeast cell wall composition and structure in response to growth conditions and mode of cultivation.** *Letters in Applied Microbiology* 2003, **37:**268–274.
4. Klis FM, Boorsma A, De Groot PWJ: **Cell wall construction in Saccharomyces cerevisiae.** *Yeast* 2006, **23:**185–202.
5. Smits JG, Kapteyn CJ, van den Ende H, Klis MF: **Cell wall dynamics in yeast.** *Current Opinion in Microbiology* 1999, **2:**348–352.
6. Dague E, Bitar R, Ranchon H, Durand F, Yken HM, François JM: **An atomic force microscopy analysis of yeast mutants defective in cell wall architecture.** *Yeast* 2010, **27:**673–684.
7. Kollár R, Reinhold BB, Petráková E, Yeh HJC, Ashwell G, Drgonová J, Kapteyn JC, Klis FM, Cabib E: **Architecture of the Yeast Cell Wall β(1 → 6)-glucan interconnects mannoprotein, β(1 → 3)-glucan, and chitin.** *J Biol Chem* 1997, **272:**17762–17775.
8. Shahinian S, Dijkgraaf GJ, Sdicu AM, Thomas DY, Jakob CA, Aebi M, Bussey H: **Involvement of protein N-glycosyl chain glucosylation and processing in the biosynthesis of cell wall beta-1,6-glucan of Saccharomyces cerevisiae.** *Genetics* 1998, **149:**843–856.
9. Levin DE: **Cell Wall Integrity Signaling in Saccharomyces cerevisiae.** *Microbiol Mol Biol Rev* 2005, **69:**262–291.
10. Gibson BR, Lawrence SJ, Leclaire JPR, Powell CD, Smart KA: **Yeast responses to stresses associated with industrial brewery handling.** *FEMS Microbiology Reviews* 2007, **31:**535–569.
11. Canetta E, Walker GM, Adya AK: **Nanoscopic morphological changes in yeast cell surfaces caused by oxidative stress: an atomic force microscopic study.** *J Microbiol Biotechnol* 2009, **19:**547–555.
12. Kobayashi N, McEntee K: **Evidence for a heat shock transcription factor-independent mechanism for heat shock induction of transcription in Saccharomyces cerevisiae.** *PNAS* 1990, **87:**6550–6554.
13. Yeh J, Haarer BK: **Profilin is required for the normal timing of actin polymerization in response to thermal stress.** *FEBS Letters* 1996, **398:**303–307.
14. Zhao XQ, Bai FW: **Mechanisms of yeast stress tolerance and its manipulation for efficient fuel ethanol production.** *Journal of Biotechnology* 2009, **144:**23–30.
15. Kim KS, Kim Y-S, Han I, Kim M-H, Jung MH, Park H-K: **Quantitative and Qualitative Analyses of the Cell Death Process in Candida albicans Treated by Antifungal Agents.** *PLoS ONE* 2011, **6:**e28176.
16. El-Kirat-Chatel S, Beaussart A, Alsteens D, Jackson DN, Lipke PN, Dufrêne YF: **Nanoscale analysis of caspofungin-induced cell surface remodelling in Candida albicans.** *Nanoscale* 2013, **5:**1105–1115.
17. Levin DE: **Regulation of Cell Wall Biogenesis in Saccharomyces cerevisiae: The Cell Wall Integrity Signaling Pathway.** *Genetics* 2011, **189:**1145–1175.
18. Cabib E, Durán A: **Synthase III-dependent Chitin Is Bound to Different Acceptors Depending on Location on the Cell Wall of Budding Yeast.** *J Biol Chem* 2005, **280:**9170–9179.
19. Valdivieso M-H, Ferrario L, Vai M, Duran A, Popolo L: **Chitin Synthesis in a gas1 Mutant ofSaccharomyces cerevisiae.** *J Bacteriol* 2000, **182:**4752–4757.
20. Lesage G, Bussey H: **Cell Wall Assembly in Saccharomyces cerevisiae.** *Microbiol Mol Biol Rev* 2006, **70:**317–343.
21. Dague E, Gilbert Y, Verbelen C, Andre G, Alsteens D, Dufrêne YF: **Towards a nanoscale view of fungal surfaces.** *Yeast* 2007, **24:**229–237.
22. Dufrêne YF: **Atomic force microscopy of fungal cell walls: an update.** *Yeast* 2010, **27:**465–471.
23. Verghese J, Abrams J, Wang Y, Morano KA: **Biology of the Heat Shock Response and Protein Chaperones: Budding Yeast (Saccharomyces cerevisiae) as a Model System.** *Microbiol Mol Biol Rev* 2012, **76:**115–158.
24. Neves MJ, Francois J: **On the mechanism by which a heat shock induces trehalose accumulation in Saccharomyces cerevisiae.** *Biochem J* 1992, **288** (Pt 3)**:**859–864.
25. Postmus J, Canelas AB, Bouwman J, Bakker BM, van Gulik W, de Mattos MJT, Brul S, Smits GJ: **Quantitative Analysis of the High Temperature-induced Glycolytic Flux Increase in Saccharomyces cerevisiae Reveals Dominant Metabolic Regulation.** *J Biol Chem* 2008, **283:**23524–23532.
26. Gasch AP, Spellman PT, Kao CM, Carmel-Harel O, Eisen MB, Storz G, Botstein D, Brown PO: **Genomic Expression Programs in the Response of Yeast Cells to Environmental Changes.** *Mol Biol Cell* 2000, **11:**4241–4257.
27. Adya AK, Canetta E, Walker GM: **Atomic force microscopic study of the influence of physical stresses on Saccharomyces cerevisiae and Schizosaccharomyces pombe.** *FEMS Yeast Research* 2006, **6:**120–128.
28. Dague E, Jauvert E, Laplatine L, Viallet B, Thibault C, Ressier L: **Assembly of live micro-organisms on microstructured PDMS stamps by convective/capillary deposition for AFM bio-experiments.** *Nanotechnology* 2011, **22:**395102.
29. Virgilio C, Hottiger T, Dominguez J, Boller T, Wiemken A: **The role of trehalose synthesis for the acquisition of thermotolerance in yeast. I. Genetic evidence that trehalose is a thermoprotectant.** *European Journal of Biochemistry* 1994, **219:**179–186.
30. Cabib E, Roh D-H, Schmidt M, Crotti LB, Varma A: **The Yeast Cell Wall and Septum as Paradigms of Cell Growth and Morphogenesis.** *J Biol Chem* 2001, **276:**19679–19682.
31. Drees BL, Sundin B, Brazeau E, Caviston JP, Chen G–C, Guo W, Kozminski KG, Lau MW, Moskow JJ, Tong A, Schenkman LR, McKenzie A, Brennwald P, Longtine M, Bi E, Chan C, Novick P, Boone C, Pringle JR, Davis TN, Fields S, Drubin DG: **A protein interaction map for cell polarity development.** *J Cell Biol* 2001, **154:**549–576.
32. Sahin A, Daignan-Fornier B, Sagot I: **Polarized Growth in the Absence of F-Actin in Saccharomyces cerevisiae Exiting Quiescence.** *PLoS ONE* 2008, **3:**E2556.
33. Futcher B: **Metabolic cycle, cell cycle, and the finishing kick to Start.** *Genome Biol* 2006, **7:**107.
34. Ziman M, Chuang JS, Schekman RW: **Chs1p and Chs3p, two proteins involved in chitin synthesis, populate a compartment of the Saccharomyces cerevisiae endocytic pathway.** *Mol Biol Cell* 1996, **7:**1909–1919.
35. Cabib E, Silverman SJ, Shaw JA: **Chitinase and chitin synthase 1: counterbalancing activities in cell separation of Saccharomyces cerevisiae.** *J Gen Microbiol* 1992, **138:**97–102.
36. Pruyne D, Bretscher A: **Polarization of cell growth in yeast. I. Establishment and maintenance of polarity states.** *J Cell Sci* 2000, **113:**365–375.
37. Lodder AL, Lee TK, Ballester R: **Characterization of the Wsc1 protein, a putative receptor in the stress response of Saccharomyces cerevisiae.** *Genetics* 1999, **152:**1487–1499.
38. Lee KS, Levin DE: **Dominant mutations in a gene encoding a putative protein kinase (BCK1) bypass the requirement for a Saccharomyces cerevisiae protein kinase C homolog.** *Mol Cell Biol* 1992, **12:**172–182.
39. Dufrêne YF, Pelling AE: **Force nanoscopy of cell mechanics and cell adhesion.** *Nanoscale* 2013, **5:**4094–4104.
40. Pruyne D, Legesse-Miller A, Gao L, Dong Y, Bretscher A: **Mechanisms of Polarized Growth and Organelle Segregation in Yeast.** *Annual Review of Cell and Developmental Biology* 2004, **20:**559–591.
41. Delley P-A, Hall MN: **Cell Wall Stress Depolarizes Cell Growth via Hyperactivation of Rho1.** *J Cell Biol* 1999, **147:**163–174.
42. Verna J, Lodder A, Lee K, Vagts A, Ballester R: **A family of genes required for maintenance of cell wall integrity and for the stress response in Saccharomyces cerevisiae.** *PNAS* 1997, **94:**13804–13809.
43. Winkler A, Arkind C, Mattison CP, Burkholder A, Knoche K, Ota I: **Heat Stress Activates the Yeast High-Osmolarity Glycerol Mitogen-Activated Protein Kinase Pathway, and Protein Tyrosine Phosphatases Are Essential under Heat Stress.** *Eukaryotic Cell* 2002, **1:**163–173.
44. Formosa C, Schiavone M, Martin-Yken H, François JM, Duval RE, Dague E: **Nanoscale effects of caspofungin against two yeast species, Saccharomyces cerevisiae and Candida albicans.** *Antimicrob Agents Chemother* 2013, **57:**3498–3506.
45. Baker Brachmann C, Davies A, Cost GJ, Caputo E, Li J, Hieter P, Boeke JD: **Designer deletion strains derived from Saccharomyces cerevisiae S288C: A useful set of strains and plasmids for PCR-mediated gene disruption and other applications.** *Yeast* 1998, **14:**115–132.
46. Chopinet-Mayeux L, Formosa C, Rols M-P, Duval RE, Dague E: **Imaging living cells surface and quantifying its properties at high resolution using AFM in QITM mode.** *Micron*. In press.
47. Hutter JL, Bechhoefer J: **Calibration of atomic force microscope tips.** *Review of Scientific Instruments* 1993, **64:**1868–1873.
48. Hertz H: **Ueber die Berührung fester elastischer Körper.** *Journal für die reine und angewandte Mathematik* 1882, **1881:**156–171.

49. Dallies N, François J, Paquet V: **A new method for quantitative determination of polysaccharides in the yeast cell wall. Application to the cell wall defective mutants of Saccharomyces cerevisiae.** *Yeast* 1998, **14:**1297–1306.
50. François JM: **A simple method for quantitative determination of polysaccharides in fungal cell walls.** *Nat Protoc* 2006, **1:**2995–3000.
51. Parrou JL, François J: **A Simplified Procedure for a Rapid and Reliable Assay of both Glycogen and Trehalose in Whole Yeast Cells.** *Analytical Biochemistry* 1997, **248:**186–188.
52. Reissig JL, Strominger JL, Leloir LF: **A Modified Colorimetric Method for the Estimation of N-Acetylamino Sugars.** *J Biol Chem* 1955, **217:**959–966.
53. Baggett J j, Shaw J d, Sciambi C j, Watson H a, Wendland B: **Fluorescent Labeling of Yeast**. In *Current Protocols in Cell Biology*. John Wiley & Sons, Inc; 2001.
54. Teparić R, Stuparević I, Mrša V: **Increased mortality of Saccharomyces cerevisiae cell wall protein mutants.** *Microbiology* 2004, **150:**3145–3150.

doi:10.1186/1741-7007-12-6
Cite this article as: Pillet *et al.*: Uncovering by Atomic Force Microscopy of an original circular structure at the yeast cell surface in response to heat shock. *BMC Biology* 2014 **12**:6.

Appendix 2:

Deletion of the α-(1,3)-glucan synthase genes induces a restructuring of the conidial cell wall responsible for the avirulence of *Aspergillus fumigatus*

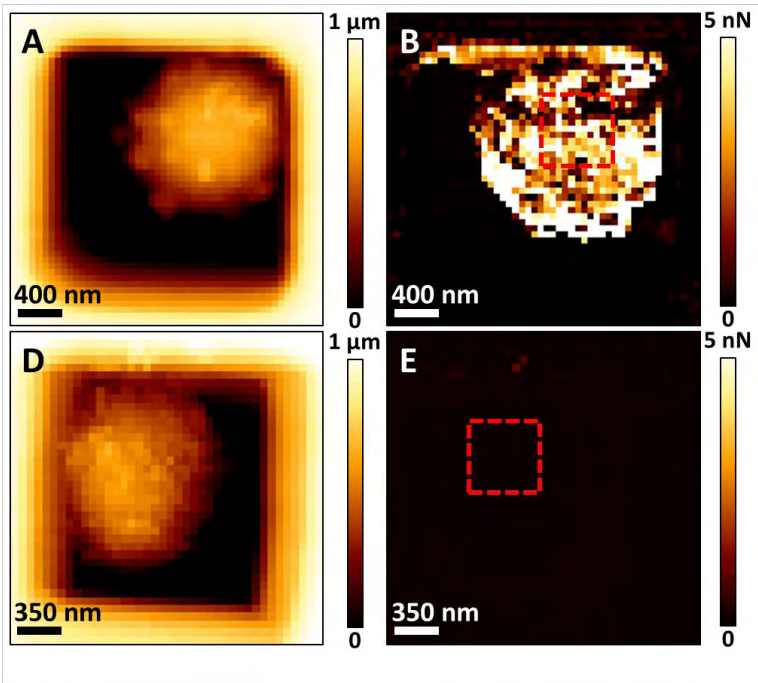

Beauvais A., Bozza S., Kniemeyer O., Formosa C., Bolloy V., Henry C., Roberson R. W., Dague E., Chignard M., Brakhage A. A., Romani L., and Latgé J. P.

Plos Pathogens, **9**, e1003716, 2014

Abstract

α-(1,3)-Glucan is a major component of the cell wall of Aspergillus fumigatus, an opportunistic human fungal pathogen. There are three genes (AGS1, AGS2 and AGS3) controlling the biosynthesis of α-(1,3)-glucan in this fungal species. Deletion of all the three AGS genes resulted in a triple mutant that was devoid of α-(1,3)-glucan in its cell wall; however, its growth and germination was identical to that of the parental strain in vitro. In the experimental murine aspergillosis model, this mutant was less pathogenic than the parental strain. The AGS deletion resulted in an extensive structural modification of the conidial cell wall, especially conidial surface where the rodlet layer was covered by an amorphous glycoprotein matrix. This surface modification was responsible for viability reduction of conidia in vivo, which explains decrease in the virulence of triple agsD mutant.

OPEN ACCESS Freely available online

PLOS | PATHOGENS

Deletion of the α-(1,3)-Glucan Synthase Genes Induces a Restructuring of the Conidial Cell Wall Responsible for the Avirulence of *Aspergillus fumigatus*

Anne Beauvais[1]*, Silvia Bozza[2], Olaf Kniemeyer[3,4], Céline Formosa[5], Viviane Balloy[6], Christine Henry[1], Robert W. Roberson[7], Etienne Dague[5], Michel Chignard[6], Axel A. Brakhage[3], Luigina Romani[2], Jean-Paul Latgé[1]

1 Unité des *Aspergillus*, Institut Pasteur, Paris, France, **2** Department of Experimental Medicine and Biochemical Sciences, University of Perugia, Perugia, Italy, **3** Molecular and Applied Microbiology, Leibniz-Institute for Natural Product Research and Infection Biology (HKI), University of Jena, Jena, Germany, **4** Integrated Research and Treatment Center, Center for Sepsis Control and Care Jena, University Hospital (CSCC), Jena, Germany, **5** CNRS, LAAS, Toulouse, France, **6** Unité de Défence Innée et Inflammation, Institut Pasteur, Inserm U874, Paris, France, **7** School of Life Sciences, Arizona State University, Tempe, Arizona, United States of America

Abstract

α-(1,3)-Glucan is a major component of the cell wall of *Aspergillus fumigatus*, an opportunistic human fungal pathogen. There are three genes (*AGS1*, *AGS2* and *AGS3*) controlling the biosynthesis of α-(1,3)-glucan in this fungal species. Deletion of all the three *AGS* genes resulted in a triple mutant that was devoid of α-(1,3)-glucan in its cell wall; however, its growth and germination was identical to that of the parental strain *in vitro*. In the experimental murine aspergillosis model, this mutant was less pathogenic than the parental strain. The *AGS* deletion resulted in an extensive structural modification of the conidial cell wall, especially conidial surface where the rodlet layer was covered by an amorphous glycoprotein matrix. This surface modification was responsible for viability reduction of conidia *in vivo*, which explains decrease in the virulence of triple *ags*Δ mutant.

Citation: Beauvais A, Bozza S, Kniemeyer O, Formosa C, Balloy V, et al. (2013) Deletion of the α-(1,3)-Glucan Synthase Genes Induces a Restructuring of the Conidial Cell Wall Responsible for the Avirulence of *Aspergillus fumigatus*. PLoS Pathog 9(11): e1003716. doi:10.1371/journal.ppat.1003716

Editor: Chad A. Rappleye, Ohio State University, United States of America

Received March 12, 2013; **Accepted** August 22, 2013; **Published** November 14, 2013

Funding: Research in the Aspergillus Unit of JP Latgé was supported by the ESF Fuminomics RNP-06132, ALLFUN FP7- 260338 and ERA-NetPathoGenoMics AntiFun. The funders had no role in study design, data collection and analysis, decision to publish, or preparation of the manuscript.

Competing Interests: The authors have declared that no competing interests exist.

* E-mail: anne.beauvais@pasteur.fr

Introduction

α-(1,3)-Glucan is a major cell wall component of most ascomycetous and basidiomycetous fungi, including the human pathogens that establish their disease upon inhalation of their infective morphotypes (e.g., *Paracoccidioides brasilisensis*, *Histoplasma capsulatum*, *Blastomyces dermatitidis*, *Cryptococcus neoformans Aspergillus fumigatus*). The role of this polysaccharide during infection has been demonstrated and the mechanisms of its involvement in establishing virulence have been forwarded [1,2]. In *C. neoformans*, α-(1,3)-glucan anchors the capsule, a well known virulence factor of this fungus, to the yeast cell wall and has been shown to be indirectly associated with virulence since a mutant devoid of α- (1,3)-glucan did not have any capsule and, most importantly, was unable to grow at 37°C [2]. In the yeast *H. capsulatum*, α-(1,3)-glucan was suggested to be essential for virulence because it masked immunogenic molecules: in the α-(1,3)-glucan synthase mutant, β-(1,3)-glucan that is recognized by Dectin-1, is exposed at the surface of the cell wall, whereas in the parental strain yeast cells, β-(1,3)-glucan is covered by α-(1,3)-glucan, preventing Dectin1-dependent immune response [1].

In *A. fumigatus*, α-(1,3)-glucan accounts for 40% and 19% of the mycelial and conidial cell wall polysaccharides, respectively [3]. It is a major adhesive involved in the aggregation of germinating conidia and in biofilm formation [4,5]. Moreover, it has been shown in experimental murine aspergillosis models that α-(1,3)-glucan has a prominent immunological function conferring a long-term survival [6]. This immune protection was associated with a reduced neutrophil recruitment in the lungs and reduced inflammatory pathology [6]. α-(1,3)-glucan, like conidia, confers a Th1/Treg protection and concomitant Th2 inhibition. These *in vivo* data were confirmed by *in vitro* experiments where dendritic cells pulsed with α-(1,3)-glucan induced Il12p70 production, a classical Th1 promoting cytokine [6]. However, the physiological role of α-(1,3)-glucan could not be further investigated in absence of the mutants devoid of α-(1,3)-glucan. In *A. fumigatus*, this polysaccharide is synthesized by three α-(1,3)-glucan synthases (Agsp) [3,7]. A triple deletion of the *AGS1*, *AGS2* and *AGS3* genes was recently generated in our lab that resulted in an *A. fumigatus* mutant lacking α-(1,3)-glucan in the cell wall. In contrast to other fungal pathogens, this triple *AGS A. fumigatus* deletion mutant did not show a distinct growth phenotype *in vitro* [8].

In the present study, three independently constructed triple *ags1*Δ*ags2*Δ*ags3*Δ (*ags*Δ) mutants devoid of α-(1,3)-glucan were used to investigate the role of α-(1,3)-glucan in *A. fumigatus* infection. As shown here, the virulence of these *A. fumigatus* triple *ags*Δ mutants was extremely attenuated in both immunocompetent and immunocompromised murine models of experimental aspergillosis tested. The defect in virulence correlated with a lack of vegetative fungal dissemination in the lungs, associated with a highly reduced

Author Summary

Aspergillus fumigatus is the predominant mold pathogen of humans, responsible for life-threatening systemic infections in patients with depressed immunity. Because of its external localization and specific composition, the fungal cell wall represents a target for recognition by and interaction with the host immune cells. In *A. fumigatus*, α-(1,3)-glucan is a key component of the extracellular matrix, which encloses the cell wall β-(1,3)-glucan-chitin fibrillar core. Interestingly, the deletion of the genes responsible for α-(1,3)-glucan synthesis resulted in a mutant that exhibited wild type phenotype *in vitro*; while the altered cell wall organization resulted in this fungus being avirulent *in vivo*. This study confirms that any modification in the cell wall components is associated with compensatory reactions developed by the fungus to counteract stress on the cell wall that may result in unexpected fungal response when challenged with the host immune system.

inflammation following conidial inoculation. Analysis of the conidia of the triple mutants showed that the lack of virulence of the mutants *in vivo* was associated to major changes occurring on the cell wall, especially on the surface of the resting and swollen conidia, which resulted in an increased killing by phagocytes.

Results

The *ags1*Δ*ags2*Δ*ags3*Δ (*ags*Δ) mutants are less virulent than the parental strain in murine model of aspergillosis

In the immunocompetent mice after four days of infection, the number of CFUs of the *ags*Δ mutants per lung was much lower than the CFUs per lung of the parental *ku80* strain (Fig. 1A; Fig. S1A). The reduced fungal burden of *ags*Δ was correlated to an absence of inflammation whereas a huge inflammatory response was observed with the parental strain (Fig. 1B, Fig. S1B). This was confirmed by the broncho-alveolar lavage (BAL) analysis, which showed a higher PMN recruitment after infection with *ku80* conidia compared with agsΔ (Fig. 1C, Fig. S1C). The reduced growth and inflammation in *ags*Δ infections was associated with an increase in the expression of the gene coding for the anti-inflammatory IL10 and a decreased expression of the gene coding for the pro-inflammatory TNFα in the lungs (Fig. 1D, Fig. S1D). In contrast, *ku80* infection was characterized by higher and lower expressions of TNFα and IL10, respectively.

The increased susceptibility of the *agsΔ* mutants was confirmed *in vitro* with murine alveolar macrophages isolated from BAL. After phagocytosis by the isolated macrophages, the killing of the *ags*Δ conidia was much higher than the parental strain. The resting conidia of *ags*Δ mutants were killed twice more than the parental strain after 2 h incubation with the macrophages (Fig. 1E). Further, after 6 h of incubation, the killing of the mutant reached 60–80% whereas a maximum of 30% of the parental strain conidia were killed at this time point (data not shown). Similar difference in the killing ratio between the mutant and parental strains was obtained when the conidia were pre-germinated (swollen conidia; after 6½ h incubation of the conidia in RPMI medium, at 37°C), suggesting that both resting and swollen conidia of the *ags*Δ mutants were more susceptible to conidial killing than the parental strain. This twofold increased killing susceptibility of the *ags*Δ mutants compared to parental strain did not change in the germinating morphotypes.

In the experimental model of aspergillosis using immunocompromised mice, the virulence of the *ags*Δ mutants was also significantly reduced. In a cyclophosphamide model of immunosuppression, infection with the *ku80* strain resulted in the mortality of all the mice within 4 days with a high inflammatory response, large foci of pneumonia and exudative bronchiolitis with destruction of bronchi and alveoli, whereas 60 to 80% mice infected by the *ags*Δ mutants survived and did not develop any inflammatory response (Fig. 2A–C, Fig. S2). Similar results were obtained when mice were immunocompromised by the injection of the RB6-8C5 MAb, which depletes circulating PMNs. Inhalation of the *ku80* conidia resulted in an extensive pulmonary fungal invasion with high inflammation (Fig. 2D–E). In contrast, in the RB6-8C5 MAb-treated mice lungs, only resting and swollen *ags*Δ conidia were observed and their incapability to grow vegetatively culminated in low inflammation (Fig. 2D–E). These results showed that the reduced virulence of the *ags*Δ mutant was due to a defect in their conidial survival or vegetative growth in the lung of the infected mice.

Susceptibility of the *ags*Δ and parental strain conidia to antifungal molecules is similar

To investigate the mechanisms responsible for the *in vivo* growth defect, the germination of *ags*Δ mutant conidia was tested *in vitro* under stress conditions mimicking the *in vivo* environment, such as, in the presence of reactive oxidants (ROS), cationic peptides, hypoxia and depletion of iron. The *ags*Δ mutants showed similar growth rates as their parental strain in the presence of Menadione, hydrogen peroxide and Luperox®101 with minimum inhibitory concentrations (MIC) of 30 μM, 10 mM and 2 μM, respectively (data not shown) irrespective of the pH of the medium (pH 7 or 4). The killing of resting conidia after 2–6 h of incubation with macrophages purified from uninfected $p47^{phox-/-}$ mice (depleted in ROS production) were similar to the killing by purified macrophages from uninfected wild type mice (C57BL6 H-2^b) (Fig. 2B, data not shown for 6 h and Fig. 3). These results suggested that the *ags*Δ mutant conidia were not more susceptible than the parental strain conidia to reactive oxidants *in vitro* as well as *in vivo*. Interestingly, these results also suggested that in our experimental models, conidia from both mutant and parental strains were efficiently killed by ROS-independent mechanisms. Moreover, the absence of iron or the presence of a hypoxic environment did not modify the survival and conidial germination of *ags*Δ mutants compared to their parental strain (data not shown). *In vitro*, the *ags*Δ conidia germinated like parental strain conidia in culture medium without supplementation with iron as well as under hypoxic conditions (<1% (v/v) O_2 and 9–13% (v/v) CO_2). The *ags*Δ mutants were not more susceptible than the parental strain to cationic peptides. At doses of 230, 100, 40 and 230 μg/ml of Cathelicidin LL-37, α HNP2 and β hBD2 defensins and lactoferrin, respectively, no germination differences were seen between parental and mutant strains (data not shown). Similarly, both mutant and parental strain conidial killing was comparable with 0.05% SDS (data not shown). In addition, no increase in the intracellular labeling of the *ags*Δ mutant conidia was seen after incubation with Calcofluor White or FITC (data not shown). These results suggested that the *ags*Δ conidia were not more permeable to extracellular toxic molecules than the parental strain. Testing of these different inhibitors in combination (such as H_2O_2 or SDS, with Lactoferrin or LL-37) did not result in a differential sensitivity between the parental and mutant strains (data not shown).

These results suggested that, *in vitro*, the triple *ags*Δ mutants were not more susceptible to environmental stresses and antifungal molecules compared to the parental strain. To further investigate the differences in virulence between the mutant and parental

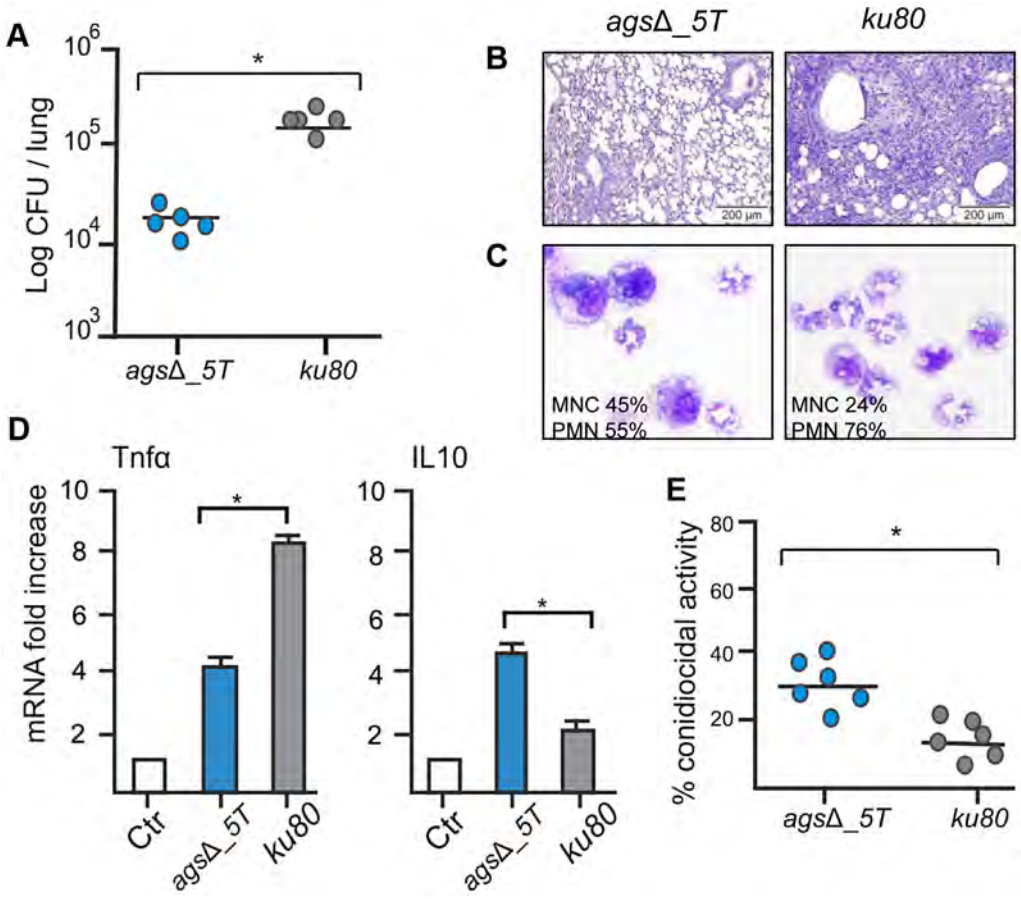

Figure 1. Immunocompetent mice infected with resting conidia of *agsΔ_5T* and parental (*ku80*) strains. Observations and analysis on mice were done four days post-infection. (A) Fungal load was expressed as log10 CFU/lung. (B) Lung histology (periodic acid-Schiff-staining). Note the polymorphonuclear cells and mononuclear infiltrates surrounding the bronchi in *ku80* infected lung. (C) After infection, percentages of monocytes and polymorphonuclear cells found in the lungs alveolar lavage (BAL). (D) Relative expression of TNFα and IL10 assessed by real time RT-PCR on lung total RNA from naïve and infected mice. (E) Conidiocidal activity by purified macrophages from uninfected mice expressed in percentage of CFU inhibition after 2 h incubation of the conidia with macrophages. Data are representative of at least three independent experiments. Ctl, naïve mice; *, $P<0.05$.
doi:10.1371/journal.ppat.1003716.g001

strains *in vivo*, we hypothesize that the killing of the *ags*Δ mutant conidia could be due to the induction of an early and strong host immune response towards the mutant conidial morphotypes.

The resting conidia of the *ags*Δ mutants are immediately recognized by the innate immune system because the surface rodlet layer is masked by a layer of glycoproteins

Resting conidia of the *ags*Δ mutant were more efficiently phagocytosed by mouse alveolar macrophages than that of the parental *ku80* strain. After 1 h incubation, an average of 3.4 and 1.4 conidia of *ags*Δ mutants and *ku80* were engulfed per macrophage, respectively (Fig. 4, Fig. S3). This result suggested that the *ags*Δ mutant and parental strain conidial surfaces are different. To investigate such structural modifications, conidial surfaces were imaged by atomic force microscopy (AFM). In contrast to the *ku80* conidia that are covered with a crystalline-like array of rodlets [9], the *ags*Δ mutant conidial surface was amorphous without any organized structure (Fig. 5A). The presence of an amorphous material covering the surface of the agsΔ conidia was further confirmed by TEM (Fig. 5B).

To investigate if the rodlet layer is still present on the *ags*Δ mutant conidial surface but masked by this amorphous material, *ku80* and *ags*Δ resting conidia were treated with hydrofluoric acid (HF) to extract the rodlet protein. Similar amount of the hydrophobic RodA protein, which constitutes the rodlet layer, could be extracted from the *ags*Δ and parental strain conidia (26.7 ± 4.9 μg and 26.5 ± 3.0 μg per 10^9 conidia, respectively). Figure 5C shows that the two bands, 16 kDa and 14.5 kDa of RodAp classically seen from HF treatment of the conidia [10] were present in the SDS-PAGE profiles of *ags*Δ and *ku80* resting conidial HF-extracts. These data confirmed AFM and TEM observations that on the *ags*Δ mutant conidial surface the rodlets were present but hidden by an amorphous material.

Because of the presence of this amorphous material covering the hydrophobic rodlets, we asked whether the observed surface changes correlated with differences in conidial adhesive properties. To understand this, we mapped and quantified the nanoscale adhesion properties of *ku80* and *ags*Δ mutant conidia by AFM using bare Si3N4 tip. Figure 6 (and Fig. S4) showed that the presence of this unorganized material on the *ags*Δ mutant conidial surface was associated with a dramatic reduction in their conidial surface adhesive properties. For the parental strain, force-distance curves recorded across the cell surface revealed large adhesion forces, with a magnitude of 0.6 ± 0.039 nN as shown by the

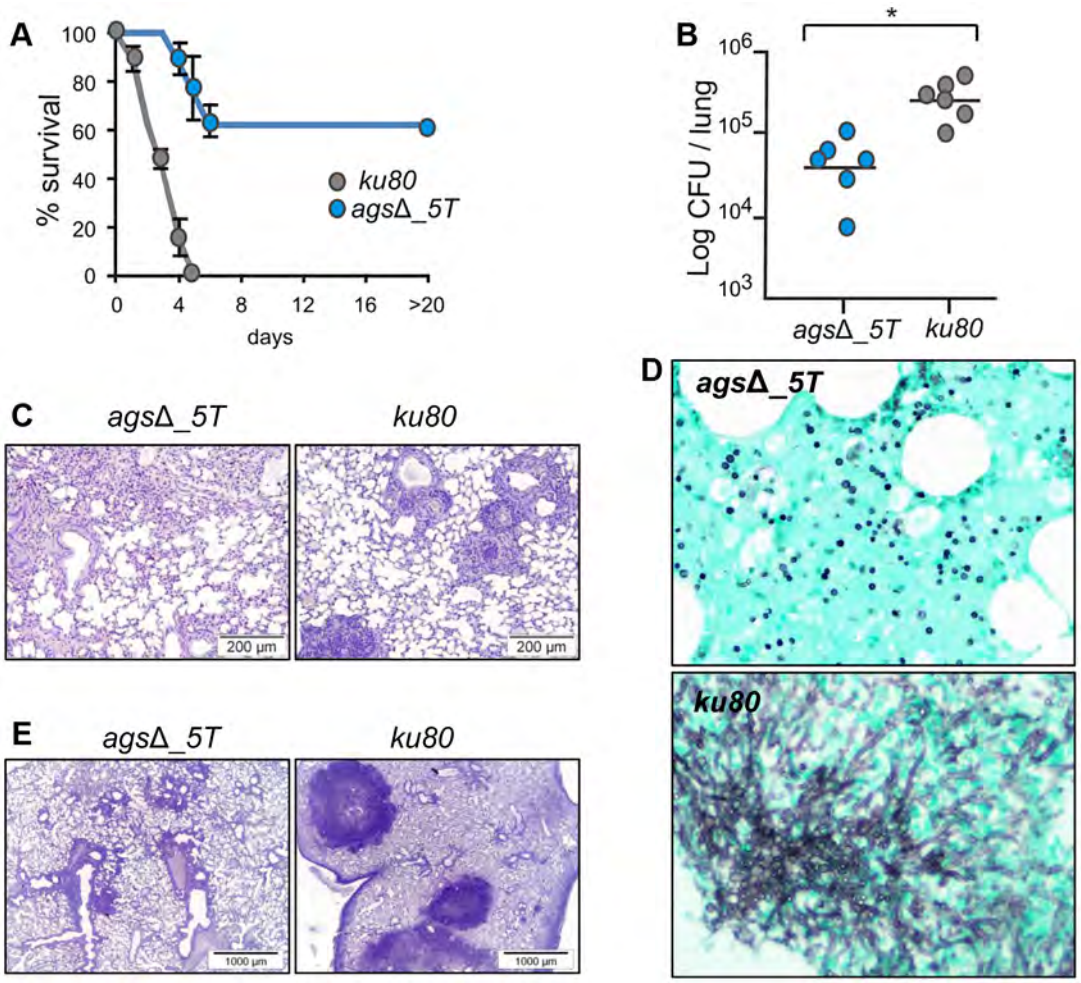

Figure 2. Cyclophosphamide immunosuppressed mice and anti-Ly6G treated neutropenic mice infected with resting conidia of *agsΔ_5T* and parental (*ku80*) strains. (A–C) Cyclophosphamide immunosuppressed mice; (D–E) anti-Ly6G treated neutropenic mice; (A) Survival (%) and (B) fungal growth estimated as CFUs in lung. (C and E) lung histology (periodic acid-Schiff-staining). Note the polymorphonuclear cells and mononuclear infiltrates surrounding the bronchi in *ku80* infected lung. (D) Histological appearance of lungs of anti-Ly6G neutropenic mice infected with conidia of *agsΔ_5T* and *ku80* (Gomori's methanamine silver-staining). Note the absence of mycelial development of *agsΔ_5T* conidia in neutropenic mice. Data are representative of at least three independent experiments. *: $p<0.05$.
doi:10.1371/journal.ppat.1003716.g002

adhesion force histogram (Fig. 6A–C). In contrast, structural changes in *agsΔ* conidia caused profound modifications of the cell surface physico-chemical properties (Fig. 6D–F, Fig. S4). Force-distance curves showed the absence of adhesion forces over the entire surface of the mutant conidia. This decrease in the *agsΔ* conidial adhesion capacities indicated a modification of the cell surface hydrophobicity that could have influenced conidial phagocytosis.

Further, chemical nature of the amorphous layer present on the *agsΔ* mutant conidial surface was investigated. It was not composed of polysaccharides since the labeling of β-(1,3)-glucan with the β-(1,3)-glucan receptor GNBP3, chitin with WGA, galactomannan (GM) with an anti-GM monoclonal antibody and galactosaminogalactan (GAG) with an anti-GAG monoclonal antibody were negative (data not shown). In contrast, a strong labeling of the resting *agsΔ* conidium with ConA was observed suggesting that the surface layer was rich in glyco-conjugates (Fig. 7).

To extract these amorphous surface materials, *agsΔ* resting conidia were incubated in 0.5 M NaCl for 2 h and the extracted materials were positive for protein assay. As shown in the Figure 8 (and Fig. S5), incubation with NaCl did not release any proteins from the parental *ku80* strain whereas the extracts from *agsΔ* mutant conidia contained 160 µg proteins per 10^{10} conidia. It was verified that the amorphous glycoprotein layer was removed after NaCl treatment because ConA labeling on the conidia after NaCl treatment was negative (data not shown). Further, extracted protein mixture was subjected to proteomic analysis. Thirty-four proteins were identified and in-silico analysis of these proteins by SigPred (http://www.cbs.dtu.dk/services/SignalP/) and CADRE (http://www.cadre-genomes.org.uk/Aspergillus_fumigatus/) revealed that all of them had a signal peptide except Sod1 (AFUA_5G09240, [11]) (Table 1, Table S1). Most of these proteins were hydrolases and the most abundant protein was a putative β-(1,4)-glucan hydrolase (AFUA_7G06140). Other glycosylhydrolases were hexosidases or N-acetylhexosaminidases (AFUA_1G05770; AFUA_1G14560, AFUA_1G10790, AFUA_8G05020, AFUA_6G10730). A unique aspartic phosphatase was identified that was different from the one previously identified as a major mycelial cell wall protein [12]. Three

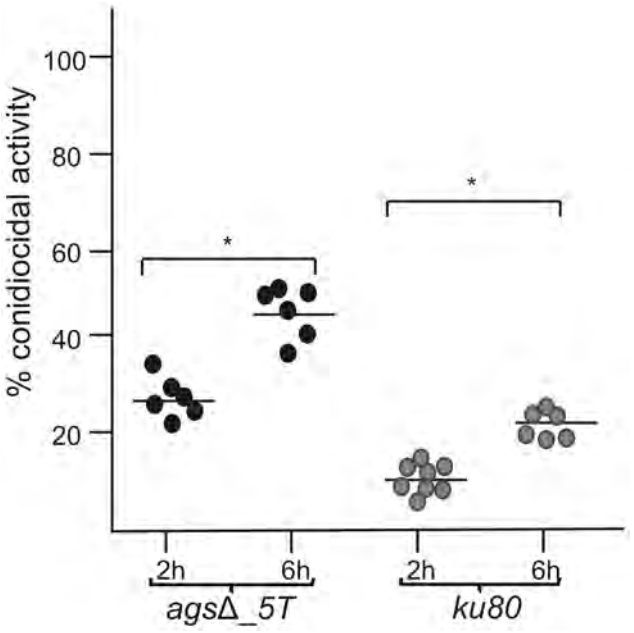

Figure 3. Conidiocidal activity of macrophages isolated from uninfected p47$^{phox-/-}$ mice against resting conidia of *agsΔ_5T* and parental (*ku80*) strains. Conidiocidal activity is expressed in percentage of CFU inhibition after 2 and 6 h incubation of the conidia with macrophages. Data are representative from at least three independent experiments. *, P<0.05.
doi:10.1371/journal.ppat.1003716.g003

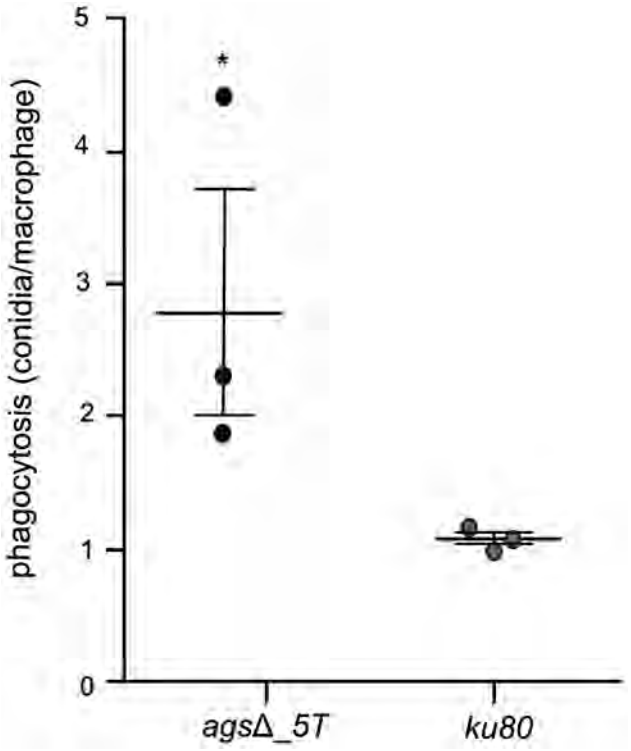

Figure 4. Phagocytosis activity by isolated macrophages from uninfected mice against resting conidia of *agsΔ_5T* and parental (*ku80*) strains. Index of phagocytosis is expressed in number of conidia per alveolar macrophage after 1 h incubation of conidia with macrophages. Data are representative of at least 3 independent experiments. *, P<0.05.
doi:10.1371/journal.ppat.1003716.g004

peptidases (AFUA_2G03510, AFUA_4G03490, AFUA_8G04120) and the two aspartic proteases, Pep1p and Pep2p (AFUA_5G13300, AFUA_3G11400), known to be associated with the conidial cell wall were found [13]. Two well known allergens of *A. fumigatus* were also detected (Aspf1 (AFUA_5G02330) and Aspf13 (AFUA_2G12630) [14]). Other protein such as oxidoreductases and enzymes of sugar metabolism (pyruvate dehydrogenase kinase AFUA_2G11900 and isopropylmalate dehydrogenase AFUA_1G15780) were present in lower amount as they were identified only once or twice in the proteomic survey. Interestingly, Sod1p and RodAp (AFUA_5G09580), known to be highly expressed in resting conidia [11], were also found in this NaCl extract. A similar SDS-PAGE profile was obtained when urea/thiourea buffer was used to extract *ags*Δ conidial surface material, indicating that the proteins recovered were not depending on the extraction buffer (data not shown). The fact that many proteins were present above the surface rodlet layer suggested that in contrast to the parental strain, the lack of α1,3 glucan has led to a different cell wall retainment of these glycoproteins in the *ags*Δ mutant conidia.

In vitro analysis of the cytokines produced during the first 5 h of incubation with alveolar macrophages showed that high amounts of pro-inflammatory TNFα cytokine were produced upon interaction with *ags*Δ mutant conidia whereas no TNFα was produced when the parental strain was incubated with macrophages under the same incubation conditions (Fig. 9A, Fig. S6A). Stimulation of the macrophages with the *ags*Δ conidial NaCl extract also induced TNFα expression (Fig. 9B; Fig. S6B). These results suggested that the surface glycoprotein layer on the resting *ags*Δ conidia was responsible for the induction of pro-inflammatory cytokine production immediately after conidial phagocytosis.

Thus, the deletion of the *AGS* genes resulted in an unexpected modification of the mutant conidial surface with the emergence of an amorphous layer on the resting conidial surface over the rodlet layer, which altered biophysical properties, consequently affecting conidial interaction with the host immune system.

Polysaccharide PAMPS are exposed on the surface of the swollen conidia of the triple *ags*Δ mutants

Increased cytokine production seen in the macrophages over a 5 h-time period could also come from changes occurring at the surface of germinating conidia since it has been shown previously that conidia starts germinating intracellularly in the macrophage lysosome after the first 2 h of phagocytosis [15]. In addition, Figure 2 shows that *ags*Δ conidia undergo swelling in the infected lungs before being killed. The structural changes of the early germ tubes resulting from the *AGS* deletion were investigated by cytochemistry. The swollen conidia of the triple *ags*Δ mutants presented an increased labeling by WGA compared to the parental strain (Fig. 10A and data not shown). In addition, swollen *ags*Δ conidia were positive with the β-(1,3)-glucan receptor GNBP3, whereas both resting and swollen conidia of the parent strain were negative (Fig. 10B and data not shown). In contrast, there were no differences in the immunolabeling of the swollen conidia of parental and *ags*Δ mutants with anti-GAG and anti-GM monoclonal antibodies (Fig. S7). These results suggest that the absence of α-(1,3)-glucan that normally hides β-(1,3)-glucan and chitin, exposes these PAMPs at the surface of the swollen *ags*Δ conidia. These results were also in agreement with the chemical analysis of the cell wall: the mycelium cell wall of the *ags*Δ contained 1.7 and 2 times more chitin and β-(1,3)-glucan, respectively, than the cell wall of the parental strain [8].

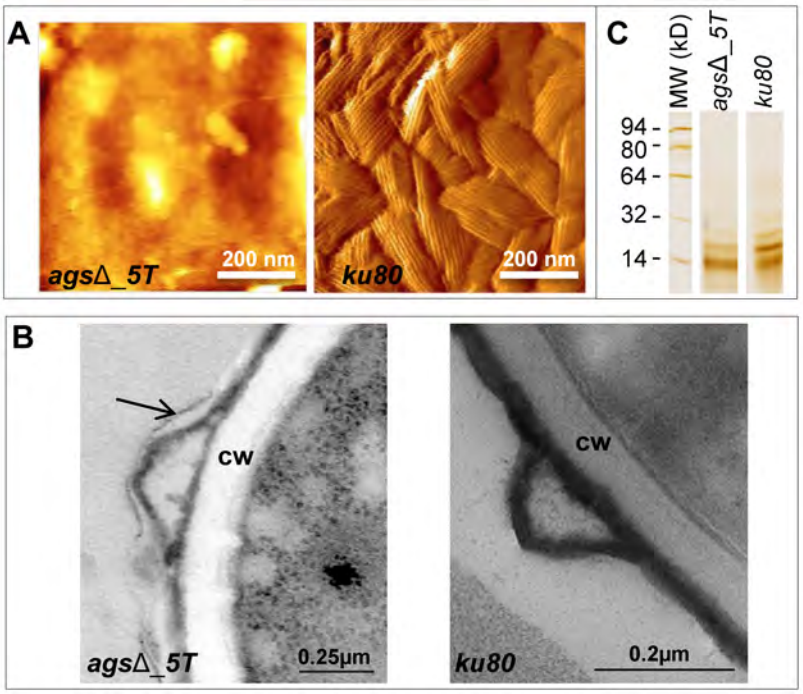

Figure 5. Surface analysis of resting conidia of *agsΔ_5T* mutant and parental (*ku80*) strains. (A): height images (z-range = 1 μm; recorded in water with silicon nitride tips). Atomic Force Microscopy (AFM) images showing the amorphous surface without the rodlet layer on the triple *agsΔ_5T* mutant conidia whereas the rodlet are observed on the parental strain conidial surface. (B): TEM observations. Note the presence of an extracellular material on the surface of the *agsΔ_5T* conidia (arrow); CW: cell wall. (C): SDS-PAGE (15% gel) of Hydrofluoric acid (HF) extracts of rodlets from resting conidia showing the two bands, 16 kDa and 14.5 kDa of RodAp classically seen from HF treatment of the conidia [10]. Data are representative of at least three independent experiments.
doi:10.1371/journal.ppat.1003716.g005

Figure 11 represents a model to explain the sequential immune events upon inhalation of the *ags*Δ mutant and parental strain conidia and their differential impact/*in vivo* fate based on our *in vitro* assays as well as *in vivo* experiments using murine aspergillosis models. The presence of glycoproteins hiding the rodlet layer increases the phagocytic rate and promotes an immediate host immunological response towards the triple *ags*Δ mutants during phagocytosis. Once the mutant conidium is internalized, the conidial swelling results in an increased exposure of PAMPs on the swollen *ags*Δ conidial surface. Such surface modifications further boosts pre-existing host defense induced by the resting *ags*Δ conidia. In contrast, the resting conidium of the parental strain are not recognized by the phagocytes and do not display major PAMPs on the surface of the conidium during the intracellular swelling. Since *ags*Δ conidia did not seem more sensitive to host antifungal molecules compared to the parental strain, we hypothesize that differences in the killing in the later growth stages resulted from an early and enhanced host response induced by the modified surface of the resting *ags*Δ conidia. This early stimulation will be responsible for the killing of the germinating *ags*Δ conidia. On the contrary, in the partially immunosuppressed experimental murine models, limited and delayed killing of the parental strain conidia enables their further vegetative growth.

Discussion

In this study we showed that the *ags*Δ mutants displayed a reduced virulence associated with an inhibition of germination *in vivo* and a reduction of the inflammatory response after 24 h infection (decreased TNFα and increased IL10 expressions and reduced recruitment of PMNs). The low level of TNFα seen with the triple *ags*Δ mutants fits with the lack of recruitment of neutrophils seen with this mutant after 24 h infection. However, during our *in vitro* experiments with macrophages incubated during 5 h with *ags*Δ or ku80 conidia, we observed the induction of pro-inflammatory cytokines. This indicated that the lack of inflammation seen at later stages of infection in mice was due to the inhibition of vegetative growth of the *ags*Δ mutants rather than a failure to stimulate inflammation. This was in agreement with the fact that *ags*Δ conidia were killed before their hyphal development.

The primary phenotype of the resting conidia of the *ags*Δ mutants was the absence of visible rodlet layer on the conidial surface. Even though the rodlets were present in the mutant conidia, their masking by a (glyco-)protein layer restored the immune sensing that is usually silenced when the rodlets are present on the surface of the wild type conidia [10,16]. The *ags*Δ conidia were covered by proteins, which are usually secreted during vegetative growth. Most hydrolases found in the additional amorphous surface layer of the resting *ags*Δ conidia were usually identified during mycelial growth in a protein-based medium [14,17]. How these proteins are able to cross the conidial cell wall remains an open question. Their presence on the surface is certainly due to the modifications of the cell wall integrity resulting from the three *AGS* deletions. Interestingly, in three independent HF extractions, the amount of 14.5 kDa RodAp was slightly higher than the 16 kDa RodAp (20–23% 16 kDa RodA in *ags*Δ mutants compared to 40–50% in the parental strain; Fig. 5C) suggesting that the rodlet structure of the mutant was less organized than the rodlet of the parental strain, which putatively modified the ionic strength of the hydrophobin layer in the *ags*Δ mutants [18]. Such structural modifications may affect the adherence of the hydrophilic glycoproteins to rodlets through

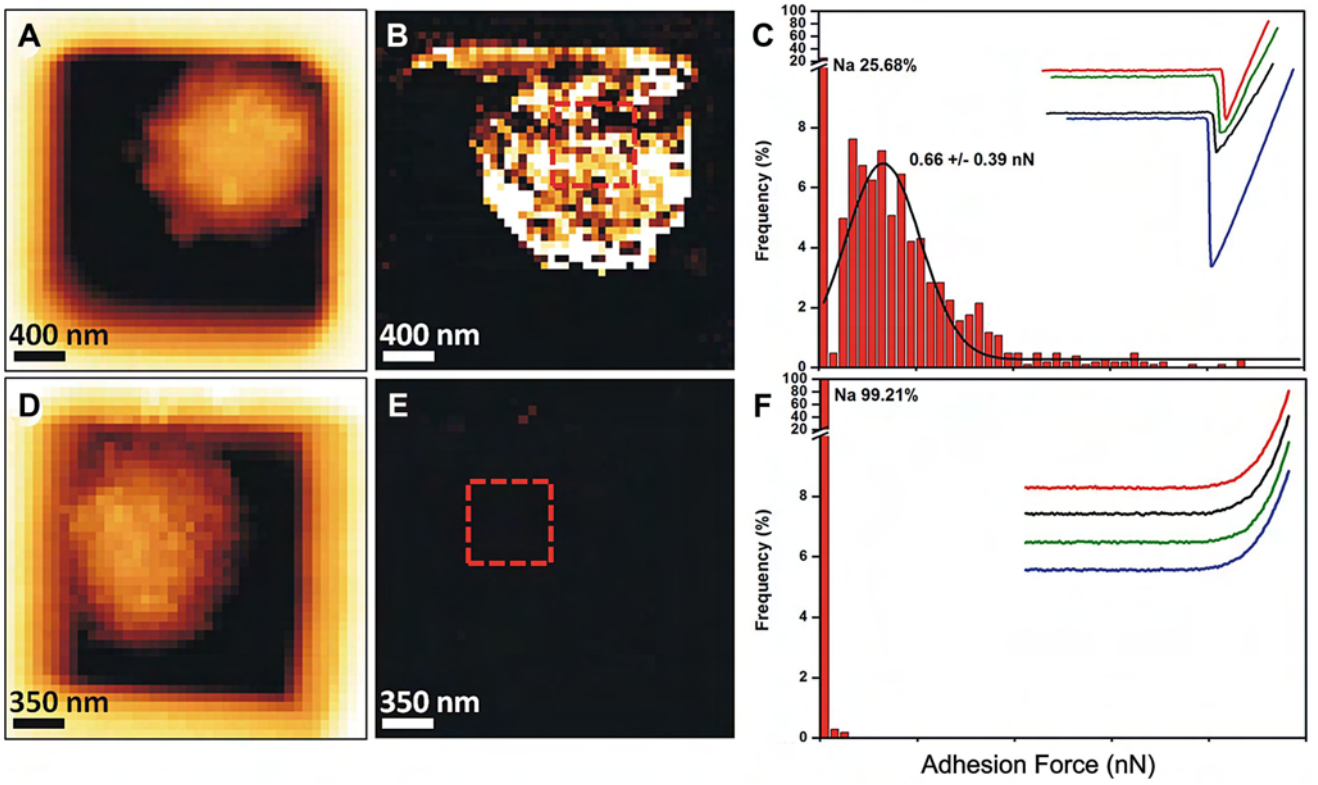

Figure 6. Imaging and adhesive properties of *A. fumigatus* resting conidia of the parental strain and *agsΔ_5T* mutant. Structural changes of *agsΔ_5T* correlate with a loss of cell surface adhesive properties. (A–C) parental strain; (D–F) *agsΔ_5T* mutant; (A, D) height images (z-range = 1 μm; recorded in water with silicon nitride tips); (B, E) adhesion force maps (z-range: 5 nN) corresponding to the height image; (C, F) Representative force-distance curves and adhesion force histograms (n = 1024) recorded on the surface of parental strain (C) and *agsΔ_5T* (F).
doi:10.1371/journal.ppat.1003716.g006

electrostatic binding, since these proteins were easily extracted by salt. How these glycoproteins reached the surface of the cell wall is still not understood. This should not be related to changes in cell wall permeability since the *ags*Δ mutants were not more permeable to FITC or drugs that affect viability such as ROS, cationic peptides or Calcofluor White than the parental strain (data not shown). Alternatively, the hydrolases, because of their enzymatic activity, may harm the cell wall structure itself and this would help the proteins to cross the cell wall barrier. The stimulation of the expression of TNFα after incubation with macrophages (isolated from naive mice BAL) with *ags*Δ mutant conidial NaCl extract showed that these proteins located on the conidial surface were sensed first by the immune system and were able to induce an immediate immune response towards *ags*Δ conidia. It was previously shown that some of these surface proteins are recognized by T cells and can induce a Th1 protective response [6]. In particular, the secreted aspartic protease Pep1 that has been found in NaCl extract from *ags*Δ conidia conferred protection against infection, associated with a reduced neutrophil recruitment in BAL and a reduced inflammatory pathology in the lung. Hiding of the rodlet layer by an amorphous glycoprotein layer that stimulates the host response is not exclusively specific to

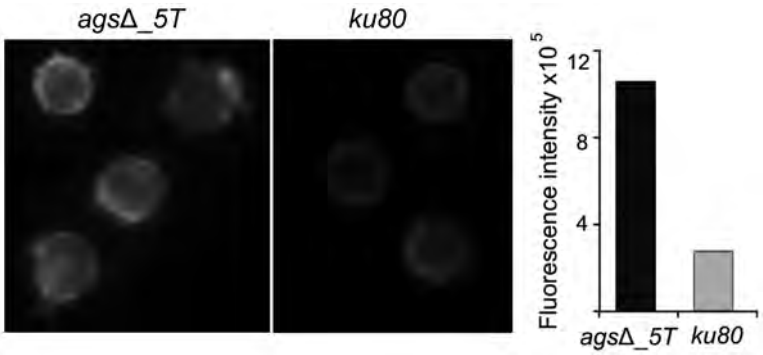

Figure 7. ConA-FITC labeling of *agsΔ_5T* mutant and parental strain (*ku80*) resting conidia. Note the increase in the ConA labeling on the *agsΔ_5T* mutant conidial surface. Histograms represent the calculated fluorescence intensity of the corresponding images, expressed in Einstein per seconds.
doi:10.1371/journal.ppat.1003716.g007

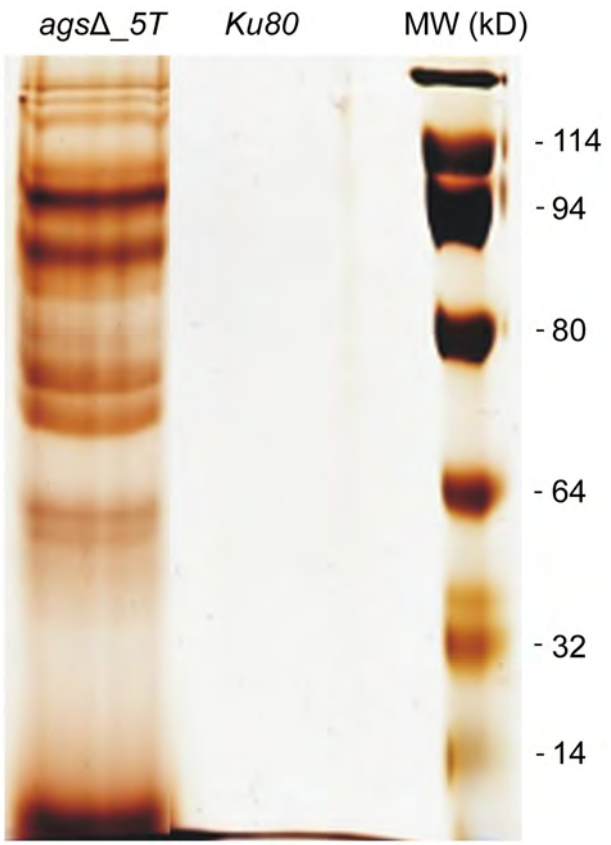

Figure 8. NaCl extracted proteins from the surface of *agsΔ_5T* resting conidia. SDS-PAGE (10% gel) of proteins extracted after 2 h incubation of *agsΔ_5T* and *ku80* resting conidia in 0.5 M NaCl.
doi:10.1371/journal.ppat.1003716.g008

the *ags*Δ deletion, since a similar conidial phenotype was observed on chitin synthase mutants [19,20]. Similarly, in *B. dermatitidis*, the absence of α-(1,3)-glucan at the surface of the yeast increased the expression of W1-1 adhesin/antigen that were bound to phagocytic cells and suppressed the generation of the pro-inflammatory cytokine TNFα [21,22].

The exposure of polysaccharide PAMPs on the surface of germinating conidia consecutively to triple *AGS* deletions also plays a role in stimulating the host innate immune response and inducing the production of antifungal molecules by the innate immune cells. The exposure of β-(1,3)-glucan at the surface of germinating *ags*Δ conidia will favor a Dectin-1-mediated host response [23]. Similarly, increased β-(1,3)-glucan exposure due to caspofungin treatment stimulated the host defense reaction against *A. fumigatus* [24,25]. In addition, the positive binding of WGA and ConA also suggested that other receptors such as the mannose or/and chitin/N-acetylglucosamine, which are known to stimulate an antifungal response, can also be involved in this modified immune response [26]. Similar to the situation with the *ags*Δ mutants, it was shown that the lack of α-(1,3)-glucan in *H. capsulatum* also led to the unmasking of PAMPs [1]. The protective role of α-(1,3)-glucan has been also shown in *B. dermatitidis* and *P. brasiliensis* where the absence of α-(1,3)-glucan at the surface of the yeast and/or its replacement by β-(1,3)-glucan stimulated the host defense reaction [21,27]. Recently, the masking of chitin by α-(1,3)-glucan has been shown to be essential for the virulence of the plant pathogen *Magnaporthe grisea* [28].

The molecules responsible for the killing of the *ags*Δ conidia remain unknown. However, it is clear that ROS were not responsible for the differences in killing between the *ags*Δ mutants and the parental strain conidia since the *ags*Δ mutants did not display a higher sensitivity to ROS *in vitro* and the killing of *ags*Δ conidia was similar in $p47^{phox-/-}$ mice compared to C57BL/6 (Fig. 3). Although a link between increased oxidative response and enhanced damage to *A. fumigatus* has been repeatedly demonstrated in the past [29,30], recent studies, especially with chronic granulomatous disease (CGD) patients, have shown that NADPH-independent mechanisms can contribute to *Aspergillus* killing as much as ROS [31,32]. Among possible mechanisms of NADPH-independent activity, D'Angelo et al. [33] have suggested that defensins and cathelicidins, known for their role in host defense, could be responsible for *A. fumigatus* killing in CGD mice. This seems however not the case for the *ags*Δ mutants as our *in vitro* studies indicated that the *ags*Δ mutants did not show a higher susceptibility to cathelicidin LL-37 or HNP2 and hBD2 defensins. Modification of the conidial surface may also lead to an increased binding of Surfactant Proteins A and D, Mannose Binding Lectin C or Penthraxin 3 that are known to be associated to an increased phagocytosis and an activation of the complement pathway known to play a major role in the killing of *A. fumigatus* [21,34,35,36,37]. Based on our data, it remains impossible to infer the killing of the *ags*Δ mutant conidia to currently known antifungal immune defense mechanisms. It can also be postulated that the killing may be due to an early burst of unknown toxic molecules or that the killing is the result of several antifungal molecules acting synergistically [38]. Our cell wall analysis suggested also that the cell wall architecture is perturbed in the inner as well as in the outer layer and that this perturbation may result in modifications of the cell wall permeability to specific antifungal molecules [8]. These could be responsible for an increased susceptibility of the *ags*Δ mutant to the host defense molecules.

The story of *A. fumigatus* α-(1,3)-glucan remains a two-sided coin. In the wild type strain, α-(1,3)-glucan induces an anti-*A. fumigatus* response as the injection of this polysaccharide into mice was immunoprotective and obviously responsible for the production of a Th1 response that is directed against *A. fumigatus* [6]. It could be expected that their removal favors the virulence of the mutant. In reality, the opposite happens due to the reorganization of the cell wall of the resting and germinating conidia upon triple *AGS* deletions. The presence of glycoproteins hiding the rodlet layer and the exposure of PAMPs in the germinating conidia modified the immunological response of the host, which increased phagocytosis and killing of the *ags*Δ mutants, and induced pro-inflammatory cytokine production. It is the structural modification of the entire cell wall consecutive to the *AGS* deletions that is responsible for an early stimulation of the host defense reactions. Interestingly, these structural modifications did not modify the survival of the fungus *in vitro* but are essential for the *in vivo* survival. The difference in the surface composition of the resting and swollen conidia of the *ags*Δ mutants led to an immediate sensing of the immunogenic molecules resulting in an early response of the phagocyte towards the *ags*Δ conidia. The deleterious effect of a delayed immune response on the microbial virulence is well known.

The α-(1,3)-glucan study tells us that the deletion of one cell wall gene does not lead only to the disappearance of the product of the encoded gene but results in a complete restructuration of the fungal cell wall. This has been shown with the deletion of the *AGS* genes in this study but also with other cell wall genes or consecutively to the use of antifungals acting on the cell wall in several fungal species [39]. Such structural and chemical

Table 1. Proteins identified in the NaCl extract of *agsΔ_5T* and *agsΔ_n8* conidia.

AFUA number	Common Name of Target	Known Gene	MW (Kd)
AFUA_7G06140	Putative secreted 1,4-β-D-glucan glucanhydrolase		78.38
AFUA_6G10130	Putative N,O-diacetyl muramidase		24.64
AFUA_1G05770	β-glucosidase ExoG2	*EXOG2*	94.75
AFUA_3G07520	Exo β-1,3-glucanase		86.72
AFUA_2G01240	Putativeβ-fructofuranosidase		57.26
AFUA_1G14560	Putative α-1,2-mannosidase, MsdS		53.84
AFUA_1G10790	Putativeα-1,2-mannosidase		92.7
AFUA_8G05020	Putative secreted α-N-acetylhexosaminidase NagA		57.4
AFUA_4G01290	Glycosyl hydrolase family 75 chitosanase		25.1
AFUA_5G13300	Secreted aspartic endopeptidase Pep1	*PEP1*	41.6
AFUA_3G11400	Secreted aspartic endopeptidase Pep2	*PEP2*	43.3
AFUA_4G03490	Putative secreted tripeptidyl-peptidase TppA, SedB	*SEDB*	65.83
AFUA_2G03380	Putative alkaline serine protease		13.4
AFUA_2G03510	Putative pheromone processing carboxypeptidase Sxa2		49.75
AFUA_8G04120	Secreted serine carboxypeptidase S1	*SCP1*	61.28
AFUA_3G07030	Putative secreted glutaminase GtaA		76.15
AFUA_2G12630	allergenic cerato-platanin Aspf13, serine alkaline protease	*ASPF13*	15.94
AFUA_5G02330	allergenic restrictocin, mitogilin Aspf1	*ASPF1*	19.59
AFUA_4G03660	Putative acid phosphatase, PhoB regulated		46.1
AFUA_5G09240	Cu,Zn superoxide dismutase Sod1	*SOD1*	16.36
AFUA_3G03450	Putative oxidoreductase		58.58
AFUA_3G08070	GMC oxidoreductase		67.61
AFUA_2G04200	4-hydroxyphenylpyruvate dioxygenase, HppD	*HPPD*	45.53
AFUA_4G13000	Putative amine oxidase		119
AFUA_4G07690	Putative phosphoribosylaminoimidazolecarboxamide formyltransferase		65
AFUA_1G16420	Uncharacterized protein		58.55
AFUA_5G09580	hydrophobin RodA	*RODA*	16.17
AFUA_1G15780	Putative 3-isopropylmalate dehydrogenase Leu2A		39
AFUA_2G11900	Putative pyruvate dehydrogenase kinase		49.43
AFUA_6G07980	Putative cyclin-dependent protein kinase		36.65
AFUA_4G03630	Putative sterol 24-c-methyltransferase		42.57
AFUA_1G11000	Putative C6 transcription factor		82.26
AFUA_1G00700	hypothetical protein		150.55
AFUA_3G06520	conserved hypothetical protein		65.71

Identification was done by MS/MS and MS with a mascot score above a threshold of 54. Details are showed in Table S1.
doi:10.1371/journal.ppat.1003716.t001

modifications in the cell wall will have an obvious impact on the immune response of the host towards the corresponding mutant. Our study also suggests, any interpretation stating that the immune response towards a cell wall mutant is only due to the lack of the product of the deleted gene should be considered with care [40,41].

Materials and Methods

Strains and culture conditions

All strains were grown in 2% (w/v) malt agar slants and 1 week-old conidia were recovered from the slants by vortexing with 0.05% (v/v) Tween 20 aqueous solution. Swollen conidia and germ tubes were produced after 5 h and 10 h, respectively, after incubation at 37°C in Brian's medium (Brian) [42]

The *A. fumigatus* parental strain AkuB^{ku80}ΔpyrG (*ku80*, [43]) and three *agsΔ* mutant strains independently obtained: *ags1Δags2-Δags3Δ_5T* (*agsΔ_5T*) obtained previously [8] and two new ones, *ags1Δags2Δags3Δn8*and *ags1Δags2Δags3Δ_n6.2* (*agsΔ_n8* and *agsΔ_n6.2*), were used in this study. Since it had been impossible to complement *agsΔ* mutant for reasons explained previously [8], two new triple *agsΔ* mutants were constructed independently using the strategy described previously to exclude the possibility that undesired mutations had occurred during the deletion process. The lack of α-(1,3)-glucan in the cell wall of mutant strains was confirmed by both chemical and immunolabeling assays (Fig. S8). Chemical analysis of the cell wall was performed as previously described [44]. For immunolabeling assays, 5–10 h germinated conidia were labeled using the MOPC 104E monoclonal antibody, which binds specifically to α-(1,3)-glucan [45] (Beauvais A. Institut

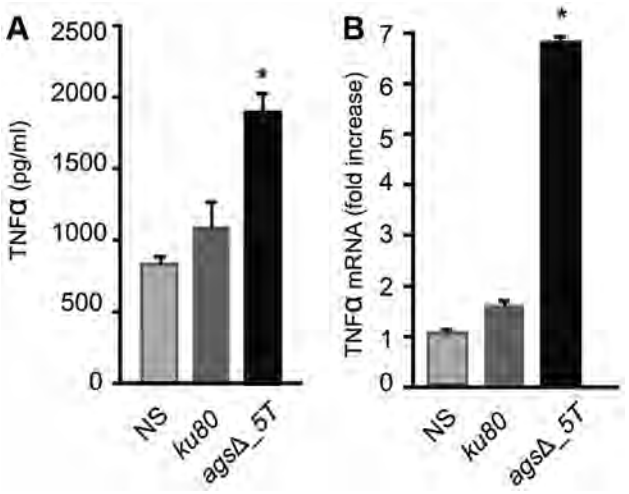

Figure 9. TNFα production or expression by macrophages (isolated from uninfected immunocompetent mice) upon interaction with resting conidia of parental (*ku80*) and *agsΔ_5T* strains or *agsΔ_5T* conidial NaCl extract (3.2 μg proteins) respectively. (A) TNFα was quantified after 5 h incubation of the conidia with macrophages; (B) Relative expression of TNFα assessed by real time RT-PCR in total RNA from macrophages after 5 h incubation of the *agsΔ_5T* conidial NaCl extract with macrophages. NaCl supernatant from *ku80* resting conidia incubated for 2 h in 0.5M NaCl was used as a control. NS: Non-stimulated. *, $P<0.05$.
doi:10.1371/journal.ppat.1003716.g009

Pasteur, Paris, France, unpublished results). Paraformaldehyde (PFA) fixed swollen and germinating conidia were permeabilized prior to immunolabeling as previously described [46]. MOPC 104E (Sigma) and control mouse IgM (Sigma) were used at a dilution of 1:25 and the goat antimouse IgG-TRITC (H+L, Sigma) was used as the secondary antibody at a dilution of 1:50. The three triple mutants used in this study germinated, sporulated and conidiated like the parental strain *in vitro* (data not shown, [8]).

Analysis of the conidial surface

Conidial surface was analyzed by Atomic Force Microscopy (AFM). The sample immobilization is achieved by assembling the living conidia within the patterns of microstructured, functionalized poly-dimethylsiloxane (PDMS, Sylgard 184) stamps using convective/capillary deposition [47]. Images and force measurements were performed in deionised water, respectively in contact mode and in Quantitative Imaging (QI) mode and Force Volume (FV) mode. For both experiments we used bare MLCT AUWH cantilever (nominal spring constant 0.01 N/m) (Bruker). Single cells were first localized and imaged and then switched over to QI and FV modes to record adhesion force maps. AFM Nanowizard II and III (JPK Instruments, Berlin, Germany) were used to capture the images. The cantilevers spring constants were measured by the thermal noise method [48] ranging from 0.0160 to 0.0190 N/m. Force curves were analyzed in order to determine the adhesion force between the conidia and the AFM tip. These adhesions were plotted as bright pixels, brighter colors indicating larger adhesion values. For each strain, images that were obtained for at least three conidia from independent cultures and analyzed with different tips, were representative of the entire conidial population inside each mutant and parental strain. The results acquired on the spores were analyzed on JPK Data Processing software.

The rodlet layer was extracted from the spore surface by incubating 10^9 dry conidia with 48% (v/v) hydrofluoric acid (HF) for 72 h at 4°C. The contents were centrifuged (10,000 rpm, 10 min) and the supernatant obtained was dried under N_2. The dried material was reconstituted in H_2O and an aliquot was subjected to 15% (w/v) SDS-PAGE analysis and visualized by silver nitrate staining. Bands were quantified using Image lab software (BioRad).

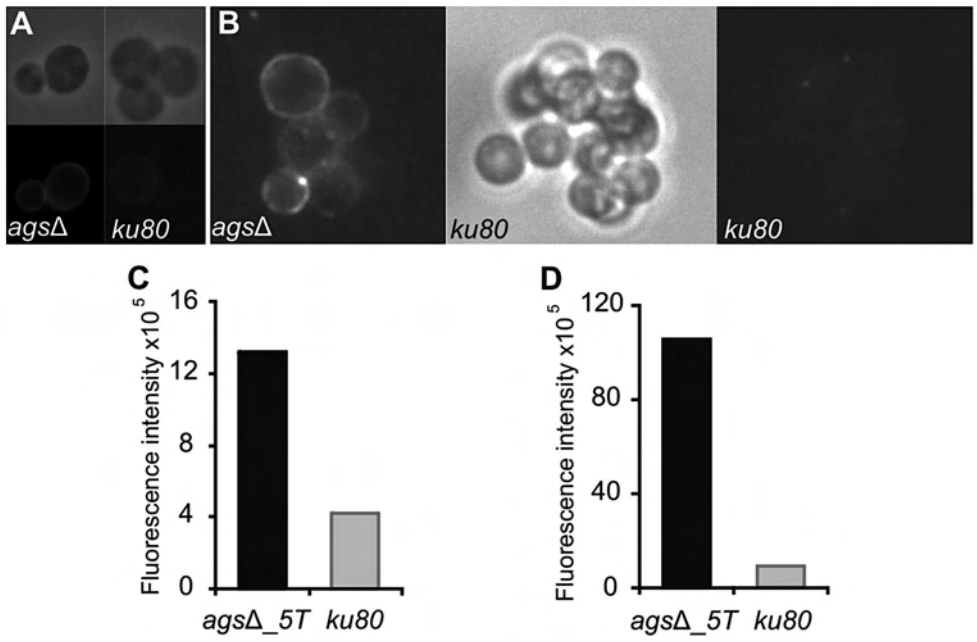

Figure 10. Labeling of the surfaces of *agsΔ_5T* and parental strain swollen conidia by WGA and the β(1,3)-glucan receptor GNBP3. The surfaces of the swollen conidia were labeled by WGA-FITC (A) and GNBP3 (B) as described in material and methods. (C, D) Histograms represented the calculated fluorescence intensity of the corresponding images (A, B respectively), expressed in Einstein per seconds.
doi:10.1371/journal.ppat.1003716.g010

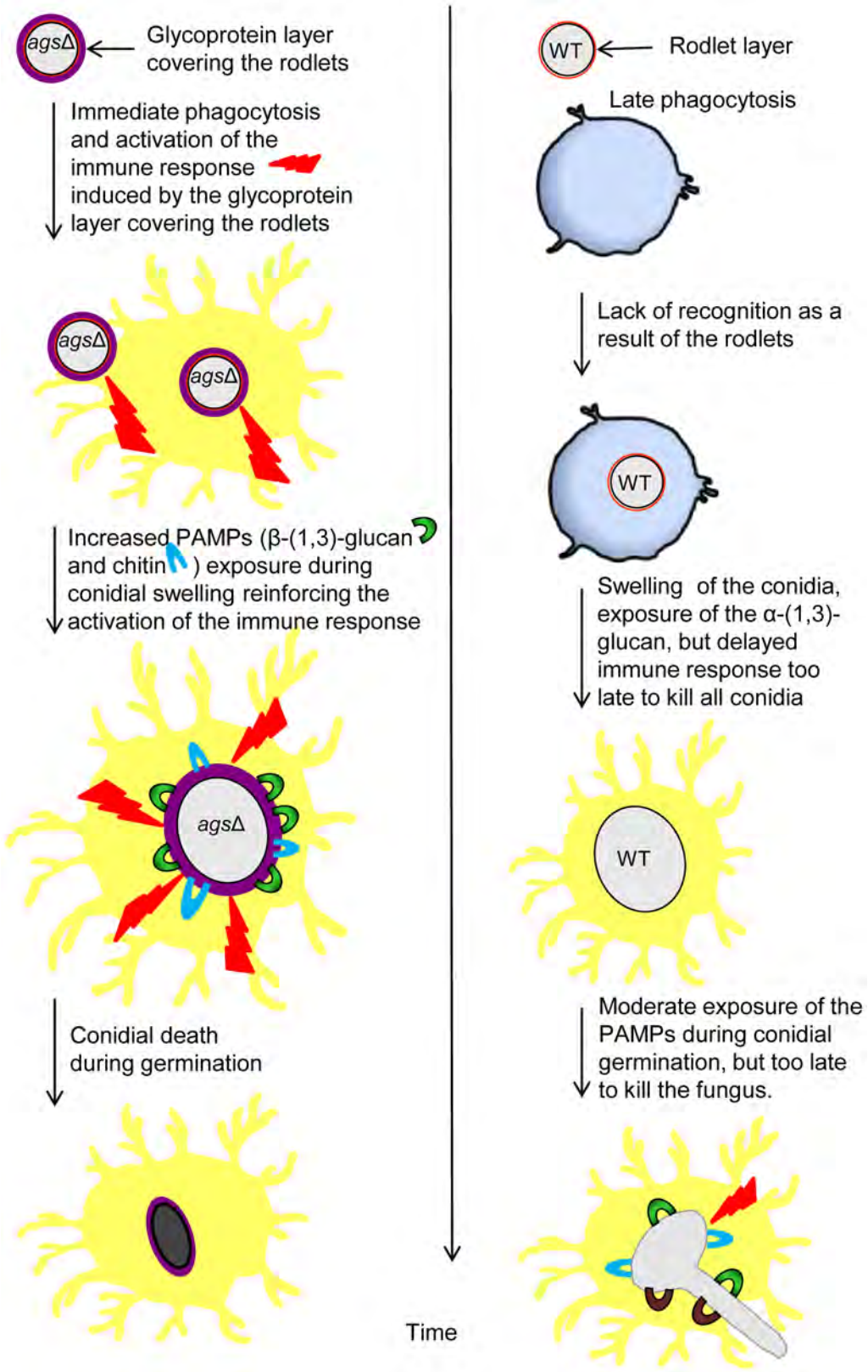

Figure 11. Working model explaining sequential and differential immune events upon inhalation of the *agsΔ* mutant and the parental (*ku80*) strain conidia. The presence of the glycoprotein layer on the triple *agsΔ* mutant conidial surface hides the rodlet layer. Increased exposure of PAMPs (WGA and ConA positive molecules and β-(1,3)-glucans) during vegetative growth in the triple *agsΔ* mutant modifies the host immunological response. This facilitates phagocytosis and killing of the triple *agsΔ* mutant and stimulates pro-inflammatory immune responses.
doi:10.1371/journal.ppat.1003716.g011

To analyze the components present on the surface, conidia were incubated in 0.5 M NaCl solution for 2 h at room temperature at a ratio of 10^{10} conidia per ml. The NaCl supernatant was recovered after centrifugation and directly subjected to 10% SDS-PAGE (w/v). The protein concentrations in the extracts were determined by the Coomassie brilliant blue method [49], using BioRad kit and BSA as the standard. Proteomic analysis of the NaCl extract was carried out as described previously with slight modifications [50]. A total amount of 50–100 µg protein was loaded onto IPG strips (11 cm, pH 3–7; GE Healthcare Life Sciences) by in-gel rehydration. After equilibration of the IPG strips, SDS-gel electrophoresis was carried out using Criterion AnykD TGX gels (Bio-RAD). Proteins were visualised by colloidal Coomassie staining [51]. After scanning, gel images were analysed with the software Delta 2D 4.3. (Decodon). Protein spots were excised and analysed by mass spectrometry using an ultrafleXtreme MALDI-TOF/TOF device (Bruker Daltonics).

Fluorescence microscopy

Resting and swollen conidia were PFA-fixed (2.5% (v/v) PFA in PBS) for one night at 4°C, washed three times with 0.1 M NH_4Cl in PBS, once with PBS and then incubated with different antibodies or lectins as described previously [52].

Galactosaminogalactan (GAG) was labeled with a monoclonal mouse antibody as described previously [53] (20 µg/ml) and a mock monoclonal antibody was used as a control. The secondary goat anti-mouse IgG-TRITC (Sigma) antibody was used at a dilution of 1:200.

Galactomannan was labeled with a rat anti-Galactofuranose (Gal*f*) monoclonal antibody (EBA2, diluted 1:1000, a kind gift of M. Tabouret from BioRad, Steenvorde [54]). Control Rat monoclonal antibody of the same isotype and the secondary goat anti-rat FITC (Sigma-Aldrich) antibody were used at a dilution of 1:1000 and 1:500, respectively.

β-(1,3)-glucan was labeled with the N-terminal β-(1,3)-glucan binding domain of *Drosophila* pattern recognition receptor, GNBP3 (homologous to Mammalian Dectin 1) at a concentration of 3 µg/ml and a polyclonal mouse antiserum against GNBP3 at 1:200 dilution (kind gifts from A. Roussel, CNRS, Orleans and D. Ferrandon, CNRS, Strasbourg, France [55]). Goat anti-mouse IgG FITC 1:200 diluted (Sigma) was used as secondary antibodies.

The glucosamine moiety of chitin/chitosan and mannose/glucose moieties of glycoproteins and glucans were labeled respectively with WGA-FITC and ConA-FITC (Sigma) at 0.1 mg/ml concentrations upon incubating the conidia for 15 min at lab temperature.

Susceptibility to oxidative stress conditions, Lactoferrin, Cathelicidin LL-37, HNP2 and hBD2 defensins, absence of iron and hypoxia

Stress conditions induced by Menadione (0 to 30 µM) and 2,5-Bis(*tert*-butylperoxy)-2,5-dimethylhexane (Luperox®101) (0 to 2 mM) were tested on both parental and mutant *A. fumigatus* strains grown on agar-RPMI (RPMI 1640, Sigma without glutamine) supplemented with 1% agar (Difco), 0.3 g/1 L-glutamine and 0.1 M MOPS or MES (to obtain a pH of 7 or 4, respectively) at 37°C for 24–48 h.

Stress conditions induced by Lactoferrin 0.45–231 µg/ml (Sigma) or Cathelicidin LL-37 0.45–231 µg/ml (Sigma), SDS (0.006–0.2%; Merck) and H_2O_2 (0.003–0.1%; Fluka) were tested on *A. fumigatus* strains grown on Brian medium without supplementation with iron or RPMI-glutamine-MOPS medium (described above) [38]. Combinations of 0.05% SDS or 0.012% H_2O_2 and Lactoferrin or Cathelicidin LL37 at concentrations of 231 µg/ml were tested in the same media, as described in Clavaud *et al* [38].

Stress condition induced by HNP2 (100 µg/ml; Sigma) and hBD2 (25 µg/ml; Sigma) defensins were also tested by incubating 10^6 conidia/ml with the defensins for 10–16 h at 37°C in RPMI-glutamine-MOPS medium.

The growth of *A. fumigatus* strains was tested in Brian medium without supplementation with iron at 37°C and under hypoxia conditions using Anaero*Gen* sachet (Oxoid), which reduces the oxygen level in a jar to below 1% that results to a CO_2 level between 9–13%.

Transmission electron microscopy (TEM)

Aliquots (20 µl) of concentrated conidia were placed onto a Formvar-coated nickel or gold mesh grids, which were then placed between the flat sides of two B-type brass planchets (Ted Pella Inc., Redding, CA). The grids were used as spacer creating a thin layer of cells that allows higher yields of well-frozen cells. The samples were immediately frozen with liquid nitrogen under high pressure (2,100 bar) using a Bal-Tec HPM 010 high pressure freezing machine (Bal-Tec Products, Middlebury, CT, USA). Following cryofixation, the samples were freeze-substituted at −85°C in 1% glutaraldehyde (Electron Microscopy Sciences, Washington, PA, USA) and 1% tannic acid in acetone for 72 h. After, the samples were rinsed thoroughly with three changes of fresh acetone at −85°C for a total of 45 min. Cells were infiltrated with 1% OsO_4 in acetone for 1 h at −85°C before being slowly warmed to room temperature over 5 h. The cells were then rinsed in acetone and slowly infiltrated with and polymerized in Spurr's resin. Embedded cells were cut into serial 70 nm thick sections with an Ultracut R Microtome (Leica, Vienna, Austria) and collected on Formvar-coated copper slot grids. Sections were post-stained with 2% uranyl acetate in 50% ethanol for 5 min followed by 5 min with Sato's lead citrate [56]. The grids were carbon-coated and viewed at 80 kV using a JEOL 1200EX transmission electron microscope (JEOL USA, Inc., Pleasanton, CA, USA).

Analysis of *ags*Δ mutant virulence

Female 8- to 10-week-old inbred C57BL6 (H-$2^{b)}$ mice were obtained from Charles River Breeding Laboratories (Calco, Italy). Experiments were performed according to the Italian Approved Animal Welfare Assurance A-3143-01. Breeding pairs of homozygous p47$^{phox-/-}$mice, raised on C57BL6 background, were purchased from Harlan Laboratories and bred under specific-pathogen free conditions at the breeding facilities of the University of Perugia, Perugia, Italy [33]. Infections were performed on one model of immunocompetent mice and in two different models of invasive pulmonary aspergillosis as previously described [6]. In the first immunosuppressed model, mice were subjected to intraperitoneal administration of cyclophosphamide (150 mg/kg body weight) one day before infection as described previously [6]. In the second immunosuppressed model, mice were treated with anti-Ly6G monoclonal antibody (clone RB6-8C5 MAb; eBienscience; 100 µg/mouse) administered intra-peritoneally one day before infection. Rat anti-*E. coli* β-galactosidase (clone GLL 113) was used as a control IgG. Treatment with the anti-Ly6G MAb is known to selectively deplete mature neutrophils, eosinophils and dendritic cells [57] and at 24 h after administration, the number of circulating neutrophils dropped to $20\pm12/mm^3$ compared to $1120\pm227/mm^3$ in controls, and the treated mice continued to be low for circulating neutrophils counts up to 5-days. Mice were monitored for survival and fungal growth (determined as colony forming unit (CFU) per organ) four days post-infection as

described previously [58]. All mice underwent necropsy for histopathological observation of fungal burden in the lungs four days post-infection. For histology, sections (3–4 μm) of paraffin-embedded lungs were stained following periodic acid-Schiff (PAS) protocol. Collection of the bronchoalveolar lavage (BAL) fluid and the morphometry [% monocytes (MNC) or polymorphonuclear (PMN) cells] was performed after four days infection as previously described [6]. Total and differential cell counts were performed after staining BAL smears with May-Grünwald Giemsa reagents (Sigma) before analysis. At least 200 cells per cytospin preparation were counted and the absolute number of each cell type was calculated. Cytospin preparations were observed using a BX51 microscope (Olympus, Milan, Italy). Histology images were captured using a high-resolution DP71 camera (Olympus).

For phagocytosis and conidiocidal activity, alveolar macrophages from uninfected mice were isolated from BAL as described [15]. For phagocytosis, macrophages were incubated at 37°C with unopsonized FITC (Sigma) labeled conidia [59] at an effector to conidial ratio of 5:1, for 1 h in RPMI medium in micro-chambers (Ibitreat). Unbound conidia were removed by washing with RPMI and cells were fixed with 3% (v/v) PFA for 1 h in PBS. After fixation, the cells were incubated with a rabbit polyclonal anti-FITC antibody (Invitrogen) diluted 1:2000 and a secondary rabbit antibody conjugated to Alexafluor 568 (dilution, 1:2000) (Invitrogen). This last procedure labels only cell surface-associated conidia and the ingested conidia remained unlabeled. The number of ingested conidia per macrophage was determined on 200 macrophages. For conidiocidal activity, macrophages isolated from uninfected C57BL6 (H-2^b) and $p47^{phox-/-}$ mice were incubated at 37°C with unopsonized resting or swollen conidia (6½ h in RPMI at 37°C), at an effector to fungal cell ratio of 1:10, for 2–6 hours in an ELISA plate wells. After removing the supernatant, Triton X100 (1%) was added to the wells and incubated at 37°C for 10 min to lyse the macrophages and to collect phagocytized conidia. The percentage of phagocytized conidia capable of further germination was determined by spotting phagocytized conidia (at suitable dilution) on a nutritive agar medium and counting those conidia capable of forming germ tube among spotted conidial population. We verified that the use of Triton X100 to lyse macrophage did not affect conidial germination as the percentage of germinations were similar (97±1%) for the *ags*Δ_*5T*, *ags*Δ_*n6.2*, *ags*Δ_*n8* mutants and the parental strain with or without Triton-treatment. The differences in the germination of the conidia from the stock solution used for macrophage conidicidal activity study permitted the calculation of conidiocidal activity.

For cytokine quantification, total RNA was extracted from lungs of immunocompetent mice four days post-infection, or from macrophages isolated from BAL fluid of uninfected mice and incubating with *ags*Δ NaCl extracts containing 3.2 μg proteins, for 5 h. The cytokines expressed and productions were quantified by Real-time PCR and ELISA, respectively as described previously [6].

Statistical significance was analyzed by one- or two-way ANOVA or paired t-test with Prism software (GraphPad software, San Diego, CA) and p-values≤0.05 were considered to be significant. Data were representative of at least two independent experiments or pooled from three to five experiments. The *in vivo* groups consisted of six mice/group and experiments were repeated at least three times. Macrophage experiments were done three times with three different batches of macrophages and conidia.

All experiments were performed using the *ags*Δ_*5T*(Figs. 1–10, Table 1, Table S1). Virulence and proteomic analyses were performed also using *ags*Δ_*n8* (Figs. S1, S2, S3, S4, S5, S6, S7, S8, Table 1 and Table S1). Major phenotypes and virulence data were verified with agsΔ_*n6.2* (Figs. S1, S5, S6, S7, S8).

Ethics statement

Mouse experiments were performed according to the Italian Approved Animal Welfare Assurance 245/2011-B. Legislative decree 157/2008-B regarding the animal license was obtained by the Italian Ministry of Health lasting for three years (2008–2011). Infections were performed under avertin anesthesia and all efforts were made to minimize suffering.

Supporting Information

Figure S1 Immunocompetent mice infected with resting conidia of *ags*Δ triple mutants and parental *ku80* strain. Observations and analysis on mice were done four days post-infection. (A) Fungal CFUs in lungs infected with conidia of *ags*Δ_*5T*, *ags*Δ_*n6.2*, *ags*Δ_*n8* and *ku80*. (B) lung histology (periodic acid-Schiff-staining) and (C) Percentages of monocytes and polymorphonuclear cells found in the lung alveolar lavage (BAL) of mice infected with conidia of *ags*Δ_*n6.2* and *ags*Δ_*n8* mutants (periodic acid-Schiff-staining and Gomori's methanamine silver-staining) (D) Relative expression of TNFα and IL10 assessed by real time RT-PCR of the total RNA extracted from the lungs of naïve and mice infected with conidia of *ags*Δ_*n6.2* and *ags*Δ_*n8* mutants and *ku80*. Data are representative of at least three independent experiments. Ctl, naïve mice; *, P<0.05.
(TIF)

Figure S2 Survival of Cyclophosphamide immunosuppressed mice infected with resting conidia of *ags*Δ_*n8* mutant and parental *ku80* strains. The survival is expressed in percentage. Data are representative of at least three independent experiments.
(TIF)

Figure S3 Phagocytosis after 1 h incubation of *ags*Δ_*n8* and parental *ku80* resting conidia by the macrophages isolated from uninfected mice. Results expressed in number of conidia per macrophages. Data are representative of at least three independent experiments. *, P<0.05.
(TIF)

Figure S4 Imaging and adhesive properties of resting conidia of *ags*Δ_*n8* mutant. Structural changes correlate with a loss of cell surface adhesive properties. (A) Height images (z-range = 1 μm; recorded in water with silicon nitride tips); (B) adhesion force maps (z-range: 5 nN) corresponding to the height image; (C) Representative force-distance curves and adhesion force histograms (n = 1024) recorded on the surface of *ags*Δ_*n8* mutant conidia.
(TIF)

Figure S5 NaCl extracted proteins from the surface of the resting *ags*Δ triple mutant conidia. SDS-PAGE (10% gel) of proteins extracted after 2 h incubation of the resting conidia in 0.5M NaCl showing that the three triple *ags*Δ mutants (agsΔ_*5T*, agsΔ_*n8*, agsΔ_*n6.2*) displayed the similar protein patterns.
(TIF)

Figure S6 TNFα production or expression by macrophages (isolated from uninfected immunocompetent mice) upon interaction with the parental strain *ku80*, *ags*Δ_*n6.2* and *ags*Δ_*n8* resting conidia, or the *ags*Δ_*n8* and *ags*Δ_*n6.2* conidial NaCl extract (3.2 μg proteins) respectively. (A) TNFα was quantified after 5 h

macrophage-conidial interaction. (B) Relative expression of TNFα assessed by real time RT-PCR in total RNA from macrophages after 5 h incubation of the *ags*Δ*_n8* and *ags*Δ*_n6.2* conidial NaCl extract with macrophages. NaCl supernatant from *ku80* resting conidia incubated for 2 h in 0.5M NaCl was used as a control. NS: Non-stimulated. *, $P<0.05$.
(TIF)

Figure S7 Immunolabeling of Galactosaminogalactan (GAG) and galactomannan (GM) on the swollen conidial surface of the triple *ags*Δ mutants and parental *ku80* strains. Note that there is no differences in the amount of GAG (A) (labeled by an anti-GAG monoclonal antibody) and GM (B) (labeled by an anti-galf monoclonal antibody) in the triple *ags*Δ mutant and parental strains.
(TIF)

Figure S8 Immunolabeling of α-(1,3)-glucan. Germinating conidia were labeled with MOPC that recognises α-(1,3)-glucan, and mouse TRITC conjugated anti-IgG was used as the secondary antibody. Note the absence of labeling on the triple *ags*Δ mutants - *ags*Δ*_5T*, *ags*Δ*_n6.2* and *ags*Δ*_n8*.
(TIF)

Table S1 Identification of NaCl extracted conidial surface proteins from the *ags*Δ*_5T* and *ags*Δ*_n8* mutants by MALDI-TOF/TOF. [(1)]Number of peptide peaks identified per protein.
(DOCX)

Acknowledgments

We thank Maria Pötsch for her excellent technical support.

Author Contributions

Conceived and designed the experiments: AB OK VB RWR ED MC LR JPL AAB. Performed the experiments: AB SB OK CF VB RWR. Analyzed the data: AB OK VB ED MC LR JPL. Contributed reagents/materials/analysis tools: AB SB OK VB CH RWR ED. Wrote the paper: AB SB OK VB RWR ED JPL.

References

1. Rappleye CA, Eissenberg LG, Goldman WE (2007) Histoplasma capsulatum alpha-(1,3)-glucan blocks innate immune recognition by the beta-glucan receptor. 2007 104: 1366–1370.
2. Reese AJ, Yoneda A, Breger JA, Beauvais A, Liu H, et al. (2007) Loss of cell wall alpha(1–3) glucan affects Cryptococcus neoformans from ultrastructure to virulence. Mol Microbiol 63: 1385–1398.
3. Maubon D, Park S, Tanguy M, Huerre M, Schmitt C, et al. (2006) AGS3, an alpha(1–3)glucan synthase gene family member of Aspergillus fumigatus, modulates mycelium growth in the lung of experimentally infected mice. Fungal Genet Biol 43: 366–375.
4. Beauvais A, Schmidt C, Guadagnini S, Roux P, Perret E, et al. (2007) An extracellular matrix glues together the aerial-grown hyphae of Aspergillus fumigatus. Cell Microbiol 9: 1588–1600.
5. Fontaine T, Beauvais A, Loussert C, Thevenard B, Fulgsang CC, et al. (2010) Cell wall alpha1-3glucans induce the aggregation of germinating conidia of Aspergillus fumigatus. Fungal Genet Biol 47: 707–712.
6. Bozza SC, Cecile; Giovannini, Gloria; Fontaine, Thierry; Beauvais, Anne; Sarfati, Jacqueline; et al (2009) Immune sensing of Aspergillus fumigatus proteins, glycolipids and polysaccharides and the impact on Th immunity and vaccination. The Journal of Immunology 183: 2407–2414.
7. Beauvais A, Maubon D, Park S, Morelle W, Tanguy M, et al. (2005) Two alpha(1–3) glucan synthases with different functions in Aspergillus fumigatus. Appl Environ Microbiol 71: 1531–1538.
8. Henry C, Latge JP, Beauvais A (2012) alpha1,3 glucans are dispensable in Aspergillus fumigatus. Eukaryot Cell 11: 26–29.
9. Dague E, Delcorte A, Latge JP, Dufrene YF (2008) Combined use of atomic force microscopy, X-ray photoelectron spectroscopy, and secondary ion mass spectrometry for cell surface analysis. Langmuir 24: 2955–2959.
10. Aimanianda V, Bayry J, Bozza S, Kniemeyer O, Perruccio K, et al. (2009) Surface hydrophobin prevents immune recognition of airborne fungal spores. Nature 460: 1117–1121.
11. Lambou K, Lamarre C, Beau R, Dufour N, Latge JP (2010) Functional analysis of the superoxide dismutase family in Aspergillus fumigatus. Mol Microbiol 75: 910–923.
12. Morelle W, Bernard M, Debeaupuis JP, Buitrago M, Tabouret M, et al. (2005) Galactomannoproteins of Aspergillus fumigatus. Eukaryot Cell 4: 1308–1316.
13. Monod M, Capoccia S, Lechenne B, Zaugg C, Holdom M, et al. (2002) Secreted proteases from pathogenic fungi. Int J Med Microbiol 292: 405–419.
14. Singh B, Oellerich M, Kumar R, Kumar M, Bhadoria DP, et al. (2010) Immuno-reactive molecules identified from the secreted proteome of Aspergillus fumigatus. J Proteome Res 9: 5517–5529.
15. Philippe B, Ibrahim-Granet O, Prevost MC, Gougerot-Pocidalo MA, Sanchez Perez M, et al. (2003) Killing of Aspergillus fumigatus by alveolar macrophages is mediated by reactive oxidant intermediates. Infect Immun 71: 3034–3042.
16. Bayry J, Aimanianda V, Guijarro JI, Sunde M, Latge JP (2012) Hydrophobins–unique fungal proteins. PLoS Pathog 8: e1002700.
17. Sriranganadane D, Waridel P, Salamin K, Reichard U, Grouzmann E, et al. (2010) Aspergillus protein degradation pathways with different secreted protease sets at neutral and acidic pH. J Proteome Res 9: 3511–3519.
18. Wang Z, Lienemann M, Qiau M, Linder MB (2010) Mechanisms of protein adhesion on surface films of hydrophobin. Langmuir 26: 8491–8496.
19. Jimenez-Ortigosa C, Aimanianda V, Muszkieta L, Mouyna I, Alsteens D, et al. (2012) Chitin synthases with a myosin motor-like domain control the resistance of Aspergillus fumigatus to echinocandins. Antimicrob Agents Chemother 56: 6121–6131.
20. Alsteens D, Aimanianda V, Hegde P, Pire S, Beau R, et al. (2013) Unraveling the Nanoscale Surface Properties of Chitin Synthase Mutants of Aspergillus fumigatus and Their Biological Implications. Biophys J 105(2):320–7.
21. Hogan LH, Klein BS (1994) Altered expression of surface alpha-1,3-glucan in genetically related strains of Blastomyces dermatitidis that differ in virulence. Infect Immun 62: 3543–3546.
22. Rappleye CA, Goldman GH (2006) Defining virulence genes in the dimorphing fungi. Ann Rev Microbiol 60: 281–303.
23. McDonald JU, Rosas M, Brown GD, Jones SA, Taylor PR (2012) Differential dependencies of monocytes and neutrophils on dectin-1, dectin-2 and complement for the recognition of fungal particles in inflammation. PLoS One 7: e45781.
24. Hohl TM, Feldmesser M, Perlin DS, Pamer EG (2008) Caspofungin modulates inflammatory responses to Aspergillus fumigatus through stage-specific effects on fungal beta-glucan exposure. J Infect Dis 198: 176–185.
25. Lamaris GA, Lewis RE, Chamilos G, May GS, Safdar A, et al. (2008) Caspofungin-mediated beta-glucan unmasking and enhancement of human polymorphonuclear neutrophil activity against Aspergillus and non-Aspergillus hyphae. J Infect Dis 198: 186–192.
26. Latge JP (2010) Tasting the fungal cell wall. Cell Microbiol 12: 863–872.
27. Feriotti C, Loures FV, Frank de Araujo E, da Costa TA, Calich VL (2013) Mannosyl-recognizing receptors induce an M1-like phenotype in macrophages of susceptible mice but an M2-like phenotype in mice resistant to a fungal infection. PLoS One 8: e54845.
28. Fujikawa T, Sakaguchi A, Nishizawa Y, Kouzai Y, Minami E, et al. (2012) Surface alpha-1,3-glucan facilitates fungal stealth infection by interfering with innate immunity in plants. PLoS Pathog 8: e1002882.
29. Roilides E, Dimitriadou-Georgiadou A, Sein T, Kadiltsoglou I, Walsh TJ (1998) Tumor necrosis factor alpha enhances antifungal activities of polymorphonuclear and mononuclear phagocytes against Aspergillus fumigatus. Infect Immun 66: 5999–6003.
30. Roilides E, Uhlig K, Venzon D, Pizzo PA, Walsh TJ (1993) Enhancement of oxidative response and damage caused by human neutrophils to Aspergillus fumigatus hyphae by granulocyte colony-stimulating factor and gamma interferon. Infect Immun 61: 1185–1193.
31. Henriet SS, Hermans PW, Verweij PE, Simonetti E, Holland SM, et al. (2011) Human leukocytes kill Aspergillus nidulans by reactive oxygen species-independent mechanisms. Infect Immun 79: 767–773.
32. Zarember KA, Sugui JA, Chang YC, Kwon-Chung KJ, Gallin JI (2007) Human polymorphonuclear leukocytes inhibit Aspergillus fumigatus conidial growth by lactoferrin-mediated iron depletion. J Immunol 178: 6367–6373.
33. D'Angelo C, De Luca A, Zelante T, Bonifazi P, Moretti S, et al. (2009) Exogenous pentraxin 3 restores antifungal resistance and restrains inflammation in murine chronic granulomatous disease. J Immunol 183: 4609–4618.
34. Kaur S, Gupta VK, Thiel S, Sarma PU, Madan T (2007) Protective role of mannan-binding lectin in a murine model of invasive pulmonary aspergillosis. Clin Exp Immunol 148: 382–389.
35. Moalli F, Doni A, Deban L, Zelante T, Zagarella S, et al. (2010) Role of complement and Fc{gamma} receptors in the protective activity of the long pentraxin PTX3 against Aspergillus fumigatus. Blood 116: 5170–5180.
36. Speth C, Rambach G (2012) Complement Attack against Aspergillus and Corresponding Evasion Mechanisms. Interdiscip Perspect Infect Dis 2012: 463794.

37. Zhang S, Fan Y, Xia YX, Keyhani NO (2010) Sulfonylurea resistance as a new selectable marker for the entomopathogenic fungus Beauveria bassiana. Appl Microbiol Biotechnol 87: 1151–1156.
38. Clavaud C, Beauvais A, Barbin L, Munier-Lehmann H, Latge JP (2012) The composition of the culture medium influences the beta-1,3-glucan metabolism of Aspergillus fumigatus and the antifungal activity of inhibitors of beta-1,3-glucan synthesis. Antimicrob Agents Chemother 56: 3428–3431.
39. Sheth CC, Hall R, Lewis L, Brown AJ, Odds FC, et al. (2011) Glycosylation status of the C. albicans cell wall affects the efficiency of neutrophil phagocytosis and killing but not cytokine signaling. Med Mycol 49: 513–524.
40. Shaler CR, Horvath C, Lai R, Xing Z (2012) Understanding delayed T-cell priming, lung recruitment, and airway luminal T-cell responses in host defense against pulmonary tuberculosis. Clin Dev Immunol 2012: 628293.
41. Svirshchevskaya EV, Shevchenko MA, Huet D, Femenia F, Latge JP, et al. (2009) Susceptibility of mice to invasive aspergillosis correlates with delayed cell influx into the lungs. Int J Immunogenet 36: 289–299.
42. Brian PW, Dawkins AW, Grove JF, Hemming HG, Lowe D, et al. (1961) Phytotoxic compounds produced by Fusarium equiseti. . J Exper Bot 12: 1–12.
43. da Silva Ferreira ME, Kress MR, Savoldi M, Goldman MH, Hartl A, et al. (2006) The akuB(KU80) mutant deficient for nonhomologous end joining is a powerful tool for analyzing pathogenicity in Aspergillus fumigatus. Eukaryot Cell 5: 207–211.
44. Mouyna I, Kniemeyer O, Jank T, Loussert C, Mellado E, et al. (2010) Members of PMT family in Aspergillus fumigatus differentially affect growth, morphogenesis, and viability. Mol Microbiol 76: 1205–1221.
45. Klimpel KR, Goldman WE (1988) Cell walls from avirulent variants of Histoplasma capsulatum lack alpha-(1,3)-glucan. Infect Immun 56: 2997–3000.
46. Harris SD, Morrell JL, Hamer JE (1994) Identification and characterization of Aspergillus nidulans mutants defective in cytokinesis. Genetics 136: 517–532.
47. Dague E, Jauvert E, Laplatine L, Viallet B, Thibault C, et al. (2011) Assembly of live micro-organisms on microstructured PDMS stamps by convective/capillary deposition for AFM bio-experiments. Nanotechnology 22: 395102.
48. Hutter S, Heinritzi K, Reich E, Ehret W (1993) [Effects of different methods of tooth resection in suckling piglets]. Tierarztl Prax 21: 417–428.
49. Bradford M (1976) A rapide and sensitive method for the quantification of microgram quantities of protein utilizing the principle of protein-dye binding. . Anal Biochem 72: 248–254.
50. Kniemeyer O, Lessing F, Scheibner O, Hertweck C, Brakhage AA (2006) Optimisation of a 2-D gel electrophoresis protocol for the human-pathogenic fungus Aspergillus fumigatus. Curr Genet 49: 178–189.
51. Candiano G, Bruschi M, Musante L, Santucci L, Ghiggeri GM, et al. (2004) Blue silver: a very sensitive colloidal Coomassie G-250 staining for proteome analysis. Electrophoresis 25: 1327–1333.
52. Lamarre C, Beau R, Balloy V, Fontaine T, Wong Sak Hoi J, et al. (2009) Galactofuranose attenuates cellular adhesion of Aspergillus fumigatus. Cell Microbiol 11: 1612–1623.
53. Fontaine T, Delangle A, Simenel C, Coddeville B, van Vliet SJ, et al. (2011) Galactosaminogalactan, a new immunosuppressive polysaccharide of Aspergillus fumigatus. PLoS Pathog 7: e 1002372.
54. Stynen D, Sarfati J, Goris A, Prevost MC, Lesourd M, et al. (1992) Rat monoclonal antibodies against Aspergillus galactomannan. Infect Immun 60: 2237–2245.
55. Mishima Y, Quintin J, Aimanianda V, Kellenberger C, Coste F, et al. (2009) The N-terminal domain of Drosophila Gram-negative binding protein 3 (GNBP3) defines a novel family of fungal pattern recognition receptors. J Biol Chem 284: 28687–28697.
56. Takagi I, Yamada K, Sato T, Hanaichi T, Iwamoto T, et al. (1990) J Electron Microsc (Tokyo) 39: 67–68.
57. Bonifazi P, D'Angelo C, Zagarella S, Zelante T, Bozza S, et al. (2010) Intranasally delivered siRNA targeting P13K/Akt/mTOR inflammatory pathways protects from aspergillosis. Mucosal Immnunol 3: 193–205.
58. Bozza S, Perruccio K, Montagnoli C, Gaziano R, Bellocchio S, et al. (2003) A dendritic cell vaccine against invasive aspergillosis in allogeneic hematopoietic transplantation. Blood 102: 3807–3814.
59. Sturtevant J, Latge JP (1992) Participation of complement in the phagocytosis of the conidia of Aspergillus fumigatus by human polymorphonuclear cells. J Infect Dis 166: 580–586.

Résumé

Mon travail de thèse consiste à utiliser les techniques de Microscopie à Force Atomique (AFM) pour étudier les microorganisms pathogènes, et leurs interactions avec des antimicrobiens. Ces dernières décennies, la résistance microbienne a augmenté de façon dramatique et s'est répandue dans le monde. Les bactéries et levures pathogènes ont développé différents moyens pour résister à presque tous les antimicrobiens utilisés. Ces pathogènes peuvent être la cause d'une large gamme d'infections superficielles ; ils sont aussi à l'origine d'infections mettant en jeu la vie de patients. Il y a donc deux urgences : la première est de trouver de nouvelles molécules antimicrobiennes, avec un mécanisme d'action innovant. Mais pour atteindre cet objectif, il est nécessaire d'acquérir des données fondamentales sur la paroi des microorganismes, afin d'identifier des cibles originales à leur surface pour de nouvelles molécules. La deuxième urgence est donc de développer des techniques pour explorer la paroi des microorganismes d'un point de vue différent, ce qui nécessite une approche expérimentale originale. Dans ce contexte, les approches biophysiques restent sous-exploitées en microbiologie clinique. Durant cette thèse, nous avons utilisé une technologie provenant de la physique, l'AFM, adapté aux conditions biologiques. Le principe de l'AFM est basé sur la mesure d'une force entre une pointe et un échantillon ; en gardant cette force constante pendant le scan de l'échantillon il est possible d'en obtenir une image tridimensionnelle. Un avantage de l'AFM est la possibilité de travailler en liquide, ce qui nous a permis d'imager l'élongation de cellules bactériennes *P. aeruginosa* traité avec de la ticarcilline, un antibiotique à cible pariétale, ainsi que la disparition des polysaccharides capsulaires de la bactérie *K. pneumoniae* traitée avec de la colistine. Cependant, l'immobilisation des échantillons est souvent un challenge, différent pour chaque type de microorganismes. L'immobilisation d'échantillons biologiques représente un domaine de recherche à part entière, qui nous a conduit à développer un timbre de polydiméthylsiloxane (PDMS) microstructuré, pour immobiliser des cellules rondes de différentes tailles, comme des levures. Une fois cette étape d'immobilisation franchie, l'AFM peut être utilisé dans les modes classiques d'imagerie et de spectroscopie de force (mode contact, mode oscillant, mode force volume), mais aussi dans des modes avancés afin d'obtenir des données à haute résolution ou multiparamétriques. En effet, l'AFM est aussi une machine de force très sensible capable d'enregistrer des courbes de force qui permettent d'accéder aux propriétés nanomécaniques et d'adhésion des cellules. Ainsi nous avons pu imager et quantifier les propriétés nanomécaniques et adhésives de microorganisms, mais aussi de cellules de mammifères vivantes et de leurs noyaux isolés. Nous avons ainsi observé les modifications des propriétés adhésives de la levure *C. albicans* traité avec de la caspofongine. Enfin pour aller plus loin dans l'étude de l'architecture des parois des microorganismes, il est possible de fonctionnaliser des pointes AFM avec des biomolécules. Une stratégie développée a consisté à lier des anticorps dirigés contre un peptide sur la pointe, et de tagguer des protéines avec ce même peptide à la surface des cellules, Ainsi nous avons localisé des protéines spécifiques à la surface de levures et cellules de mammifères vivantes. Une autre stratégie développée consiste à directement lier une biomolécule sur la pointe, qui interagit naturellement avec un composé pariétal. Nous avons utilisé cette stratégie pour étudier la paroi de la bactérie *P. aeruginosa* traité par un antibactérien innovant, le Cx1, et ainsi mieux comprendre l'architecture de son peptidoglycane. Pour conclure, cette thèse a permis d'adresser spécifiquement la contribution de la biophysique en microbiologie clinique.